Dynamics of stream and groundwater exchange using environmental tracers

submitted by

Jodie Lee Pritchard BSc (Hons)

As requirement in full for the degree of

Doctor of Philosophy

in the

School of Chemistry, Physics and Earth Sciences,

Faculty of Science and Engineering

Flinders University of South Australia

August 2005

TABLE OF CONTENTS

LIST OF FIGURES

LIST OF TABLES

LIST OF SYMBOLS

C^0	^{222}Rn activity upstream	(Bq L^{-1})
$C^0_{\max}$	Maximum predicted upstream ^{222}Rn activity	(Bq L^{-1})
C_{ss}	Steady state ^{222}Rn activity of groundwater	(Bq L^{-1})
C_{ss}^{AGW}	Steady state ^{222}Rn emanation from alluvial aquifer sands	(Bq L^{-1})
C^B	Background ^{222}Rn activity in stream water	(Bq L^{-1})
$C_{\max}^{RGW}$	Maximum ^{222}Rn activity measured in regional groundwater	(Bq L^{-1})
$C_{\min}^{RGW}$	Minimum ^{222}Rn activity measured in regional groundwater	(Bq L^{-1})
C^{gw}	^{222}Rn activity of groundwater	(Bq L^{-1})
C^{i-1}	^{222}Rn activity upstream of a distance interval, i	(Bq L^{-1})
C_R^i	^{222}Rn activity downstream of a distance interval, i, due to radioactive decay losses	(Bq L^{-1})
C_T^i	^{222}Rn activity downstream of a distance interval, i, due to turbulent losses	(Bq L^{-1})
$C_{\min}^i$	Minimum ^{222}Rn activity of groundwater input to streamflow	(Bq L^{-1})
C^j	^{222}Rn activity of stream water lost to the adjacent aquifer	(Bq L^{-1})
c_m	^{222}Rn activity within aquifer matrix	(Bq L^{-1})
C_m	Cl^- concentration of mixed pore water and deionised water	(mg L^{-1})
C_{pw}	Cl^- concentration of pore water	(mg L^{-1})
C^n	^{222}Rn activity downstream	(Bq L^{-1})
C_R^n	^{222}Rn activity downstream due to radioactive decay	(Bq L^{-1})
C_T^n	^{222}Rn activity downstream	(Bq L^{-1})
C_{TR}^n	Predicted ^{222}Rn activity downstream after turbulent and radioactive losses	(Bq L^{-1})
C^{222}	The ^{222}Rn concentration in a closed system	(Bq L^{-1})
C^{226}	^{222}Rn concentration produced by the radioactive decay of ^{226}Ra	(Bq L^{-1})
D	Molecular diffusivity of ^{222}Rn	(at 23°C 1.2×10^{-9} m^2 s^{-1})

E	^{222}Rn emanation rate	(Bq kg^{-1})
ε	Porosity	(cm^3 cm^{-3})
f	Fraction of surface water lost to the adjacent aquifer	
f_{aq}	Porosity of aquifer material (expressed as a fraction)	
f^0	Fraction of surface water lost to the adjacent aquifer that originates from Q^0	
$1-f^0$	Fraction of surface water lost to the adjacent aquifer that originates from Q^{gw}	
h	Average depth of stream	(m)
h_{eq}	Equivalent freshwater head	(m)
h_m	Measured head	(m)
i	Interval number, integer fraction of n	
L_n^0	^{222}Rn loss from stream water between consecutive surface water sampling stations (i.e. between *0* and *n*)	(Bq L^{-1})
L_n^{gw}	^{222}Rn loss from groundwater that contributes to stream flow between consecutive surface water sampling stations (i.e. between *0* and *n*)	(Bq L^{-1})
L_j^0	^{222}Rn loss from stream water before it discharges to the adjacent aquifer	(Bq L^{-1})
L_j^{gw}	^{222}Rn loss from groundwater that contributes to stream flow and later recharges the adjacent aquifer	(Bq L^{-1})
λ	^{222}Rn decay constant	(2.098 × 10^{-5} s^{-1})
M_{cw}	Mass of wet soil and chipette	(g)
M_{cd}	Mass of dry soil and chipette	(g)
M_c	Mass of chipette	(g)
M_d	Mass of oven-dried soil	(g)
M_{dw}	Mass of deionised water	(g)
M_{pw}	Mass of pore water ($M_{pw} = \theta_g \times M_w$)	(g)
M_w	Mass of wet soil	(g)
n	Number of equal sections over a constant distance, x	
Q^0	Stream discharge at upstream sampling station	(m^3 s^{-1})

Q^j	Stream water discharged (lost) to the adjacent aquifer	(m^3 s^{-1})
Q^n	Stream discharge at downstream sampling station	(m^3 s^{-1})
Q^{gw}	Groundwater discharged to stream flow	(m^3 s^{-1})
Q^{sw}	Stream discharge	(m^3 s^{-1})
Q^{gw}/Q^{sw}	Fraction of groundwater in stream water at downstream sampling station	
$^{222}R_{meas}$	^{222}Rn activity measured in groundwater	(Bq L^{-1})
ρ_b	Bulk density	(g cm^{-3})
ρ_{fw}	Density of freshwater	(1 kg m^{-3})
ρ_m	Density of measured groundwater	(kg m^{-3})
ρ_s	Particle density	(g cm^{-3})
θ_g	Gravimetric water content of soils	(g^{-1} g^{-1})
t	Travel time between consecutive sampling stations	(s)
T	Time of ^{222}Rn ingrowth	(s)
TDS	Total dissolved solids	(mg L^{-1})
TDS_m	Total dissolved solids measured in groundwater	(kg m^{-3})
v	Velocity of stream water	(m s^{-1})
V	Volume of soil core	(cm^{-3})
V^{gw}	Volume of groundwater discharged to the stream channel	(L)
x	Distance between sampling stations	(m)
z	Thickness of stagnant film	(m)
$\%AGW_{\min}$	Minimum percentage of stream water sourced from alluvial groundwater	
$\%RGW_{\min}$	Minimum percentage of stream water sourced from regional groundwater	
$\%AGW_{\max}$	Maximum fraction of stream water sourced from alluvial groundwater	
$\%RGW_{\max}$	Maximum fraction of stream water sourced from regional groundwater	

ABSTRACT

Regions of surface water and groundwater exchange are major sites for the transfer and transformation of solutes and nutrients between stream and subsurface environments. Conventional stream and groundwater exchange investigations are limited by methodologies that require intensive field investigations and/or the set-up of expensive infrastructure. These difficulties are exacerbated where hydraulic gradients are very low and stream discharge highly variable. This thesis uses a suite of environmental tracers (Cl^-, ^{222}Rn, δ^2H & $\delta^{18}O$, $^{87}Sr/^{86}Sr$) to characterise the extent of stream and groundwater exchange between a sand bed stream and adjacent alluvial aquifer in a subtropical catchment (the Wollombi Brook) of eastern Australia. The aims were to identify sources and relative contributions of different sources of groundwater to stream discharge and specifically to improve the methodology of using ^{222}Rn to obtain quantitative estimate of groundwater fluxes.

The sensitivity of the ^{222}Rn technique for identifying groundwater discharge based on the ^{222}Rn concentration in stream water was improved via an iterative numerical approach to account for ^{222}Rn loss from stream water via turbulent gas exchange and radioactive decay. Optimal distances between stream sampling points for defining the magnitude of groundwater discharge to stream flow based on ^{222}Rn concentrations in stream water is a function of average stream velocity and water depth. The maximum allowable distance between sampling points for determining the magnitude of groundwater discharge to the Wollombi Brook was 2 km. This work showed that groundwater discharged to all reaches of the Wollombi Brook during baseflow and flood recession conditions. Alluvial groundwater contributed <30% of water to stream flow in the mid Wollombi Brook catchment.

Dilution of steady-state ^{222}Rn concentrations measured in transects from the stream to the alluvial sediments showed that significant surface water and groundwater exchange occurs even when gradients between surface water and groundwater are low. Lateral stream water influx to the adjacent alluvial aquifer was more extensive in the lowland areas of the Wollombi Catchment during low flow than flood recession conditions. Extensive stream water influx to the adjacent alluvial aquifer occurs contrary to the net direction of surface water and groundwater flux (as indicated by hydraulic gradients toward the stream channel). The rate of stream and groundwater exchange within the adjacent alluvial aquifer appears to be greatest during baseflow conditions. Fresh alluvial groundwater appeared to provide a buffer against higher salinity regional groundwater discharge to the alluvial aquifer in some reaches of the Wollombi Brook catchment. Pumping of the alluvial aquifer and diversions of surface water may jeopardise the water quality and volume of the alluvial aquifer and induce water flow from the regional aquifer toward the stream, potentially salinising the fresh alluvial aquifer and subsequently the stream.

The change in the Cl^- concentration and the variation in slope of the δ^2H-$\delta^{18}O$ line between consecutive stream sampling points could be used to differentiate between regional and alluvial groundwater discharge to stream flow. Incorporating this information with three-component end-member mixing using $[Sr^{2+}]$ and $^{87}Sr/^{86}Sr$ showed that stream and alluvial groundwater exchange within the stream channel was highest in the lowland floodplains during low flow conditions. The least stream and alluvial groundwater exchange occurred in the low streambed gradient mid reaches of the Wollombi Brook regardless of stream stage. The greatest difference in the degree of stream and alluvial groundwater exchange between high and low stream stages occurred in the lowland floodplains of the Wollombi Brook.

DECLARATION OF ORIGINALITY

I certify that this thesis does not incorporate without acknowledgement any material previously submitted for a degree or diploma in any university; and that to the best of my knowledge and belief it does not contain any material previously published or written by any other person except where due reference is made in the text.

Jodie Lee Pritchard

August 2005

PUBLICATIONS ASSOCIATED WITH THIS THESIS

JOURNAL PAPERS

Lamontagne S, Herczeg A L, Dighton J C, Jiwan J S, **Pritchard J L** (2005). Patterns in nitrogen concentration in the floodplain of a subtropical stream (Wollombi Brook, New South Wales). *Biogeochemistry*, **72(2)**: 169-190.

Pritchard J L, Herczeg A L (in prep). Dynamics of exchange of water between alluvial groundwater ↔ regional groundwater and surface water ↔ alluvial groundwater: Testing conceptual flow processes in near-stream subsurface. Journal of Hydrology.

Pritchard J L, Herczeg A L, Lamontagne S (in prep). Comparison of sources of water to stream flow during baseflow and flood recession. Hydrological Processes.

TECHNICAL REPORTS

Lamontagne S, Herczeg A, Dighton J C, **Pritchard J L**, Jiwan J S, Ullman W J (2003). Groundwater-surface water interactions between streams and alluvial aquifers: Results from the Wollombi Brook (NSW) study (Part II – Biogeochemical processes). CSIRO Land and Water, Technical Report 42/03, July 2003, pp. 64.

CONFERENCE PAPERS

Pritchard J, Herczeg A, Lamontagne S (2003). Comparison of environmental isotopes for tracing groundwater-surface water interactions in a sand-bed stream. Proceedings from the International Symposium on Isotope Hydrology and Integrated Water Resources Management, IAEA, May 19 - 23, Vienna, Austria: 153-154.

Pritchard J L, Herczeg A L (2003). Tracing sources of water to an alluvial aquifer using strontium isotopes and radon. Proceedings from the EGS - AGU - EUG Joint Assembly, April 7 - 11, Nice, France: 297.

Pritchard J, Herczeg A, Lamontagne S (2003). Tracing seasonal groundwater contributions to stream flow using a suite of environmental isotopes. Proceedings from the EGS - AGU - EUG Joint Assembly, April 7 - 11, Nice, France: 295.

Pritchard J, Herczeg A, Lamontagne S (2002). The use of environmental tracers for estimating the seasonal contributions of groundwater to streamflow. Proceedings from the International Conference on balancing the water budget, IAH, May 12 – 17, Darwin, NT, Australia. pp 6.

Pritchard J, Herczeg A, Lamontagne S (2001). Tracing exchange of water between streams and alluvial aquifers using environmental isotopes. Proceedings from the 7th Australasian conference on Isotopes in the Environment, 24 - 26 September 2001, Robertson, NSW, Australia: 37-38.

Lamontagne S, Herczeg A, Leaney F, Dighton J, **Pritchard J**, Ullman W, Jiwan J (2001). Nitrogen attenuation by stream riparian zones: Prospects for Australian landscapes. Proceedings of the 8th Murray-Darling Basin groundwater workshop 2001, 4 – 6 September 2001, Victor Harbour, SA, Australia.

Herczeg A, Lamontagne S, **Pritchard J**, Leaney F, Dighton J, Jiwan J, Smith P (2001). Groundwater – surface water interactions: testing conceptual models with environmental tracers. Proceedings of the 8th Murray-Darling Basin groundwater workshop 2001. 4 – 6 September 2001, Victor Harbour, SA, Australia.

Lamontagne S, Herczeg A, Conway C, **Pritchard J**, Leaney F, Dighton J, Jiwan J (2001). Exchange of water and nutrient transformations in a sub-tropical stream-alluvial aquifer system. 28th congress of the International Society for Limnology, 4-10 February 2001, Melbourne, Vic, Australia.

Pritchard J L, Lamontagne S, Herczeg A L (2001). Tracing exchange of water between streams and alluvial aquifers using stable isotopes of water. 28th congress of the International Society for Limnology, 4-10 February 2001, Melbourne, Vic, Australia.

ACKNOWLEDGEMENTS

The work presented in this thesis was realised through the support of numerous organisations and individuals. I wish to thank Land and Water Australia for funding the project (Project No. CLW7), the New South Wales Government Department of Natural Resources (DIPNR), CSIRO Land & Water, Flinders University and Centre for Groundwater Studies for financial and in-kind support they provided for this project.

I owe a great deal of thanks to my supervisor Dr. Andrew Herczeg (CSIRO Land & Water, Adelaide) for sharing his vast geochemical knowledge and for his continual guidance and encouragement. Especially in the last six months, when exploring Europe would have been far more appealing than reviewing chapters of my thesis. Thank you to my co-supervisor Dr. Corinne Le Gal La Salle (Flinders University) for managing the university administration.

I thank my colleagues at CSIRO Land & Water (Adelaide) for their invaluable knowledge, support and encouragement. Specifically I would like to thank Dr. Sébastien Lamontagne for our countless biogeochemistry discussions and for his enthusiastic approach to field expeditions. Thank you to my dear friend John Dighton for his moral support, encouragement and tremendous technical skill and help in the field and laboratory. John and Sébastien made field trips a real joy with their impromptu folk music renditions. I wish to thank Dr. Peter Cook for his technical help in measuring ^{222}Rn emanation. Thank you to Megan Lefournour and Michelle Caputo for teaching me the delicate art of deuterium and oxygen-18 analyses and for making laboratory work a party.

My sincere thanks to Dr. John Foden (Adelaide University) for opening up his laboratories to me and to David Bruce (Adelaide University) for his attentive instruction in strontium isotope analysis.

I benefited enormously from philosophical discussions with staff from Flinders University and with my fellow PhD students. A special thanks to Dr. John Hutson for his help and enthusiasm during the inception phase of my research. Many thanks to Rebecca Doble for sharing the highs and lows of every step of the PhD experience with me.

Thank you to my employer, REM, for supporting me in my studies over the last year and a half and for allowing me the flexibility to finish writing up.

My family have provided vital ongoing support throughout my studies. Thank you to my parents Teresa and Don for their unreserved support and encouragement, and my sister Mandy for her love and cheer.

Last but not least I thank my extraordinarily patient companion Doug Weatherill. He has helped me by taking on mundane tasks such as formatting my references through to discussing the finer points of numerical modelling with me.

1 INTRODUCTION

1.1 SCOPE

Stream and groundwater exchange processes influence the chemical and biological conditions of stream and groundwater ecosystems. In many stream systems, flow is sustained by groundwater discharge during low flow conditions (e.g. Freeze and Cherry 1979). In addition, groundwater discharge delivers essential nutrients to streams for ecosystem function (e.g. Fiebig *et al.* 1990, Triska *et al.* 1993). From the opposite perspective, stream water influxes can deliver dissolved oxygen and organic matter to anaerobic groundwater systems, which activates a myriad of biogeochemical reactions that attenuate some chemicals whilst mobilising others (e.g. nitrification). Because chemical transformations prompted by stream water influxes to the groundwater system may in turn deliver essential chemical constituents back to the stream (e.g. Hendricks and White 1991, Valett *et al*. 1990), the dynamic regimes of stream and groundwater exchange need to be understood.

One area that has received relatively little attention is the interface between groundwater and streams – the hyporheic zone. Changes in hyporheic exchange can limit (1) the delivery of essential chemicals to streams and subsurface environments for ecosystem function, and (2) the capacity of the hyporheic zone to attenuate potential pollutants prior to recharging the aquifer system or discharging to streams leading to water quality problems (e.g. eutrophication). Subsurface refuges may no longer be suitable for surface biota, changing their ability to recover after disturbances, and reducing reproductive success of fish dependent on hydrological exchange (e.g. aeration of sediments). Knowing the mechanisms and rates of dynamic hydrologic exchange processes is an essential component underpinning the investigation of more complex biogeochemical processes that will aid in the

development of water resource management plans that protect stream and subsurface ecosystems. This study evaluates the use of environmental tracers for determining the direction and magnitude of stream and groundwater exchange under low hydraulic gradient conditions.

1.1 PREVIOUS WORK

Exchange of water through the hyporheic zone is driven by a number of processes including:

1. The distribution and magnitude of hydraulic conductivities both within the stream channel and the associated alluvial sediments (e.g. Dahm *et al*. 1998, Winter *et al*. 1998, Wroblicky *et al*. 1998);
2. The relation of stream stage to groundwater levels in the adjacent aquifer (e.g. Winter *et al*. 1998); and
3. The morphology and position of the stream channel within the alluvial sediments (e.g. Harvey and Bencala 1993, Woessner 2000).

As a result stream and groundwater exchange varies spatially due to aquifer heterogeneity and temporally due to changes in stream and groundwater levels. For example, hydrometric studies have found that, in gravel-bed streams where high gradients between groundwater and surface water exists, hyporheic exchange is reduced during high flows (Harvey *et al.* 1996, Wroblicky *et al.* 1998).

Exchange between streams and groundwater has been characterised in previous studies by:

1. Measuring water levels in piezometers installed within the streambed and adjacent alluvial aquifer (e.g. Lee and Cherry 1978, Triska *et al*. 1989, Wondzell and Swanson 1996, Woessner 2000);

2. Gauging stream flows at a number of cross sections over a short period of time and comparing discharge measurements (e.g. Woessner 2000);
3. Comparing groundwater and stream water geochemistry (e.g. Rutherford and Hynes 1987, Hoehn and von Gunten 1989, Benner *et al*. 1995, Woessner 2000); and
4. Conducting stream channel tracer injection studies (e.g. Harvey *et al*. 1996, Harvey and Wagner 2000).

Hyporheic exchange surveys have been confined to the reach-scale, to low order streams and to where hydraulic gradients between streams and adjacent aquifers are high. Investigations have been limited by methodologies that require intensive field investigations and/or the set-up of expensive infrastructure. These challenges and others associated with heterogeneity and methodological access to hyporheic zones have limited the general understanding of dynamic water fluxes between streams and adjacent aquifers and the processes that contribute to them. Spatial and temporal dynamics of stream and groundwater exchange in relation to geomorphology are poorly understood (Dahm *et al*. 1998). Robust methodology is required to characterise the direction and magnitude of surface water and groundwater exchange that (1) can be applied to low gradient environments, (2) can be extrapolated from reach-scale to the catchment-scale, and (3) does not need expensive infrastructure.

1.2 AIMS OF THE THESIS

The broad objective of this thesis is to apply environmental tracer methods to determine the direction and magnitude of water exchange between streams and adjacent aquifers in low gradient environments. A suite of environmental tracers (Cl^-, ^{222}Rn, δ^2H & $\delta^{18}O$, $^{87}Sr/^{86}Sr$) were used to define (1) the extent of stream water influx to the adjacent alluvial aquifer, (2) identify areas of preferred groundwater

discharge to stream flow, (3) identify the main sources and relative contributions of groundwater discharge to stream flow.

The specific aims are as follows:

1. Determine the direction and fluxes of exchange between surface water and groundwater in highlands to lowland floodplains during high and low stream discharge;
2. Develop a numerical approach to solve ^{222}Rn losses due to radioactive decay and turbulent gas exchange from surface water simultaneously to improve the identification of groundwater discharge to stream flow;
3. Determine optimal distances between stream water sampling stations for ^{222}Rn sampling so that the magnitude, in addition to the location, of groundwater discharge to stream flow can be estimated from ^{222}Rn concentrations in stream water; and
4. Develop a systematic multi-tracer approach (Cl^-, ^{222}Rn, δ^2H & $\delta^{18}O$, $^{87}Sr/^{86}Sr$) to differentiate between sources of water contributing to stream flow based on changes in stream water chemistry between sampling intervals.

The main hypotheses that are evaluated are (1) that the alluvial aquifer provided the dominant source of groundwater to stream flow under baseflow conditions, and (2) the relative contribution of regional groundwater to stream flow is greater in the highlands than in the lowland floodplains.

1.3 APPLICATION OF ENVIRONMENTAL TRACERS

Water exchange between streams and alluvial aquifers can be difficult to characterise by conventional (hydrodynamic) methods if hydraulic gradients are low. An alternative approach for characterising near-stream flow processes is to apply

environmental or artificial tracer techniques. Environmental tracers are naturally occurring chemical, isotopic and physical properties of water that can be used to trace the movement of water through catchments. Some practical tracers include (1) common dissolved constituents, such as major cations and anions; (2) stable isotopes of the water molecule (^{16}O, ^{18}O, ^{1}H and ^{2}H); (3) isotopes of strontium ($^{87}Sr/^{86}Sr$); (4) radioactive isotopes such as tritium (^{3}H) and radon (^{222}Rn); and (5) water temperature. When used in end-member mixing analysis and hydrologic transport calculations, environmental tracers can be used to (1) determine the origin of water and dissolved chemicals in a catchment, (2) calculate hydrologic and chemical fluxes between groundwater and surface water, (3) calculate residence times of water and dissolved chemicals, and (4) determine average rates of chemical reactions that take place during transport (Winter *et al.* 1998).

The effectiveness of these tracers at delineating the mixing between river water and groundwater is related to the chemical and isotopic differences between the end members and reactions that may occur between water and aquifer materials after mixing. Geochemical models, incorporating these chemical and isotopic data and analyses of aquifer mineralogy can be used for testing hypotheses on hydrological and dominant geochemical processes and to estimate the amount of mixing of river water with groundwater (e.g. NETPATH: Plummer *et al.* 1994) that occurs in the hyporheic zone.

A multi-tracer approach for hydrologic investigations has the advantage that different tracers can reveal different processes that occur in a catchment. Conservative (or unreactive) tracers (e.g. Cl^-, δ^2H & $\delta^{18}O$) can be used to validate flowpath prediction based on hydrologic measurements (e.g. Hunt *et al.* 1998) whereas solute (or reactive) tracers (e.g. $^{87}Sr/^{86}Sr$) can provide information about the reactions that occur along a specific flowpath (e.g. Krabbenhoft *et al.* 1994, Bullen *et al.* 1996).

Stable isotopes of water can often provide information about residence times and relative contributions from different water sources. However, flowpaths cannot always be identified using $\delta^{18}O$ or $\delta^{2}H$ data and simple hydrograph separation techniques because water travelling along a single flowpath can originate from several different sources (Ogunkoya and Jenkins 1991). Furthermore, if subsurface waters have variable isotopic compositions (e.g. from different recharge events) and variable residence times before discharging into a stream, two and three-component, constant composition mixing models can complicate hydrologic interpretations. Reactive solute isotopes (e.g. ^{87}Sr) can provide valuable information about flowpaths because they can reflect the reactions that are characteristic along specific flowpaths (Bullen *et al.* 1996, Bullen and Kendall 1998). Waters flowing through mineralogically distinctive horizons can be uniquely labelled by the chemical and isotopic compositions of their solutes (Douglas *et al.* 1995). Solute isotope applications are most revealing for tracing the relative contributions of potential sources to groundwater or surface water. Because solute isotope tracers are usually affected by a smaller number of processes than chemical constituents are, interpretations of changes in isotopic composition are less ambiguous than simultaneous changes in solute concentrations (Kendall *et al.* 1995).

1.4 OUTLINE OF ENVIRONMENTAL TRACERS USED

1.4.1 Chloride

Chloride (Cl^-) is often used in preference to other major ion chemical species as a solute tracer in hydrologic studies because it is widely considered to behave conservatively (e.g. Hayashi *et al.* 1998). There is some suggestion that Cl^- can be bound by adsorption processes during surface runoff (Chen *et al*. 2002). However, the impacts of groundwater discharge and evaporative processes on the Cl^-

concentration of stream water are likely to be magnitudes greater than adsorption processes in the current study.

Groundwaters tend to have higher Cl^- concentrations than stream waters and therefore increases in the Cl^- concentration of stream water can indicate locations of groundwater discharge. However, extended residence of water in the stream channel can also produce elevated Cl^- concentrations due to evaporative concentration, making the interpretation of this tracer more ambiguous. Therefore, additional tracers are valuable for differentiating between evaporative processes and groundwater discharges to the streams (e.g. stable isotopes of water).

1.4.2 Radon-222

^{222}Rn is an inert, naturally occurring radioactive gas (½-life 3.83 days), produced by the radioactive decay of ^{226}Ra (½-life 1.6×10^3 years). ^{226}Ra is part of the ^{238}U decay series and is present in sediments and sedimentary rocks. ^{222}Rn begins to diffuse through the crystal lattice of the enclosing mineral as soon as it is produced, however, because it has such a short half-life, most ^{222}Rn that is produced decays before it escapes the mineral. ^{222}Rn escapes from solid material by a process termed emanation. The emanating power (fraction of ^{222}Rn atoms produced that escape the crystalline structure of the rock) is usually greater for small-grained sediments than coarser-grained sediments (Kraemer and Genereux 1998). Salomons, Leaney and Herczeg (1991) associated low ^{222}Rn activities with low clay contents in soils. The concentration of ^{238}U (or ^{226}Ra) near the mineral surface also governs the rate of ^{222}Rn release from rocks and sediments. Cecil and Green (2000) summarise the potential processes by which ^{222}Rn emanates from the crystalline structure of a rock. Once it has escaped the sediment or rock, ^{222}Rn can freely migrate and accumulate in groundwater. In saturated soils it takes approximately three weeks for ^{222}Rn

activities in water to reach steady state. Since ^{222}Rn is chemically inert, its migration is primarily dependent on physical processes (Cecil and Green 2000). Table 1.1 demonstrates the range of ^{222}Rn activities encountered in groundwater residing in sedimentary aquifers.

Table 1.1 ^{222}Rn activity of groundwater from sedimentary and alluvial aquifers (adapted from Faure 1986).

Reference	**Location**	**Aquifer description**	**No. wells**	**^{222}Rn range (Bq kg^{-1})**	**^{222}Rn mean (Bq kg^{-1})**
Tanner (1964)	Utah	Alluvial sands	11	8 - 30	13
Andrews & Wood (1972)	England	Milford sand	9	18 - 28	22
		Red sandstone	4	6 - 24	18
		Limestone	15	1 - 15	6
Andrews & Lee (1979)	England	Sandstone	24	2 - 22	9
Gorgoni *et al.* (1982)	Italy Emilia	Alluvial deposits	43	4 - 15	7
	Lombardy	Sand - gravels	21	10 - 41	15
Gilkeson *et al.* (1983)	Illinois	Sandstone	80	1 - 25	
Prichard & Gesell (1983)	Midwest USA	Sedimentary	209		4 - 8
Heaton (1984)	South Africa	Sandstone	14	12 - 120	45
Hussain & Krishnaswami (1980)	India	Sandstone	12	4 - 15	12

^{222}Rn migrates primarily by liquid diffusion in small pores, whereas in larger pore spaces ^{222}Rn movement is dominated by advective transport (Tanner 1980). When ^{222}Rn enters the unsaturated zone it can move readily in a gaseous state. Groundwater pumping can create a space for the diffusion of ^{222}Rn by lowering the water table (LeGrand 1987). With cyclic pumping, the fluctuating water table causes

advective gas transport, and may enhance radon transport through the unsaturated zone (Cecil and Green 2000).

Atmospheric ^{222}Rn concentrations vary with location, season (generally minimum during spring and maximum during summer), time of day (maximum at sunrise and minimum during the afternoon) and decrease with height above ground (Gesell 1983). Concentrations of atmospheric ^{222}Rn typically range from less than 10 to 100 mBq L^{-1} (Snow and Spalding 1997, Table 1.2). ^{222}Rn rapidly outgases from water exposed to the atmosphere because it has a low ambient partial pressure. Therefore ^{222}Rn concentrations in surface waters are generally low in relation to groundwaters (e.g. Bourg and Bertin 1993), however points of groundwater discharge are marked by abrupt increases in ^{222}Rn concentration (e.g. Ellins *et al.* 1990). Comparisons of surface and ground water concentrations of ^{222}Rn have enabled locations of groundwater discharge to be identified, and determination of discharge rates (e.g. Ellins *et al.* 1990, Lee and Hollyday 1993). ^{222}Rn has also been used to identify bank infiltration into alluvial aquifers (e.g. Hoehn and von Gunten 1989, Bertin and Bourg 1994). The first-order radioactive decay law was used to describe increases in ^{222}Rn activity in alluvial water with increasing distance from the stream channel and determine rates of stream water infiltration. Previous groundwater studies have also analysed ^{222}Rn concentrations over short time-scales to estimate groundwater residence times by analysis of the growth or decay curves (Hoehn *et al.* 1992, Cecil and Green 2000).

Table 1.2 Atmospheric ^{222}Rn concentrations.

Location	**^{222}Rn mBq L^{-1}**	**Reference**
USA	3.5 to 14	Gesell (1983)
Jabiru, NT, Australia	39 ± 5	Akber and Pfitzner (1994)
Mauna Loa Observatory, Hawaii	0.02 to 0.7	Whittlestone, Robinson and Ryan (1992)

1.4.3 Stable isotopes of water

Stable oxygen (^{16}O & ^{18}O) and hydrogen (^{1}H & ^{2}H) isotopes are highly effective tracers of mixing between different water sources because they constitute and move with water molecules. The different masses of the water molecule species causes them to have different reaction rates, which can lead to isotopic fractionation as water cycles through the environment.

Oxygen and hydrogen isotope data are generally reported in delta (δ) notation in parts per thousand (‰) relative to the standard VSMOW (Vienna Standard Mean Ocean Water, Gonfiantini 1978). The $\delta^{2}H$ and $\delta^{18}O$ signatures of continental rainfall derived from oceanic moisture generally correlate with the straight line relationship (1.1, Craig 1961) referred to as the Global Meteoric Water Line (GMWL).

$$\delta^{2}H = 8 \times \delta^{18}O + 10 \qquad \text{‰, VSMOW} \qquad \textbf{1.1}$$

Moisture recycling by evaporation causes differential enrichment in ^{2}H and ^{18}O causing water to deviate from the GMWL (equation 1.1). Deuterium excess is an index ($d-excess$, equation 1.2, Dransgaard 1964) often used to identify different sources of evaporated water by way of departure from the GMWL. The $d-excess$ of the GMWL is 10 (equation 1.1).

$$d-excess = \delta^{2}H - 8 \times \delta^{18}O \qquad \textbf{1.2}$$

Interaction between surface water and groundwater can often be traced using the stable isotopes of water because water that remains at the surface for any length of time is usually subjected to evaporation and is consequently enriched in ^{2}H and ^{18}O relative to groundwater. The stable isotopes of the water molecule can also be useful

for distinguishing the sources of surface water following a storm. Potential sources include overland flow, throughflow, and groundwater discharge. The stable isotopic compositions of different rainfall events are typically quite different from groundwater and soil water compositions. Groundwaters and soil waters integrate the long-term isotopic composition of several storm events, whereas single rainfall events depend on temperature and storm trajectory (e.g. McDonnell *et al.* 1990). In addition, different sources of groundwater may have characteristic isotopic signatures depending on the altitude that recharge occurred.

Water that recharges in arid or semi-arid regions can have long residence times in the top few metres of soil. Kinetic effects by vapour diffusion can be greater during extensive evaporation from the unsaturated zone than evaporation from surface water (Dinçer *et al.* 1974). Therefore, evaporation from the unsaturated zone and the water table is often characterised by stronger evaporative enrichment with a lower slope (e.g. $m = 2.1$, Dinçer *et al.* 1974) for the $\delta^{18}O$-$\delta^{2}H$ relationship. Allison (1982) found that during evaporation from the surface of unsaturated water columns kinetic isotope effects were enhanced as soil moisture decreased. As evaporation proceeded, the drying front moved down through the soil. With greater water loss, the tension head increased causing the upward movement of water through the soil by capillary action. As the zone of vapour diffusion became wider than that typical from surface water bodies, kinetic diffusion increased. Under steady-state conditions $^{1}H_{2}{}^{18}O$ and $^{2}H^{1}HO$ that has accumulated in the unsaturated zone moves downward to the water table by aqueous diffusion, giving an exponential profile (e.g. Clark and Fritz 1997). Such profiles are disturbed when infiltration occurs flushing the isotopically enriched water down into the saturated sediments. Allison *et al.* (1984) showed that groundwater recharged under such conditions of direct infiltration often have a $\delta^{18}O$-$\delta^{2}H$ composition that plots below, but parallel to the meteoric water line.

The rate of evaporation from bare soil surfaces can be calculated from the shape of the isotope profile. Allison and Barnes (1983, 1985) measured moisture content and the isotopic composition of water with depth in unsaturated soil profiles to estimate evaporation from a dry salt lake, Lake Frome, in South Australia. $\delta^{2}H$ and $\delta^{18}O$ signatures in the soil water of the lakebed increased exponentially from about 0.5 m below the surface, to a peak at or near the surface. The isotope profiles were explained as a balance between the upwards-advective flux of isotopes caused by evaporation and the downwards diffusive flux of isotopes due to concentration gradients resulting from evaporative enrichment at the surface.

1.4.4 Strontium isotopes and concentrations

Strontium is a trace element that occurs in measurable quantities in most rocks, which has four naturally occurring stable isotopes: ^{84}Sr, ^{86}Sr, ^{87}Sr and ^{88}Sr whose relative abundances are 0.55%, 9.86%, 6.99% and 82.59% respectively. The relative proportions of ^{84}Sr, ^{86}Sr and ^{88}Sr are preserved within minerals, however the proportion of ^{87}Sr in minerals increases after formation because it is also produced by the β-decay of ^{87}Rb (½-life of 4.8×10^{10} years). Therefore ^{87}Sr in rocks can originate from two sources; (1) that incorporated during formation of the material and (2) that produced by the radioactive decay of ^{87}Rb (radiogenic Sr).

The present-day $^{87}Sr/^{86}Sr$, which is often reported in geologic research, represents the relative proportion of radiogenic strontium produced since the formation of a mineral. This is a function of the original mineral $^{87}Sr/^{86}Sr$, the proportion of rubidium in the mineral ($^{87}Rb/^{86}Sr$) and the age of the mineral. For example, each mineral crystallised from the same magma would have the same initial $^{87}Sr/^{86}Sr$, but different proportions of Rb/Sr depending on the lattice-site preference for incorporating the different elements. Rb/Sr typically increases in the order

plagioclase, hornblende, K-feldspar, muscovite, biotite (Faure and Powell 1972). Therefore, different materials within a catchment can develop distinct $^{87}Sr/^{86}Sr$ values due to different ages or different initial Rb/Sr and $^{87}Sr/^{86}Sr$ (e.g. Table 1.3).

Table 1.3 Estimated dissolution times and likely ranges of $^{87}Sr/^{86}Sr$ assuming an initial ratio of 0.705 and Rb/Sr typical for Palaeozoic granites of eastern Australia (0.3 – 2.0). Modified from Douglas *et al*. (1995).

Rock/mineral	**Dissolution time (years required to dissolve 1 mm crystal at 298 K, pH = 5)**	**$^{87}Sr/^{86}Sr$**
muscovite	2.6 × 106	>1
K-feldspar	2.9 × 104 - 9.2 × 106	0.730 – 0.800
albite	5.6 × 105	0.706 – 0.715
diopside	6.8 × 103	0.706 – 0.708
anorthite	110	0.707 – 0.708

Solutes receive inputs of strontium from atmospheric fallout. Coastal rainfall tends to have $^{87}Sr/^{86}Sr$ similar to that of marine water, whereas water vapour that moves progressively further inland tends to acquire greater proportions of more radiogenic Sr from terrestrial dust (e.g. Seimbille *et al.* 1988, Quade *et al.* 1995). Therefore, rainfall-fed surface water systems near the coast have $^{87}Sr/^{86}Sr$ similar to that of marine water, ranging from 0.7087 (Hamilton 1966) to 0.7097 (Bogard *et al.* 1967), whereas rainfall-fed systems further inland will tend to approach 0.715 (Seimbille *et al.* 1988).

Strontium isotopic ratios of groundwaters incorporate rainfall signatures that subsequently tend to become more radiogenic relative to contact time with particular rock types. Solutes that derive Sr solely from mineral weathering reactions acquire the same $^{87}Sr/^{86}Sr$ signature as the mineral (e.g. Bullen and Kendall 1998). Surface water systems that drain areas composed mainly of silicate rocks have $^{87}Sr/^{86}Sr$ that range between 0.712 and 0.726 (Faure and Powell 1972). Whereas strontium

released by the weathering of basalts impart much lower $^{87}Sr/^{86}Sr$ on water (0.702 – 0.706, Faure and Powell 1972). Unlike isotopes of lighter elements (e.g. ^{1}H, ^{2}H, ^{16}O and ^{18}O), strontium isotopes are not fractionated by phase changes (i.e. evaporation or condensation), chemical speciation or biological uptake (Graustein 1989). Therefore $^{87}Sr/^{86}Sr$ of water in alluvial aquifer systems, which have relatively short residence times, could be caused by either (1) the mixing between inwelling stream water and regional groundwater; or (2) chemical reactions that release Sr into solution within the alluvial aquifer. Therefore strontium isotopes ($^{87}Sr/^{86}Sr$) can be effective tracers of solute sources to alluvial aquifer systems providing groundwaters and surface waters develop distinct $^{87}Sr/^{86}Sr$, and residence times are short relative to the radioactive decay of ^{87}Rb to ^{87}Sr. Such contrasts in $^{87}Sr/^{86}Sr$ could potentially be used to identify rainfall versus groundwater derived streamflow.

1.4.5 Tracer comparison

Table 1.4 lists the advantages and limitations of the environmental tracers used in this research for identifying the magnitude and direction of stream and groundwater exchange.

Table 1.4 Advantages and limitations of Cl^-, ^{222}Rn, δ^2H & $\delta^{18}O$ and Sr^{2+} & $^{87}Sr/^{86}Sr$ for distinguishing between water reservoirs and for interpreting stream and groundwater interactions.

Tracer	Advantages	What it reveals	Limitations
Cl^-	•Low cost •Often part of standard sampling regime •Low concentration in rainfall •Relatively high concentration in groundwater •Tends to behave conservatively with aquifer material	•Points of groundwater discharge to stream flow •Extent of surface water intrusion into aquifer system •Relative proportion of water sources using two-component end-member mixing model	•Becomes concentrated due to evaporation making interpretation of surface water data ambiguous •Insensitive to small changes in water fluxes
^{222}Rn	•Low concentration in atmosphere •Generally low concentration in surface water •Generally high concentration in groundwater •Short half-life •Degasses rapidly from surface water •Behaves conservatively with aquifer material •Quick, easy analysis	•Water interaction with aquifer material •If concentrations are elevated in surface water, indicates points of groundwater discharge •Can indicate extent of surface water infiltration into adjacent aquifer over short time periods	•Surface water sampling not trivial •Must be analysed within a week of sampling
δ^2H-$\delta^{18}O$	•Behaves conservatively with aquifer material •Moves as part of water molecule •Simple to sample and store	•If water has experienced evaporation •Under what conditions water has recharged groundwater •Different aquifers can have characteristic signatures due to recharge environment	•Fractionated by evaporation •Expensive analysis
Sr^{2+} & $^{87}Sr/^{86}Sr$	•Low Sr^{2+} concentration in rainfall •Relatively high Sr^{2+} concentration in groundwater •Characteristic ratios related to aquifer geology •Is not fractionated by evaporation, biological uptake or chemical speciation	•Water interaction with aquifer of specific geology	•Non-conservative •Expensive analysis

1.5 STUDY AREA OVERVIEW

1.5.1 Physical Setting

The Wollombi Brook Catchment is a sub-catchment of the Hunter River and is located approximately 150 km north of Sydney in eastern Australia and its' eastern-most boundary is approximately 30 km west from the coast (Figure 1.1). The Wollombi Brook is the main southern tributary to the Hunter River and has a catchment area of approximately 1200 km^2. The Wollombi Brook Catchment has steep topography, bounded to the south-east by the Watagan Range where the highest peak is 640 m AHD (Australian Height Datum) at Mt Warrawalong. To the south-west, the Wollombi Brook Catchment is surrounded by the Hunter Ranges and both the Broken Back and Myall Ranges dominate the eastern catchment topography. The Wollombi Brook and tributaries in the southern catchment area are characterised by deeply incised stream channels surrounded by steep mountain ranges. Further north, the topography of the Wollombi Brook Catchment flattens and the stream channels broaden into alluvial floodplains. The lowest point in the Wollombi Brook Catchment is at its northern boundary where the Wollombi Brook meets the Hunter River (60 m AHD).

1.5.2 Climate

The Wollombi Catchment has a sub-tropical climate, characterised by hot summers and mild winters. Daily maximum temperatures average around 29ºC during summer and 18ºC during winter at Broke (1957 to 2002). Average minimum temperatures range between 17ºC during summer and 6ºC in winter.

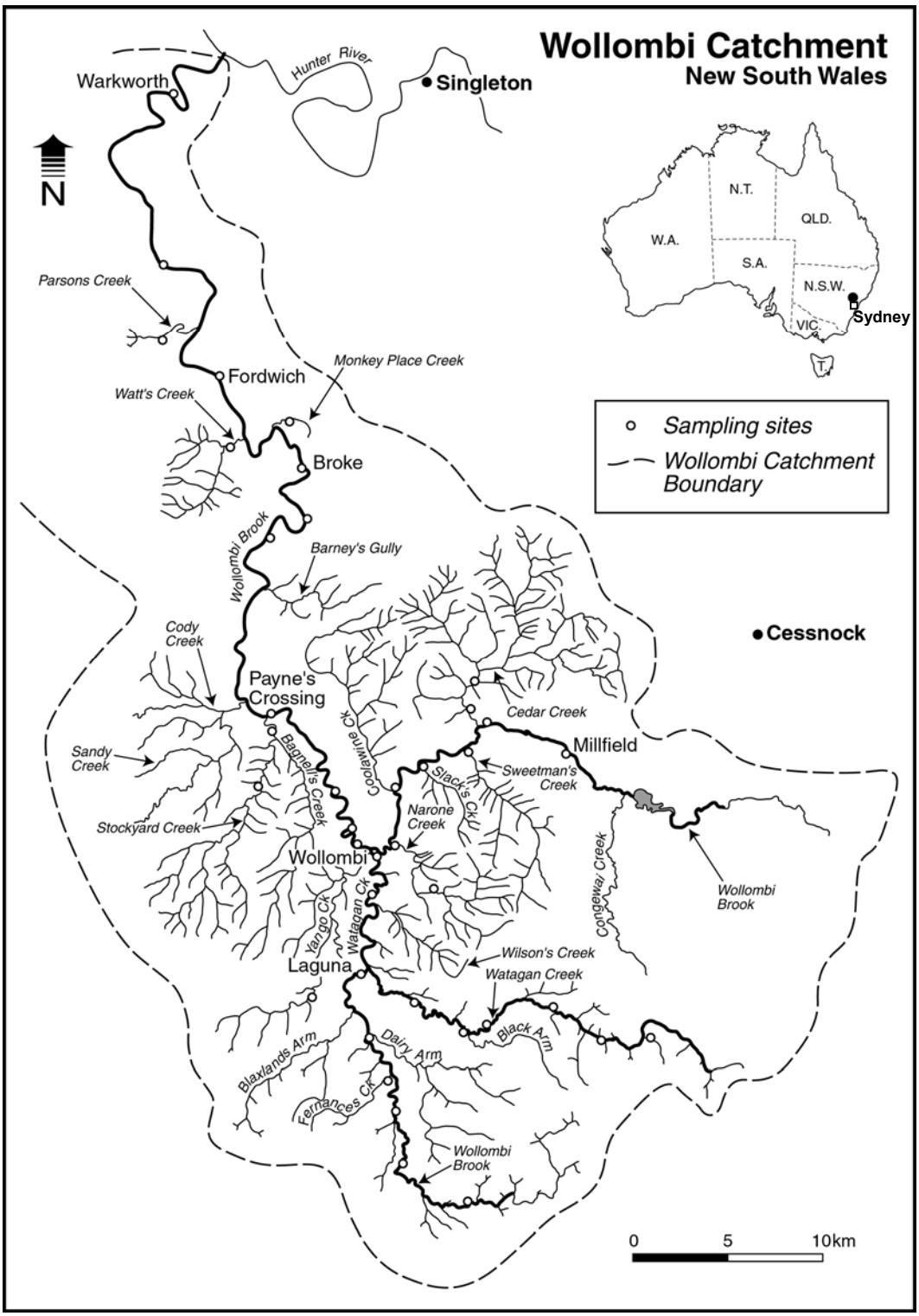

Figure 1.1 Location map of the Wollombi Brook Catchment.

Mean annual rainfall (over a period of 111 years) in the lower Wollombi Catchment at Broke is 651 mm (1889 to 2002), however precipitation increases with elevation. In the upland ranges to the east of the Wollombi Brook Catchment (at Cooranbong, Figure 1.2) the average annual rainfall is 1122 mm (111 year average). Rainfall is summer-dominated, with more than 30% of annual rainfall occurring between December and February at Broke (Figure 1.3). Less than 20% of annual rainfall typically occurs during winter. The mean annual rainfall at Broke is exceeded by the mean potential evaporation (1510 mm), however average monthly rainfall exceeds potential evaporation between April and July.

The average monthly relative humidity at Singleton and Cessnock ranged from 63 to 85% at 9 am and from 40 to 62% at 3 pm (from 9 to 14 year records respectively, Table 1.5). Relative humidity is generally highest during late autumn to early winter and lowest during late spring to early summer.

Table 1.5 Average monthly and annual relative humidity (%) measured daily at 9 am and 3 pm.

		J	F	M	A	M	J	J	A	S	O	N	D	Annual
Singleton	9 am	72	77	74	75	80	81	77	71	64	61	65	63	72
Army	3 pm	49	52	51	49	56	56	52	42	42	42	43	40	48
Cessnock	9 am	71	81	84	77	85	85	81	77	72	65	66	68	76
Airport	3 pm	51	57	58	53	62	61	54	48	49	49	49	49	53

Figure 1.2 Satellite image of Wollombi Brook Catchment (Wollombi township marker: 32º57'00'00" S, 151º08'00" E).

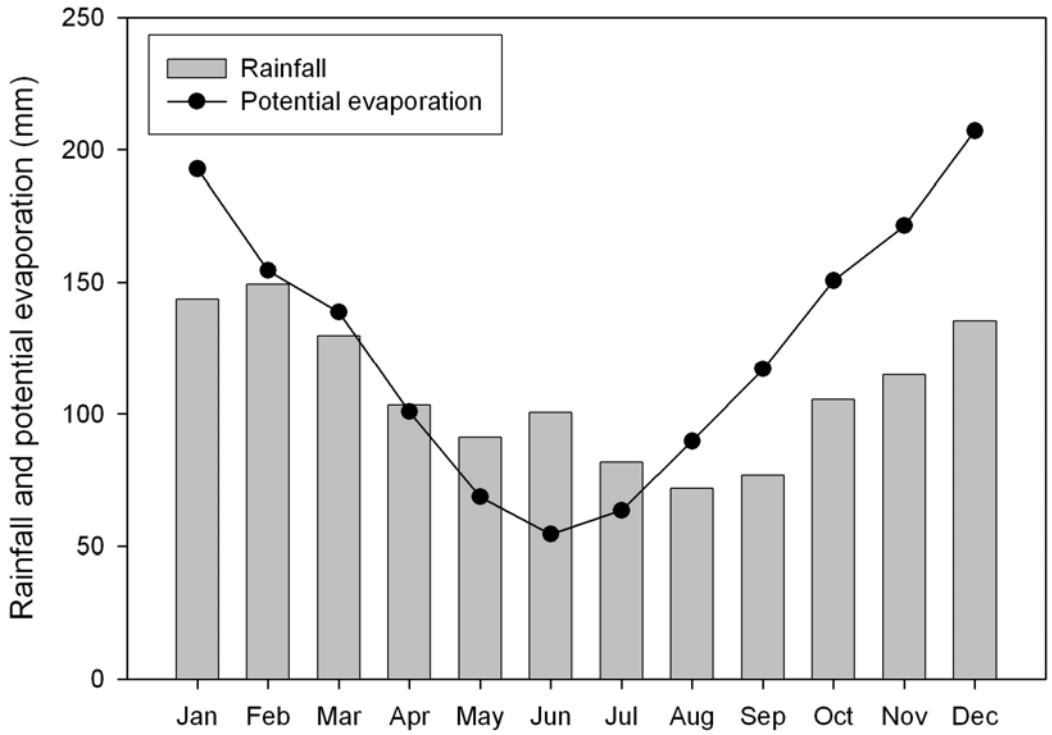

Figure 1.3 Average monthly rainfall (1889 to 2002) and potential evaporation (1972 to 2002) at Broke (lower Wollombi Brook).

1.5.3 Hydrology

Stream flow in the lower Wollombi Brook is perennial, with peak stream flows typically occurring during summer and early autumn (January to March) and gradually decreasing flows throughout the rest of the year (Warkworth, Figure 1.4). Stream flow upstream of Warkworth is intermittent (e.g. Brickman's Bridge), with the Wollombi Brook often becoming a series of disconnected pools toward late spring and early summer before the commencement of summer storms.

The Wollombi Brook exhibits large flood variability with the Flash Flood Magnitude Index (standard deviation of the logarithms to base 10 of the annual maximum flood series, Baker 1977) ranging from 0.61 in the upper Wollombi Brook to 0.9 in the lower Wollombi Brook (Erskine 1994). The mean Flash Flood Magnitude Index in

the Wollombi Brook is more than double the mean for rivers throughout the world (Webb and Erskine 2003).

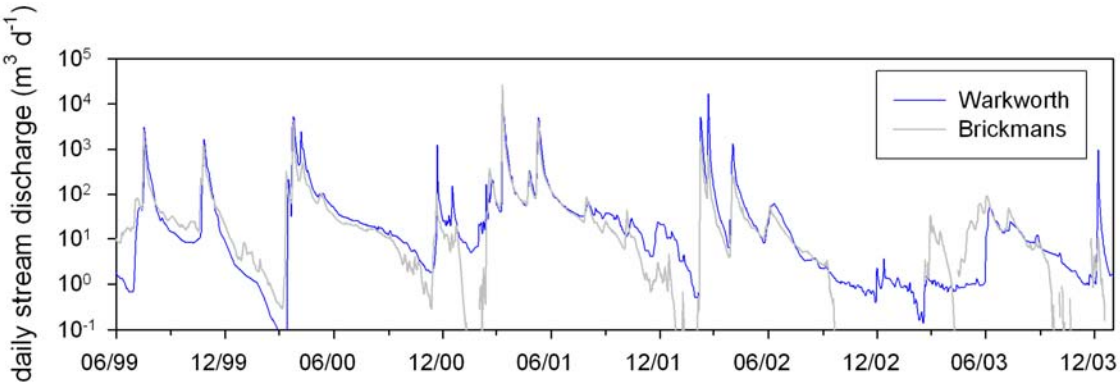

Figure 1.4 Stream discharge (m^3 d^{-1}) in the lower Wollombi Brook (Warkworth) and in a mid-catchment tributary (Brickmans).

A series of large floods between 1949 and 1956 caused widespread stream bank erosion creating deeply incised stream channels in the mid to upper Wollombi Brook (Erskine 1994). The floods destroyed riparian vegetation and caused extensive sand deposition in the lowland floodplains forming the active sand-bed stream.

1.5.4 Hydrogeology

Two main aquifer systems exist in the Wollombi Brook Catchment, these are the shallow alluvial aquifers associated with the Wollombi Brook and tributaries, and the regional hard rock aquifer (MER 2000). The shallow alluvial aquifer is comprised of unconsolidated Quaternary alluvium (interlayered silty to coarse sands and silty to coarse gravels) generated by flood erosion and deposition (Erskine 1994). The alluvial aquifer overlies the regional aquifer system that predominantly consists of Triassic sandstone with some shale (which is the main surficial aquifer in the south-western catchment area) and Permian sediments (sandstone, shale, mudstone, conglomerate and coal) derived from ancient marine sediments (which outcrops

upstream of Millfield and downstream of Broke; in the north-eastern catchment area). The regional aquifer also contains Tertiary basalts that outcrop east of Fordwich, and Permian tuff, lava sandstone, siltstone and conglomerate, and Carboniferous sediments with some volcanics that outcrop north of Millfield (Erskine 1994).

Groundwater in the alluvial aquifer appears to be stratified exhibiting increasing salinity with depth. Shallow alluvial groundwater is fresh to brackish (electrical conductivity, EC <2500 $\mu S\ cm^{-1}$) and is utilised for domestic, stock and irrigation supply whilst deeper alluvial groundwater (EC: 3500 to 11000 $\mu S\ cm^{-1}$) and regional groundwater is generally brackish to saline (MER 2000).

1.5.5 Land use

Development of the Wollombi Brook Catchment for wheat production began in the 1830s (Bennett and Mooney 2003). Much of the original native vegetation was removed, especially in the lowland floodplains and riparian zones (Webb and Erskine 2003). During the 1860s land-use shifted toward dairy farming (Bennett and Mooney 2003). Stock grazing is still common in the mid to upland areas of the Wollombi Brook catchment, however, extensive vineyards have been cultivated in the lowland areas of the Wollombi Brook catchment in recent years. The Wollombi Brook catchment also supports a growing coal mining industry.

1.6 CHAPTER DESCRIPTIONS

1.6.1 Chapter 1: Introduction

An overview of the importance of stream and groundwater interactions and previous hyporheic studies demonstrates the need for improved methods for defining

hydrologic processes that govern hyporheic exchange. Selected environmental tracers are described and their advantages and disadvantages for characterising stream and groundwater interactions are compared. The climate, hydrology, hydrogeology and land use of the study area (Wollombi Brook Catchment, eastern Australia) is described.

1.6.2 Chapter 2: Methods

Rationale for site selection and the characteristics of surface water and groundwater sampling sites are described. Field set-up, instrumentation and the timing of monitoring is presented. Sampling and preservation of surface water, groundwater, pore water and soil samples are described. Field measurements (EC, pH, temperature and alkalinity) and analytical methods performed on water (major ion chemistry concentration, ^{222}Rn activity, $\delta^{2}H$ & $\delta^{18}O$, Sr^{2+} concentration and $^{87}Sr/^{86}Sr$) and soil (pore water extraction, ^{222}Rn ingrowth, Cl^{-} concentration, moisture content, bulk density and porosity) samples are detailed.

1.6.3 Chapter 3: Dynamics of stream and groundwater exchange using ^{222}Rn

The short-term (<12 days) residence time of groundwater in the alluvial aquifer was estimated by comparison of ^{222}Rn emanation from alluvial aquifer material to ^{222}Rn concentrations in surface water and groundwater. This technique showed that surface water and groundwater exchange within the alluvial aquifer occurred when low hydraulic gradients indicated (1) net surface water flux into the alluvial aquifer, (2) no net flux between surface water and the alluvial aquifer, and (3) net alluvial groundwater flux into the stream channel. ^{222}Rn-based estimates of groundwater residence time showed that lateral surface water and groundwater exchange within

the alluvial aquifer was more extensive during baseflow than flood recession conditions, whilst vertical exchange was more extensive during flood recession than baseflow conditions. The same methodology showed that any regional groundwater leakage to the monitored areas of the alluvial aquifer system occurred over longer flow pathways than the technique was able to measure.

1.6.4 Chapter 4: Quantifying groundwater discharge to streams using ^{222}Rn

^{222}Rn concentrations in stream water were used to identify locations of groundwater discharge to stream flow. The sensitivity of the ^{222}Rn technique for identifying groundwater discharge was improved via an iterative numerical approach to account for ^{222}Rn loss from stream water via turbulent gas exchange and radioactive decay simultaneously. This technique showed that groundwater discharged into the stream channel between all sampling stations along the Wollombi Brook. Furthermore, it enabled estimation of the percentage of groundwater discharged to stream flow between sampling stations via analysis of ^{222}Rn concentrations in stream water, alluvial groundwater and regional groundwater. Recommendations for improving field set-up were made, based on numerical modelling, to maximise information from minimum ^{222}Rn sampling.

1.6.5 Chapter 5: Sources of water to streams using tracer techniques

A multi-tracer approach (Cl^-, ^{222}Rn, δ^2H & $\delta^{18}O$, $^{87}Sr/^{86}Sr$) was used to identify the sources of water (surface runoff, alluvial groundwater or regional groundwater) contributing to stream flow. ^{222}Rn losses from stream water due to turbulent gas exchange and radioactive decay were incorporated into a ^{222}Rn mass balance equation to determine the ^{222}Rn concentration of groundwater contributing to stream

flow. This technique showed that the source of groundwater contribution to stream flow in the mid Wollombi Brook catchment was the alluvial aquifer. A framework was developed to identify sources of water to stream flow based on the slope of the δ^2H-$\delta^{18}O$ line and the change in Cl^- concentration of stream water between sampling intervals. This method of interpreting δ^2H and $\delta^{18}O$ data indicated whether increases in the Cl^- concentration of stream water were due to (1) evaporation within the stream channel, (2) discharge of shallow evaporated groundwater, or (3) discharge of regional groundwater to stream flow. Strontium concentrations and $^{87}Sr/^{86}Sr$ were utilised in three-component end-member mixing to differentiate between alluvial and regional sources of groundwater discharge to stream flow. Sources of groundwater discharge to stream flow were compared to stream stage and typical stream channel morphology in the lower, mid and upper regions of the Wollombi Brook Catchment.

1.6.6 Chapter 6: Reach scale interpretation of tracer data

Chapter 6 provides a more detailed investigation of data presented in Chapter 5. A point-to-point interpretation of in-stream Cl^-, δ^2H and $\delta^{18}O$, ^{222}Rn and $^{87}Sr/^{86}Sr$ data was used to differentiate between and quantify the proportions of surface water, alluvial groundwater and regional groundwater discharges to stream flow at the reach-scale.

1.6.7 Chapter 7: Conclusions

The concluding chapter outlines the main findings and methodological development addressed by this thesis. Insights into stream and groundwater exchange processes revealed in this research are described. Advances in methodology for understanding stream and groundwater interactions are outlined.

2 SAMPLING AND ANALYTICAL METHODS

2.1 SITE SELECTION

The Department of Land and Water Conservation (DLWC 1999) identified the Wollombi Brook Catchment as an area with a high level of both water extraction and environmental stress. It was recognised that surface water diversions impacted the ecological health and tourism value of the Wollombi Brook. Subsequent restrictions on surface water diversions throughout NSW were put in place by the implementation of the Water Management Act 2000. Historically, surface water and groundwater resources in the Wollombi Catchment (as in many other areas) have been managed separately. As a result of the restrictions placed on surface water resources, water use shifted from the Wollombi Brook and tributaries to groundwater pumped from the adjacent alluvial aquifer system. Groundwater abstraction was limited to the alluvial aquifer because it was the only source of fresh groundwater within a more saline regional groundwater basin. It was feared that groundwater abstraction from the alluvial aquifer adjacent to the Wollombi Brook undermined the surface water restrictions by depleting a major source of water to stream flow. If this were the case, there would be little, if any, ecological or tourism benefit associated with the shift from surface water to groundwater use. Thus commenced the quest for a better understanding of the degree of interaction between the surface water and groundwater resources.

2.2 BORE AND PIEZOMETER NETWORK

Three sites (Figure 2.1) were selected along the Wollombi Brook for detailed groundwater monitoring to study water exchange between the stream, alluvial aquifer and regional aquifer systems. Sites were selected to cover a range of areas between

the upper and the lower reaches of the Wollombi Brook catchment. Secondary criteria for site selection were ease of accessibility and site security.

Site 1 (Figure 2.1) was established at the first secure and accessible location upstream of the confluence between the Wollombi Brook and the Hunter River (Warkworth, ~50 m AHD). The Wollombi Brook meanders through a broad and flat sandy alluvial floodplain at Warkworth that is characteristic of stream channel morphology in the lower reaches of the Wollombi Brook Catchment. The alluvial floodplain is partially confined by bedrock (basalt and sedimentary rocks) and cemented terrace sediments (Erskine 1994). The stream channel contains sequences of pool and riffle structures and the streambed consists of fine to medium grained silty sands. Sparse reedy vegetation grows on the stream bank and thinner vegetation grows on the sandy floodplain (Figure 2.2***a***). Denser scrub and trees grow on the slopes between the floodplain and surrounding terraces.

The site near the township of Wollombi (site 10, ~85 m AHD, Figure 2.1) was chosen to represent stream water and groundwater interactions in the mid to upper region of the Wollombi Brook Catchment. It is located immediately downstream from the confluence between the southern and eastern branches of the Wollombi Brook. Deeply incised Triassic sandstones (Erskine 1994) that have formed sinuous gullies at Wollombi are characteristic of stream channel morphology in the mid to upper reaches of the Wollombi Brook Catchment. Pool and riffle structures have developed in the poorly sorted, coarse-grained silty sand streambed sediments. Thick grasses grow on the stream bank and occasional trees grow within the incised gullies (Figure 2.2***c***).

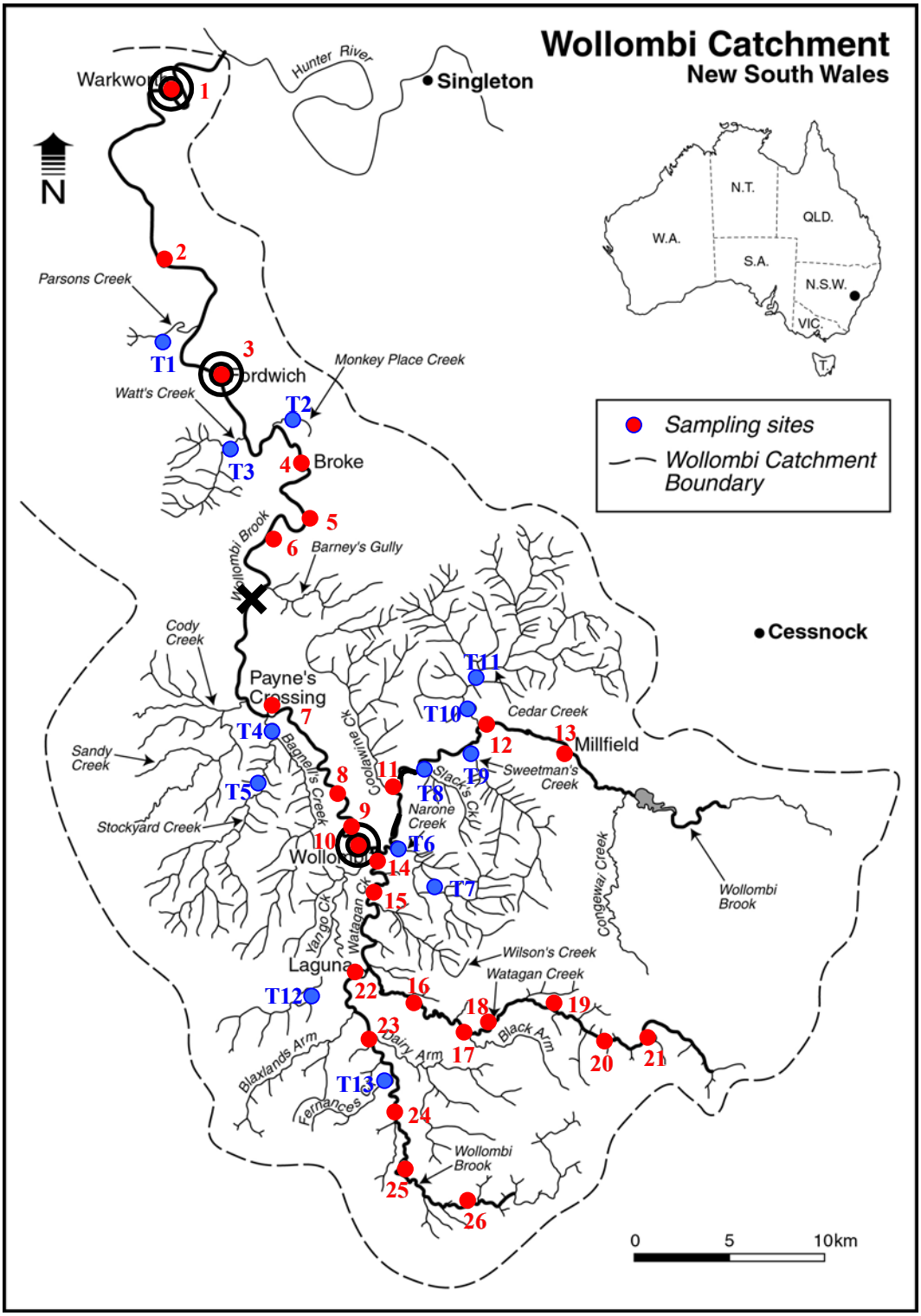

Figure 2.1 Location of catchment-scale surface water, 'run of river' sampling sites from the Wollombi Brook (1 to 26) and its tributaries (T1 to T13). Targets indicate locations of piezometer networks and bores (Warkworth, Fordwich and Wollombi). The cross indicates the site of the weekly "time-series" sampling.

The third site at Fordwich (site 3, ~65 m AHD, Figure 2.1) was selected because it was the most easily accessible and secure location part-way between Warkworth (site 1) and Wollombi (site 10). Stream channel morphology at Fordwich closely resembled that at Warkworth, however, the stream channel was broader and shallower at Fordwich due to higher sediment accumulation (Figure 2.2***b***). At low flows the stream channel was often braided and there were no evident pool and riffle structures. A line of trees bordered the floodplain at the break in slope between the floodplain and surrounding terraces, but there was no vegetation on the sandy alluvial floodplain.

Each site was instrumented with a series of boreholes and piezometers on the eastern side of the Wollombi Brook (left bank facing upstream) between January and May 2000 with the aim of monitoring groundwater in cross-sectional transects (Figure 2.3). Two boreholes were installed at the edge of the upper terrace and a network of piezometers was installed in the alluvial floodplain at each site. Shallow bores were screened at the interface between the upper unconfined aquifer and the regional bedrock aquifer (15 to 17 m below ground level) and deeper boreholes were screened (50 m below ground surface) in the regional aquifer. The Department of Land and Water Conservation oversaw the installation of the boreholes, which were drilled using a rotary air drill. Incomplete bore construction information was available, however, it is believed that bores were constructed with 4 m screens, with sand packs around the screens followed by bentonite plugs.

Six to seven piezometers were installed at each site at varying depths (from <0.5 to 4 m below ground level) into the alluvial floodplain and at various distances (from 0 to 40 m) from the stream channel. Piezometers were constructed with 0.05 m ID PVC that was slotted to 0.5 m from the base and covered with a filter sock. The non-cohesive nature of the alluvial sands made it difficult to install piezometers to depths

greater than four metres below the ground surface. Several piezometers were damaged during the study due to high flood flows. Therefore, two or three additional drivepoints (Lamontagne *et al.* 2003) were installed in the alluvial floodplain at each site during October 2000 to sample groundwater at depths of three to six metres below ground level. Three mini-piezometer bundles were installed at Warkworth (site 1) during May 2001 to collect groundwater samples at 0.25 to 0.5 m intervals for up to three metres below the water table (Lamontagne *et al.* 2003). Details of the construction and installation of drivepoints and mini-piezometer bundles are reported in Lamontagne *et al.* (2003).

2.3 RUN OF RIVER SITES

During May 2000 seven run of river sites (sampling stations 2, 4, 6, 7, 9, 12 and 13, Figure 2.1), in addition to the three groundwater monitoring sites, (1) Warkworth, (3) Fordwich, and (10) Wollombi, were selected for sampling surface water from the main branch of the Wollombi Brook. Run of river sampling sites were selected primarily for ease of access to the Wollombi Brook and were therefore predominantly located at river crossings. In March 2001, run of river sampling expanded to incorporate three more sites (8, 11 and 14) along the main branch of the Wollombi Brook and six tributary streams (sites T1, T2, T6, T8, T9 and T10). During November 2001, surface water levels were low enabling access to the upper Wollombi Catchment. Run of river sampling was undertaken at an additional twelve sites (sampling stations 15 to 26) along the Watagan and Southern branches of the Wollombi Brook and at seven additional sites along tributaries (T3, T4, T5, T7, T11, T12 and T13).

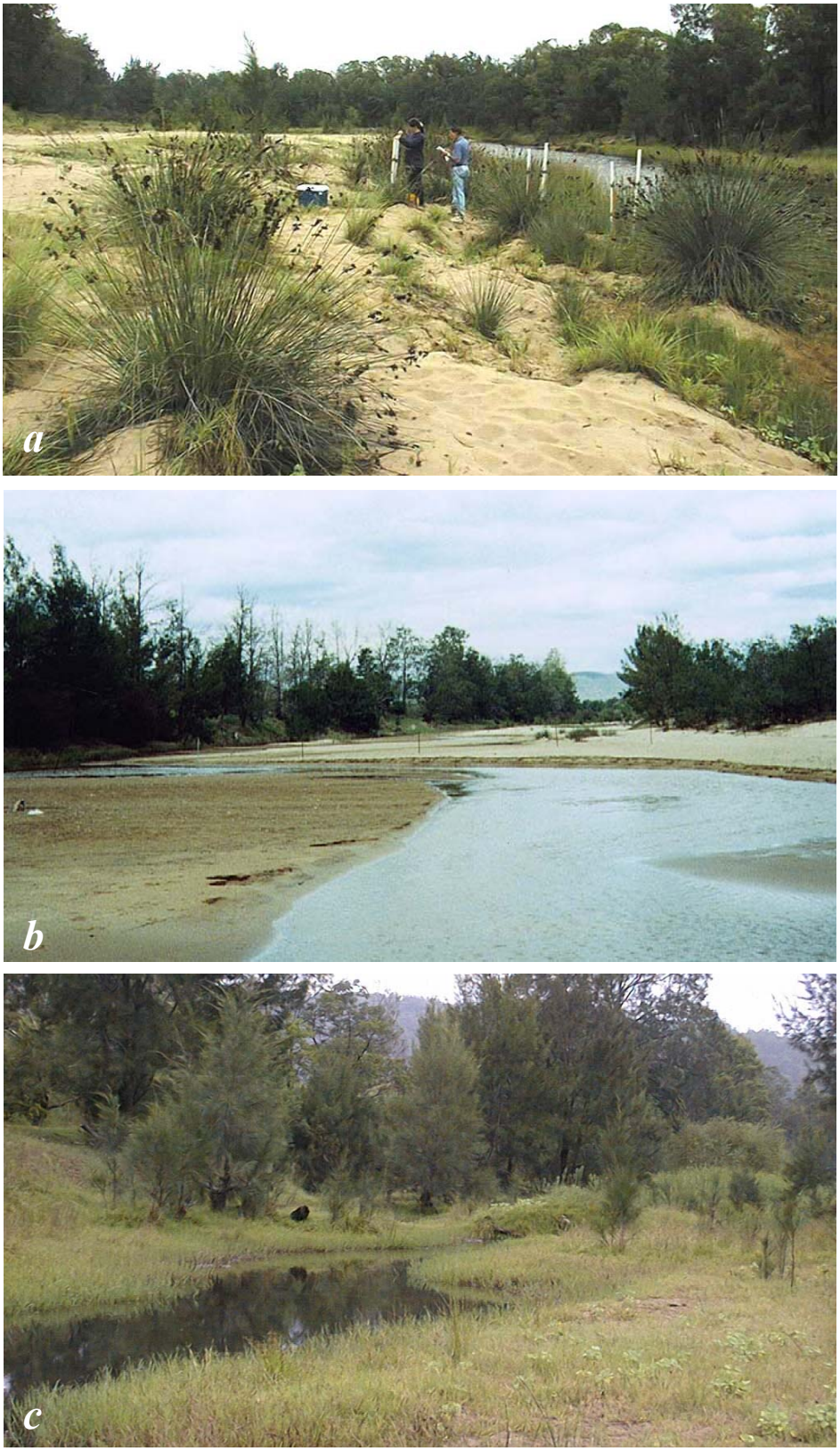

Figure 2.2 Groundwater monitoring sites: (***a***) Warkworth (site 1), (***b***) Fordwich (site 3) and (***c***) Wollombi (site 10).

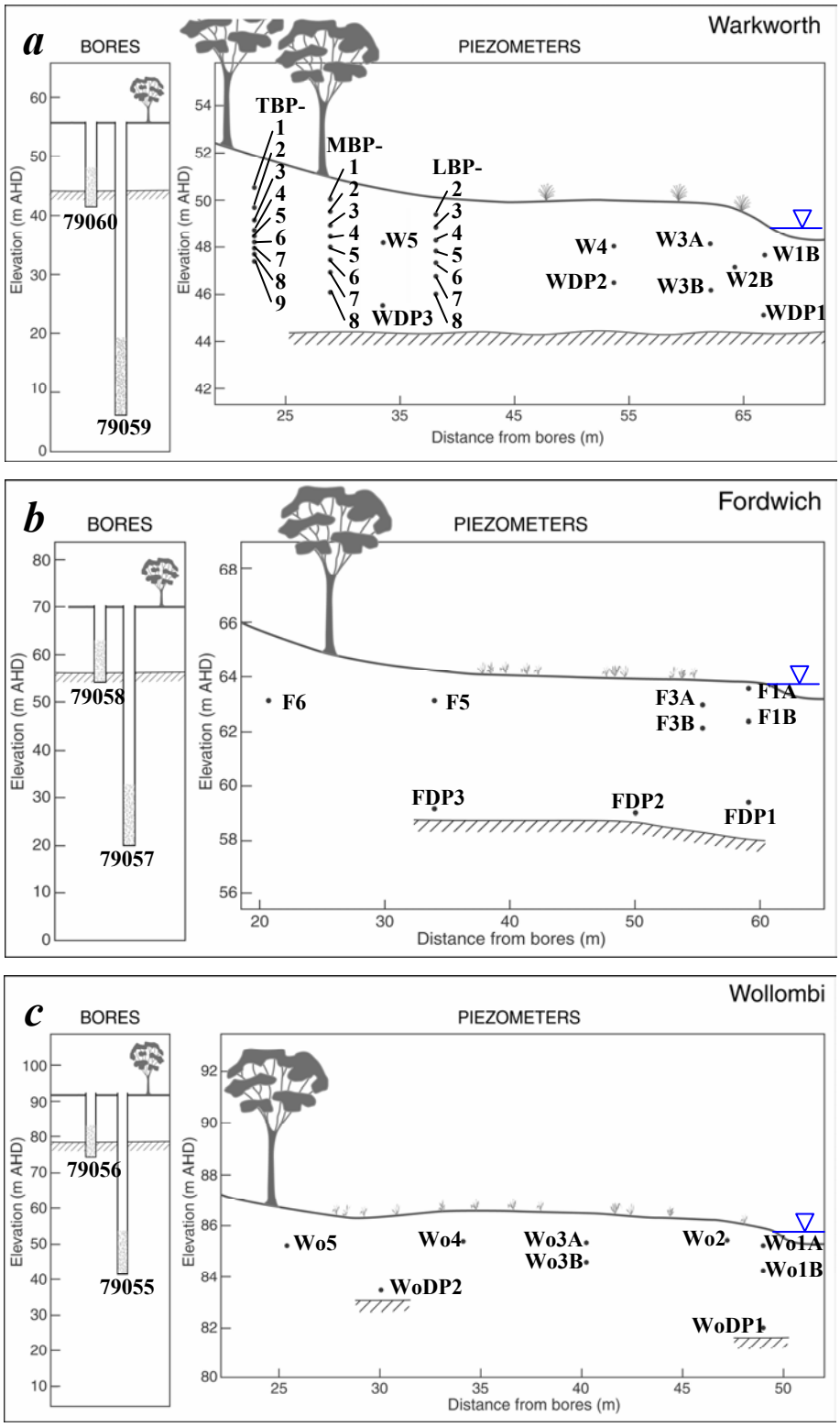

Figure 2.3 Cross-sections of the piezometer and bore network set-up at (***a***) Warkworth (site 1, lower Wollombi Brook), (***b***) Fordwich (site 3, lower Wollombi Brook) and (***c***) Wollombi (site 10, mid to upper Wollombi Brook). Known extent of the bedrock aquifer is represented by hatched line. Note vertical and lateral scales differ at each site.

During November 2001 surface water in the southern branch of the Wollombi Brook commenced as a series of ponds (sampling station 26, Figure 2.1) in a valley cleared for grazing that was encompassed by undisturbed native vegetation in the surrounding Triassic sandstone hill slopes (Erskine 1994). The stream channel at sampling station 26 is narrow, shallow and overgrown with grass. The Wollombi Brook gradually becomes wider and deeper (sampling station 25) as it meanders into a broader sandy alluvial floodplain that is extensively cleared for grazing (stations 24, 23 and T13) and the stream banks are comprised of bare unconsolidated sands. Further downstream, the southern branch of the Wollombi Brook gradually becomes rocky, deeper and narrower and the stream banks are densely vegetated (sampling station 22) before its confluence with the Watagan branch of the Wollombi Brook.

In the upper Watagan branch of the Wollombi Brook (sampling station 21, Figure 2.4***a***) surface water seeped from Triassic sandstone boulders in a steep and narrow stream channel surrounded by dense native vegetation during November 2001. The densely vegetated, rocky stream channel is broader and deeper at sampling station 20 where the streambed gradient abruptly lowers (Figure 2.4***b***). Further downstream (at sampling station 19) the stream channel narrows and deepens through less rocky and less densely vegetated terrain. Further down gradient the stream channel meanders through a sandy alluvial floodplain (at sampling station 18) that has been cleared for grazing and is surrounded by densely vegetated sandstone hill slopes. The low gradient sandy stream channel is broader and deeper (at sampling station 18) than the rocky stream channel further upstream. The sandy alluvial stream channel narrows downstream and is infested with blackberry bushes (sampling stations 17 to 15), then becomes deeper and rockier and has a steeper streambed gradient (at sampling station 14) before its confluence with the main stem of the Wollombi Brook (upstream of sampling station 10).

Figure 2.4 Surface water sampling stations (***a***) 21, and (***b***) 20, located along the Watagan branch of the Wollombi Brook.

The upper reaches of the main stem of the upper Wollombi Brook transform from a wide valley with Triassic sandstone walls to broad lowlands (sampling station 13, Figure 2.1) developed on Permian sandstones, siltstones and conglomerates (Erskine 1994). The Wollombi Brook has a low gradient at sampling station 13 flowing through a broad and deep sandy alluvial stream channel. The stream banks are densely vegetated with reeds and grasses and are surrounded by sandy terraces that are extensively cleared for grazing. Downstream from sampling station 13, the stream channel gradient steepens and is more deeply incised into Triassic sandstones forming a narrow sinuous gully (Erskine 1994), extending from sampling station 12 to 6. The streambed sediments gradually become less rocky and sandier between sampling stations 12 and 10. Streambed gradients are low at sampling stations 9 and 7 resulting in broad and deep stream channels within the sinuous gully, whereas the streambed is rocky and the gradient is relatively high at sampling station 8 causing the stream channel to be relatively narrow and shallow. Downstream from station 6, the Wollombi Brook opens out from the Tertiary sandstone gullies into broad lowland floodplains developed in soft Permian sedimentary rocks (Erskine 1994). The lower reaches of the Wollombi Brook (including sampling stations 5 through to 1) are characterised by low gradient stream channels that meander through broad sandy alluvial floodplains with sparsely vegetated stream banks and narrow strips of riparian vegetation.

Tributary streams that enter the main stem of the Wollombi Brook from the south (between sampling stations 13 and 10) are typically steep and narrow with rocky stream channels (at T6, T8 and T9, Figure 2.1) and thin strips of native riparian vegetation lining the stream banks. Further upstream tributary channels are shallower and narrower (T7). The tributary stream that flows into the main stem of the Wollombi Brook on the northern side (T10) is broad and rocky and is completely

cleared of native vegetation. Further upstream the tributary channel (T11) is narrower and shallower where surface water flows through a pine forest plantation.

Yango Creek commences as a series of ponds (sampling station T12, Figure 2.1) that are swamped with dense grasses in narrow and shallow stream channels that meander through partially cleared grazing land. Tributary stream channels toward the mid to lower Wollombi Brook (i.e. entering the Wollombi Brook down-gradient from sampling station 8, Figure 2.1) are typically broader and shallower than tributaries discharging into the upper reaches of the Wollombi Brook. Lower Wollombi Brook catchment tributary stream channels typically meander through unconsolidated alluvial sands that are surrounded by extensively cleared land with only narrow strips of native vegetation on the stream banks (T1 to T5). Monkey Place Creek and Stockyard Creek were not flowing during October 2001, but surface water was present in permanent pools at sampling stations T2, T4 and T5.

2.4 TIME SERIES SITE

One site was selected for higher frequency (approximately weekly) "time-series" surface water sampling. The time-series site was located in the deeply incised Triassic sandstone gully approximately 5 km upstream from the transition to broad lowland floodplains (Figure 2.1). Pool and riffle structures have developed in the fine to medium grained silty sand sediments. The streambed gradient is low and deep ponds were historically used as swimming holes (personal communication Jim Maher, property owner and time-series surface water sampler). However, high stream flow events carrying high sediment loads have deposited alluvial sands in the low gradient streambed environment which have gradually infilled the water holes.

2.5 SURFACE WATER AND GROUNDWATER MONITORING

Bores and selected piezometers were equipped with capacitance probes and electronic loggers in February 2000. Memory capacity of the electronic loggers, battery longevity and the expected time between sampling trips determined the frequency of groundwater level recording. Groundwater levels were logged a minimum of once every eight hours up to a maximum of once hourly. Groundwater levels were also measured manually in all bores and piezometers at the beginning of every field trip, using a dip meter, before any groundwater sampling commenced.

As part of the HITS (Hunter Integrated Telemetry System, http://hits.nsw.gov.au/) network, stream flow was electronically logged at three locations in the lower to mid Wollombi catchment. These were sited in the vicinity of the surface water sampling stations at Warkworth (site 1) and Bulga (site 3), and at Brickman's Creek (between the time-series site and site 6, Figure 2.1). Stream water level and discharge was monitored at all three sites and stream water electrical conductivity (EC) and temperature was monitored at sites 1 and 3. Surface water electronic logging systems frequently failed due to high stream flow events. When the electronic logging systems were operational, stream water parameters were monitored daily and sometimes hourly.

Stream discharge was also measured at selected surface water sampling stations (Table 2.1) using a pycnometer during May 2000, October 2000, March 2001 and November 2001.

Table 2.1 Average stream height (h), average stream velocity (v) and stream discharge (Q) measured at selected sites using a pycnometer.

Site	h (m)	v (m s^{-1})	Q (m^3 s^{-1})	Measurement time
Warkworth (1)	0.10	0.001	0.002	May-00
	0.09	0.001	0.001	Oct-00, Nov-01
Fordwich (3)	0.08	0.07	0.012	Nov-01
Wollombi (10)	0.13	0.07	0.015	May-00
	0.06	0.07	0.009	Nov-01
Coolawine (11)	0.05	0.10	0.005	Nov-01
Parsons Creek (T1)	0.05	0.09	0.018	Mar-01

Field trips were timed to sample surface water and groundwater under a variety of stream flow conditions. Bore and piezometer networks were sampled five times during a 20 month period; March 2000, May 2000, October 2000, March 2001 and November 2001. May 2000 and March 2001 sampling trips were timed during receding limbs of high stream flow events (herein referred to as flood recession conditions, Figure 2.5). March 2000, October 2000 and November 2001 sampling trips were undertaken during prolonged dry periods when stream flow was derived from groundwater discharge without a component of rainfall generated runoff (herein referred to as baseflow conditions).

If there was any surface water present, the Wollombi Brook was sampled at the bore and piezometer sites every time groundwater was sampled. During March 2000 and October 2000 the surface water had ceased flowing in many reaches of the Wollombi Brook. Surface water persisted as a series of disconnected ponds at Warkworth (site 1) and Wollombi (site 10), however, the stream channel was completely dry at Fordwich (site 3) during March 2000 and October 2000.

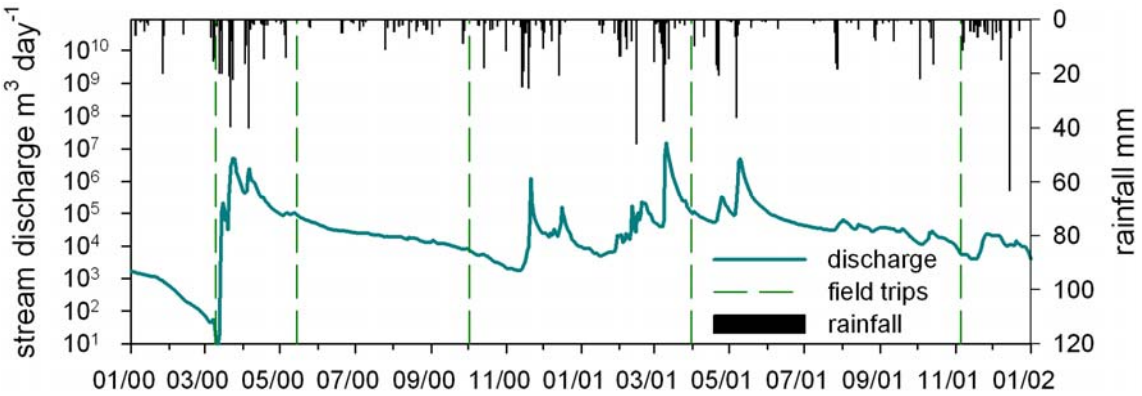

Figure 2.5 Timing of field trips (dashed lines) compared to daily rainfall at Broke (bar graph) and stream discharge at Warkworth (site 1).

Extensive surface water 'run of river' sampling was undertaken during three field trips, two of which were timed with flood recession conditions (May 2000 and March 2001) and one coincided with baseflow conditions (November 2001). Surface water from the Wollombi Brook was generally sampled at the 'time-series' site once per week, however, during high stream stages surface water was sampled up to three times per week. 'Time-series' sampling commenced during October 2000 and was concluded during January 2002.

2.6 SAMPLING METHODOLOGY

2.6.1 Groundwater sampling

One day before groundwater sampling, three well volumes were generally pumped from all bores, piezometers, drive points and mini-piezometer bundles. The groundwater flow rates to some piezometers were too low to allow removal of three well volumes. In such cases piezometers were pumped to dryness the day before sampling.

Groundwater samples were collected from piezometers using a Whale 12 V submersible pump and polyethylene tubing. To enable groundwater collection with minimal exposure to the atmosphere, the end of the pump line was inserted into the bottom of a large Erlenmeyer flask and allowed to overflow. Groundwater samples were collected from the bottom of the flask using a syringe connected to a three-way valve. Groundwater was sampled from drive points and mini-piezometer bundles using a sipper (6 mm OD nylon tubing) and a peristaltic pump.

Groundwater samples were also collected using a transportable pore water profiler, which enabled shallow groundwater sampling without setting up permanent infrastructure. The construction of the pore water profiler is described in Lamontagne *et al.* (2003). The pore water profiler was simply pushed into streambed sediments by hand and groundwater samples were collected every 0.1 m to a maximum depth of one metre using the peristaltic hand pump. This method was utilised for sampling groundwater from saturated streambed sediments at the edge of the stream channel at Wollombi (site 10) during March 2001 and at Warkworth (site 1) during March and November 2001.

2.6.2 Surface water sampling

Surface water samples were collected from near the middle of the stream channel by either (1) wading into the middle of the channel and sampling up gradient, or (2) where water was too deep for wading, using a submersible (whale) pump over the side of bridges. Shallow surface water bodies (i.e. <1 m deep) were sampled mid-depth, whilst deeper surface water features were sampled approximately 0.5 m below the stream surface.

Rainwater samples were collected from a rainwater tank near Broke (site 4) during March and November 2001. Two rainfall samples were opportunistically collected (in assorted pots and pans) over two consecutive nights near Monkey Place Creek (site T2) during the November 2001 field trip.

2.6.3 Soil and unsaturated zone pore water sampling

Soil samples were collected for three purposes: (1) for extracting pore water from unsaturated soils for chemical analysis ($\delta^{18}O$, $\delta^{2}H$ and Cl^{-}), (2) for determining physical parameters of alluvial aquifer material (bulk density and soil moisture content, and (3) for estimating ^{222}Rn emanation from alluvial aquifer material. Unsaturated alluvial aquifer sediments were sampled: (1) from the face of pits excavated down to the water table, and (2) from push tubes used to take soil cores.

A total of six unsaturated zone sediment profiles were collected from pits excavated down to the water table on the Warkworth floodplain (site 1). Three of these were collected during flood recession conditions (Mar-01) along a transect parallel to the piezometer transect. The pits were excavated distances of 2, 6 and 21 m from the stream channel, to depths of 0.18, 0.65 and 1.4 m respectively. Similarly, three unsaturated zone soil profiles were collected along a transect parallel to the piezometer transect at distances 4, 10 and 23 m from the stream channel, to depths of 0.5, 0.8 and 1.8 m respectively during baseflow (Nov-01). Sediments were collected as quickly as possible from pits dug immediately before sampling to minimise redistribution of water throughout the profile and evaporation whilst sampling took place. Samples were taken at 2 cm intervals from the soil surface to the water table.

Soil cores were taken adjacent to the stream channel at Warkworth (site 1) and Wollombi (site 10) and one was taken 9.5 m from the stream channel at Wollombi

during March 2001. Soil cores were collected by hammering a 0.1 m diameter, 0.5 m length PVC push tube into the alluvial aquifer sediments and immediately digging them out. Unsaturated soils were sampled from soil cores directly after retrieval at 0.02 m intervals. Intact soil cores were collected in 0.07 × 0.07 m brass rings to determine the bulk density of alluvial aquifer material.

2.7 SAMPLE PRESERVATION

2.7.1 Major ion chemistry

Surface water and groundwater samples were syringe filtered (0.45 μm Supor© membrane) immediately after sampling. A 125 ml filtered sample was stored in a polyethylene bottle for laboratory Cl^-, Si and alkalinity analyses. Another 125 ml sample was stored in an acid-washed polyethylene bottle and acidified (with 2M HCl) to a pH <2 in the field for major ion analyses.

Soil sampled for investigating the Cl^- concentration of pore water from unsaturated alluvial aquifer material was sub-sampled from soil collected for $\delta^{18}O$ and $\delta^{2}H$ analysis of unsaturated zone pore water (section 2.7.3). Unsaturated sediments collected for analysing the Cl^- concentration of pore water were sealed in air-tight containers to prevent evaporative losses.

2.7.2 Radon

Different techniques were used for sampling ^{222}Rn in surface waters and groundwaters. Groundwater samples were collected from piezometers using a hand-peristaltic pump to limit degassing. 14 ml groundwater samples were injected using a glass syringe beneath 7 ml of a (pre-weighed) mineral oil based scintillation cocktail (produced by Packard) and stored in a low-diffusion scintillation vial.

Because surface water samples are likely to have lower ^{222}Rn concentrations, larger water samples were equilibrated with the scintillant in the field. Approximately 1.1 L surface water samples were agitated with 20 ml of (pre-weighed) Packard's high efficiency mineral oil scintillant for 4 mins to degas the ^{222}Rn and equilibrate it between the water, gas and scintillant phases. The scintillant was allowed to coalesce for another 4 mins then separated and stored in pre-weighed low-diffusion scintillation vials.

Surface water and groundwater sampling times were recorded to resolve losses due to radioactive decay between sampling and analysis. To assess the accuracy of the technique, ^{222}Rn samples were duplicated for at least one in ten surface water and groundwater samples.

Soil sampled for investigating rates of ^{222}Rn emanation from alluvial aquifer material was sub-sampled from soil collected for $\delta^{18}O$ and $\delta^{2}H$ analysis of unsaturated zone pore water (section 2.7.3). There are no special storage requirements (other than preventing cross-contamination) for soil samples collected for ^{222}Rn emanation analysis. Duplicate ^{222}Rn emanation measurements were run on splits taken from the same soil samples.

2.7.3 Stable isotopes of water

Surface water and groundwater samples were stored in 30 ml glass McCartney bottles. Samples were inverted to prevent isotope fractionation if any leakage occurred before analysis. Unsaturated sediments were stored at a constant temperature, in 0.75 L glass jars sealed with electrical tape to prevent evaporative losses until analysis.

2.7.4 Strontium

Rainwater, stream water and groundwater samples collected for $^{87}Sr/^{86}Sr$ and Sr^{2+} concentration analysis were filtered (0.45 μm Supor© membrane) and acidified (2M HCl) to a pH ≈ 2 in the field and stored in acid-washed polyethylene bottles. Rainwater (3 L) and stream water samples (0.5 L) were larger than groundwater samples (0.125 L) because they were expected to contain much lower concentrations of Sr^{2+}. At least 2 μg L^{-1} of Sr^{2+} was required for $^{87}Sr/^{86}Sr$ analysis (section 2.8.5).

2.8 ANALYTICAL TECHNIQUES

2.8.1 Field analysis

Field EC, pH and temperature were measured using a WTW Multine P4 Universal meter. The alkalinity of surface water and groundwater was measured on filtered (0.45 μm Supor© membrane) samples in the field using a Hach® titration kit. Surface water and groundwater samples (section 2.7.1) were also collected for alkalinity analysis in the laboratory (section 2.8.2).

2.8.2 Major ion chemistry

Major cation concentrations (Ca^{2+}, Mg^{2+}, Na^{+} and K^{+}) of surface water and groundwater samples were determined by Inductively Coupled Plasma (ICP) emission spectrometry (Method 3120, SMEWW 1999). The Cl^{-} and SO_4^{2-} concentrations of surface water and groundwater samples were measured by ion chromatography (IC) using chemical suppression and electrical conductivity detection (Method 4110, SMEWW 1999). Filterable reactive Si concentrations in surface water and groundwater samples were analysed by segmented flow analysis (SFA) using ammonium molybdate and oxalic acid then reduced with ascorbic acid and measured colorimetrically at 815 nm (modified Method 4500-SiO_2, Lamontagne

et al. 2003). The alkalinity of surface water and groundwater samples was measured by Gran Titration with 0.1M H_2SO_4 using an Orion® 960 Autochemistry System.

Measured groundwater levels in piezometers and bores containing high salinity groundwater were corrected for density affects to equivalent freshwater heads using equation 2.1.

$$h_{eq} = h_m \times \left(\frac{\rho_m}{\rho_{fw}} \right) \qquad \textbf{2.1}$$

h_{eq}	Equivalent freshwater head	(m)
h_m	Measured head	(m)
ρ_m	Density of measured groundwater	(kg m^{-3})
ρ_{fw}	Density of freshwater	(1 kg m^{-3})

The density of measured groundwater was calculated by summing the measured concentration of total dissolved solids (TDS) in groundwater and the density of freshwater (equation 2.2).

$$\rho_m = TDS_m + \rho_{fw} \qquad \textbf{2.2}$$

TDS_m	Total dissolved solids measured in groundwater	(kg m^{-3})

The Cl^- concentration of pore water was analysed on sub-samples taken from sandy alluvial aquifer material sampled from the unsaturated zone for $\delta^{18}O$ and $\delta^{2}H$ analysis (section 2.7.3). Approximately 50 ml of deionised water was added to 10 g of sand and shaken for two hours. The resulting pore water – deionised water

solution was titrated with $AgNO_3$ using an Orion® 960 Autochemistry System. The Cl^- concentration of pore water was calculated using equation 2.3.

$$C_{pw} = C_m \times \left(\frac{M_{pw} + M_{dw}}{M_{pw}} \right) \qquad \textbf{2.3}$$

C_{pw}	Cl^- concentration of pore water	(mg L^{-1})
C_m	Cl^- concentration of mixed pore water and deionised water	(mg L^{-1})
M_{pw}	Mass of pore water ($M_{pw} = \theta_g \times M_w$)	(g)
M_{dw}	Mass of deionised water	(g)
θ_g	Gravimetric water content of soils (section 2.8.6)	(g^{-1} g^{-1})
M_w	Mass of wet soil	(g)

2.8.3 Radon

The ^{222}Rn activity of surface water and groundwater samples was analysed within 48 hours of sampling using a KLB Wallac (1220) Quantulus liquid scintillation counter with 70 to 200 min sampling times (depending on count rates). The pulse shape analysis program was used to differentiate alpha from beta decay (Herczeg *et al.* 1994). After initial ^{222}Rn analysis, surface water and groundwater samples were sealed and stored for a month and reanalysed to check for ^{222}Rn ingrowth. This method has a precision of ± 3% at 10 Bq L^{-1} or 3-15% at 10-0.3 Bq L^{-1}.

Rates of ^{222}Rn emanation from alluvial aquifer sands were measured following the method outlined by Cook and Dighton (2000). Samples of approximately 40 g of air-dried sand were sealed in 60 ml brass airtight chambers with 20 ml of Packard's high efficiency mineral oil scintillant and filled with approximately 20 ml of distilled water. Samples were left for 4 months to allow them to reach steady state (this

probably takes only 3 weeks) before the mineral oil was removed and its ^{222}Rn concentration was measured by liquid scintillation counting (as per surface water and groundwater method of analysis above). Cook and Dighton (2000) determined the efficiency of the analysis to be approximately 61%.

Assuming that radium is evenly distributed throughout the aquifer material, the ^{222}Rn activity within the aquifer matrix (c_m) is related to the ^{222}Rn emanation rate (E) by equation 2.4.

$$E = \frac{c_m \varepsilon}{\rho_s (1-\varepsilon)} \qquad \textbf{2.4}$$

E	^{222}Rn emanation rate	(Bq kg^{-1})
c_m	^{222}Rn activity within aquifer matrix	(Bq L^{-1})
ρ_s	Particle density (section 2.8.6)	(g cm^{-3})
ε	Porosity (section 2.8.6)	(cm^3 cm^{-3})

2.8.4 Stable isotopes of water

Pore water was extracted from the sediment samples using azeotropic distillation with kerosene substituted for toluene (Revesz and Woods 1990). Deuterium analysis of surface water, groundwater and pore water samples was carried out via high temperature (800°C) reduction of water (25 μL) to H_2 gas over depleted uranium turnings. For ^{18}O analysis, prior to July 2001, 2 ml water samples were equilibrated with CO_2 gas by shaking at a constant temperature (~30°C) in a water-bath for several hours (2< hr <24). The ^{2}H/^{1}H and ^{18}O/^{16}O ratios of H_2 and CO_2 gases respectively, were measured on a Europa Scientific® GEO 20-20 mass spectrometer. Since July 2001, the set-up of an automated on-line CO_2 gas equilibration system

simplified ^{18}O analysis. 1 ml water samples were flushed with CO_2 gas at atmospheric pressure. These samples were left stationary to equilibrate with the sample for 8 hours at 50°C. The gas samples were then passed through a cold trap before entering the mass spectrometer. The results are expressed in delta (δ) notation, relative to the standard VSMOW (Vienna Standard Mean Ocean Water) in parts per mil (‰, Gonfiantini 1978, equations 2.5 and 2.6). The precision of $\delta^{18}O$ and $\delta^{2}H$ results were 0.1 and 1 ‰ respectively.

$$\delta^{18}O = \left(\frac{^{18}O / ^{16}O_{\text{sample}}}{^{18}O / ^{16}O_{\text{standard}}} - 1 \right) \times 10^{3} \qquad \textbf{‰, VSMOW} \qquad \textbf{2.5}$$

$$\delta^{2}H = \left(\frac{^{2}H / ^{1}H_{\text{sample}}}{^{2}H / ^{1}H_{\text{standard}}} - 1 \right) \times 10^{3} \qquad \textbf{‰, VSMOW} \qquad \textbf{2.6}$$

2.8.5 Strontium

Rainwater, stream water and groundwater samples were analysed for Sr^{2+} concentrations using inductively coupled plasma (ICP) spectroscopic methods, with an analytical detection limit of 0.1 mg L^{-1}. The Foden *et al.* (1995) methodology for analysing the strontium isotopic composition ($^{87}Sr/^{86}Sr$) and Sr^{2+} concentration of rocks was modified to analyse water samples.

Sample preparation for $^{87}Sr/^{86}Sr$ and Sr^{2+} concentration analyses was performed in teflon beakers that had been washed systematically in boiling 6M HNO_3, 6M HCl, deionised (DI) water, and rinsed three times with DI water after each stage. Rainwater (3 L), stream water (0.5 L) and groundwater (0.125 L) samples were evaporated down to dryness (180°C) to concentrate the salts and were then redissolved with 1.5 ml of 2M distilled HCl.

Samples were split for two different analyses: (1) isotopic composition (IC) and (2) isotopic concentration (ID). A strontium spike that was 81.4% enriched in ^{84}Sr was added to the ID samples, then all IC and ID samples were evaporated to dryness and redissolved in 1.5 ml 2M HCl.

Samples were centrifuged for five minutes at 3000 rpm and 1 ml of the supernatant was passed through a cation exchange resin with HCl as the eluent. The elution was evaporated to dryness then reconstituted in 1 ml of 2M HCl and passed through the resin a second time to ensure all ^{87}Rb was removed from the elution. Residual ^{87}Rb in the sample would complicate analysis of the mass spectrometer $^{87}Sr/^{86}Sr$ measurements.

The samples were evaporated to dryness and the purified Sr was reconstituted in ~2 μL of Birck® Solution (Paris, composed primarily TaO and minor components of HF, HNO_3 and phosphoric acid) and loaded onto a single tantalum (Ta) filament using the sandwich technique for mass spectrometric measurement. The isotopic composition of Sr (IC) was measured on a Finnigan MAT® 262 thermal ionisation mass spectrometer (TIMS). Isotopic concentrations (ID) were measured on a Finnigan MAT® 261 TIMS. $^{87}Sr/^{86}Sr$ analyses had a mean measurement error of 0.000013 (2σ, n=60). The standard SRM 987 gave a mean value of 0.710278 ± 0.000026 (2σ, n=45) and the total procedural Sr^{2+} blanks were less than 1 ng $g,^{-1}$ which is negligible in comparison to the sample with the lowest Sr^{2+} concentration (rainwater).

2.8.6 Soils

The soil moisture content was determined for soil samples that were preserved for $\delta^{18}O$ and $\delta^{2}H$ analysis of pore water (section 2.7.3). Small soil sub-samples (20 to

30 g) were placed in pre-weighed chipettes and weighed before and after they were oven-dried at 105°C for 24 hours. The gravimetric water content of the soils was calculated using equation 2.7.

$$\theta_g = \frac{M_{cw} - M_{cd}}{M_{cd} - M_c} \qquad \textbf{2.7}$$

θ_g	Gravimetric water content of soils	(g^{-1} g^{-1})
M_{cw}	Mass of wet soil and chipette	(g)
M_{cd}	Mass of dry soil and chipette	(g)
M_c	Mass of chipette	(g)

Bulk density was measured by oven drying undisturbed soil cores at 105°C for 24 hours. The bulk density of soil samples was calculated by dividing the mass of the dry soil by the volume of the soil core (equation 2.8).

$$\rho_b = \frac{M_d}{V} \qquad \textbf{2.8}$$

ρ_b	Bulk density	(g cm^{-3})
M_d	Mass of oven-dried soil	(g)
V	Volume of soil core	(cm^{-3})

Porosity was calculated as a function of soil bulk density and particle density (ρ_s), equation 2.9 (after Kutilek and Nielsen 1994).

$$\frac{f_{aq}}{100} = 1 - \frac{\rho_b}{\rho_s} \qquad \textbf{2.9}$$

f_{aq} Porosity of aquifer material (expressed as a fraction)

ρ_s Particle density (g cm^{-3})

Particle density was estimated from the literature for sand to range between 2.52 and 2.59 g cm^{-3}.

The mineralogy and chemical composition of rock samples from the alluvial aquifer were determined by X-Ray Diffraction (XRD) and X-Ray Fluorescence (XRF) respectively.

2.9 RESULTS

Complete results of field (EC, pH and temperature), major ion chemistry, ^{222}Rn, δ^2H and $\delta^{18}O$ analyses are tabulated and presented as appendices. Results are presented as "run of river" (Tables A.1 to A.4), "time-series" (Table A.5) and piezometer and bore network (Tables A.6 to A.10) datasets and are sub-divided by sampling time.

3 DYNAMICS OF EXCHANGE BETWEEN STREAM WATER, ALLUVIAL GROUNDWATER AND REGIONAL GROUNDWATER USING ^{222}Rn

3.1 INTRODUCTION

Alluvial aquifers that have good hydraulic connection with an adjacent river system are used in many countries as major water supply resources (e.g. Bourg and Bertin 1993). In the Wollombi Brook catchment, groundwater abstraction from the alluvial aquifer provides a precious fresh water supply within a larger more saline groundwater system. The impact of mining the alluvial groundwater resource is a major concern for water policy makers and environmental groups. Excessive alluvial groundwater abstraction will reduce fresh water discharge to stream flow and lower stream discharge particularly during dry seasons. If an increased proportion of the more saline regional groundwater discharges to stream flow following the removal of the fresh alluvial groundwater buffer zone stream salinity will also increase. In order to better understand the risks associated with alluvial groundwater abstraction, we need to investigate the dynamic exchange between the surface water, alluvial groundwater and regional groundwater reservoirs.

Previous studies have characterised stream water and groundwater exchange by:

1. Monitoring differences in surface water and groundwater levels (e.g. Woessner 2000),
2. Conducting stream channel tracer injection studies (e.g. Harvey *et al.* 1996, Harvey and Wagner 2000), or
3. Comparing groundwater and stream water geochemistry (e.g. Hoehn and von Gunten 1989, Benner *et al.* 1995, Woessner 2000).

Surface water and groundwater interactions become difficult to characterise using hydrometric techniques alone when there are low hydraulic gradients between water reservoirs. Injection of artificial chemicals can be used to trace water movement and exchanges between reservoirs, however, it can alter the hydrologic system, can take a long time to reach equilibrium, can be expensive and only represents a short time scale. Natural variation in solute concentrations and isotopic content of catchment waters can be useful for determining solute sources and hydrological pathways and they are already at equilibrium with the environment.

Because ^{222}Rn has very low atmospheric concentrations and has a short half-life (3.8 days), it is useful for understanding surface water and groundwater interactions on time scales of a few days up to 3 weeks. ^{222}Rn concentrations in groundwater have been used in previous studies (Hoehn and von Gunten 1989, Bertin and Bourg 1994, Hoehn 1998) to estimate the residence time and velocity of groundwater in downwelling zones of river channels. ^{222}Rn concentrations in groundwater have also been used to estimate rates of leakage from artificially recharged spreading basins (Snow and Spalding 1997). Hoehn *et al.* (1992) used ^{222}Rn to estimate residence times and flow velocities in sand in a laboratory study.

Although there were low gradients between surface water, alluvial groundwater and regional groundwater systems in the Wollombi Brook Catchment, it was hypothesised that both surface water and regional groundwater recharged the alluvial aquifer system. It was assumed that surface water recharged the alluvial aquifer during high stream flow events and that regional groundwater discharged to the alluvial aquifer during baseflow conditions.

This chapter investigates the use of ^{222}Rn to understand the extent of short-term interactions between Wollombi Brook, the adjacent alluvial aquifer and regional

aquifer system. The objectives of the study were to define the extent of surface water versus regional groundwater infiltration to the alluvial aquifer during flood recession and baseflow conditions and to estimate the rate of surface water infiltration.

3.2 RESULTS

3.2.1 Water level gradients

For the purposes of this study, the term "baseflow" represents stream flow that is not generated by rainfall runoff in which hydraulic gradients indicate that there is no net loss of surface water to the adjacent groundwater system. "Flood recession" represents a high stream flow stage shortly following peak stream flows generated by a high rainfall runoff event.

There were very low gradients between the near-stream alluvial groundwater (within about 40 m of the stream channel) and stream water at the three monitored sites Warkworth (site 1), Fordwich (site 3) and Wollombi (site 10), during both flood recession (Mar-01) and baseflow (Nov-01, Figure 3.1).

During flood recession (Mar-01) there was a relatively high hydraulic gradient (0.0048) between the alluvial aquifer and the stream channel at Warkworth (Figure 3.1***a***), indicating potential for alluvial groundwater discharge to stream flow. There was a lower hydraulic gradient (0.0008) within the alluvial aquifer toward the stream channel during baseflow (Nov-01, Figure 3.1***d***) indicating diminished potential for alluvial groundwater discharge to the stream channel under baseflow conditions at Warkworth. The groundwater levels in the deeper bores were always lower than both alluvial groundwater and stream water levels, indicating that regional

groundwater did not contribute to stream flow at Warkworth during either baseflow or flood recession.

At Fordwich, there was a small hydraulic gradient (0.0013) from the stream channel into the alluvial aquifer, indicating alluvial aquifer recharge from stream water during flood recession (Figure 3.1***b***). During baseflow there was no gradient between the alluvial groundwater and stream water, making it difficult to ascertain the interaction between the two water reservoirs (Figure 3.1***e***). The groundwater level in the shallow bore was always lower than alluvial groundwater and stream water levels, however, the water level in the deeper bore was always higher than stream water and alluvial groundwater levels, indicating potential for regional groundwater leakage into the surface water system.

During flood recession at Wollombi, there was no hydraulic gradient between the alluvial groundwater and stream water, indicating a close hydraulic connection between the two reservoirs (Figure 3.1***c***). There was a small hydraulic gradient (0.0018) from the alluvial aquifer toward the stream channel, indicating the potential for alluvial groundwater discharge to stream flow under baseflow conditions (Figure 3.1***f***). The groundwater levels in the bores were always lower than alluvial groundwater and stream water levels, indicating that regional groundwater was unlikely to contribute to stream flow.

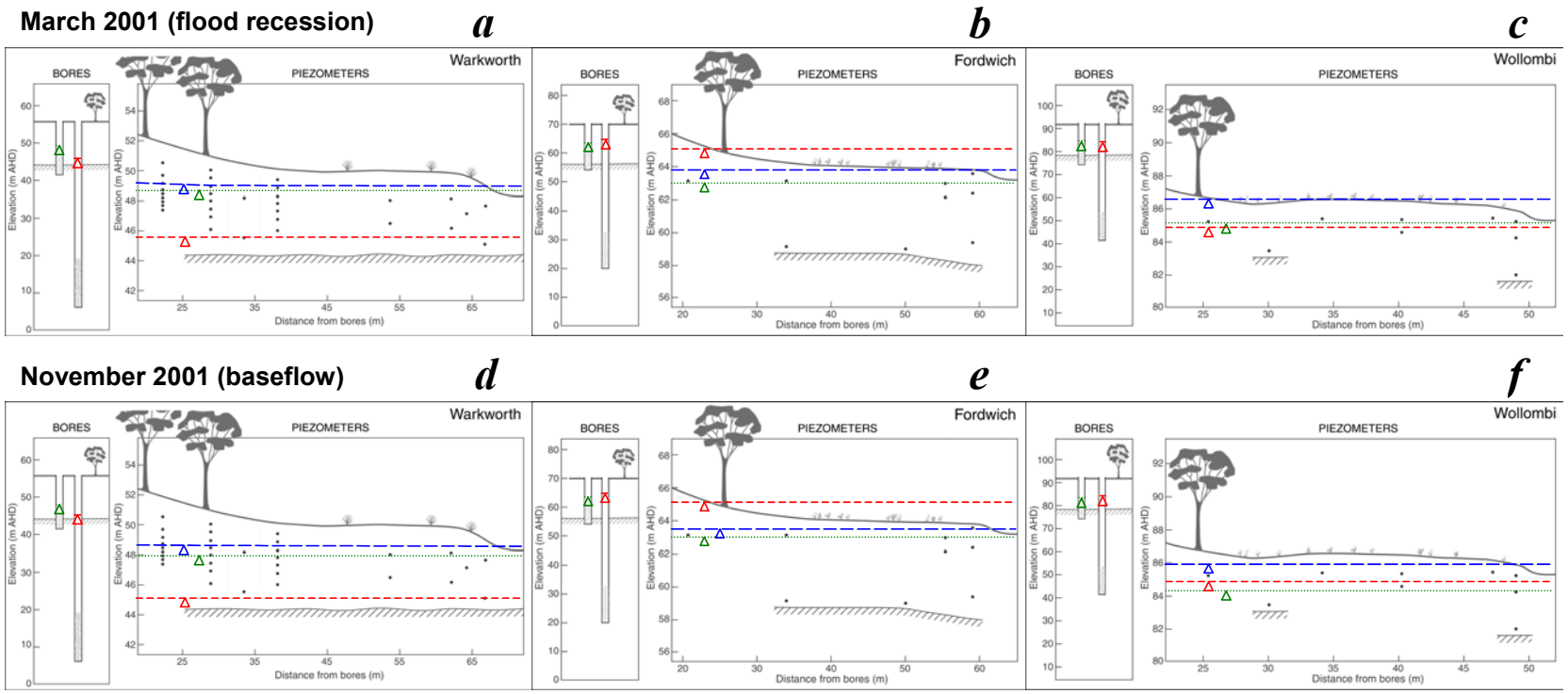

Figure 3.1 Water levels in the Wollombi Brook and adjacent alluvial aquifer (– – –) compared to groundwater levels in deep (----) and shallow (·····) bores in the lower (Warkworth site 1 and Fordwich site 3) and mid to upper (Wollombi site 10) Wollombi Brook measured during flood recession (***a***, ***b***, ***c***, Mar-01) and baseflow (***d***, ***e***, ***f***, Nov-01) conditions.

Low gradients made it difficult to determine the degree of interaction between alluvial groundwater and stream water, particularly during baseflow. Regional groundwater levels were generally lower than the alluvial groundwater and surface water levels indicating that it was unlikely to contribute to stream flow. However, at Fordwich, regional groundwater levels were higher showing potential for discharge, but it was not obvious when or whether it did actually contribute water to stream flow. Furthermore, groundwater level monitoring networks did not have enough coverage to determine the sources of water to stream flow on the catchment scale. To gain a better understanding of the seasonal sources of water to stream flow on a catchment scale, it was necessary to investigate the chemistry of the stream water and the potential sources of water to stream flow.

3.2.2 End-member ^{222}Rn concentrations

Average ^{222}Rn concentrations in alluvial groundwater (3.7 Bq L^{-1}) were one order of magnitude higher than stream water (0.47 Bq L^{-1}) and one order of magnitude lower than regional groundwater average concentrations (11.1 Bq L^{-1}, Figure 3.2). Ranges of ^{222}Rn concentration in stream water compared to alluvial groundwater were narrow and distinctly lower. The ^{222}Rn concentration in regional groundwater was typically much higher than both stream water and alluvial groundwater, but it was highly variable. The ^{222}Rn concentration in regional groundwater overlapped alluvial groundwater values and partially overlapped stream water values.

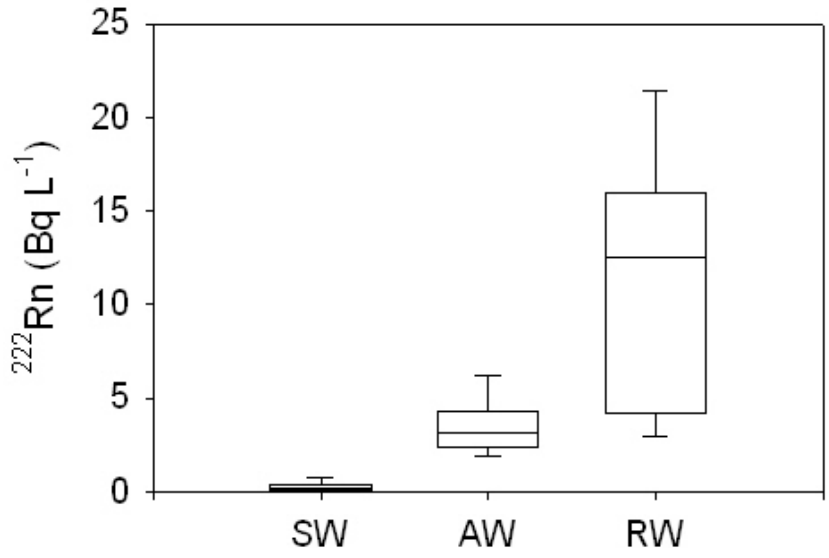

Figure 3.2 The 10th, 25th, 75th and 90th percentiles represent the variation throughout the two-year sampling period (2000-01) of ^{222}Rn measured in stream water (SW), alluvial groundwater (AW) and regional groundwater (RW) sampled across the Wollombi Catchment.

3.2.3 Flood recession and baseflow ^{222}Rn concentrations

During flood recession in May 2000, the ^{222}Rn activity of alluvial groundwater in the piezometer network at Warkworth (site 1, Figure 3.3***a***) increased linearly with increasing distance from the stream channel (R^2=0.98, Figure 3.4***a***). ^{222}Rn activities ranged from 1.8 Bq L^{-1} only 0.5 m from the stream channel up to 12.5 Bq L^{-1} at approximately 70 m from the stream channel (measured in the shallow bore). The ^{222}Rn concentration in the deep bore was anomalously low (0.6 Bq L^{-1}). This was not considered to be representative of the regional aquifer and the low ^{222}Rn value was probably caused by difficulties associated with sampling (e.g. aeration) at greater depths (~40 m).

During the March 2001 flood recession, ^{222}Rn activities in the alluvial aquifer at Warkworth (site 1, Figure 3.3***b***) were more variable with distance from the stream channel than during May 2000. ^{222}Rn in alluvial groundwater sampled directly

beneath the stream channel (0.2 to 0.9 m) ranged between 0.2 and 5.0 Bq L^{-1}. Within 35 m of the stream channel the ^{222}Rn activity generally increased linearly with increasing distance from the stream channel (R^2=0.53, Figure 3.4***b***). The ^{222}Rn activity of alluvial groundwater at Warkworth during March 2001 peaked (8.5 Bq L^{-1}) at a distance of 35 m from the stream channel. At distances of 45 to 65 m from the stream channel, ^{222}Rn activities in alluvial groundwater were significantly lower, varying between 2.3 and 4.1 Bq L^{-1}. The ^{222}Rn activity of the regional aquifer (12.9 Bq L^{-1}) was higher than levels measured in the alluvial aquifer.

During baseflow (Nov-01) the ^{222}Rn activity of alluvial groundwater (Figure 3.3***c***) increased linearly with increasing distance from the stream channel (R^2=0.57, Figure 3.4***c***). Alluvial groundwater ^{222}Rn activities ranged from 2.0 Bq L^{-1} measured 0.2 m beneath the stream channel, up to 15.0 Bq L^{-1} measured 70 m from the stream channel. There was little variation in the ^{222}Rn activity of shallow (<1.2 m below the water table) alluvial groundwater (2.0 to 3.1 Bq L^{-1}) sampled within 15 m from the stream channel. At greater distances from the stream channel the ^{222}Rn activity of alluvial groundwater was higher, varying from 3.5 to 15 Bq L^{-1}.

At a distance of 31 m from the stream channel, ^{222}Rn activities in alluvial groundwater increased from 5.9 to 13.0 Bq L^{-1} with depth over less than 2 m. At distances between 35 and 40 m from the stream channel, alluvial groundwater increased from 3.5 to 5.8 Bq L^{-1} with depth over a 2.4 m interval. There were no vertical trends in the alluvial groundwater ^{222}Rn activity profile located 48 m from the stream channel. The ^{222}Rn activity in regional groundwater was slightly higher (16.2 Bq L^{-1}) than maximum ^{222}Rn activities measured in alluvial groundwater during baseflow.

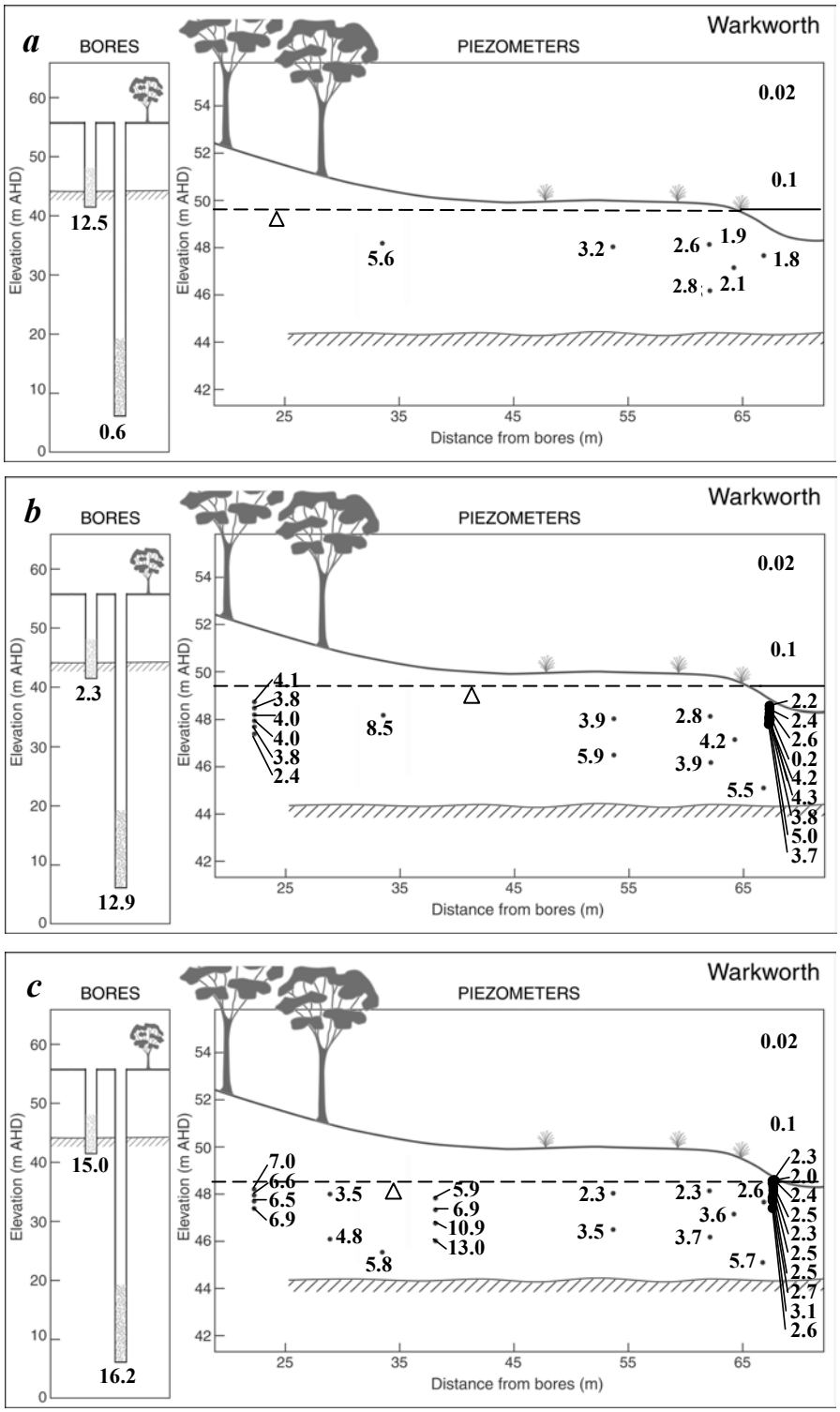

Figure 3.3 Warkworth (site 1): ^{222}Rn activity (Bq L^{-1}) of groundwater sampled from piezometer network during flood recession (***a***) May-00, (***b***) Mar-01 and (***c***) low flow conditions (baseflow) Nov-01. The ^{222}Rn concentration in stream water was consistently 0.1 Bq L^{-1} at Warkworth and the atmospheric ^{222}Rn concentration was assumed to be 0.02 Bq L^{-1}.

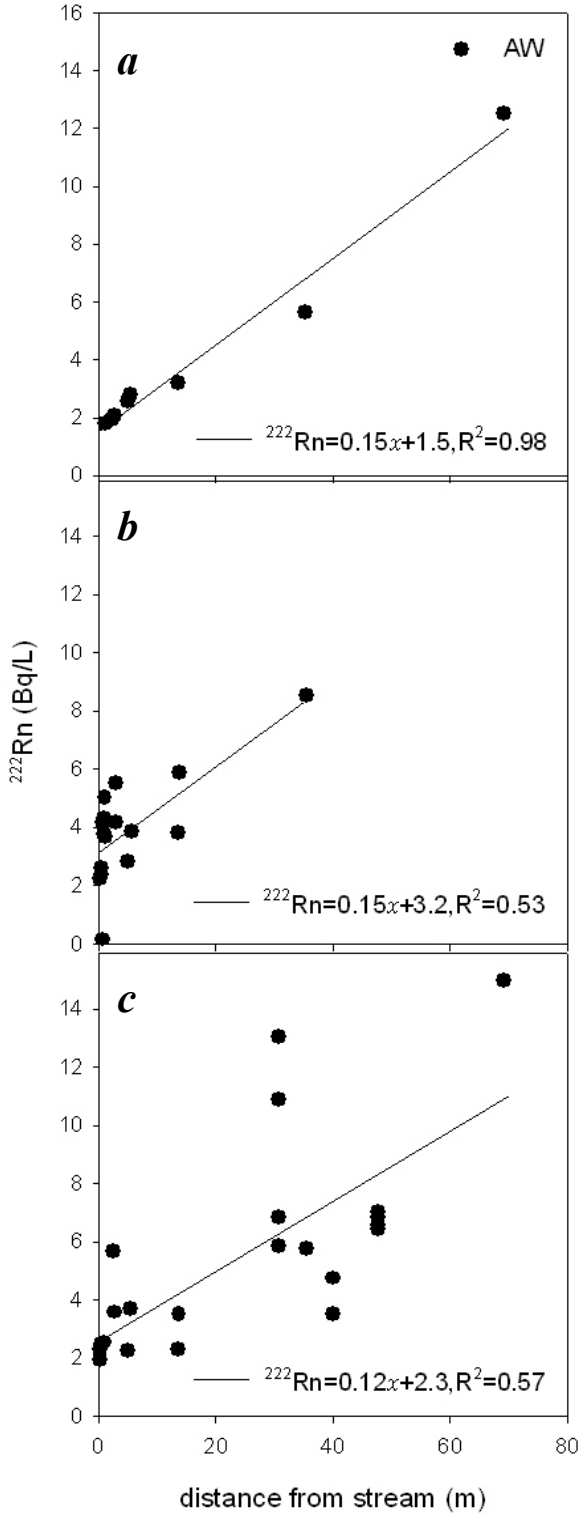

Figure 3.4 ^{222}Rn activity (Bq L^{-1}) in alluvial groundwater (AW) relative to distance (x) from the stream channel (m) during (***a***) May-00 flood recession, (***b***) Mar-01 flood recession and (***c***) Nov-01 baseflow.

There were no trends in the ^{222}Rn activity of alluvial groundwater with distance from the stream channel during either flood recession (May-00, Figure 3.5***a***) or baseflow (Nov-01, Figure 3.5***b***) at Fordwich (site 3). Alluvial groundwater sampled less than 1.3 m below the water table had ^{222}Rn activities ranging from 1.6 to 2.9 Bq L^{-1}. The ^{222}Rn activity of alluvial groundwater sampled more than 1.3 m below the water table was higher ranging from 3 to 4.8 Bq L^{-1}. The shallower of the two bores at Fordwich had consistently higher ^{222}Rn levels than the deeper bore (Figure 3.5).

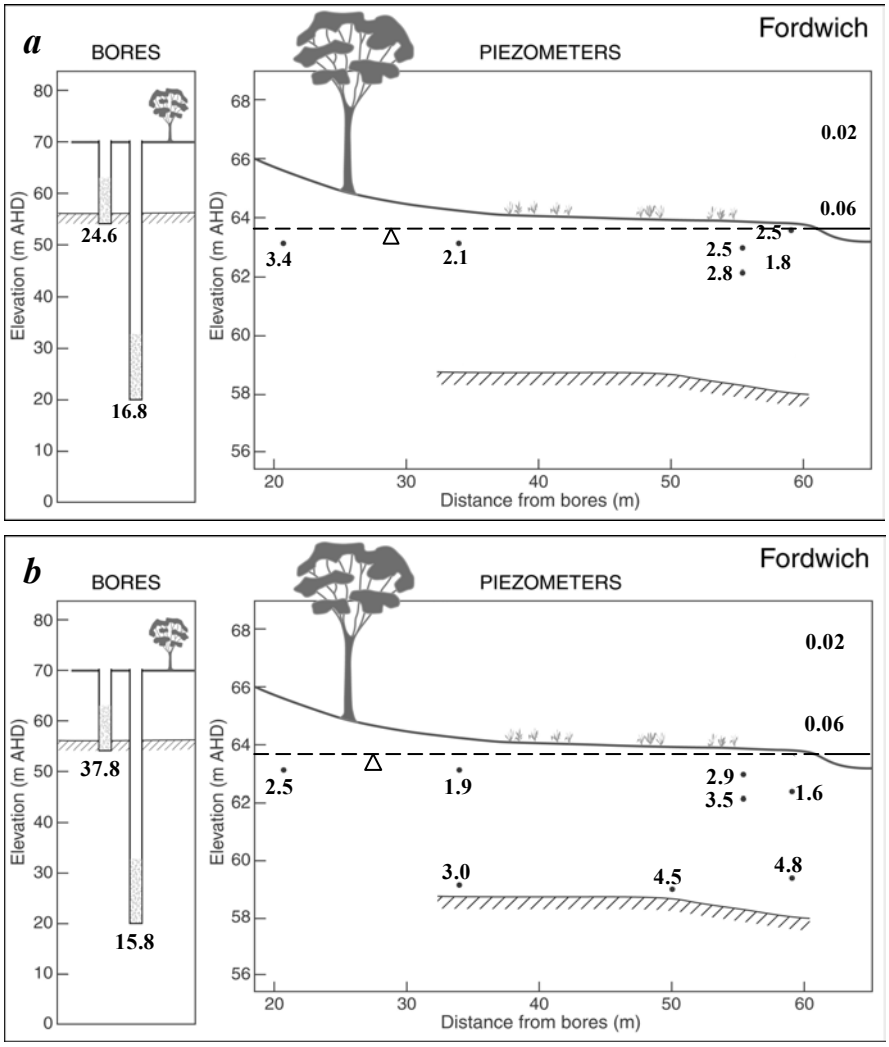

Figure 3.5 Fordwich site: ^{222}Rn activity (Bq L^{-1}) of groundwater sampled from piezometer network during (***a***) Mar-01 flood recession and (***b***) Nov-01 low flow (baseflow). The ^{222}Rn concentration in stream water was consistently 0.06 Bq L^{-1} at Fordwich and the atmospheric ^{222}Rn concentration was assumed to be 0.02 Bq L^{-1}.

^{222}Rn activities measured in alluvial groundwater at Wollombi (site 10) ranged from 0.2 to 4.6 Bq L^{-1} during flood recession (Mar-01, Figure 3.6***a***) and 1.6 to 6.2 during baseflow (Nov-01, Figure 3.6***b***). There were no obvious trends in ^{222}Rn activity with either distance from the stream channel or depth into the aquifer system. The range of ^{222}Rn activity measured in regional groundwater (varying from 0.8 to 4.6 Bq L^{-1}) was no higher than levels measured in alluvial groundwater.

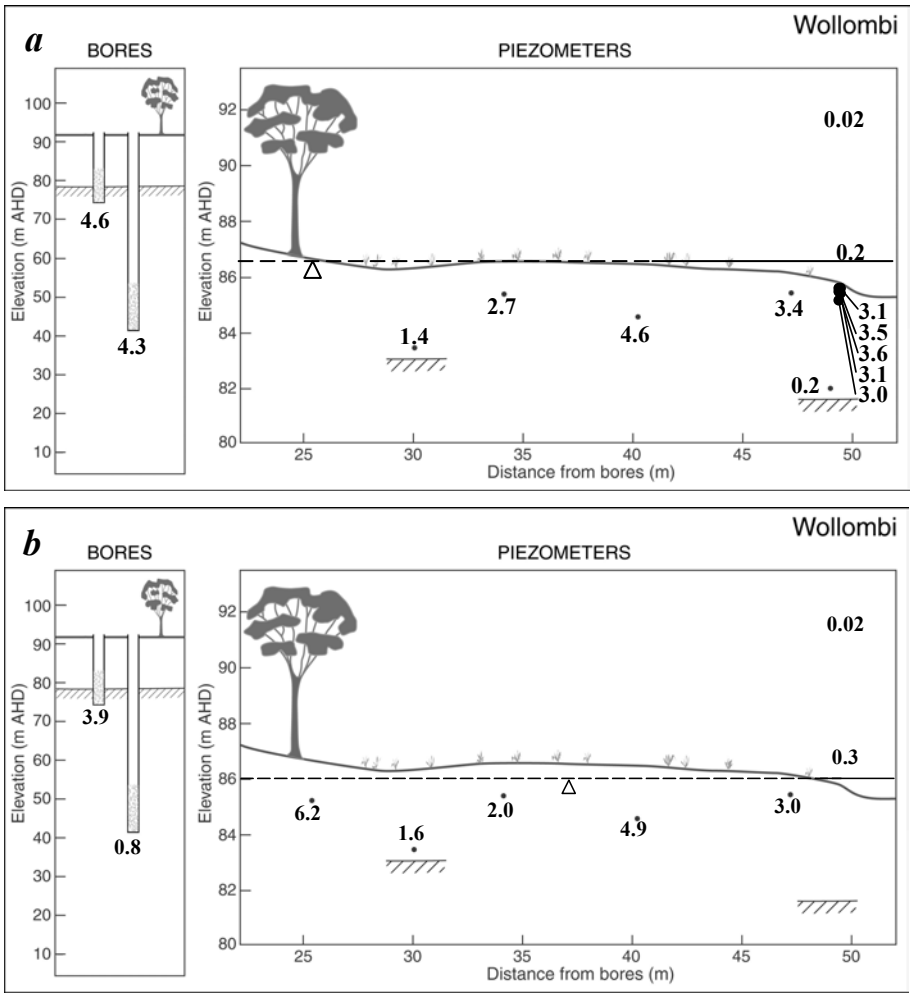

Figure 3.6 Wollombi site: ^{222}Rn activity (Bq L^{-1}) of groundwater sampled from piezometer network during (***a***) Mar-01 flood recession and (***b***) Nov-01 low flow (baseflow) conditions. The ^{222}Rn concentration in stream water was 0.2 Bq L^{-1} during Mar-01 and 0.3 Bq L^{-1} during Nov-01 at Fordwich and the atmospheric ^{222}Rn concentration was assumed to be 0.02 Bq L^{-1}.

3.2.4 Emanation of ^{222}Rn from alluvial aquifer material

The steady state ^{222}Rn emanation (C_{ss}) from alluvial aquifer sediments was measured at 0, 4 and 23 m from the stream channel at Warkworth (site 1) and 0 and 9 m from the stream channel at Wollombi (site 10) at various depths into the sediment profile (Table 3.1).

Table 3.1 Steady state ^{222}Rn concentration (C_{ss}, Bq L^{-1}) in alluvial aquifer material at Warkworth (site 1). Bracketed numbers indicate replicate analyses.

Site	Distance from Brook (m)	Sediment depth (cm)	Steady state ^{222}Rn concentration in water C_{ss} (Bq L^{-1})
Warkworth Site 1	0	0-2	3.6
	0	4-6	2.7
	0	6-8	3.4
	0	8-10	4.4
	0	10-12	3.3
	0	12-14	2.8
	0	16-18	1.6
	0	18-20	3.8
	0	20-22	2.2 (2.0)
	0	22-24	2.4
	0	24-26	3.2
	0	26-28	4.1
	4	0-2	5.6
	4	35-40	3.8
	4	75-80	2.7
	23	40-50	3.8 (3.9)
	23	90-100	4.0
	23	160-180	3.0
Wollombi Site 10	0	16-18	4.6
	0	36-38	2.4
	9.5	0-2	6.7 (3.8)
	9.5	24-26	4.7
	9.5	45-50	4.7
Median			**3.7**

The C_{ss} measured in alluvial aquifer material ranged from 1.6 to 5.6 Bq L^{-1} at Warkworth (site 1) and from 2.4 to 6.7 Bq L^{-1} at Wollombi (site 10, Table 3.1). The median C_{ss} value of alluvial aquifer material at Wollombi (4.6 Bq L^{-1}) was higher

than at Warkworth (3.3 Bq L^{-1}). The median C_{ss} for alluvial aquifer material sampled at both sites was 3.7 Bq L^{-1}.

There was less than 6% variation between duplicate C_{ss} in the well-sorted sandy alluvial aquifer material at Warkworth (Table 3.1). There was a large difference (2.9 Bq L^{-1}) between duplicate analyses of C_{ss} in the alluvial aquifer material sampled at Wollombi (site 10).

There were no trends in C_{ss} with depth in alluvial aquifer profiles (e.g. Figure 3.7). In the sediment profile located 0 m from the stream channel, the C_{ss} of alluvial aquifer material fluctuated between 1.6 and 4.2 Bq L^{-1}. The highest C_{ss} value measured in the alluvial aquifer material at Warkworth (5.6 Bq L^{-1}) was sampled in the unsaturated zone of the profile located 4 m from the stream channel. The ranges of C_{ss} values in the saturated zone overlapped all other C_{ss} values measured in the unsaturated zone at Warkworth. Ranges in the C_{ss} value of alluvial aquifer material measured at 0, 4 and 23 m from the stream channel were similar. There were no trends in C_{ss} values of alluvial aquifer material with distance from the stream channel.

3.3 DISCUSSION

3.3.1 Origin of ^{222}Rn in alluvial aquifer

^{222}Rn in alluvial groundwater originates from either (1) ^{222}Rn emanation from alluvial aquifer material (Table 3.1), or (2) influxes of higher ^{222}Rn concentration regional groundwater (Figure 3.2). Since the ^{222}Rn concentrations in alluvial groundwater tended to increase with increasing distance from the stream channel (c.f. section 3.2.3), it was hypothesised that either:

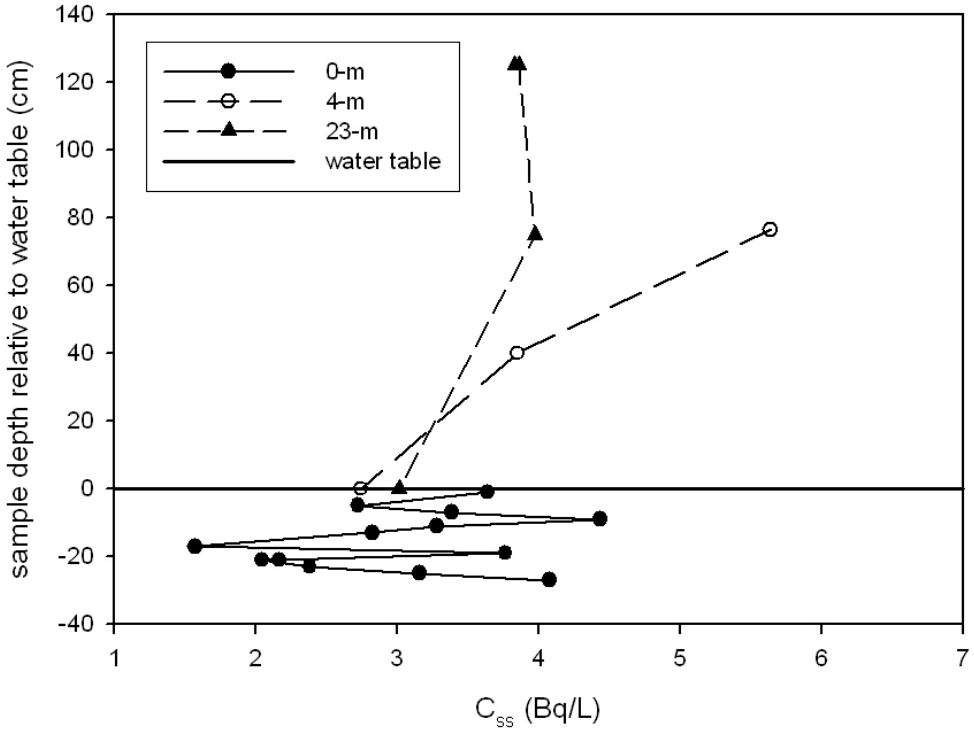

Figure 3.7 Steady state ^{222}Rn activity (C_{ss}, Bq L^{-1}) in alluvial aquifer sediment profiles located distances of 0, 4 and 23 m from the stream channel at Warkworth.

1. Low ^{222}Rn concentration stream water recharged the alluvial aquifer and the ^{222}Rn concentration of the newly recharged alluvial groundwater gradually increased along its flow path (due to ^{222}Rn ingrowth and mixing with "old" alluvial groundwater) until the ^{222}Rn concentration reached equilibrium with the alluvial sediments; or
2. High ^{222}Rn concentration regional groundwater leaked into the alluvial aquifer causing localised peaks in the ^{222}Rn concentration of alluvial groundwater. Assuming that the high ^{222}Rn concentration regional groundwater flowed through the alluvial aquifer toward the stream channel, the ^{222}Rn concentration in the groundwater gradually decreased due to radioactive decay until the ^{222}Rn concentration reached equilibrium with the alluvial sediments.

Potential influxes of regional groundwater to the alluvial aquifer were identified by "hotspots" of relatively high ^{222}Rn concentration alluvial groundwater in comparison to ^{222}Rn emanation from alluvial aquifer material. Influxes of surface water to the alluvial groundwater system typically lower the ^{222}Rn concentration of alluvial groundwater (Figure 3.2). Therefore, influxes of surface water to the alluvial aquifer were identified by low alluvial groundwater ^{222}Rn concentrations relative to ^{222}Rn emanation from alluvial aquifer material.

Steady state ^{222}Rn emanation (C_{ss}) from alluvial aquifer material varied between 1.6 and 5.6 Bq L^{-1} at Warkworth (site 1) and 2.4 and 6.7 Bq L^{-1} at Wollombi (site 10, Table 3.1). C_{ss} was considered to be more representative of the steady state ^{222}Rn concentration of alluvial groundwater (A_{222}^{ss}) than ^{222}Rn concentrations measured in alluvial groundwater because it was not certain that alluvial groundwater was sampled under steady state conditions. A_{222}^{ss} was assumed to be less variable than C_{ss} due to molecular diffusion within alluvial groundwater. Therefore, median C_{ss} values were considered to best represent A_{222}^{ss} at Warkworth (3.3 Bq L^{-1}) and Wollombi (4.6 Bq L^{-1}).

Differences in C_{ss} values between Warkworth and Wollombi were probably caused by differences in particle size distribution and amount of organic matter in alluvial aquifer material. Alluvial aquifer material at Warkworth contained well-sorted sands, whereas alluvial aquifer material at Wollombi contained a wider particle size distribution and more organic particles (i.e. clay and chunks of charcoal). ^{222}Rn emanation from aquifer material depends on its ^{226}Ra concentration and the size and crystal structure of the particles (Cecil and Green 2000). Clays tend to have greater ^{222}Rn emanation potential than sands, even though sands tend to have higher ^{238}U concentrations. This is because ^{222}Rn emanation potential is highly dependent on soil sediment size (Jönsson 1999, Baixeras *et al.* 2001) and is usually greater for

small-grained sediments than coarser-grained sediments (Kraemer and Genereux 1998).

Duplicate C_{ss} measurements of alluvial aquifer material were more variable at Wollombi than Warkworth because of the wider particle size distribution. Inclusion or exclusion of a single "pebble" in the experimental set-up causes greater variability in duplicate C_{ss} measurements of alluvial aquifer material. There was insufficient C_{ss} data collected at Wollombi to indicate whether the C_{ss} of the alluvial aquifer material was statistically different from that at Warkworth.

Hydraulic gradients indicated that neither stream water nor regional groundwater were likely to recharge the alluvial aquifer at Warkworth (site 1) in the lower Wollombi Catchment during either flood recession (Mar-01) or baseflow sampling (Nov-01, Figure 3.1***a***, ***d***). However, ^{222}Rn concentrations in alluvial groundwater were generally lowest within 10 m of the stream channel indicating that some surface water exchange had occurred during both flood recession (May-00, Mar-01, Figures 3.3***a***, ***b***) and baseflow (Nov-01, Figure 3.3***c***) conditions. In addition, high ^{222}Rn concentrations (exceeding steady state alluvial sediment emanation, Table 3.1) indicated potential for regional groundwater discharge into the alluvial aquifer approximately 30 m from the stream channel during flood recession (Mar-01, Figure 3.3***b***) and at approximately 30 and beyond 40 m from the stream channel during baseflow conditions (Nov-01, Figure 3.3***c***).

At Fordwich (site 3) hydraulic gradients indicated potential for regional groundwater discharge to the alluvial aquifer during both flood recession (Mar-01, Figure 3.1***b***) and baseflow conditions (Nov-01, Figure 3.1***e***). However, ^{222}Rn concentrations in alluvial groundwater (Figure 3.5) were not elevated in comparison to ^{222}Rn emanation from alluvial aquifer material (Table 3.1). Hydraulic gradients indicated

that the alluvial aquifer at Fordwich (site 3) was potentially recharged by surface water during flood recession (Mar-01, Figure 3.1***b***), but not during baseflow (Nov-01, Figure 3.1***e***) sampling. ^{222}Rn concentrations in alluvial groundwater at Fordwich were low relative to ^{222}Rn emanation indicating potential surface water recharge into the alluvial aquifer up to 30 m from the stream channel during flood recession. During baseflow ^{222}Rn concentrations in shallow alluvial groundwater (<1.3 m below the water table) were lower than steady state ^{222}Rn emanation indicating potential for infiltration of surface water into the alluvial aquifer up to 40 m from the stream channel.

During flood recession alluvial groundwater and surface water elevations were level indicating that there was no net gain or loss of alluvial groundwater from or to the stream channel in the mid to upper Wollombi Catchment (at Wollombi site 10, Figure 3.1***c***). During baseflow hydraulic gradients indicated that the major water flow pathway was from alluvial groundwater to the Wollombi Brook (Figure 3.1***f***). However, low alluvial groundwater ^{222}Rn concentrations relative to the median steady state ^{222}Rn emanation from alluvial sands at Wollombi (Table 3.1) indicated that there was some surface water infiltration into the alluvial aquifer during both flood recession (Figure 3.6***a***) and baseflow conditions (Figure 3.6***b***). Regional groundwater levels were consistently lower than alluvial groundwater levels indicating that regional groundwater was unlikely to contribute to the alluvial aquifer.

Hydraulic gradients between the surface water, alluvial groundwater and regional groundwater systems indicated that there was minimal, if any surface water or regional groundwater contribution to the alluvial aquifer. However, comparison of ^{222}Rn concentrations in alluvial groundwater to steady state ^{222}Rn emanation from alluvial aquifer sediments indicated that surface water recharged the alluvial aquifer

during flood recession and baseflow conditions in the lower (Warkworth site 1 and Fordwich site 3) and mid to upper (Wollombi site 10) Wollombi Catchment. Differences between ^{222}Rn concentrations in alluvial groundwater and steady state ^{222}Rn emanation from alluvial aquifer sediments indicated potential for regional groundwater contribution to the alluvial aquifer during flood recession and baseflow conditions in the lower Wollombi Catchment (Warkworth site 1).

3.3.2 Extent of surface water influx to alluvial aquifer

If alluvial aquifer sediments are completely flushed with low ^{222}Rn concentration (e.g. 0.2 Bq L^{-1}) surface water, the ^{222}Rn concentration of newly recharged alluvial groundwater gradually increases (due to ^{222}Rn ingrowth) until it reaches equilibrium with alluvial aquifer material (equation 3.1).

$$C^{222} = C^{226}\left(1 - e^{-\lambda T}\right) \qquad \textbf{3.1}$$

C^{222}	The ^{222}Rn concentration in a closed system	(Bq L^{-1})
C^{226}	^{222}Rn concentration produced by the radioactive decay of ^{226}Ra	(Bq L^{-1})
λ	Rate of ^{222}Rn decay	(2.098 × 10^{-6} s^{-1})
T	Time of ^{222}Rn ingrowth	(s)

Radioactive steady state occurs after 20 to 25 days (5 to 6 half-lives of ^{222}Rn) due to the large difference in decay rates between ^{222}Rn and ^{226}Ra. Since the concentration of ^{222}Rn in groundwater approaches C^{226} under steady state conditions (97 to 99%, Snow and Spalding 1997) the steady state ^{222}Rn concentration (C_{ss}) can be used to approximate C^{226}. Therefore, the time of ^{222}Rn ingrowth (T) can be estimated using equation 3.2.

$$T = \frac{\ln\left(1 - {}^{222}R_{meas} / C_{ss}\right)}{-\lambda} \qquad \textbf{3.2}$$

$^{222}R_{meas}$	^{222}Rn activity measured in groundwater	(Bq L^{-1})
C_{ss}	Steady state ^{222}Rn activity of groundwater	(Bq L^{-1})

Since ^{222}Rn ingrowth increases exponentially with time (T, Figure 3.8) and ^{222}Rn emanation from alluvial aquifer material was inhomogeneous (Table 3.1), the residence time of newly recharged alluvial groundwater was estimated for up to 12 days (Figures 3.9 to 3.11). If alluvial groundwater is not completely flushed by surface water infiltration (i.e. mixing between "old" and "new" alluvial groundwater occurs), the residence time of "new" alluvial groundwater within the alluvial aquifer will be overestimated. Therefore, estimates of the extent of surface water infiltration into the alluvial aquifer within a 12 day period are conservative.

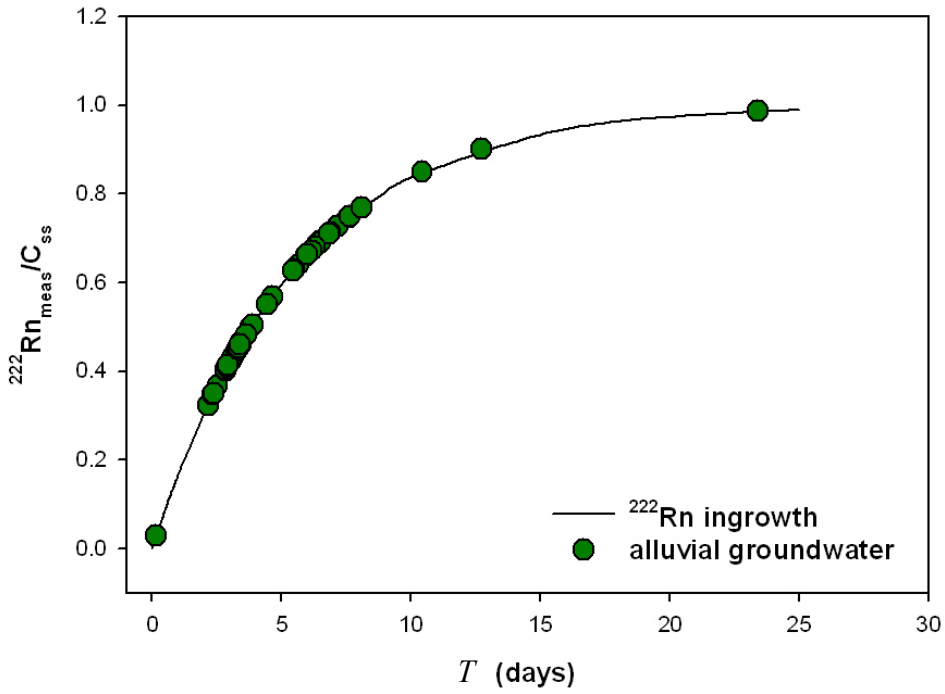

Figure 3.8 Residence time (T) of water within the alluvial aquifer and the fraction of ^{222}Rn ingrowth represented by the ^{222}Rn concentration measured in the alluvial aquifer ($^{222}R_{meas}$) divided by the steady state ^{222}Rn emanation from alluvial aquifer material (C_{ss}).

In the lower Wollombi catchment (Warkworth site 1, Figure 3.9***a***, ***b***) surface water infiltrated up to 10 m horizontally into the alluvial aquifer within 12 days during flood recession. The vertical infiltration of surface water into the alluvial aquifer was 3 m during the May 2000 flood recession, whilst surface water infiltrated less then 2 m vertically into the alluvial aquifer during the March 2001 flood recession. The extent of horizontal surface water infiltration into the alluvial aquifer was higher during baseflow (Nov-01, Figure 3.9***c***) than during flood recession conditions in the lower Wollombi Catchment (Warkworth, site 1). Surface water infiltrated up to 20 m horizontally and 1 m vertically into the alluvial aquifer within 12 days during baseflow. This translates to horizontal groundwater velocities in the order of 3 cm hr^{-1} during flood recession (Mar-01) and 7 cm hr^{-1} during baseflow (Nov-01) and vertical groundwater velocities of less than 1 cm hr^{-1} during both flood recession and baseflow conditions at Warkworth. Groundwater velocities are underestimates because they were based on the shortest distances from the stream channel.

At Fordwich (site 3) in the lower Wollombi Catchment surface water infiltrated approximately 30 m horizontally and 2 m vertically into the alluvial aquifer within 12 days during flood recession (May-00, Figure 3.10***a***). During baseflow (Nov-01, Figure 3.10***b***), surface water infiltration was more extensive horizontally (approximately 40 m) and less extensive vertically (up to 1 m) within 12 days than during flood recession conditions. Therefore, horizontal groundwater velocities in the alluvial aquifer at Fordwich ranged between approximately 10 cm hr^{-1} during flood recession and 14 cm hr^{-1} during baseflow sampling. Vertical alluvial groundwater velocities were less than 1 cm hr^{-1} during both flood recession and baseflow sampling.

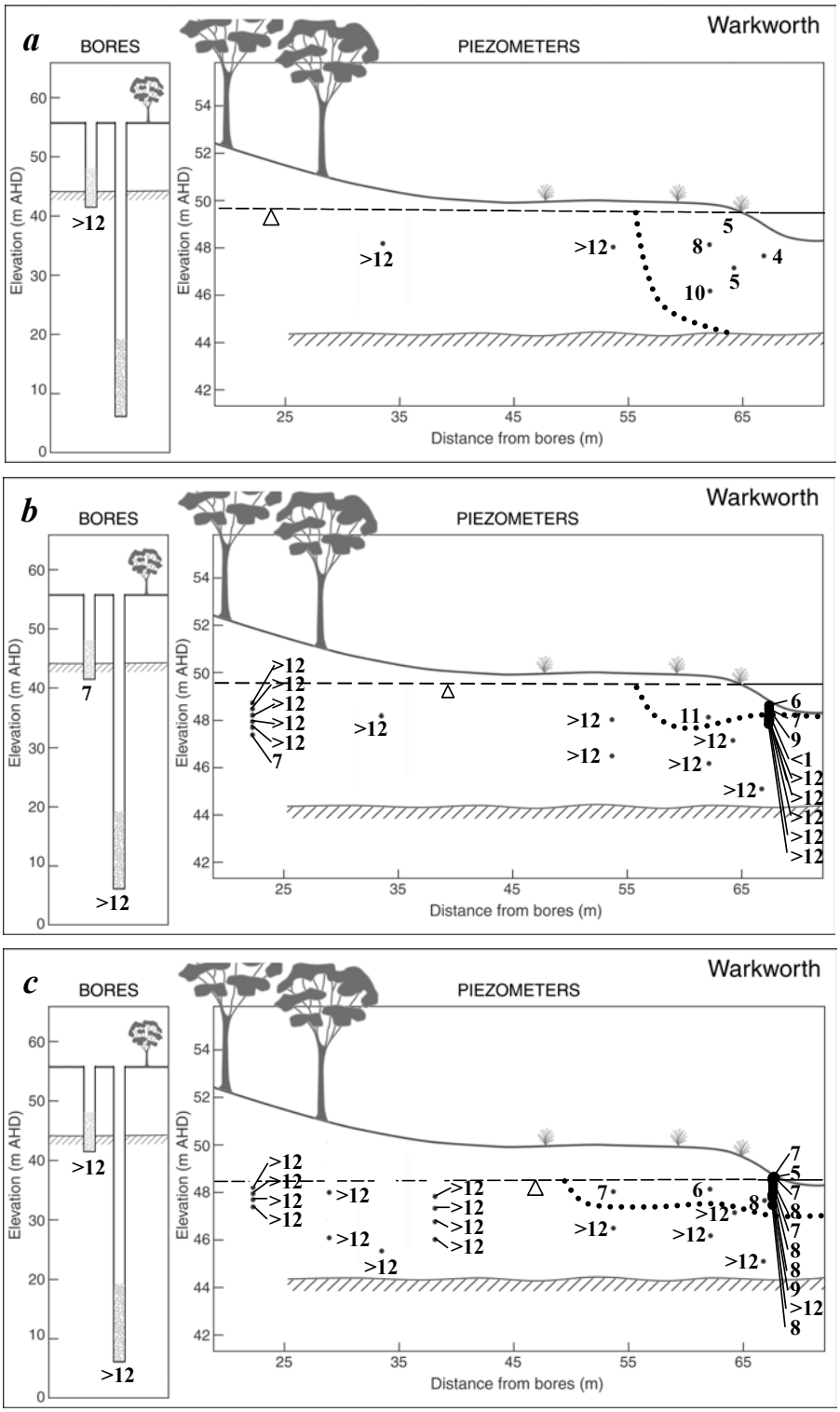

Figure 3.9 Residence time (days) of stream water in the alluvial aquifer at Warkworth during the (***a***) May-00 and (***b***) Mar-01 flood recessions and during the (***c***) Nov-01 low stream flow (baseflow) conditions based on ^{222}Rn ingrowth estimates. Dashed line indicates the interpreted groundwater level. Dotted line indicates the extent of surface water infiltration into the alluvial aquifer within 12 days.

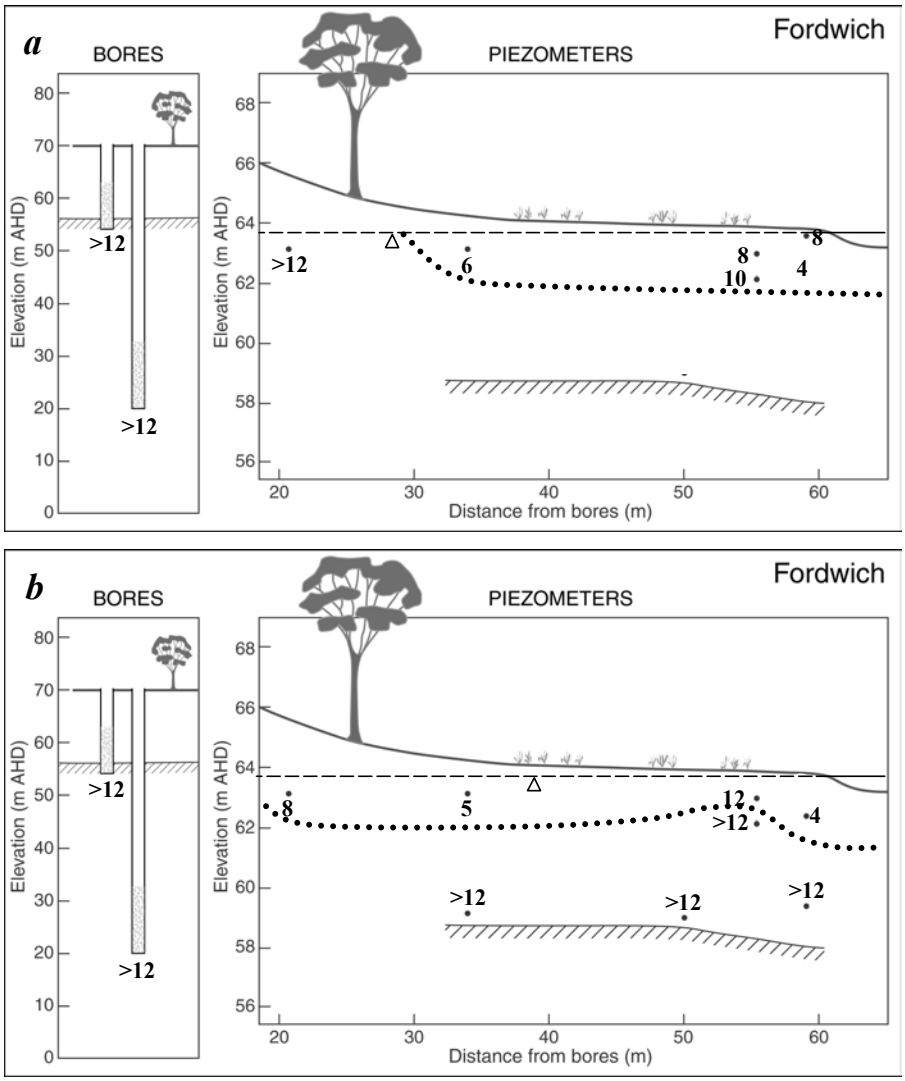

Figure 3.10 Residence time (days) of stream water in the alluvial aquifer at Fordwich during the (***a***) May-00 flood recession and (***b***) Nov-01 low flow (baseflow) conditions based on ^{222}Rn ingrowth estimates. Dashed line indicates the interpreted groundwater level. Dotted line indicates the extent of surface water infiltration into the alluvial aquifer within 12 days.

In the mid to upper Wollombi Catchment the horizontal extent of surface water infiltration was not bounded by the piezometer network because surface water extended beyond the piezometer network during flood recession (Mar-01, Wollombi, site 10, Figure 3.11***a***). Surface water infiltrated up to 4 m vertically within 12 days during flood recession. During baseflow surface water infiltrated approximately 20 m horizontally and at least 2.5 m vertically into the alluvial aquifer (Figure 3.11***b***). Groundwater velocities were in the order of 1 cm hr^{-1} vertically during flood recession and 7 cm hr^{-1} horizontally during baseflow sampling.

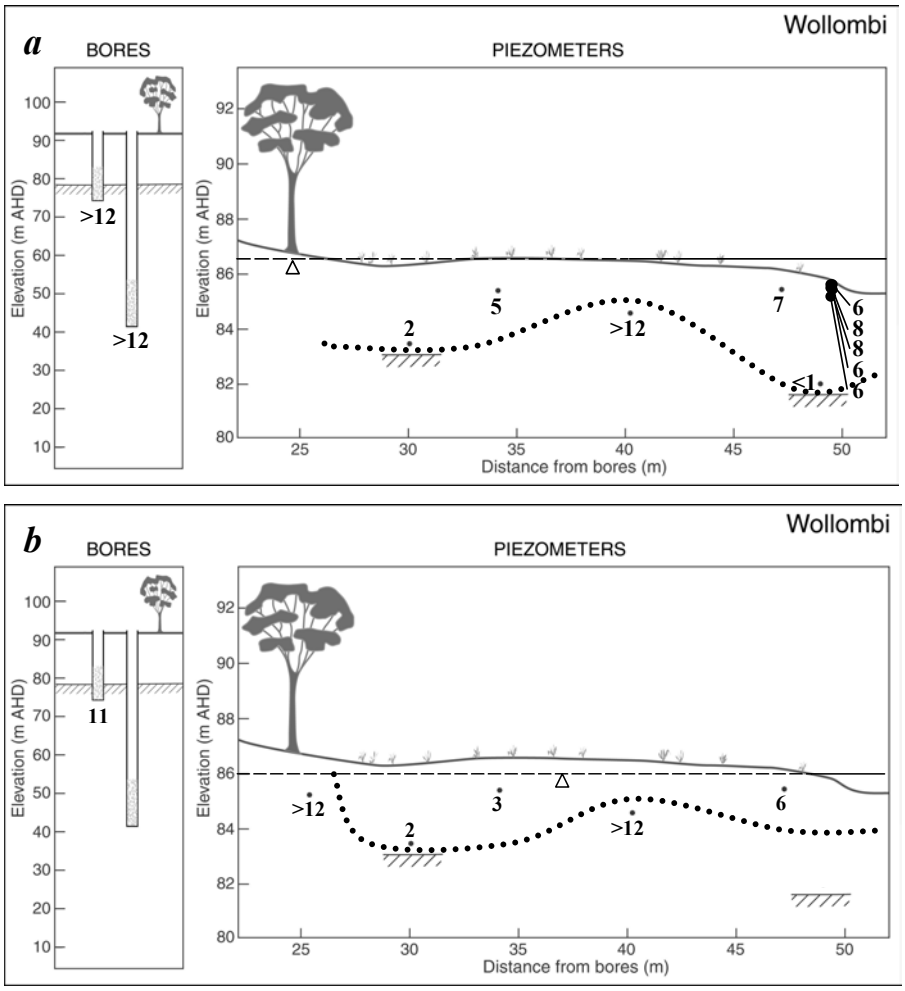

Figure 3.11 Residence time (days) of stream water in the alluvial aquifer at Wollombi during the (***a***) Mar-01 flood recession and the (***b***) Nov-01 low stream flow (baseflow) conditions based on ^{222}Rn ingrowth estimates. Dashed line indicates the interpreted groundwater level. Dotted line indicates the extent of surface water infiltration into the alluvial aquifer within 12 days.

Hydraulic gradients indicated that surface water only recharged the alluvial aquifer in the lower Wollombi Catchment at Fordwich (site 3) during flood recession conditions (Mar-01). However, estimates of groundwater residence time in the alluvial aquifer, based on steady state ^{222}Rn emanation and ^{222}Rn concentrations in alluvial groundwater, showed surface water infiltrated (up to 40 m horizontally and 3 m vertically) into the alluvial aquifer in the lower (Warkworth, site 1 and Fordwich, site 3) and mid to upper (Wollombi, site 10) Wollombi Catchment during all sampling periods. Estimated alluvial groundwater velocities based on extent of surface water infiltration into the alluvial aquifer within 12 days were similar to

groundwater velocities measured in the mid Wollombi Catchment alluvial aquifer using the point dilution method (0.5 to 3 cm hr^{-1}, Lamontagne *et al.* 2002) and to pore velocities in sands measured in laboratory experiments (1.6 to 3.4 cm hr^{-1}, Hoehn *et al.* 1992).

In the lower Wollombi Brook, surface water infiltrated further horizontally into the alluvial aquifer within 12 days during baseflow than during flood recession conditions. Correspondingly, horizontal alluvial groundwater velocities were higher during baseflow than flood recession conditions in the lower Wollombi Catchment. This is consistent with previous hydrometric studies that found hyporheic exchange was reduced during high flows (Harvey *et al.* 1996, Wroblicky *et al.* 1998). The lateral extent and rate of surface water ingress to the alluvial aquifer at Warkworth is most likely related to the hydraulic gradient between the surface water and alluvial groundwater systems. Hydraulic gradients from the alluvial aquifer toward the Wollombi Brook were highest during flood recession conditions (Figure 3.1***a***, ***d***), which probably limited (or created greater resistance to) the lateral extent and rate of surface water influx to the alluvial aquifer. The same argument, however, did not apply for Fordwich. Hydraulic gradients indicated greater potential for surface water influx to the alluvial aquifer at Fordwich during flood recession than baseflow sampling (Figure 3.1***b***, ***e***). However, ^{222}Rn-based estimates of alluvial groundwater residence times indicated greater lateral influx of surface water to the alluvial aquifer during baseflow than flood recession at Fordwich.

Assuming that the extent of surface water influx to the alluvial aquifer within 12 days based on estimated residence times is correct, the hydraulic gradient was not the key factor driving surface water ingress to the alluvial aquifer system at Fordwich. Less extensive and lower rates of lateral surface water ingress to the alluvial aquifer during flood recession could potentially be associated with the higher flood recession

stream flow rates. Shorter residence times of water in the stream channel during high flow conditions may increase hydraulic uptake lengths (e.g. Morrice *et al.* 1997) and reduce the extent of hyporheic flows (e.g. Legrand-Marcq and Laudelot 1985). Alternatively less extensive and lower rates of lateral surface water ingress to the alluvial aquifer during flood recession may be related to stream channel morphology. Stream water tends to infiltrate the streambed (into the hyporheic zone) at the head of riffles (where streambed gradients increase) and discharges back into the stream channel in down gradient pools (where streambed gradients decrease, e.g. Harvey and Bencala 1993). Hyporheic flows may be inhibited when pool and riffle structures become submerged during high stream stages (e.g. Hinkle *et al.* 2001), reducing surface water infiltration to the alluvial aquifer system at Fordwich during flood recession. In Rio Calaveras, Wroblicky *et al.* (1998) found that hyporheic flows through streambed meanders were high during low stream flows, but decreased or ceased altogether during higher stream flows.

The vertical extent of surface water infiltration into the alluvial aquifer within 12 days was greater during flood recession than baseflow conditions in the lower Wollombi Catchment. In the mid to upper Wollombi Catchment available data indicated that the extent of surface water infiltration into the alluvial aquifer was similar during flood recession and baseflow conditions. High stream flow events are likely to scour the stream channel, removing low hydraulic conductivity material that has accumulated during low stream flow conditions. This would be inclined to increase the hydraulic conductivity of the streambed and therefore increase surface water infiltration beneath the stream channel during flood recession in comparison to baseflow conditions.

Lower rates of lateral surface water exchange with alluvial groundwater in the lower reaches of the Wollombi Catchment during flood recession compared to baseflow conditions were most likely related in varying degrees to:

1. The steepness of hydraulic gradients within the alluvial aquifer,
2. The hydraulic gradient between the alluvial aquifer and the stream channel,
3. Stream flow rates, and
4. Stream channel morphology.

Greater vertical surface water exchange with alluvial groundwater during flood recession in comparison to baseflow conditions was probably influenced by scouring and deposition processes within the stream channel related to high and low stream flow conditions. Hyporheic flow paths that have long contact times (in the order of days) with aquifer material are important for biogeochemical transformations to occur (e.g. nitrogen transformations, Duff and Triska 2000). Extensive surface water and groundwater interaction between the Wollombi Brook and adjacent alluvial aquifer probably facilitate biogeochemical reactions, which maintain high water quality (low nutrient concentration, Lamontagne *et al.* 2003) in the Wollombi Brook, particularly during low stream flow conditions.

3.3.3 Regional groundwater leakage into the alluvial aquifer

The occurrence of higher than steady state ^{222}Rn concentrations in alluvial groundwater could potentially be caused by influxes of regional groundwater to the alluvial aquifer system. Variable rates of ^{222}Rn emanation from alluvial aquifer material may also cause points of high ^{222}Rn concentration in alluvial groundwater. The following discussion assumes that (1) measured steady state ^{222}Rn emanation from alluvial aquifer material (1.6 to 6.7 Bq L^{-1}, Table 3.1) was representative of the range of steady state alluvial groundwater ^{222}Rn concentrations, and (2) ^{222}Rn concentrations (Figures 3.3, 3.5 and 3.6) and groundwater levels (Figure 3.1)

measured in the bore network were representative of the regional groundwater system. If the above assumptions are valid and regional groundwater was the source of higher than steady state ^{222}Rn concentration alluvial groundwater, the time (t, within 12 days) that regional groundwater has taken to reach the alluvial aquifer can be estimated using equation 3.3.

$$C^t = C^0 e^{-\lambda t} \qquad \textbf{3.3}$$

C^t	^{222}Rn concentration at time, t, after radioactive decay	(Bq L^{-1})
C^0	Initial ^{222}Rn concentration	(Bq L^{-1})
λ	^{222}Rn decay constant	(2.098 × 10^{-6} s^{-1})
t	Time of ^{222}Rn decay	(s)

Higher than steady state ^{222}Rn concentrations in alluvial groundwater occurred in the lower Wollombi Catchment at Warkworth (site 1) during flood recession (Mar-01 Figure 3.3***b***) and baseflow sampling (Nov-01 Figure 3.3***c***). Travel times (t) for regional groundwater to reach alluvial aquifer piezometers were estimated assuming (1) ^{222}Rn concentrations between 13 and 16 Bq L^{-1} (Figure 3.3) were representative of regional groundwater at Warkworth, and (2) the maximum steady state ^{222}Rn emanation from alluvial aquifer material at Warkworth was 6 Bq L^{-1} (Table 3.1). It takes 4 to 6 days (equation 3.3) for regional groundwater (13 to 16 Bq L^{-1}) to decay to steady state ^{222}Rn emanation concentrations (6 Bq L^{-1}). Therefore, any regional groundwater induced elevated ^{222}Rn concentrations in alluvial groundwater would have occurred due to recent (<6 days) regional groundwater influxes to the alluvial aquifer.

Elevated ^{222}Rn concentration alluvial groundwater occurred 34 m from bores during flood recession (8.5 Bq L^{-1}, Figure 3.3***b***) and 20 and 38 m from bores (Figure 3.3***c***) during baseflow. If regional groundwater leakage caused the elevated ^{222}Rn concentrations in alluvial groundwater, it would have taken between 1 and 5 days (equation 3.3) to reach the points of elevated ^{222}Rn concentration in the alluvial aquifer during baseflow and approximately 3 days during flood recession. However, differences in groundwater levels between the regional groundwater and alluvial groundwater systems indicated that elevated ^{222}Rn concentrations in alluvial groundwater were unlikely to be caused by regional groundwater leakage. It is more likely that elevated ^{222}Rn concentrations measured in alluvial groundwater during flood recession and baseflow sampling originated from zones of high ^{222}Rn emanation within the alluvial aquifer.

^{222}Rn concentrations of 16 to 38 Bq L^{-1} were assumed to be representative of regional groundwater at Fordwich (site 3, Figure 3.5) and the maximum steady state ^{222}Rn emanation from alluvial aquifer material was assumed to be 6 Bq L^{-1}. Therefore, it would take 5 to 10 days for regional groundwater ^{222}Rn concentrations to decay to steady state alluvial groundwater ^{222}Rn concentrations at Fordwich (equation 3.3). ^{222}Rn concentrations in alluvial groundwater were not elevated with respect to steady state ^{222}Rn emanation values at Fordwich during flood recession or baseflow sampling. Therefore, any regional groundwater influxes to the alluvial aquifer must have taken more than 5 days to reach the Fordwich alluvial groundwater piezometer network during flood recession (Mar-01) and baseflow (Nov-01) sampling.

^{222}Rn concentrations in regional groundwater (1 to 5 Bq L^{-1}, Figure 3.6) were not elevated with respect to steady state ^{222}Rn emanation from alluvial aquifer material (4 to 7 Bq L^{-1}, Table 3.1) in the upper Wollombi Catchment (at Wollombi, site 10).

Differences between regional groundwater and alluvial groundwater ^{222}Rn concentrations were insufficient to identify areas of regional groundwater influxes to the alluvial aquifer in the upper Wollombi Catchment. Therefore, short-term regional groundwater influxes to the alluvial aquifer at Wollombi were not estimated.

Hydraulic gradients indicated potential for regional groundwater leakage into the alluvial aquifer system at Fordwich. However, ^{222}Rn concentrations indicated that any regional groundwater leakage had not reached the piezometer network less than 10 days prior to flood recession (May-00) or baseflow (Nov-01) sampling at Fordwich. Hydraulic gradients between regional and alluvial aquifer systems indicated that regional groundwater did not contribute to the alluvial aquifer at Warkworth (site 1) or Wollombi (site 10) during flood recession (Mar-01) or baseflow (Nov-01) sampling.

Alluvial groundwater mounds in the Wollombi catchment (Figure 3.1) appear to function as buffer zones between the Wollombi Brook and the regional groundwater system. Alluvial groundwater abstraction will lower water levels in the Wollombi Brook, particularly during low rainfall seasons, and could potentially induce regional groundwater flows toward the Wollombi Brook. Regional groundwater influxes would increase the salinity of alluvial groundwater and subsequently increase the salinity of groundwater discharge to stream flow.

3.4 CONCLUSIONS

Whilst hydraulic gradients indicated the net direction of surface water and groundwater fluxes, the use of ^{222}Rn for estimating residence times of water in the alluvial aquifer showed the extent of short-term (less than 12 days) surface water and groundwater interaction within the alluvial aquifer. Surface water and groundwater

interaction within the alluvial aquifer was not limited to conditions of net surface water influx to the alluvial aquifer. ^{222}Rn-based estimates of groundwater residence time showed that surface water and groundwater exchange occurred within the alluvial aquifer when low hydraulic gradients indicated (1) net surface water flux into the alluvial aquifer, (2) no net flux between surface water and the alluvial aquifer, and (3) net alluvial groundwater flux into the stream channel.

^{222}Rn-based estimates of groundwater residence time showed that lateral surface water and groundwater exchange within the alluvial aquifer was more extensive during baseflow (Nov-01) than flood recession (Mar-01) sampling in the lower Wollombi Catchment. In addition, estimates of groundwater velocity indicated that the rates of surface water and groundwater exchange within the alluvial aquifer were higher during baseflow than flood recession sampling. The lateral extent of the surface water and alluvial groundwater mixing zone (hyporheic zone) in the lower Wollombi Catchment was probably highest during baseflow sampling due to (1) lower hydraulic gradients within the alluvial aquifer (i.e. between the hill slope and floodplain) rather than between the near-stream alluvial aquifer and stream channel (2) lower stream flow rates and therefore greater water residence times (shorter uptake lengths) within the stream channel, and (3) greater impact of stream channel morphological features (i.e. meanders, pools and riffles) during low stream stages.

Vertical surface water and groundwater interaction within the alluvial aquifer was more extensive during flood recession (Mar-01) than baseflow (Nov-01) sampling in the lower Wollombi Catchment. Flood flows probably scoured low hydraulic conductivity streambed material creating greater short-term vertical hydraulic conductivities beneath the stream channel during flood recession sampling. Conversely, siltation of the streambed sediments probably occurred during lower stream flows causing lower streambed hydraulic conductivities, resulting in less

extensive surface water and groundwater interaction in the alluvial aquifer beneath the stream channel.

Differences in ^{222}Rn concentration and water levels between the alluvial groundwater and regional groundwater systems indicated that regional groundwater did not leak into the near-stream alluvial aquifer (covered by the piezometer network) in the week prior to flood recession (Mar-01) or baseflow (Nov-1) sampling in the lower Wollombi Catchment. Any regional groundwater leakage to the monitored areas of the alluvial aquifer system must have occurred along longer than 6 day flow pathways.

4 QUANTIFYING GROUNDWATER DISCHARGE TO STREAM FLOW USING ^{222}Rn

4.1 INTRODUCTION

Groundwater discharge to stream ecosystems influences the volume and persistence of stream discharge and the chemical conditions in and near streams. Each of these factors plays an important role in sustaining biological activity and biodiversity within the stream ecosystem. For example, stream flow is often maintained by groundwater discharge during periods of low flow (Freeze and Cherry 1979). Constant temperature stream water zones induced by groundwater discharge provide a desirable habitat for fish spawning (e.g. Dent *et al.* 2000). Groundwater also delivers essential nutrients to the riverine environment for ecosystem function (Fiebig *et al.* 1990, Triska *et al.* 1993). If the source of groundwater discharge to stream flow is reduced or contaminated it is likely to damage ecosystem biodiversity (e.g. Neilsen *et al.* 1980).

Groundwater abstraction can reduce groundwater discharge to stream flow and in some cases reverse groundwater flows inducing surface water to recharge the adjacent aquifer system (e.g. Winter *et al.* 1998). Alluvial groundwater abstraction may prolong no flow conditions in the Wollombi Brook applying pressure on ecosystem health and potentially reducing biodiversity. In addition, alluvial groundwater abstraction reduces the freshwater buffer between the Wollombi Brook and the saline regional groundwater system potentially inducing more saline groundwater discharge to stream flow. If the nature of groundwater discharge to stream flow is identified, then groundwater pumping can be managed to minimise detrimental impacts on stream ecosystem health.

Previous studies have used hydrometric measurements (e.g. Woessner 2000), seepage meters (e.g. Cey *et al.* 1998), measurements of stream flow increments (e.g. Devito *et al.* 1996) and tracer techniques (e.g. Uliana and Sharp 2001) to investigate groundwater discharge to surface water systems. The dynamics of stream water and groundwater exchange are difficult to ascertain using hydrometric techniques when hydraulic gradients are low (c.f. Chapter 3). Point-scale seepage and hydraulic property measurements provide limited useful information for catchment-scale investigations (Cey *et al.* 1998). Intensive monitoring is required when using differences in stream flow to identify locations of groundwater discharge. Chemical or isotopic mass balance techniques cannot be used to identify locations of groundwater discharge to stream flow if it is derived completely from groundwater discharge during periods of baseflow (Cey *et al.* 1998).

The radon (^{222}Rn) activity in groundwater can be several orders of magnitude higher than surface water. Therefore groundwater discharge to stream flow usually causes localised increases in the ^{222}Rn activity of stream water. Downstream of a groundwater discharge zone, the ^{222}Rn activity rapidly decreases in stream water as ^{222}Rn decays or is lost to the atmosphere.

Previous studies have used ^{222}Rn concentrations in surface water to identify locations of groundwater discharge to streams (e.g. Rogers 1958, Cook *et al.* 2001, 2003) and lakes (e.g. Al-Masri and Blackburn 1999). Few studies have attempted to estimate the magnitude of groundwater discharge (e.g. Lee and Hollyday 1987, 1993) and fewer have incorporated ^{222}Rn loss from stream or lake water (e.g. Ellins 1988, Ellins *et al.* 1990, Corbett *et al.* 1997) into their estimations. None have simultaneously incorporated both radioactive decay and gas exchange losses of ^{222}Rn from surface water. In this chapter existing methodology for estimating ^{222}Rn loss from stream

water, via gas exchange and radioactive decay, is advanced by numerically incorporating both processes simultaneously.

This chapter investigates the use of ^{222}Rn to understand the extent of short-term interactions between Wollombi Brook and the adjacent aquifers. Because ^{222}Rn has very low atmospheric concentrations and has a short half-life (3.8 days), it is useful for understanding surface water and groundwater interactions on time scales of a few days up to 3 weeks. ^{222}Rn concentrations in stream water in excess of background atmospheric levels are used to indicate locations of groundwater discharge to stream flow.

The aims of this chapter are to:

1. Identify locations of groundwater discharge to stream flow;
2. Solve ^{222}Rn losses from surface water due to turbulent gas exchange and radioactive decay simultaneously;
3. Estimate the magnitude of groundwater discharge to stream flow; and
4. Recommend strategies (field and analytical) that can be applied to other catchments for improving estimates of the magnitude of groundwater discharge to stream flow using ^{222}Rn concentrations stream water.

4.2 BACKGROUND THEORY

4.2.1 Estimating groundwater discharge to stream flow

4.2.1.1 Introduction

There are two potential sources of ^{222}Rn to stream water. The major source of ^{222}Rn input to stream water is typically groundwater discharge (e.g. Cook *et al.* 2003). Sediment flux from streambed (or lakebed) sediments can also be significant (e.g.

Par Pond, Corbett *et al.* 1997), however, such a source of ^{222}Rn to stream water is likely to be relatively constant.

If a single pulse of ^{222}Rn (e.g. from a groundwater discharge point) is injected into stream water and there are no further sources of ^{222}Rn to stream flow, the ^{222}Rn activity in stream water will gradually decrease due to gas exchange and radioactive decay (e.g. Lee and Hollyday 1993, Cook *et al.* 2003) until it reaches equilibrium with the atmosphere (average 4 to 15 Bq m^{-3}, Gesell 1983). If, in addition to the former scenario, there were a constant flux of ^{222}Rn into the stream water from ^{226}Ra-rich streambed sediments, the ^{222}Rn activity of stream water would gradually decrease until equilibrium was reached between the rate of ^{222}Rn loss from stream water and the rate of ^{22}Rn generation from stream sediments. In both scenarios net increases in the ^{222}Rn activity of stream water as it flows downstream are indicative of groundwater discharge to stream flow.

Even in stream reaches where there are net declines in the ^{222}Rn activity in stream water from upstream to downstream sampling stations there can still be significant groundwater contributions to stream flow. If ^{222}Rn losses from stream water are greater than ^{222}Rn inputs via groundwater contribution to stream flow then the net decline in ^{222}Rn from upstream to downstream sampling stations conceals groundwater discharge. Therefore, in order to better estimate groundwater discharge to stream flow between sampling stations ^{222}Rn loss via radioactive decay and gas exchange need to be accounted for.

In turbulent systems gas exchange is the primary mechanism of ^{222}Rn loss in surface water systems (e.g. Ellins 1988). In Par Pond (Cobett *et al.* 1997), which is a deeper and less turbulent system, radioactive decay was the primary ^{222}Rn loss mechanism. Surface water flow rates in the Wollombi Brook catchment are highly variable from

season to season and in different reaches of the catchment. Both ^{222}Rn loss mechanisms are likely to be significant in different parts of the catchment and under varying stream flow conditions.

4.2.1.2 Radon gas exchange

The stagnant film model (Lewis and Whitman 1924, Broecker and Peng 1982, Ellins *et al.* 1990) was used to estimate the transfer of ^{222}Rn from the Wollombi Brook to the atmosphere. In this model both stream water and the atmosphere are considered well mixed reservoirs, with constant vertical concentrations, separated by a hypothetical stagnant film of water (boundary layer, Figure 4.1) of thickness 2.5 to 500μm. The net transfer of ^{222}Rn from stream water to the atmosphere is assumed to occur via molecular diffusion. The ^{222}Rn concentration gradient between the two reservoirs, and the thickness of the boundary layer (z) separating them, determines the rate of ^{222}Rn diffusion from the stream to the atmosphere.

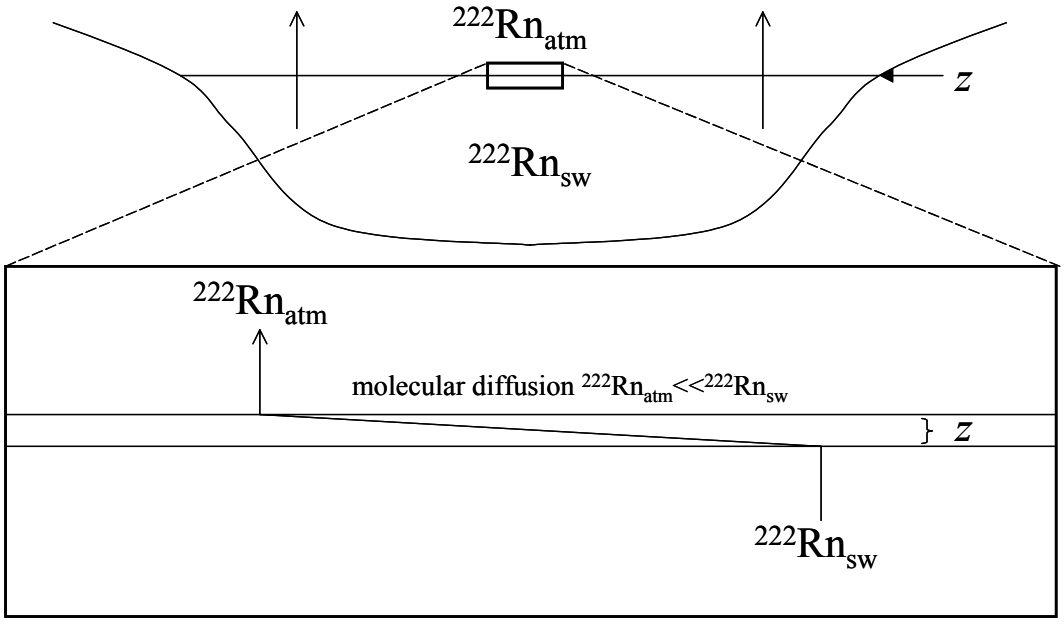

Figure 4.1 Stream cross-section, where the radon concentration in stream water ($^{222}Rn_{sw}$) is much higher than the radon concentration in the atmosphere ($^{222}Rn_{atm}$) and radon transfer occurs via molecular diffusion across the hypothetical stagnant boundary layer (z).

High ^{222}Rn concentration gradients occur between streams and the atmosphere when relatively high ^{222}Rn concentration groundwater discharges to stream flow. Inland atmospheric concentrations of ^{222}Rn typically range between 8 Bq m^{-3} (New Jersey) and 28 Bq m^{-3} (Colorado) (Gesell 1983). In contrast, surface water ^{222}Rn concentrations have been measured as high as 887 Bq L^{-1} (8.87×10^5 Bq m^{-3}) in fluvial springs in the Himalayas (Choubey *et al.* 2000). Reported ^{222}Rn concentrations in Australian surface waters range from 0.1 to 2.5 Bq/L (100 to 2500 Bq m^{-3}) in the Barron River (north-eastern Australia, Cook *et al.* 2001) and up to 10 Bq/L in springs flowing into the Daly River (northern Australia, Cook *et al.* 2003).

The thicker the boundary layer, the more slowly that ^{222}Rn is transferred from surface water to the atmosphere. For example, in a surface water system where radioactive decay is the dominant mechanism of ^{222}Rn loss, the stagnant film model considers the stagnant film layer to be exceedingly thick such that ^{222}Rn loss via molecular diffusion to the atmosphere is prohibited. The thickness of the stagnant film (z) is estimated (equation 4.1) by comparing upstream and downstream ^{222}Rn concentrations in a section of the stream where it can be assumed that there is no groundwater contribution to stream flow (Figure 4.2).

$$z = \frac{xD}{\ln\left(C^0 / C_T^n\right) hv} \qquad \textbf{4.1}$$

z	Thickness of stagnant film	(m)
x	Distance between sampling stations	(m)
D	Molecular diffusivity of ^{222}Rn	(at 23°C 1.2×10^{-9} m^2 s^{-1})
C^0	^{222}Rn activity upstream	(Bq L^{-1})
C_T^n	^{222}Rn activity downstream	(Bq L^{-1})

h	Average depth of stream	(m)
v	Velocity of stream water	(m s^{-1})

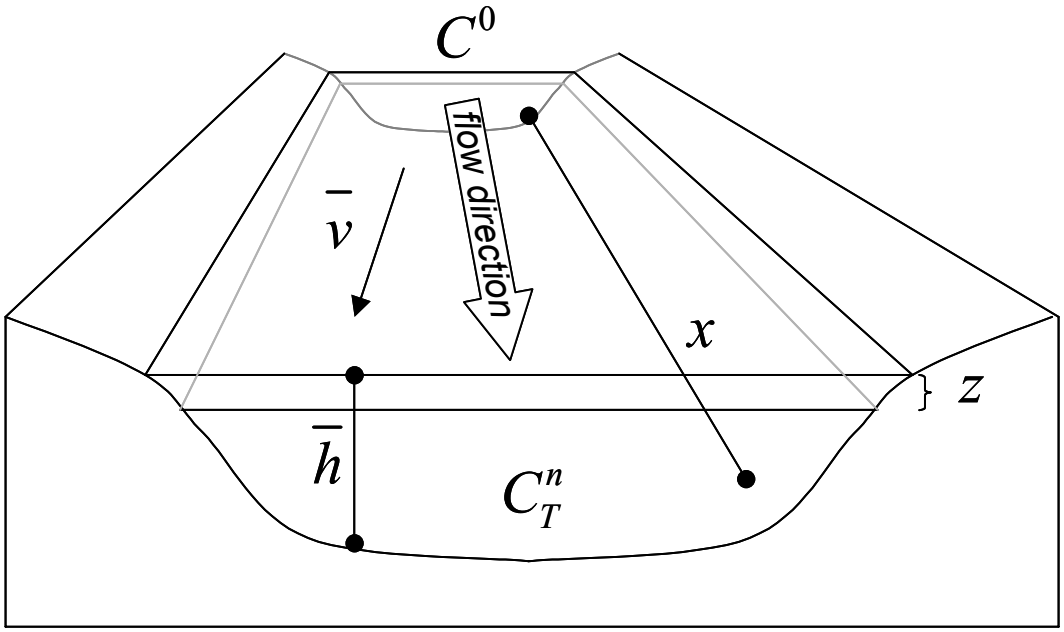

Figure 4.2 Stream section showing parameters measured for estimation of stagnant film thickness (z , equation 4.1) in a section of the stream in which there is no groundwater discharge to stream flow.

Thicknesses of stagnant film layers were estimated for the experimental lakes in Ontario (Emerson and Broecker 1975), assuming that the primary control on ^{222}Rn exchange was wind, and ranged between 500 and 700 μm. However, ^{222}Rn transfer from most streams to the atmosphere is generated primarily by stream turbulence (O'Connor and Dobbins 1957). Elsinger and Moore (1983) estimated stagnant film thicknesses for the Pee Dee River in South Carolina that ranged between 19 and 48 μm. Similarly Ellins *et al.* (1990) reported stagnant film thicknesses for the Rio Grande de Manati in Puerto Rico that ranged between 2.5 and 41 μm.

Once the thickness of the stagnant film is known, the ^{222}Rn activity at any distance (x) downstream (C_T^n) can be predicted accounting for turbulent ^{222}Rn losses from stream water using equation 4.2.

$$C_T^n = C^0 . e^{-Dx/zhv} \quad \textbf{4.2}$$

The difference between the predicted ^{222}Rn activity downstream (C_T^n) and the actual downstream ^{222}Rn activity (C^n) is proportional to the concentration and amount of groundwater entering the stream channel over the measured interval (equation 4.3).

$$C^n - C_T^n \propto C^{gw} V^{gw} \quad \textbf{4.3}$$

C^n	^{222}Rn activity downstream	(Bq L^{-1})
C^{gw}	^{222}Rn activity of groundwater	(Bq L^{-1})
V^{gw}	Volume of groundwater discharged to the stream channel	(L)

In a reach of the catchment where there is no groundwater contribution to stream flow equation 4.4 (Ellins *et al.* 1990) can be used to estimate the background ^{222}Rn activity of stream water due to sediment flux.

$$C^B = C^n - C_T^n \quad \textbf{4.4}$$

C^B	Background ^{222}Rn activity in stream water	(Bq L^{-1})

Equations 4.2 and 4.4 describe ^{222}Rn loss from surface water systems in which losses via radioactive decay are negligible. If ^{222}Rn loss via radioactive decay were significant, estimates of groundwater discharge to stream flow based on these

equations would be over-estimates. The following section (4.2.1.3) investigates the significance of ^{222}Rn loss from stream water due to radioactive decay.

4.2.1.3 Radon decay

^{222}Rn loss from stream water due to radioactive decay can be estimated using equation 4.5 if the time taken for water to flow between sampling stations is known.

$$C_R^n = C^0 . e^{-\lambda t} \qquad \textbf{4.5}$$

C_R^n	^{222}Rn activity downstream due to radioactive decay	(Bq L^{-1})
λ	^{222}Rn decay constant	(2.098×10^{-5} s^{-1})
t	Travel time between consecutive sampling stations	(s)

Equation 4.5 is converted to a function of distance (x, equation 4.6) between stream water sampling stations by substituting t for x/v.

$$C_R^n = C^0 . e^{-\lambda x / v} \qquad \textbf{4.6}$$

^{222}Rn losses from the Martha Brae (Jamaica) and Rio Manati (Puerto Rico) due to radioactive decay were considered negligible (Ellins 1988) because distances between sampling points were short (50 to 300 m) and the flow rates were relatively high (1 m s^{-1}). Whereas the distance between surface water sampling stations in the Wollombi Brook catchment were much higher (ranging from 900 to 15,500 m) and stream velocities much lower (<0.3 m s^{-1}).

Travel times for stream water to flow between Wollombi Brook sampling stations are likely to vary from 2 hours up to 4 weeks. This represents up to seven ^{222}Rn half-lives (3.8 days). If an initial ^{222}Rn concentration in stream water were 600 Bq L^{-1}, and there were no additional sources of ^{222}Rn to stream flow, after seven half lives only 5 Bq L^{-1} would remain in stream water. Therefore, due to the large distance between sampling stations in the Wollombi Brook catchment, ^{222}Rn loss from stream water due to radioactive decay was significant.

4.2.2 Percentage groundwater discharge to stream flow

The conventional use of ^{222}Rn in streams has been to identify the location of groundwater input to streams (e.g. Ellins *et al.* 1990, Lee and Holliday 1987, 1993). In the absence of discharge data it is difficult to convert the results of ^{222}Rn longitudinal transects to groundwater discharge estimates. It is easier to convert the data to the ratio of groundwater discharge (Q^{gw}) to stream discharge (Q^{sw}) using expression 4.7.

$$\frac{Q^{gw}}{Q^{n}} = \frac{\left(C^{n} - C^{n}_{TR}\right)}{\left(C^{gw} - C^{n}_{TR}\right)} \qquad \textbf{4.7}$$

Q^{gw} Groundwater discharged to stream flow ($m^3\ s^{-1}$)

Q^{sw} Stream discharge ($m^3\ s^{-1}$)

C^{n}_{TR} Predicted ^{222}Rn activity downstream after turbulent and radioactive losses ($Bq\ L^{-1}$)

Q^{gw}/Q^{sw} Fraction of groundwater in stream water at downstream sampling station

One of the largest sources of error in using equation 4.7 is estimated ^{222}Rn loss caused by gas exchange and radon decay along a given reach. All previous work that

has used naturally occurring ^{222}Rn activities to investigate groundwater discharges to surface water systems have, for the sake of simplicity, disregarded one of the two mechanisms for ^{222}Rn loss from surface water (e.g. Ellins *et al.* 1990, Corbett *et al.*1997). In the Wollombi Brook catchment, however, both mechanisms need to be solved simultaneously.

4.3 FIELD RESULTS

4.3.1 End-member characteristics

Median ^{222}Rn concentrations in stream water (0.17 Bq L^{-1}) were one order of magnitude lower than alluvial groundwater (3.2 Bq L^{-1}) and two orders of magnitude lower than regional groundwater median concentrations (13 Bq L^{-1}, Figure 4.3).

There were several tributaries (T5, T7, T9, T11 & T12, Figure 2.1) in the upper Wollombi Brook Catchment measured during baseflow (Nov-01) that had relatively high ^{222}Rn concentrations (Figure 4.4). The highest ^{222}Rn concentration measured in surface water was 6.4 Bq L^{-1}. This value was reached in a small spring (T5) that lost surface water connection with the Wollombi Brook during baseflow. T12 also lost surface water connection with Wollombi Brook during baseflow. Both T7 and T11 were still flowing into the Brook during baseflow, but their ^{222}Rn concentrations decreased significantly before they reached the Wollombi Brook. Only T9 discharged high concentration ^{222}Rn surface water into the Wollombi Brook during baseflow. By the time water from T9 (3.9 Bq L^{-1}) had mixed with Wollombi Brook water and flowed 5 km downstream to the next sampling station it had decreased to less than 10% of it's original value (0.34 Bq L^{-1}). The minimum ^{222}Rn concentration measured in stream water was 0.02 Bq L^{-1} and this was considered to represent background ^{222}Rn levels.

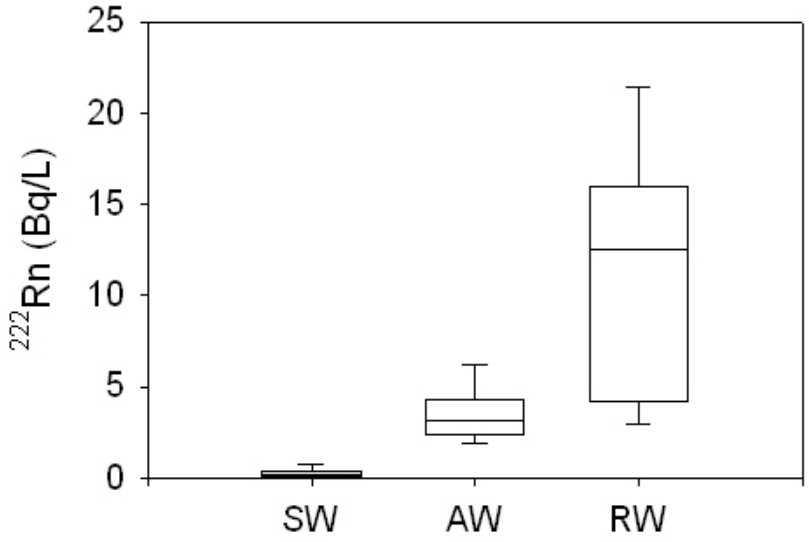

Figure 4.3 The 10th, 25th, 75th and 90th percentiles represent the variation throughout the two-year sampling period (2000-01) of radon (^{222}Rn) measured in stream water (SW), alluvial groundwater (AW) and regional groundwater (GW) sampled across the Wollombi Catchment.

Ranges of ^{222}Rn concentration in stream water compared to alluvial groundwater were narrow and distinctly different (Figure 4.3). The ^{222}Rn concentration in regional groundwater was typically much higher than both stream water and alluvial groundwater, but it was highly variable. The ^{222}Rn concentration in regional groundwater overlapped alluvial groundwater.

4.3.2 In-stream transects

^{222}Rn sampling during May 2000 and March 2001 were conducted shortly after flood conditions, and the longitudinal transects were virtually identical (Figure 4.5). Above the 80 km point ^{222}Rn activities were relatively low (~0.15 Bq L^{-1}), and ^{222}Rn activities peaked at about 0.21 Bq L^{-1} between 75 and 65 km. ^{222}Rn activities rapidly decreased from 65 and 55 km plateauing at about 0.08 Bq L^{-1}. ^{222}Rn activities remained relatively constant between 55 and 20 km, then increased to reach another lower peak of about 1.1 Bq L^{-1} at the 13 km point.

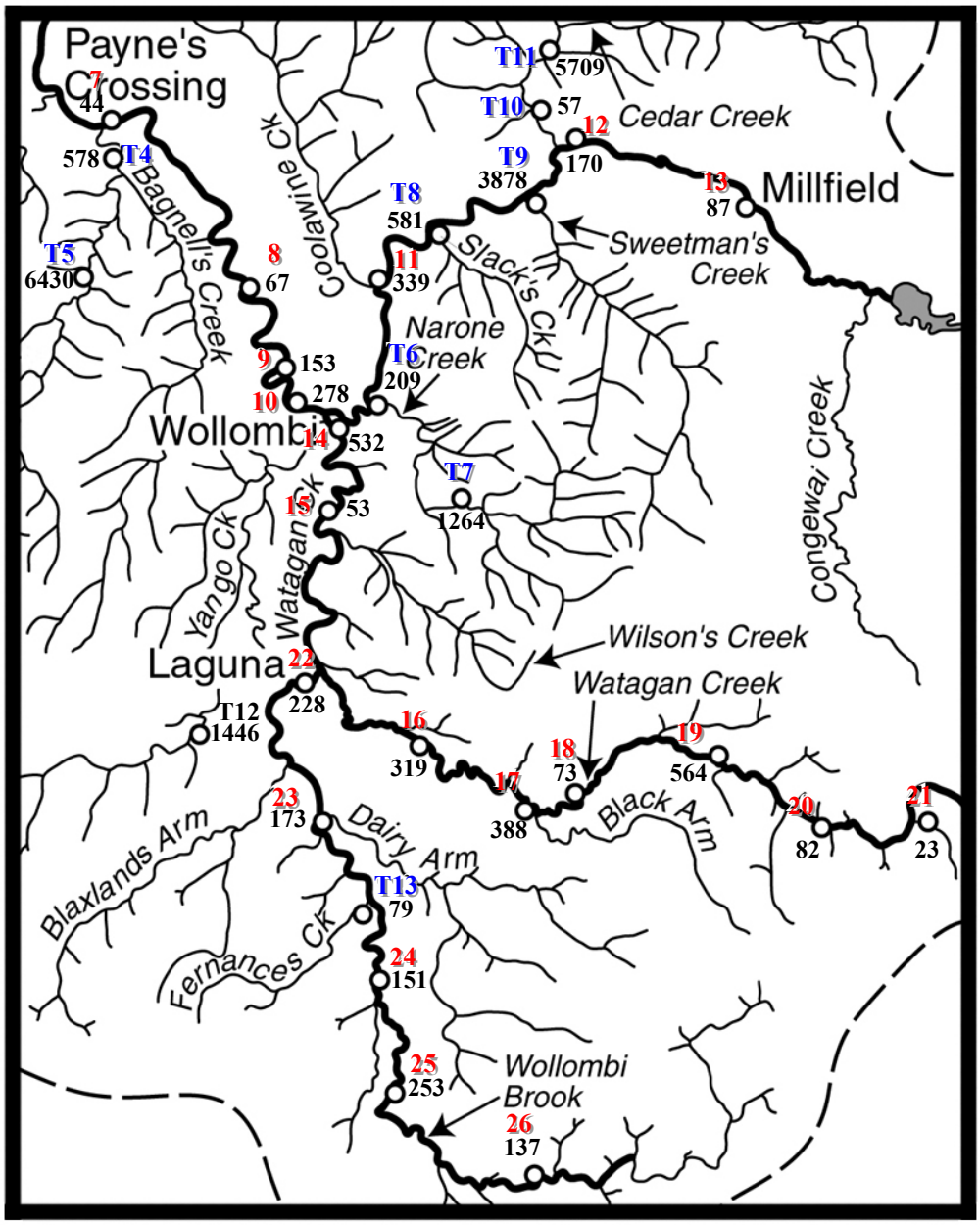

Figure 4.4 ^{222}Rn concentrations (mBq L^{-1}), shown in black, measured in the upper Wollombi Catchment during baseflow conditions (Nov-01).

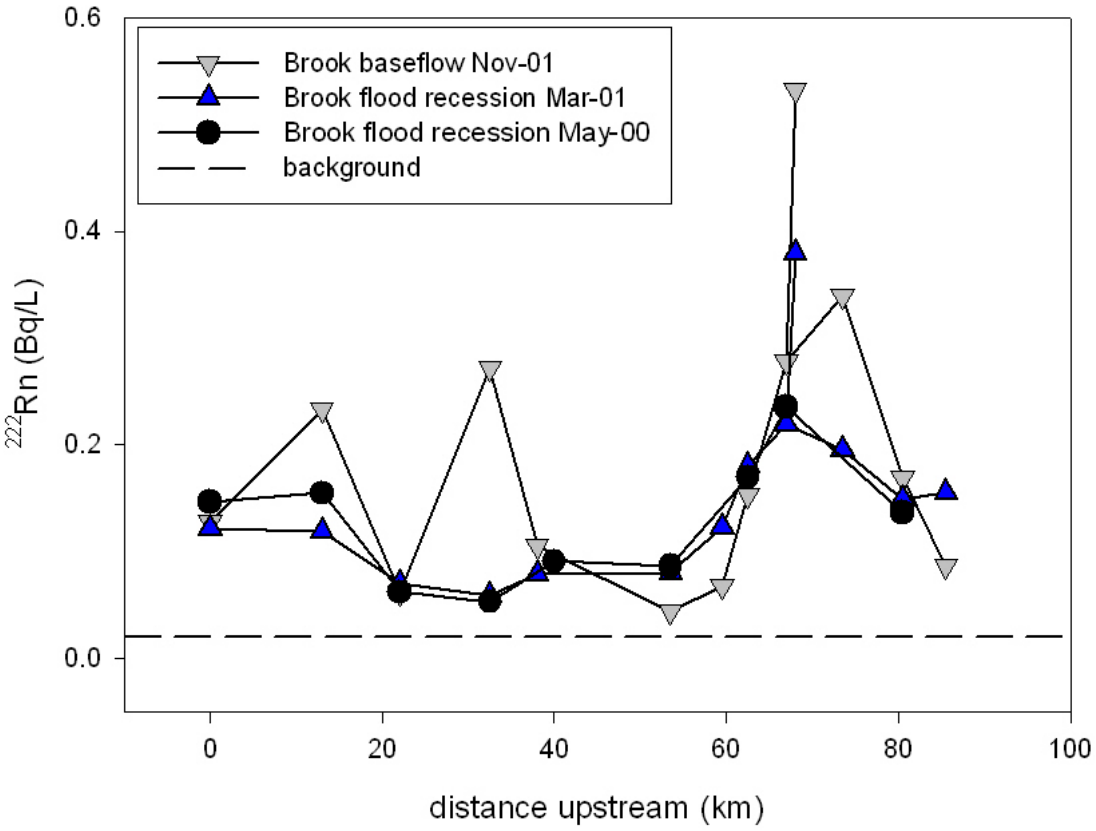

Figure 4.5 Radon (^{222}Rn) activities (Bq L^{-1}) in stream water measured during flood recession (May-00 & Mar-01) and baseflow (Nov-01) in the Wollombi Brook and tributaries compared background levels.

Under baseflow conditions (Nov-01) the general shape of the longitudinal ^{222}Rn transect was similar to those during flood recession (Figure 4.5), but peak ^{222}Rn concentrations were higher and occurred further upstream. There were also greater fluctuations in ^{222}Rn activity between sequential sampling stations, particularly in the lower reaches of the catchment (0 to 20 km). ^{222}Rn activities were consistently higher between the 40 to 60 km points during flood recession than during baseflow conditions. ^{222}Rn activities in stream water were typically higher in the upper (65 to 90 km) catchment than in the lower (0 to 60 km) catchment.

Stream reaches in which the ^{222}Rn activity at the upstream sampling station was lower than the ^{222}Rn activity at the downstream sampling station indicate that several reaches of the Wollombi Brook received groundwater contributions to stream flow. ^{222}Rn activities were higher in stream water than in the atmosphere in all stream water sampled throughout the catchment, showing that groundwater influxes impacted all reaches of the Wollombi Brook Catchment.

4.4 PARAMETERS FOR ESTIMATING ^{222}Rn PERSISTENCE IN STREAM WATER

4.4.1 Stagnant film thickness

Stagnant film thicknesses were estimated (equation 4.1) for the Wollombi Brook during flood recession (May-00 and Mar-01) and baseflow (Nov-01) conditions (Table 4.1).

Table 4.1 Stagnant film thickness (z) estimates and variable parameters (upstream and downstream ^{222}Rn concentrations; C^0, C_T^n, distance and travel time between sampling stations; x, t, average stream height and velocity; h, v) for each run of river transect in the Wollombi Brook (flood recessions May-00 and Nov-01, and baseflow Mar-01) based on ^{222}Rn gas exchange equation (4.1).

Sampling time	z	C^0	C_T^n	x	h	v	t
	μm	Bq L^{-1}	Bq L^{-1}	m	m	m s^{-1}	days
May 2000 Flood recession	92	170	85	9000	2.5	0.07	1.5
March 2001 Flood recession	40	180	125	3000	1.2	0.23	0.2
November 2001 Baseflow	67	155	70	3000	0.9	0.07	0.5

The Wollombi Brook stagnant films (ranging from 40 to 92 μm) were typically thicker than the Rio Grande de Manati (19 to 48 μm, Ellins *et al.* 1990) and Pee Dee

River (2.5 to 41 μm, Elsinger and Moore 1983) stagnant films. The most probable explanation for the thicker Wollombi Brook stagnant film estimates is the lower average stream velocity.

The greatest risk for error in estimating the stagnant film thickness (equation 4.1) is associated with the assumptions (1) ^{222}Rn is only lost from stream water via gas exchange and (2) there are no additional sources of ^{222}Rn contributing to stream flow over the stream section in which z is estimated. If ^{222}Rn losses due to radioactive decay were significant over the distances (x) that stagnant film thicknesses were estimated, the ^{222}Rn concentrations downstream due to gas exchange losses would be greater than the actual ^{222}Rn concentrations measured downstream (i.e. $C_T^n > C^n$). This would cause the thickness of the stagnant film to be underestimated. Therefore, the longer the travel time between sampling stations, the greater the potential error in estimating the stagnant film thickness.

Confidence in the assumption that groundwater does not discharge to stream flow within the stream section that z is estimated decreases over larger distances between sampling stations (x). If groundwater discharged to stream flow within the stream section that the stagnant film thickness was estimated, the downstream ^{222}Rn concentration due to gas exchange losses would be less than the actual ^{222}Rn concentration measured downstream (i.e. $C_T^n < C^n$). This would cause the theoretical stagnant film thickness to be overestimated. Therefore the greater the distance between sampling stations the lower the confidence in the z estimation.

Although the distances between sampling stations in the Wollombi Brook catchment were relatively large (3 to 9 km) the estimates of stagnant film thickness were comparable to those for the Rio Grande de Manati (Ellins *et al.* 1990) and Pee Dee River (Elsinger and Moore 1983). The stagnant film thickness estimated for the May

2000 flood recession during (Table 4.1) was thicker than stagnant film thicknesses estimated during baseflow (Nov-01) and flood recession (Mar-01). The May 2000 stagnant film thickness was probably overestimated due to the relatively large travel time between sampling stations (Table 4.1). Therefore only March 2001 and November 2001 sampling trips are discussed in subsequent sections. It is recommended that shorter time intervals between sampling stations be established for future estimations of stagnant film thickness.

4.4.2 Background ^{222}Rn concentration in stream water

Background stream water ^{222}Rn concentration estimates, based on turbulent gas exchange ^{222}Rn losses alone (equation 4.4), were very low or negative (Table 4.2). This is because predicted estimates of ^{222}Rn activity downstream due to turbulent loss alone do not account for losses due to radioactive decay, therefore the predicted downstream ^{222}Rn activity is overestimated. A new technique for predicting the ^{222}Rn activity downstream and the background ^{222}Rn activity in stream water is developed in section 4.5.3, which utilises a numerical modelling approach that incorporates both turbulent gas exchange and radioactive decay losses.

Table 4.2 Background ^{222}Rn concentrations in stream water (C^B) due to sediment flux (Bq L^{-1}) were estimated using equation (4.4).

Sampling time	**Background ^{222}Rn concentration in stream water** (C^B) **mBq L^{-1}**
May 2000 Flood recession	-0.00001
March 2001 Flood recession	0.0001
November 2001 Baseflow	-0.0004

4.5 MODELLING ^{222}Rn PERSISTENCE IN STREAM WATER

4.5.1 Introduction

The persistence of ^{222}Rn in stream water is controlled by (1) the rate of ^{222}Rn influx into stream water (via groundwater discharge) and (2) the rate of ^{222}Rn emission and decay from stream water. Both gas exchange and radioactive decay equations (4.2 and 4.6 respectively) used to estimate ^{222}Rn losses from stream water assume that the rate of ^{222}Rn loss is constant over the distance (x) between sampling stations. The rate of ^{222}Rn loss from stream water, however, depends on the ^{222}Rn activity within stream water. As ^{222}Rn is lost from stream water, the ^{222}Rn activity within stream water decreases, as a result, the rate of ^{222}Rn decay also decreases. Therefore, without additional ^{222}Rn contributions to stream flow, the rate of ^{222}Rn loss from stream water decreases as it flows further downstream.

It is a good approximation to assume a constant rate of ^{222}Rn loss over the distance between sampling stations if either ^{222}Rn decay (e.g. Ellins *et al.* 1990) or ^{222}Rn gas exchange (e.g. Corbett *et al.* 1997) are negligible in the study environment. However, ^{222}Rn loss via both gas exchange and radioactive decay were significant processes owing to the relatively large distances between sampling stations in the Wollombi Brook catchment. Therefore it could not be assumed that ^{222}Rn was lost from the Wollombi Brook at a constant rate for this investigation.

To the author's knowledge, all previous studies have considered ^{222}Rn losses due to radioactive decay and turbulent gas exchange exclusively. Due to the relatively large distances between stream water sampling stations in the Wollombi Brook catchment, ^{222}Rn loss via gas exchange was significantly diminished by radioactive decay losses and vice versa.

A numerical technique was developed to simultaneously solve the two previously independently analysed solutions (equations 4.2 and 4.6) for the dependent processes (^{222}Rn loss via gas exchange and radioactive decay respectively). This was achieved by subtracting equations 4.2 and 4.6 from the initial concentration (C^0) over n progressively smaller intervals of length x/n (equation 4.8, Figure 4.6), until the predicted downstream ^{222}Rn concentration (C_{TR}^n) converged.

$$C_{TR}^n = C^0 - \sum_{i=1}^{n} (C^{i-1} - C_T^i) + (C^{i-1} - C_R^i) \qquad \textbf{4.8}$$

n Number of equal sections over a constant distance, x

C^{i-1} ^{222}Rn activity upstream of a distance interval, i (Bq L^{-1})

C_T^i ^{222}Rn activity downstream of a distance interval, i, due to turbulent losses, equation 4.2 $C_T^i = C^0.e^{-Dx/zhv}$ (Bq L^{-1})

C_R^i ^{222}Rn activity downstream of a distance interval, i, due to radioactive decay losses, equation 4.6 $C_R^i = C^0.e^{-\lambda x/v}$ (Bq L^{-1})

i Interval number, integer fraction of n

Convergence was deemed once further spatial discretisation had minimal impact (< 10^{-4} Bq/L) on the solution. This is demonstrated in Figure 4.7, in which the estimated value for C_{TR}^n converged after x was subdivided into greater than 200 intervals (n).

The rate of ^{222}Rn loss from each interval of x (i) was progressively smaller with increasing distance from the upstream station. In other words, as i approached n (Figure 4.6), the value subtracted from C^0 $\left(C^{i-1} - C_T^i + C^{i-1} - C_R^i\right)$ became progressively smaller.

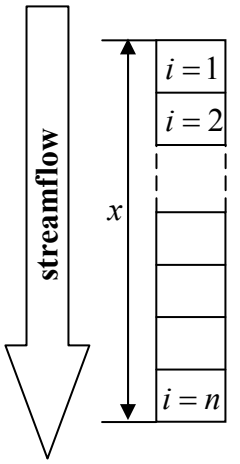

$$C^0$$

$$C^1_{TR} = C^0 - (C^0 - C^1_T) - (C^0 - C^1_R)$$

$$C^2_{TR} = C^0 - (C^1 - C^2_T) - (C^1 - C^2_R) - (C^0 - C^1_T) - (C^0 - C^1_R)$$

$$C^n_{TR} = C^0 - \sum_{i=1}^{n} (C^{i-1} - C^i_T) + (C^{i-1} - C^i_R)$$

Figure 4.6 The downstream ^{222}Rn concentration was predicted (C^n_{TR} **,** equation 4.8) for n progressively smaller intervals of x until C^n_{TR} converged.

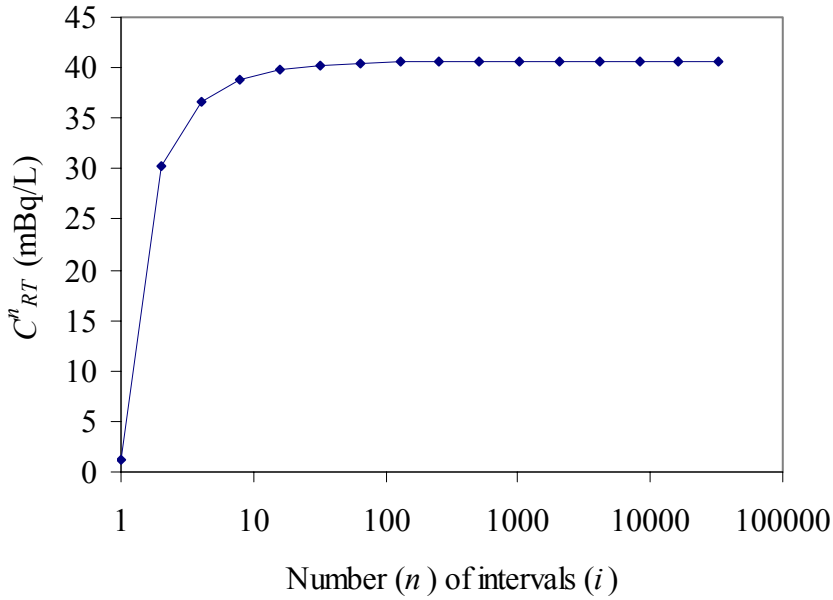

Figure 4.7 Example of model output. The predicted ^{222}Rn concentration (C^n_{TR}) in stream water converged at approximately 40 mBq L^{-1} where C^0 = 280 mBq L^{-1}, x = 4.5 km (divided into >100 equal intervals, i), v = 0.05 m s^{-1}, h = 0.93 m, z = 6.7 × 10^{-5} m.

In the following sub-sections, numerical models based on equation 4.8 which combined ^{222}Rn losses via turbulent gas exchange and radioactive decay were used to predict:

1. Downstream ^{222}Rn activities (C^n) in section 4.5.2;
2. Background ^{222}Rn concentrations in stream water due to sediment flux in section 4.5.3; and
3. Distances of ^{222}Rn persistence in stream water (x) in section 4.5.4.

Slight alterations to the numerical methodology described in this section were made for estimating other parameters and are described in the relevant subsections.

4.5.2 Predicting downstream ^{222}Rn concentrations in stream water

Downstream ^{222}Rn concentrations (C_{TR}^n) in stream water were estimated based on measured upstream ^{222}Rn concentrations (C^0) and estimates of ^{222}Rn loss due to radioactive decay and gas exchange (equation 4.8). For this calculation it is assumed that there is no groundwater contributing to streamflow in between sampling stations. Differences between predicted downstream ^{222}Rn estimates and measured downstream ^{222}Rn concentrations (C^n) in stream water indicate locations of groundwater discharge to the stream channel.

Predicted in-stream ^{222}Rn concentrations (C_{TR}^n, Figure 4.8) depend on average stream velocity (v, equations 4.2 and 4.6) and average stream height (h, equation 4.2). However, limited stream flow data was available for the lower Wollombi Brook catchment and none in the upper-most reaches of the catchment (refer to Chapter 2). Therefore average stream velocities (v) and average stream heights (h) were estimated from limited real data. Because of the large error associated with stream flow estimates, the sensitivity of the predicted ^{222}Rn concentrations (C_{TR}^n) to

order of magnitude changes in average stream velocity (v) and average stream height (h) was tested. Error associated with average stream height and velocity is unlikely to be as much as an order magnitude, however, this represents the worst-case scenario.

If both average stream velocity (v) and average stream height (h) were an order of magnitude higher than the estimates used to predict downstream ^{222}Rn concentrations (C_{TR}^{n}) there is little change in the magnitude or shape of the longitudinal C_{TR}^{n} transects (C_{TR}^{n} order high, Figure 4.8). On the other hand, if both v and h were an order of magnitude lower than the estimates used to predict downstream ^{222}Rn concentrations (C_{TR}^{n}) then there was little change in shape but the magnitude of the longitudinal C_{TR}^{n} transects (C_{TR}^{n} order high, Figure 4.8) were significantly reduced.

Predicted downstream ^{222}Rn concentrations (C_{TR}^{n}) in stream water were close to background concentrations at most surface water sampling stations (Figure 4.8, Table 4.3). Therefore, the predictions suggest that stream flow conditions were conducive to high ^{222}Rn loss via turbulent gas exchange and radioactive decay in between most of the surface water sampling stations. There were three sampling stations in between 40 and 65 km upstream in which predicted downstream ^{222}Rn concentrations (C_{TR}^{n}) in stream water were significantly higher than background concentrations (Figure 4.8). ^{222}Rn concentrations (C_{TR}^{n}) in stream water peaked at about 60 km upstream during both flood recession and baseflow conditions. Peak C_{TR}^{n} concentrations were 120 m Bq L^{-1} during flood recession (Figure 4.8***a***) and 60 m Bq L^{-1} during baseflow (Figure 4.8***b***) conditions.

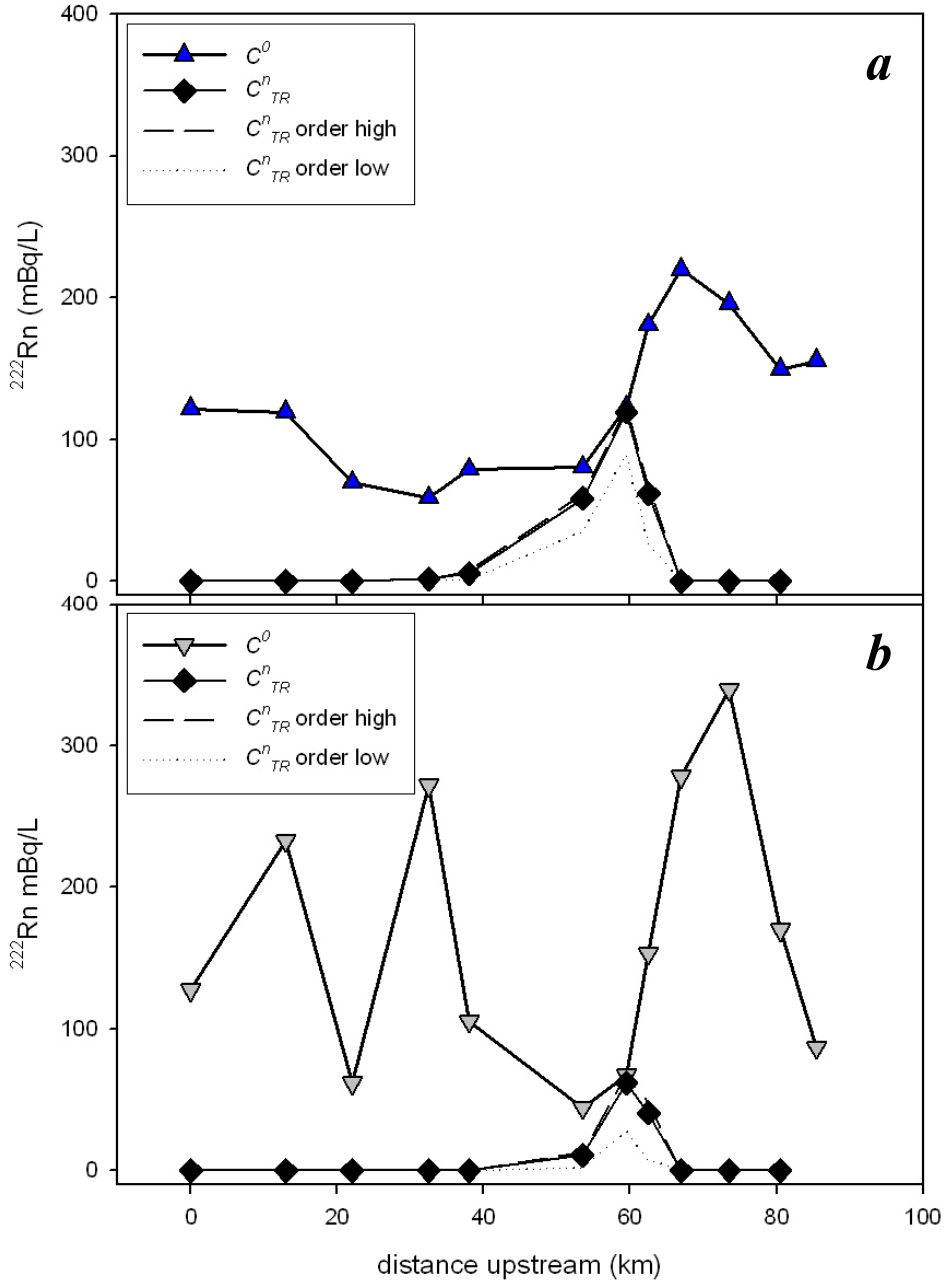

Figure 4.8 ^{222}Rn concentrations (mBq L^{-1}) measured in stream water (C^0) during (***a***) the March-2001 flood recession and (***b***) under baseflow conditions (Nov-2001) compared to predicted ^{222}Rn concentrations (C^n_{TR}), based on upstream ^{222}Rn concentrations and gas exchange and radioactive decay ^{222}Rn losses. C^n_{TR} order high and C^n_{TR} order low demonstrate the sensitivity of the predicted ^{222}Rn concentrations (C^n_{TR}) to order of magnitude changes in both average stream velocity (v) and average stream height (h).

Even if there were order of magnitude errors associated with estimated v and h values, the predicted ^{222}Rn concentrations (C_{TR}^{n}) in stream water were lower than the corresponding measured ^{222}Rn concentrations (C^{0}) in stream water at all sampling stations (Figure 4.8). Measured ^{222}Rn concentrations were consistently higher than predicted stream water ^{222}Rn concentrations at each sampling station (i.e. $C^{0} > C_{TR}^{n}$) indicating that groundwater contributed ^{222}Rn to stream flow in all reaches of the catchment.

4.5.3 Background ^{222}Rn concentration in stream water

Background ^{222}Rn concentrations in stream water (C^{B}) presented in section 4.4.2 (Table 4.2) were estimated using the methodology described by Ellins *et al.* (1990), which considered losses due to turbulent gas exchange alone. Because there were relatively long travel times (t, up to 4 weeks, section 4.2.1.3) between Wollombi Brook sampling stations, radioactive decay ^{222}Rn losses from stream water were also significant for estimating C^{B}. Therefore C^{B} values recorded in Table 4.2 are considered to be very low estimates. In order to better estimate C^{B}, equation 4.4 was altered replacing C_{T}^{n} with C_{TR}^{n} (modelled results from section 4.5.2) giving equation 4.9.

$$C^{B} = C^{n} - C_{TR}^{n} \qquad \textbf{4.9}$$

Predicted ^{222}Rn activity (C_{TR}^{n}) remaining in stream water after gas exchange and radioactive decay losses peaked at approximately 55 to 60 km upstream (Figure 4.8). The peak C_{TR}^{n} value was not, however, a location of high groundwater discharge. The stream channel was deeper at 60 km upstream than in other parts of the catchment and the stream velocity was significantly lower. Both these factors caused

lower ^{222}Rn losses from stream water via gas exchange. Therefore the high C_{TR}^{n} value was primarily a result of low ^{222}Rn loss from stream water due to changes in stream channel morphology.

If ^{222}Rn loss is estimated accurately C_{TR}^{n} will never be greater than C^{n}. Presuming that ^{222}Rn loss is accurately estimated, C_{TR}^{n} equals C^{n} when there is no groundwater contribution to stream flow. Groundwater discharge to stream flow is indicated when measured ^{222}Rn activities are greater than predicted values (i.e. $C_{TR}^{n} < C^{n}$). The smallest difference between predicted (C_{TR}^{n}) and measured ^{222}Rn concentrations (C^{n}) occurred approximately 60 km upstream (Figure 4.8). Although the peak C_{TR}^{n} occurred 60 km upstream, it was the location that received the least groundwater discharge to stream flow and was therefore used to estimate C^{B} due to sediment flux (equation 4.9, Table 4.3).

Table 4.3 Background ^{222}Rn concentrations (C^{B}) in stream water (Bq L^{-1}) estimated using equation (4.9).

Sampling time	**Background ^{222}Rn concentration in stream water (C^{B}) Bq L^{-1}**
May 2000 Flood recession	0.021
March 2001 Flood recession	0.004
November 2001 Baseflow	0.005

Background ^{222}Rn concentrations in stream water (C^{B}), delivered via sediment flux to the overlying water, ranged from 0.004 to 0.021 Bq L^{-1} (Table 4.3). This range in C^{B} values is higher than those estimated in section 4.4.2, however they are still

much lower than values published by Ellins *et al.* (1990), which ranged from 0.184 to 0.284 Bq L^{-1}. The differences in the C^B values between the two sites are most probably due to differences in the ^{226}Ra concentration and ^{222}Rn emanation potential (refer to Chapter 3) from sediment material at the different sites.

4.5.4 Distance of ^{222}Rn persistence in stream water

Stream water sampled at any point in a stream channel may contain ^{222}Rn from groundwater that discharged into the stream channel over a large range of distances from further upstream. The distance over which ^{222}Rn remains in the stream channel (x) depends upon the ^{222}Rn activity of stream water at the point of groundwater discharge (C^0), the background ^{222}Rn activity in stream water (C^B) and the rate of ^{222}Rn loss from stream water due to turbulent gas exchange and radioactive decay.

The distance (x) that ^{222}Rn would remain in stream water that was subjected to turbulent gas exchanges losses was estimated by rearranging equation 4.2 to give:

$$x = -\frac{zhv}{D}\ln\left(\frac{C_T^n}{C^0}\right) \qquad \textbf{4.10}$$

For example, if alluvial groundwater discharge increased the ^{222}Rn concentration in stream water to 3.3 Bq L^{-1} (median ^{222}Rn activity of steady state alluvial groundwater, C_{ss}, in the lower Wollombi Brook, Table 3.1) at one point in the lower Wollombi Brook, then over a distance (x), ^{222}Rn would be lost from stream water until it reached background concentrations (0.005 Bq L^{-1}, Table 4.3). If $C^0 = 3.3$ Bq L^{-1} and $C^B = 0.005$ Bq L^{-1} (substituting C^B for C_T^n in equation 4.10) the distance (x) that ^{222}Rn would persist in the stream channel (above background

concentrations) can be estimated after turbulent gas loss to the atmosphere using equation 4.10 and parameters listed in Table 4.4.

Table 4.4 Summary of parameters required for estimation of the distance of ^{222}Rn persistence (x) in stream water following groundwater discharge based on ^{222}Rn gas exchange with the atmosphere (equation 4.10). Values were measured (h and v, c.f. Chapter 2) and estimated from real data (z, C^n, C^0) from the upper Wollombi Brook during flood recession (Wollombi, site 10, Mar-01) and from lower Wollombi Brook during baseflow (Fordwich, site 3, Nov-01).

Parameters	**Flood recession**	**Baseflow**
	March 2001	**November 2001**
z (μm)	40	67
h (m)	0.13	0.08
v (m s^{-1})	0.07	0.07
C^B (Bq L^{-1})	0.004	0.005
C^0 Alluvial groundwater (Bq L^{-1})	4.6	3.3
C^0 Regional groundwater (Bq L^{-1})	5.6	16.2
D (m^2 s^{-1})	1.2×10^{-9}	1.2×10^{-9}
λ (s^{-1})	2.098×10^{-5}	2.098×10^{-5}

Discharge of ^{222}Rn into the stream channel from alluvial groundwater would persist in stream water for up to 2.0 km downstream in the lower catchment (Fordwich, site 3) during baseflow (Nov-01) due to turbulent ^{222}Rn losses alone (equation 4.10). Similarly, the distance (x) of ^{222}Rn persistence in the stream channel during flood recession (Mar-01) in the mid-upper catchment (Wollombi, site 10) can be estimated. If $C^0 = 4.6$ Bq L^{-1} (median steady state ^{222}Rn concentration of alluvial aquifer material, C_{ss}, at site 10 was 4.6 Bq L^{-1}, Table 3.1), $C^B = 0.004$ Bq L^{-1} (substituting C^B for C_T^n in equation 4.10) and using the parameters listed in Table 4.4, then the distance of ^{222}Rn persistence (x, equation 4.10) from alluvial groundwater discharge

into the stream channel during flood recession (Mar-01) in the mid-upper catchment (Wollombi, site 10) would be 2.1 km.

If ^{222}Rn concentrations in stream water were only altered by radioactive decay losses, then the distance of ^{222}Rn persistence (x) in the stream channel can be estimated by rearranging equation 4.6 to give:

$$x = -\frac{v}{\lambda}\ln\left(\frac{C_R^n}{C^0}\right) \qquad \textbf{4.11}$$

Applying equation 4.11 to the parameters listed in Table 4.4, the distance of ^{222}Rn persistence (x) in the stream channel in the upper catchment (Wollombi, site 10) during flood recession (Mar-01) would be 23.5 km. Similarly, the distance of ^{222}Rn persistence (x) in the stream channel in the lower catchment (Fordwich, site 3) during baseflow conditions (Nov-01) would be 21.7 km.

Distance estimates of ^{222}Rn persistence (x , Table 4.5) in the stream channel due to ^{222}Rn loss from stream water as a result of radioactive decay (equation 4.11) were an order of magnitude higher than distance estimates based on turbulent ^{222}Rn loss (equation 4.10). Under these conditions (Table 4.4) turbulent gas exchange caused greater ^{222}Rn loss from stream water than radioactive decay.

Table 4.5 Summary of the distance of ^{222}Rn persistence in stream water estimates (x km) for the upper Wollombi Brook during flood recession (Wollombi, site 10, Mar-01) and the lower Wollombi Brook during baseflow (Fordwich, site 3, Nov-01).

Solutions for x km		Flood recession	Baseflow
Equation	**Groundwater reservoir**	**March 2001**	**November 2001**
4.10 C_T^n	Alluvial	2.14	2.03
4.11 C_R^n	Alluvial	23.5	21.7
4.8 C_{TR}^n	Alluvial	2.12	2.01
4.10 C_T^n	Regional	2.20	2.53
4.11 C_R^n	Regional	24.2	27.0
4.8 C_{TR}^n	Regional	2.18	2.50

Since elevated ^{222}Rn concentrations (above background concentrations) persisted in stream water in the order of kilometres (Table 4.5), ^{222}Rn loss due to turbulent gas exchange (C_T^n, equation 4.10) and radioactive decay (C_R^n, equation 4.11) were both significant. The distance (x) of ^{222}Rn persistence in the stream channel incorporating both gas exchange (equation 4.10) and radioactive decay (equation 4.11) was estimated by incrementally modifying the value for x within equation 8 until C_{TR}^n converged at the background ^{222}Rn concentration (C^B) in stream water.

If alluvial groundwater discharged ^{222}Rn into the stream channel in the lower catchment under baseflow conditions, it would persist in stream water for up to 2.0 km downstream (equation 4.8). During flood recession elevated ^{222}Rn concentrations in stream water due to alluvial groundwater discharge in the upper catchment persisted for 2.1 km downstream (equation 4.8).

If regional groundwater contributed to stream flow in the lower catchment (maximum ^{222}Rn activity measured in the lower catchment 16.2 Bq L^{-1}) under

baseflow conditions ^{222}Rn would persist in stream water above background levels for up to 2.5 km downstream. If regional groundwater contributed to stream flow during flood recession in the upper part of the catchment (maximum ^{222}Rn activity measured in the upper catchment 5.6 Bq L^{-1}), then ^{222}Rn would persist in stream water above background levels for up to 2.2 km downstream.

Estimates of the distance ^{222}Rn persistence in stream water were lowest when both gas exchange and radioactive ^{222}Rn losses were accounted for (equation 4.8, Table 4.5). However, the incorporation of both gas exchange and radioactive decay ^{222}Rn losses (equation 4.8) to estimate the distance of ^{222}Rn persistence in stream water only shortened the distance of ^{222}Rn persistence by 20 to 30 m compared to ^{222}Rn losses via gas exchange alone (equation 4.10, Table 4.5).

Estimates of the distance of ^{222}Rn persistence in stream water were highly sensitive to variation in average stream velocity (v) and height (h). Therefore the distance of ^{222}Rn persistence in stream water was only estimated for reaches where measured v and h data was available.

If ^{222}Rn activities in stream water were higher than background levels then either alluvial or regional groundwater discharges into the stream channel would have occurred within 2.5 km in either the upper catchment during flood recession or in the lower catchment during baseflow. This suggests that for streams with similar flow characteristics as the Wollombi Brook, estimates of groundwater contribution (based on ^{222}Rn concentrations in stream water) can only be made when distances between sampling stations are within 2.0 km of each other.

4.5.5 Constraining groundwater discharge to stream flow

Rather than using average groundwater ^{222}Rn concentrations to estimate percentages of groundwater discharge to streamflow, observed minimum and maximum ^{222}Rn concentrations in groundwater were used to constrain the fraction of groundwater discharge contribution to streamflow. Minimum percentages of (alluvial and regional) groundwater discharge required to reproduce measured stream water ^{222}Rn concentrations were estimated based on steady state ^{222}Rn emanation from alluvial aquifer (C_{ss}^{AGW}) sediments (C_{ss}, Table 3.1) and maximum ^{222}Rn activities measured in regional groundwater ($C_{\max}^{RGW}$, Table 4.6).

Table 4.6 Summary of steady state ^{222}Rn emanation from alluvial aquifer material, maximum and minimum ^{222}Rn concentrations measured in regional groundwater in the lower, mid and mid-upper regions of the Wollombi Brook Catchment.

Catchment region	**Lower**	**Mid**	**Mid-upper**
Distance upstream (km)	0 - 20	20 - 50	50 - 90
C_{ss}^{AGW} (Bq L^{-1})	3.3	3.3	4.6
$C_{\max}^{RGW}$ (Bq L^{-1})	16.2	37.8	5.6
$C_{\min}^{RGW}$ (Bq L^{-1})	12.5	15.8	0.8

The minimum percentage of groundwater discharging into the stream channel ($C_{\min}^{i}$) was estimated assuming that the difference between the ^{222}Rn concentration measured in stream water (C^{n}) and predicted ^{222}Rn concentrations in stream water (C_{TR}^{n}, section 4.5.2 using equation 4.8) was the minimum ^{222}Rn input ($C_{\min}^{i}$, via groundwater discharge) to that stream reach using equation 4.12.

$$C^{i}_{\min} = C^{n} - C^{n}_{TR} \qquad \textbf{4.12}$$

$C^{i}_{\min}$ Minimum ^{222}Rn activity of groundwater input to streamflow (Bq L^{-1})

It was assumed that the minimum ^{222}Rn activity of the groundwater discharge ($C^{i}_{\min}$) did not experience radioactive decay or gas exchange losses between entering the stream channel and being sampled at the downstream water sampling station. The tacit assumption is that all groundwater discharge to the steam channel occurred in very close proximity to the downstream surface water sampling station.

The minimum ^{222}Rn input ($C^{i}_{\min}$) was either converted to a minimum percentage of alluvial or regional groundwater discharge to stream flow. Minimum alluvial groundwater discharge was estimated using equation 4.13, assuming no regional groundwater contribution to stream flow.

$$\%AGW_{\min} = 100 \times \left(\frac{C^{i}_{\min}}{C^{AGW}_{ss} - C^{n}_{TR}} \right) \qquad \textbf{4.13}$$

$\%AGW_{\min}$ Minimum percentage of stream water sourced from alluvial groundwater

C^{AGW}_{ss} Steady state ^{222}Rn emanation from alluvial aquifer sands (Bq L^{-1})

Minimum regional groundwater input was estimated using equation 4.14, assuming no alluvial groundwater contribution to stream flow.

$$\%RGW_{\min} = 100 \times \left(\frac{C^{i}_{\min}}{C^{RGW}_{\max} - C^{n}_{TR}} \right) \qquad \textbf{4.14}$$

$\%RGW_{\min}$ Minimum percentage of stream water sourced from regional groundwater

$C^{RGW}_{\max}$ Maximum ^{222}Rn activity measured in regional groundwater (Bq L^{-1})

This technique treats alluvial groundwater and regional groundwater independently. For example it assumes that if alluvial groundwater contributes to stream flow then regional groundwater does not. This may not necessarily be the case in all reaches of the catchment. If both alluvial and regional groundwater contribute to stream flow, then the actual fraction of alluvial groundwater discharge to stream flow could be lower than $\%AGW_{\min}$ estimates. Similarly, the actual fraction of regional groundwater discharge to stream flow could also be lower than $\%RGW_{\min}$ estimates. However the combined alluvial and regional groundwater discharge to stream flow would always be greater than $\%RGW_{\min}$ (i.e. $\%AGW + \%RGW > \%RGW_{\min}$). In other words $\%RGW_{\min}$ represents the absolute minimum groundwater contribution to stream flow. This includes both alluvial and regional groundwater sources because it incorporates the maximum ^{222}Rn activities measured in groundwater throughout the entire catchment.

The minimum percentage of either alluvial ($\%AGW_{\min}$) or regional groundwater ($\%RGW_{\min}$) discharge to stream flow was >0% in all reaches of the catchment during both flood recession and baseflow conditions (Figure 4.9). Even though this technique treats alluvial groundwater and regional groundwater exclusively, it is evident that groundwater of some type discharges into the stream channel in all reaches of the catchment during both flood recession and baseflow conditions.

The minimum fraction of regional groundwater ($\%RGW_{\min}$) discharge to stream flow was consistently lower than $\%AGW_{\min}$ contributions to stream flow. This was because the maximum ^{222}Rn activities measured in the regional aquifer ($C_{\max}^{RGW}$) were higher than steady state ^{222}Rn emanation activities (C_{ss}^{AGW}) in the alluvial aquifer throughout the catchment (Table 4.6). However, there was relatively little difference between the maximum ^{222}Rn activity measured in the regional aquifer ($C_{\max}^{RGW}$) and the steady state ^{222}Rn emanation activity in the alluvial aquifer (C_{ss}^{AGW}) in the upper catchment. Therefore estimated minimum fractions of alluvial and regional groundwater ($\%AGW_{\min}$ and $\%RGW_{\min}$) discharge to stream flow were similar in the upper catchment (Figure 4.9).

Estimates of the minimum fraction of regional groundwater ($\%RGW_{\min}$) discharge to stream flow were higher in the upper catchment (65 to 80 km) than in the lower catchment (0 to 60 km) during both flood recession and baseflow (Figure 4.9***b***). Similarly $\%AGW_{\min}$ estimates were relatively high in the upper catchment (65 to 80 km) and low in the mid-catchment (40 to 60 km, Figure 4.9***a***). However, in the lower catchment (0 to 40 km) $\%AGW_{\min}$ estimates were relatively high in comparison to $\%RGW_{\min}$ estimates of groundwater contribution to stream flow. The minimum percentage of groundwater discharge to stream flow was consistently higher during baseflow than during flood recession. It is possible that floodwater that recharged the alluvial aquifer resided within the alluvial sands for insufficient time to reach steady state with respect to ^{222}Rn. Therefore alluvial groundwater discharge to stream flow during flood recession may have much lower ^{222}Rn activities than steady state. This could cause the minimum amount of alluvial groundwater discharge into the stream channel to be underestimated during flood recession.

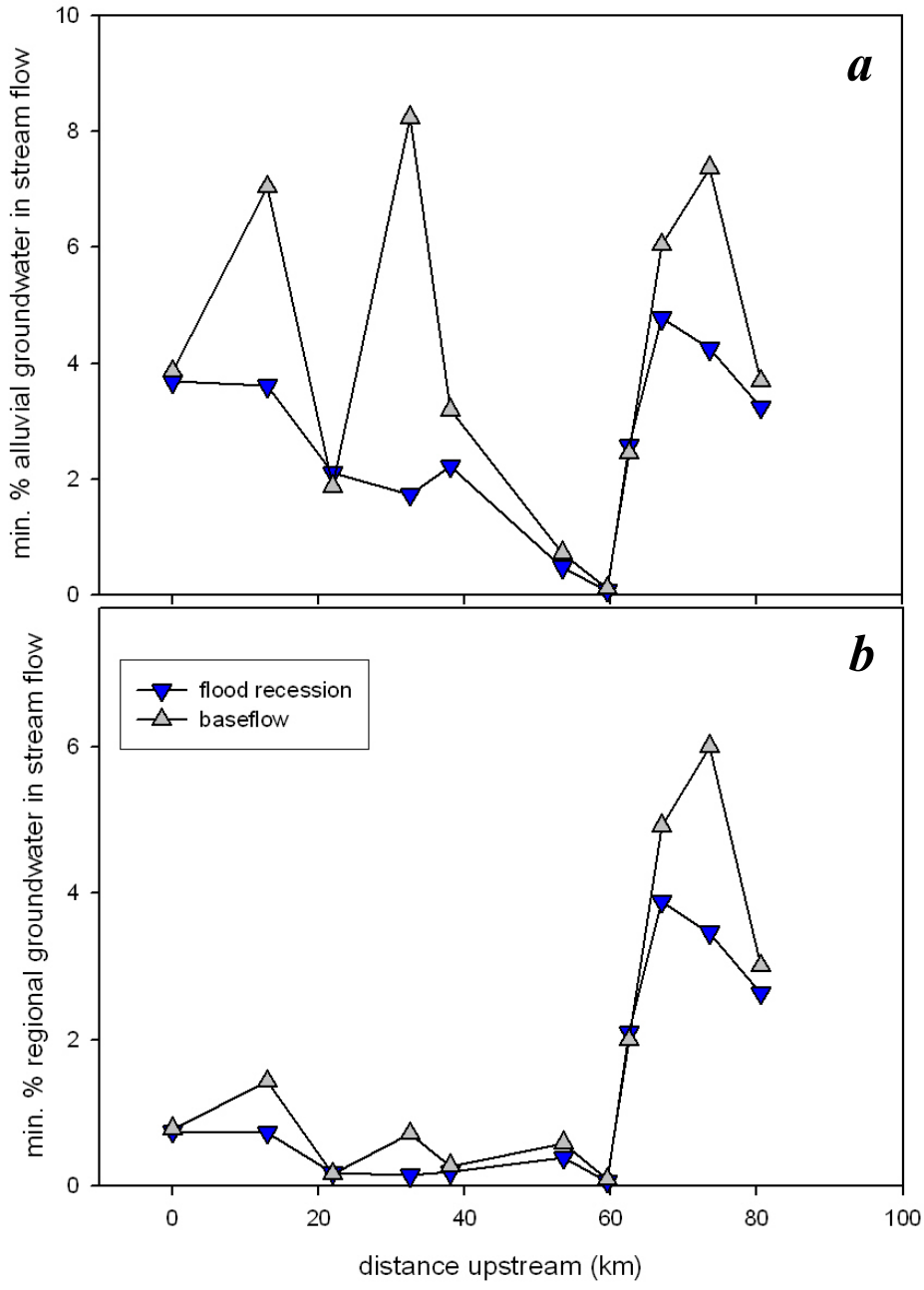

Figure 4.9 Minimum percentages of (***a***) alluvial groundwater ($\%AGW_{\min}$) and (***b***) regional groundwater ($\%RGW_{\min}$) discharges to stream flow during flood recession (Mar-01) and baseflow (Nov-01).

To estimate the maximum percentage of groundwater discharge to stream flow it was assumed that groundwater entered the stream channel at a maximum distance between sampling stations (x). Under this scenario groundwater discharge would be subjected to maximum radioactive decay and gas exchange losses. The ^{222}Rn activity required at the groundwater discharge point ($C^0_{\max}$) to reproduce the ^{222}Rn activity measured at the downstream sampling station (C^n) was estimated incorporating ^{222}Rn losses via both gas exchange (equation 4.2) and radioactive decay (equation 4.6). This was achieved by adding equations 4.2 and 4.6 to the measured downstream concentration (C^n) over n progressively smaller intervals of length x/n (equation 4.15), until $C^0_{\max}$ converged. Equation 4.15 is an adaptation of equation 4.8. Substituting $C^0_{\max}$ for C^0 and C^n for C^n_{TR} into equation 4.8 and rearranging to make $C^0_{\max}$ the subject gives equation 4.15.

$$C^0_{\max} = C^n + \sum_{i=1}^{n} (C^{i-1} - C^i_T) + (C^{i-1} - C^i_R) \qquad \textbf{4.15}$$

$C^0_{\max}$ Maximum predicted upstream ^{222}Rn activity (Bq L^{-1})

The maximum fractions of alluvial groundwater ($\%AGW_{\max}$) and regional groundwater ($\%RGW_{\max}$) discharge to stream flow required to reproduce measured downstream ^{222}Rn activities were estimated independently. The maximum fraction of alluvial groundwater discharge ($\%AGW_{\max}$) to stream flow was based on steady state emanation of ^{222}Rn from alluvial aquifer material (C^{AGW}_{ss}, equation 4.16).

$$\%AGW_{\max} = 100 \times \left(\frac{C^0_{\max} - C^n}{C^{AGW}_{SS} - C^n} \right) \qquad \textbf{4.16}$$

$\%AGW_{\max}$ Maximum fraction of stream water sourced from alluvial groundwater

The maximum fraction of regional groundwater discharge ($\%RGW_{\max}$) to the Wollombi Brook was based on minimum ^{222}Rn concentrations measured in regional groundwater ($C^{RGW}_{\min}$, equation 4.17).

$$\%RGW_{\max} = 100 \times \left(\frac{C^0_{\max} - C^n}{C^{RGW}_{\min} - C^n} \right) \qquad \textbf{4.17}$$

$\%RGW_{\max}$ Maximum fraction of stream water sourced from regional groundwater

$C^{RGW}_{\min}$ Minimum ^{222}Rn activity measured in regional groundwater (Bq L^{-1})

In the mid-catchment (40 to 70 km) $C^0_{\max}$ values were similar to the ranges of both alluvial and regional groundwater ^{222}Rn concentrations measured in the Wollombi Brook catchment (Figure 4.10). In the upper (70 to 90 km) and lower (0 to 40 km) reaches of the Wollombi Brook $C^0_{\max}$ values were much higher than ^{222}Rn activities measured in both alluvial and regional groundwater during both flood recession (Mar-01) and baseflow (Nov-01).

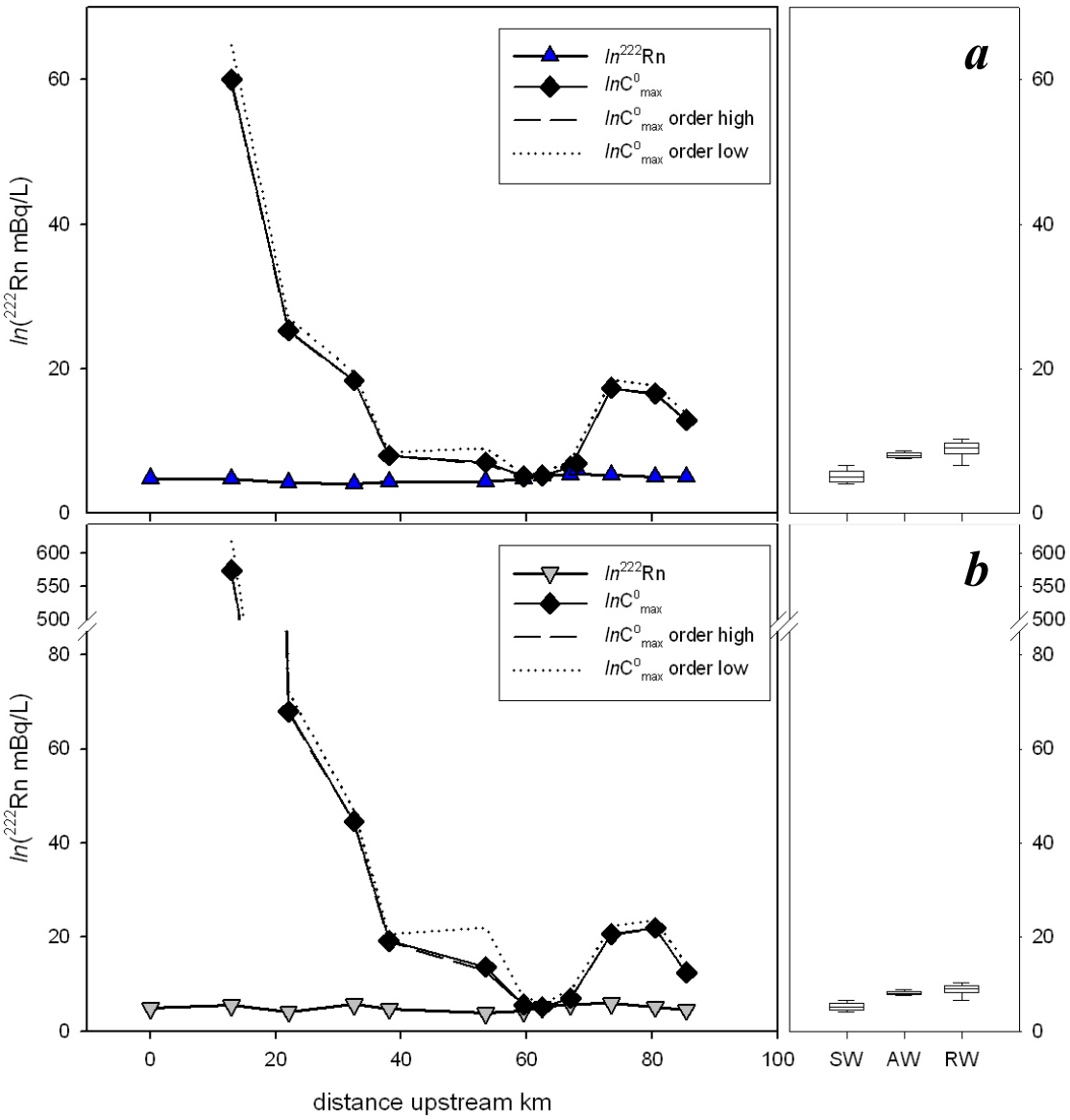

Figure 4.10 ^{222}Rn activities (m Bq L^{-1}) during (***a***) flood recession (Mar-01) and (***b***) baseflow (Nov-01) compared to predicted ^{222}Rn activities ($C^0_{\max}$) required at the upstream sampling station (due to gas exchange and radioactive decay losses) to reproduce actual ^{222}Rn activities downstream (C^n). $C^0_{\max}$ order high and $C^0_{\max}$ order low demonstrate the sensitivity of the predicted ^{222}Rn activities (C^n_{TR}) to order of magnitude changes in both average stream velocity (v) and average stream height (h).

Alluvial and regional groundwater contributions to stream water are likely to be significant in different parts of the catchment and under different stream flow conditions. Since the ^{222}Rn concentrations measured in stream water were too low to distinguish between the alluvial and regional discharges to stream flow, their potential contributions were estimated separately in all reaches of the Wollombi Brook.

If it is assumed that only alluvial groundwater discharged into the Wollombi Brook, then during flood recession (Mar-01) groundwater contributed >2% in the lower catchment (0 to 35 km), 1 to 30% in the mid catchment (35 to 65 km) and >4% in the upper catchment (65 to 90 km) of water to streamflow (Figure 4.11***a***). Similarly, during baseflow (Nov-01) groundwater contributed >2% in the lower catchment (0 to 40 km), 1 to 20% in the mid catchment (40 to 65 km) and >4% in the upper catchment (65 to 90 km) of water to streamflow (Figure 4.11***b***). Conversely, if it is assumed that only regional groundwater contributed to the Wollombi Brook then groundwater contributed >1% in the lower catchment (0 to 35 km), 1 to 13% in the mid catchment (35 to 60 km) and >3% in the upper catchment (60 to 90 km) to streamflow during flood recession (Figure 4.12***a***). In the same way groundwater contributed >1% in the lower catchment (0 to 40 km), 1 to 20% in the mid catchment (40 to 65 km) and >3% in the upper catchment (65 o 90 km) to stream flow during baseflow conditions (Figure 4.12***b***).

Estimated maximum fractions of groundwater discharge to stream flow were considered well constrained for defining appropriate distances between sampling stations if they were <100%. The fractions of stream water that were sourced from alluvial groundwater (Figure 4.11***a***) and regional groundwater (Figure 4.12***a***) were well constrained ($\%AGW_{\max}$ and $\%RGW_{\max}$ <100%) in the mid-catchment (35 to 65 km) of the Wollombi Brook during flood recession. During baseflow,

percentages of alluvial groundwater and regional groundwater in stream water were only <100% at three sites in the mid-catchment (55 to 65 km, Figures 4.11***b*** and 4.12***b***). The lower (0 to 20 km) and upper-most (70 to 90 km) reaches of the Wollombi Brook were poorly constrained ($\%AGW_{\max}$ and $\%RGW_{\max}$ >100%) during both flood recession (Mar-01) and baseflow (Nov-01) conditions.

Estimation of $C^0_{\max}$ was useful for constraining the upper limit of groundwater discharge to stream flow into the mid-catchment region of the Wollombi Brook (Figures 4.11 and 4.12). This technique indicated that there was potentially 100% exchange of water between the stream channel and the groundwater system in upper and lower reaches of the stream channel. In reality, the fraction of groundwater discharge to stream flow was likely to be much less in between consecutive sampling stations. The large distances between sampling stations, in the upper (70 to 90 km) and lower (0 to 40 km) reaches of the Wollombi Brook, caused estimated $C^0_{\max}$ values to be unrealistically large. Therefore the fraction of groundwater discharge to stream flow versus surface water runoff from upstream was poorly constrained in the lower reaches (0 to 35 km) and upper reaches (65 to 80 km) of the Wollombi Brook catchment.

Estimates of the magnitude of groundwater discharge to stream flow could have been better constrained if ^{222}Rn concentrations distinguished between the two potential sources of groundwater discharge. Maximum percentages of groundwater influxes to stream flow could be more tightly constrained if the distances between surface water sampling stations were shorter (e.g. let x <2.5 km, section 4.5.4). This would lessen ^{222}Rn losses via radioactive decay and gas exchange in comparison to groundwater discharge to stream flow and therefore lower $C^0_{\max}$, $\%AGW_{\max}$ and $\%RGW_{\max}$ values.

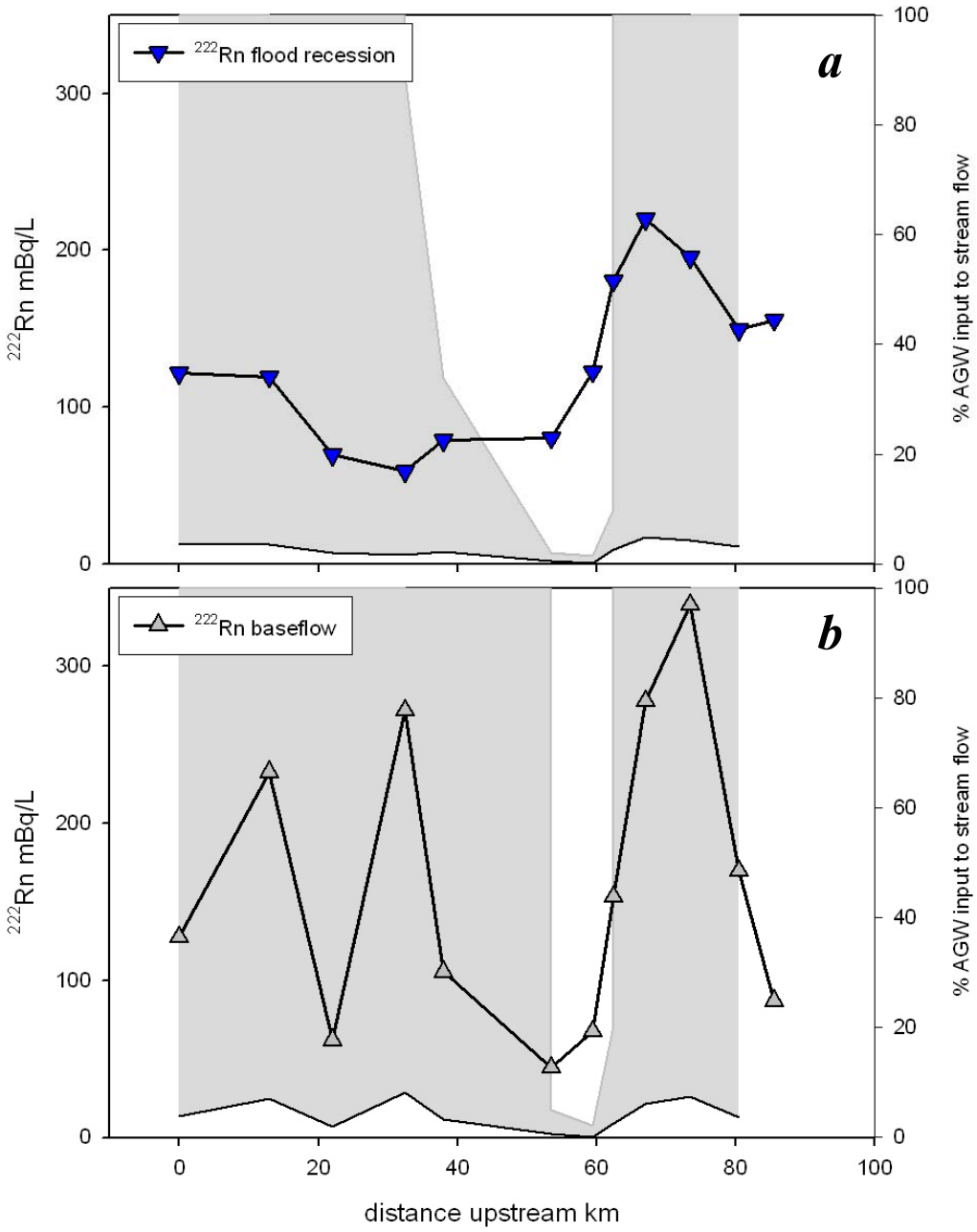

Figure 4.11 Maximum and minimum percentages of alluvial groundwater contribution to stream flow during (***a***) flood recession (Mar-01) and (***b***) baseflow (Nov-01).

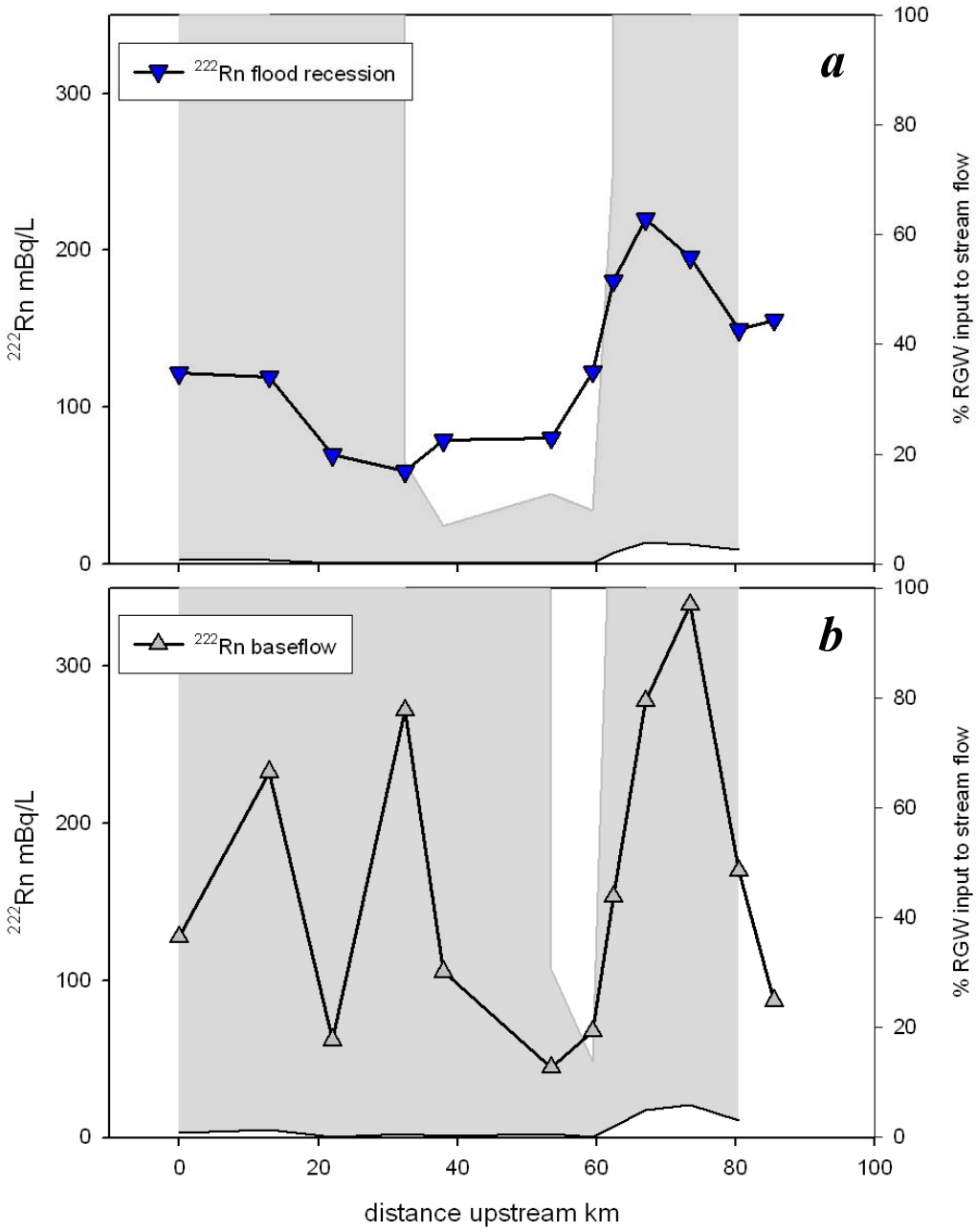

Figure 4.12 Maximum and minimum percentages of regional groundwater contribution to stream flow during (***a***) flood recession (Mar-01) and (***b***) baseflow (Nov-01).

4.5.6 Optimal intervals for sampling ^{222}Rn in stream water

Maximum groundwater contributions to stream flow ($\%AGW_{\max}$ and $\%RGW_{\max}$) were <100% where distances in between sampling stations were relatively short (3 to 6 km) during baseflow conditions (Nov-01, Figures 4.11***b*** and 4.12***b***). However, during flood recession (Mar-01) $\%AGW_{\max}$ and $\%RGW_{\max}$ were <100% where distances between sampling stations varied from 3 to 15.5 km (Figures 4.11***a*** and 4.12***b***). If distances between sampling stations in the upper and lower reaches of the Wollombi Brook catchment were shortened, the maximum percentage of groundwater contribution to stream flow would have been better constrained (<100%). However, the maximum percentage of groundwater contribution to stream flow was not only <100% when distances in between sampling stations were short. The minimum distance required in between sampling stations varied in different parts of the Brook. Therefore additional variables contributed to whether $\%AGW_{\max}$ and $\%RGW_{\max}$ were <100% or not.

The reaches of the Wollombi Brook where the maximum fraction of groundwater input to stream flow was <100% were compared to those that were not (i.e. $\%AGW_{\max}$ and $\%RGW_{\max}$ >100%) to identify which parameters (in addition to distance between sampling stations, x) could better constrain the maximum percentages of groundwater input to stream flow. The lower the value of $C^0_{\max}$ (equation 4.15), the lower $\%AGW_{\max}$ and $\%RGW_{\max}$ will be (equations 4.16 and 4.17 respectively).

Comparing average stream velocity (v) and height (h) to distance (x) between sampling stations (Figure 4.13***a***) showed that regardless of the distance between sampling stations (x), if the product of v and h was sufficiently high (>0.045 $m^2\ s^{-1}$) then the maximum percentage of groundwater discharge to stream

flow was <100%. Similarly, if vh/x >7.8 × 10^{-6} (Figure 4.13***b***), then the percentage of groundwater contribution to stream flow was well constrained ($\%AGW_{\max}$ and $\%RGW_{\max}$ <100%). Therefore in the Wollombi Brook catchment, the optimal spacing between surface water sampling stations (x, equation 4.18) can be estimated from average stream velocity (v) and height (h) values.

$$x < \frac{v.h}{7.8\times10^{-6}} \qquad \textbf{4.18}$$

x	Optimal distance between stream water sampling stations	(m)
7.8 × 10^{-6}	Empirically derived constant	(m s^{-1})

A simple methodology for setting up ^{222}Rn field-sampling programs (i.e. estimating the maximum distance that can be left in between stream water sampling stations) for estimating groundwater contribution to stream flow would be practical for transferral of the technique to different catchments. A numerical solution for estimating the maximum fraction of groundwater discharge to stream flow that incorporates site-specific information would be more accurately transferred to other catchments than the empirical relationship (equation 4.18) established for the Wollombi Brook catchment. This is because there are ranges of ^{222}Rn concentrations in surface water and groundwater and stagnant film thicknesses that are characteristic of the Wollombi Brook catchment that are embedded into equation 4.18.

Maximum percentages of groundwater discharge to stream flow (i.e. $\%AGW_{\max}$, equation 4.16) are better constrained (<100%) if the maximum predicted ^{222}Rn concentrations ($C^{0}_{\max}$, equation 4.15) in stream water are less than the minimum ^{222}Rn concentrations measured in groundwater (i.e. C_{ss}^{AGW}, equation 4.19).

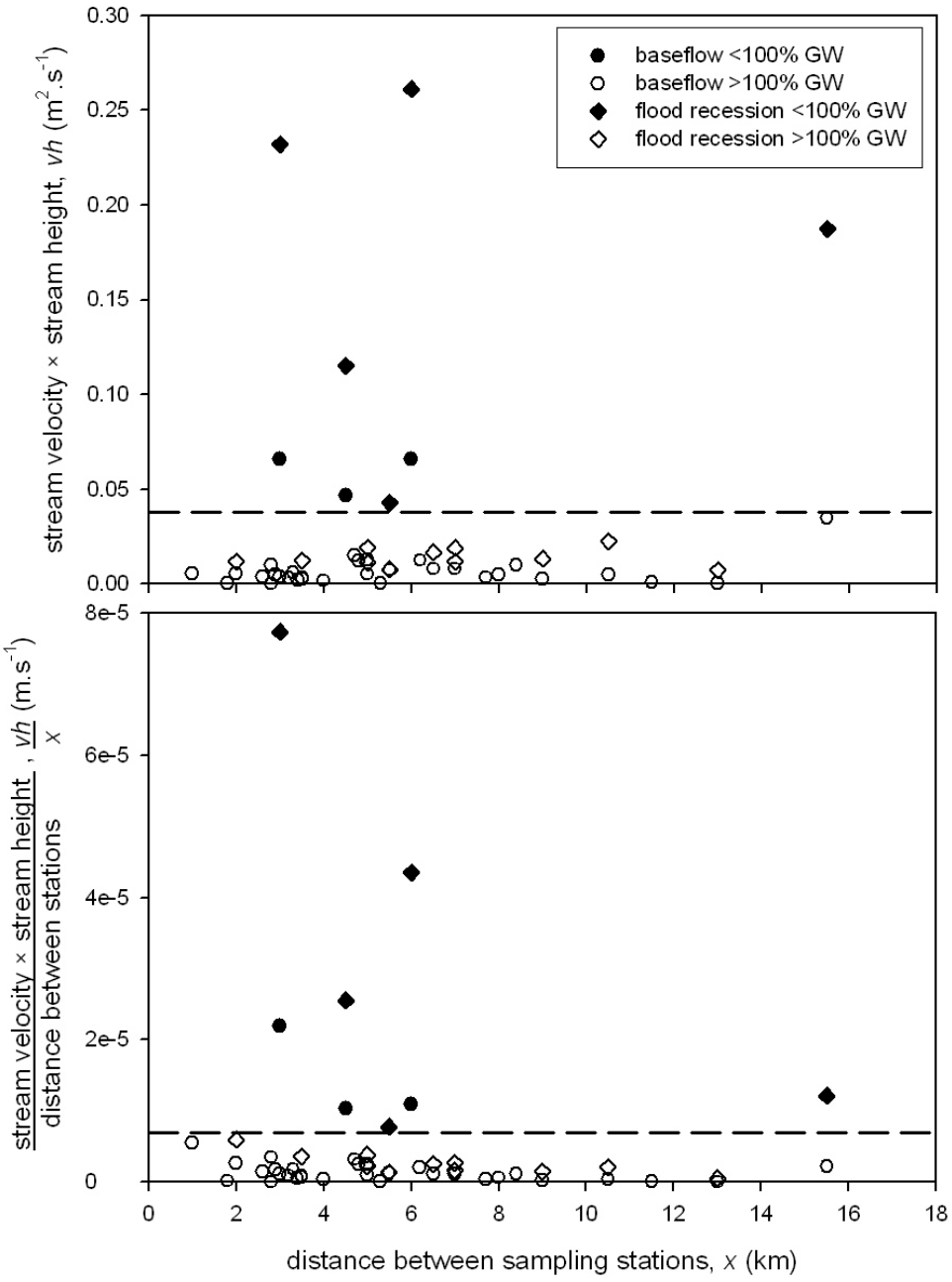

Figure 4.13 Relationships between average stream velocity (v), average stream height (h) and distance between sampling stations (x) for constraining limits of alluvial and regional groundwater discharge to stream flow. Well-constrained percentages of groundwater contribution to stream flow (<100% GW) are represented by solid symbols. Poorly constrained groundwater contributions to stream flow (>100% GW) are represented by open symbols. Dashed lines indicate divisions between well-constrained and poorly constrained percentages of groundwater contribution to stream flow.

$$C_{ss}^{AGW} > C_{\max}^{0} \qquad \text{if } \%AGW < 100\% \qquad \textbf{4.19}$$

Substituting $C_{\max}^{0}$ in equation 4.19 with equation 4.15 gives relationship 4.20.

$$C_{ss}^{AGW} > C^{n} + \sum_{i=1}^{n} (C^{i-1} - C_{T}^{i}) + (C^{i-1} - C_{R}^{i}) \qquad \textbf{4.20}$$

The maximum distance (x) that could be left between steam water sampling stations for constraining alluvial groundwater discharge to stream flow (such that $\%AGW_{\max}$ <100%) was estimated by iterating equation 4.20 for incrementally modified values of x, until equation 4.20 converged at the steady state ^{222}Rn concentration in the alluvial aquifer (C_{ss}^{AGW}). The maximum distance that can be left between stream water sampling stations for constraining fractions of regional groundwater discharge to stream flow was estimated (equation 4.21) using the same approach.

$$C_{\min}^{RGW} > C^{n} + \sum_{i=1}^{n} (C^{i-1} - C_{T}^{i}) + (C^{i-1} - C_{R}^{i}) \qquad \textbf{4.21}$$

Using this methodology the distances between sampling stations (x) can be adjusted (equations 4.20 and 4.21) such that $C_{\max}^{0}$ is less than C_{ss}^{AGW} and $C_{\min}^{RGW}$ (Table 4.6). Maximum distances (x) that could be left between stream water ^{222}Rn-sampling stations for constraining maximum groundwater discharges to stream flow were estimated using both empirical (equation 4.18) and numerical solutions (4.20 and 4.21). Wollombi (site 10) during flood recession (Mar-01) and Fordwich (site 3) during baseflow (Nov-01) were selected to test the numerical solution because

accurate stream flow data was available for those times in those locations (Table 4.7).

Table 4.7 Comparison of empirical (equation 4.18) and numerical (equations 4.20 and 4.21) estimates of the maximum distance (x) in between stream water ^{222}Rn sampling stations such that estimates of maximum groundwater (equations 4.16 and 4.17) contribution to stream flow are well constrained (<100%). Maximum distances were estimated from real data from the upper Wollombi Brook during flood recession (Wollombi, site 10, Mar-01) and the lower Wollombi Brook during baseflow (Fordwich, site 3, Nov-01). Parameter values used in equations 4.18, 4.20 and 4.21 are recorded in Tables 4.4 and 4.6.

	Flood recession	**Baseflow**
	March 2001	**November 2001**
C^n (Bq L^{-1})	0.22	0.06
x (km), equation 4.18	1.2	0.7
x (km), equation 4.20	0.9	1.2
x (km), equation 4.21	0.4	1.6

For both empirical (equation 4.18) and numerical (equations 4.20 and 4.21) solutions, the higher the product of average stream velocity and stream height ($v \times h$), the greater the maximum distance (x) allowable between sampling stations for constraining the percentage of maximum groundwater discharge to stream flow ($\%AGW_{\max}$ and $\%RGW_{\max}$). However, the higher $v \times h$ the thinner the stagnant film, z (equation 4.1), becomes and the shorter the maximum distance, x, in between sampling stations required for constraining maximum groundwater discharges to stream flow (equations 4.20 and 4.21).

Even though $v \times h$ was higher during flood recession than during baseflow (Table 4.4), the numerical estimates of maximum distance, x, between stream water sampling stations were shorter during flood recession than during baseflow (Table 4.7). This is partially due to the thinner stagnant film, z, during flood recession than baseflow (Table 4.4). However, the ^{222}Rn concentration in stream water was much higher in the upper Wollombi Brook during flood recession (C^n = 0.22 Bq L^{-1}) than in the lower Wollombi Brook during baseflow (C^n = 0.06 Bq L^{-1}, Table 4.7). If all parameters in equation 4.15 are held constant $C^0_{\max}$ is highest when the distance between sampling stations, x, is largest. Similarly, if C^n is the only variable in equation 4.15 $C^0_{\max}$ is highest when C^n is highest. Therefore, if all other parameters were constant, the higher the downstream ^{222}Rn concentration measured in stream water, C^n, the shorter the maximum distance required between sampling stations to constrain groundwater discharge to stream water.

In order to recommend maximum distances between steam water ^{222}Rn sampling stations (for constraining the maximum estimates of groundwater discharge to stream flow), accurate estimates of average stream velocity (v) and height (h) and prior knowledge of the ranges of ^{222}Rn concentrations in stream water and groundwater are required. Without such data, the most accurate information that can be extracted from transects of ^{222}Rn concentration in stream water are the locations and minimum percentages of groundwater contribution to stream flow. However, in general the higher the product of the average stream velocity with average stream height ($v \times h$), the greater the distance (x) that can be left in between stream water sampling stations (for constraining the percentage of groundwater discharge to stream flow).

4.6 CONCLUSIONS

Increases in ^{222}Rn concentrations between consecutive stream water sampling stations indicated that groundwater discharged to stream flow in the upper (73 to 86 km), mid (32 to 54 km) and lower (13 to 22 km) reaches of the Wollombi Brook during baseflow (Nov-01). Considering ^{222}Rn concentrations in the same manner indicated that groundwater discharge occurred in the upper (67 to 81 km) and lower (0 to 33 km) reaches of the Wollombi Brook during flood recession (Mar-01).

Comparison of ^{222}Rn concentrations in stream water to predicted ^{222}Rn concentrations after radioactive decay and gas exchange losses indicated that groundwater discharged into the Wollombi Brook in all reaches of the catchment. The numerical methodology developed to estimate downstream ^{222}Rn concentrations in stream water due to radioactive decay and gas exchange losses was resilient to order of magnitude error in average stream height and velocity.

^{222}Rn concentrations in stream water were too low to distinguish between regional and alluvial sources of groundwater discharge. However, groundwater contributed a maximum of 30% of water to streamflow during both flood recession and baseflow in the mid region of the Wollombi Brook catchment. Fractions of groundwater discharge to stream flow would be better constrained in the upper and lower regions of the Wollombi Brook catchment if stream water sampling stations were placed <2.0 km apart. However, the allowable maximum distance between sampling stations for constraining the magnitude of groundwater contribution to stream flow varied in different reaches of the Wollombi Brook and is likely to be just as variable in other catchments.

If stream flow information is available, site specific estimates of maximum allowable distance between stream sampling stations for constraining groundwater discharge to stream flow can be made. An empirical relationship based on average stream height and velocity was found for estimating the maximum distance that could be left in between stream water sampling stations in the Wollombi Brook catchment. This empirical method, however, would be limited to transferral to other catchments with similar hydrogeology (i.e. ^{222}Rn concentrations in groundwater).

A numerical method was developed to estimate the maximum allowable distance between stream water sampling stations for constraining the fraction of groundwater discharge to stream flow for transferral to other catchments. This method requires prior knowledge of ranges of ^{222}Rn concentrations in stream water and groundwater in addition to streamflow information, however, the methodology is widely transferable to other catchments.

5 APPLICATION OF TRACER TECHNIQUES TO IDENTIFY SOURCES OF WATER TO STREAM FLOW DURING BASEFLOW & FLOOD RECESSION

5.1 INTRODUCTION

5.1.1 Background

Surface water diversions, groundwater pumping and land clearing have altered the volume and seasonal fluctuation of water flowing in many river systems. This in turn has changed the amount and rate (and in some cases direction) of surface water and groundwater interaction with potential impacts on river water quality and ecosystems (e.g. Winter *et al.* 1998). For example, abstraction of fresh groundwater from near-stream alluvial aquifer systems can induce the "intrusion" of more saline regional groundwater into the alluvial aquifer system, increasing river salinity (e.g. Nobi and Das Gupta 1997).

Many studies have compared differences in water levels between streams and aquifers to estimate the relative contributions of groundwater and surface water to stream flow (e.g. Mosley 1979, Onda *et al.* 2001, Burt *et al.* 2002). However, in environments where there are low gradients between surface water and groundwater reservoirs (e.g. the near-stream zone), it is necessary to employ other techniques for distinguishing between the potential sources of water to stream flow. In such cases, it is common to investigate the major ion chemistry or stable isotopes of water of the various potential surface water and groundwater sources of water to stream flow to estimate their relative contributions (e.g. Pinder and Jones 1969, Uliana and Sharp 2001). If the various water bodies were recharged under similar conditions, they can have very similar ionic ratios and therefore become indistinguishable on reaching the stream channel.

Chloride (Cl^-) concentrations, radon (^{222}Rn), stable isotopes of water (^{1}H, ^{2}H, ^{16}O & ^{18}O), and strontium isotope ratios ($^{87}Sr/^{86}Sr$) were measured in stream water to estimate the relative contributions of potential water sources contributing to stream flow. It was hypothesised that there were three water reservoirs potentially contributing to stream flow at any one point in the Wollombi Brook (Figure 5.1).

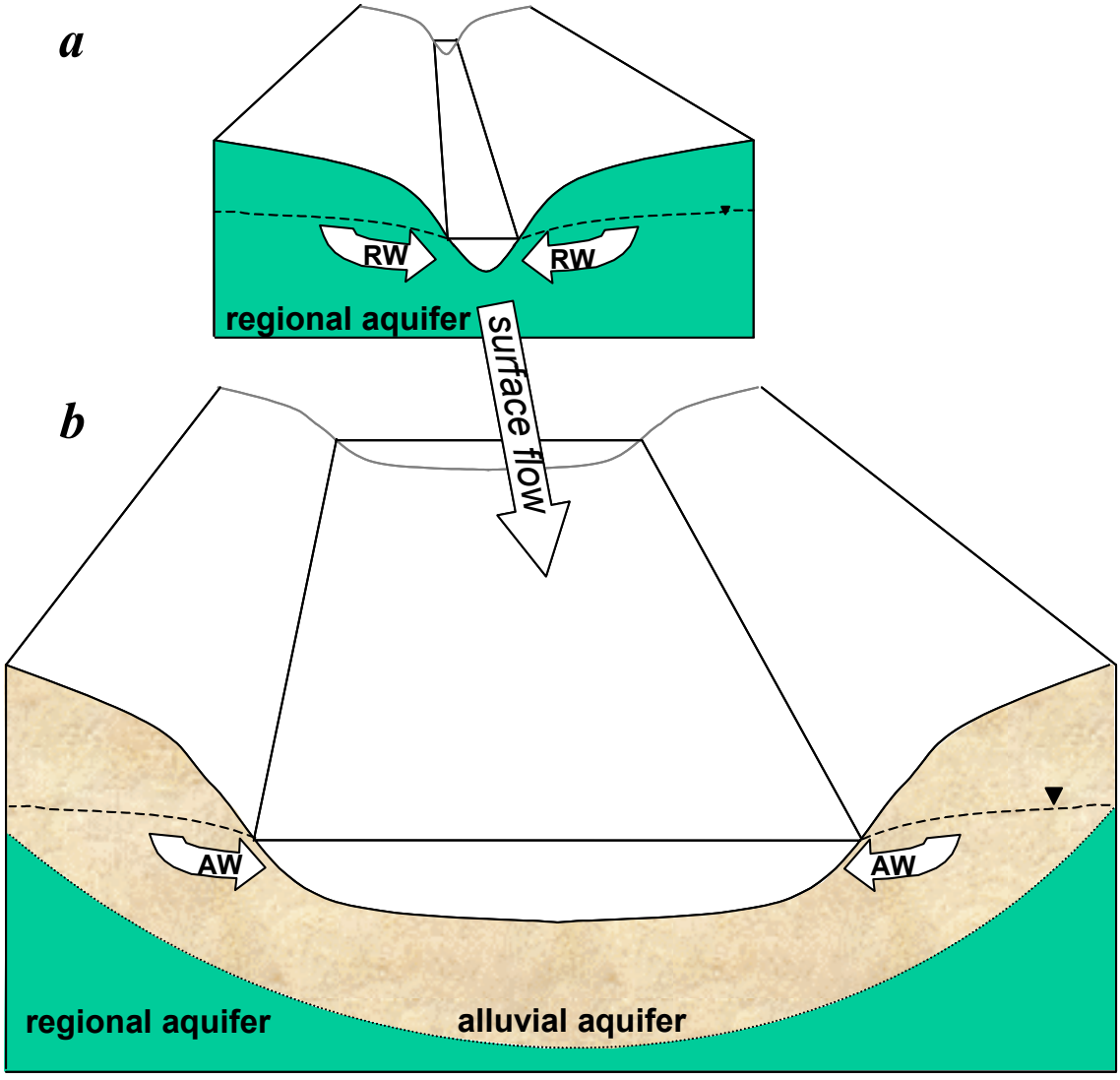

Figure 5.1 Conceptual diagram of alluvial groundwater (AW) or regional groundwater (RW) discharge to stream flow. Groundwater discharge to the Wollombi Brook is presumed to vary between two extremes; (***a***) in the absence of an alluvial aquifer (e.g. in the upper catchment) only regional groundwater discharges to stream flow, and (***b***) when extensive alluvial aquifers exist (e.g. in the lower catchment) alluvial groundwater is the primary source of groundwater discharge to stream flow.

Alluvial groundwater and regional groundwater were assumed to supplement surface water flows in the Wollombi Brook (e.g. Figure 5.1). The source and location of groundwater discharge to the Wollombi Brook was assumed to vary under different stream flow conditions. If there are distinct differences in stream water, alluvial groundwater and regional groundwater chemistry, the sources of groundwater discharge to streamflow can be identified by detection of changes in stream water chemistry. However, processes that occur within the stream channel can also alter stream water chemistry. Therefore, groundwater discharge induced changes to stream water chemistry may have secondary changes superimposed on them by processes that occur within the stream channel. Surface water processes that are likely to alter stream water chemistry differ under high and low stream flow conditions.

In this chapter, a series of naturally occurring environmental tracers (salinity, ^{222}Rn, $\delta^{2}H$ & $\delta^{18}O$ and $^{86}Sr/^{87}Sr$) were measured in stream water to investigate the sources and proportions of groundwater discharge to stream flow under low hydraulic gradient conditions. Two specific snapshots in time were compared: during the receding limb of a flood (Mar-2001) and during baseflow conditions (Nov-2001).

5.1.2 Objectives

The aims of this chapter were to:

1. Describe how environmental tracer signatures (salinity, ^{222}Rn, $\delta^{2}H$ & $\delta^{18}O$ and $^{86}Sr/^{87}Sr$) would be expected to change in stream water in response to (1) groundwater discharge to the Wollombi Brook, and (2) surface processes during high and low stream flow conditions;

2. Develop methodology to differentiate between alluvial groundwater and regional groundwater discharges to stream flow based on changes in environmental tracer signatures of stream water;
3. Identify sources of water that contribute to stream flow;
4. Investigate the use of long-term (time-series) and short-term (Mar-01 flood recession and Nov-01 baseflow) datasets to relate stream hydrograph stage to the sources of water to stream flow;
5. Compare the relative importance of the water sources within the upper and lower reaches of the Wollombi Brook catchment;
6. Investigate whether these relatively quick and easy techniques lend themselves to use in ungauged catchments for understanding surface water and groundwater interactions rather than setting up expensive stream discharge and groundwater level monitoring networks;

and to test the following hypothesis:

7. Alluvial groundwater contributed the greatest proportion of groundwater to stream flow during baseflow and flood recession conditions.

5.1.3 Sampling Strategy

Surface water samples from the Wollombi Brook and its tributaries were collected from several locations throughout the Wollombi Catchment during three 'run-of-river' surveys (Figure 2.1). This approach represents a 'snapshot' in time where preferential zones of surface water, alluvial groundwater or regional groundwater inflow to the Wollombi Brook were identified using the suite of environmental tracers described above. The first reconnaissance trip in May 2000 was followed by a detailed survey in March 2001 (during flood recession) and another following a prolonged drought period at baseflow (November 2001). The 'run-of-river' surveys were carried out over two to three days, in which stream water was analysed for pH,

temperature, electrical conductivity and alkalinity in the field. Water samples were collected for major ion chemistry, water isotopes (δ^2H & $\delta^{18}O$), radon (^{222}Rn) and strontium isotope ($^{87}Sr/^{86}Sr$) analyses.

To complement the 'run of river' snapshots during flood recession (Mar-01) and baseflow (Nov-01) conditions, stream water was sampled at one location (Figure 2.1, 'time-series' sampling point) once a week (or more frequently following high stream flows), from October 2000 to January 2002. 'Time-series' stream water samples were analysed for a limited range of chemical species (major ions, δ^2H and $\delta^{18}O$). These data give a more dynamic perspective of the changes in stream water chemistry (and sources of groundwater discharge) in response to changes in stream flow than 'run of river' data. Sampling and analytical techniques are described in detail in Chapter 2.

During baseflow (Nov-01) stream water sampling was more extensive than during flood recession (Mar-01) because the higher reaches of the catchment were more accessible. In addition to the main branch of the Wollombi Brook (stations **1** to **13**), two other branches were sampled in greater detail: the Watagan branch (stations **14** to **21**) and the South branch (stations **22** to **26**).

During the March 2001 flood recession, rainwater, the Wollombi Brook, alluvial groundwater and regional groundwater were sampled in the lower catchment (Warkworth, site 1) to determine whether the strontium isotope signatures of the different water reservoirs were distinctive enough to differentiate between alluvial and regional groundwater discharges to stream flow.

During baseflow (Nov-01) Wollombi Brook water samples were collected for strontium isotope ratio ($^{87}Sr/^{86}Sr$) analysis from stations that were suspected of

receiving groundwater contributions to stream flow based on peak in-stream ^{222}Rn activities (see 4.4.3). The piezometer and bore networks at the three equipped sites (Warkworth - site 1, Fordwich - site 3 and Wollombi - site 10) were sampled to characterise the local alluvial groundwater and regional groundwater $^{87}Sr/^{86}Sr$ ratios in the lower up to the mid-upper catchment.

5.2 RESULTS

5.2.1 Stream hydrograph

As part of the HITS (Hunter Integrated Telemetry System, http://hits.nsw.gov.au/) network, stream flow was electronically logged at three locations in the lower to mid Wollombi catchment. These were sited in the vicinity of stream sampling stations Warkworth (site 1), Bulga (site 3) and Brickman's Creek (between the time-series site and site 6, Figure 2.1). Warkworth station was nearest the Wollombi Brook mouth. Bulga station monitored Wollombi Brook discharge approximately 13 km upstream from Warkworth. Brickman's Bridge station was located on a small tributary stream approximately 44 km upstream from Warkworth.

Wollombi Brook flowed continuously at Warkworth throughout the sampling period (Mar-00 to Jan-02, Figure 5.2). Surface water stopped flowing at Bulga in early Oct-00 and resumed flowing in late Nov-00. Stream flow at Bulga stopped flowing a second time in late Dec-00 and restarted flowing in mid Feb-01. The Brickman's Bridge tributary stream to the Wollombi Brook stopped flowing for two weeks during Nov-00, resumed flow during late Nov-00. It ceased flowing again in early Jan-01 for one month and recommenced flowing during early Feb-01. In total the Wollombi Brook stopped flowing for approximately 3 months at Bulga and the tributary stream at Brickman's Bridge stopped flowing for about 1.5 months during the monitoring period.

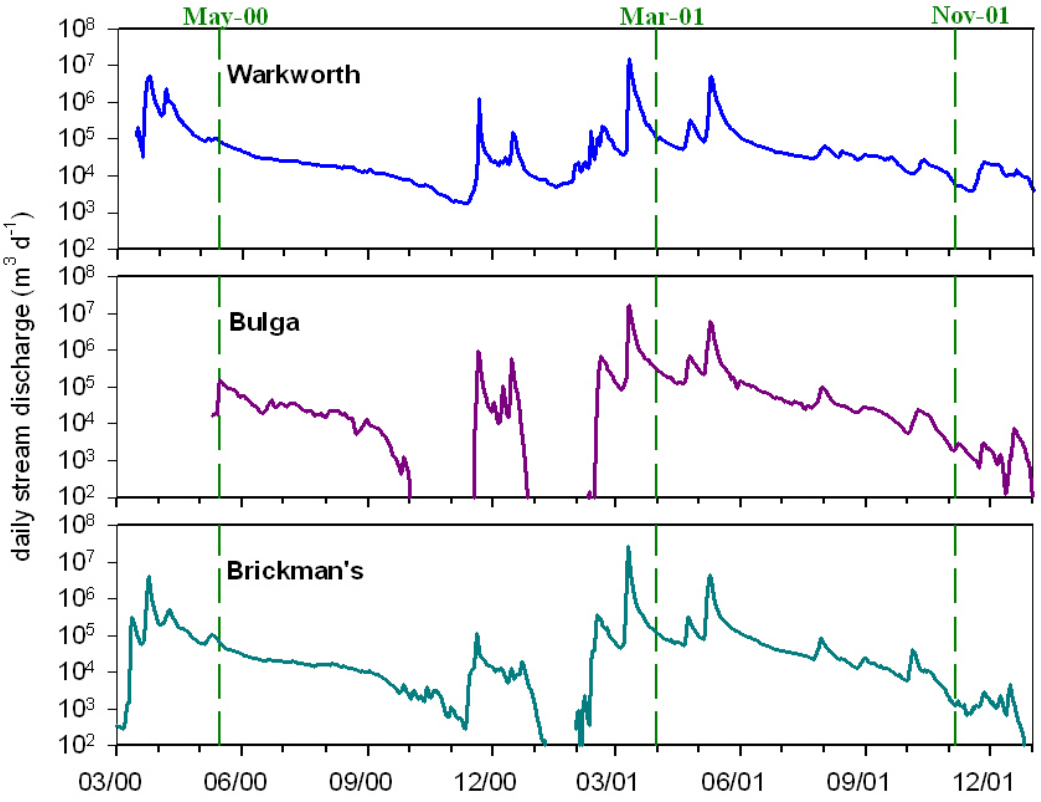

Figure 5.2 Stream discharge (m^3 d^{-1}) hydrographs monitored in the lower Wollombi Brook (Warkworth and Bulga) and in a mid-catchment tributary (Brickman's Bridge). Run of river sampling was carried out during May-00, Mar-01 and Nov-01 (indicated by dashed lines).

Peak stream flow typically arrived at the Brickman's Bridge tributary first, then in the Wollombi Brook at Bulga and lastly at Warkworth. Similarly high stream stages receded more slowly at Warkworth than at Bulga, and more slowly at Bulga than at Brickman's Bridge.

Stream water discharge was not continuously monitored in the upper-most reaches of the Wollombi Brook catchment. However, the occurrence of stream flow in the upper catchment is likely to be similar to that monitored at Brickman's Bridge (Figure 5.2), rapidly rising and receding in response to streamflow generation events (e.g. high rainfall). Stream flow was reported by local residents to cease in the Wollombi Brook and tributaries during prolonged dry periods transforming the stream channel into a series of disconnected pools.

May-00 and Mar-01 'run of river' sampling surveys took place during receding limbs of high stream flow events (during flood recession conditions). The Nov-01 'run of river' survey coincided with a very low stream stage during which stream flow was supplied by groundwater discharge (baseflow conditions).

5.2.2 Chloride

During flood recession (Mar-01) the Cl^- concentration in stream water varied from 110 mg L^{-1} in the upper catchment (81 to 67 km) down to a minimum of 85 mg L^{-1} in the mid catchment (63 to 74 km) and increased up to 110 mg L^{-1} again in the lower catchment (Figure 5.3). The Cl^- concentration in tributaries during flood recession were similar to those in the main channel, however, at 28 km (T2) the Cl^- concentration was much higher (230 mg L^{-1}) than any other surface water measured throughout the catchment. Chloride concentrations within the stream channel were generally higher during baseflow than flood recession sampling.

During baseflow (Nov-01) the Cl^- concentration in stream water gradually decreased from 226 mg L^{-1} in the upper catchment (at 80 km) to a minimum of 117 mg L^{-1} in the mid catchment (50 to 70 km). The Cl^- concentration in stream water rapidly increased from the mid catchment minimum up to a maximum of 420 mg L^{-1} at 22 km. By 13 km the Cl^- concentration in stream water had plummeted down to 204 mg L^{-1}, but increased again at 0 km (321 mg L^{-1}). During baseflow the Cl^- concentration of stream water in the tributaries were typically lower than those measured in the main stream channel. However, two tributaries in the lower catchment at 28 and 44 km (T2 and TB) were significantly higher (971 and 291 mg L^{-1} respectively) than stream water in the main channel. The maximum surface water Cl^- concentration measured in tributary T2 at 28 km is not plotted in Figure 5.3 because it was disconnected from the mainstream channel during baseflow sampling.

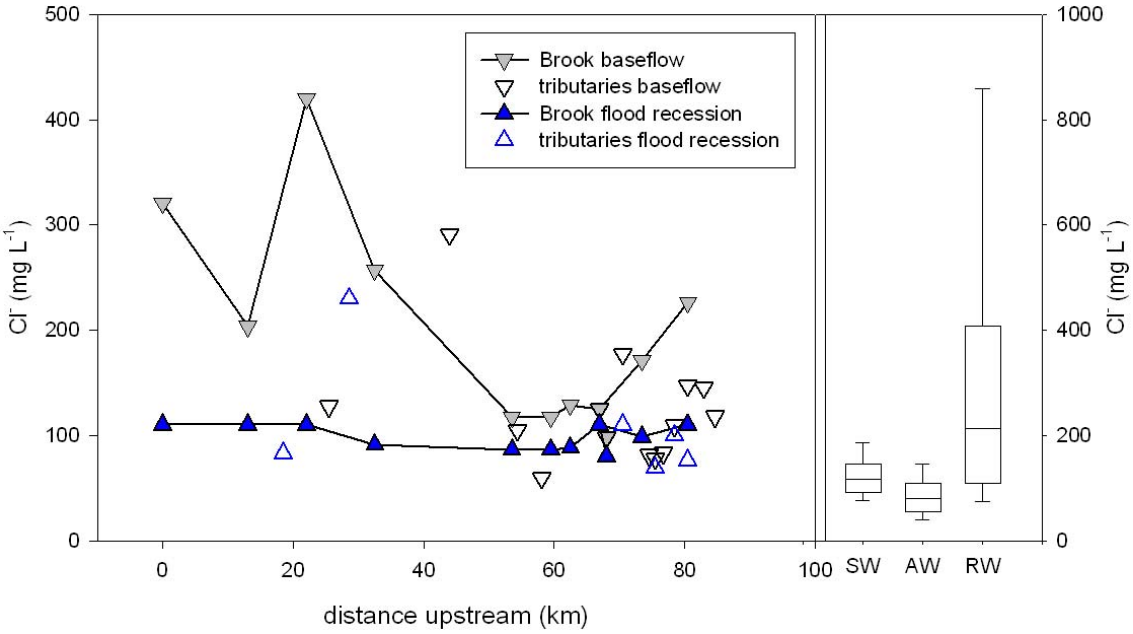

Figure 5.3 Chloride (Cl^-) concentrations (mg L^{-1}) in stream water measured during flood recession (Mar-01) and baseflow (Nov-01) in the Wollombi Brook and tributaries. The 10th, 25th, 75th and 90th percentiles represent the variation throughout a two-year sampling period (2000-01) of Cl^- measured in surface water (SW), alluvial groundwater (AW) and regional groundwater (RW) sampled across the Wollombi Catchment.

The Cl^- concentration of regional groundwater ranged over two orders of magnitude (71 to 1740 mg L^{-1}), but was generally higher than both surface water and alluvial groundwater (Figure 5.3). Chloride concentration in shallow alluvial groundwater (13 to 320 mg L^{-1}) was generally lower than in surface water (46 to 971 mg L^{-1}) but their ranges overlapped.

5.2.3 Radon-222

^{222}Rn concentrations measured in the Wollombi Brook typically ranged from 0.06 to 0.69 Bq L^{-1} (Figure 5.4). ^{222}Rn was not detected in stream water samples one month after sample collection. Alluvial groundwater ^{222}Rn concentrations (2 to 6 Bq L^{-1}) were generally an order of magnitude higher than surface water values. Regional groundwater ^{222}Rn concentrations typically ranged between 4 and 22 Bq L^{-1}. The median ^{222}Rn concentration in regional groundwater (13 Bq L^{-1}) was one order of

magnitude higher than median alluvial groundwater (3.2 Bq L^{-1}) and two orders of magnitude higher than the median surface water value (0.17 Bq L^{-1}).

^{222}Rn concentrations in surface water from the Wollombi Brook and tributaries were characteristically low and had a narrow range of values compared to alluvial and regional groundwaters (Figure 5.4). Alluvial groundwater had a relatively narrow range of ^{222}Rn concentrations in comparison to regional groundwater concentrations, but were not unique. Although ^{222}Rn concentrations in regional groundwater were typically an order of magnitude higher than alluvial groundwater values, they were highly variable and overlapped the upper range of alluvial groundwater ^{222}Rn concentrations.

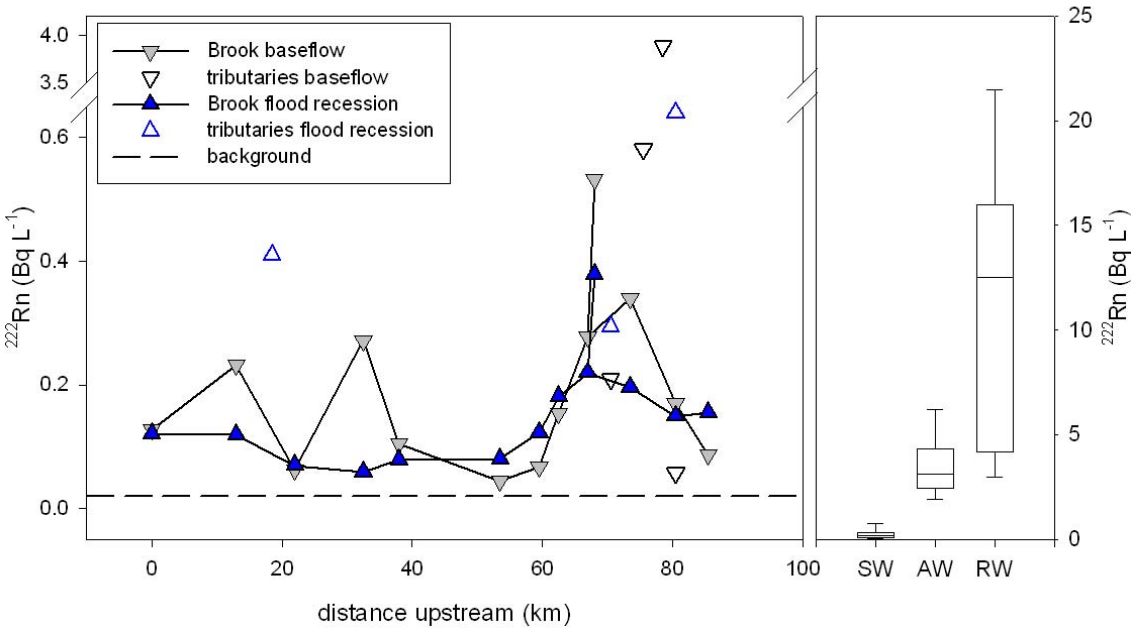

Figure 5.4 Radon (^{222}Rn) activities (Bq L^{-1}) measured in stream water during flood recession (Mar-01) and baseflow (Nov-01) in the Wollombi Brook and tributaries compared to background concentrations. The 10th, 25th, 75th and 90th percentiles represent the variation throughout a two-year sampling period (2000-01) of ^{222}Rn measured in surface water (SW), alluvial groundwater (AW) and regional groundwater (RW) sampled across the Wollombi Catchment.

^{222}Rn sampling during May 2000 and March 2001 was conducted shortly after flood conditions and the longitudinal transects were virtually identical. Therefore the March 2001 flood recession transect is presented in Figure 5.4 and the May 2000 flood recession is omitted from further discussion. ^{222}Rn activities in stream water during flood recession were approximately 0.15 Bq L^{-1} in the upper catchment (80 to 85 km) and gradually increased peaking at 0.22 Bq L^{-1} at 67 km. This peak (0.22 Bq L^{-1}) was located 1 km downstream of the confluence between the main eastern branch (0.20 Bq L^{-1}) and the southern branch of the Wollombi Brook (0.38 Bq L^{-1}, Figure 2.1). The ^{222}Rn concentration in stream water rapidly decreased between 67 and 53 km remaining between 0.06 and 0.08 Bq L^{-1} until it increased to 0.12 Bq L^{-1} at 13 km. During flood recession the ^{222}Rn activities in surface water tributaries (0.29 to 0.77 Bq L^{-1}) were typically higher than those measured in the Wollombi Brook.

Under baseflow conditions (Nov-01) the general shape of the longitudinal transect was similar to those during flood recession (Figure 5.4). There was, however, greater fluctuation in ^{222}Rn activity between sequential sampling stations during baseflow than during flood recession, particularly in the lower reaches of the catchment. The ^{222}Rn activity in stream water rapidly increased from 0.09 Bq L^{-1} at 86 km to a peak of 0.34 Bq L^{-1} at 74 km. The ^{222}Rn concentration in stream water rapidly decreased downstream to a minimum of 0.04 Bq L^{-1} at 54 km. The ^{222}Rn concentration in stream water gradually increased until it reached a second peak of 0.27 Bq L^{-1} at 33 km. There was a sharp decline in the ^{222}Rn concentration in stream water at 22 km followed by a third peak of 0.23 Bq L^{-1} at 13 km. ^{222}Rn concentrations in several surface water tributaries in the upper catchment were an order of magnitude higher than those measured in the Wollombi Brook during baseflow.

^{222}Rn activities measured in stream water were typically higher during baseflow than during flood recession. However, ^{222}Rn activities were consistently higher from 45 to 65 km during flood recession than during baseflow. ^{222}Rn activities in stream water were typically higher in the upper part of the catchment than in the lower part of the catchment.

5.2.4 Stable isotopes of water

5.2.4.1 Deuterium and Oxygen-18

Regional groundwater $\delta^{18}O$ values typically ranged between –5.02 to –6.46 ‰ and $\delta^{2}H$ values ranged between –31 to –39 ‰ (Figure 5.5). Alluvial groundwater was more enriched in ^{18}O and ^{2}H than regional groundwater ranging from –2.82 to -4.74 ‰ for $\delta^{18}O$ and –14 to –26 ‰ for $\delta^{2}H$. Much larger variations were observed in surface water: $\delta^{18}O$ varied between –0.52 and -3.91 ‰ and $\delta^{2}H$ varied between –5 and -20 ‰.

Ranges of regional groundwater $\delta^{18}O$ and $\delta^{2}H$ values were relatively constant and were distinctly lower than the ranges of alluvial groundwater and evaporated surface water values. On average, alluvial groundwater $\delta^{18}O$ and $\delta^{2}H$ values were lower than surface water values, however their ranges overlapped. $\delta^{18}O$ and $\delta^{2}H$ values in the Wollombi Brook and tributaries were consistently higher during baseflow than during flood recession.

During flood recession (Mar-01) $\delta^{18}O$ and $\delta^{2}H$ values were relatively constant within the Wollombi Brook. $\delta^{18}O$ varied by only 1.1 ‰ (-2.38 to -3.48 ‰, Figure 5.5***a***) and $\delta^{2}H$ varied by 5.4 ‰ (-11.6 to –17.0, Figure 5.5***b***) within the Wollombi Brook during flood recession. During baseflow (Nov-01) $\delta^{18}O$ and $\delta^{2}H$ values were more variable

than during flood recession. $\delta^{18}O$ ranged between -0.59 and –1.90‰ (1.31 ‰ variation) and $\delta^{2}H$ ranged between –5.1 and –11.8 ‰ (6.7 ‰ variation).

During flood recession the $\delta^{18}O$ value in the Wollombi Brook slightly increased by 0.25 ‰ from 85 to 80 km and then gradually decreased (by 0.42 ‰) to -3.00 ‰ at 60 km (Figure 5.5***a***). The minimum $\delta^{18}O$ value measured within the Wollombi Brook during flood recession (–3.48 ‰) occurred in the southern branch at approximately 70 km. Between 60 and 38 km the $\delta^{18}O$ value in stream water gradually increased by 0.44 ‰, decreased by 0.06 ‰ at 22 km, then increased up to the flood recession maximum (–2.38 ‰) at 13 km. The $\delta^{18}O$ value in the Wollombi Brook decreased by 0.28 ‰ in between 13 and 0 km.

The longitudinal $\delta^{2}H$ (Figure 5.5***b***) and $\delta^{18}O$ (Figure 5.5***a***) transects were very similar in shape between 85 and 22km in the Wollombi Brook during flood recession. However the shape of the $\delta^{2}H$ and $\delta^{18}O$ transects diverged between 22 and 13 km. The $\delta^{2}H$ value in the Wollombi Brook decreased significantly (by 1.2 ‰) from –11.6 to –12.9 ‰ between 22 and 13 km, whereas $\delta^{18}O$ values increased significantly (by 0.20 ‰) over the same interval.

Overall, $\delta^{18}O$ values in the Wollombi Brook increased from the upper to the lower catchment during baseflow (Figure 5.5***a***). There were four sections along the Wollombi Brook (in between sampling stations) where decreases in $\delta^{18}O$ values occurred. These decreases in $\delta^{18}O$ values occurred between 74 and 67 km, 60 and 54 km, 38 and 33 km, and 22 and 13 km.

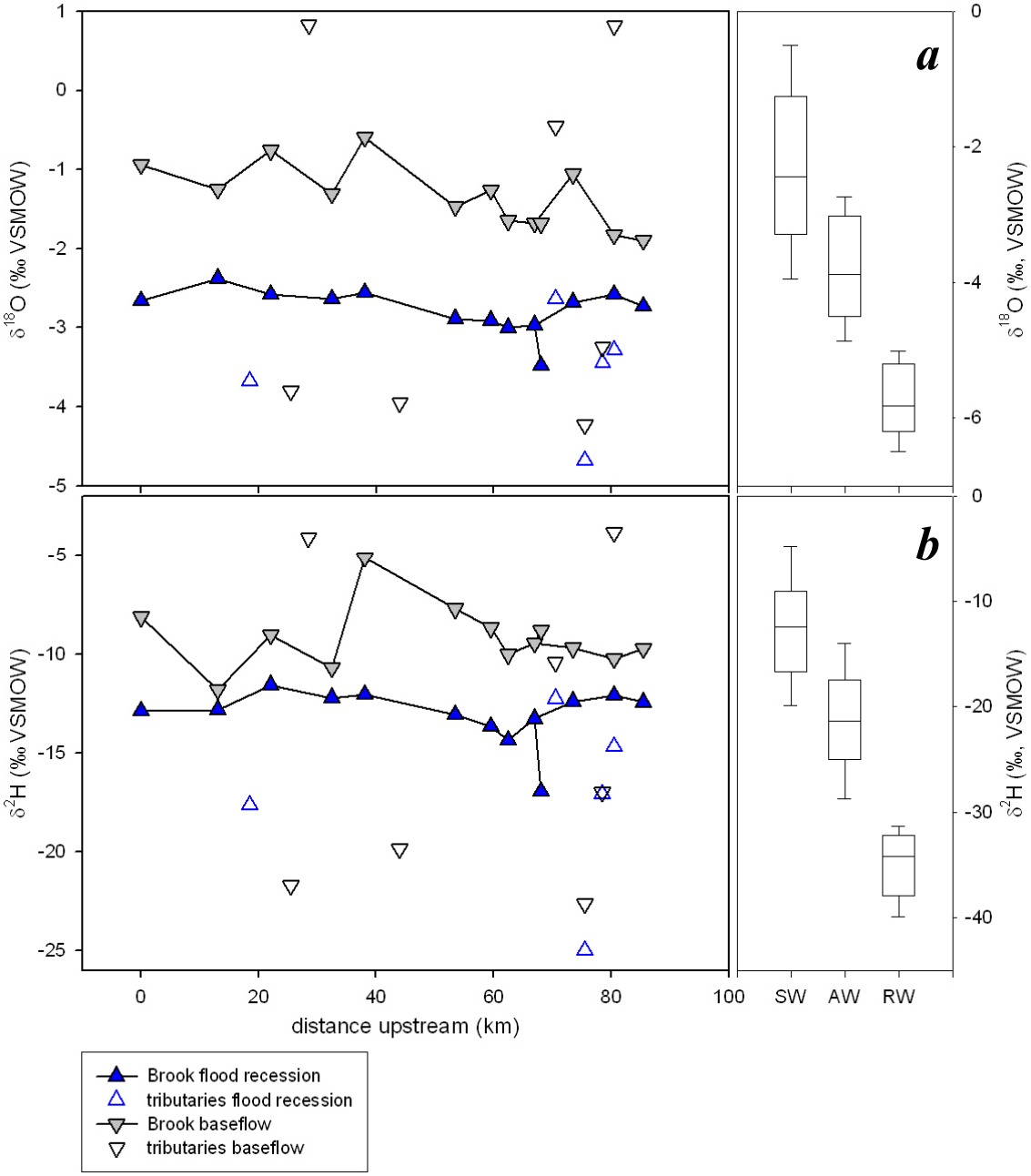

Figure 5.5 (***a***) Oxygen-18 ($\delta^{18}O$) and (***b***) deuterium ($\delta^{2}H$) values (‰ VSMOW) in stream water measured during flood recession (Mar-01) and baseflow (Nov-01) in the Wollombi Brook and tributaries. The 10th, 25th, 75th and 90th percentiles represent the variation throughout a two-year sampling period (2000-01) of $\delta^{18}O$ and $\delta^{2}H$ measured in surface water (SW), alluvial groundwater (AW) and regional groundwater (RW) sampled across the Wollombi Catchment.

δ^2H values typically increased in the upper to mid catchment (85 to 38 km) during baseflow (Figure 5.5***b***). However two small decreases in δ^2H occurred in the Wollombi Brook between 86 and 81 km and between 67 and 63 km. These two sections in the upper to mid catchment in which δ^2H values decreased corresponded with increases in $\delta^{18}O$ values. Similarly the two sections along the Wollombi Brook in which $\delta^{18}O$ values decreased in the upper to mid catchment coincided with increases in δ^2H values. There was an overall decrease in δ^2H values n the lower Wollombi Brook (33 to 0 km). Two significant decreases in δ^2H values occurred in the Wollombi Brook between 38 and 33 km and 22 and 13 km. These δ^2H decreases in the lower Wollombi Brook corresponded with the locations of $\delta^{18}O$ decreases during baseflow.

5.2.4.2 Deuterium-excess

The lowest deuterium excess (*d*-excess) value measured in the Wollombi catchment throughout the two-year (2000 – 01) sampling period occurred in surface water (Wollombi Brook and tributaries) in which the median *d*-excess was 7.2 ‰ (Figure 5.6). Median *d*-excess values in alluvial groundwater (9.9 ‰) and regional groundwater (11.1 ‰) were progressively higher than surface water. Surface waters exhibited the broadest range of *d*-excess values (–2.0 and 12.0 ‰) and overlapped most alluvial groundwater (6.2 to 13.2 ‰) and regional groundwater (7.8 to 14.2 ‰) values. There was, however, a large range of *d*-excess values that was unique to surface waters (-2.0 to 6.2 ‰). Alluvial groundwater *d*-excess values were completely overlapped by surface waters in the lower range and regional groundwater values in the upper range. There was a small range of *d*-excess values that was unique to regional groundwaters (13.2 to 14.2 ‰).

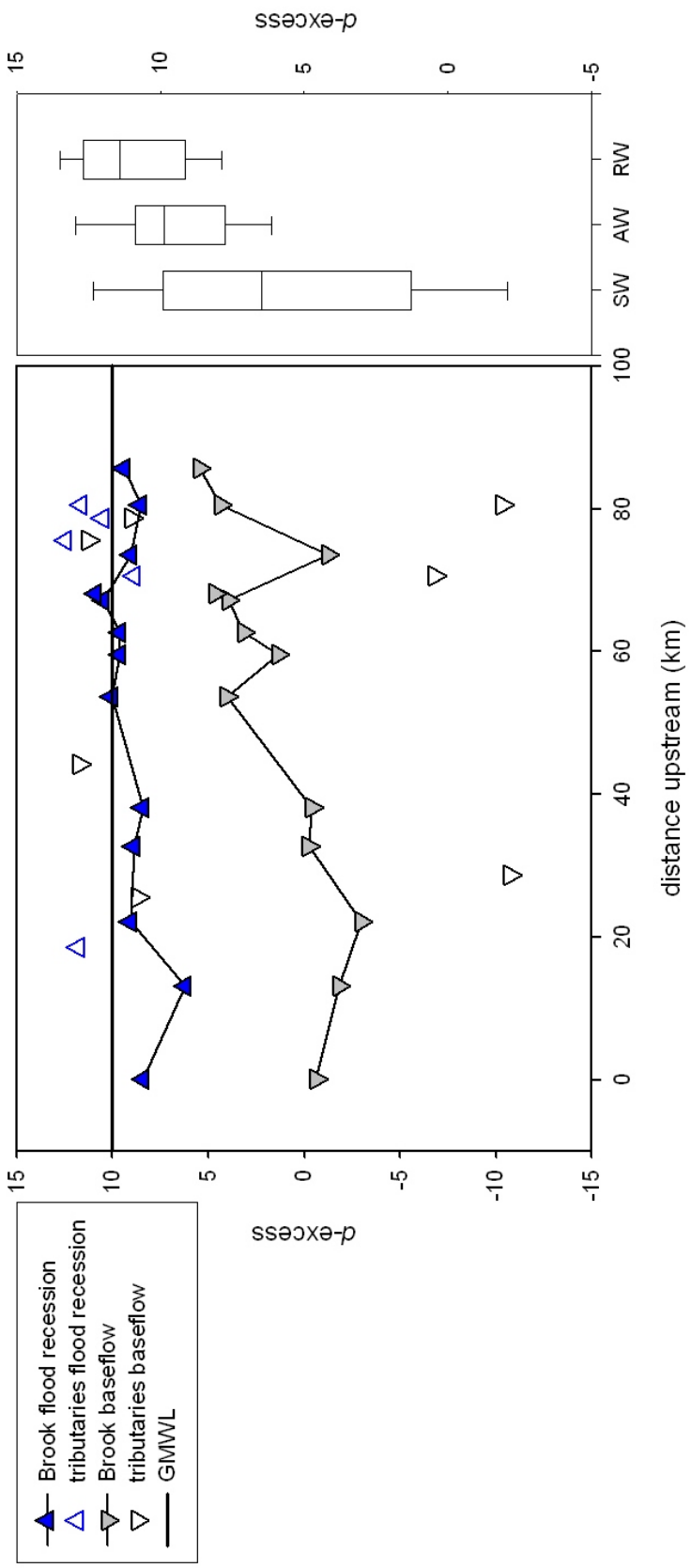

Figure 5.6 Deuterium excess (*d*-excess) values in stream water measured during flood recession (Mar-01) and baseflow (Nov-01) in the Wollombi Brook and tributaries compared to the Global Meteoric Water Line (GMWL). The 10th, 25th, 75th and 90th percentiles represent the variation throughout a two-year sampling period (2000-01) of *d*-excess measured in surface water (SW), alluvial groundwater (AW) and regional groundwater (RW) sampled across the Wollombi Catchment.

d-excess in the Wollombi Brook was significantly lower during baseflow (Nov-01) than during flood recession (Mar-01, Figure 5.6). *d*-excess in the Wollombi Brook was relatively constant (~9.5 ‰) along the longitudinal transect during flood recession until it reached 13 km and decreased significantly (to 6.2 ‰). The *d*-excess value in the Wollombi Brook subsequently increased significantly (by 2.2 ‰) in between 13 and 0 km. The overall decrease in *d*-excess from the upper to lower Wollombi Brook was 1 ‰ during flood recession. The range of *d*-excess values measured in the Wollombi Brook and tributaries during flood recession (6.2 to 12.5 ‰) fell completely within the range of *d*-excess values measured in alluvial groundwater.

Overall, the *d*-excess values in the Wollombi Brook decreased by 6.1 ‰ from the upper (5.5 ‰) to lower catchment (-0.6 ‰) during baseflow (Figure 5.6). There were, however, three reaches along the Wollombi Brook in which *d*-excess increased significantly during baseflow. These increases in *d*-excess occurred in the Wollombi Brook between 74 to 67 km, 60 to 54 km, and 22 to 0 km. The *d*-excess values in the Wollombi Brook were significantly higher in the upper catchment (85 to 50 km, ~4 ‰, excluding two low points at 60 and 74 km that can be attributed to surface water inflows from tributary streams) than in the lower catchment (50to 0 km, ~-1 ‰) under baseflow conditions.

The range of *d*-excess values in the Wollombi Brook during baseflow (5.2 to -3.0 ‰) were lower than the *d*-excess ranges measured in both alluvial groundwater and regional groundwater. There were four tributaries (at 79, 75, 44 and 26 km) that fell within alluvial groundwater and regional groundwater values during baseflow. There were an additional three tributaries (at 81, 71 and 28 km) that had much lower *d*-excess values (-6.8 to –10.7) than values measured in the Wollombi Brook during baseflow.

5.2.4.3 Unsaturated zone

Unsaturated zone δ^2H, *d*-excess and soil moisture profiles measured during flood recession (Mar-01) and baseflow (Nov-01) conditions are presented in Figures 5.7 and 5.8. Because δ^2H and $\delta^{18}O$ profiles were similar, only δ^2H profiles are described. Unsaturated zone $\delta^{18}O$ profiles are presented in Figure A.1.

Unsaturated zone thicknesses were 0.16, 0.65 and 1.4 m in soil profiles located 2, 6 and 21 m from the stream channel respectively during flood recession (Mar-01, Figure 5.7***a***, ***b***, ***c***). Maximum δ^2H values occurred in the top 0.02 m of unsaturated soil profiles during flood recession. In the soil profile located 6 m from the stream channel δ^2H decreased with depth from -4.2 ‰ reaching a minimum of –30.9 ‰ at 0.12 m below the ground surface (Figure 5.7***b***). Secondary maximum (-20.8 ‰) and minimum (-29.4 ‰) δ^2H values occurred at depths of 0.16 and 0.18 m respectively below which δ^2H increased down into the capillary fringe. δ^2H decreased slightly approximately 0.1 m above the water table. Unsaturated zone profiles located 2, 6 and 21 m from the stream channel displayed similar trends in the δ^2H of soil water during flood recession (Figure 5.7***a***, ***b***, ***c***).

During baseflow (Nov-01) unsaturated zone thicknesses were 0.55, 0.8 and 1.7 m in soil profiles located 4, 10 and 23 m respectively from the stream channel (Figure 5.7***d***, ***e***, ***f***). Dry surface layers developed in the top 0.1 m of unsaturated soil profiles located 10 and 23 m from the stream channel and maximum δ^2H values (-29.9 ‰ and –31.4 ‰ respectively) occurred 0.12 m below ground surface (Figure 5.7***e***, ***f***). δ^2H decreased exponentially with depth until at the top of the capillary fringe it decreased sharply to a minimum of -31.9 ‰ 0.1 m above the water table in the unsaturated soil profile located 6 m from the stream channel (Figure 5.7***e***). The vertical trends in the δ^2H values of soil water were similar in unsaturated soil profiles located 6 and 23 m from the stream channel (Figure 5.7***e***, ***f***). There was much less

variation in the δ^2H values in the shallower unsaturated zone profile (Figure 5.7***d***). The δ^2H in soil water ranged from a maximum of –13.6 ‰ 0.04 m below the ground surface to a minimum of 24.3 ‰ just above the capillary fringe (Figure 5.7***d***).

The *d*-excess of soil water from unsaturated zone profiles ranged between –37 and 17 ‰ during flood recession (Mar-01) and -58 and 13 ‰ during baseflow (Nov-01, Figure 5.8). Minimum *d*-excess values occurred near the ground surface and increased sharply with depth toward the Global Meteoric Water Line (*d*-excess = 10). During flood recession soil water in the unsaturated profile nearest the stream channel exceeded 10 ‰ at 0.06 m below the ground surface, however, *d*-excess of soil water decreased to 8 ‰ at a depth of 0.1 m then increased to 10 ‰ at the top of the water table (Figure 5.8***a***). *d*-excess exceeded 10 ‰ at 0.16 m below the ground surface in soil water from the unsaturated profile located 6 m from the stream channel, but *d*-excess was highly variable below this point ranging between 4 and 12 ‰ (Figure 5.8***b***). The *d*-excess of soil water was consistently higher than 10 ‰ below a depth of 0.55 m in the unsaturated profile located 21 m from the stream channel during flood recession (Figure 5.8***c***). During baseflow *d*-excess exceeded 10 ‰ below 0.24, 0.65 and 1.7 m in the unsaturated profiles located 4, 10 and 23 m from the stream channel respectively (Figure 5.8***c***, ***d***, ***e***).

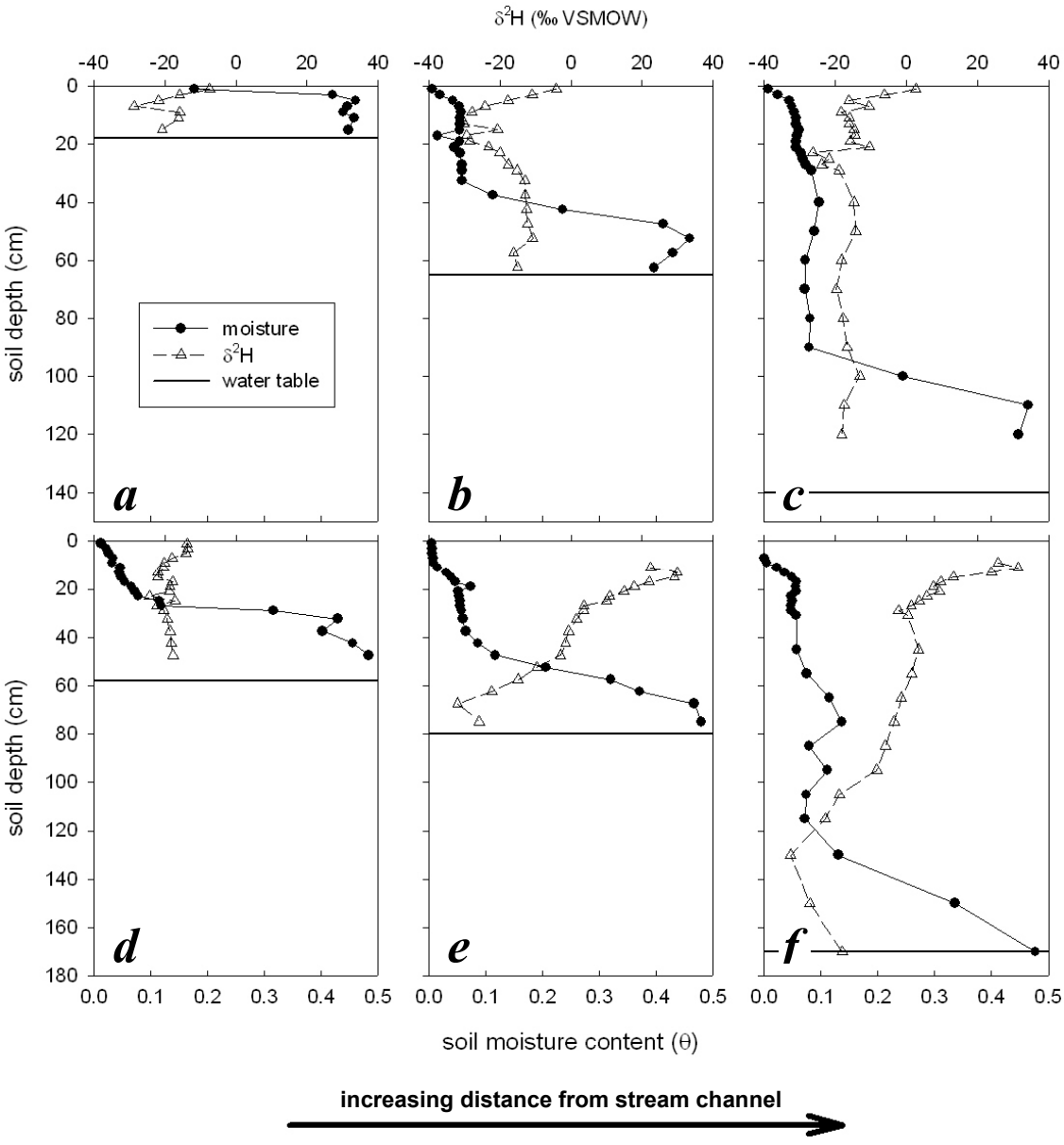

Figure 5.7 Soil moisture content and δ^2H signature in unsaturated soils located (***a***) 2 m, (***b***) 6 m, (***c***) 21 m, (***d***) 4 m, (***e***) 10 m and (***f***) 23 m from the stream channel at sampling station 1 (Warkworth) during (***a, b, c***) flood recession (Mar-01) and (***d, e, f***) baseflow (Nov-01) conditions.

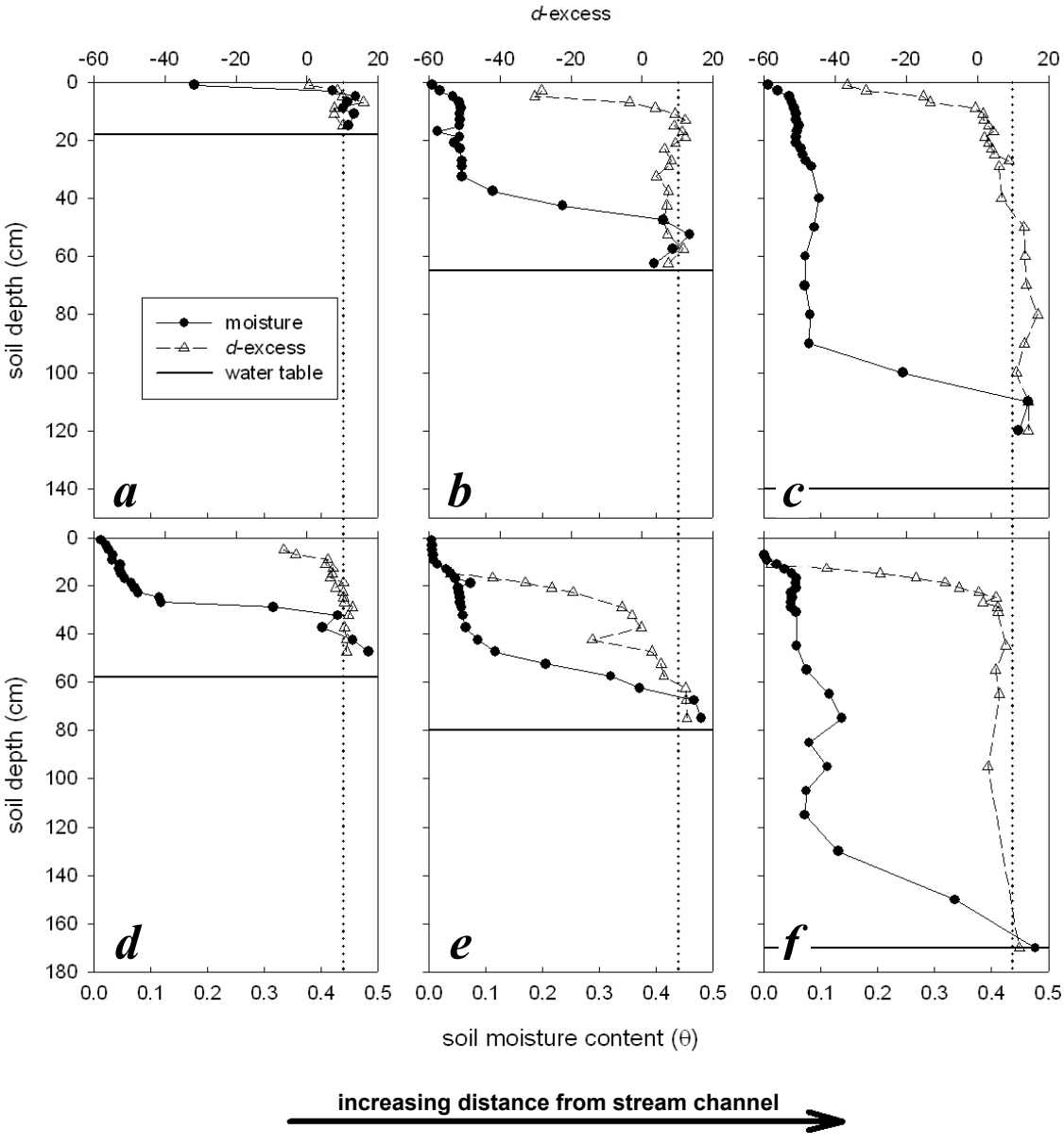

Figure 5.8 Soil moisture content and *d*-excess in unsaturated soils located (***a***) 2 m, (***b***) 6 m, (***c***) 21 m, (***d***) 4 m, (***e***) 10 m and (***f***) 23 m from the stream channel at sampling station 1 (Warkworth) during (***a, b, c***) flood recession (Mar-01) and (***d, e, f***) baseflow (Nov-01) conditions. Dotted lines represent the Global Meteoric Water Line (*d*-excess = 10).

5.2.5 Strontium and $^{87}Sr/^{86}Sr$

The strontium concentration in stream water typically ranged between <0.1 mg L^{-1} (analytical detection limit) and 0.38 mg L^{-1} (Figure 5.9). Alluvial groundwater Sr^{2+} concentrations generally varied between 0.09 and 0.45 mg L^{-1}. The Sr^{2+} concentration in regional groundwater typically ranged from 0.30 to 2.38 mg L^{-1}.

The range Sr^{2+} concentrations in stream water was similar to alluvial groundwater values. Regional groundwater Sr^{2+} concentrations were typically higher than both surface water and alluvial groundwater values. However, there was a narrow range of values (0.22 to 0.39 mg L^{-1}) in which the Sr^{2+} concentrations in all three water reservoirs overlapped.

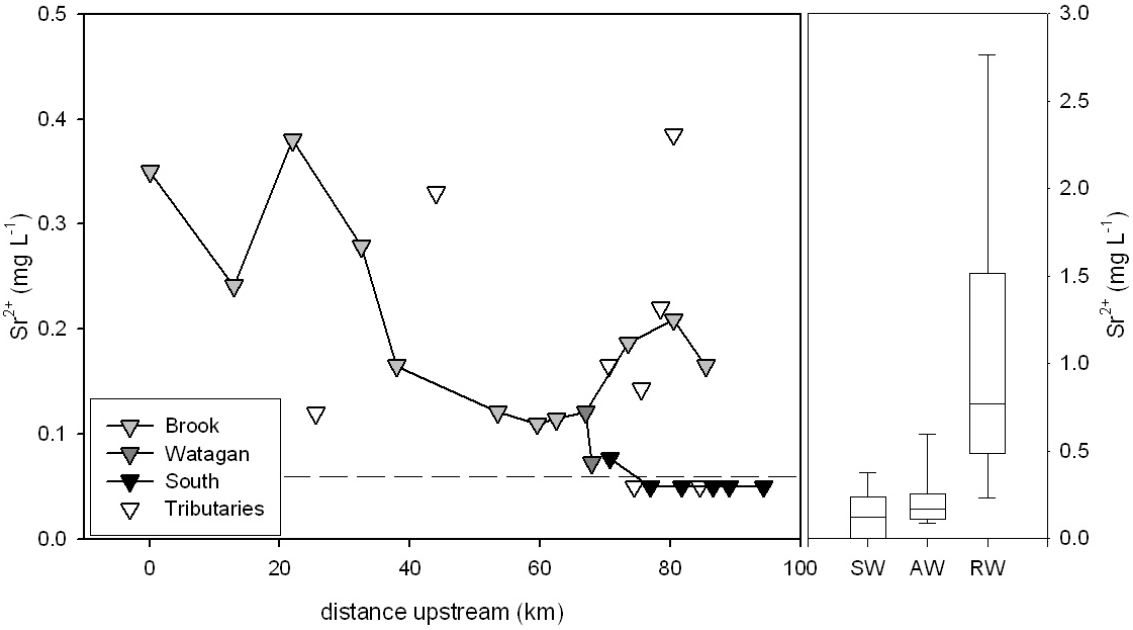

Figure 5.9 The strontium concentration (Sr^{2+} mg L^{-1}) in stream water measured during baseflow (Nov-01) separated into the main stem (Brook), two major branches (Watagan and South) and tributaries. Points below the dashed line were below the laboratory detection limit. The 10th, 25th, 75th and 90th percentiles represent the variation throughout a two-year sampling period (2000-01) of Sr^{2+} measured in surface water (SW), alluvial groundwater (AW) and regional groundwater (RW) sampled across the Wollombi Catchment.

During baseflow (Nov-01) the Sr^{2+} concentration in the Wollombi Brook was higher in the lower catchment (0 to 33 km) than in the mid (38 to 67 km) and upper regions of the catchment (74 to 95 km, Figure 5.9). The Sr^{2+} concentration of stream water in the main stem of the Wollombi Brook increased by 0.04 mg L^{-1} between 86 and 81 km, then decreased by 0.1 mg L^{-1} between 81 and 63 km. The Sr^{2+} concentration in the Wollombi Brook remained relatively constant between 63 and 54 km, and then gradually increased (by 0.26 mg L^{-1}) to a maximum Sr^{2+} concentration of 0.38 mg L^{-1} at 22 km. The maximum Sr^{2+} concentration in the Wollombi Brook was followed by a sharp decrease (of 0.14 mg L^{-1}) at 13 km and then a sharp increase (of 0.11 mg L^{-1}) at 0 km.

The Sr^{2+} concentrations in the Watagan and South branches were lower than the Sr^{2+} concentrations in the main stem of the Wollombi Brook. The Sr^{2+} concentration in the South branch of the Wollombi Brook was below detection limit in between 95 and 77 km. Tributary Sr^{2+} concentrations typically corresponded with Wollombi Brook values measured in the same region of the catchment. However, there was one tributary in the upper catchment that had an elevated Sr^{2+} concentration (at 81 km) in comparison to the Wollombi Brook in the upper catchment (70 to 90 km).

The $^{87}Sr/^{86}Sr$ ratio within the Wollombi Brook typically ranged between 0.7095 and 0.7139 (Figure 5.10). Alluvial groundwater $^{87}Sr/^{86}Sr$ ratios generally ranged between 0.7093 and 0.7113 and regional groundwaters typically ranged between 0.7053 and 0.7096. The relatively large range of $^{87}Sr/^{86}Sr$ ratios measured in the Wollombi Brook was overlapped by both alluvial groundwater and regional groundwater values. However, there was a range of $^{87}Sr/^{86}Sr$ values (0.7113 to 0.7139) that was unique to the Wollombi Brook. The narrow range of alluvial groundwater $^{87}Sr/^{86}Sr$ values was completely overlapped by stream water and regional groundwater values. Regional groundwater $^{87}Sr/^{86}Sr$ values were overlapped in the upper range by both

stream water and alluvial groundwater. However, a large range of $^{87}Sr/^{86}Sr$ values (0.7053 to 0.7093) was exclusive to regional groundwater.

There was a net decrease (of 0.0023) in the $^{87}Sr/^{86}Sr$ ratio from the upper to lower reaches of the main stem of the Wollombi Brook (Figure 5.10). There were, however, two significant increases in the $^{87}Sr/^{86}Sr$ ratio of stream water in the main stem of the Wollombi Brook at 67 and 13 km. The peak $^{87}Sr/^{86}Sr$ in the main stem of the Wollombi Brook at 67 km occurred approximately 1 km downstream of its confluence with the Watagan and South branches. The $^{87}Sr/^{86}Sr$ ratios in the Watagan and South branches were significantly higher (by 0.0018) than those in the main stem of the Wollombi Brook.

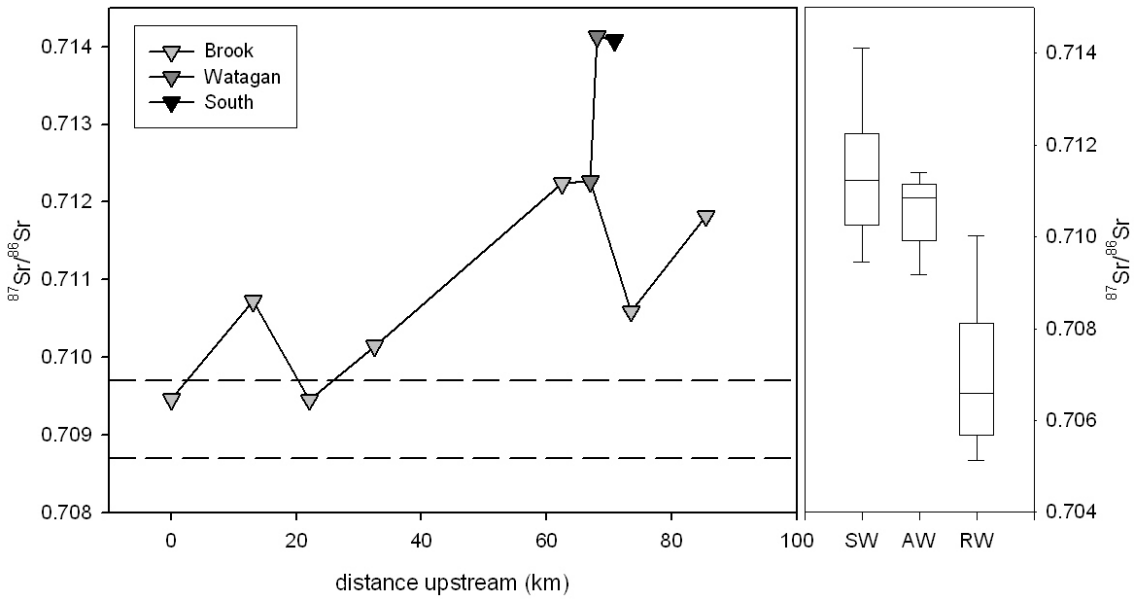

Figure 5.10 Strontium isotope ratios ($^{87}Sr/^{86}Sr$) in stream water measured during baseflow (Nov-01) separated into the main stem (Wollombi Brook) and two major branches (Watagan and South). The 10th, 25th, 75th and 90th percentiles represent the variation throughout a two-year sampling period (2000-01) of $^{87}Sr/^{86}Sr$ measured in surface water (SW), alluvial groundwater (AW) and regional groundwater (RW) sampled across the Wollombi Catchment. The dashed lines encompass the range of values expected for near coastal rainfall.

Stream water $^{87}Sr/^{86}Sr$ ratios were typically much higher than values expected for rainfall (0.7087 to 0.7097) in the region (Figure 5.10). The $^{87}Sr/^{86}Sr$ ratios in the upper reaches of the Wollombi Brook (63 to 71 km) were typically higher than any values measured in either alluvial groundwater or regional groundwater. In the lower Wollombi Brook (0 to 33 km), stream water $^{87}Sr/^{86}Sr$ ratios were completely within the range of alluvial groundwater values. At 0 and 22 km the Wollombi Brook $^{87}Sr/^{86}Sr$ ratios were within both (1) the upper range of regional groundwater values, and (2) the range of expected rainfall values.

The peak Sr^{2+} concentration measured in the Wollombi Brook (at 22 km, Figure 5.9) corresponded with the lowest $^{87}Sr/^{86}Sr$ ratio measured in the stream channel (Figure 5.10). Sr^{2+} concentrations were commonly below analytical detection limit (<0.1 mg/L) in the Watagan and South branches of the Wollombi Brook, which coincided with the highest $^{87}Sr/^{86}Sr$ ratios observed in the catchment (Figure 5.10). Alluvial groundwater typically Sr^{2+} concentration and $^{87}Sr/^{86}Sr$ ratios were typically similar to stream water values. In contrast, regional groundwater typically contained much higher Sr^{2+} concentrations and much lower $^{87}Sr/^{86}Sr$ ratios than stream water.

$^{87}Sr/^{86}Sr$ in rainwater sampled from the same rain tank was 0.7097 during flood recession (Mar-01) and 0.7105 during baseflow (Nov-01). Rainfall was sampled during two storms (12 hours apart) in November 2001. The $^{87}Sr/^{86}Sr$ and Sr^{2+} concentration of the first storm rainfall sample was 0.7104, 0.002 mg L^{-1} and the second storm rainfall sample was 0.7105, 0.005 mg L^{-1}.

5.2.6 Time series data

At the 'time-series' stream water sampling station (in the mid catchment, Figure 2.1) Cl^- concentrations were lowest in stream water during peak stream flows (Figure

5.11***a***). As high stream flow events receded, Cl^- concentrations gradually increased in stream water reaching a maximum concentration (260 mg L^{-1}) when stream flow ceased in January 2001. Cl^- concentrations in stream water increased at a much faster rate once stream flow had ceased.

Cl^- concentrations were gradually increasing in the Wollombi Brook during the receding limb of a high stream flow event when flood recession (Mar-01) 'run of river' sampling was undertaken (Figure 5.11***a***). Baseflow (Nov-01) 'run of river' sampling commenced following a prolonged low flow period in which Cl^- concentrations were gradually increasing in stream water.

δ^2H and $\delta^{18}O$ values in stream water had matching responses to seasonal changes in stream flow conditions (Figure 5.11***b***). Maximum stream water δ^2H and $\delta^{18}O$ values occurred in the Wollombi Brook shortly before stream flow ceased in January 2001. Stream water δ^2H and $\delta^{18}O$ values decreased before the Wollombi Brook recommenced flowing, coinciding with January (summer) rainfall. δ^2H and $\delta^{18}O$ values in stream water initially decreased when the Wollombi Brook started flowing in February 2001, followed by large increases in δ^2H and $\delta^{18}O$ values as stream flow increased. There were large decreases in δ^2H and $\delta^{18}O$ values in stream water during the receding limb of the February 2001 high stream flow event. A smaller increase in δ^2H and $\delta^{18}O$ values occurred in the Wollombi Brook coinciding with the second (March 2001) high stream flow event. δ^2H and $\delta^{18}O$ values in the Wollombi Brook decreased significantly during the third (April 2001) and fourth (May 2001) peak stream flow events. δ^2H and $\delta^{18}O$ values in stream water initially decreased after the first and second high stream flow events, whereas, δ^2H and $\delta^{18}O$ values increased in stream water after the third and fourth high stream flow events. δ^2H and $\delta^{18}O$ values generally increased in the Wollombi Brook after May 2001 as stream flow started receding.

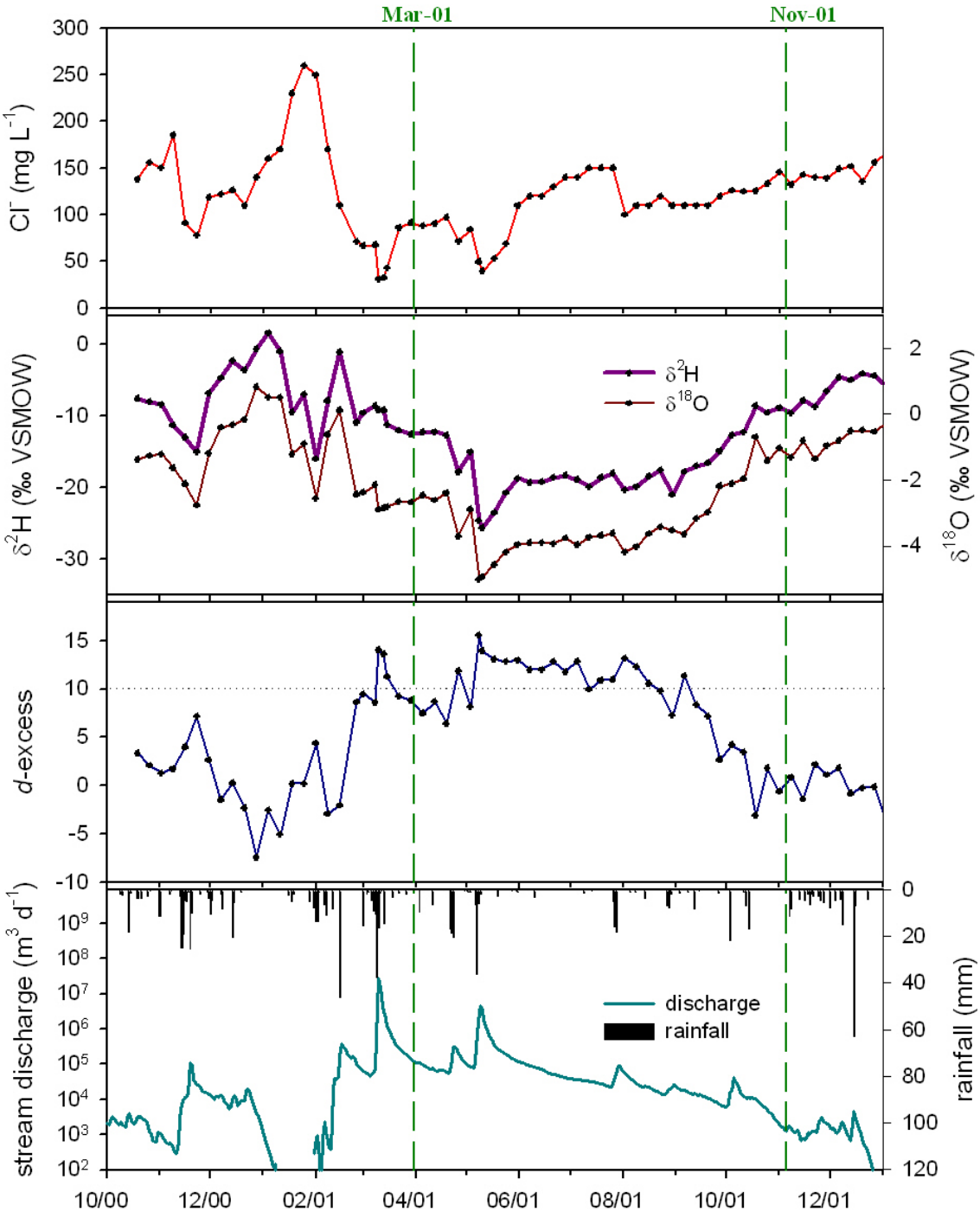

Figure 5.11 'Long-term' changes in (***a***) Cl^- concentrations, (***b***) δ^2H and $\delta^{18}O$, and (***c***) *d*-excess in the Wollombi Brook in comparison to (***d***) stream water discharge at Brickman's Bridge (site 'TB', tributary to the Wollombi Brook) and daily rainfall at Broke (site '4').

The lowest *d*-excess value measured in stream water (-7.4 ‰) occurred just before stream flow ceased in January 2001 (Figure 5.11***c***). The *d*-excess value in stream water increased before the stream recommenced flowing, coinciding with a small rainfall event. The *d*-excess of water in the Wollombi Brook increased rapidly when low stream flow commenced in February 2001, but decreased rapidly as stream flow receded. There was a large increase in *d*-excess in stream water when the first 2001 high stream stage occurred. *d*-excess remained high (around 10 ‰) until September 2001 stream flow dropped below 10^4 m^3 day^{-1}. Decreases in the *d*-excess value of stream water were associated with decreases in stream flow, however, increases in the *d*-excess of stream water did not always coincide with increases in stream flow.

5.3 METHODOLOGY FOR USE OF ENVIRONMENTAL TRACERS TO IDENTIFY SOURCES OF GROUNDWATER DISCHARGE TO STREAM FLOW

5.3.1 Stream water salinity as an indicator of groundwater discharge to stream flow

Depending on the source of groundwater, discharge to stream flow can cause either increases or decreases in stream water salinity. For example, average Cl^- concentrations were lower in alluvial groundwater than in stream water (Figure 5.3) and would generally cause decreases in stream water Cl^- concentration when it discharged to stream flow. On the other hand, average regional groundwater Cl^- concentrations were much higher than average stream water Cl^- concentrations. Therefore, regional groundwater discharge to stream flow would typically increase the Cl^- concentrations of stream water.

During low flows stream water remains in the stream channel for prolonged periods of time (e.g. during Nov-01 stream water took more than two weeks to flow from the

headwaters to the mouth of the Wollombi Brook) and is subjected to significant evaporative losses. Salinity becomes progressively more concentrated in stream water as it flows downstream due to the evaporative concentration of salts. Therefore, increases in stream water salinity during low flow conditions can be caused by either (1) regional groundwater discharge to stream flow, or (2) evaporative concentration of salts, making identification of regional groundwater discharge to stream flow ambiguous. During high stream flows (e.g. Mar-01) evaporative concentration of salts is less likely to significantly increase stream water salinity. Therefore, increases in stream water salinity during high stream flow events are more likely to be caused by groundwater contributions to stream flow than evaporative concentration of salts.

In-stream Cl^- data is used in preference to other major ion chemical species to identify sources of groundwater discharge to stream flow because it is widely considered to behave conservatively in stream water (e.g. Stone 1992). In order to explain the difference between Cl^- concentrations in rainfall events and the Cl^- response of stream water Chen *et al.* (2002) suggested that Cl^- was bound by adsorption processes generating an additional Cl^- store within the catchment. However, the impacts of groundwater discharge and evaporative processes on the Cl^- concentration of stream water in the Wollombi Brook are likely to be magnitudes greater than adsorption processes.

Decreases in stream water salinity during low flow conditions (e.g. Nov-01 baseflow), are likely to be caused by alluvial groundwater discharge to stream flow. However, during flood recession (Mar-01) Cl^- concentrations in stream water and alluvial groundwater were very similar (Figure 5.3). Therefore alluvial groundwater discharge to stream flow does not necessarily cause distinct decreases in the Cl^- concentration of stream water during high flows.

5.3.2 Radon-222 in stream water as an indicator of groundwater discharge to stream flow

Groundwater is the major source of ^{222}Rn to the Wollombi Brook (Chapter 4). Diffusion of ^{222}Rn from streambed sediments was found to impart background stream water ^{222}Rn concentrations of only 0.02 Bq L^{-1} or less (Table 4.3). Dissolved ^{226}Ra in surface water can also provide a source of ^{222}Rn. However, ^{222}Rn was not detected in stream water samples one month after collection, indicating that there was minimal dissolved ^{226}Ra in stream water sustaining high ^{222}Rn concentrations in the Wollombi Brook.

Both alluvial groundwater and regional groundwater discharge to stream flow increase the ^{222}Rn concentration of stream water (Figure 5.4). Regional groundwater would typically cause greater increases in the ^{222}Rn concentration of stream water in the Wollombi Brook than alluvial groundwater per unit volume of groundwater discharge. Distinct increases in the ^{222}Rn concentration of stream water between consecutive surface water sampling stations indicated points of groundwater discharge to stream flow (Figure 5.4). However, ^{222}Rn concentrations were consistently lower in stream water than alluvial groundwater and regional groundwater. Therefore alluvial groundwater discharge could not be distinguished from regional groundwater discharge to the Wollombi Brook based on raw changes in stream water ^{222}Rn concentration data. However, if surface water discharge data is available, the ^{222}Rn concentration of groundwater discharge can be estimated (C^{gw}, equation 5.1).

$$C^{gw} = \left(Q^n C^n - Q^0 C^0\right) \Big/ Q^{gw} \qquad \textbf{5.1}$$

Q^0	Stream discharge at upstream sampling station	($m^3\ s^{-1}$)
C^0	^{222}Rn activity in upstream sampling station	(Bq L^{-1})
Q^{gw}	Groundwater discharged to stream flow	($m^3\ s^{-1}$)
C^{gw}	^{222}Rn activity of groundwater	(Bq L^{-1})
Q^n	Stream discharge at downstream sampling station	($m^3\ s^{-1}$)
C^n	^{222}Rn activity at downstream sampling station	(Bq L^{-1})

Equation 5.1 is based on the following assumptions:

1. Stream water does not discharge from the Wollombi Brook into the adjacent aquifer;
2. ^{222}Rn is not lost from the Wollombi Brook via gas exchange or radioactive decay;
3. Groundwater discharge to the Wollombi Brook is the difference between stream discharge between consecutive surface water sampling points ($Q^{gw} = Q^n - Q^0$) where $Q^n > Q^0$; and
4. The ^{222}Rn concentration of groundwater that discharges to the Wollombi Brook is the difference in ^{222}Rn concentration of stream water between consecutive surface water sampling points ($C^{gw} = C^n - C^0$) where $C^n > C^0$.

Since alluvial groundwater (2.0 to 6.0 Bq L^{-1}) and regional groundwater (4.0 to 22 Bq L^{-1}) have distinct ^{222}Rn concentrations (Figure 5.4), equation 5.1 could be used to differentiate between alluvial groundwater and regional groundwater discharge to stream flow. However the Wollombi Brook is a variably gaining and losing stream system. This means that the Wollombi Brook can lose water to and gain water from

the adjacent aquifer system within a single sampling reach (i.e. between consecutive stream water sampling stations). If stream water is lost to the adjacent aquifer (Q^j) the actual groundwater discharge (Q^{gw}) to stream flow is greater than net change in stream discharge ($Q^n - Q^0$, equation 5.2).

$$Q^{gw} = Q^n - Q^0 + Q^j \quad \textbf{5.2}$$

Q^j Stream water discharged (lost) to the adjacent aquifer ($m^3\ s^{-1}$)

Therefore loss of stream discharge to the adjacent aquifer needs to be incorporated into an estimate of the ^{222}Rn concentration of groundwater discharge (equation 5.3).

$$C^{gw} = \left(Q^n C^n - Q^0 C^0 + Q^j C^j\right) \Big/ Q^{gw} \quad \textbf{5.3}$$

where

$$Q^j = f\left(f^0 Q^0 + \left(1 - f^0\right) Q^{gw}\right) \quad \textbf{5.4}$$

$$C^j = f^0 C^0 + \left(1 - f^0\right) C^{gw} \quad \textbf{5.5}$$

$$f = Q^j \Big/ \left(Q^0 + Q^{gw}\right) \quad \textbf{5.6}$$

$$f^0 = Q^j / Q^0 \quad \textbf{5.7}$$

C^j ^{222}Rn activity of stream water lost to the adjacent aquifer ($Bq\ L^{-1}$)

f Fraction of surface water lost to the adjacent aquifer

f^0 Fraction of surface water lost to the adjacent aquifer that originates from Q^0

$1 - f^0$ Fraction of surface water lost to the adjacent aquifer that originates from Q^{gw}

Both equations 5.1 and 5.3 are based on the assumption that the ^{222}Rn concentration in surface water is stable and alluvial groundwater and regional groundwater reservoirs are at equilibrium with respect to ^{222}Rn. However, in the absence of a continuous ^{222}Rn supply, stream water ^{222}Rn concentrations are rapidly depleted due to radioactive decay and turbulent gas exchange (Chapter 4). Therefore, the estimate of C^{gw} needs to incorporate ^{222}Rn loss from surface water (L_n^0) and groundwater that contributes to stream flow (L_n^{gw}) between consecutive surface water sampling stations (equation 5.8, Figure 5.12).

$$C^{gw} - L_n^{gw} = \left(\mathrm{Q}^n C^n - \mathrm{Q}^0\left(C^0 - L_n^0\right) + \mathrm{Q}^j C^j\right) \Big/ \mathrm{Q}^{gw} \qquad \textbf{5.8}$$

where

$$\mathrm{Q}^j = f\left(f^0 \mathrm{Q}^0 + \left(1 - f^0\right)\mathrm{Q}^{gw}\right) \qquad \textbf{5.9}$$

$$C^j = f^0\left(C^0 - L_j^0\right) + \left(1 - f^0\right)\left(C^{gw} - L_j^{gw}\right) \qquad \textbf{5.10}$$

L_n^0 ^{222}Rn loss from stream water between consecutive surface water sampling stations (i.e. between *0* and *n*) (Bq L^{-1})

L_n^{gw} ^{222}Rn loss from groundwater that contributes to stream flow between consecutive surface water sampling stations (i.e. between *0* and *n*) (Bq L^{-1})

L_j^0 ^{222}Rn loss from stream water before it discharges to the adjacent aquifer (Bq L^{-1})

L_j^{gw} ^{222}Rn loss from groundwater that contributes to stream flow and later recharges the adjacent aquifer (Bq L^{-1})

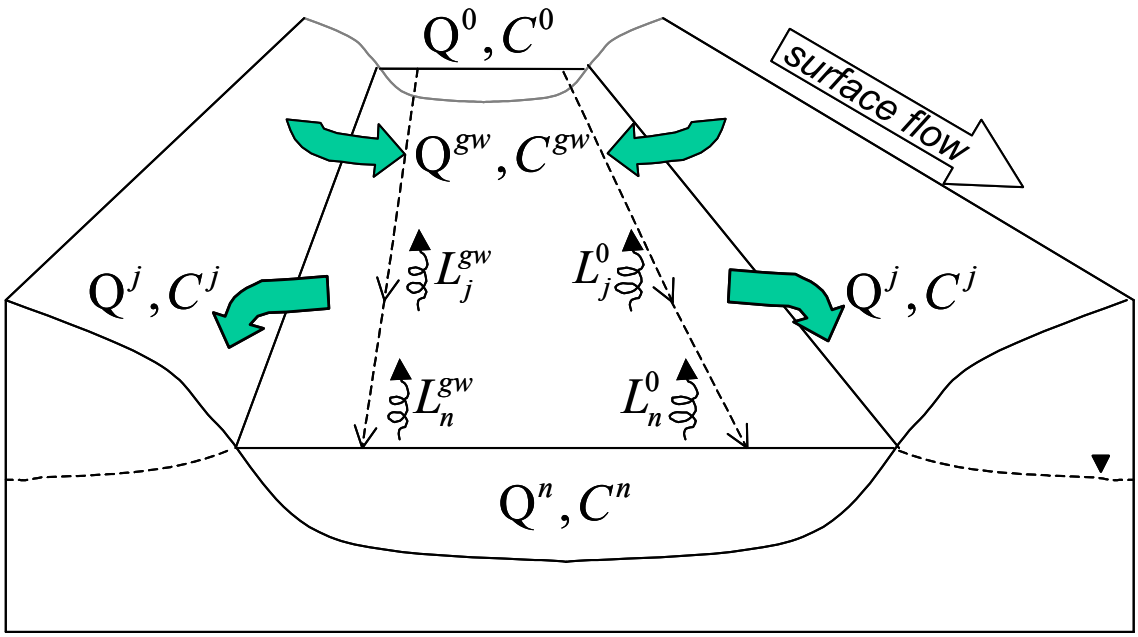

Figure 5.12 Conceptual diagram of ^{222}Rn loss and gain from the Wollombi Brook between surface water sampling stations 0 and *n*. Q^0 and Q^n represent stream discharge at consecutive stream water sampling stations, Q^{gw} is groundwater discharge into the stream channel, Q^j is discharge from the stream channel into the adjacent aquifer and $C^{0,n,gw,j}$ represents the ^{222}Rn concentration of water associated with discharges. ^{222}Rn loss from surface water (at *j* and *n*) that originated from station 0 and groundwater discharge is represented by $L_{j,n}^0$ and $L_{j,n}^{gw}$ respectively, where surface water recharges the adjacent aquifer at *j*.

The ^{222}Rn concentration that remains in stream water after ^{222}Rn loss due to radioactive decay and turbulent exchange (C_{TR}^n) was estimated in Chapter 4 using equation 4.8. Modification of equation 4.8 (equation 5.11) can also be used to estimate ^{222}Rn loss from groundwater that has discharged into the stream channel (L_n^{gw}).

$$L^{gw} = \sum_{i=1}^{n} (C^{i-1} - C_T^i) + (C^{i-1} - C_R^i) \qquad \textbf{5.11}$$

n Number of equal sections over a constant distance, x

C^{i-1} ^{222}Rn activity of the groundwater component of stream water, upstream of a distance interval, i (Bq L^{-1})

C_T^i ^{222}Rn activity of the groundwater component of stream water downstream of a distance interval, i, due to turbulent losses, modified from equation 4.2 $C_T^i = C^{gw}.e^{-Dx/zhv}$ (Bq L^{-1})

C_R^i ^{222}Rn activity of the groundwater component of stream water, downstream of a distance interval, i, due to radioactive decay losses, modified from equation 4.6 $C_R^i = C^{gw}.e^{-\lambda x/v}$ (Bq L^{-1})

i Interval number, integer fraction of n

D Molecular diffusivity of ^{222}Rn (at 23ºC 1.2×10^{-9} m^2 s^{-1})

x Distance between surface water sampling stations (m)

z Thickness of stagnant film (m)

h Average depth of stream (m)

v Velocity of stream water (m)

An intimate knowledge of the locations of groundwater discharge and the location and fraction of surface water that recharges the adjacent aquifer is required to solve equation 5.8. This level of data is not available between consecutive surface water sampling stations in the Wollombi Brook catchment. The approach is better suited to a reach-scale than a catchment-scale investigation. However, if it can be assumed that specific reaches of the Wollombi Brook do not lose surface water to the adjacent aquifer (i.e. $Q^j = 0$ and $Q^n > Q^0$) during flood recession (Mar-01) or baseflow (Nov-01) conditions, and $C^0 - L^0$ in equation 5.8 is substituted with C_{TR}^n from equation 4.8, then equation 5.8 simplifies to equation 5.12.

$$C^{gw} = \frac{Q^n C^n - Q^0 C_{TR}^n}{Q^n - Q^0} + L_n^{gw} \qquad \textbf{5.12}$$

The initial ^{222}Rn concentration of groundwater that discharged to stream flow (C^{gw}) between consecutive surface water sampling stations can be estimated by solving equation 5.12 using the numerical model technique developed in section 4.5.1. The initial ^{222}Rn concentration of groundwater that discharged to stream flow (C^{gw}) in equation 5.11 was modified over n progressively smaller intervals of length x/n, until it converged with C^{gw} in equation 5.12.

Alluvial groundwater ^{222}Rn concentrations may not reach equilibrium prior to discharge to the Wollombi Brook due to short residence times (Chapter 3) in the alluvial aquifer (e.g. during Nov-01 high flow conditions). This would lower the estimate of C^{gw} in equation 5.12, and make the differentiation between alluvial groundwater and regional groundwater more distinct.

Evaporative processes do not affect ^{222}Rn concentrations in stream water. However, the rate of turbulent ^{222}Rn loss is likely to be greater during high stream flows than low stream flows. In contrast, ^{222}Rn loss from stream water due to radioactive decay is likely to be greater during low than high stream flows because of longer residence times in the stream channel. Even though the rate of ^{222}Rn loss from stream water is higher during high flows than low flow conditions, it applies for shorter time periods. Therefore, net ^{222}Rn loss from stream water may potentially be higher during low flow than high flow conditions in the Wollombi Brook. Regardless of ^{222}Rn losses from surface water, in-stream ^{222}Rn data enabled the detection groundwater discharge to the Wollombi Brook if it occurred less than 2 km upstream from the sampling point (Table 4.5).

5.3.3 Stable isotopes of water as indicators of groundwater discharge to stream flow

Both alluvial groundwater and regional groundwater discharge to stream flow would generally lower δ^2H-$\delta^{18}O$ (Figure 5.5) and increase *d*-excess signatures in stream water (Figure 5.6). However, during low flows evaporation causes stream water δ^2H-$\delta^{18}O$ values to increase and *d*-excess values to decrease (Figure 5.4). In this way groundwater discharge generated δ^2H-$\delta^{18}O$ decreases and *d*-excess increases in stream water are overwritten by evaporative increases in δ^2H-$\delta^{18}O$ and decreases in *d*-excess. Therefore, identification of locations of groundwater discharge to stream flow by detection of decreases in δ^2H-$\delta^{18}O$ or increases in *d*-excess in stream water may only be possible short distances from groundwater discharge points during low flow conditions. During high stream flows (e.g. Mar-01 flood recession) evaporative increases in δ^2H-$\delta^{18}O$ values and decreases in *d*-excess are unlikely to be significant due to the relatively short residence time of surface water in the Wollombi Brook.

Identification of alluvial groundwater discharge to stream flow based on in-stream δ^2H-$\delta^{18}O$ and *d*-excess data is complicated by the potential for alluvial groundwater to develop evaporated δ^2H-$\delta^{18}O$ and *d*-excess signatures during low stream flow conditions. If alluvial groundwater developed a similar δ^2H-$\delta^{18}O$ signature to stream water, alluvial groundwater discharge to stream flow would not necessarily be indicated by decreases in the δ^2H-$\delta^{18}O$ signatures in stream water. Three processes could potentially increase δ^2H-$\delta^{18}O$ and decrease *d*-excess signatures in alluvial groundwater during low flow conditions:

1. Small increases in stream height induce evaporated surface water to recharge into the alluvial aquifer;
2. Evaporation directly from the alluvial aquifer through saturated sands adjacent to the Wollombi Brook (e.g. Zimmermann *et al.* 1967); or

3. Evaporated soil water in unsaturated alluvial sands is leached down into the alluvial aquifer during recharge events (e.g. Clark and Fritz 1997).

If alluvial groundwater that was recharged by evaporated surface water subsequently discharges back into the stream channel during a lower stream stage, it can potentially be identified by decreases in the δ^2H-$\delta^{18}O$ and increases in the *d*-excess values in stream water. However, if alluvial groundwater discharge and recharge into and from the stream channel continuously changes direction, alluvial groundwater discharge may not cause any distinct change in the δ^2H-$\delta^{18}O$ and *d*-excess signatures in stream water.

Identification of alluvial groundwater (that was recharged by evaporated surface water) discharges to stream flow will depend on its residence time and extent of mixing with older groundwater within the alluvial aquifer. If evaporated stream water is subjected to greater evaporative losses after alluvial aquifer recharge has occurred, stream water will acquire higher δ^2H-$\delta^{18}O$ values than alluvial groundwater. Subsequent alluvial groundwater discharge (after relatively long residence in the alluvial aquifer, i.e. in the order of weeks) to stream flow will lower the ^2H-$\delta^{18}O$ values in stream water. If groundwater within the alluvial aquifer is well mixed, evaporated surface water recharge will increase alluvial groundwater δ^2H-$\delta^{18}O$ values, but they will remain lower than surface water δ^2H-$\delta^{18}O$. Even if evaporated surface water resides in the alluvial aquifer for short time periods (i.e. in the order of days) alluvial groundwater discharge from a well-mixed aquifer would cause identifiable decreases in the δ^2H-$\delta^{18}O$ values of stream water.

Alluvial groundwater can potentially develop an evaporated δ^2H-$\delta^{18}O$ signature via evaporation directly from saturated soil (e.g. Zimmermann *et al.* 1967) or through unsaturated sand (e.g. Allison *et al.* 1984) adjacent to the Wollombi Brook. Groundwaters that develop an evaporated signature in this way can be differentiated from evaporated surface waters because they tend to develop lower sloped evaporation lines on δ^2H-$\delta^{18}O$ plots (Figure 5.13). Because surface water is exposed to atmospheric turbulence, evaporation can approach equilibrium conditions such that fractionation of δ^2H-$\delta^{18}O$ is minimised. In contrast δ^2H-$\delta^{18}O$ is strongly fractionated via molecular diffusion during the evaporation of soil water (Allison *et al.* 1985). Therefore the slopes of δ^2H-$\delta^{18}O$ evaporation lines are typically higher in surface water than soil water.

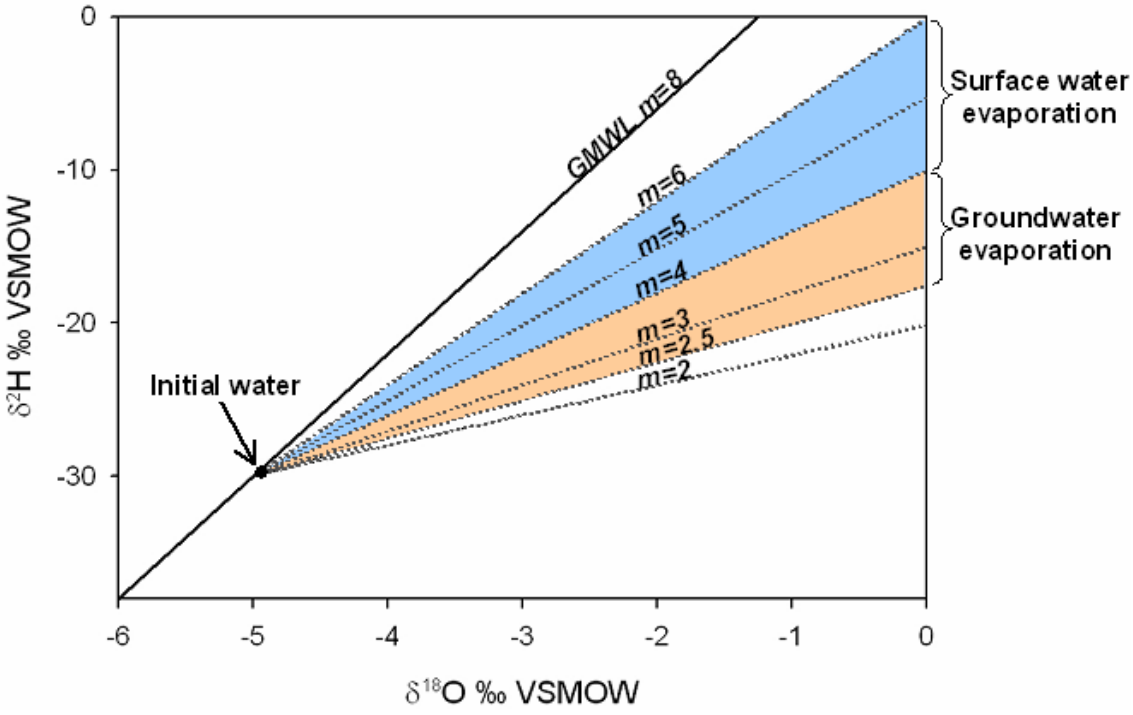

Figure 5.13 Schematic δ^2H-$\delta^{18}O$ plot demonstrating the difference in slope (m) between surface water and groundwater evaporation lines in a temperate climate from an initial water signature of $\delta^{18}O$ = -5 and δ^2H = -30 on the Global Meteoric Water Line (GMWL).

Surface water evaporation causes residual water to develop characteristic δ^2H-$\delta^{18}O$ slopes depending on the humidity, temperature and δ^2H-$\delta^{18}O$ composition of moisture in the area (Gat 1996). Theoretically at 100% humidity equilibrium evaporation occurs and the slope (*m*) of δ^2H-$\delta^{18}O$ in surface water approaches 8 (i.e. the Global Meteoric Water Line). As humidity approaches 0%, δ^2H-$\delta^{18}O$ is strongly fractionated during evaporation and *m* in residual surface water approaches 3.7 (Gonfiantini 1986). In measured surface waters *m* ranges between 3 and 5 in semi-arid environments (Clark and Fritz 1997) and 4 and 6 in temperate climates (Allison *et al.* 1985). According to the Gonfiantini (1986) relationship and relative humidity data (Table 1.5) evaporated surface water δ^2H-$\delta^{18}O$ slopes would range between 4.4 and 5.6 in the Wollombi Catchment region. Assuming that the Gonfiantini (1986) relationship holds for the Wollombi Catchment, δ^2H-$\delta^{18}O$ slopes of less than 4.4 in stream water would indicate locations of evaporated alluvial groundwater discharge.

Evaporation has been shown to occur directly from the ground surface where soils are saturated (Zimmermann *et al.* 1967, Allison *et al.* 1983). However, the δ^2H-$\delta^{18}O$ slope for groundwater evaporated directly from saturated soils is poorly characterised in the literature. Allison *et al.* (1983) reported a groundwater δ^2H-$\delta^{18}O$ slope of 4.2 in sand that was saturated to the surface. If a δ^2H-$\delta^{18}O$ slope of 4.2 were characteristic of evaporation from saturated sands, discharge of evaporated alluvial groundwater to stream flow would not be distinguishable from evaporation within the stream channel during low stream flow conditions (e.g. Nov-01 baseflow). During high stream flow conditions (e.g. Mar-01 flood recession) evaporated alluvial groundwater discharge would lower in-stream δ^2H-$\delta^{18}O$ values, but the process of evaporation (e.g. from saturated soils) would not be obvious.

Slopes of δ^2H-$\delta^{18}O$ evaporation lines in unsaturated zone soil water have been reported to range between 2.5 and 3.9 in a temperate climate (Allison *et al.* 1983)

and approximately 2 in an arid environment (Dinçer *et al.* 1974). Limited data (from Allison *et al.* 1983, 1984) indicates that the thicker the dry surface layer and the lower the soil moisture content, the lower the slope of δ^2H-$\delta^{18}O$ soil water evaporation line. Rainfall recharge that mixes with and displaces evaporated soil water downwards in the unsaturated zone has produced soil water profiles that plot to the right but parallel to the GMWL (Allison *et al.* 1984).

Increases in the *d*-excess of stream water (in time or between consecutive stream water sampling stations) indicate mixing with less evaporated source water (Figure 5.14). The less evaporated source water could be rainfall, alluvial groundwater or regional groundwater. In this case the alluvial groundwater may be evaporated, but to a lesser extent than stream water. Decreases in the *d*-excess of stream water (in time or between consecutive stream water sampling stations) either indicate (1) evaporation of water within the stream channel, or (2) mixing with a more evaporated water source (potentially alluvial groundwater). Therefore, observation of the change in *d*-excess of stream water in isolation cannot be used to differentiate between the potential sources of water to stream flow. Observation of the δ^2H-$\delta^{18}O$ slope in conjunction with the change in δ^2H or $\delta^{18}O$ between consecutive surface water sampling stations (or between sampling times) is more indicative of the sources of water to stream flow (Figure 5.15)

Shifts in δ^2H and the δ^2H-$\delta^{18}O$ slope (m) of surface water between consecutive surface water sampling stations or between successive sampling times (Figure 5.15, from point 1 to point 2) indicated that:

1. Regional groundwater potentially discharged to stream flow where $0 \leq m \leq 8$ and δ^2H_2-$\delta^2H_1 \leq 0$ (Figure 5.15***f***) and where $m \leq 0$ and δ^2H_2-$\delta^2H_1 \geq 0$ (Figure 5.15***g***);

2. Alluvial groundwater potentially discharged to stream flow where $m \leq 0$ and $^2H_2\text{-}\delta^2H_1 \geq 0$ or where $0 \leq m \leq 8$ and $\delta^2H_2\text{-}\delta^2H_1 \leq 0$ (Figure 5.15***g***, ***f***);
3. Evaporated alluvial groundwater discharged to stream flow where $2 \leq m \leq 4$ and $\delta^2H_2\text{-}\delta^2H_1 > 0$ (Figure 5.15***b***);
4. Alluvial groundwater discharge to stream flow that was either evaporated prior to stream discharge of subsequently evaporated within the stream channel potentially occurred where $m \geq 6$ and $\delta^2H_2\text{-}\delta^2H_1 > 0$, $0 \leq m \leq 2$ and $^2H_2\text{-}\delta^2H_1 \geq 0$, where $m \leq 0$ and $\delta^2H_2\text{-}\delta^2H_1 \leq 0$, or where $m \geq 8$ and $\delta^2H_2\text{-}\delta^2H_1 \leq 0$ (Figure 5.15***h***, ***c***, ***d***, ***e***); and
5. Rainfall recharge potentially occurred where $0 \leq m \leq 8$ and $\delta^2H_2\text{-}\delta^2H_1 \leq 0$, where $m \leq 0$ and $^2H_2\text{-}\delta^2H_1 \geq 0$, or where $m > 6$ and $\delta^2H_2\text{-}\delta^2H_1 > 0$ (Figure 5.15***f***, ***g***, ***h***).

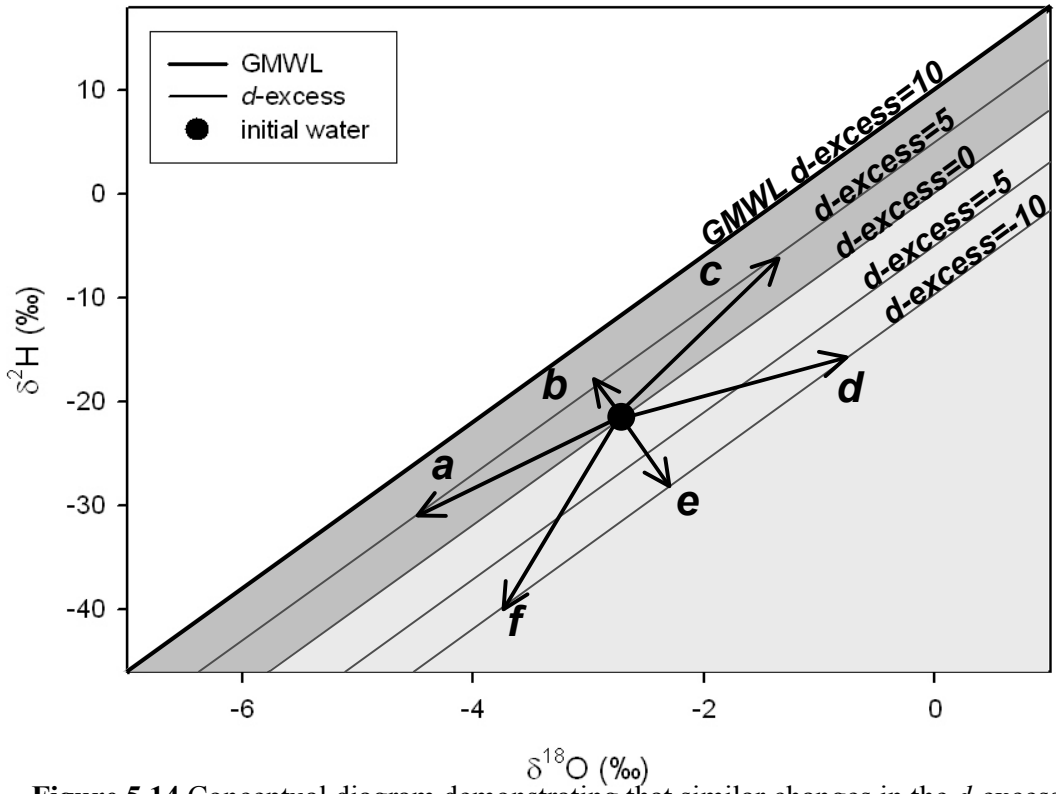

Figure 5.14 Conceptual diagram demonstrating that similar changes in the *d*-excess of stream water can be caused by different processes (indicated by arrows). Assuming there are no surface water tributaries contributing to stream flow, *d*-excess in stream water increases from the initial signature due to (***a***) regional groundwater or alluvial groundwater discharge, (***b***) rainfall recharge, or (***c***) evaporated alluvial groundwater discharge or groundwater discharge followed by evaporation within the stream channel. *d*-excess in stream water decreases from the initial value due to (***d***) evaporation from within the stream channel, or (***e***, ***f***) mixing with evaporated groundwater or groundwater discharge followed by evaporation within the stream channel.

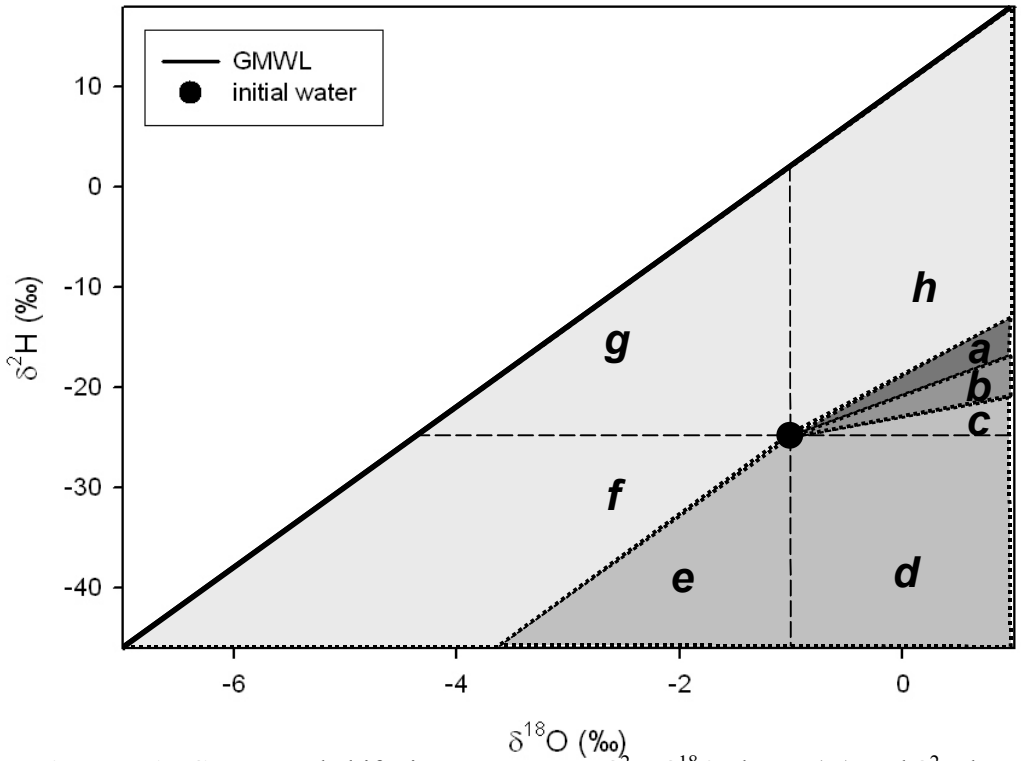

Figure 5.15 Conceptual shifts in stream water δ^2H-$\delta^{18}O$ slopes (m) and δ^2H between consecutive surface water sampling stations (from point 1 to 2), or between successive sampling times from an initial (evaporated) signature. Shifts from the initial δ^2H-$\delta^{18}O$ signature towards sections ***a***, ***b***, ***c***, ***d***, ***e***, ***f***, ***g***, and ***h*** indicate: (***a***) surface water evaporation where $4 \leq m \leq 6$ and δ^2H_2-$\delta^2H_1 > 0$, (***b***) discharge of evaporated groundwater where $2 \leq m \leq 4$ and δ^2H_2-$\delta^2H_1 > 0$, (***c***, ***d***, ***e***) mixing with evaporated groundwater or groundwater discharge followed by evaporation within the stream channel where (***c***) $0 \leq m \leq 2$ and δ^2H_2-$\delta^2H_1 \geq 0$, (***d***) where $m \leq 0$ and δ^2H_2-$\delta^2H_1 \leq 0$, or (***e***) where $m \geq 8$ and δ^2H_2-$\delta^2H_1 < 0$, (***f***, ***g***, ***h***) shift toward the Global Meteoric Water Line (GMWL) indicating: (***f***) rainfall recharge or groundwater discharge where $0 \leq m \leq 8$ and δ^2H_2-$\delta^2H_1 \leq 0$, (***g***) rainfall recharge or groundwater discharge where $m \leq 0$ and δ^2H_2-$\delta^2H_1 \geq 0$, and (***h***) rainfall recharge or alluvial groundwater discharge followed by evaporation within the stream channel where $m \geq 6$ and δ^2H_2-$\delta^2H_1 > 0$.

5.3.4 Strontium and $^{87}Sr/^{86}Sr$ as indicators of groundwater discharge to stream flow

Regional groundwater discharge would typically increase the strontium (Sr^{2+}) concentration (Figure 5.9) and lower $^{87}Sr/^{86}Sr$ (Figure 5.10) in stream water. Average alluvial groundwater and stream water Sr^{2+} concentrations and $^{87}Sr/^{86}Sr$ were very similar. However, stream water Sr^{2+} concentrations and $^{87}Sr/^{86}Sr$ were much more variable and largely overlapped alluvial groundwater values. Alluvial groundwater discharge would cause either increases or decreases to the Sr^{2+}

concentration and $^{87}Sr/^{86}Sr$ of stream water depending on the stream water values immediately upstream from the discharge point.

The Sr^{2+} concentration of stream water is likely to increase during baseflow conditions (e.g. Nov-01) due to evaporative concentration of salts. Sr^{2+} concentrations in stream water are likely to be affected by biogeochemical reactions (Stewart *et al*. 1998). However, the general shape of the stream water Sr^{2+} transect (Figure 5.9) was similar to the Cl^- transect (considered to have low reactivity, Figure 5.3), suggesting that any biogeochemical reactions that release Sr^{2+} into or remove Sr^{2+} from stream water were minimal or at least consistent throughout the catchment. Fractionation of the $^{87}Sr/^{86}Sr$ signature in stream water by evaporative or biogeochemical processes is negligible (Bullen *et al.* 1996). Therefore, any change in the $^{87}Sr/^{86}Sr$ signature of stream water is caused by groundwater discharge to stream flow. Decreases in the $^{87}Sr/^{86}Sr$ of stream water can be caused by either alluvial groundwater or regional groundwater discharge to stream flow.

The $^{87}Sr/^{86}Sr$ measured in surface waters and groundwater in the Wollombi Brook catchment ranged between values that were characteristic of groundwater from silicate aquifers (0.7141) and values that were characteristic of groundwater from basalt aquifers (0.7056, section 5.2.5). The highest $^{87}Sr/^{86}Sr$ values were measured in the upper Watagan and Southern reaches of the Wollombi Brook during baseflow (Nov-01) conditions (Figure 5.10), which coincided with low Sr^{2+} concentrations (<0.08 mg L^{-1}). All $^{87}Sr/^{86}Sr$ measured in groundwater in the Wollombi Brook catchment were below those reported in the literature for silicate aquifers (0.712 to 0.726, Faure and Powell 1972). Therefore the source of the high $^{87}Sr/^{86}Sr$ groundwater that discharged to stream flow in the upper reaches of the Wollombi Brook was not characterised by groundwater sampling from the piezometer and bore network. However, the source of the high $^{87}Sr/^{86}Sr$ values is assumed to be

groundwater from a silicate aquifer with a Sr^{2+} concentration less than 0.07 mg L^{-1}. Therefore groundwater discharge from a silicate aquifer into the Wollombi Brook would generally increase the $^{87}Sr/^{86}Sr$ and decrease the Sr^{2+} concentration of stream water (Figure 5.16). The lowest $^{87}Sr/^{86}Sr$ values measured in the Wollombi Brook were sampled from the regional bores and deep alluvial piezometers. The Sr^{2+} concentration of groundwater sampled in the Wollombi Brook catchment that contained characteristic $^{87}Sr/^{86}Sr$ of groundwater from basalt aquifers (0.702 to 0.706, Faure and Powell 1972) was high, ranging between 0.5 and 1.4 mg L^{-1}. Therefore groundwater discharge from a basalt aquifer into the Wollombi Brook would generally decrease the $^{87}Sr/^{86}Sr$ and increase the Sr^{2+} concentration of stream water (Figure 5.16).

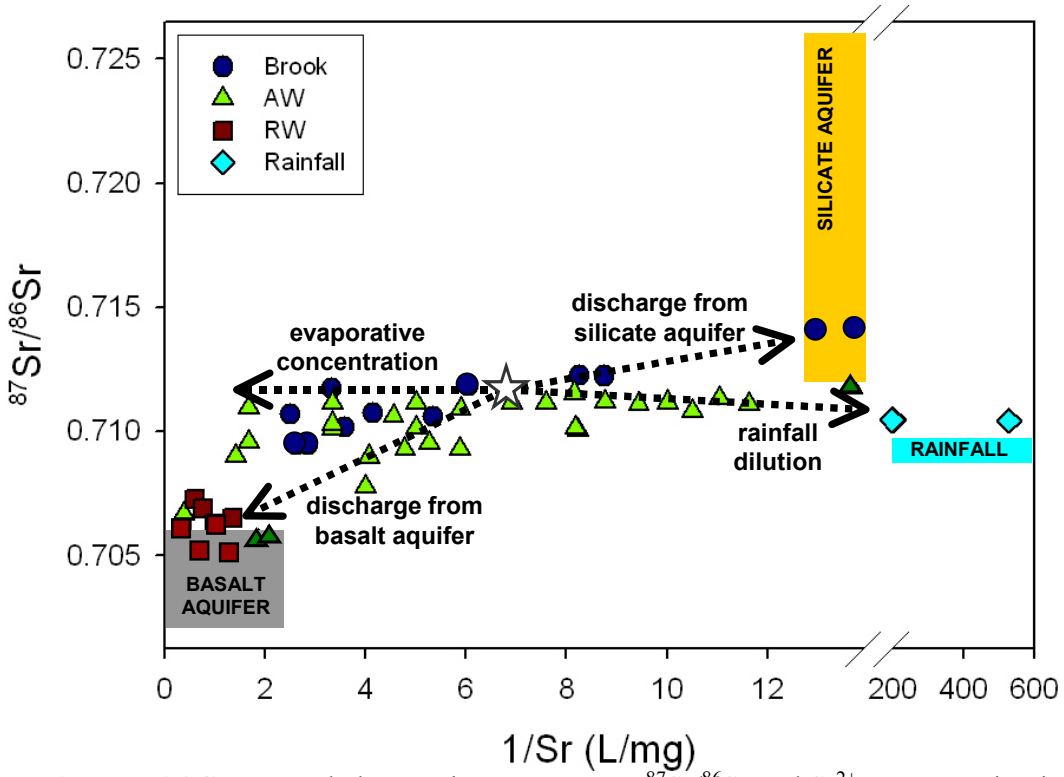

Figure 5.16 Conceptual changes in stream water $^{87}Sr/^{86}Sr$ and Sr^{2+} concentration in response to evaporation from the stream channel, rainfall dilution and groundwater discharge from basalt and silicate aquifers. Measured $^{87}Sr/^{86}Sr$ and Sr^{2+} concentrations in the Wollombi Brook (Brook), rainfall, alluvial groundwater (AW) and regional groundwater (RW) were sampled during flood recession (Mar-01) and baseflow (Nov-01) conditions. Boxed $^{87}Sr/^{86}Sr$ ranges for rainfall and groundwater from basalt and silicate aquifers were taken from the literature. Boxed ranges of Sr^{2+} concentrations in rainfall and groundwater from basalt and silicate aquifers were based on data from the Wollombi Brook catchment.

$^{87}Sr/^{86}Sr$ in rainfall is reported to range between 0.7087 (Hamilton 1966) and 0.7097 (Bogard *et al.* 1967). Limited $^{87}Sr/^{86}Sr$ and Sr^{2+} concentration rainfall data collected in the Wollombi Brook catchment ranged between 0.7097 and 0.7105 and 0.002 and 0.005 mg L^{-1} respectively (section 5.2.5). Therefore rainfall recharge to the Wollombi Brook would generally decrease $^{87}Sr/^{86}Sr$ and drastically reduce the Sr^{2+} concentration of stream water during flood recession (Mar-01) and baseflow (Nov-01) conditions (Figure 5.16). $^{87}Sr/^{86}Sr$ is not fractionated within the Wollombi Brook, therefore during evaporation the Sr^{2+} concentration of stream water will increase whilst the $^{87}Sr/^{86}Sr$ in stream water remains the same (Figure 5.16).

Decreases in $^{87}Sr/^{86}Sr$ associated with large increases in the Sr^{2+} concentration of stream water are either caused by (1) regional groundwater discharge, or (2) alluvial groundwater discharge that is subsequently concentrated by evaporation (Figure 5.16). Simultaneous decreases in both the $^{87}Sr/^{86}Sr$ and Sr^{2+} concentrations of stream water are most likely caused by alluvial groundwater discharges to stream flow. In the lower reaches of the Wollombi Brook increases in the $^{87}Sr/^{86}Sr$ of stream water would most likely be caused by alluvial groundwater discharge (excluding the possibility of surface water discharge) to stream flow. However, in the upper reaches of the Wollombi Brook increases in the $^{87}Sr/^{86}Sr$ of stream water is most likely caused by groundwater discharge from a silicate aquifer.

5.4 SOURCES OF GROUNDWATER DISCHARGE TO STREAM FLOW

5.4.1 Long-term monitoring

The strategy for interpreting "time series" stream water data, based on changes in δ^2H-$\delta^{18}O$ and Cl^- between successive sampling events (Figure 5.17), indicated that alluvial groundwater potentially contributed to the Wollombi Brook throughout the duration of sampling (October 2000 to January 2002, Figure 5.18). However,

sources of groundwater discharge to stream flow were not always distinct. Evaporation (E) affected stream water δ^2H-$\delta^{18}O$ and Cl^- signatures such that, over a small number of time periods, it was not evident whether there were any additional sources of water contributing to stream flow (Figure 5.18). The evaporated stream water signature was generally detected when stream discharge was decreasing and there may not have been any rainwater, alluvial groundwater or regional groundwater contributing to stream flow. However, in late November 2001 the evaporated surface water signature was associated with an increase in stream discharge indicating that there was an additional source of water contributing to stream flow (Figure 5.18). Therefore evaporation from the stream channel potentially concealed alluvial groundwater and/or regional groundwater discharge to stream flow as stream discharge was decreasing.

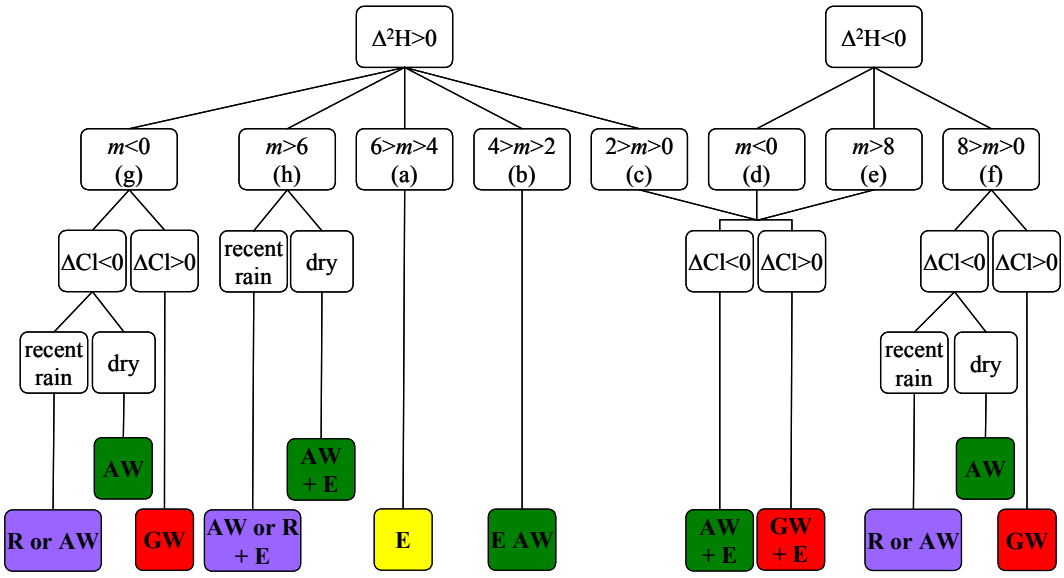

Figure 5.17 Strategy used for identifying sources of water to stream flow between sampling periods based on δ^2H-$\delta^{18}O$ and Cl^- data. Δ^2H (δ^2H_2-δ^2H_1) is the change in the δ^2H signature of stream water between successive sampling events. The δ^2H-$\delta^{18}O$ slopes (*m*) between sampling periods are categorised (***a***, ***b***, ***c***, ***d***, ***e***, ***f***, ***g***, ***h***) according to Figure 5.15. ΔCl ($Cl^-_{(2)}$-$Cl^-_{(1)}$) is the difference in the Cl^- concentration of stream water between sampling periods. "Recent rain" and "dry" represent the rainfall conditions between stream water sampling. The potential sources of water to stream flow are rainfall (R), alluvial groundwater (AW), evaporated alluvial groundwater (E AW) and regional groundwater (RW). "GW" represents alluvial groundwater and/or regional groundwater discharge to stream flow. "E" signifies that evaporation has concealed any potential groundwater discharge to stream flow.

During peak stream flow events the Cl^- concentration in stream water decreased and the δ^2H-$\delta^{18}O$ signature typically shifted toward the Global Meteoric Water Line (GMWL, Figure 5.15), indicating that either one or both rainfall and alluvial groundwater (R or AW) contributed to stream flow. Since rainfall recharge and alluvial groundwater discharge to the Wollombi Brook caused similar changes to the δ^2H-$\delta^{18}O$ and Cl^- signatures of stream water, the occurrence (or non-occurrence) of rainfall between sampling periods was the key distinguishing factor for identifying alluvial groundwater contributions to stream flow (Figures 5.17 and 5.18). If there was no (or minimal) rainfall recorded between sampling periods, it was assumed that alluvial groundwater was the main source of water contributing to stream flow.

There were no stages along the stream hydrograph over which regional groundwater definitely contributed to stream flow (identified by the "time series" strategy, Figure 5.18). However, there was potential for regional groundwater and/or alluvial groundwater (GW) discharge to the Wollombi Brook during the receding limb of high stream stages.

Alluvial groundwater (AW) discharge to stream flow was detected at many stages along the stream hydrograph: near peak stream discharge stages; during the receding limb of high stream stages; and when stream water ceased flowing during January 2001 (Figure 5.18). It was not always possible to identify a single source of water to stream flow. However, a component of alluvial groundwater discharge to stream flow could explain all observed changes in the δ^2H-$\delta^{18}O$ and Cl^- signatures of stream water.

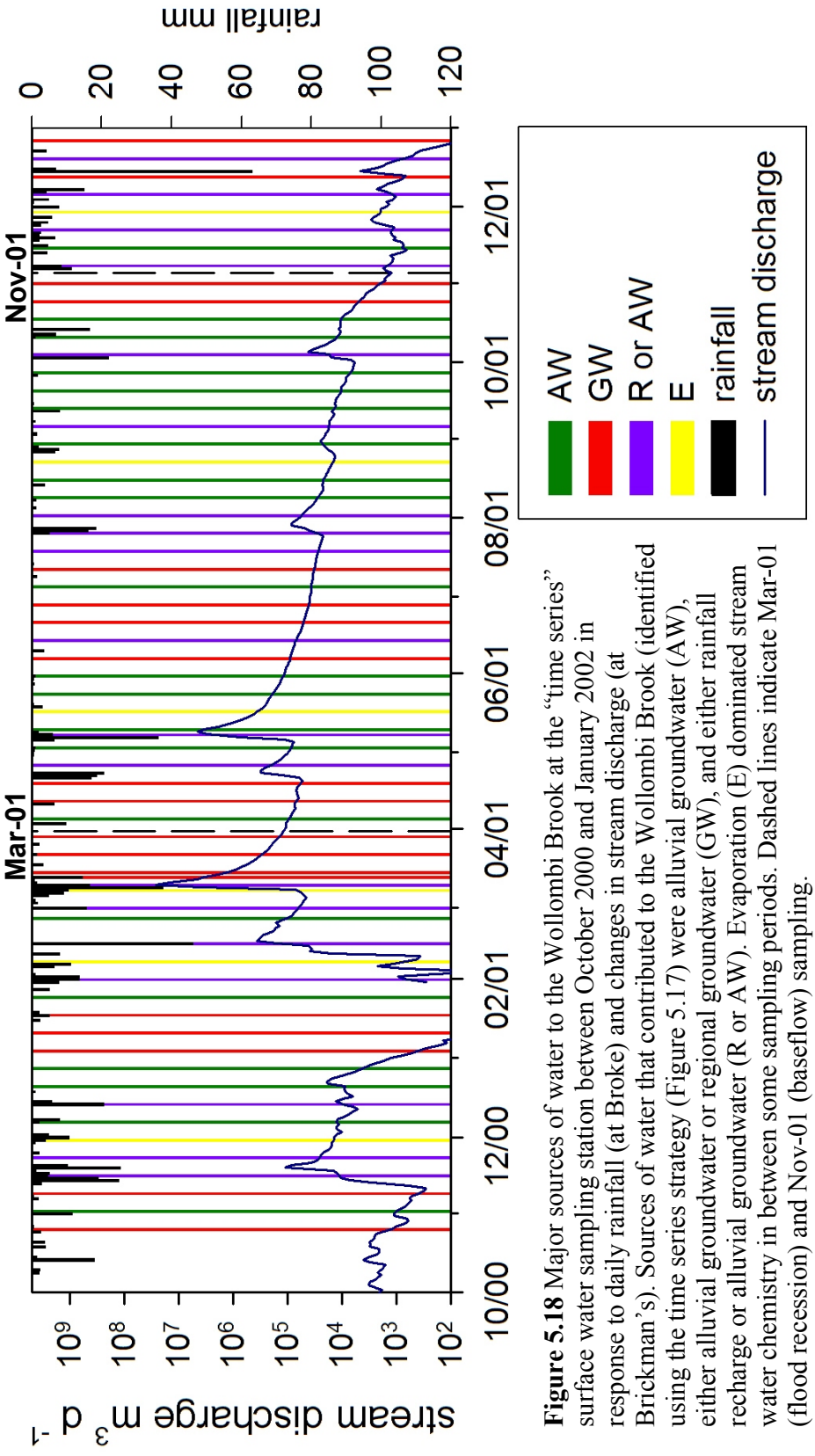

Figure 5.18 Major sources of water to the Wollombi Brook at the "time series" surface water sampling station between October 2000 and January 2002 in response to daily rainfall (at Broke) and changes in stream discharge (at Brickman's). Sources of water that contributed to the Wollombi Brook (identified using the time series strategy (Figure 5.17) were alluvial groundwater (AW), either alluvial groundwater or regional groundwater (GW), and either rainfall recharge or alluvial groundwater (R or AW). Evaporation (E) dominated stream water chemistry in between some sampling periods. Dashed lines indicate Mar-01 (flood recession) and Nov-01 (baseflow) sampling.

5.4.2 Flood recession

Since flood recession (Mar-01) stream discharge was fairly high (in the order of 10^5 m^3 day^{-1}) stream water was unlikely to experience large evaporative losses between sampling stations. Therefore flood recession δ^2H-$\delta^{18}O$ signatures would be expected to sit on or close to the Global Meteoric Water Line (GMWL). Although flood recession stream water δ^2H-$\delta^{18}O$ values were close to the GMWL, an evaporation line slope of 5.7 indicated that there was a component of evaporated water in some reaches of the stream channel (Figure 5.19). A δ^2H-$\delta^{18}O$ slope of 5.7 would generally indicate evaporation from the open stream channel (Allison *et al*. 1985, Figure 5.13). However, the δ^2H-$\delta^{18}O$ values of water in the Wollombi Brook were encompassed by highly variable alluvial groundwater values during flood recession (Figure 5.20***a***). Some alluvial groundwater δ^2H-$\delta^{18}O$ values sat to the right of the GMWL indicating that some water in the alluvial aquifer had experienced evaporation. Therefore, evaporated alluvial groundwater discharge, rather than evaporation directly from the stream channel, could also have given stream water an evaporated δ^2H-$\delta^{18}O$ signature in some reaches of the Wollombi Brook.

Evaporation was evident in unsaturated zone soil water during flood recession (Figure 5.21***a***). A δ^2H-$\delta^{18}O$ slope of 4.7 was similar to slopes reported by Allison *et al*. (1983) for evaporation from saturated sands. Therefore discharge of evaporated alluvial groundwater from saturated sands adjacent to the Wollombi Brook could potentially have given stream water an evaporated δ^2H-$\delta^{18}O$ signature in some reaches of the catchment. However, δ^2H in flood recession unsaturated zone soil water indicated that evaporation had extended no more than 0.1 m into the unsaturated zone since the last recharge event (Figure 5.7***a***, ***b***, ***c***). Therefore it was unlikely that alluvial groundwater received an evaporated signature via evaporation directly from shallow groundwater. Downward movement of evaporated soil water during previous recharge events explains the low *d*-excess values below the

evaporation front (Figure 5.8***b***). Alluvial groundwater with δ^2H-δ^{18}O signatures that were almost parallel to but displaced to the right of the GMWL (Figure 5.22) support the theory that evaporated soil water was displaced downward by recharge water giving shallow groundwater an evaporated signature (Allison *et al.* 1984). Therefore, it is likely that a component of alluvial groundwater that developed an evaporated δ^2H-δ^{18}O signature due to downward leaching of evaporated soil water contributed to stream flow in some reaches of the Wollombi Brook during flood recession.

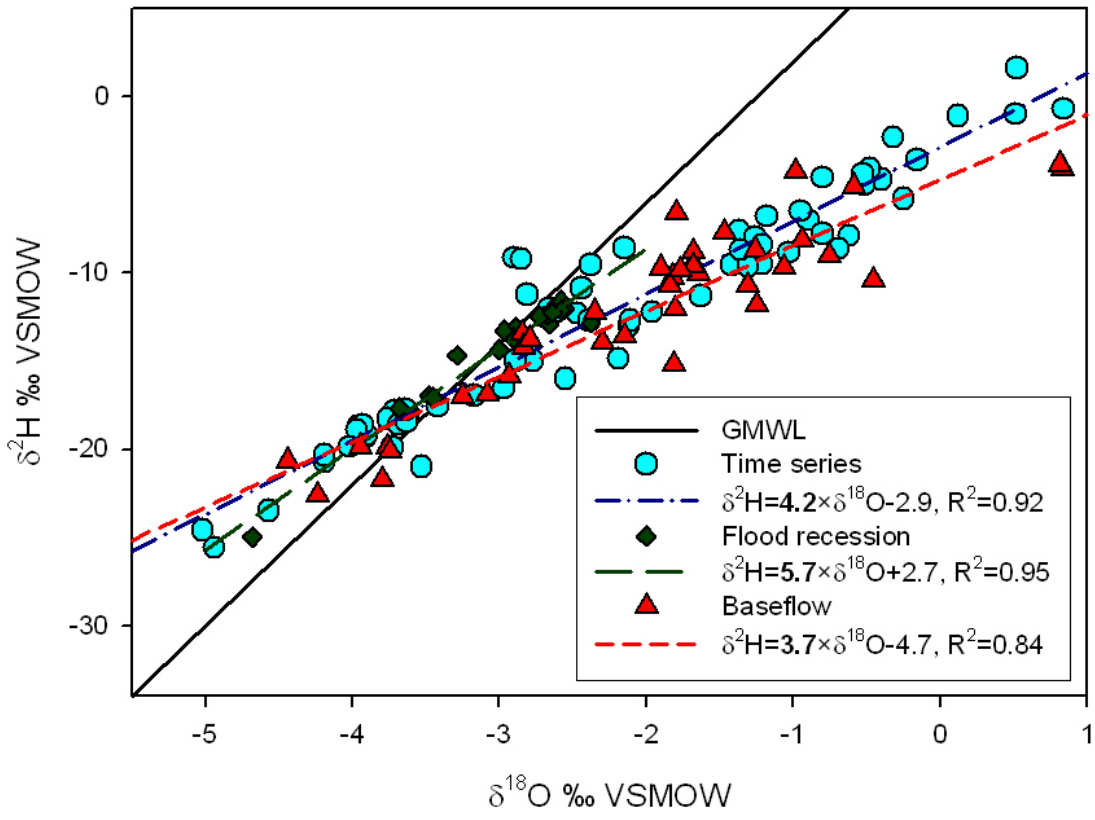

Figure 5.19 Surface water δ^2H-δ^{18}O evaporation lines for long-term "time series" sampling, and "snapshot" flood recession (Mar-01) and baseflow (Nov-01) sampling.

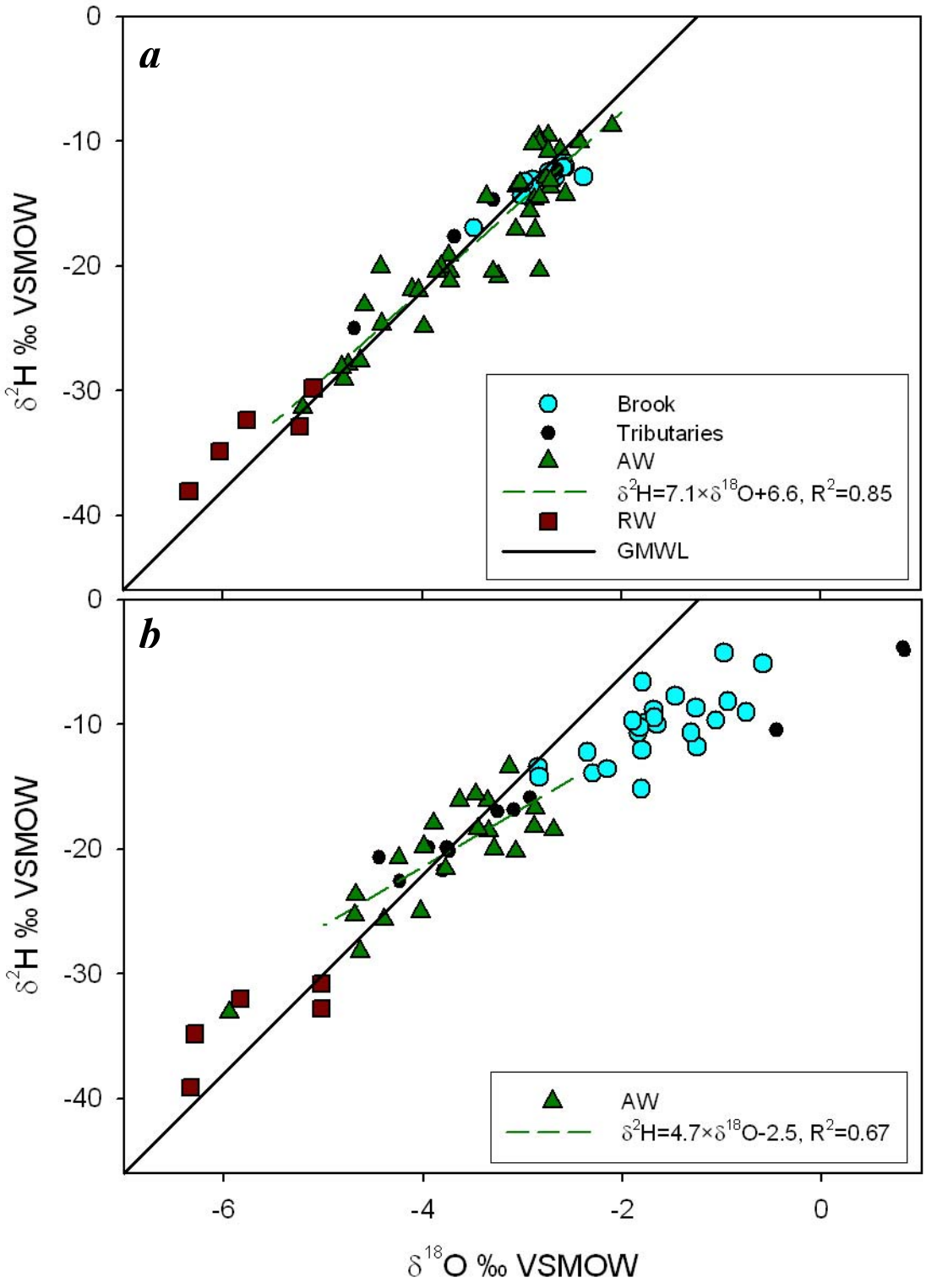

Figure 5.20 δ^2H-δ^{18}O signatures measured in alluvial groundwater (AW), regional groundwater (RW), the Wollombi Brook (Brook) and tributaries in relation to the Global Meteoric Water Line (GMWL) during (***a***) flood recession (Mar-01) and (***b***) baseflow (Nov-01) conditions. Dashed lines indicate alluvial groundwater evaporation lines.

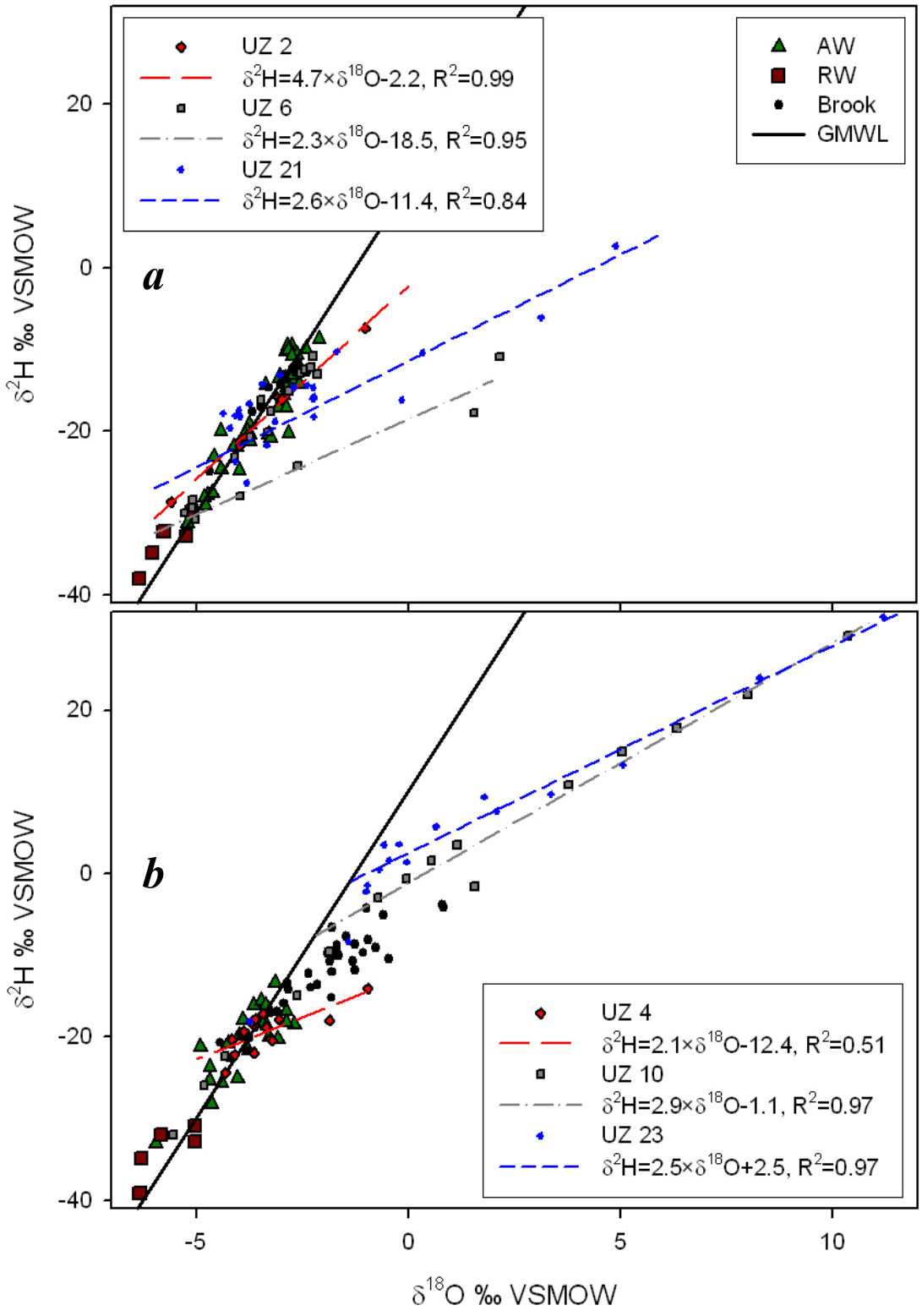

Figure 5.21 Unsaturated zone (UZ) δ^2H-$\delta^{18}O$ signatures compared to δ^2H-$\delta^{18}O$ signatures in the Wollombi Brook (Brook), alluvial groundwater (AW), regional groundwater (RW) and the Global Meteoric Water Line (GMWL) during (***a***) flood recession (Mar-01, located 2, 6 and 21 m from the stream channel) and (***b***) baseflow (Nov-01, located 4, 10 and 23 m from the stream channel) conditions.

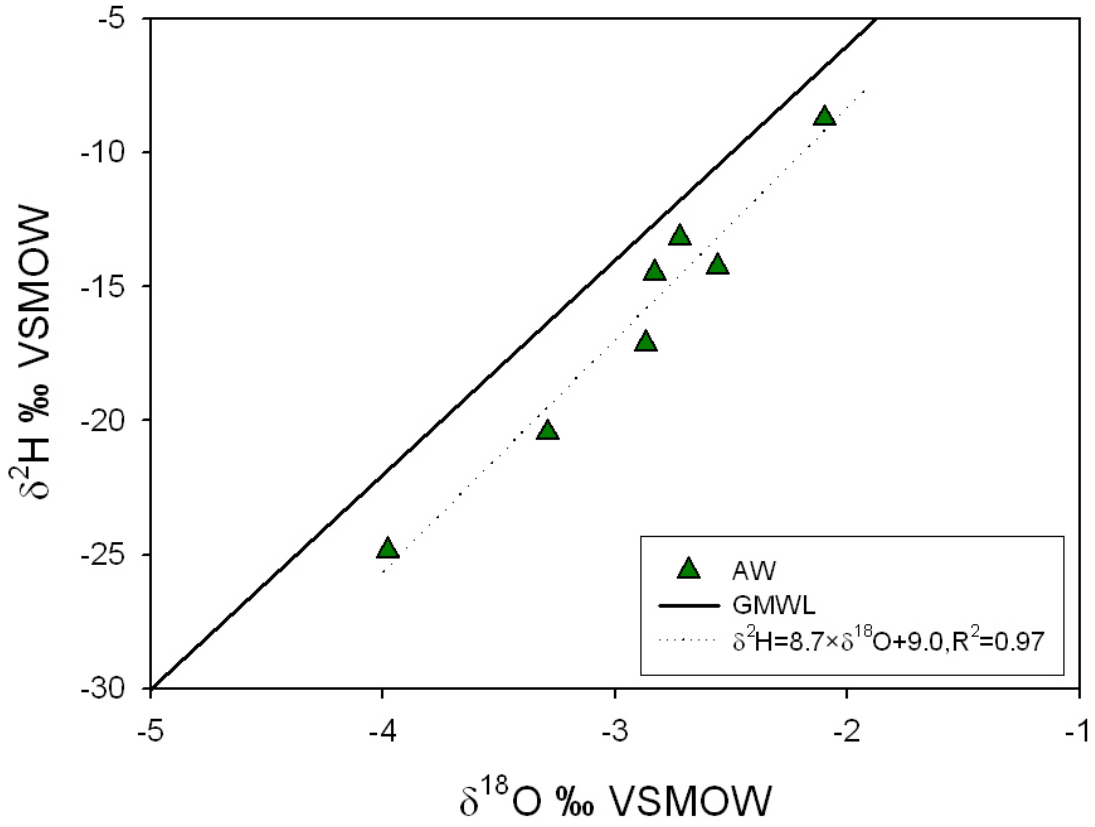

Figure 5.22 Alluvial groundwater (AW) δ^2H-$\delta^{18}O$ evaporation line at Fordwich (station site 3) during flood recession (Mar-01) in relation to the Global Meteoric Water Line (GMWL).

Alluvial groundwater discharge to stream flow was indicated by small decreases in the Cl^- concentration of stream water in the mid (63 km) and upper (74 km) Wollombi Brook (Mar-01, Figure 5.3). In addition, estimates of the initial ^{222}Rn concentration of groundwater that discharged to stream flow (C^{gw} , equation 5.12) indicated that alluvial groundwater discharged to the Wollombi Brook in the mid catchment (54 km and 63 km). Limited flood recession $^{87}Sr/^{86}Sr$ and Sr^{2+} data indicated that stream water $^{87}Sr/^{86}Sr$ and Sr^{2+} concentrations were similar to alluvial groundwater values and much higher than regional groundwater values (Figure 5.23***a***).

There was little evidence of regional groundwater discharge to stream flow during flood recession. Small increases in the Cl^- concentration of stream water in the mid

to upper (67 km) and lower (22 km) Wollombi Brook could potentially have been caused by regional groundwater discharge to stream flow (Mar-01, Figure 5.3). A $^{87}Sr/^{86}Sr$ and Sr^{2+} concentration mixing line constructed between surface water and regional groundwater end-members indicated that regional groundwater contributed a maximum of 4% of water to stream flow (Figure 5.23***a***). Time series data also indicated that there was potential for regional groundwater discharge to stream flow prior to flood recession sampling (Figure 5.18). However, alluvial groundwater discharge would equally explain the small increases in the Cl^- concentration of stream water.

Analysis of ^{222}Rn data showed that groundwater contributed to stream flow in all reaches of the Wollombi Brook during flood recession (section 4.5.2). Minimal changes in the Cl^- concentration (Figure 5.3) and δ^2H-$\delta^{18}O$ signature of stream water throughout the Wollombi Brook indicated that the major source of groundwater discharge to stream flow was alluvial groundwater and that a small component of alluvial groundwater was evaporated prior to discharge. Regional groundwater potentially contributed a minor component of stream discharge during flood recession (Mar-01).

5.4.3 Baseflow

High evaporative stream water loss was expected during baseflow conditions because stream discharge was low (in the order of 10^3 m^3 day^{-1}). However, the slope of the δ^2H-$\delta^{18}O$ evaporation line (m = 3.7, Figure 5.19) was lower than expected for evaporation from an open water channel (4 to 6, Allison *et al.* 1985), which indicated that there was a component of evaporated groundwater contributing to stream flow during baseflow conditions (Figure 5.13).

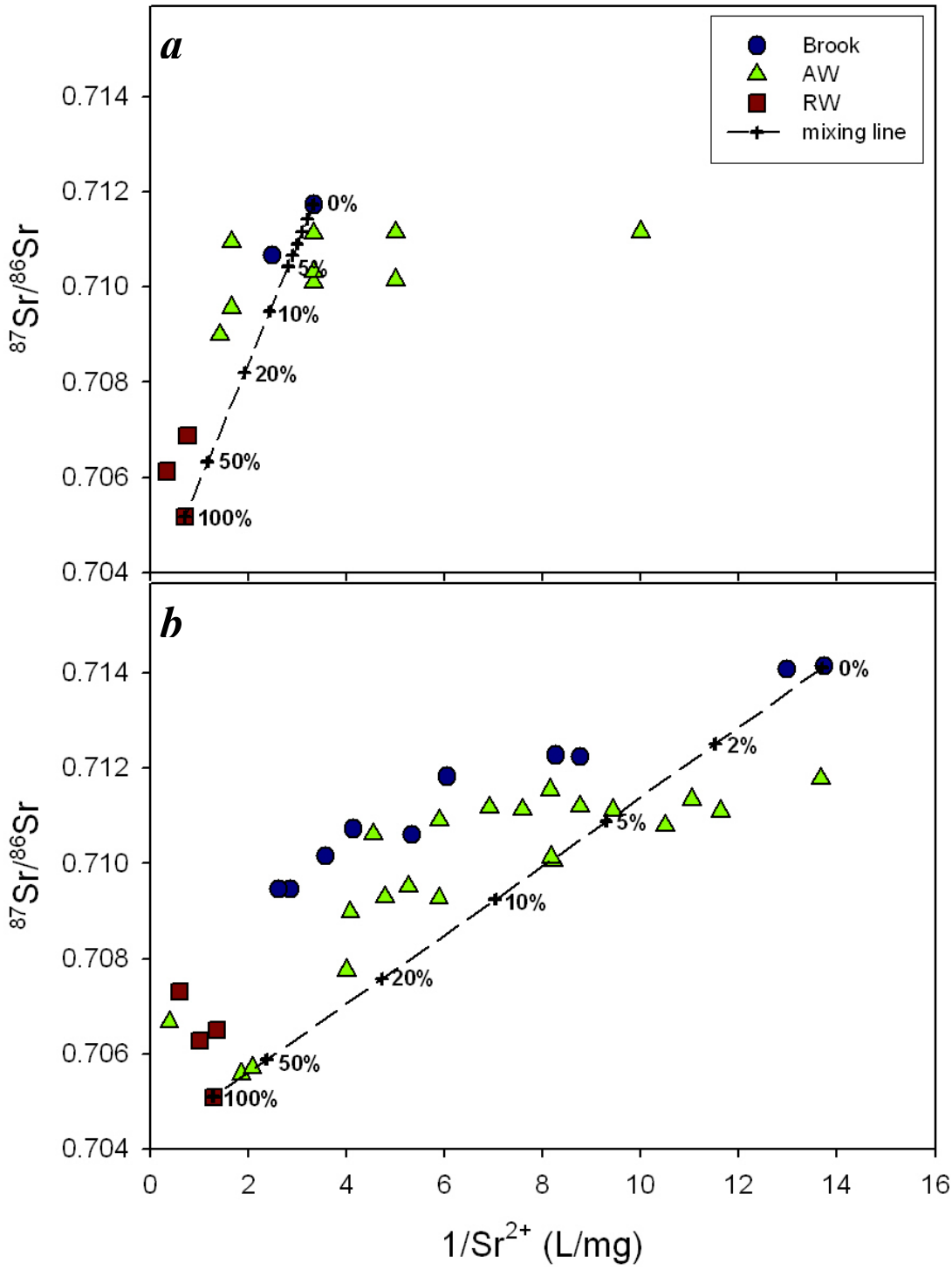

Figure 5.23 $^{87}Sr/^{86}Sr$ versus inverse Sr^{2+} concentration of stream water (Brook), alluvial groundwater (AW) and regional groundwater (RW) during (***a***) flood recession (Mar-01) and (***b***) baseflow (Nov-01) conditions. Theoretical mixing lines were constructed between stream water and regional groundwater end-members demonstrating potential percentages of regional groundwater discharge to stream flow.

Alluvial groundwater δ^2H-$\delta^{18}O$ signatures were distinctly lower and closer to the Global Meteoric Water Line (GMWL) than stream water in the Wollombi Brook (Figure 5.20***b***). Therefore alluvial groundwater discharge would typically shift the δ^2H-$\delta^{18}O$ signature of stream water toward the GMWL. The slope of the alluvial groundwater δ^2H-$\delta^{18}O$ evaporation line (m=4.7, poorly correlated R^2=0.67) was indicative of surface water evaporation suggesting that alluvial groundwater was recharged by evaporated surface water. Therefore, subsequent alluvial groundwater discharge would be expected to increase the δ^2H-$\delta^{18}O$ evaporation slope of stream water in the Wollombi Brook during baseflow. Since this was not the case, the δ^2H-$\delta^{18}O$ signature of alluvial groundwater sampled in the piezometer network was not exclusively representative of the alluvial groundwater that discharged to stream flow. Deep alluvial groundwater with relatively unevaporated δ^2H-$\delta^{18}O$ signatures was less likely to discharge to stream flow than shallower evaporated alluvial groundwater and potentially skewed the alluvial groundwater δ^2H-$\delta^{18}O$ slope upwards (Figure 5.20***b***). Evaporated surface water probably recharges the alluvial aquifer at some stages of the stream hydrograph (particularly when groundwater is pumped from the alluvial aquifer adjacent to the stream channel). However, the δ^2H-$\delta^{18}O$ evaporation slope of alluvial groundwater (recharged by evaporated surface water) was too high to cause the low δ^2H-$\delta^{18}O$ evaporation slope observed in the Wollombi Brook during baseflow conditions.

The baseflow (Mar-01) δ^2H-$\delta^{18}O$ evaporation slope of 3.7 in the Wollombi Brook is consistent with evaporation from unsaturated soils with dry surface layers of varying thicknesses (2.5 to 3.9) reported by Allison *et al.* (1983). Unsaturated zone soil water in the alluvial aquifer adjacent to the Wollombi Brook had strong evaporation signatures with δ^2H-$\delta^{18}O$ slopes ranging between 2.1 and 2.9 during baseflow conditions (Nov-01, Figure 5.21***b***). One unsaturated zone soil water δ^2H profile (where the depth to groundwater was approximately 0.8 m below the ground surface)

indicated that evaporation extended down to the capillary fringe during baseflow conditions (Figure 5.7***e***). Therefore, alluvial groundwater was potentially evaporated through shallow unsaturated sands during baseflow conditions. In another unsaturated zone soil profile (where the depth to groundwater was approximately 1.7 m below the ground surface) relatively low *d*-excess values beneath the evaporation front indicated downward movement of evaporated soil water during previous recharge events (Figure 5.8***f***). Therefore alluvial groundwater potentially develops an evaporated signature via downward leaching of evaporated soil water during recharge events. If alluvial groundwater that developed an evaporated δ^2H-$\delta^{18}O$ signature via (1) evaporation through the unsaturated zone, or (2) downward displacement of evaporated soil water during recharge events, discharged to stream flow and mixed with evaporated surface water, it would lower the δ^2H-$\delta^{18}O$ evaporation slope of stream water. Therefore, the low baseflow δ^2H-$\delta^{18}O$ evaporation slope in the Wollombi Brook can be explained by evaporated surface water mixing with evaporated alluvial groundwater discharge to stream flow.

Stream water $^{87}Sr/^{86}Sr$ in the Watagan and Southern branches of the Wollombi Brook were higher than values expected for rainfall (0.7087 to 0.7097) and higher than values measured in alluvial groundwater and regional groundwater (Figure 5.10). Sr^{2+} concentrations in the Watagan and Southern branches of the Wollombi Brook were higher than values measured in rainfall (Figure 5.16), but much lower than alluvial groundwater and regional groundwater values (Figure 5.9). Therefore stream water in the Watagan and Southern branches of the Wollombi Brook probably originated from a third aquifer-type that was not characterised by the piezometer or bore networks within the Wollombi catchment. In-stream $^{87}Sr/^{86}Sr$ data indicated that groundwater from a silicate aquifer (Faure and Powell 1972) with low Sr^{2+} lability or short residence times (i.e. allowing minimal Sr^{2+} dissolution) discharged into the Watagan and Southern branches of the Wollombi Brook.

Stream water $^{87}Sr/^{86}Sr$ within the main branch of the Wollombi Brook was lower and Sr^{2+} concentrations were higher than values in the Watagan and Southern branches of the Wollombi Brook (Figure 5.10). $^{87}Sr/^{86}Sr$ in the main branch of the Wollombi Brook and alluvial groundwater were similar, however, Sr^{2+} concentrations were marginally higher in stream water than alluvial groundwater (Figure 5.22***b***). This suggests that alluvial groundwater was the dominant source of water to the main branch of the Wollombi Brook and that evaporation increased the concentration of Sr^{2+} in stream water. Rainfall and subsequent evaporation could potentially produce similar $^{87}Sr/^{86}Sr$ and Sr^{2+} concentrations to those in the main branch of the Wollombi Brook. However, there were no rainfall generated surface flows at least three weeks prior to sampling (Figure 5.18).

Decreases in the Cl^- concentration of stream water indicated alluvial groundwater discharge to the lower (13 km) and mid to upper (60, 70 and 74 km) Wollombi Brook during baseflow (Nov-01, Figure 5.3). In addition, estimates of the initial ^{222}Rn concentration of groundwater that discharged to stream flow (C^{gw}, equation 5.12) indicated that alluvial groundwater discharged to the Wollombi Brook in the mid catchment (54 and 63 km).

Regional groundwater discharge to stream flow followed by evaporation could explain the $^{87}Sr/^{86}Sr$ and Sr^{2+} concentrations in the main branch of the Wollombi Brook (Figure 5.23***b***). Theoretical mixing between surface water and regional groundwater end-members indicated that regional groundwater contributed a maximum of 10% of water to stream flow. Decreases in $^{87}Sr/^{86}Sr$ (Figure 5.10) associated with sharp increases in the Cl^- concentration (Figure 5.3) and shifts in *d*-excess toward the GMWL (Figure 5.6) of stream water indicated potential for regional groundwater discharge to stream flow in the lower Wollombi Brook (0 and 33 km). Time series data also indicated that there was potential for regional

groundwater discharge to stream flow prior to baseflow sampling (Figure 5.18). However, alluvial groundwater discharge and subsequent evaporation within the stream channel could potentially cause similar changes in stream water $^{87}Sr/^{86}Sr$, Cl^- and *d*-excess signatures.

Based on ^{222}Rn data, groundwater discharged to stream flow in all reaches of the Wollombi Brook during baseflow (Nov-01, section 4.5.2). Even though there was significant evaporation of stream water directly from the stream channel, the low slope of the stream water δ^2H-$\delta^{18}O$ evaporation line (Figure 5.19) and the generally low Cl^- concentration of stream water (Figure 5.3) indicated that shallow alluvial groundwater was the major source of groundwater discharge to stream flow during baseflow conditions. However, regional groundwater potentially contributed a major proportion (up to 10%) of water to stream flow in some reaches of the Wollombi Brook during baseflow (Mar-01).

5.5 SPATIAL DISTRIBUTION OF ALLUVIAL GROUNDWATER AND REGIONAL GROUNDWATER CONTRIBUTIONS TO STREAM FLOW

The alluvial aquifer was absent in the upper-most reaches of the Wollombi Brook, but its depth and lateral extent were assumed to become progressively greater in the mid and lower reaches of the Wollombi Brook (Figure 5.24). The stream channel in the upper Wollombi Brook was assumed to be in direct contact with the regional aquifer. As the alluvial aquifer became progressively more extensive in the mid and lower reaches of the Wollombi Brook, it was assumed that the direct connection between the stream channel and regional aquifer may be less evident. Therefore, conceptually regional groundwater discharge dominates stream flow in the upper reaches of the Wollombi Brook whilst alluvial groundwater is the principal source of discharge to stream flow in the lower reaches of the Wollombi Brook.

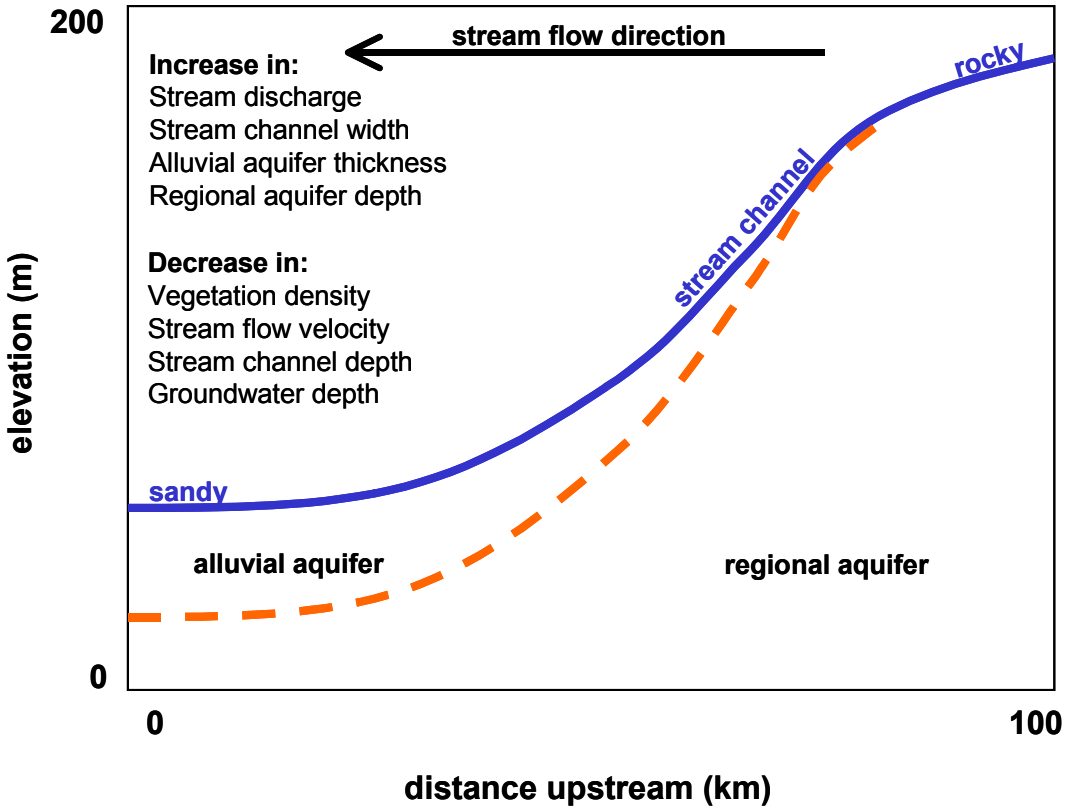

Figure 5.24 Conceptual diagram of changes in stream channel morphology and discharge characteristics from the upper to the lower Wollombi Brook. The bold line indicates the elevation of the stream channel and the dashed line represents the conceptual boundary between the alluvial and regional aquifers.

The generally low Cl^- concentrations in stream water indicated that alluvial groundwater was the dominant source of groundwater discharge to the Wollombi Brook during flood recession (Mar-01) and baseflow conditions (Nov-01, Figure 5.3). However, increases in the Cl^- concentration of stream water indicated potential for regional groundwater discharge to stream flow in the mid (67 km) and lower reaches (22 km) of the Wollombi Brook during flood recession and in the upper (86 km), mid (63 km) and lower (0, 22 and 33 km) reaches of the Wollombi Brook during baseflow.

Cl^- concentrations in stream water were lowest in the mid to lower (33 to 63 km) reaches of the Wollombi Brook during flood recession (Figure 5.3). Since minimal

surface water evaporation occurred during flood recession conditions, the proportion of alluvial groundwater to regional groundwater discharge was higher in the mid to lower reaches than in any other reaches of the Wollombi Brook. The Cl^- concentrations in stream water were similar in the upper (67 to 80 km) and the lower (0 to 22 km) Wollombi Brook. In the upper (74 to 81 km) and lower (0 to 38 km) Wollombi Brook *d*-excess was marginally lower than the Global Meteoric Water Line (GMWL) indicating that there was some evaporated water in the stream channel (Figure 5.6). However, the decrease in *d*-excess in the upper Wollombi Brook was associated with a decrease in Cl^- concentration indicating that the relatively low *d*-excess was caused by evaporated alluvial groundwater discharge to stream flow. Conversely, the increases in Cl^- concentration in the upper and lower Wollombi Brook coincided with an increase in *d*-excess indicating a regional groundwater contribution to stream flow. Further changes in *d*-excess in the lower Wollombi Brook were not associated with increases in Cl^- concentration indicating that both evaporated and unevaporated alluvial groundwater contributed to stream flow in the lower Wollombi Brook during flood recession.

During baseflow Cl^- concentrations were lowest in the mid reaches of the Wollombi Brook (56 to 67 km, Figure 5.3) indicating that either (1) much less surface water evaporation occurred from the mid reaches than in any other reaches of the Wollombi Brook, or (2) the mid region of the Wollombi Brook received a much higher ratio of alluvial groundwater to regional groundwater discharge than in any other location of the Wollombi Brook. Cl^- concentrations were generally highest in the lower Wollombi Brook (0 to 33 km) during baseflow conditions. Therefore, either (1) the evaporative concentration of Cl^-, or (2) the proportion of regional groundwater discharge to stream flow, was highest in the lower reaches than in any other part of the Wollombi Brook during baseflow conditions. Decreases in the Cl^- concentration of stream water indicated that alluvial groundwater contribution to

stream flow occurred in some reaches of the upper Wollombi Brook. The *d*-excess of stream water was generally higher in the mid to upper (54 to 86 km) than in the lower to mid (0 to 38 km) Wollombi Brook during baseflow (Figure 5.6). This indicated that stream water was typically less evaporated in the mid to upper than in the lower to mid Wollombi Brook. Therefore, a greater proportion of alluvial groundwater discharged to stream flow in the mid than the upper Wollombi Brook during baseflow. Furthermore, the high Cl^- concentrations in the upper Wollombi Brook were more likely to be associated with regional groundwater discharge to stream flow than the high Cl^- concentrations in the lower Wollombi Brook during baseflow. However, the decreases in $^{87}Sr/^{86}Sr$ associated with increases in Cl^- concentration of stream water pointed to regional groundwater discharge into the lower Wollombi Brook during baseflow conditions (Figure 5.10).

Cl^- concentrations were higher and *d*-excess values were lower in stream water during baseflow than flood recession. This is partially because greater evaporative concentration of Cl^- occurred in the Wollombi Brook during baseflow than flood recession. However, the large difference between baseflow and flood recession Cl^- concentrations may also be caused by higher relative proportions of regional groundwater discharge to stream flow during baseflow than flood recession conditions.

Alluvial groundwater and regional groundwater both contributed to stream flow in the upper and lower regions of the Wollombi Brook during baseflow and flood recession conditions. Alluvial groundwater was shown to discharge into the mid Wollombi Brook during both baseflow and flood recession conditions. There was no evidence of regional groundwater discharge into the mid Wollombi Brook during either baseflow or flood recession conditions. The ratio of alluvial groundwater to regional groundwater discharge to stream flow was higher in the mid than in the

upper Wollombi Brook during both flood recession and baseflow conditions. The ratio of alluvial groundwater to regional groundwater discharge to stream flow was also higher in the mid than in the lower Wollombi Brook during flood recession.

The relationship between alluvial groundwater and regional groundwater discharge to stream flow and the stream channel morphology is more complicated than the conceptual model proposed (Figure 5.24). Although the extent of the alluvial aquifer in the upper Wollombi Brook is relatively small (where it exists), it still provides a source of water to stream flow during baseflow and flood recession conditions. The mid Wollombi Brook appears to receive negligible regional groundwater, relying on alluvial groundwater to sustain stream flow. Both evaporated and non-evaporated sources of alluvial groundwater discharge to stream flow in the lower Wollombi Brook. Even though the alluvial aquifer is most extensive in the lower Wollombi catchment, there is still potential for regional groundwater to contribute to stream flow. A reach-scale approach (Chapter 6) gives a more detailed understanding of the relationships between stream channel morphology and sources of groundwater discharge to stream flow.

5.6 CONCLUSIONS

Because there were large differences between the Cl^- concentrations of alluvial groundwater and regional groundwater, changes in the Cl^- concentration of stream water (between surface water sampling stations or between sampling periods) gave a good indication of the source of groundwater discharge to stream flow unless significant surface water evaporation occurred. The slope of the δ^2H-$\delta^{18}O$ evaporation line between sampling intervals indicated whether increases in the Cl^- concentration of stream water were due to (1) evaporation within the stream channel, (2) discharge of evaporated alluvial groundwater, or (3) discharge of regional

groundwater to stream flow. Low estimates of the initial ^{222}Rn concentrations of groundwater that discharged to stream flow (equation 5.12) showed that only alluvial groundwater discharged to streamflow in some mid reaches of the Wollombi Brook. The $^{87}Sr/^{86}Sr$ of stream water indicated the aquifer-type from which groundwater discharge to stream flow was derived.

Alluvial groundwater was the dominant source of groundwater contributing to stream flow in the Wollombi Brook during flood recession (Mar-01), baseflow (Nov-01) and for the duration of weekly sampling in the mid to lower Wollombi Brook (Oct-00 to Jan-02, Figure 2.1). Alluvial groundwater often contained an evaporated δ^2H-$\delta^{18}O$ signature prior to discharge to the Wollombi Brook. Regional groundwater contributed to stream flow in the upper and lower regions of the Wollombi Brook during flood recession and potentially contributed to the upper and lower Wollombi Brook during baseflow conditions. A low Sr^{2+} concentration high $^{87}Sr/^{86}Sr$ silicate aquifer potentially discharged groundwater to stream flow in the Watagan and Southern branches of the Wollombi Brook.

The proportion of alluvial groundwater versus regional groundwater discharge was highest for the mid region of the Wollombi Brook during both flood recession and baseflow conditions. The ratio of alluvial groundwater to regional groundwater discharge was also higher in the mid than the lower Wollombi Brook during flood recession conditions.

Groundwater contributed to stream flow in the Wollombi Brook during the receding limb of all high stream discharge events throughout the long-term 'time series' sampling period (Oct-00 to Jan-02, Figure 5.17). Alluvial groundwater discharged into the upper, mid and lower regions of the Wollombi Brook during "snap-shot" flood recession (Mar-01) and baseflow (Nov-01) sampling and was the principal

source of groundwater discharge to stream flow in the mid catchment. Even though the alluvial aquifer was relatively narrow and shallow in the upper Wollombi Brook, it continued to contribute to stream flow during baseflow conditions (Nov-01).

The potential for regional groundwater discharge to the lower Wollombi Brook may be enhanced by ungauged alluvial groundwater pumping from spear-points adjacent to the stream channel. Such pumping causes local depressions in alluvial groundwater, which reduces alluvial groundwater discharge to the Wollombi Brook and increases hydraulic gradients between regional groundwater and the stream channel inducing regional groundwater flows toward the Wollombi Brook. Depletion of the "fresh" alluvial groundwater buffer zone will potentially reduce duration and frequency of stream flow and induce higher salinity groundwater discharge to the Wollombi Brook.

6 REACH-SCALE INTERPRETATION OF TRACER DATA

6.1 INTRODUCTION

This chapter describes a point-to-point interpretation of environmental tracer information for Wollombi Brook from the "headwaters" to its confluence with the Hunter River during flood recession (Mar-01, section 6.2) and baseflow (Nov-01, section 6.3) conditions. The purpose is to provide a rigorous methodology for the application and interpretation of in-stream tracers to infer subsurface pathways. This methodology has potential applications to low gradient systems where directions of surface water and groundwater exchange are indistinct and to surface water systems where surface water and groundwater information is unavailable.

Locations of alluvial groundwater and regional groundwater discharge to stream flow were identified by measuring major ion chemistry, ^{222}Rn, δ^2H & $\delta^{18}O$ and $^{87}Sr/^{86}Sr$ changes in stream water between consecutive sampling stations. Proportions of alluvial and regional groundwater discharge to stream flow were estimated by two component end-member mixing analyses of the major ion concentrations measured in consecutive stream water sampling stations (equation 6.1, Figure 6.1).

$$M = (C_1 \times f_1) + (C_2 \times f_2) \qquad \textbf{6.1}$$

M Tracer concentration (e.g. Cl^-) in stream water (mg L^{-1})

$C_{1,2}$ Tracer concentrations in surface water (C_1), and groundwater (C_2) that contribute to stream flow at M (mg L^{-1})

$f_{1,2}$ Fractions of surface water (f_1), and groundwater (f_2) that contribute to stream flow at M, where $f_2 = 1 - f_1$

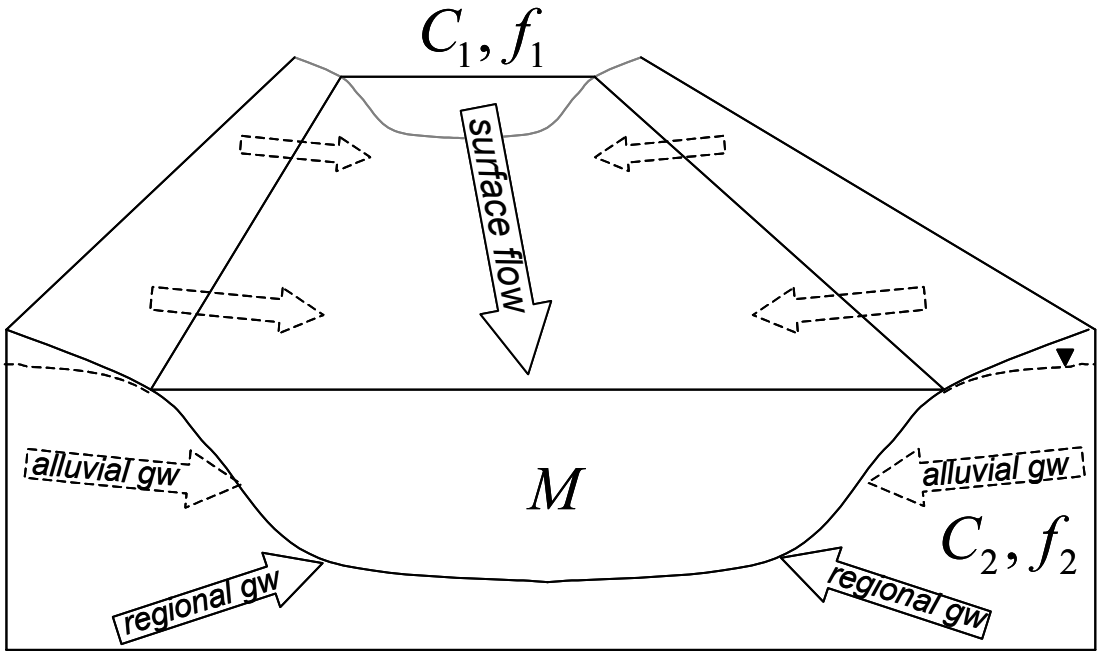

Figure 6.1 Schematic diagram of two-component end-member mixing. Stream water at M is a mixture of surface water and groundwater (alluvial and/or regional) inflows. The tracer concentration (M) results from the proportions (f) and the tracer concentrations (C) of surface water (C_1, f_1) and groundwater (C_2, f_2) contributions to stream flow.

Possible ranges of alluvial and regional groundwater discharge to stream flow were estimated (major ion chemistry, equation 6.1) assuming that only one groundwater source contributed to stream flow between consecutive sampling stations. However, it is likely that both alluvial and regional groundwater contributed to stream flow in some stream reaches of the Wollombi Brook. Therefore, maximum and minimum major ion concentrations measured in alluvial groundwater and regional groundwater were used in two component end-member analysis to give comprehensive ranges of the possible proportions of groundwater discharge to stream flow. Ranges of estimated groundwater contributions to stream flow for each measured chemical species are summarised in the appendices (Tables A.11 and A12).

Estimates of groundwater discharge to stream flow were calculated assuming that dissolution, precipitation and biogeochemical reactions did not affect the stream

water chemistry between consecutive sampling stations. Geochemical modelling (PHREEQC, Appendix B) indicated that neither stream water nor groundwater was supersaturated with respect to soluble minerals, including carbonates. Therefore, precipitation reactions were unlikely to occur within stream water. However, several of the major ion species analysed were likely to be involved in biogeochemical reactions within the stream channel, i.e. SO_4^{2-}, K^+ (e.g. Wetzel 2001) and $SiO_{2\,(aq)}$ (e.g. Miretzky and Cirelli 2004), and therefore were not used as primary evidence of groundwater discharge to stream flow.

6.2 FLOOD RECESSION

6.2.1 Stations 13 to 12

Between stations **13** and **12** (86 to 81 km, Figure 2.1), there was a small decrease in the ^{222}Rn concentration in stream water (from 0.16 to 0.15 Bq L^{-1}, Figure 5.4). However, the ^{222}Rn loss between stations 13 and 12 was less than that estimated to be caused by radioactive decay and gas exchange over the distance travelled (86 to 81 km, Figure 4.8***a***). The stream must have gained additional ^{222}Rn via groundwater discharge over this reach. Considering ^{222}Rn exchange between the stream and atmosphere, alluvial groundwater or regional groundwater potentially contributed between 3 and 100% of water to stream flow in this reach of the catchment.

The groundwater discharge was associated with a decrease in stream water alkalinity (Table A.2), which (excluding biogeochemical reactions) suggested an influx of between 19 and 100% alluvial groundwater (Table A.11). δ^2H and $\delta^{18}O$ increased (Figure 5.5) and *d*-excess decreased (Figure 5.6) over this reach indicating that stream water was subject to evaporation as it flowed from station 13 to 12. These evaporated δ^2H-$\delta^{18}O$ and *d*-excess signatures in stream water could either have been

caused by (1) evaporation from the open stream channel, or (2) the influx of alluvial groundwater with an evaporated signature.

The residence time of water within this reach of the stream channel was most probably too short to affect the δ^2H-δ^{18}O signature of stream water. Furthermore, the slope (m) of the δ^2H-δ^{18}O plot between stations 13 and 12 ($m = 2.3$, Figure 6.2) was lower than that expected for open water evaporation ($m = 3$ to 5, Clark and Fritz 1997). Therefore the most probable cause of the δ^2H and δ^{18}O increase in stream water between stations 13 and 12 was the influx of 3 to 100% alluvial groundwater.

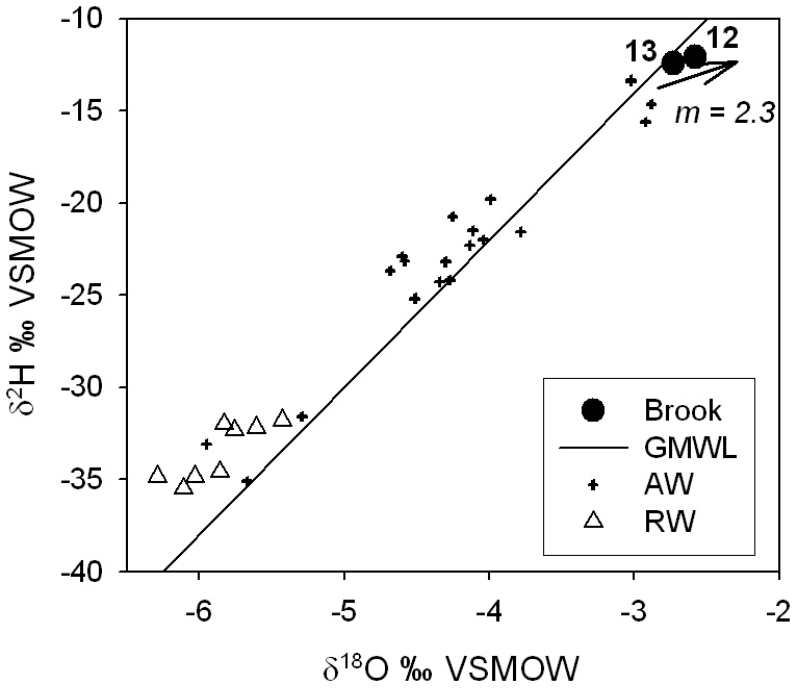

Figure 6.2 δ^2H and δ^{18}O (‰ VSMOW) composition of stream water (Brook), alluvial groundwater (AW) and regional groundwater (RW) in relation to the Global Meteoric Water Line (GMWL) during flood recession (Mar-01). The arrow indicates the direction of stream flow between stations 13 and 12. m is the slope of the evaporation line.

6.2.2 Stations 12 to 11

Discerning sources of water to stream flow between stations **12** and **11** (81 to 74 km) was complicated by discharge from three tributary streams (**T8**, **T9** and **T10**, Figure 2.1). Stream water between stations 12 and 11 was simultaneously diluted with respect to all major ions except alkalinity and $SiO_{2\,(aq)}$ (e.g. Cl^-, Figure 5.3, Table A.2). Measured dilutions between stations 12 and 11 could have been caused by:

1. Tributary "T8" contributing 28 to 100% of water to stream flow (based on changes in Cl^- concentration, Table A.11); or
2. Alluvial groundwater contributing 24 to 64% of water to stream flow (based on changes in Na^+ concentration, Table A.11); or
3. Lesser percentages of both "T8" and alluvial groundwater contributing to stream flow.

Regional groundwater discharge to stream flow would cause the Cl^-, and major cation concentrations to increase (rather than the measured decrease) between stations 12 and 11. Similarly, if tributaries "T9" and "T10" were the exclusive sources of additional water to the Wollombi Brook between stations 12 and 11 the salinity would have increased (rather than the measured decrease) in stream water. Therefore any regional groundwater, tributary "T9" or "T10" discharges to the Wollombi Brook between stations 12 and 11 (causing concentration of ions) must have been diluted by additional alluvial groundwater or tributary "T8" discharge.

The measured increases in alkalinity and $SiO_{2\,(aq)}$ concentrations in stream water between stations 12 and 11 could have been caused by alluvial groundwater contributing 60 to 100% (based on changes in $SiO_{2\,(aq)}$ concentration, Table A.11) to stream flow. The alkalinity concentrations in "T8" were too low to have caused the measured increase in the Wollombi Brook between station 12 and 11. However,

since stream water alkalinity does not always behave conservatively (e.g. increased stream water alkalinity due to calcite dissolution, Fairchild *et al.* 1999), this does not rule out "T8" as the major source of water to the Wollombi Brook.

Increased ^{222}Rn values between stations 12 and 11 (Figure 5.4), indicated there was an additional source of water contributing ^{222}Rn to stream flow. However, it was not obvious from the raw data whether this source of ^{222}Rn was from the tributary streams (T8, T9 and T10) or groundwater discharges to stream flow. Estimates of ^{222}Rn decay and gas exchange from stream water indicated that the concentrations of ^{222}Rn in the tributaries were too low to have caused the observed ^{222}Rn increase in between stations 12 and 11 (Table C.1). Therefore either alluvial groundwater contributed 5 to 100% or regional groundwater contributed 4 to 100% of water to stream flow.

Based on changes in the major ion chemistry of stream water, it is unlikely that regional groundwater contributed much, if any, water to stream flow between stations 12 and 11. Therefore, alluvial groundwater must have been the source of additional ^{222}Rn discharge to stream flow. Although tributaries "T8", "T9" and "T10" all contribute to stream flow within the Wollombi Brook, alluvial groundwater is most probably the dominant source contributing approximately 24 to 64% of water to stream flow between stations 12 and 11.

6.2.3 Stations 11 to 10

There were two tributary streams (**14** and **T6**) that flowed into the Wollombi Brook between stations **11** to **10** (Figure 2.1). However, neither of these tributaries could have caused the observed shift in δ^2H and δ^{18}O from station 11 to 10 without an additional source of non-evaporated groundwater discharging to stream flow (Figure

6.3). The shift in δ^2H and $\delta^{18}O$ suggested an alluvial rather than a regional groundwater contribution to stream flow. However, the Cl^- and Na^+ concentrations in alluvial groundwater were too low to have caused the observed in-stream increases between stations 11 and 10 (74 to 67 km, Figure 5.3). Furthermore, δ^2H and $\delta^{18}O$ indicated that stream water was not subjected to evaporation, therefore Cl^- and Na^+ ions were not evapo-concentrated within the stream channel. The measured increases in the Cl^- and Na^+ concentrations of stream water between stations 11 and 10 could only have been caused by 5 to 7% regional groundwater contribution (excluding inputs from all other potential sources of water discharge) to stream flow (Table A.11). Increases in SO_4^{2-} concentrations as water flowed downstream from station 11 to 10 also indicated regional groundwater discharge to stream flow, but in much higher proportions (32 to 100%, excluding biogeochemical reactions).

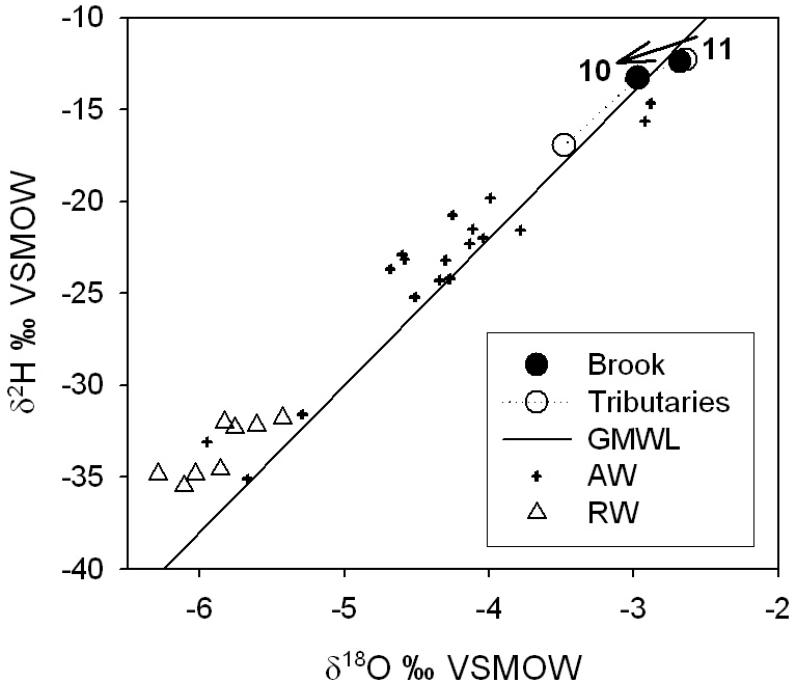

Figure 6.3 δ^2H and $\delta^{18}O$ (‰ VSMOW) composition of stream water (Brook) and tributaries, alluvial groundwater (AW) and regional groundwater (RW) in relation to the Global Meteoric Water Line (GMWL) during flood recession (Mar-01). The arrow indicates the direction of stream flow between stations 11 and 10.

Dilutions in stream water alkalinity from station 11 to 10 indicated that either:

1. Tributary "14" contributed 40% of water to stream flow; or
2. Alluvial groundwater discharged 25 to 100% to stream flow; or
3. Both tributary "14" and alluvial groundwater discharged smaller proportions of water stream flow.

If stream water at station 10 was comprised of up to 40% of water from tributary "14" or 25 to 100% alluvial groundwater, a maximum of 37% (by simple mass balance calculations, equation 6.1) regional groundwater contribution would be required to reproduce the measured Cl^- and Na^+ concentrations in stream water.

Regional groundwater discharge to the stream channel strongly influenced the stream water chemistry between sampling stations 11 and 10 in the Wollombi Brook, contributing 5 to 37% of water to stream flow. Alluvial groundwater potentially discharged into the stream channel, but its contribution could not be estimated because tributaries "14" and "T6" complicated the interpretation of the data set.

6.2.4 Stations 10 to 9

Lower major ion concentrations and negative shifts in the δ^2H and $\delta^{18}O$ composition of stream water (Table A.2) all indicated that alluvial groundwater discharged into the stream channel between stations **10** and **9**. Alluvial groundwater must contribute 55 to 100% (based on the change in Ca^{2+} concentration) of water to stream flow to satisfy the decrease in salinity between stations 10 and 9. The Ca^{2+}-based estimate of alluvial groundwater discharge to the stream channel is high, however the change in the Cl^- concentration (considered the least chemically reactive solute, e.g. Christophersen and Neal 1990) of stream water also indicated an alluvial groundwater dilution of 42 to 100%. None of the major ion tracers indicated regional groundwater discharge to the stream channel in this reach of the catchment.

There was a net decrease in the ^{222}Rn concentration in stream water between stations 10 and 9 (Table A.2). However, estimates of radioactive decay and exchange of ^{222}Rn within this reach indicated that 3 to 10% alluvial groundwater discharged to stream flow (Figure 4.11***a***). The alluvial groundwater discharge to stream flow estimate was based on steady state ^{222}Rn emanation from alluvial sands (4.6 Bq $^{-1}$, refer Chapter 4). However, during flood recession the residence time of alluvial groundwater may have been insufficient (<20 days, Hoehn and von Gunten 1989, Krishnaswami *et al.* 1982) to reach steady state ^{222}Rn concentrations. For example, if floodwater (e.g. ^{222}Rn < 0.2 Bq $^{-1}$) recharged the alluvial aquifer (completely displacing residual alluvial groundwater), it would acquire a ^{222}Rn concentration of 1.4 Bq L^{-1} after residence of approximately two days (equation 4.1). Coincidently, the minimum ^{222}Rn concentration measured in alluvial groundwater at Wollombi station (#10) was 1.4 Bq L^{-1} during flood recession. Substituting the steady state alluvial groundwater ^{222}Rn concentration (C_{ss}^{AGW} in equation 4.13, 4.6 Bq L^{-1}) with the non-steady state (1.4 Bq L^{-1}, two day residence) alluvial groundwater ^{222}Rn concentration, the estimate of alluvial groundwater discharge to stream flow is 3 to 36%. This is approaching the range of alluvial groundwater discharge percentages indicated by the major ion dilutions in stream water.

All measured environmental tracers indicated alluvial groundwater discharge to stream flow occurred between stations 10 and 9. The disparity between Cl$^-$ and ^{222}Rn estimates of the percentage of alluvial groundwater in stream flow suggested that floodwater had short residence times in the alluvial aquifer (in the order of a couple of days) before discharging into the stream channel between stations 10 and 9. Stream water was comprised of at least 42% alluvial groundwater that was discharged into the stream channel between stations 10 and 9 during flood recession.

6.2.5 Stations 9 to 8

There was very little change in stream water chemistry between stations **9** and **8** during flood recession (Table A.2). Minor increases and decreases in the major ion chemistry (excluding K^+ and $SiO_{2\,(aq)}$) could have been caused by 7 to 100% alluvial groundwater discharge to stream flow between stations 9 and 8 (Table A.11). The positive, non-evaporated shift in the δ^2H and $\delta^{18}O$ composition of stream water also indicated alluvial groundwater discharge to stream flow. There was no indication of regional groundwater discharge to stream flow within this reach of the Wollombi Brook.

There was a net decrease in ^{222}Rn concentration between stations 9 and 8, however, estimates of radioactive decay and the rate of gas exchange indicated that there was a small component of alluvial groundwater discharge to stream flow (up to 1.5%, Figure 4.11***a***). This estimate of alluvial groundwater discharge to stream flow was based on steady state ^{222}Rn concentrations in the alluvial aquifer (4.6 Bq^{-1}, refer Chapter 4) and was lower than estimates based on changes in salinity. Correcting the alluvial groundwater discharge estimate for non steady state ^{222}Rn concentrations (as between stations 10 and 9, section 6.2.4) yields an estimate of up to 5% alluvial groundwater discharge to stream flow. Incorporating potential error involved with estimates of radioactive decay and the rate of gas exchange yields an estimate of a maximum of 10% alluvial groundwater discharge to stream flow.

Alluvial groundwater discharge into the stream channel between sampling stations 9 and 8 comprised 7 to 10% of streamflow. The alluvial groundwater that discharged to stream flow between stations 9 and 8 during flood recession had a short residence time (in the order of days) in the alluvial aquifer prior to discharge.

6.2.6 Stations 8 to 7

There was very little change in stream water chemistry between sampling stations **8** and **7** (Table A.2). It is unlikely that regional groundwater discharged to stream flow because even a very small amount would have significantly increased the stream water TDS and Cl^- concentrations. The measured changes in stream water major ion chemistry can all be explained by 4 to 100% alluvial groundwater contribution to stream flow (Table A.11). The positive, non-evaporated shift in the δ^2H and $\delta^{18}O$ signature of stream water between stations 8 and 7 indicated that alluvial groundwater contributed to stream flow.

There was a net decrease in the ^{222}Rn concentration in stream water between stations 8 and 7 (60 to 54 km, Figure 5.4), however, estimates of ^{222}Rn loss via gas exchange and radioactive decay indicated that there was a source of groundwater contributing to stream flow (Figure 4.8***a***). Based on ^{222}Rn loss from stream water estimates either alluvial groundwater contributed up to 2% under steady state conditions, up to 7% under non-steady state conditions or regional groundwater contributed up to 13% of water to stream flow (Figure 4.11***a*** and 4.12***b***). Having established that alluvial groundwater discharged 4 to 100% of water to stream flow (via δ^2H, $\delta^{18}O$ and major ion chemistry), alluvial groundwater must not have reached steady state with respect to ^{222}Rn concentrations prior to discharge. Therefore the residence of water within the alluvial aquifer was short (in the order of a couple of days) between stations 8 and 7 during flood recession. An estimated 4 to 7% of stream flow was comprised of alluvial groundwater.

6.2.7 Stations 7 to 4

There was very little change in stream water chemistry between sampling stations **7** and **4** (Table A.2). TDS and Cl^- concentrations in stream water were slightly higher

at station 4 than station 7. A negative shift in the δ^2H and $\delta^{18}O$ signatures of stream water between stations **5** and **4** (38 and 33 km, Figure 5.5) indicated groundwater discharge to stream flow. However, the net positive shift in the δ^2H and $\delta^{18}O$ signature of stream water showed that evaporative processes dominated stream water chemistry between stations 7 and 4 (Figure 6.4). This made it difficult to identify and constrain groundwater discharges to stream flow by observation of major ion chemistry alone. However, it did indicate that if significant evapo-concentration of stream water occurred between stations 7 and 4, significant dilutions must also have occurred (due to the small change in stream water chemistry). Regional groundwater major ion chemistry concentrations were much higher than stream water concentrations (excluding SO_4^{2-}). As such, regional groundwater discharge to stream flow would not cause dilutions in stream water chemistry. Therefore any groundwater contribution to stream flow would have discharged from the alluvial aquifer system.

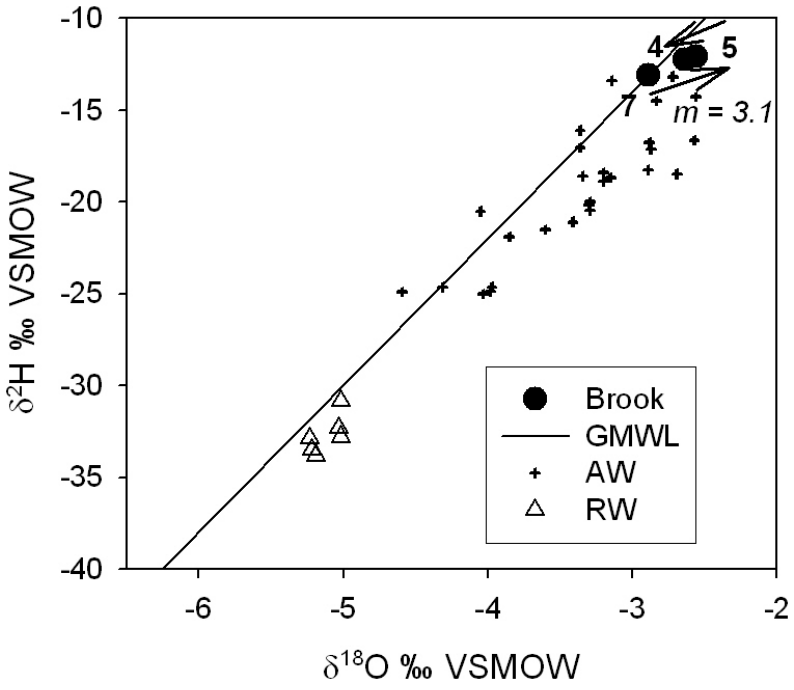

Figure 6.4 δ^2H and $\delta^{18}O$ (‰ VSMOW) values in stream water (Brook), alluvial groundwater (AW) and regional groundwater (RW) in relation to the Global Meteoric Water Line (GMWL) during flood recession (Mar-01). Arrows indicate the direction of stream flow between stations 7, 5 and 4. *m* is the slope of the evaporation line.

The ^{222}Rn concentration in stream water decreased between consecutive down-gradient surface water sampling stations 7 through to 4. However, estimated ^{222}Rn losses from stream water showed that there was a component of groundwater contributing to stream flow between stations 7, 5 and 4. Assuming that alluvial groundwater had reached steady state conditions prior to discharge into the stream channel, stream water was comprised of 2 to 34% alluvial groundwater between stations 7 and 5, and 2 to 89% alluvial groundwater between stations 5 and 4.

6.2.8 Stations 4 to 3

Significant increases in major ion concentrations (excluding K^+ and $SiO_{2\,(aq)}$) occurred in stream water between stations **4** and **3** (Table A.2, i.e. 33 to 22 km, Figure 5.3). The increased concentrations could all potentially have been caused by (1) surface water inflow from tributary "T2", (2) evapo-concentration, (3) alluvial groundwater discharge to stream flow, or (4) regional groundwater discharge to stream flow. However, it was believed that tributary "T2" had ceased flowing into the Wollombi Brook at the time of sampling (Mar-01).

Both δ^2H and $\delta^{18}O$ values increased between stations 4 and 3. However, the shift was toward the Global Meteoric Water Line (Figure 6.5) suggesting that even though stream water was affected by evaporative processes there was also a component of groundwater discharge to stream flow within the reach. Both δ^2H and $\delta^{18}O$ values increased in stream water between stations 4 and 3, and because regional groundwater values were typically much lower than alluvial groundwater values, it seems most probable that the source of groundwater discharge was from the alluvial aquifer system.

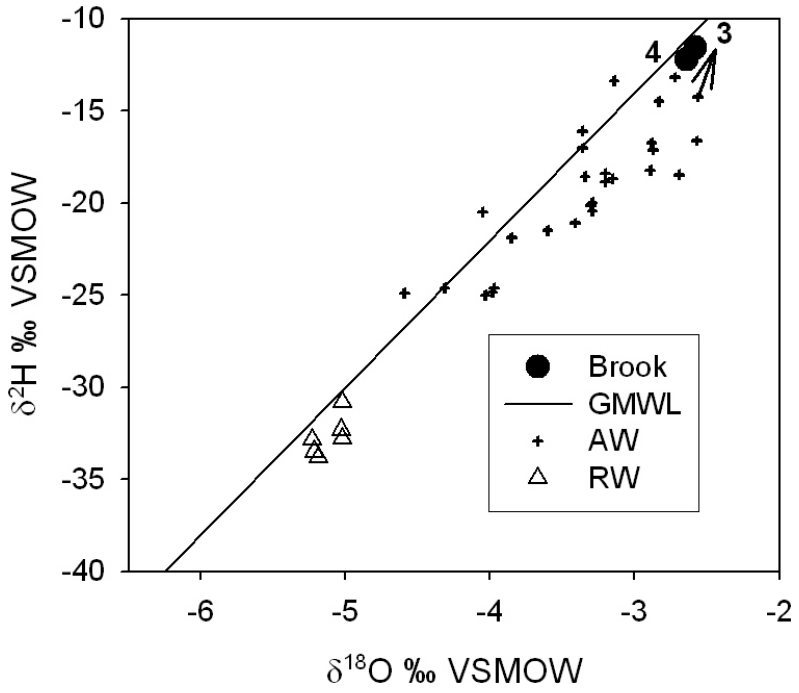

Figure 6.5 δ^2H and $\delta^{18}O$ (‰ VSMOW) values in stream water (Brook), alluvial groundwater (AW) and regional groundwater (RW) in relation to the Global Meteoric Water Line (GMWL) during flood recession (Mar-01). The arrow indicates the direction of stream flow between stations 4 and 3.

The ^{222}Rn concentration increased in stream water between stations 4 and 3, which supported the interpretation that there was a component of groundwater discharge to stream flow. However, estimates of the possible range of proportions of groundwater discharge to stream flow (after correcting for ^{222}Rn gas exchange and decay) between stations 4 and 3 (33 and 22 km, Figure 4.11***a***) were broad (2 to 100% alluvial groundwater or 1 to 100% regional groundwater).

The shift in stream water δ^2H and $\delta^{18}O$ values suggested an alluvial groundwater source of water to stream flow between stations 4 and 3. However, there was insufficient difference between measured stream water and groundwater chemistry to differentiate between alluvial and regional groundwater sources. Estimates based on Cl^- two component end-member mixing analysis indicated that either alluvial

groundwater contributed 7 to 100% of water to stream flow or regional groundwater discharged up to 6% of water to stream flow (Table A.11).

6.2.9 Stations 3 to 2

Increases in major ion concentrations (excluding SO_4^{2-}) and ^{222}Rn (22 to 13 km, Figure 5.4) occurred in stream water between stations **3** and **2** (Table A.2), however, the Cl^- concentration remained constant (Figure 5.3). A small tributary "**T1**" discharged into the Wollombi Brook in between stations 3 and 2. The concentration of all measured major ions (with the exception of alkalinity and $SiO_{2\,(aq)}$) were lower in tributary "T1" water than in stream water at stations 3 and 2 (Table A.2).

δ^2H decreased and $\delta^{18}O$ increased in stream water between stations 3 and 2 (Figure 6.6). The shift in the δ^2H and $\delta^{18}O$ signature of stream water between stations 3 and 2 was caused by either (1) mixing with water from tributary "T1" coupled with evaporation or (2) groundwater discharge to stream flow and evaporation. Major ion concentrations (excluding alkalinity, SO_4^{2-} and $SiO_{2\,(aq)}$) in "T1" were all too low to cause the increases in stream water concentration observed between stations 3 and 2. Evaporation could potentially have caused the increases in concentration, however stream water residence times within the stream channel were probably too short during flood recession (Mar-01) for significant evapo-concentration of major ions to have occurred.

Accounting for ^{222}Rn losses between stations 3 and 2, the ^{222}Rn activity of "T1" was too low to have caused the increase in ^{222}Rn activity in this reach of the catchment (Table C.1). The changes in ^{222}Rn activity showed that either alluvial groundwater contributed 4 to 100% or regional groundwater contributed 1 to 100% of water to stream flow (13 km, Figure 4.9).

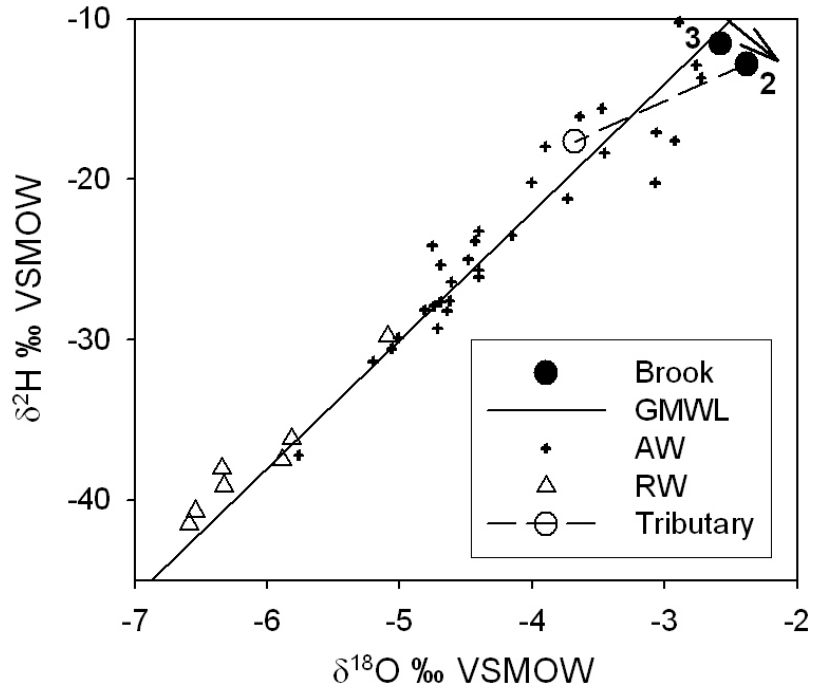

Figure 6.6 δ^2H and $\delta^{18}O$ (‰ VSMOW) values in stream water (Brook), tributary "T1", alluvial groundwater (AW) and regional groundwater (RW) in relation to the Global Meteoric Water Line (GMWL) during flood recession (Mar-01). The arrow indicates the direction of stream flow between stations 3 and 2.

The change in stream water $^{87}Sr/^{86}Sr$ versus $1/Sr^{2+}$ relationship showed that there was a component of groundwater discharge to stream flow between sampling stations 3 and 1 (Figure 6.7). The $^{87}Sr/^{86}Sr$ and $1/Sr^{2+}$ signature of stream water was very similar to the alluvial groundwater signature. However, theoretical end-member mixing analysis showed that the change in stream water $^{87}Sr/^{86}Sr$ and $1/Sr^{2+}$ signature between stations 3 and 1 could have been caused by (1) approximately 20% alluvial groundwater discharge (Figure 6.7***a***), or (2) approximately 3% regional groundwater discharge to stream flow (Figure 6.7***b***).

Changes in stream water chemistry between stations 3 and 2 was most likely caused by 8 to 20% alluvial groundwater discharge to stream flow. The estimates of regional groundwater discharge to stream flow between stations 3 and 2 were inconsistent between the chemical species, indicating that regional groundwater was

unlikely to contribute water to stream flow in this part of the catchment during flood recession.

6.2.10 Stations 2 to 1

There was very little change in stream water chemistry between sampling stations **2** and **1** (Table A.2). The Cl^- concentration in stream water remained constant as water flowed downstream (13 to 0 km, Figure 5.3). This tends to indicate a lack of groundwater contribution to stream flow. However, all changes in the major ion concentrations (excluding SO_4^{2-}, K^+ and $SiO_{2\,(aq)}$) of stream water could be explained by 6 to 100% alluvial groundwater discharge to stream flow (Table A.11).

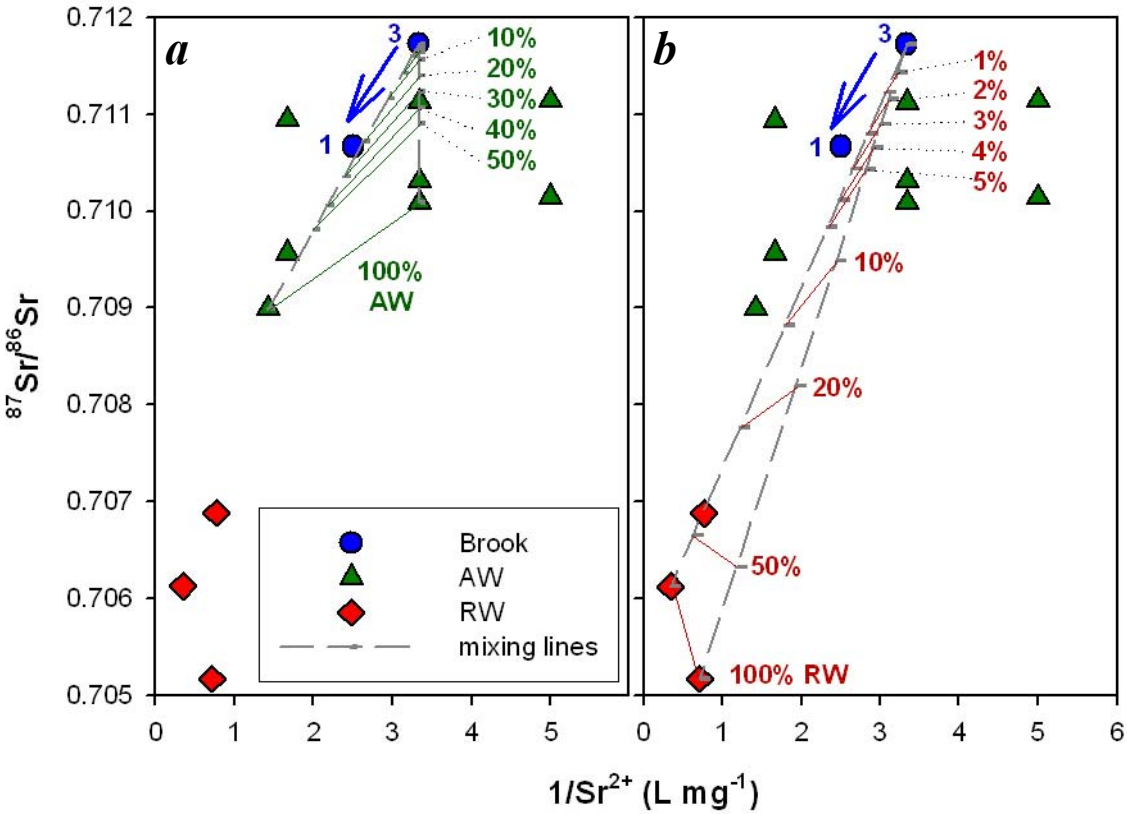

Figure 6.7 Changes in the strontium isotope ratio ($^{87}Sr/^{86}Sr$) and inverse strontium concentration ($1/Sr^{2+}$, L mg^{-1}) in the Wollombi Brook between stream water sampling stations 3 and 1 in comparison to alluvial groundwater (AW) and regional groundwater (RW) values during flood recession (Mar-01). Arrows indicate stream flow direction. Theoretical mixing lines were constructed between stream water at sampling station 3 and (***a***) alluvial groundwater, and (***b***) regional groundwater, to estimate the potential proportions of groundwater discharge to stream flow between stations 3 and 1.

An increase in the ^{222}Rn concentration of stream water indicated that there was a component of groundwater discharging to the stream channel. Estimates of ^{222}Rn loss from stream water indicated that there was either an alluvial groundwater contribution of 4 to 100% or a regional groundwater contribution of 1 to 100% to stream flow (Figure 4.9). However, a regional groundwater contribution to stream flow between stations 2 and 1 is highly unlikely. Even as little as 1% regional groundwater discharge would increase the Cl^- concentration in stream water. Furthermore, both δ^2H and $\delta^{18}O$ values decreased in stream water between stations 2 and 1, making a large shift toward the Global Meteoric Water Line (Figure 6.8). The shift in the δ^2H and $\delta^{18}O$ signature of stream water was very similar to the δ^2H and $\delta^{18}O$ signature of alluvial groundwater measured at site 1.

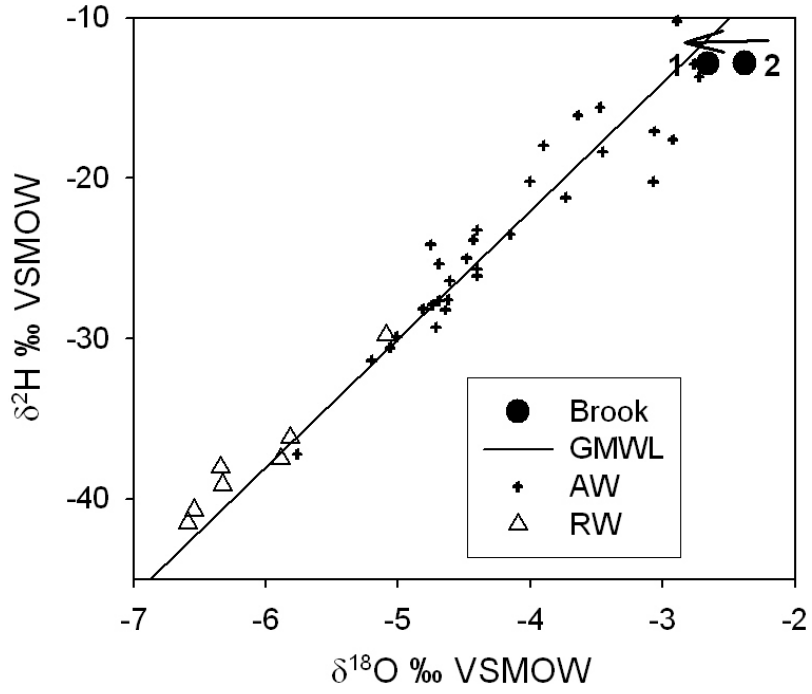

Figure 6.8 δ^2H and $\delta^{18}O$ (‰ VSMOW) values in stream water (Brook), alluvial groundwater (AW) and regional groundwater (RW) in relation to the Global Meteoric Water Line (GMWL) during flood recession (Mar-01). The arrow indicates the direction of stream flow between stations 2 and 1.

The $^{87}Sr/^{86}Sr$ and $1/Sr^{2+}$ signature of stream water indicated that alluvial groundwater comprised approximately 20% of stream flow between stations 3 and 1 (as per explanation section 6.2.9, Figure 6.7). Therefore 6 to 20% alluvial groundwater discharged to stream flow between stations 2 and 1 during flood recession.

6.3 BASEFLOW

6.3.1 Stations 13 to 12

Major ion concentrations increased significantly in stream water between sampling stations **13** and **12** (Table A.4, i.e. 86 to 81 km, Figure 5.3). Alluvial groundwater major ion concentrations (excluding $SiO_{2\,(aq)}$) were much lower than stream water concentrations during baseflow in the upper catchment. Therefore, alluvial groundwater discharge would have caused significant decreases in the salinity of stream water. Increases in the major ion concentrations in stream water could potentially have been caused by either (1) evapo-concentration, or (2) regional groundwater contributions to stream flow. Based on Cl^- two-component end-member mixing estimates, regional groundwater contributed 22 to 92% of water to stream flow (Table A.12). If alluvial groundwater discharged into the stream channel (diluting the chemical concentrations in stream water), additional regional groundwater discharge (i.e. higher than the estimated range 22 – 92%) would be required to generate the major ion concentrations measured in stream water.

The increase in the ^{222}Rn concentration of stream water as it flowed downstream (86 to 81 km, Figure 5.4) indicated that there was a component of groundwater discharge to stream flow. Estimates of ^{222}Rn loss indicated that either alluvial groundwater contributed 4 to 100% or regional groundwater contributed 3 to 100% of water to stream flow (Figure 4.9).

The $\delta^{18}O$ value in stream water increased in between stations 13 and 12 indicating that stream water was affected by evaporative process during baseflow (86 to 81 km, Figure 5.5***a***). However, $\delta^{2}H$ decreased in stream water between stations 13 and 12 indicating that there was also a component of groundwater discharge to stream flow (Figure 5.5***b***). The shift in the $\delta^{2}H$ and $\delta^{18}O$ signature of stream water between stations 13 and 12 could have been caused by either alluvial or regional groundwater discharge to stream flow followed by evaporation within the stream channel (Figure 6.9).

Alluvial groundwater strontium isotope ratios (0.7112 to 0.7118) were too high to cause the large $^{87}Sr/^{86}Sr$ decrease in stream water between stations 13 (0.7118) and 11 (0.7106, Figure 6.10). Only regional groundwater discharge to stream flow could have caused the large measured $^{87}Sr/^{86}Sr$ decrease in stream water.

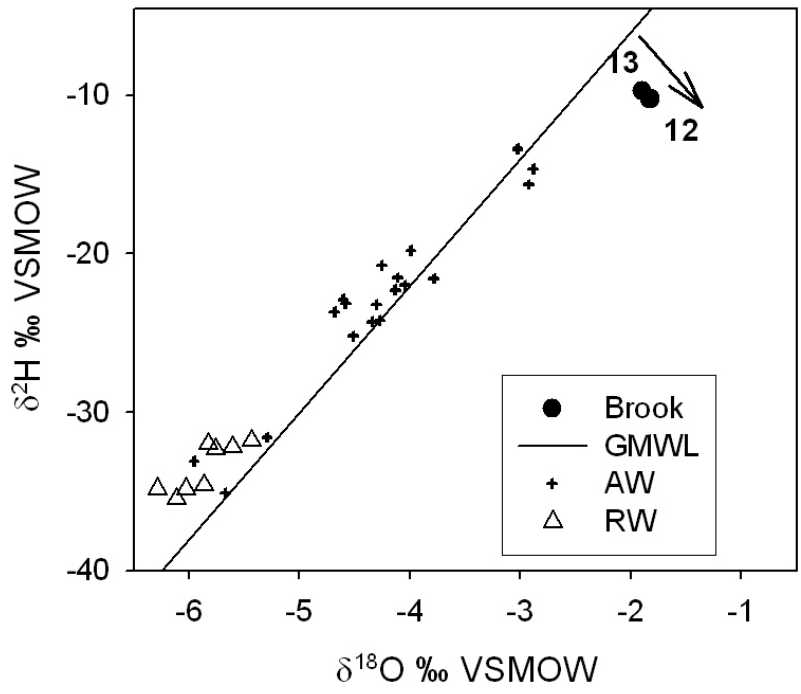

Figure 6.9 $\delta^{2}H$ and $\delta^{18}O$ (‰ VSMOW) values in stream water (Brook), alluvial groundwater (AW) and regional groundwater (RW) in relation to the Global Meteoric Water Line (GMWL) during baseflow (Nov-01). The arrow indicates the direction of stream flow between stations 13 and 12.

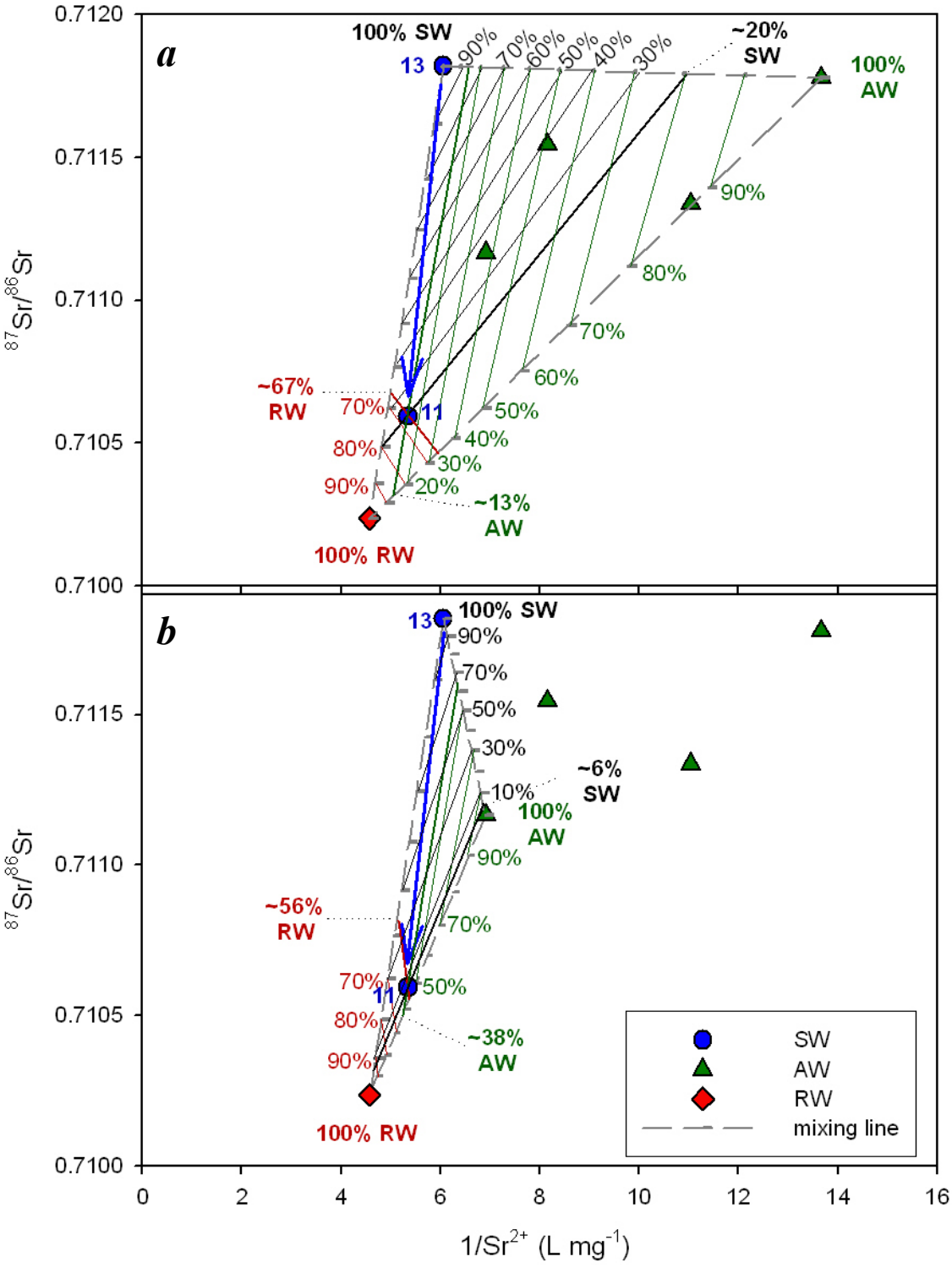

Figure 6.10 Change in $^{87}Sr/^{86}Sr$ and inverse Sr^{2+} concentration of stream water (SW) in between stations 13 and 11 (arrow indicates stream flow direction) compared to alluvial groundwater (AW) and regional groundwater (RW) values. Theoretical mixing lines were constructed between SW at station 13, RW and (***a***) maximum AW, and (***b***) minimum AW to estimate the proportions of each water source present in stream water at sampling station 11.

Proportions of the potential sources of water to stream flow at station 11 were estimated by constructing theoretical $^{87}Sr/^{86}Sr$ and inverse Sr^{2+} mixing lines and three component end-member mixing calculations (equation 6.2, Figure 6.11) between stream water (at station 13), alluvial groundwater and regional groundwater end-members (Figure 6.10).

$$(R_m \times C_m) = (R_1 \times C_1 \times f_1) + (R_2 \times C_2 \times f_2) + (R_3 \times C_3 \times f_3) \qquad \textbf{6.2}$$

$R_{1,2,3,m}$ $^{87}Sr/^{86}Sr$ of surface water (R_1), alluvial groundwater (R_2) and regional groundwater (R_3) that contribute to stream flow (at m)

$C_{1,2,3,m}$ Sr^{2+} concentrations in surface water (C_1), alluvial groundwater (C_2) and regional groundwater (C_3) that contribute to stream flow (at m) (mg L^{-1})

$f_{1,2,3}$ Fractions of surface water (f_1), alluvial groundwater (f_2) and regional groundwater (f_3) that contribute to stream flow (at m)

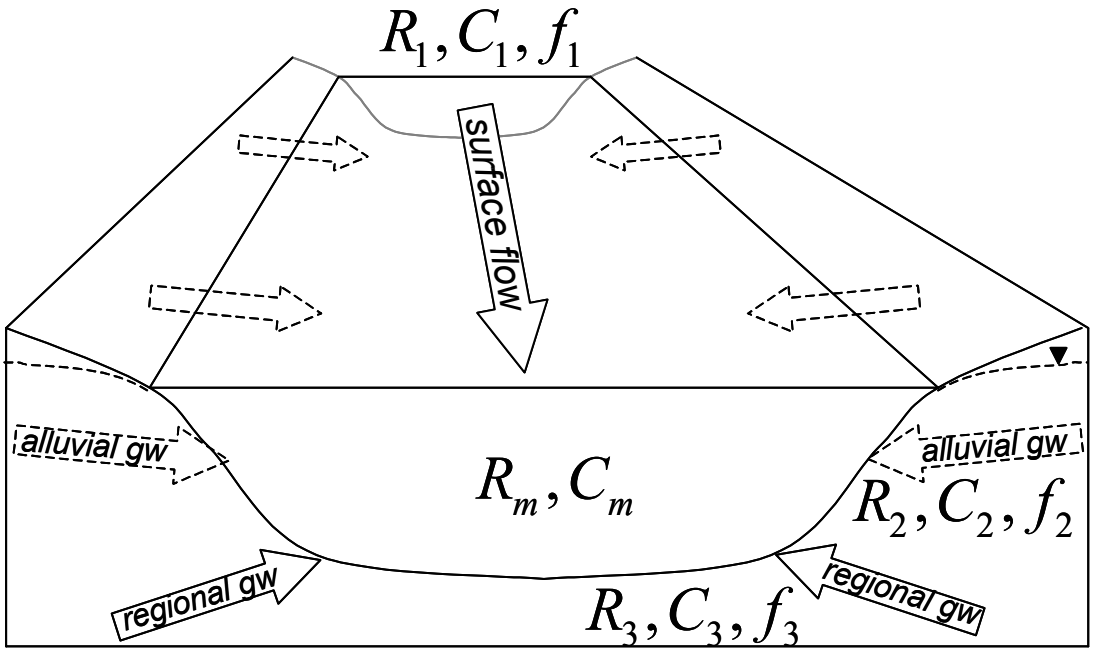

Figure 6.11 Schematic diagram of three-component end-member mixing. Stream water is a mixture of surface water, alluvial groundwater and regional groundwater inflows. The $^{87}Sr/^{86}Sr$ and Sr^{2+} concentration in stream water (R_m, C_m) results from the proportions (f), the $^{87}Sr/^{86}Sr$ (R), and Sr^{2+} concentrations (C) of surface water (R_1, C_1, f_1), alluvial groundwater (R_2, C_2, f_2) and regional groundwater (R_3, C_3, f_3) contributions to stream flow.

Figure 6.10 indicated that stream water at station 11 was comprised of 6 to 20% surface water from station 13, 13 to 38% alluvial groundwater and 56 to 67% regional groundwater. Since there was limited strontium isotope data, discharge points were not obvious from $^{87}Sr/^{86}Sr$ data alone. However, changes in the Cl^-, δ^2H and $\delta^{18}O$ signatures of stream water indicated that (1) alluvial groundwater discharged up to 39% of water to stream flow between stations **12** and **11** (refer to section 6.3.2), and (2) regional groundwater did not enter the stream channel via any of the tributaries (**T8**, **T9** or **T10**) or discharge directly into the stream channel between stations **12** and **11** (refer to section 6.3.2). Therefore alluvial groundwater contributed up to 38% of water to stream flow and regional groundwater discharge only occurred between stations 13 and 12. Stream water at station 12 was comprised of up to 44% stream water from station 13, up to 38% alluvial groundwater and 56 to 67% regional groundwater.

6.3.2 Stations 12 to 11

Decreases in major ion and Sr^{2+} concentrations (excluding SO_4^{2-}) in stream water between stations **12** and **11** (81 to 74 km, Figure 5.3, Figure 5.9, Table A.4) could have been caused by either alluvial groundwater or tributary '**T8'** contributions to stream flow. Two additional tributary streams ('**T9**' and '**T10**') also flowed into the Wollombi Brook during the sampling period. However, the alkalinity, $Mg^{2+}$and Sr^{2+} concentrations were too high in both T9 and T10 to have caused the observed dilutions in stream water concentrations between stations 12 and 11. In addition Ca^{2+}, K^+ and $SiO_{2\,(aq)}$ concentrations were also too high in T10 to have caused the observed dilutions in stream water concentrations. Regional groundwater discharge to stream flow would have increased the concentrations of all the aforementioned chemical constituents in stream water between stations 12 and 11.

Estimated proportions of the potential sources of water discharge to stream flow based on changes in stream water chemistry, were highly variable probably owing to the non-conservative behaviour of many of the ions (Table A.12). Since Cl^- is considered the most conservative ion amongst these, the dilution in stream water chemistry between stations 12 and 11 was caused by either (1) 36 to 39% alluvial groundwater discharge, (2) T8 contributing 37 to 100%, (3) T9 contributing 47 to 100%, (4) T10 contributing 69 to 100% of water to stream flow. The reality was probably a lesser proportion of alluvial groundwater, T8, T9 and T10 all contributing to stream flow.

The ^{222}Rn concentration increased in stream water indicating that there was a component of groundwater discharge to stream flow in between stations 12 and 11. The ^{222}Rn concentrations in tributaries T8 (0.6 Bq L^{-1}) and T9 (3.9 Bq L^{-1}) were high, but not high enough to have caused the observed increases in ^{222}Rn concentration in stream water between stations 12 and 11 (Table C.2). Therefore stream water was comprised of either 7 to 100% alluvial groundwater or 6 to 100% regional groundwater that discharged directly into the Wollombi Brook through stream bank discharge in between stations 12 and 11 (Figures 4.11***b*** and 4.12***b***).

Both δ^2H and $\delta^{18}O$ values increased in stream water between stations 12 and 11 indicating that evaporation was a significant process within this reach of the catchment (Figure 6.12). Water in T10 was highly evaporated, however, water in both T8 and T9 had relatively unevaporated signatures that were very similar to alluvial groundwater values. Since evapo-concentration was likely to be a significant process, additional alluvial groundwater discharge (i.e. 36 to 100%) or tributary dilution would be required to reproduce the dilution in stream water chemistry measured between stations 12 and 11.

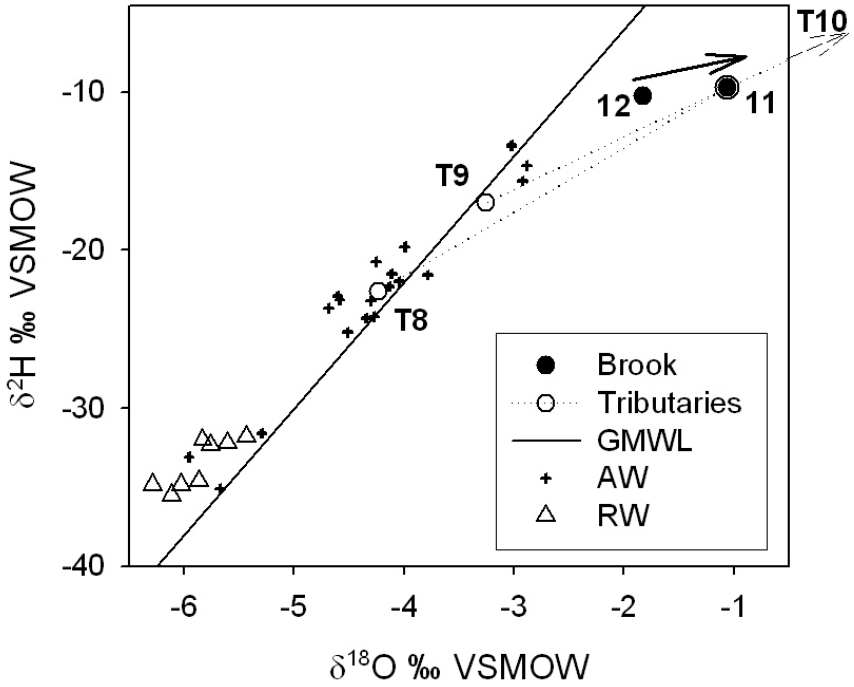

Figure 6.12 δ^2H and $\delta^{18}O$ (‰ VSMOW) values in stream water (Brook), tributaries (T8, T9 and T10) alluvial groundwater (AW) and regional groundwater (RW) in relation to the Global Meteoric Water Line (GMWL) during baseflow (Nov-01). The arrow indicates the direction of stream flow between stations 12 and 11.

The strontium isotope ratios and Sr^{2+} concentrations indicated that stream water at station 11 was comprised of approximately 6 to 20% surface water from station 13, 13 - 38% alluvial groundwater and 56 to 67% regional groundwater (section 6.3.1, Figure 6.10). However, Cl^- concentrations, δ^2H and $\delta^{18}O$ indicated that regional groundwater did not discharge to stream flow in between stations 12 and 11. Therefore all the regional groundwater discharge to stream flow occurred between stations 13 and 12. Stream water at station 11 was comprised of 6 to 20% of stream water from station 12, between 13 and 38% alluvial groundwater and 42 to 81% surface water from tributaries "T8", "T9" and "T10".

6.3.3 Stations 11 to 10

There were two tributaries (**14** and **T6**) that contributed to stream flow between Wollombi Brook sampling stations **11** and **10** (Figure 2.1). Major ion (excluding

$SiO_{2\,(aq)}$) and Sr^{2+} concentrations decreased in stream water in between stations 11 and 10 (i.e. 74 to 67 km, Figure 5.3, Figure 5.9, Table A.4). The ion concentrations in regional groundwater and tributary T6 were too high to have caused the measured dilutions in stream water chemistry between stations 11 and 10. Therefore regional groundwater and T6 discharged negligible water to the Wollombi Brook during baseflow. The ion concentrations in alluvial groundwater and tributary 14 were sufficiently low to have caused all the measured dilutions in stream water chemistry. Two-component end-member mixing (based on Cl^- concentrations, Table A.12) indicated that stream water at station 10 was comprised of either (1) 48 to 53% alluvial groundwater or (2) 63 to 100% surface water from tributary 14.

There was a net decrease in the ^{222}Rn concentration of stream water between stations 11 and 10 (74 to 67 km, Figure 5.4). However, the predicted ^{222}Rn loss from stream water between stations 11 and 10 was much higher than the net ^{222}Rn loss actually measured (67 km, Figure 4.8***b***). Therefore an additional water source contributed ^{222}Rn to stream flow. High predicted ^{222}Rn loss from surface water tributaries 14 or T6 suggests that they did not contribute the additional ^{222}Rn to stream flow in the Wollombi Brook (Table C.2). Therefore ^{222}Rn concentrations in stream water indicated that there was a component of groundwater discharge to stream flow in between stations 11 and 10. Changes in ^{222}Rn concentration in stream water indicated that either (1) alluvial groundwater contributed 6 to 100%, or (2) regional groundwater contributed 5 to 100% of water to streamflow (Figures 4.11***b*** and 4.12***b***).

The shift in δ^2H and $\delta^{18}O$ of stream water between stations 11 and 10 (Figure 6.13) indicated that tributary 14 was the most significant contributor of additional water to the Wollombi Brook during baseflow. The δ^2H and $\delta^{18}O$ values in stream water at station 10 were slightly more negative than tributary 14 indicating that a component

of non-evaporated groundwater also contributed to stream flow in between stations 11 and 10.

The $^{87}Sr/^{86}Sr$ of stream water increased considerably from 0.7106 to 0.7123 in between stations 11 and 10 respectively (74 to 67 km, Figure 5.10). The $^{87}Sr/^{86}Sr$ values measured in alluvial groundwater and regional groundwater were too low to have caused the observed increase in the $^{87}Sr/^{86}Sr$ of stream water between stations 11 and 10. The $^{87}Sr/^{86}Sr$ of surface water in tributary 14 was much higher than $^{87}Sr/^{86}Sr$ values measured in the Wollombi Brook, alluvial groundwater and regional groundwater. Therefore the increase in the $^{87}Sr/^{86}Sr$ of stream water between stations 11 and 10 was strongly influenced by surface water discharge from tributary 14.

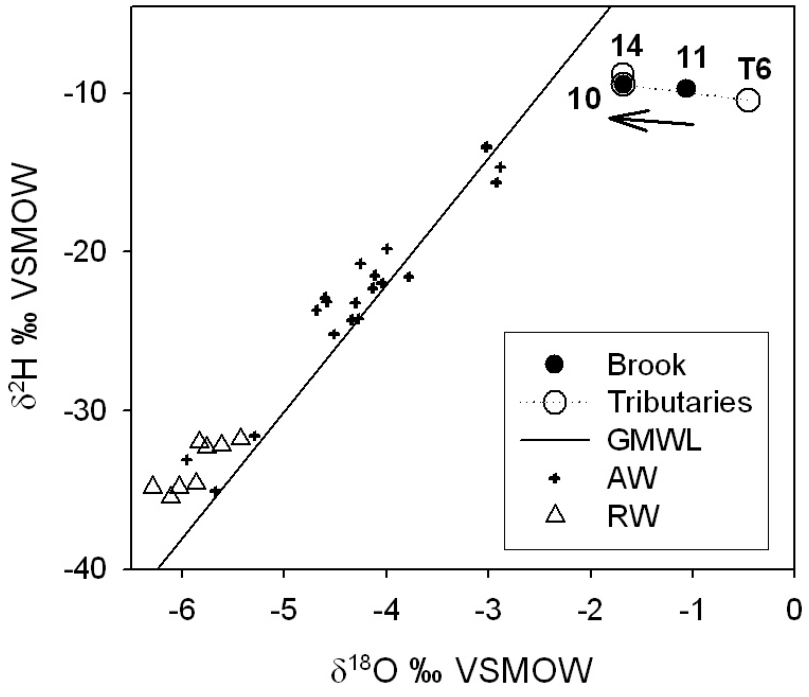

Figure 6.13 δ^2H and $\delta^{18}O$ (‰ VSMOW) values in stream water (Brook), tributary water (14 and T6), alluvial groundwater (AW) and regional groundwater (RW) in relation to the Global Meteoric Water Line (GMWL) during baseflow (Nov-01). The arrow indicates the direction of stream flow between stations 11 and 10.

The potential proportions of the sources of water that contributed to stream flow at station 10 were estimated by constructing theoretical $^{87}Sr/^{86}Sr$ and inverse Sr^{2+} mixing lines between stream water at station 11, surface water from tributary 14 and alluvial groundwater end-members (Figure 6.14). These indicated that stream water at station 10 was comprised of 0 to 30% surface water from station 11, 20 to 70% surface water from tributary 14 and 0 to 80% alluvial groundwater. However, ^{222}Rn data indicated that at least 6% of water at station 10 was comprised of alluvial groundwater. Therefore stream water at station 10 was composed of 0 to 28% surface water from station 11, 20 to 66% of tributary water from station 14 and 6 to 80% alluvial groundwater.

6.3.4 Stations 10 to 9

Small increases in TDS, Cl^- and major cation concentrations occurred in stream water between stations 10 and 9 during baseflow (Table A.4, i.e. 67 to 63 km, Figure 5.3). Alluvial groundwater TDS, Cl^- and major cation concentrations were typically lower than stream water concentrations (Table A.10). Therefore alluvial groundwater discharge to stream flow would have caused dilutions rather than the observed concentration of ions in stream water. Two-component end-member mixing indicated that the small increase in the Cl^- concentration of stream water between stations 10 and 9 was caused by 2 to 4% regional groundwater discharge (Table A.12). Alternatively, the small increases in stream water chemistry could potentially have been caused by evaporative concentration.

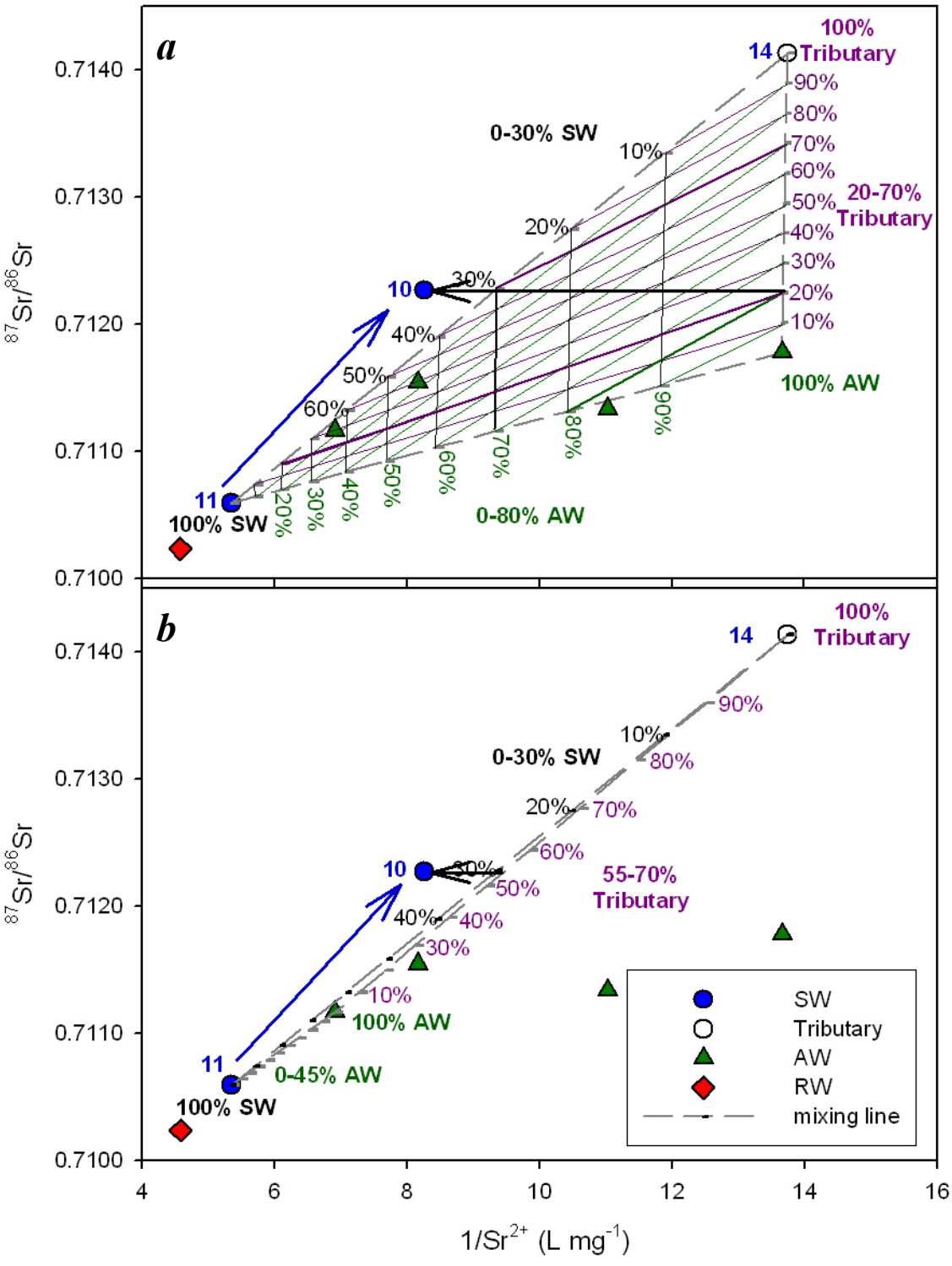

Figure 6.14 Change in $^{87}Sr/^{86}Sr$ and inverse Sr^{2+} concentration in stream water (SW) between stations 11 and 10 (arrow indicates stream flow direction) compared to tributary water (14) alluvial groundwater (AW) and regional groundwater (RW) values. Theoretical mixing lines were constructed between SW at station 11, tributary 14 and (***a***) maximum AW, and (***b***) minimum AW values to estimate proportions of each water source present in stream water at sampling station 10.

The ^{222}Rn concentration in stream water decreased in between stations 10 and 9 (67 to 63 km, Figure 5.4). However, the predicted ^{222}Rn concentration in stream water at station 9 was lower than the measured value (63 km, Figure 4.8***b***). Therefore there was a component of groundwater discharge that contributed additional ^{222}Rn to stream flow in between stations 10 and 9. Changes in ^{222}Rn concentration in stream water indicated that either (1) alluvial groundwater contributed 3 to 20% (63 km, Figure 4.11***b***), or (2) regional groundwater contributed 2 to 100% of water to streamflow (63 km, Figure 4.12***b***).

The δ^2H value decreased and the $\delta^{18}O$ value increased in stream water in between stations 10 and 9 (67 to 63 km, Figure 5.5). This indicates that either (1) groundwater discharged to stream flow and was subsequently evaporated, or (2) shallow alluvial groundwater (with an evaporated signature) discharged to stream flow.

Construction of theoretical $^{87}Sr/^{86}Sr$ and inverse Sr^{2+} mixing lines between stream water at station 10, alluvial groundwater and regional groundwater end-members (Figure 6.15) indicated that stream water at station 9 contained very little groundwater. Figure 6.15 indicates that alluvial groundwater contributed 2 to 14% of water to stream flow and the remaining stream water at station 9 originated from surface runoff from further upstream (station 10).

Stream water at station 9 was comprised of 3 to 14% alluvial groundwater, based on ^{222}Rn data (minimum) and $^{87}Sr/^{86}Sr$ and inverse Sr^{2+} mixing lines (maximum). Therefore 86 to 97% of stream water at station 9 originated from surface water flow at station 10. The observed increase in the Cl^- concentration of stream water between stations 10 and 9 was caused by evaporative concentration rather than regional groundwater discharge to stream flow.

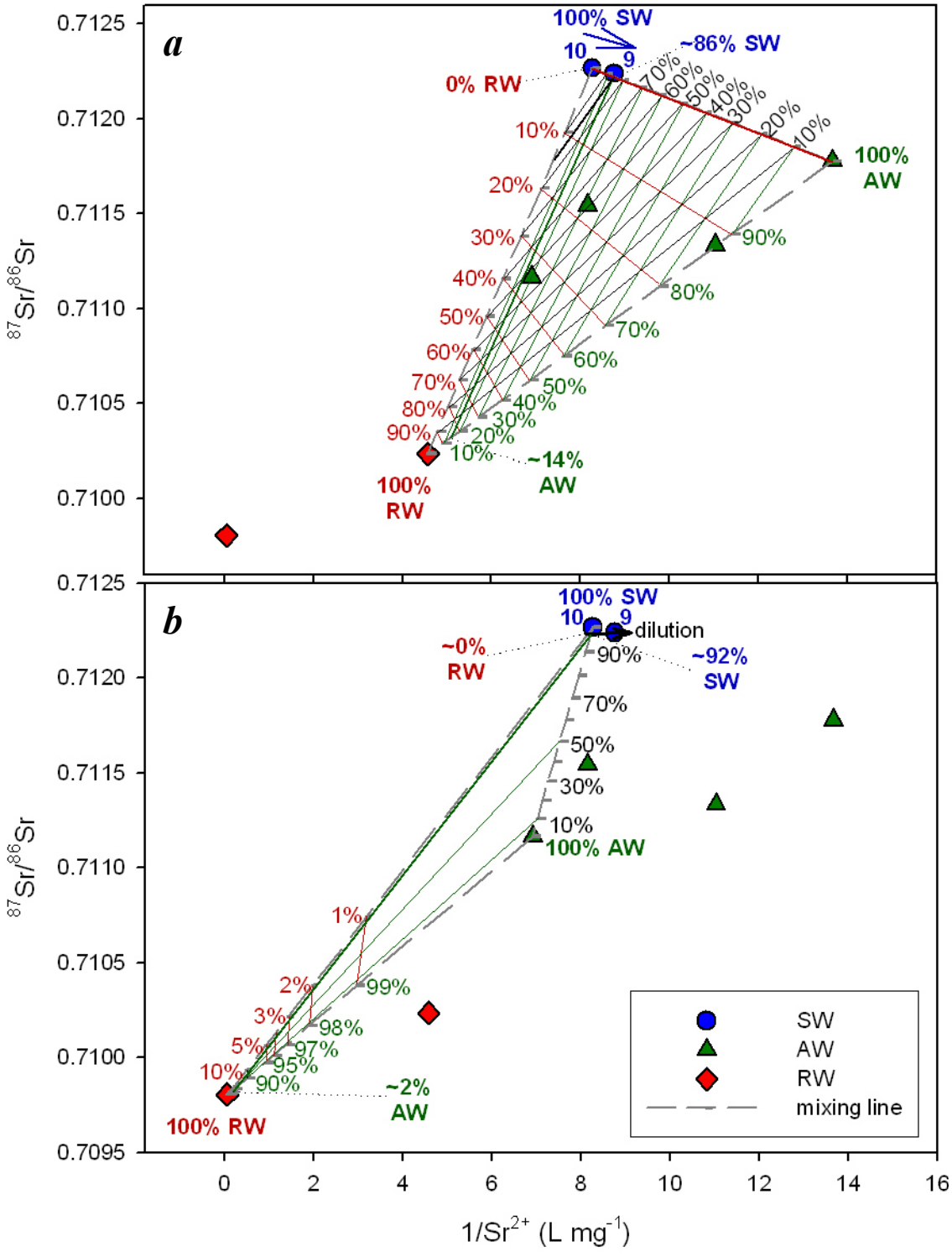

Figure 6.15 Change in $^{87}Sr/^{86}Sr$ and inverse Sr^{2+} concentration in stream water (SW) in between stations 10 and 9 (arrow indicates stream flow direction) compared to alluvial groundwater (AW) and regional groundwater (RW) values. Theoretical mixing lines were constructed between SW at station 10, (***a***) maximum AW and minimum RW values, and (***b***) minimum AW and maximum RW values to estimate proportions of each water source present in stream water at sampling station 9.

6.3.5 Stations 9 to 8

Stream water salinity and major ion (excluding K^+ and $SiO_{2\,(aq)}$), concentrations decreased between stations 9 and 8 (Table A.4, i.e. 60 to 54 km, Figure 5.3). If there was a component of (more saline) regional groundwater discharge to stream flow in between stations 9 and 8, there would have to be additional alluvial groundwater discharge to dilute the chemical concentrations in stream water. Assuming that regional groundwater did not discharge to stream flow, two-component end-member mixing based on Cl^- concentrations indicated that alluvial groundwater contributed 25 ± 2% of water to stream flow (Table A.12).

The ^{222}Rn concentration in stream water decreased in between stations 9 and 8 (60 to 54 km, Figure 5.4). The predicted ^{222}Rn concentration in stream water was marginally lower at station 8 than the measured ^{222}Rn concentration. This indicated that there was very little ^{222}Rn addition to stream flow via groundwater discharge. Changes in ^{222}Rn concentration in stream water indicated that either (1) alluvial groundwater contributed up to 2% (60 km, Figure 4.11***b***), or (2) regional groundwater contributed a maximum of 14% of water to streamflow (60 km, Figure 4.12***b***).

Both δ^2H and $\delta^{18}O$ values increased in stream water between stations 9 and 8 (Figure 6.16). The slope of the evaporation line (3.4) indicated that stream water was subjected to evaporative concentration within the stream channel between stations 9 and 8 during baseflow. Therefore the estimates of stream water dilution via alluvial groundwater discharge based on Cl^- concentrations may be underestimates. This suggests that alluvial groundwater discharge to stream flow between stations 9 and 8 was marginally higher than the Cl^--based estimate (25 ± 2%).

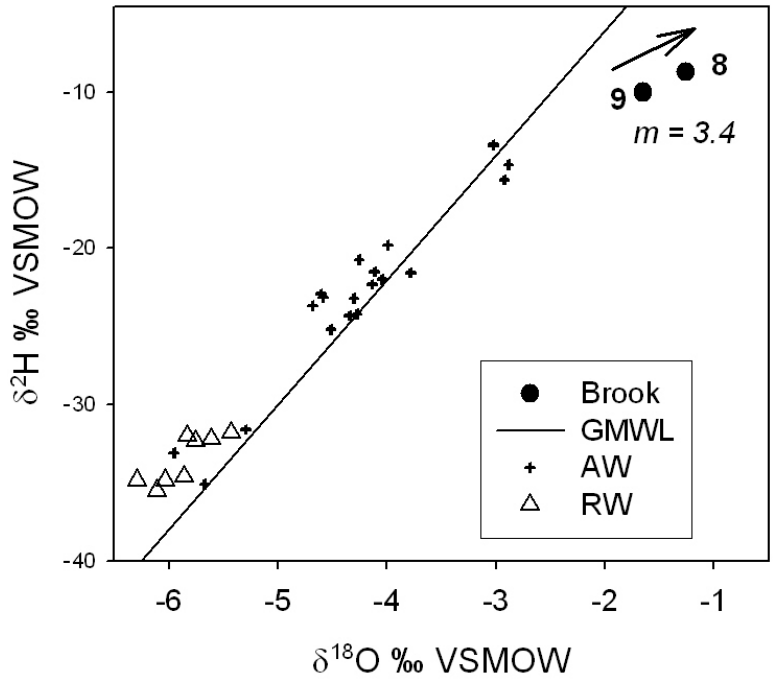

Figure 6.16 δ^2H and δ^{18}O (‰ VSMOW) values in stream water (Brook), alluvial groundwater (AW) and regional groundwater (RW) in relation to the Global Meteoric Water Line (GMWL) during baseflow (Nov-01). The arrow indicates the direction of stream flow between stations 9 and 8. *m* is the slope of the evaporation line.

There was a significant difference between Cl^--based estimates (25 ± 2%) and ^{222}Rn-based estimates (up to 2%) of the proportion of alluvial groundwater discharge to stream flow in between stations 9 and 8. This large discrepancy could be expected if there were an additional low Cl^- and low ^{222}Rn concentration surface water contribution to stream flow. However, there were no evident tributary channels in this area of the catchment (Figure 2.1). Furthermore, if there was an additional surface water tributary that was not detected, it is unlikely that it would still be flowing during baseflow conditions. It is more probable that the discrepancy was caused by (potentially) lower ^{222}Rn concentrations in alluvial groundwater discharge to stream flow between stations 9 and 8 than at station 10 (where it was measured).

Lower ^{222}Rn concentrations in alluvial groundwater could result from short residence times in the alluvial aquifer (e.g. ~3 weeks to reach steady state concentrations),

however this is unlikely during baseflow conditions. It is more likely that the alluvial aquifer had lower steady state ^{222}Rn emanation in between stations 9 and 8 than was measured at station 10 (5 km upstream). Lower steady state ^{222}Rn emanation (C_{SS}^{AGW}, equation 4.16) from alluvial aquifer sands results in higher estimates of alluvial groundwater discharge to stream flow.

Alluvial groundwater discharged approximately 25 ± 2% of water to stream flow in between stations 9 and 8 during baseflow. ^{222}Rn concentrations were low in stream water most probably due to low steady state ^{222}Rn emanation rates from the alluvial aquifer in this reach of the catchment.

6.3.6 Stations 8 to 7

There was negligible change in the concentrations of Cl^- (60 to 54 km, Figure 5.3), and major cations in stream water between stations **8** and **7** during baseflow (Table A.4). Alluvial groundwater discharge to stream flow would have caused small decreases and regional groundwater discharge would have caused significant increases in the concentrations in the aforementioned ions (Table A.10).

There was a net decrease in the ^{222}Rn concentration in stream water between stations 8 and 7 (Figure 5.4). However, the predicted ^{222}Rn concentration in stream water at station 7 was lower than the measured value (54 km, Figure 4.8***b***). Therefore there was a component of groundwater discharge to stream flow in between stations 8 and 7. Changes in ^{222}Rn concentration in stream water indicated that either (1) alluvial groundwater contributed up to 5% (54 km, Figure 4.11***b***), or (2) regional groundwater contributed a maximum of 31% of water to streamflow (54 km, Figure 4.12***b***). Since regional groundwater discharge to stream flow would have caused a

marked increase in the major ion concentrations in stream water, the source of groundwater discharge must have been alluvial groundwater.

δ^2H increased while $\delta^{18}O$ decreased in stream water between stations 8 and 7 (Figure 6.17). The net δ^2H - $\delta^{18}O$ shift was toward the global meteoric water line indicating that there was a component of groundwater discharge to streamflow that was subsequently evaporated. Therefore, during baseflow stream water was comprised of up to 5% alluvial groundwater that discharged to stream flow and was subsequently evaporated within the stream channel between stations 8 and 7.

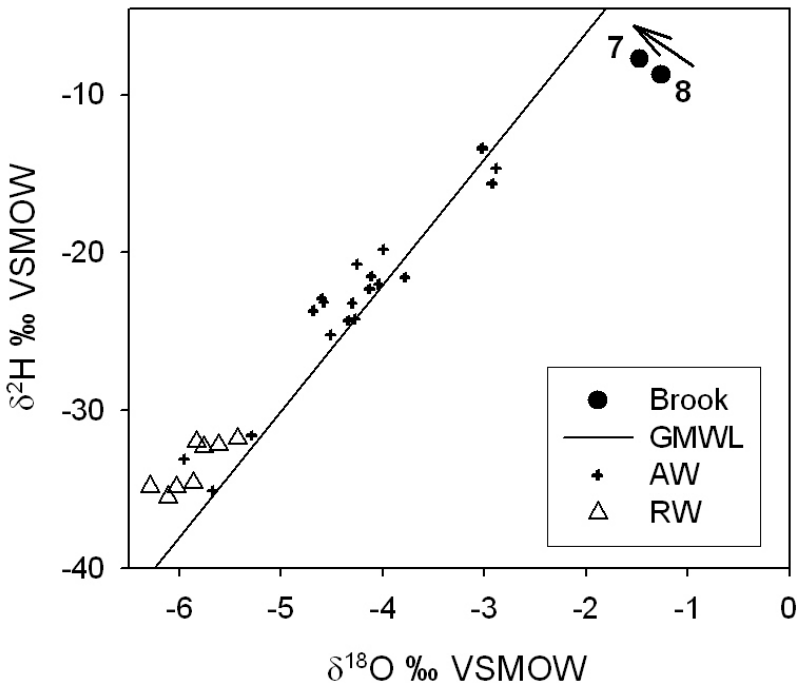

Figure 6.17 δ^2H and $\delta^{18}O$ (‰ VSMOW) values in stream water (Brook), alluvial groundwater (AW) and regional groundwater (RW) in relation to the Global Meteoric Water Line (GMWL) during baseflow (Nov-01). The arrow indicates the direction of stream flow between stations 8 and 7.

6.3.7 Stations 7 to 5

The salinity and major ion concentrations in stream water increased significantly between stations **7** and **5** during baseflow (Table A.4, i.e. 54 to 38 km, Figure 5.3). This reach of the Wollombi Brook was located approximately half way between stations 3 and 10, where alluvial and regional groundwater was sampled (Figure 2.1). However the geological and landscape setting was most similar to the conditions at station 3. Therefore, in the following discussion it is assumed that alluvial groundwater and regional groundwater have similar chemical characteristics to those monitored at station 3.

The Cl^- concentrations measured in deep regional groundwater bores (79057 and 79058, Table A.10) were lower than those measured in stream water, therefore deep regional groundwater did not discharge water to stream flow (assuming insufficient evapo-concentration). Similarly, shallow alluvial groundwater contained lower Cl^- concentrations than stream water, which would have caused stream water Cl^- dilution if it had discharged into the stream channel. Shallow regional groundwater contained much higher Cl^- concentrations (i.e. 1740 mg/L measured in F6) and could potentially have caused the observed increase in Cl^- concentration in stream water if it contributed 2% of water to stream flow (Table A.12). Similarly, if deep alluvial groundwater (i.e. 310 mg/L measured in FDP1) discharged 20 to 26% of water to stream flow the observed Cl^- concentration in stream water could have been reproduced without evaporative concentration.

The ^{222}Rn concentration increased in stream water between stations 7 and 5 (54 to 38 km, Figure 5.4) indicating that there was a component of groundwater discharge to stream flow. However, the distances between stations 7 and 5 were too large (38 km, Figure 2.1) for estimates of ^{222}Rn loss due to gas exchange and decay to further constrain groundwater discharge to stream flow.

There were large increases in both the δ^2H and $\delta^{18}O$ values in stream water between stations 7 and 5 (54 to 38 km, Figure 5.5). This indicates that there was a strong evaporative loss of water from the stream channel and potentially high evaporative concentration of Cl^- (and other ions) in stream water.

It is certain that groundwater discharged to stream flow between stations 7 and 5 during baseflow. However, evaporation of stream water from the open channel and large distances between sampling stations rendered estimation of the sources and their magnitude uncertain.

6.3.8 Stations 5 to 4

Increases in the salinity and major ion concentrations of stream water were observed between stations **5** and **4** during baseflow (Table A.4, i.e. 38 to 33 km, Figure 5.3). The Cl^- concentrations measured in deep regional groundwater bores (79057 and 79058, Table A.10) and shallow alluvial groundwater were lower than those measured in stream water. Therefore, if they discharged to stream flow they would have caused decreases in the Cl^- concentration of stream water. It is unlikely that deep regional groundwater discharged water to stream flow. Shallower regional groundwater had much higher Cl^- concentrations (i.e. 1740 mg/L measured in F6) and could potentially have caused the observed increase in Cl^- concentration in stream water if it contributed 6% of water to stream flow (Table A.12). If deep alluvial groundwater discharged 66 - 95% of water to stream flow the observed increase in the Cl^- concentration of stream water could have occurred without evaporative concentration.

The ^{222}Rn concentration increased in stream water between stations 5 and 4 (38 to 33 km, Figure 5.4) indicating that there was a component of groundwater discharge

to stream flow; either (1) alluvial groundwater contributed 8 to 100% (38 km, Figure 4.11***b***), or (2) regional groundwater contributed 1 to 100% of water to streamflow (38 km, Figure 4.12***b***).

Large decreases in both the δ^2H and $\delta^{18}O$ values in stream water indicated that groundwater discharged to stream flow between stations 5 and 4 (38 to 33 km, Figure 5.5). The slope of the mixing ling between stations 5 and 4 was nearly parallel to the Global Meteoric Water Line (Figure 6.18). This indicated that the source of groundwater either (1) had an evaporated signature (i.e. shallow alluvial groundwater), or (2) was evaporated subsequent to discharge into the stream channel. Therefore the change in the δ^2H and $\delta^{18}O$ signature of stream water could have been caused by either alluvial groundwater or regional groundwater discharge to stream flow.

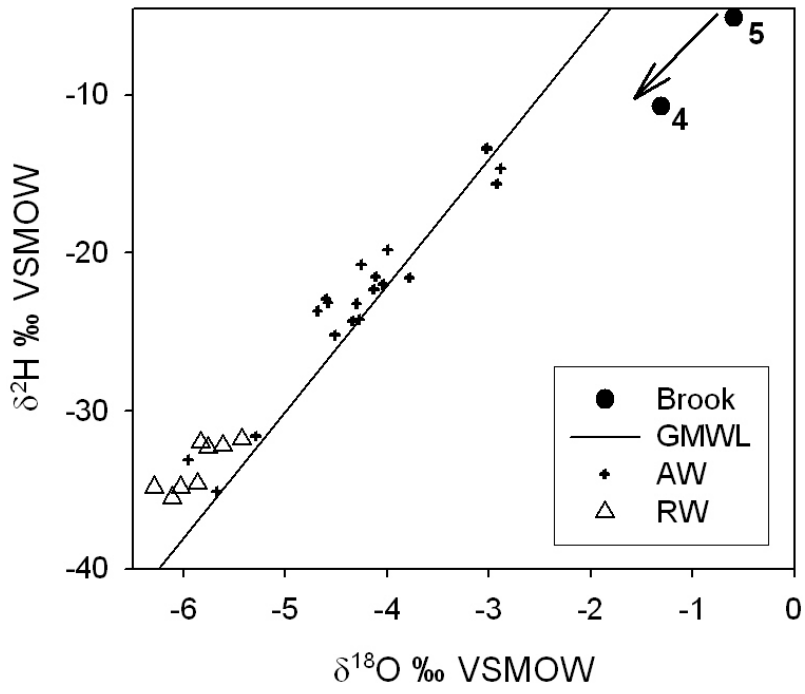

Figure 6.18 δ^2H and $\delta^{18}O$ (‰ VSMOW) values in stream water (Brook), alluvial groundwater (AW) and regional groundwater (RW) in relation to the Global Meteoric Water Line (GMWL) during baseflow (Nov-01). The arrow indicates the direction of stream flow between stations 5 and 4.

There was a large decrease in the $^{87}Sr/^{86}Sr$ of stream water (from 0.7122 to 0.7101) between stations **9** and **4** (63 to 33 km, Figure 5.10). The decrease in the $^{87}Sr/^{86}Sr$ of stream water could have been caused by either alluvial groundwater or regional groundwater discharge to stream flow. Three-component end-member mixing of $^{87}Sr/^{86}Sr$ and Sr^{2+} concentrations between stream water and potential sources of groundwater discharge are presented in Figures 6.19 and 6.20. If shallow alluvial groundwater were the source of groundwater discharge to stream flow it would have to contribute greater than 57% of water to stream flow and undergo significant evaporation to cause the measured changes in $^{87}Sr/^{86}Sr$ and Sr^{2+} in stream water between stations 9 and 4 (Figure 6.19***a***). Alternatively, approximately 3% shallow regional groundwater discharge to stream flow and evaporative concentration of Sr^{2+} would cause the measured changes in $^{87}Sr/^{86}Sr$ and Sr^{2+} in stream water between stations 9 and 4 (Figure 6.19***b***). The measured changes in $^{87}Sr/^{86}Sr$ and Sr^{2+} in stream water could also have been caused by 9 to 29% deep alluvial groundwater discharge to stream flow between stations 9 and 4 (Figure 6.20).

Alluvial groundwater contributed 25±2% of water to stream flow between stations 9 and 8, and up to 5% between stations 8 and 7. If alluvial groundwater were the sole source of water that contributed to stream flow between stations 9 and 4, then 25% to 34% (i.e. $57-27-5=25\%$ or $57-23-0=34\%$) of alluvial groundwater discharge to stream flow would have occurred between stations 7 and 4. This would have been followed by strong evaporative concentration of Sr^{2+} in stream water.

In order to estimate the potential proportions of either deep alluvial groundwater or shallow regional groundwater to stream flow between stations 7 and 4 it was necessary to estimate the $^{87}Sr/^{86}Sr$ value in stream water at station 7. A range of $^{87}Sr/^{86}Sr$ values in stream water at station 7 was estimated via three-component end-member mixing (equation 6.2) of $^{87}Sr/^{86}Sr$ and Sr^{2+} concentrations between surface

water and estimated alluvial groundwater contributions between stations 9, 8 and 7. Three-component end-member mixing lines of the $^{87}Sr/^{86}Sr$ and Sr^{2+} concentrations in stream water at station 7 and deep alluvial groundwater and shallow regional groundwater were constructed to estimate their potential contributions to stream flow between station 7 and 4 (Figures 6.21 and 6.22).

If shallow regional groundwater was the only source of water that contributed to stream flow between stations 7 and 4 it would have contributed 2±1% of water to stream flow followed by evaporative concentration of Sr^{2+} in stream water (Figure 6.21). Alternatively, if the source of water to stream flow between stations 7 and 4 was deep alluvial groundwater it would have contributed 9 - 29% of water to stream flow (Figure 6.22) followed by evaporative concentration of Sr^{2+} in stream water.

6.3.9 Stations 4 to 3

Major ion concentrations increased significantly in stream water between stations **4** and **3** during baseflow (Table A.4, i.e. 33 to 22 km, Figure 5.3). The Cl^- concentrations measured in deep regional groundwater bores (79057 and 79058, Table A.10) and alluvial groundwater were lower than those measured in stream water. Therefore, if they discharged to stream flow they would have diluted Cl^- in stream water. It is unlikely that deep regional groundwater discharged water to stream flow. Shallower regional groundwater had much higher Cl^- concentrations (i.e. 1740 mg/L measured in F6) and could potentially have caused the observed increase in Cl^- concentration in stream water if it contributed 11% of water to stream flow (Table A.12).

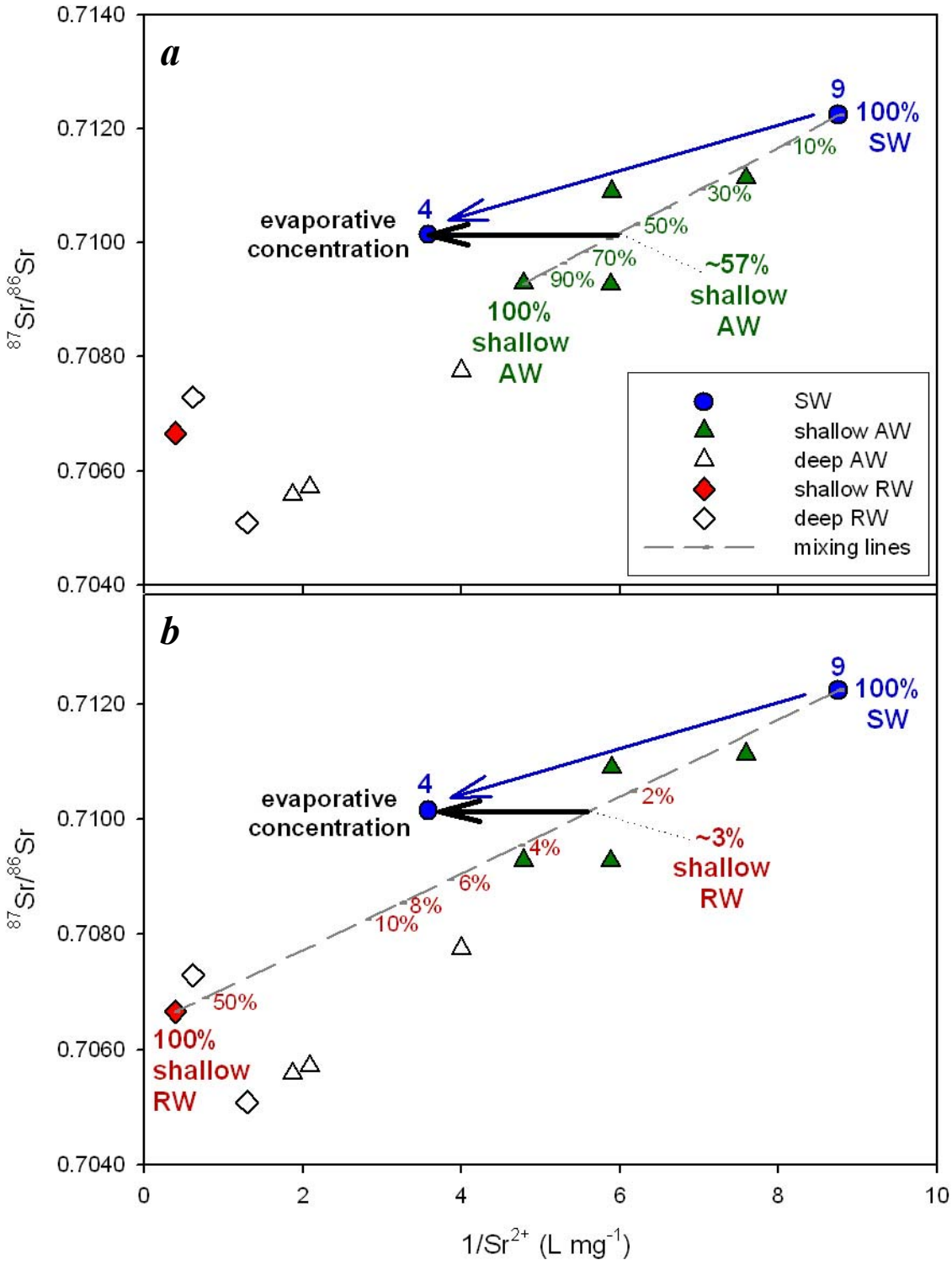

Figure 6.19 Change in $^{87}Sr/^{86}Sr$ and inverse Sr^{2+} concentration in stream water (SW) in between stations 9 and 4 (arrows indicate stream flow direction) compared to alluvial groundwater (AW) and regional groundwater (RW) values. Theoretical mixing lines were constructed between SW at station 9 and (***a***) shallow AW, and (***b***) shallow RW to estimate the potential proportions of each water source present in stream water at sampling station 4.

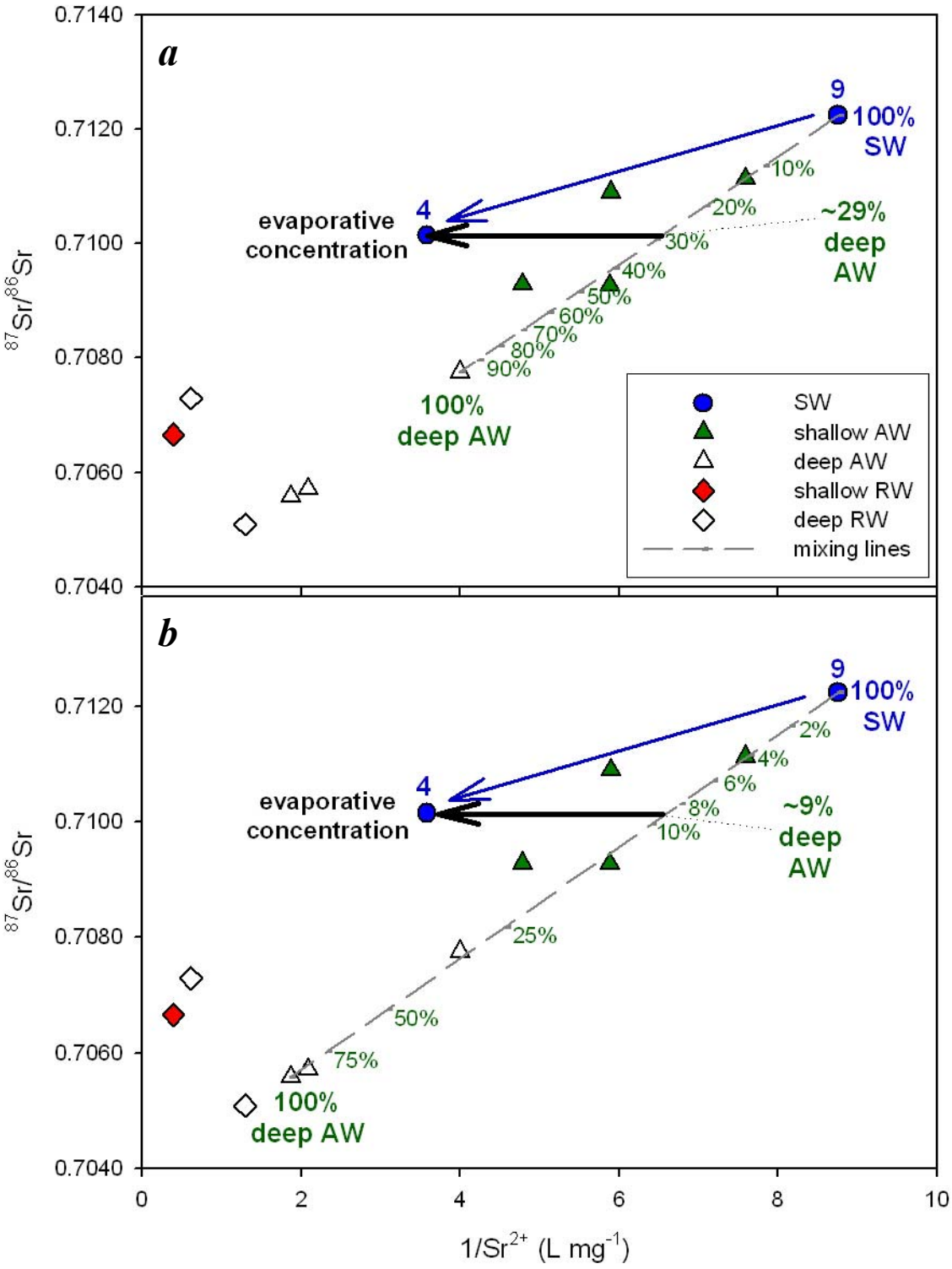

Figure 6.20 Change in $^{87}Sr/^{86}Sr$ and inverse Sr^{2+} concentration in stream water (SW) in between stations 9 and 4 (arrows indicate stream flow direction) compared to alluvial groundwater (AW) and regional groundwater (RW) values. Theoretical mixing lines were constructed between SW at station 9 and (***a***) minimum deep AW, and (***b***) maximum deep AW values to estimate the potential proportion of deep AW present in stream water at sampling station 4.

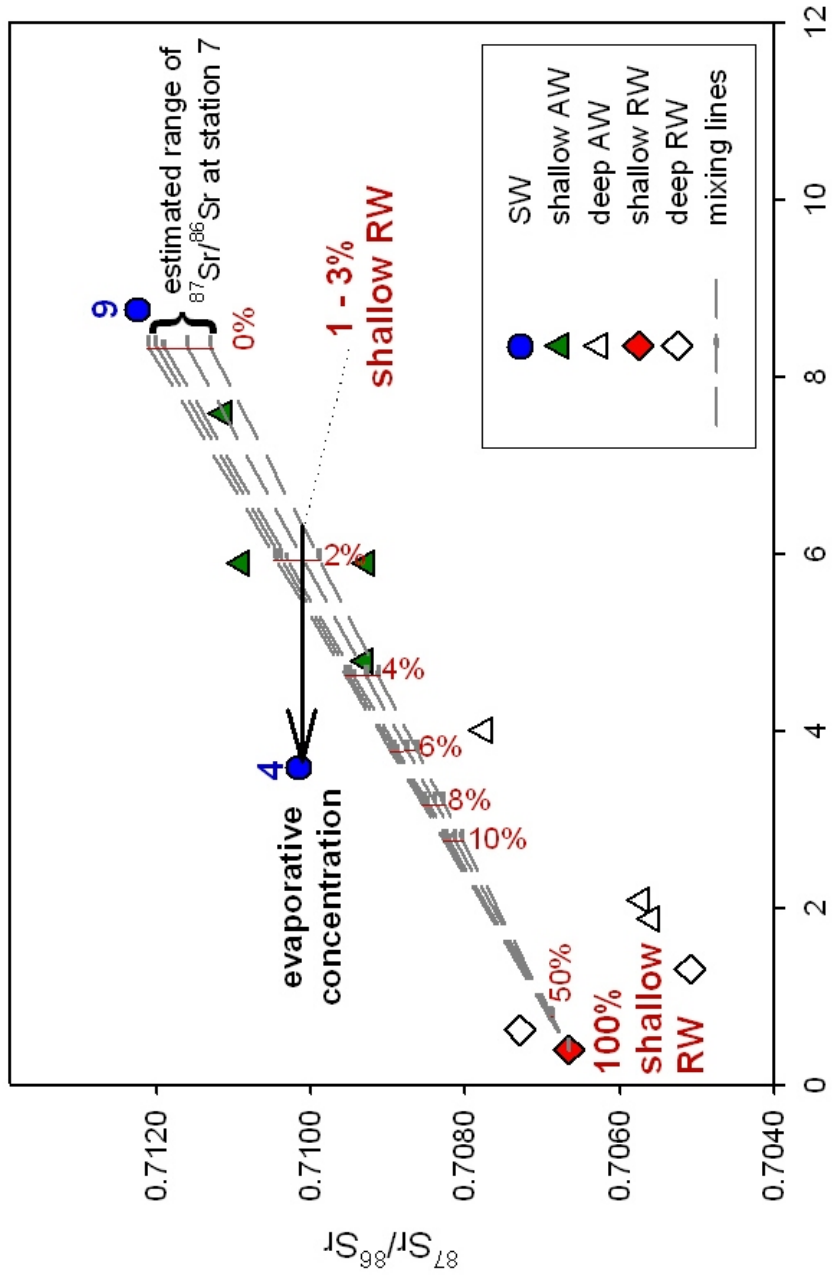

Figure 6.21 Change in $^{87}Sr/^{86}Sr$ and inverse Sr^{2+} concentration in stream water (SW) in between stations 9 and 4 compared to alluvial groundwater (AW) and regional groundwater (RW) values. Theoretical mixing lines were constructed between SW at station 7 and shallow RW to estimate potential shallow RW discharge to stream flow between stations 7 and 4.

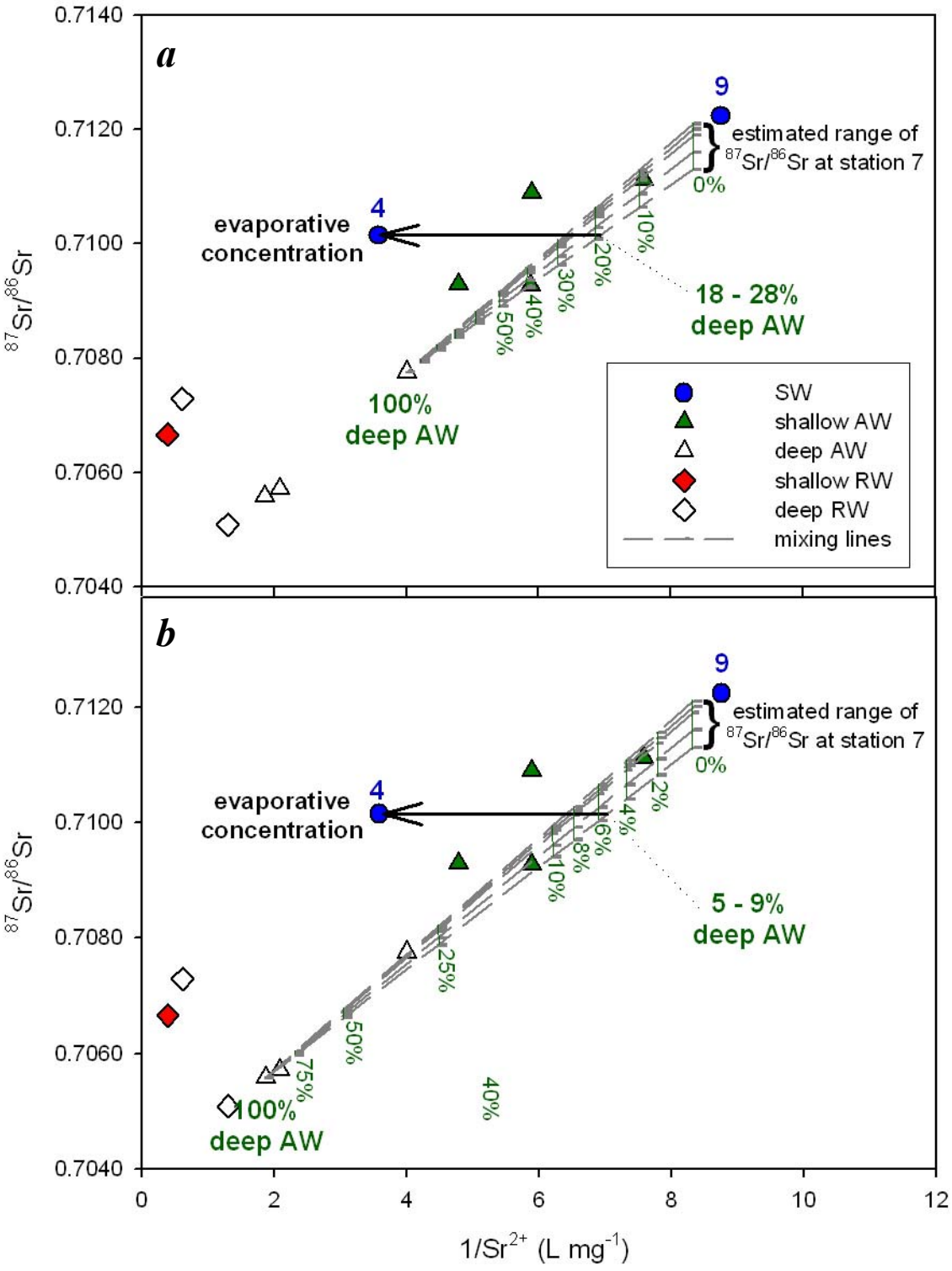

Figure 6.22 Change in $^{87}Sr/^{86}Sr$ and inverse Sr^{2+} concentration in stream water (SW) in between stations 9 and 4 compared to alluvial groundwater (AW) and regional groundwater (RW) values. Theoretical mixing lines were constructed between SW at station 7 and (***a***) minimum, and (***b***) maximum deep AW values to estimate potential deep AW discharge to stream flow between stations 7 and 4.

There was a net decline in the ^{222}Rn concentration in stream water between stations 4 and 3 (33 to 22 km, Figure 5.4). However, estimates of ^{222}Rn loss from stream water due to gas exchange and radioactive decay indicated that groundwater discharged to stream flow between stations 4 and 3 (22 km, Figures 4.9***b*** and 4.10***b***). The proportions of either alluvial groundwater (2 to 100%) or regional groundwater (0.5 to 100%) discharge to stream flow were not well constrained due to the relatively large distance between sampling stations.

Both δ^2H and $\delta^{18}O$ values in stream water increased between stations 4 and 3 (33 to 22 km, Figure 5.5). Therefore evaporative processes influenced stream water chemistry in this reach of the catchment during baseflow. This means that there could potentially be a low Cl^- groundwater source contributing to stream flow that is subsequently evapo-concentrated.

Theoretical $^{87}Sr/^{86}Sr$ and inverse Sr^{2+} mixing lines between stream water at station 4, alluvial groundwater and regional groundwater end-members (Figure 6.23) were constructed to estimate the proportions of the potential sources of groundwater discharge to stream flow. Figure 6.23 indicated that the Sr^{2+} concentration in stream water increased due to evaporative concentration between stations 4 and 3 following either (1) 85% shallow alluvial groundwater, (2) 9 - 31% deep alluvial groundwater, or (3) approximately 3% shallow regional groundwater contribution to stream flow.

6.3.10 Stations 3 to 2

Large decreases in the salinity and major ion concentrations (excluding $SiO_{2\,(aq)}$) occurred in stream water between stations **3** and **2** during baseflow (Table A.4, i.e. 22 to 13 km, Figure 5.3). Regional groundwater concentrations were too high to have caused the measured decreases in stream water salinity between stations 3 and 2 (Table A.10). Two-component end-member mixing indicated that the decrease in

stream water Cl^- concentration was caused by 65±6% alluvial groundwater discharge to stream flow between stations 3 and 2 (Table A.12).

There was a large net increase in the ^{222}Rn concentration in stream water between stations 3 and 2 (22 to 13 km, Figure 5.4) indicating significant groundwater discharge to stream flow. The increase in ^{222}Rn concentration was the result of either (1) alluvial groundwater contributing 7 to 100% (13 km, Figure 4.11***b***), or (2) regional groundwater contributed 1 to 100% of water to streamflow (13 km, Figure 4.12***b***).

Both the δ^2H and $\delta^{18}O$ values in stream water decreased significantly between stations 3 and 2 (22 to 13 km, Figure 5.5). This indicated that groundwater discharged to stream flow between stations 3 and 2. The change in the δ^2H and $\delta^{18}O$ signature of stream water could have been caused by either alluvial groundwater or regional groundwater discharge to stream flow.

The $^{87}Sr/^{86}Sr$ in stream water increased significantly between stations 3 and 2 (22 to 13 km, Figure 5.10). The $^{87}Sr/^{86}Sr$ values measured in deep alluvial groundwater and regional groundwater were lower than the $^{87}Sr/^{86}Sr$ values measured in stream water at station 2 (Figure 6.24). Therefore it is unlikely that either deep alluvial groundwater or regional groundwater contributed to stream flow between stations 3 and 2. Three component $^{87}Sr/^{86}Sr$ and Sr^{2+} end-member mixing lines were constructed to estimate how much shallow alluvial groundwater discharge to stream flow would be required to cause the observed changes in the $^{87}Sr/^{86}Sr$ and Sr^{2+} concentration in stream water between station 3 and 2. Figure 6.24 indicates that 90 to 100% exchange between stream water and alluvial groundwater followed by significant evaporative concentration of Sr^{2+} would be required to cause the measured increase in the $^{87}Sr/^{86}Sr$ and decrease in Sr^{2+} concentration in stream water between station 3 and 2.

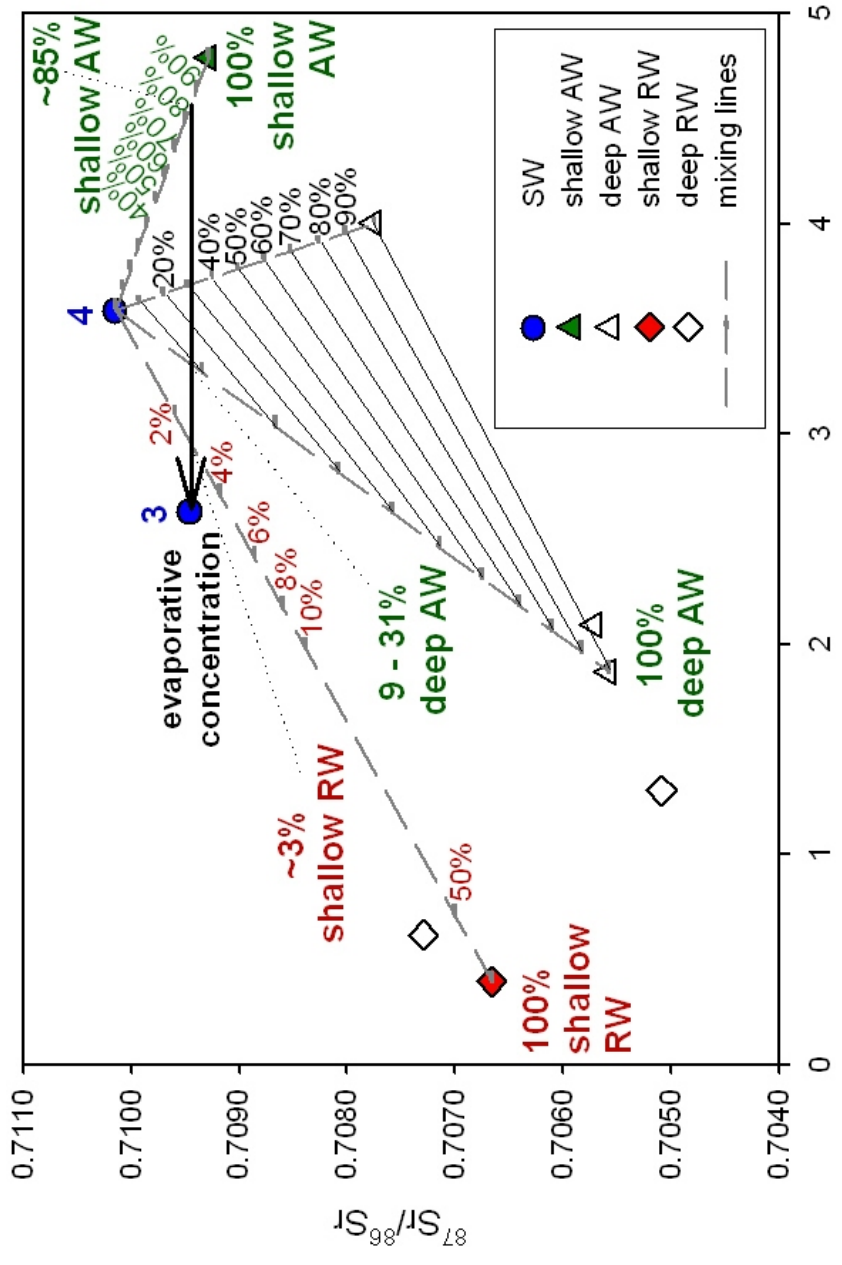

Figure 6.23 Change in $^{87}Sr/^{86}Sr$ and inverse Sr^{2+} concentration in stream water (SW) in between stations 4 and 3 compared to alluvial groundwater (AW) and regional groundwater (RW) values. Theoretical mixing lines were constructed between SW at station 4, shallow AW, deep AW and shallow RW to estimate potential proportions of groundwater discharge to stream flow between stations 4 and 3.

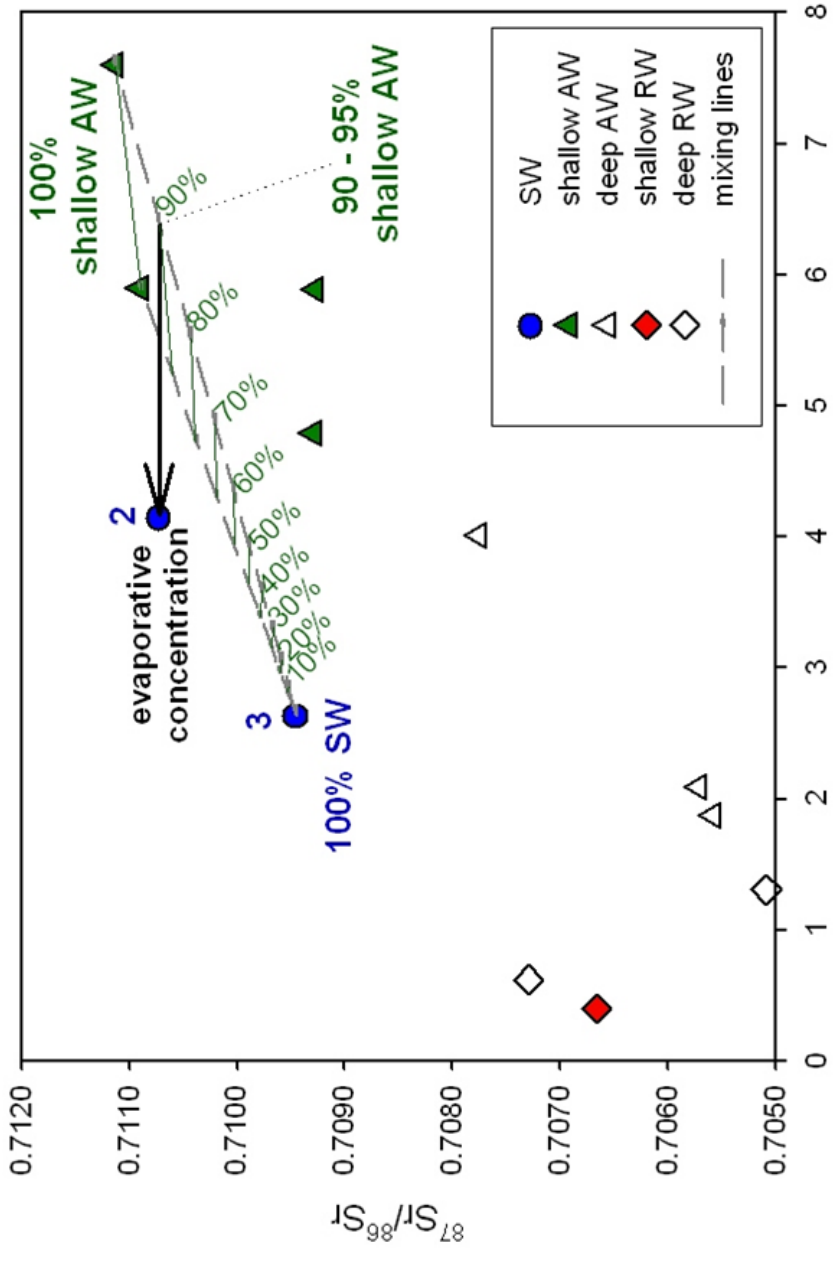

Figure 6.24 Change in $^{87}Sr/^{86}Sr$ and inverse Sr^{2+} concentration in stream water (SW) in between stations 3 and 2 compared to alluvial groundwater (AW) and regional groundwater (RW) values. Theoretical mixing lines were constructed between SW at station 3 and shallow to estimate potential proportions of groundwater discharge to stream flow between stations 3 and 2.

6.3.11 Stations 2 to 1

The salinity and major ion concentrations increased in stream water between stations **2** and **1** during baseflow (Table A.4, i.e. 13 to 0 km, Figure 5.3). The salinities of alluvial groundwater were lower than those measured in stream water (Table A.10). Therefore, unless significant evaporative concentration occurred within the stream channel, it is unlikely that alluvial groundwater discharge to stream flow caused the changes in stream water chemistry between stations 2 and 1. Two-component end-member mixing indicated that the increase in stream water Cl^- concentration was caused by 4 to 100% regional groundwater discharge to stream flow between stations 2 and 1 (Table A.12). However, both δ^2H and $\delta^{18}O$ increased in stream water indicating that evaporation (and therefore evaporative concentration) was a significant process between stations 2 and 1 during baseflow (Figure 5.5).

There was a net decrease in the ^{222}Rn concentration of stream water between stations 2 and 1 (13 to 0 km, Figure 5.4). However, after correction for ^{222}Rn loss from stream water due to gas exchange and radioactive decay, ^{222}Rn data indicated that either (1) 4 to 100% alluvial groundwater, or (2) 1 to 100% regional groundwater discharged to stream flow between stations 2 and 1 (13 km, Figures 4.9***b*** and 4.10***b***).

Theoretical $^{87}Sr/^{86}Sr$ and inverse Sr^{2+} mixing lines between stream water at station 2, alluvial groundwater and regional groundwater end-members (Figure 6.25) were constructed to estimate the proportions of the potential sources of groundwater discharge to stream flow. The results indicated that the Sr^{2+} concentration in stream water increased due to evaporative concentration between stations 2 and 1 following either (1) 72 to 100% alluvial groundwater, or (2) 11±2% regional groundwater contribution to stream flow (Figure 6.25).

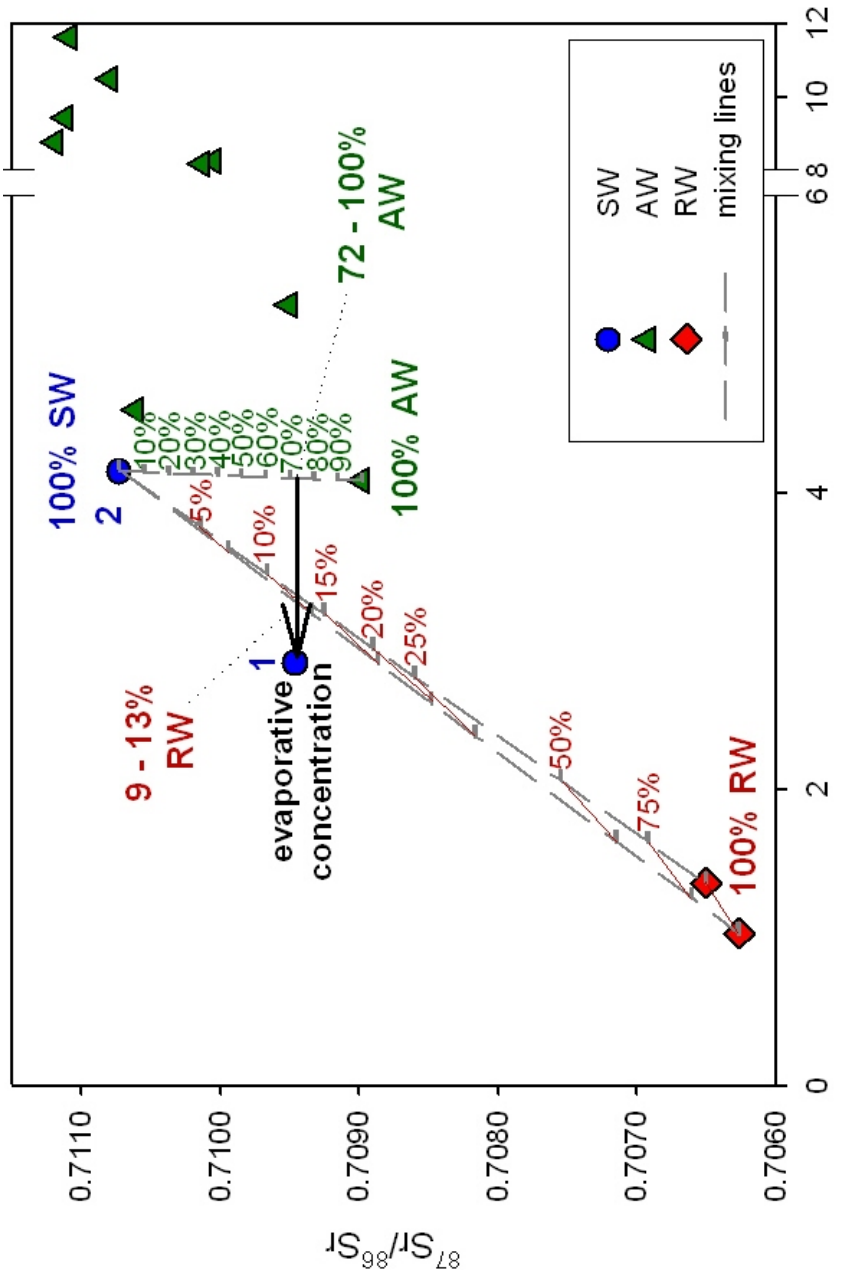

Figure 6.25 Change in $^{87}Sr/^{86}Sr$ and inverse Sr^{2+} concentration in stream water (SW) in between stations 2 and 1 compared to alluvial groundwater (AW) and regional groundwater (RW) values. Theoretical mixing lines were constructed between SW at station 2, deep AW and RW to estimate potential proportions of groundwater discharge to stream flow between stations 2 and 1.

6.4 SPATIAL DISTRIBUTION OF GROUNDWATER DISCHARGE TO STREAM FLOW

Estimates of groundwater contribution to streamflow in between each surface water sampling station during flood recession (Mar-01) and baseflow (Nov-01) are summarised in Table 6.1.

Table 6.1 Summary of the percentages of alluvial groundwater (**AGW**) and regional groundwater (**RGW**) discharges to stream flow between consecutive stream water sampling stations (1 to 13) during flood recession (Mar-01) and baseflow (Nov-01).

Sampling Interval	Distance upstream (km)	Flood recession	Baseflow
1 – 2	0	**AGW:** 6 - 20%	**AGW:** 72 - 100% or
		RGW: -	**RGW:** 11±2%
2 – 3	12	**AGW:** 8 - 20%	**AGW:** 90 - 100%
		RGW: -	**RGW:** -
3 – 4	22	**AGW:** 7 - 100% or	**AGW:** 9 - 85% or
		RGW: up to 6%	**RGW:** 3%
4 – 7	33	**AGW:** 2 - 89%	**AGW:** 9 - 100% or
		RGW: -	**RGW:** 2±1%
7 – 8	54	**AGW:** 6±2%	**AGW:** up to 5%
		RGW: -	**RGW:** -
8 – 9	60	**AGW:** 9±2%	**AGW:** 25±2%
		RGW: -	**RGW:** -
9 – 10	63	**AGW:** 42 - 100%	**AGW:** 3 - 14%
		RGW: -	**RGW:** -
10 – 11	67	**AGW:** possible	**AGW:** 6 - 80%
		RGW: 5 - 37%	**RGW:** -
11 – 12	74	**AGW:** 24 - 64%	**AGW:** 13 - 38%
		RGW: -	**RGW:** -
12 – 13	81	**AGW:** 3 - 100%	**AGW:** 0 - 38%
		RGW: -	**RGW:** 56 - 67%

Groundwater discharged to stream flow along all monitored stream reaches of the Wollombi Brook during both flood recession (Mar-01) and baseflow (Nov-01) conditions. Alluvial groundwater was the dominant source of groundwater discharge to stream flow during both flood recession and baseflow conditions. However, regional groundwater discharged to stream flow in the upper reaches of the Wollombi Brook during both flood recession (between stations 11 and 10, 74 to 67 km) and baseflow (between stations 13 and 12, 86 to 81 km). It is also possible that regional groundwater discharged to stream flow in the lower catchment during both flood recession (between stations 4 and 3, 33 to 22 km) and baseflow (between stations 7 and 1, 54 to 0 km).

In some reaches of the Wollombi Brook the ranges in estimates of groundwater discharge to stream flow were large (i.e. 3 to 100% alluvial groundwater discharge to stream flow between stations 12 to 13 during flood recession, Table 6.1). However, the ranges were generally more tightly constrained by examining the suite of environmental tracers (Cl^-, δ^2H and $\delta^{18}O$, ^{222}Rn, $^{87}Sr/^{86}Sr$, Figure 6.26) than by using ^{222}Rn alone (Chapter 6, e.g. Figures 4.11 and 4.12). Furthermore, by analysing the suite of tracers rather than simply ^{222}Rn, it was generally possible to distinguish between alluvial groundwater and regional groundwater sources of discharge to stream flow.

During flood recession (Mar-01) stream water in the lower (6 to 20% from 0 to 13 km) and mid (4 to 11% from 54 to 60 km and negligible at 67 km) Wollombi Brook was comprised of relatively low proportions of alluvial groundwater (Figure 6.26***a***). Stream water in the mid to upper Wollombi Brook contained higher proportions of alluvial groundwater (24 to 100% at 63 and 74 km) and potentially high proportions of alluvial groundwater discharged into the lower to mid Wollombi Brook (7 to 100%, from 22 to 33 km). Regional groundwater did not contribute to

stream flow along most reaches of the Wollombi Brook (Figure 6.26***b***). However, stream water in the mid to upper Wollombi Brook contained a comparatively high proportion of regional groundwater (5 to 37% at 67 km) and in the lower Wollombi Brook (at 33 km) up to 6% of stream water potentially originated from regional groundwater.

During baseflow (Nov-01) the highest proportion of alluvial groundwater discharge to stream flow occurred in the lower Wollombi Brook (90 to 100% at 22 km). Stream water in the mid Wollombi Brook contained relatively low proportions of alluvial groundwater that discharged to stream flow (up to 14%, at 54 and 63 km, Figure 6.26***c***). Moderately high proportions of alluvial groundwater discharged into the stream channel in the mid to upper Wollombi Brook (13 to 38% at 60 and 74 km) and potentially discharged into the lower to mid (9 to 100%, at 33 km) and mid to upper (6 to 80% at 67 km) Wollombi Brook. Regional groundwater did not contribute to stream flow in the mid reaches of the Wollombi Brook (54 to 74 km, Figure 6.26***d***). However, stream water contained a high proportion of regional groundwater in the mid to upper Wollombi Brook during baseflow (56 to 67% at 81 km) and regional groundwater potentially contributed approximately 3% of water to stream flow in the lower Wollombi Brook (0 km and 22 to 33 km).

In general, stream flow was comprised of higher proportions of groundwater during baseflow than during flood recession. However, in the mid Wollombi Brook (33 to 54 km) there was little discernable difference between baseflow and flood recession proportions of groundwater discharge to stream flow. In addition, alluvial groundwater discharge accounted for higher percentages of stream flow during flood recession than during baseflow at two points (at 63 and 74 km) in the mid to upper Wollombi Brook.

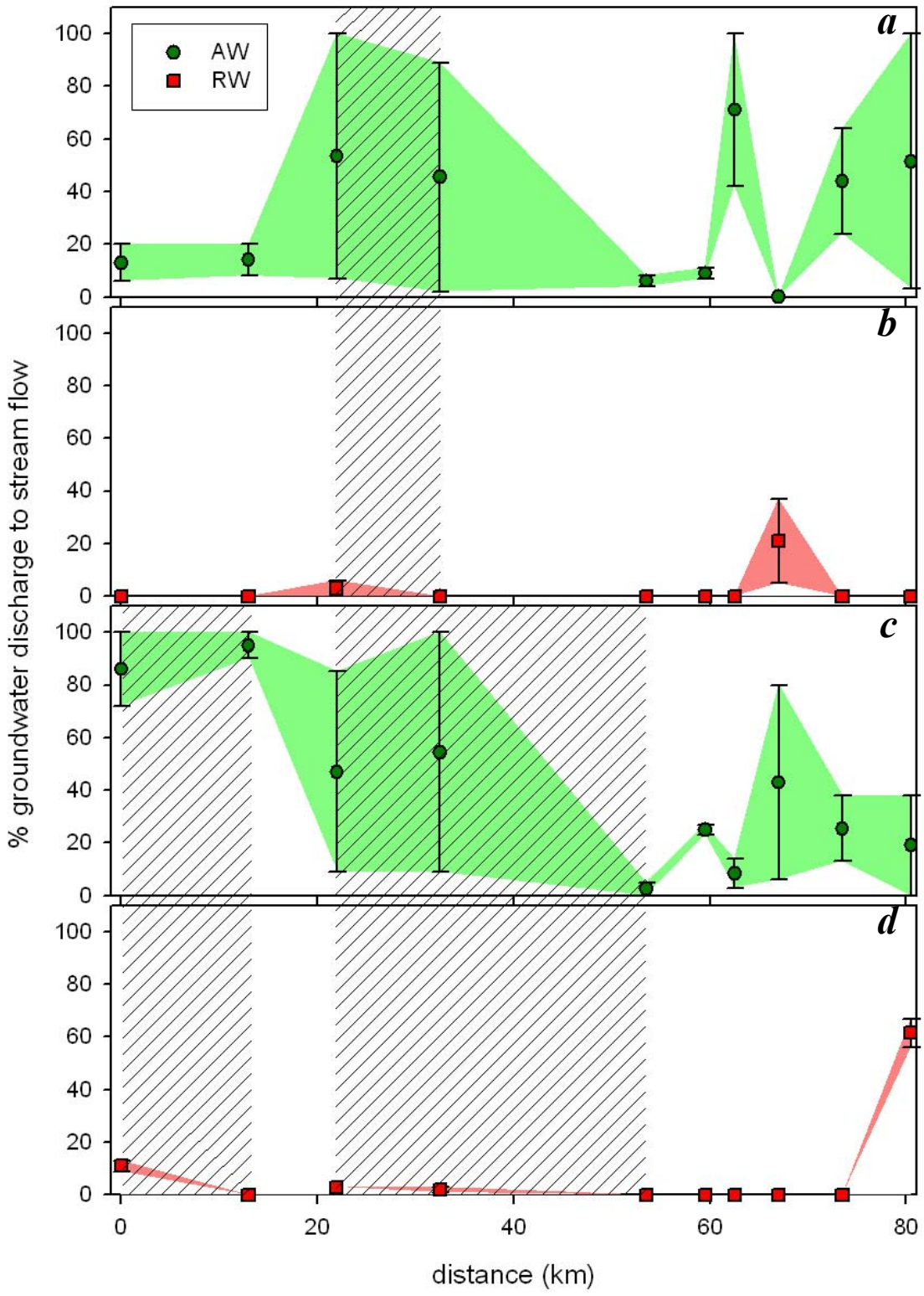

Figure 6.26 Estimated ranges of alluvial groundwater (AW), and regional groundwater (RW) discharge to stream flow during (***a*** and ***b***) flood recession (Mar-01), and (***c*** and ***d***) baseflow (Nov-01). Shaded areas indicate reaches where AW and RW discharges were indistinguishable and one source was assumed. If AW and RW both discharged to stream flow in the shaded reaches, lesser percentages of both AW and RW discharge would have occurred.

In one mid to upper reach of the Wollombi Brook the source of groundwater discharge to stream flow switched from regional groundwater during flood recession to alluvial groundwater discharge during baseflow (at 74 km, Figure 6.26). Conversely, in another the mid to upper reach of the Wollombi Brook (81 km) the source of groundwater discharge to stream flow switched from alluvial groundwater during flood recession to predominantly regional groundwater during baseflow.

Surface water inflows from further upstream contributed more water to stream flow than groundwater discharge between sampling stations in the lower (0 to 13 km) and mid (54 to 60 km) Wollombi Brook during flood recession (Mar-01). During baseflow conditions (Nov-01) surface water discharge contributed the majority of water to stream flow in the mid (54 to 63 km) and upper (74 km) Wollombi Brook.

6.5 CONCLUSIONS

Examination of changes in stream water chemistry (Cl^-, δ^2H & $\delta^{18}O$, ^{222}Rn, $^{87}Sr/^{86}Sr$) at several locations along the Wollombi Brook enabled the identification of locations, sources and relative contributions of groundwater discharge to stream flow. This methodology showed that groundwater discharged to stream flow between all stream water sampling stations during both flood recession (Mar-01) and baseflow (Nov-01) conditions.

As conceptually expected, stream water generally contained higher percentages of groundwater during baseflow than during flood recession. Alluvial groundwater was the dominant source of groundwater discharge to stream flow during both flood recession and baseflow conditions. Regional groundwater discharged in discrete reaches of the mid to upper Wollombi Brook during both flood recession and

baseflow and potentially discharged smaller percentages to the lower reaches of the Wollombi Brook.

There were distinct differences in groundwater contribution to stream flow between flood recession and baseflow conditions. Changes in groundwater contribution to stream flow were commonly associated with differences in stream channel morphology (and landscape position). In the lower Wollombi Brook, stream flow was comprised of much larger percentages of alluvial groundwater during baseflow than during flood recession. In the mid catchment there was little variation in the baseflow and flood recession percentages of alluvial groundwater discharge to stream flow. Conversely, groundwater discharge to stream flow in the mid to upper Wollombi Brook was more variable. In one reach stream water was comprised of a higher percentage of alluvial groundwater during baseflow than during flood recession. Stream water in two reaches was comprised of a higher percentage of alluvial groundwater during flood recession than during baseflow. The source of groundwater discharge to stream flow switched from alluvial groundwater during flood recession to regional groundwater during baseflow in one reach of the mid to upper Wollombi Brook. In another stream reach groundwater discharge switched from a regional groundwater to an alluvial groundwater source between flood recession and baseflow conditions.

The lower Wollombi Brook received the highest percentages of groundwater discharge during baseflow, whereas the mid to upper Wollombi Brook typically received the highest percentage of groundwater discharge to stream flow during flood recession. Surface water inflows from further upstream dominated stream flow in some lower and mid reaches of the Wollombi Brook during flood recession and in some mid and upper reaches during baseflow conditions.

The point-to-point interpretation of environmental tracers in stream water has provided a powerful technique for understanding groundwater flows in the riverine environment of the Wollombi Brook catchment. In-stream water chemistry sampling is a viable alternative for understanding the dynamic exchanges between stream and groundwater systems particularly within ungauged catchments (i.e. catchments that lack groundwater level monitoring wells), facilitating water management decisions without expensive infrastructure.

7 CONCLUSIONS

7.1 OVERVIEW

The development of surface water and groundwater resources has altered the quality and quantity of groundwater discharging to surface water systems around the world. Many stream systems have transformed from net groundwater gaining to net groundwater losing stream systems. Groundwater abstraction from the alluvial aquifer adjacent to the Wollombi Brook (in eastern Australia) has modified the surface water – groundwater flow regime, threatening ecosystem health and biodiversity. Whilst an understanding of surface water and groundwater interactions is frequently sought, characterisation of stream water and groundwater interactions in low gradient conditions has been limited by methodology that requires intensive monitoring and expensive infrastructure.

The broad objective of this research was to develop methodology for determining the direction and magnitude of surface water and groundwater interactions in low gradient systems. A suite of environmental tracers were applied to (1) characterise the extent of stream water and groundwater interaction within an alluvial aquifer adjacent to a stream, (2) detect locations of groundwater discharge to stream flow, and (3) identify sources and relative contributions of different sources of groundwater to stream flow. These methods were used to compare surface water and groundwater interactions during high and low stream stages. In-stream tracer methodology was extended to establish the relative importance of groundwater discharge to stream flow in upland and lowland reaches of a stream system.

7.2 STREAM WATER AND GROUNDWATER EXCHANGE PROCESSES

7.2.1 Extent of stream water and groundwater interaction in alluvial aquifers

Environmental tracer data showed that significant surface water and groundwater exchange can occur contrary to the net direction of surface water and groundwater flux (as indicated by hydraulic gradients) when gradients between surface water and groundwater are low. Radon-222 concentrations in the alluvial aquifer were persistently lower than that estimated by secular equilibrium with aquifer minerals indicating extensive stream water penetration into the alluvial aquifer on a time scale of <12 days. The results during high and low discharge conditions show that higher stream flows do not necessarily generate more extensive stream water and groundwater exchange within the adjacent alluvial aquifer (Chapter 3). Lateral stream water and groundwater exchange within the alluvial aquifer adjacent to the Wollombi Brook was more extensive (over a 12 day period) and the groundwater velocity was faster during low stream flow (baseflow) than during higher stream flow (flood recession) conditions. In contrast, vertical stream water and groundwater exchange within the adjacent alluvial aquifer (over a 12 day period) was more extensive during flood recession than baseflow conditions.

7.2.2 Regional groundwater contribution to alluvial aquifers

It was hypothesised that the alluvial aquifer adjacent to the Wollombi Brook was recharged by stream water during flood flows and by regional groundwater during low stream flows. Regional groundwater levels were higher than alluvial groundwater levels at one of the three piezometer and bore network sites in the Wollombi Brook catchment. Alluvial groundwater did not exhibit elevated ^{222}Rn concentrations in response to regional groundwater contribution to the alluvial

aquifer. Therefore, any regional groundwater discharge to the alluvial aquifer occurred along flowpaths that took longer than one week to arrive at the alluvial groundwater monitoring sites during flood recession (Mar-01) and baseflow (Nov-01) conditions (Chapter 3).

Fresh alluvial groundwater that has recharged from surface water appears to provide a buffer against higher salinity regional groundwater discharge to the alluvial aquifer in some reaches of the Wollombi Brook catchment. Abstraction of alluvial groundwater in these areas may result in increased saline regional groundwater discharge to the alluvial aquifer and subsequently discharge higher salinity groundwater to the Wollombi Brook.

7.2.3 Groundwater contribution to stream flow

Chloride, ^{222}Rn, $\delta^{2}H$, $\delta^{18}O$, $[Sr^{2+}]$ and $^{87}Sr/^{86}Sr$ data showed that alluvial groundwater contributed to streamflow between most surface water sampling stations along the length of the Wollombi Brook during flood recession (Mar-01) and baseflow (Nov-01) conditions (Chapters 4 and 6) and for the majority of the time-series monitoring (Oct-00 to Jan-02, Chapter 5). Regional groundwater discharged to discrete segments in the upper reaches and potentially to discrete reaches in the lower Wollombi Brook during both flood recession and baseflow conditions (Chapters 5 and 6). Regional groundwater was most likely to contribute to stream flow in the lower reaches of the Wollombi Brook during the receding limb of high stream stage events and unlikely to contribute during any other stages of the stream hydrograph (Chapter 5).

In upper reaches of stream systems, where alluvial aquifers tend to be narrow and shallow, regional groundwater was hypothesised to provide the dominant source of

groundwater to stream flow. However, this thesis has shown that even where alluvial aquifers may appear to be of little consequence in the mid to upper reaches of stream systems, they can still provide an important component of water to sustain stream flow. On average stream flow in the mid to upper reaches of the Wollombi Brook catchment (in the incised Triassic sandstone gullies) was comprised of similar proportions of alluvial groundwater during flood recession (15 to 36%) and baseflow (9 to 33%) conditions (Chapter 6). During flood recession stream flow was comprised of a high proportion (up to 37%) of regional groundwater in only one reach of the upper Wollombi Brook. During baseflow a high proportion of stream flow (56 to 67%) was comprised of regional groundwater in one other reach of the upper Wollombi Brook. However, overall alluvial groundwater was the dominant source of groundwater contributing to stream flow in the upper reaches of the Wollombi Brook during both flood recession and baseflow conditions.

Alluvial groundwater was the only source of groundwater that discharged to stream flow in the mid reaches of the Wollombi Brook during both flood recession and baseflow conditions (Chapters 5 and 6). However, the proportion of stream water derived from alluvial groundwater discharge within the mid reaches was much lower than alluvial groundwater discharge in the upper and lower reaches of the Wollombi Brook. There was little variation between flood recession and baseflow proportions of alluvial groundwater discharge to the mid reaches of the Wollombi Brook. These characteristics were probably generated by the abrupt change in stream channel morphology between the upper and mid reaches of the Wollombi Brook.

Similar to the mid reaches of the Wollombi Brook, there was little variation in the proportions of groundwater contributing to stream flow in the mid to lower Wollombi Brook between flood recession and baseflow conditions (Chapter 6). However, in contrast to the mid reaches of the Wollombi Brook, there was potential

for both alluvial groundwater and regional groundwater discharge to stream flow in the mid to lower reaches of the Wollombi Brook. The potential proportions of alluvial groundwater discharge to stream flow were higher in the mid to lower reaches than in the mid reaches of the Wollombi Brook. These changes in groundwater discharge to stream flow were associated with the transition from deeply incised Triassic sandstone gullies to broad and shallow stream channels that meander through lowland floodplains.

In the lower Wollombi Brook average alluvial groundwater discharge to stream flow was much higher during baseflow (80 to 100%, Chapter 6) than during flood recession (7 to 20%) conditions. Since hydraulic gradients from the alluvial aquifer to the stream are higher during flood recession than baseflow, the lower proportion of alluvial groundwater in the lower Wollombi Brook is probably largely due to the greater surface runoff that dilutes alluvial groundwater that is discharged to the stream during flood recession.

7.3 METHOD DEVELOPMENT FOR INVESTIGATING SURFACE WATER AND GROUNDWATER EXCHANGE

7.3.1 Surface water and groundwater exchange

Tracer methodology developed for this thesis enabled point-scale (on the order of 100 m) investigation of the extent of surface water and groundwater interaction within aquifer systems adjacent to surface water bodies. Naturally occurring ^{222}Rn concentrations in groundwater were compared to steady state ^{222}Rn emanation from aquifer material to estimate the short-term residence time (<12 days) of groundwater within the aquifer (Chapter 3). The technique assumes that the initial ^{222}Rn concentration of surface water influxes to the adjacent aquifer is negligible and that the "new" groundwater gradually acquires the ^{222}Rn concentration of "old"

groundwater via ^{222}Rn emanation from aquifer material. The technique assumes that "new" groundwater completely displaces "old" groundwater rather than mixing with it. As such, estimates of the extent of surface water infiltration into the adjacent aquifer within a 12 day period are conservative.

This method of investigating the extent of surface water and groundwater exchange within aquifers adjacent to streams is particularly useful for, but is not limited to, low hydraulic gradient systems and enables an estimate of groundwater flow velocity. It is, however, limited to short-term surface water and groundwater exchange processes (<12 days) and by the distance between groundwater sampling points.

7.3.2 Groundwater discharge to stream flow

A suite of naturally occurring environmental tracers (Cl^-, ^{222}Rn, δ^2H-$\delta^{18}O$ and $^{87}Sr/^{86}Sr$) were measured in stream water to identify locations, sources and proportions of groundwater discharge to stream flow. The effectiveness of these tracers for characterising groundwater discharge to stream flow depends on the ability to precisely characterise the end members and processes that modify them within the stream channel (i.e. evaporation and gas exchange). A numerical approach to account for ^{222}Rn losses from stream water was developed to identify locations, sources and proportions of groundwater discharge to stream flow. A method for interpreting δ^2H-$\delta^{18}O$ signatures in stream water based on the slope between successive sampling points was developed to identify sources of groundwater discharge to stream flow.

Previous investigations have used ^{222}Rn concentrations in stream water to identify groundwater discharge to stream flow at the point-scale (on the order of 50 m, e.g. Ellins *et al.* 1990). The sensitivity of the ^{222}Rn technique was refined via an iterative

numerical approach to account for ^{222}Rn loss from stream water via radioactive decay and gas exchange simultaneously (Chapter 4). This enabled the expansion of the technique to identify groundwater discharge to stream flow on the reach-scale (e.g. at the scale of 1 to 10 km). The numerical approach was further developed to estimate the magnitude and to differentiate between sources of groundwater discharge to stream flow (Chapter 4).

The ^{222}Rn method for identifying groundwater discharge to stream flow involves measuring series ("run of river") of ^{222}Rn concentrations in stream water at appropriate intervals along the length of the stream system. Corrections for ^{222}Rn loss from stream water (requiring some knowledge of average stream depth and velocity) highlight reaches of the stream system where ^{222}Rn concentrations surpass background levels indicating groundwater discharge to stream flow. Selection of intervals between stream water sampling points becomes critical if magnitudes and sources of groundwater discharge to stream flow are sought. The strategy devised for selecting optimal intervals between stream water sampling points for estimating the magnitude and sources of groundwater discharge to stream flow requires prior knowledge of stream velocity, stream depth and ^{222}Rn concentrations in stream water and groundwater (Chapter 4). Sources of groundwater discharge to stream flow can only be differentiated if they have distinctively different ^{222}Rn concentrations (e.g. order of magnitude) and if the distances between stream water sampling points are sufficiently small (e.g. for the Wollombi Brook <2 km).

In the Wollombi Brook catchment, the optimal interval between stream water sampling points was 2 km (Chapter 4). Since this distance was formulated subsequent to the field program in the Wollombi Brook catchment, the interval between many stream water sampling points exceeded 2 km. Therefore, the magnitude of groundwater discharge to stream flow based on ^{222}Rn concentrations in

stream water was not well constrained in all reaches of the Wollombi Brook. The intervals between stream water sampling stations were also too large to use ^{222}Rn concentrations in stream water for differentiating between the potential sources of groundwater discharge to stream flow. Changes in Cl^- concentration, slopes of δ^2H-$\delta^{18}O$ lines and changes in $^{87}Sr/^{86}Sr$ signatures between consecutive stream water sampling points gave a better indication of the sources of groundwater discharge to stream flow (Chapter 5). Whilst two component end-member mixing of Cl^- concentrations and three component end-member mixing of Sr^{2+} concentrations and $^{87}Sr/^{86}Sr$ gave better indications of the proportions of groundwater discharge to stream flow between consecutive stream water sampling points (Chapter 6).

The slope of the δ^2H-$\delta^{18}O$ evaporation line in conjunction with the changes in δ^2H signature and Cl^- concentration of stream water between sampling points was used to differentiate between stream water that (1) was evaporated within the stream channel, (2) was evaporated through unsaturated soils (i.e. shallow alluvial groundwater) prior to discharge to stream flow, or (3) mixed with non-evaporated groundwater (i.e. regional groundwater or deep alluvial groundwater) prior to evaporation within the stream channel (Chapter 5). Low slopes (2 to 4) indicte evaporation from the unsaturated zone within the alluvial aquifer, slopes of 4 to 6 indicate evaporation from the open water, and intermediate slopes (approximately 4) can be caused by evaporation from the shallow water table.

REFERENCES

Akber R A, Pfitzner J L (1994). Atmospheric concentrations of radon and radon daughters in Jabiro East. Technical Memorandum 45. Supervising Scientist for the Alligator Rivers Region, AGPS, Canberra.

Allison G B (1982). The relationship between 18O and deuterium in water in sand columns undergoing evaporation. *Journal of Hydrology* **55**: 163-169.

Allison G B, Barnes C J (1983). Estimation of evaporation from non-vegetated surfaces using natural deuterium. *Nature* **301**: 143-145.

Allison G B, Barnes C J (1985). Estimation of evaporation from the normally "dry" Lake Frome in South Australia. *Journal of Hydrology* **78**: 229-242.

Allison G B, Barnes C J, Hughes M W (1983). The distribution of deuterium and ^{18}O in dry soils 2. Experimental. *Journal of Hydrology* **64**: 377-397.

Allison G B, Barnes C J, Hughes M W, Leaney F W J (1984). Effect of climate and vegetation on oxygen-18 and deuterium profiles in soils. In *Isotope Hydrology*, IAEA Symposium, September 1983, Vienna, 270/20: 105-123.

Allison G B, Gat J R, Leaney F W J (1985). The relationship between deuterium and oxygen-18 delta values in leaf water. *Chemical Geology* **58**: 145-156.

Al-Masri M S, Blackburn R (1999). Radon-222 and related activities in surface waters of the English Lake District. *Applied Radiation Isotopes* **50**: 1137-1143.

Andrews J N, Lee D J (1979). Inert gases in ground water from the Bunter Sandstone of England as indicators of age and paleoclimatic trends. *Journal of Hydrology* **41**: 233-252.

Andrews J N, Wood D F (1972). Mechanism of radon release in rock matrices and entry in groundwater. *Transactions Institution of Mining and Metallurgy*. **81**: 197-209.

Baker V R (1977). Stream-channel response to floods, with examples from central Texas. *Geological Society of America Bulletin* **88**: 1057-1071.

Baixeras C, Erlandsson B, Font Ll, Jönsson, G (2001). Radon emanation from soil samples. *Radiation Measurements* **34**: 441-443.

Benner S G, Smart E W, Moore J N (1995). Metal behaviour during surface-groundwater interaction, Silver Bow Creek, Montana. *Environmental Science & Technology* **29**: 1789-1795.

Bennett P, Mooney S D (2003). A palynological reconstruction of pre-European riparian vegetation at Wollombi, New South Wales and its application to stream bank management and revegetation. *Ecological Management & Restoration* **4**: S69-S78.

Bertin C, Bourg A C M (1994). Radon-222 and chloride as natural tracers of the infiltration of river water into an alluvial aquifer in which there is significant river/groundwater mixing. *Environmental Science & Technology*, **28**: 794-798.

Bogard D D, Gurnett D S, Eberhardt P, Wasserburg G J (1967). Rb^{87}-Sr^{87} isochron and K^{40}-Ar^{40} ages of the Norton County Chondrite. *Earth and Planetary Science Letters* **3**: 179-189.

Bourg A C M, Bertin C (1993). Biogeochemical processes during the infiltration of river water into an alluvial aquifer. *Environmental Science & Technology* **27**:661-666.

Broecker W S, Peng T H (1982). *Tracers in the Sea*. Eldigio Press, Palisades, NY, pp 689.

Bullen T D, Kendall C (1998). Tracing of weathering reactions and water flowpaths: A multi-isotope approach. In *Isotope Tracers in Catchment Hydrology* (editors Kendall C, McDonnell J J), Elsevier, Amsterdam, pp. 610-646.

Bullen T D, Krabbenhoft D P, Kendall C (1996). Kinetic and mineralogic controls on the evolution of groundwater chemistry and $^{87}Sr/^{86}Sr$ in a sandy silicate aquifer, northern Wisconsin, USA. *Geochimica et Cosmochimica Acta* **60(10)**: 1807-1821.

Burt T P, Bates P D, Stewart M D, Claxton A J, Anderson M G, Price D A (2002). Water table fluctuations within the floodplain of the River Severn, England. *Journal of Hydrology* **262**: 1-20.

Cecil L D, Green J R (2000). Radon-222. In *Environmental tracers in subsurface hydrology* (editors Cook P G, Herczeg A L). Kluwer Academic Publishers, USA, pp. 175-194.

Cey E E, Rudolph D L, Parkin G W, Aravena R (1998). Quantifying groundwater discharge to a small perennial stream in southern Ontario, Canada. *Journal of Hydrology* **210**: 21-37.

Chen J, Wheater H S, Lees M J (2002). Identification of processes affecting stream chloride response in the Hafren catchment, mid-Wales. *Journal of Hydrology* **264**: 284-290.

Choubey V M, Bartarya S K, Ramola R C (2000). Radon in Himalayan springs: a geohydrological control. *Environmental Geology* **39(6)**: 523-530.

Christophersen N, Neal C (1990). Linking hydrological, geochemical, and soil chemical processes on the catchment scale: An interplay between modeling and field work. *Water Resources Research* **26(12)**: 3077-3086.

Clark I, Fritz P (1997). *Environmental Isotopes in Hydrology*. Lewis Publishers, New York, pp 328.

Cook P G, Dighton J C (2000). Dissolved radon concentrations in fractured rock aquifers. In *Groundwater: Past achievements and future challenges* (editors: Sililo O *et al.*). Proceedings of the 30th IAH Congress, Cape Town, South Africa, 26 November – 1 December 2000, Balkema, Rotterdam, 475-480.

Cook P G, Favreau G, Dighton J C, Tickell S (2003). Determining natural groundwater influx to a tropical river using radon, chlorofluorocarbons and ionic environmental tracers. *Journal of Hydrology* **277**: 74-88.

Cook P G, Herczeg A L, McEwan K L (2001). Groundwater recharge and stream base flow. CSIRO Land and Water Technical Report 08/01, pp 84.

Corbett D R, Burnett W C, Cable P H, Clark S B (1997). Radon tracing of groundwater input into Par Pond, Savannah River Site. *Journal of Hydrology* **203**: 209-227.

Craig H (1961). Isotopic variations in natural waters. *Science* **133**: 1702-1703.

Dahm C N, Grimm N B, Marmonier P, Valett H M, Vervier P (1998). Nutrient dynamics at the interface between surface waters and groundwaters. *Freshwater Biology* **40**: 427-451.

Dent C L, Schade J D, Grimm N B, Fisher S G (2000). Subsurface influences on surface biology. In *Streams and Ground Waters* (editors Jones J B, Mulholland P J), Academic Press, London, pp 381-401.

Devito K J, Hill A R, Roulet N (1996). Groundwater-surface water interactions in headwater forested wetlands of the Canadian Shield. *Journal of Hydrology* **181**: 127-147.

Dinçer T, Al-Mugrin A, Zimmermann U (1974). Study of the infiltration and recharge through the sand dunes in arid zones with special reference to the stable isotopes and thermonuclear tritium. *Journal of Hydrology* **23**: 79-109.

DLWC (1999). Stressed Rivers Assessment Report. Hunter Catchment. Department of Land and Water Conservation, Sydney, HO/17/98.

Douglas G B, Gray C M, Hart B T,Beckett R (1995). A strontium isotopic investigation of the origin of suspended particulate matter (SPM) in the Murray-Darling River system, Australia. *Geochimica et Cosmochimica Acta* **59(18)**: 3799-3815.

Dransgaard W (1964). Stable isotopes in precipitation. *Tellus* **16**: 436-468.

Duff J H, Triska F J (2000). Nitrogen biogeochemistry and surface-subsurface exchange in streams. In *Streams and Ground Waters* (editors Jones J B, Mulholland P J) Academic Press, London, pp 197-220.

Ellins K K (1988). Isotope Hydrology of Karst Drainage Basins in Jamaica and Puerto Rico. Ph.D. thesis, Colombia University.

Ellins K K, Romas-Mas A, Lee R (1990). Using ^{222}Rn to examine groundwater/surface discharge interaction in the Rio Grande de Manati, Puerto Rico. *Journal of Hydrology* **115**: 319-341.

Elsinger R J, Moore W (1983). Gas exchange in the Pee Dee River based on ^{222}Rn evasion. *Geophysical Research Letters* **10**: 443-446.

Emerson S, Broecker W S (1973). Gas exchange rates in a small lake as determined by the radon method. *Journal of the Fisheries Research Board of Canada* **30**: 1475-1484.

Erskine W D (1994). Flood-driven channel changes on Wollombi Brook, NSW since European settlement. In *The way of the river: Environmental perspectives on the*

Wollombi (editors: Mahony D, Whitehead J). Newey and Beath Printers Pty. Ltd, Newcastle, Australia, pp 41-69.

Fairchild I J, Killawee J A, Hubbard B, Dreybrodt W (1999). Interactions of calcareous suspended sediment with glacial meltwater: A field test of dissolution behaviour. *Chemical Geology* **155**: 243-263.

Faure G, Powell J L (1972). Strontium Isotope Geology. In *Minerals, Rocks and Inorganic Materials* (editors W von Engelhardt, T Hahn, R Roy, P J Wyllie). Monograph Series of Theoretical Studies, 5. Springer – Verlag, Berlin. pp 180.

Fiebig D M, Lock M A, Neal C (1990). Soil water in the riparian zone as a source of carbon for a headwater stream. *Journal of Hydrology* **116**: 217-237.

Foden J, Mawby J, Kelly S, Turner S, Bruce D (1995). Metamorphic events in the eastern Arunta Inlier, Part 2. Nd-Sr-Ar isotopic constraints. *Precambrian Research* **71**: 207-227.

Freeze R A, Cherry J A (1979). *Groundwater*. Prentice-Hall, New Jersey.

Gat J R (1996). Oxygen and hydrogen isotopes in the hydrologic cycle. *Annual Review of Earth and Planetary Sciences* **24**: 225-262.

Gesell T F (1983). Background atmospheric ^{222}Rn concentrations outdoors and indoors: a review. *Health Physics* **45(2)**: 289-302.

Gilkeson R H, Cartwright K, Cowart J B, Holtzman R B (1983). Hydrologic and geochemical studies of selected natural radioisotopes and barium in groundwater.

Bureau of Reclamation, U.S. Department of the Interior, Washington, DC, (UILU-WRC-83-0180).

Gonfinatini R (1978). Standards for stable isotope measurements in natural compounds. *Nature* **271**: 534-536.

Gonfiantini R (1986). Environmental isotopes in lake studies. In *Handbook of Environmental Isotope Geochemistry* (editors Fritz P, Fontes J Ch) Vol. 2, *The Terrestrial Environment.* Elsevier Scientific, Amsterdam, pp. 113-168.

Gorgoni C, Martinelli G, Sighinolfi G P (1982). Radon distribution in groundwater in the Po sedimentary basin (Italy). *Chemical Geology* **35**: 297-309.

Graustein W C (1989). $^{87}Sr/^{86}Sr$ ratios measure the sources and flow of strontium in terrestrial ecosystems. In *Stable Isotopes in Ecological Research* (editors Rundel P W, Ehleringer J R, Nagy K A). Springer-Verlag, New York, pp. 491-512.

Hamilton E I (1966). The isotopic composition of strontium in Atlantic Ocean water. *Earth and Planetary Science Letters* **1**: 435-436.

Harvey J W, Bencala K E (1993). The effect of streambed topography on surface-subsurface water exchange in mountain catchments. *Water Resources Research* **29(1)**: 89-98.

Harvey J W, Wagner B J (2000). Quantifying hydrologic interactions between streams and their subsurface hyporheic zones. In *Streams and Ground Waters* (editors Jones J B, Mulholland P J) Academic Press, London, pp 3-41.

Harvey J W, Wagner B J, Bencala K E (1996). Evaluating the reliability of the stream tracer approach to characterize stream-subsurface water exchange. *Water Resources Research* **32(8)**: 2441-2451.

Hayashi M, van der Kamp G, Rudolph D L (1998). Water and solute transfer between a prairie wetland and adjacent uplands, 2. Chloride cycle. *Journal of Hydrology* **207**: 56-67.

Heaton T H E (1984). Rates and sources of ^{4}He accumulation in groundwater. *Hydrological Sciences Journal* **29(1)**: 29-47.

Hendricks S P, White D S (1991). Physiochemical patterns within the hyporheic zone of a northern Michigan river, with comments on surface water patterns. *Canadian Journal of Fisheries and Aquatic Sciences* **48**: 1645-1654.

Herczeg A L, Dighton J C, Easterbrook M L, Salomons E (1994). Measurement of radon-222 and radium-226 in ground water by liquid scintillation counting. Radon and Radon Progeny Measurements in Australia Symposium, Canberra, 18 February 1994, pp 79-82.

Hinkle S R, Duff J H, Triska F J, Laenen A, Gates E B, Bencala K E, Wentz D A, Silva S R (2001). Linking hyporheic flow and nitrogen cycling near the Willamette River - a large river in Oregon, USA. *Journal of Hydrology* **244**:157-180.

Hoehn E (1998). Solute exchange between river water and groundwater in headwater environments. In *Hydrology, Water Resources and Ecology in Headwaters* (editors Kovar K, Tappeiner U, Peters N E, Craig R G), IAHS Press, Oxfordshire, UK, pp 165-171.

Hoehn E, von Gunten H R (1989). Radon in groundwater: A tool to assess infiltration from surface waters to aquifers. *Water Resources Research*, **25(8)**: 1795-1803.

Hoehn E, von Gunten H R, Stauffer F, Dracos T (1992). Radon-222 as a groundwater tracer: A laboratory study. *Environmental Science & Technology*, **26**: 734-738.

Hunter Integrated Telemetry System, http://hits.nsw.gov.au/

Hunt R J, Bullen T D, Krabbenhoft D P, Kendall C (1998). Using stable isotopes of water and strontium to investigate the hydrology of a natural and constructed wetland. *Ground Water* **36(3)**: 434-443.

Hussain N, Krishnaswami S (1980). U-238 series radioactive disequilibrium in groundwaters: implications to the origin of U-234 excess and fate of reactive pollutants. *Geochimica et Cosmochimica Acta* **44(9)**: 1287-1291.

Jönsson G (1999). Experience from using plastic film in radon measurement. *Radiation Measurements* **31**: 265-270.

Kendall C, Sklash M, Bullen T D (1995). Isotope tracers of water and solute sources in catchments. In *Solute Modelling in Catchment Systems* (editor Trudgill S T). Wiley, New York, pp 261-303.

Krabbenhoft D P, Bowser C J, Kendall C, Gat J R (1994). Use of oxygen-18 and deuterium to assess the hydrology of groundwater-lake systems. In *Environmental*

Chemistry of Lakes and Reservoirs (editor L A Baker) ACS Advances in Chemistry Series No. 237. American Chemical Society, Washington, D C, 67-90.

Kraemer T F, Genereux D P (1998). Applications of uranium- and thorium-series radionuclides in catchment hydrology studies. In *Isotope Tracers in Catchment Hydrology* (editors Kendall C, McDonnell J J), Elsevier, Amsterdam, pp 679-722.

Krishnaswami S, Graustein W C, Turekian K K (1982). Radium, thorium, and radioactive lead isotopes in groundwaters: Application to the in-situ determination of adsorption-desorption rate constants and retardation factors. *Water Resources Research* **18(6)**: 1633-1675.

Kutilek M, Nielsen D R (1994). *Soil Hydrology*. Catena Verlag, Germany, pp 370.

Lamontagne S, Dighton J, Ullman W (2002). Estimation of groundwater velocity in riparian zones using point dilution tests. CSIRO Land and Water Technical Report 14/02, 1-16.

Lamontagne S, Herczeg A L, Dighton J C, Pritchard J L, Jiwan, J S, Ullman W J (2003). Groundwater-surface water interactions between streams and alluvial aquifers: Results from the Wollombi Brook (NSW) study (Part II – Biogeochemical processes). CSIRO Land and Water Technical Report 42/03, 1-64.

Lee D R, Cherry J A (1978). A field exercise on groundwater flow using seepage meters and mini-piezometers. *Journal of Geological Education* **27**:6-10.

Lee R W, Hollyday E F (1987). Radon measurement in streams to determine location and magnitude of ground-water seepage. In *Radon, Radium and other Radioactivity in Ground Water* (editor Graves B), Lewis Publishers Inc, USA, pp. 241-249.

Lee R W, Hollyday E F (1993). Use of radon measurements in Carter Creek, Maury County, Tennessee, to determine location and magnitude of groundwater seepage. In *Field studies of radon in rocks, soils and water* (editors Gunderson L C S, Wanty R B), E C Coley, USA, pp. 237-242.

LeGrand H E (1987). Radon and radium emanations from fractured crystalline rocks – A conceptual hydrological model. *Ground Water* **25(1)**: 59-69.

Legrand-Marcq C, Laudelot H (1985). Longitudinal dispersion in a forest stream. *Journal of Hydrology* **78**: 317-324.

Lewis W K, Whitman W C (1924). Principles of gas absorbtion. *Industrial & Engineering Chemistry Research* **17**: 1215-1220.

McDonnell J J, Bonell M, Stewart M K, Pearce A J (1990). Deuterium variations in storm rainfall: implications for stream hydrograph separation. *Water Resources Research* **26**: 455-458.

MER (2000). South Bulga Colliery proposed south east extension groundwater and hydrogeological studies. *Mackie Environmental Research*, pp 27.

Miretzky P, Cirelli A F (2004). Silica dynamics in a pampean lake (Lake Chascoumús, Argentina). *Chemical Geology* **203**: 109-122.

Morrice J A, Valett H M, Dahm C N, Campana M E (1997). Alluvial characteristics, groundwater-surface water exchange and hydrological retention in headwater streams. *Hydrological Processes* **11**: 253-267.

Mosley M P (1979). Streamflow generation in a forested watershed, New Zealand. *Water Resources Research* **15(4)**: 795-806.

Neilsen G H, Culley J L, Cameron D R (1980). Nonpoint N runoff from agricultural watersheds into the Great Lakes. *Journal of Great Lakes Research* **6**: 195-202.

Nobi N, Das Gupta A (1997). Simulation of regional flow and salinity intrusion in an integrated stream-aquifer system in coastal region: southwest region of Bangladesh. *Ground Water* **35(5)**: 786-796.

O'Connor D J, Dobbins W E (1958). Mechanism of reaeration in natural streams. *Transactions of the American Society of Civil Engineers* **2394**: 641-684.

Ogunkoya O O, Jenkins A (1991). Analysis of runoff pathways and flow contributions using deuterium and stream chemistry. *Hydrological Processes* **5**: 271-282.

Onda Y, Komatsu Y, Tsujimura M, Fujihara J (2001). The role of subsurface runoff through bedrock on storm flow generation. *Hydrological Processes* **15**: 1693-1706.

Pinder G F, Jones J F (1969). Determination of the ground-water components of peak discharge from the chemistry of total runoff. *Water Resources Research* **5**: 438-445.

Plummer L N, Prestemon E C, Parkhurst D L (1994). An interactive code (NETPATH) for modeling NET geochemical reactions along FLOW path Version 2.0. US Geological Survey Water Resources Investigations Report 94-4169.

Prichard H, Gesell T F (1983). Radon-222 in municipal water supplies in the central United States. *Health Physics.* **45**: 991.

Quade J, Chivas A R, McCulloch M T (1995). Strontium and carbon isotope tracers and the origins of soil carbonate in South Australia and Victoria. *Palaeogeography, Palaeoclimatology, Palaeoecology* **113**: 103-117.

Revesz K, Woods P H (1990). A method to extract soil water for isotopic analyses. *Journal of Hydrology* **115**: 397-406.

Rogers A S (1958). Physical behaviour and geologic control of radon in mountain streams. U.S. Geological Survey Bulletin 1052-E, pp187.

Rutherford J E, Hynes H B N (1987). Dissolved organic carbon in streams and groundwater. *Hydrobiologia* **154**: 33-48.

Salomons E R, Leaney F W, Herczeg A L (1991). Naturally occurring ^{222}Rn as a tracer for throughflow separation on a hill slope. Centre for Groundwater Studies, Adelaide, Report No. 36.

Seimbille F, Manhes G, Allegre C J (1988). Isotopic composition and content of strontium in rainwater. *Chemical Geology* **70(1-2)**: 16.

Snow D D, Spalding R F (1997). Short-term aquifer residence times estimated from ^{222}Rn disequilibrium in artificially recharged ground water. *Journal of Environmental Radioactivity*, **37(3)**: 307-325.

Standard Methods for the Examination of Water and Wastewater (1999). 20th edition American Public Health Association, American Water Works Association, Water Environment Federation.

Stewart B W, Capo R C, Chadwick O A (1998). Quantitative strontium isotope models for weathering, pedogenesis and biogeochemical cycling. *Geoderma* **82**: 173-195.

Stone W J (1992). Estimating contamination potential at waste-disposal sites using a natural tracer. *Environmental Geology and Water Sciences* **19(3)**: 139-145.

Tanner A B (1964). Radon migration in the ground: A review. In *Natural Radiation Environment* (editors Adams J A S, Lowder W M). University of Chicago Press, Chicago, pp. 161-190.

Tanner A B (1980). Radon migration in the ground: A supplementary review. Proceedings of the Symposium on Third Natural Radiation Environment, Vol. 1., Houston, Texas, April 1978, pp. 5-56.

Triska F J, Duff J H, Avanzino R J (1993). The role of water exchange between a stream channel and its hyporheic zone in nitrogen cycling at the terrestrial-aquatic interface. *Hydrobiologia* **251**: 167-184.

Triska F J, Kennedy V C, Avanzino R J, Zellweger GW, Bencala K E (1989). Retention and transport of nutrients in a third-order stream in northwestern California: Hyporheic processes. *Ecology* **70(6)**: 1893-1905.

Uliana M W, Sharp J M Jr. (2001). Tracing regional flow paths to major springs in Trans-Pecos Texas using geochemical data and geochemical models. *Chemical Geology* **179**: 53-72.

Valett H M, Fisher S G, Stanley E H (1990). Physical and chemical characteristics of the hyporheic zone of a Sonoran Desert stream. *Journal of the North American Benthological Society* **9(3)**: 201-215.

Webb A A, Erskine W D (2003). A practical scientific approach to riparian vegetation rehabilitation in Australia. *Journal of Environmental Management* **68**: 329-341.

Wetzel R G (2001). Salinity of inland waters. In *Limnology, Lake and River Systems*. Academic Press, USA, 169-204.

Whittlestone S, Robinson E, Ryan S (1992). Radon at the Manua Loa Observatory. Transport from distant continents. *Atmospheric Environment* **26(2)**: 251-260.

Winter T C, Harvey J W, Lehn Franke O, Alley W M (1998). Groundwater and surface water: A single resource. *U.S. Geological Survey Circular* **1139**, pp79.

Woessner W W (2000). Stream and fluvial plain ground water interactions: Rescaling hydrogeologic thought. *Ground Water* **38(3)**: 423-429.

Wondzell S M, Swanson F J (1996). Seasonal and storm dynamics of the hyporheic zone of a 4th order mountain stream; I: Hydrologic processes. *Journal of the North American Benthological Society* **15(1)**: 3-19.

Wroblicky G J, Campana M E, Valett H M, Dahm C N (1998). Seasonal variation in surface-subsurface water exchange and hyporheic area of two stream-aquifer systems. *Water Resources Research* **34(3)**: 317-328.

Zimmermann U, Ehhalt D, Münnich K O (1967). Soil - water movement and evapotranspiration: Changes in the isotopic composition of the water. In*: Isotopes in Hydrology*, IAEA Conference proceedings 14-18 November 1966, Vienna, 567-585.

APPENDIX A:
SURFACE WATER & GROUNDWATER CHEMISTRY

Table A.1 Run of river survey, Trip 2 (May 2000).

Location code	Temperature °C	Field pH	EC µS/cm	TDS mg/L	Cl^- mg/L	SO_4^{2-} mg/L	Alkalinity as HCO_3^- mg/L	Ca^{2+} mg/L	K^+ mg/L	Mg^{2+} mg/L	Na^+ mg/L	Si mg/L	^{222}Rn mBq/L
1	10.5	7.99	643	396	146	17.0	101	13	4.5	17	95	2.7	147
2	12.5	7.68	536	-	-	-	-	-	-	-	-	-	155
3	9.2	7.53	510	325	124	7.3	74.0	14	4.9	16	83	2.2	62
4	15.0	7.58	404	233	91	6.4	58.1	9.2	3.9	11	52	1.9	53
6	14.0	7.33	370	217	84	6.5	53.9	8.9	4.0	10	48	2.0	91
7	13.7	6.71	367	220	86	7.3	53.7	8.9	4.0	10	48	2.1	87
9	13.2	9.83	373	-	-	-	-	-	-	-	-	-	169
10	8.5	7.73	388	252	96	12.0	59.2	11	3.9	12	56	2.1	235
12	12.2	6.96	462	237	106	17.0	20.3	11	4.2	12	64	3.0	137
13	12.2	6.91	448	-	-	-	-	-	-	-	-	-	-
14	-	-	-	-	-	-	-	-	-	-	-	-	140
	13.2	7.34	426	256	96	14.0	60.0	11	4.0	12	57	1.9	166
	15.5	6.78	246	-	-	-	-	-	-	-	-	-	-

Table A.2 Run of river survey, Trip 5 (March-April 2001).

Location code	EC µS/cm	TDS mg/L	Cl^- mg/L	SO_4^{2-} mg/L	Alkalinity as HCO_3^- mg/L	Ca^{2+} mg/L	K^+ mg/L	Mg^{2+} mg/L	Na^+ mg/L	Si mg/L	^{222}Rn mBq/L	$\delta^{18}O$ ‰	δ^2H ‰
1	484	302	110	13.4	[1]74	11	5.8	13	67	3.9	122	-2.70	-12.9
2	493	293	110	6.6	77.6	11	5.5	13	65	3.6	119	-2.38	-12.8
3	462	274	110	7.4	66.3	11	5.3	12	59	3.5	70	-2.58	-11.6
4	405	237	91	7.0	59.0	9.5	5.3	11	50	3.5	59	-2.64	-12.2
5	397	-	-	-	-	-	-	-	-	-	79	-2.56	-12.1
7	387	230	86	7.6	58.6	9.6	5.1	11	49	3.6	80	-2.89	-13.1
8	389	227	86	7.6	58.4	9.5	4.9	11	48	1.9	123	-2.91	-13.7
9	393	229	88	7.2	57.7	9.3	4.9	11	48	2.8	181	-3.00	-14.4
10	400	283	110	17.9	60.8	13	5.2	12	60	4.6	220	-2.97	-13.3
11	461	273	99	14.9	69.6	12	5.0	12	56	3.9	196	-2.68	-12.4
12	481	285	110	16.4	63.8	13	5.4	12	63	1.8	149	-2.58	-12.1
13	472	-	-	-	70.5	-	-	-	-	-	156	-2.73	-12.4
14	344	200	80	4.6	47.5	6.9	4.6	9.8	43	4.0	379	-3.48	-17.0
T1	398	250	83	3.8	82.6	6.3	5.1	12	53	4.1	410	-3.68	-17.7
T2	-	724	230	7.4	265	33	15	41	[2]129	2.9	-	-	-
T7	472	284	110	2.6	78.5	9.8	8.2	14	58	2.9	294	-2.64	-12.3
T8	307	187	69	5.9	50.0	9.6	1.8	11	35	5.5	770	-4.68	-25.0
T9	468	282	100	0.6	92.0	13	6.2	16	50	3.6	769	-3.45	-17.1
T10	442	292	76	14.6	114	19	3.8	14	48	2.9	639	-3.29	-14.7

[1] Alkalinity estimated from differences between total cations and anions

[2] Na^+ estimated = 0.56 × Cl^-

Table A.3 Run of river survey, Trip 6 (September 2001).

Location code	Cl^- mg/L	$\delta^{18}O$ ‰	$\delta^{2}H$ ‰
1	265	-2.67	-14.68
3	292	0.54	-14.34
4		-2.45	
7	122	-2.63	-15.27
9	132	-2.96	-16.11
10	159	-3.06	-15.78
12	185	-2.82	-15.5
13	180	-2.98	-16.5
14	91	-2.86	-16.2
T2	820	-1.14	-12.09

Table A.4 Run of river survey, Trip 7 (October-November 2001).

Location code	Temperature °C	Field pH	EC µS/cm	TDS mg/L	Cl^- mg/L	SO_4^{2-} mg/L	Alkalinity as HCO_3^- mg/L	Ca^{2+} mg/L	K^+ mg/L	Mg^{2+} mg/L	Na^+ mg/L	Si mg/L	^{222}Rn mBq/L	$\delta^{18}O$ ‰	δ^2H ‰
1	24.5	7.87	1373	981	321	196.8	196	21	6.2	32	205	2.7	127	-0.94	-8.2
2	23.6	7.48	838	508	204	7.6	142	15	5.0	19	113	2.6	233	-1.25	-11.8
3	26.4	8.14	1584	967	420	52.4	195	30	6.4	40	220	2.5	62	-0.76	-9.0
4	19.2	7.21	1011	592	257	11.9	137	16	5.2	21	143	1.9	272	-1.31	-10.7
5	26.3	7.87	631	364	155	7.4	90.7	11	5.1	14	79	1.0	105	-0.59	-5.1
7	21.1	7.03	481	289	117	7.0	78.8	9.4	4.5	11	59	1.7	44	-1.47	-7.7
8	26.3	7.45	484	285	117	8.1	73.1	9.5	4.8	12	60	1.3	67	-1.26	-8.7
9	22.3	7.21	520	312	129	8.5	79.0	11	4.7	13	66	1.3	153	-1.65	-10.0
10	25.1	7.17	502	307	125	8.7	79.0	10	4.4	12	65	1.7	278	-1.68	-9.5
11	24.7	7.19	727	433	171	20.4	111	16	4.5	16	92	1.5	339	-1.06	-9.7
12	21.9	7.40	963	571	226	41.3	129	21	4.6	21	127	1.5	170	-1.83	-10.2
13	20.1	7.35	826	495	196	30.7	116	20	3.9	19	109	1.0	87	-1.90	-9.7
14	18.0	6.71	405	240	98	4.4	63.9	7.2	4.3	11	50	1.3	532	-1.68	-8.8
15	19.8	6.81	373	218	95	3.6	53.6	6.3	3.8	9.3	45	1.3	53	-2.35	-12.2
16	15.9	6.65	438	262	106	3.7	75.1	8.6	3.6	12	52	0.9	319	-2.85	-13.4
17	15.8	6.72	398	256	98	3.3	83.5	8.8	3.2	12	46	1.5	388	-2.84	-14.2
18	19.2	6.76	395	249	93	5.7	80.1	10	3.1	11	44	2.0	73	-2.30	-13.9
19	17.7	6.74	476	302	107	5.7	101	13	4.2	14	53	3.5	564	-1.81	-15.2
20	17.6	6.80	329	180	77	4.2	39.3	6.1	3.8	9.2	37	3.5	82	-2.15	-13.6
21	15.8	6.79	550	201	[3]92	5.6	19.9	7.4	6.1	14	51	4.3	23	-1.80	-6.6
22	22.3	6.67	366	216	92	3.4	55.0	6.2	3.9	8.6	43	3.2	228	-1.80	-12.1
23	22.3	6.60	303	190	76	3.1	53.2	4.9	3.9	8.0	39	1.6	173	-1.84	-10.7

[3] Cl^- estimated = $Na^+ \div 0.56$

Location code	Temperature °C	Field pH	EC µS/cm	TDS mg/L	Cl^- mg/L	SO_4^{2-} mg/L	Alkalinity as HCO_3^- mg/L	Ca^{2+} mg/L	K^+ mg/L	Mg^{2+} mg/L	Na^+ mg/L	Si mg/L	^{222}Rn mBq/L	$\delta^{18}O$ ‰	δ^2H ‰
24	21.5	6.79	276	172	72	3.0	47.0	4.9	3.7	7.7	33	1.4	151	-1.69	-9.6
25	18.9	6.73	271	178	73	3.6	52.9	5.2	4.3	7.6	30	1.1	253	-1.77	-9.9
26	19.3	6.38	159	121	46	0.4	45.7	4.1	3.9	5.2	15	0.5	137	-0.98	-4.3
T2	20.5	7.76	3520	2152	971	10.1	475	43	16	58	577	0.2	59	0.83	-4.1
T3	21.6	6.80	594	407	128	12.5	152	11	4.1	18	76	5.8	455	-3.80	-21.7
TB	22.4	6.88	1168	726	291	54.0	168	31	3.9	31	141	6.9	255	-3.95	-19.9
T4	22.8	6.77	407	283	105	0.4	105	7.9	4.1	11	46	3.4	578	-2.93	-15.9
T5	19.2	5.72	197	117	60	3.6	15.6	1.5	3.4	5.1	23	5.2	6430	-4.44	-20.7
T6	16.7	6.85	700	422	177	2.1	117	12	6.5	17	87	2.5	209	-0.45	-10.4
T7	15.2	6.30	337	190	81	1.5	46.3	5.2	3.5	8.5	39	4.9	1264	-3.76	-19.9
T8	19.4	7.15	320	216	78	7.3	70.6	9.2	1.6	11	33	5.2	581	-4.24	-22.6
T9	15.8	6.75	568	342	109	0.8	138	13	4.4	18	52	5.2	3878	-3.25	-17.0
T10	20.3	7.88	751	515	147	24.3	209	27	4.8	24	79	0.1	57	0.81	-3.8
T11	16.5	6.82	745	503	146	35.3	186	27	4.8	23	76	4.9	5709	-3.09	-16.9
T12	21.5	6.14	300	195	83	0.3	49.6	6.9	3.7	8.6	38	4.2	1446	-3.74	-20.1
T13	22.4	6.88	443	250	118	8.4	43.9	6.3	3.5	8.5	59	3.2	79	-2.79	-13.8

Table A.5 Time series data.

Date	EC	TDS	Cl^-	SO_4^{2-}	Alkalinity as HCO_3^-	Ca^{2+}	K^+	Mg^{2+}	Na^+	Si	$\delta^{18}O$	δ^2H
	µS/cm	mg/L	mg/L	mg/L	mg/L	mg/L	mg/L	mg/L	mg/L	mg/L	‰	‰
19/10/00	476	303	138	6.4	62.0	9.6	4.2	13	69	0.8	-1.37	-7.6
26/10/00	482	340	156	5.8	72.8	10	4.5	14	76	0.9	-1.26	-8.0
02/11/00	505	336	150	5.3	69.4	11	4.6	14	81	1.1	-1.21	-8.4
09/11/00	645	426	186	3.7	93.7	17	5.3	18	102	1.8	-1.63	-11.3
16/11/00	333	209	91	5.2	46.2	6.2	4.0	9.0	46	1.7	-2.12	-13.0
23/11/00	279	187	78	5.6	45.9	4.8	4.4	7.4	38	2.3	-2.77	-15.0
30/11/00	414	271	119	4.8	59.5	9.8	4.2	12	60	1.5	-1.18	-6.8
07/12/00	446	243	122	3.7	27.5	9.8	4.3	12	62	1.4	-0.40	-4.7
14/12/00	427	291	126	3.5	70.4	9.8	4.4	12	63	1.5	-0.32	-2.3
21/12/00	490	309	110	2.9	103	10	4.8	13	64	1.8	-0.16	-3.6
28/12/00	600	333	140	5.6	71.6	12	4.7	15	82	1.9	0.84	-0.7
04/01/01	680	374	160	4.3	82.1	13	5.1	16	92	1.8	0.52	1.6
11/01/01	730	408	170	3.8	99.1	14	5.4	17	97	1.9	0.51	-1.0
18/01/01	990	525	230	1.9	106	24	7.0	23	130	2.8	-1.21	-9.5
25/01/01	1080	577	260	1.4	113	27	7.6	25	140	3.0	-0.90	-7.0
01/02/01	1100	572	250	0.9	115	29	7.8	26	140	3.1	-2.55	-16.0
08/02/01	760	416	170	4.0	100	15	5.8	18	100	2.3	-0.62	-7.9
15/02/01	500	276	110	4.6	67.0	10	4.9	12	63	3.0	0.12	-1.1
25/02/01	310	191	71	12.0	41.9	7.4	4.8	8.3	42	3.4	-2.44	-10.9
01/03/01	290	199	67	8.6	57.4	8.0	4.6	9.0	41	3.7	-2.38	-9.6
08/03/01	290	195	67	5.4	56.7	8.1	4.2	8.9	41	3.2	-2.15	-8.6
10/03/01	140	79	31	6.5	8.0	2.8	4.2	3.3	20	3.3	-2.90	-9.1
13/03/01	140	85	33	8.6	7.7	3.5	4.6	3.8	21	3.6	-2.85	-9.2
15/03/01	190	130	43	9.3	31.6	5.0	5.1	5.5	27	4.2	-2.81	-11.2
22/03/01	350	225	86	8.4	51.8	8.6	5.5	9.3	50	4.2	-2.66	-12.0
29/03/01	360	238	91	8.0	57.5	9.0	5.3	10	52	4.2	-2.67	-12.5
05/04/01	360	235	88	7.0	59.2	9.5	5.2	11	51	3.8	-2.47	-12.3

Date	EC	TDS	Cl^-	SO_4^{2-}	Alkalinity as HCO_3^-	Ca^{2+}	K^+	Mg^{2+}	Na^+	Si	$\delta^{18}O$	δ^2H
	µS/cm	mg/L	mg/L	mg/L	mg/L	mg/L	mg/L	mg/L	mg/L	mg/L	‰	‰
12/04/01	360	235	91	5.6	58.2	9.2	5.1	11	52	3.4	-2.61	-12.2
19/04/01	390	249	97	6.2	61.2	9.7	4.9	11	56	3.1	-2.39	-12.7
26/04/01	300	179	71	7.6	36.1	6.6	5.0	7.9	41	3.3	-3.71	-17.8
03/05/01	340	218	84	9.0	49.2	8.6	4.7	9.5	50	3.0	-2.89	-15.0
08/05/01	220	133	49	8.2	24.8	5.2	5.0	5.6	31	3.4	-5.02	-24.6
10/05/01	140	107	39	9.0	16.1	4.0	4.2	4.1	27	3.4	-4.94	-25.6
17/05/01	220	153	53	10.5	36.0	5.7	4.2	6.2	33	3.8	-4.57	-23.5
24/05/01	300	182	69	10.1	39.3	6.9	4.0	8.0	41	3.7	-4.19	-20.7
31/05/01	363	240	110	10.0	46.7	9.2	4.0	9.5	48	2.9	-3.96	-18.7
07/06/01	352	251	120	10.0	45.3	8.9	4.1	9.9	50	2.6	-3.91	-19.3
14/06/01	371	252	120	9.1	47.9	9.2	4.1	9.9	49	2.4	-3.90	-19.2
21/06/01	364	266	130	9.2	48.8	9.4	4.1	10	52	2.2	-3.93	-18.6
28/06/01	422	286	140	9.6	51.0	10	4.1	11	58	2.1	-3.76	-18.3
05/07/01	422	283	140	9.9	50.1	9.8	4.1	11	56	2.0	-3.97	-18.9
12/07/01	424	296	150	10.0	51.8	10	4.1	12	57	1.8	-3.73	-19.9
19/07/01	432	298	150	11.0	52.4	10	4.0	12	57	1.6	-3.69	-18.6
26/07/01	429	297	150	11.0	52.0	10	3.9	12	57	1.5	-3.62	-18.0
02/08/01	340	239	100	11.0	45.8	9.1	4.3	11	56	1.6	-4.19	-20.3
09/08/01	370	260	110	14.0	48.9	9.8	4.5	12	59	1.5	-4.02	-19.9
16/08/01	390	272	110	15.0	51.7	11	4.5	13	65	1.2	-3.63	-18.5
23/08/01	400	288	120	15.0	56.2	11	4.5	13	67	1.2	-3.42	-17.6
30/08/01	380	265	110	13.0	53.4	9.6	4.2	12	62	1.1	-3.53	-21.0
06/09/01	380	270	110	13.0	53.9	11	4.3	13	64	0.9	-3.64	-17.8
13/09/01	400	271	110	11.0	59.8	9.9	4.4	12	63	0.8	-3.17	-17.0
20/09/01	390	274	110	11.0	58.1	10	4.6	13	66	0.8	-2.97	-16.6
27/09/01	410	294	120	11.0	63.0	12	4.8	14	68	0.7	-2.19	-14.9
04/10/01	520	293	126	9.8	64.1	9.9	4.5	13	65	0.8	-2.11	-12.7
11/10/01	510	285	125	10.5	59.5	9.4	4.4	12	64	0.8	-1.96	-12.2

Date	EC	TDS	Cl^-	SO_4^{2-}	Alkalinity as HCO_3^-	Ca^{2+}	K^+	Mg^{2+}	Na^+	Si	$\delta^{18}O$	δ^2H
	µS/cm	mg/L	mg/L	mg/L	mg/L	mg/L	mg/L	mg/L	mg/L	mg/L	‰	‰
18/10/01	490	276	126	7.1	59.2	8.6	4.3	11	59	0.9	-0.69	-8.6
25/10/01	540	297	134	6.6	62.3	9.6	4.6	13	67	1.0	-1.42	-9.6
01/11/01	600	333	146	6.5	71.7	11	5.0	14	78	1.2	-1.03	-8.9
08/11/01	530	317	132	5.8	71.5	12	4.9	14	76	1.2	-1.31	-9.6
15/11/01	540	337	143	5.9	73.8	12	5.1	15	82	1.2	-0.80	-7.8
22/11/01	540	328	140	5.9	72.2	11	4.8	14	78	1.2	-1.36	-8.7
29/11/01	520	328	139	5.4	74.3	11	4.9	14	77	1.1	-0.95	-6.5
06/12/01	560	344	149	4.9	77.6	12	5.2	14	80	1.4	-0.80	-4.6
13/12/01	570	357	152	4.5	81.7	12	5.3	15	85	1.3	-0.52	-5.0
20/12/01	530	325	136	4.6	76.3	11	5.1	14	75	1.5	-0.48	-4.1
27/12/01	600	380	156	3.9	93.5	14	5.6	16	89	1.9	-0.53	-4.4
03/01/02	650	414	166	3.3	106	16	5.9	17	97	2.1	-0.25	-5.8

Table A.6 Piezometer water and stream water chemistry measured during March 2000.

Location	Temperature	Field pH	EC	TDS	Cl^-	SO_4^{2-}	Alkalinity as HCO_3^-	Ca^{2+}	Mg^{2+}	Na^+	K^+	Si
code	°C		µS/cm	mg/L	mg/L	mg/L	mg/L	mg/L	mg/L	mg/L	mg/L	mg/L
W Brook	22.7	7.2	1867	1148	440	121.7	179.8	29.4	44.4	320	9.1	3.4
W1A	23.9	6.77	255	150	35	17.2	49.2	7.6	6.1	29	2.0	4.0
W1B	23.2	6.45	316	179	59	10.2	52.5	11.1	11.1	27	3.5	4.4
W2A	23.8	6.29	259	146	40	14.2	40.3	6.7	4.4	32	3.1	5.0
W2B	21.9	6.57	262	165	45	12.3	57.1	9.3	8.9	25	3.0	4.3
W3A	22.9	6.66	263	149	40	8.7	49.2	8.1	5.1	28	5.0	5.2
W3B	21.1	6.47	278	172	40	1.2	77.0	9.6	8.5	29	3.1	3.6
W4	21.4	6.11	235	124	43	15.0	21.5	7.8	4.2	23	3.7	5.0
W5	21.2	6.16	524	211	[4]122	37.4	21.5	15.7	14.4	68	5.3	5.0
F1A	24.9	6.41	482	322	90	9.7	117.1	13.6	16.2	66	5.9	3.1
F1B	22.1	6.42	578	360	120	1.4	119.2	16.3	17.1	78	5.6	2.9
F2	25.3	7.02	509	326	98	6.7	113.2	14.0	14.9	68	7.0	3.5
F3A	24.6	6.67	475	308	99	4.4	102.3	13.0	13.8	66	6.6	3.6
F3B	22.2	6.56	654	417	140	1.5	138.3	16.0	19.2	94	5.9	2.5
F4	25.6	6.48	545	339	110	6.9	115.0	14.0	16.4	67	6.4	3.0
F5	24.5	6.53	314	197	62	11.3	59.4	11.3	10.8	32	5.8	4.1
F6	21.6	6.52	1216	765	240	9.7	256.9	36.4	30.7	180	3.0	8.6
Wo Brook	21.7	6.51	495	302	110	3.8	82.1	14.5	13.9	70	4.4	3.3
Wo1A	23.4	6.48	485	260	62	14.6	105.7	20.4	7.8	44	3.0	2.5
Wo1B	24.6	6.38	461	263	74	1.1	105.1	15.6	11.4	47	3.9	4.6

[4] Cl^- estimated = $Na^+ \div 0.56$

Location	Temperature	Field pH	EC	TDS	Cl^-	SO_4^{2-}	Alkalinity as HCO_3^-	Ca^{2+}	Mg^{2+}	Na^+	K^+	Si
code	°C		µS/cm	mg/L	mg/L	mg/L	mg/L	mg/L	mg/L	mg/L	mg/L	mg/L
Wo2	24.3	6.48	470	278	62	14.3	118.3	23.5	9.5	43	3.0	3.9
Wo3A	22.8	6.41	467	258	66	9.6	107.6	15.8	7.9	45	2.9	2.6
Wo3B	24.5	6.35	443	237	74	4.4	83.8	11.7	11.0	46	3.6	1.6
Wo4	21.0	6.42	492	251	60	63.0	49.7	16.4	9.3	47	3.2	2.1
Wo5	21.7	6.10	417	242	68	49.2	44.2	15.5	11.0	47	2.5	4.2

Table A.7 Piezometer water, bore water and stream water chemistry measured during May 2000.

Location code	Temperature	Field pH	EC	TDS	Cl^-	SO_4^{2-}	Alkalinity as HCO_3^-	Ca^{2+}	Mg^{2+}	Na^+	K^+	Si	^{222}Rn	Error	$\delta^{18}O$	δ^2H
	°C		µS/cm	mg/L	mg/L	mg/L	mg/L	mg/L	mg/L	mg/L	mg/L	mg/L	Bq/L	Bq/L	‰	‰
W Brook	10.5	7.99	643	396	146	17.0	101.2	13.0	17.0	95	4.5	2.7	0.1	0.01	-3.41	-21.1
W1A			457													
W1B	15.2	7.90	312	202	71	7.9	60.3	9.1	12.0	35	3.2	3.3	1.8	0.13	-5.76	-37.2
W2A	14.7	7.83	236	162	36	7.5	71.2	8.8	6.3	23	3.8	5.5	1.9	0.13	-4.48	-25.0
W2B	16.8	7.93	286	245	64	1.3	110.7	19.0	8.5	35	2.3	4.3	2.1	0.13	-4.00	-20.2
W3A	14.7	7.83	236	163	41	14.2	60.1	9.6	7.1	20	5.6	5.6	2.6	0.15	-4.61	-26.4
W3B	18.9	7.47	337	212	64	0.5	83.8	12.0	11.0	32	3.6	5.1	2.8	0.16	-6.82	-45.2
W4	18.6	7.87	187	113	31	12.6	30.1	5.8	2.7	22	3.5	5.0	3.2	0.17	-4.15	-23.5
W5	19.0	7.66	258	157	43	28.0	32.3	5.3	6.3	34	3.2	5.1	5.6	0.23	-4.40	-26.1
79059	20.2	7.44	8000	3818	[5]3339	5.2	637.7	31.0	24.0	1870	14.0	6.0	12.5	0.33	-6.54	-40.7
79060	19.4	7.29	1027	584	[5]546	11.9	39.0	23.0	17.0	306	5.7	6.6	0.6	0.12	-5.82	-36.2
F Brook	9.2	7.53	510	325	124	7.3	74.0	14.0	16.0	83	4.9	2.2	0.1	0.00	-	-
F1A	12.4	7.65	331	205	40	7.5	98.7	9.3	9.6	32	3.3	5.0	2.5	0.13	-4.05	-20.5
F1B	14.4	7.47	539	332	99	2.4	133.5	15.0	19.0	55	4.5	3.8	-	-	-3.85	-21.9
F2	-	-	-		-	-	-	-	-	-	-	-	1.8	0.11	-	-
F3A	11.7	7.71	439	307	110	5.3	95.7	14.0	16.0	57	5.7	3.3	2.5	0.14	-3.41	-21.1
F3B	13.5	7.53	696	448	154	0.7	158.0	16.0	23.0	88	5.3	3.5	2.8	0.14	-3.20	-18.4
F5	-	-	-	-	-	-	-	-	-	-	-	-	2.1	0.13	-4.59	-24.9
F6	17.1	7.10	2920	1203	973	22.0	[6]10.8	72.0	67.0	413	4.7	9.5	3.34	0.16	-3.60	-21.5

[5] Cl^- estimated = $Na^+ \div 0.56$

[6] Cl^- estimated = E.C. ÷ 3

Location code	Temperature	Field pH	EC	TDS	Cl^-	SO_4^{2-}	Alkalinity as HCO_3^-	Ca^{2+}	Mg^{2+}	Na^+	K^+	Si	^{222}Rn	Error	$\delta^{18}O$	δ^2H
	°C		µS/cm	mg/L	mg/L	mg/L	mg/L	mg/L	mg/L	mg/L	mg/L	mg/L	Bq/L	Bq/L	‰	‰
79057	9.3	7.19	1229	1190	74	20.0	776.2	18.0	21.0	270	3.2	8.1	16.8	0.40	-5.03	-32.3
79058	19.0	7.01	968	387	323	20.0	[7]41.5	74.0	39.0	95	1.4	23.0	24.6	0.57	-5.19	-33.8
Wo Brook	8.5	7.73	388	252	96	12.0	59.2	11.0	12.0	56	3.9	2.1	0.2	0.01	-	-
Wo1B	9.4	7.70	510	-	-	-	-	-	-	-	-	-	-	-	-	-
Wo1C	10.3	6.62	448	185	42	11.8	78.3	9.4	9.3	26	3.0	5.3	2.7	0.15	-4.11	-21.5
Wo2	13.0	7.30	383	-	-	-	-	-	-	-	-	-			-	-
Wo3A	14.2	6.90	388	-	-	-	-	-	-	-	-	-	-	-	-	-
Wo3B	15.6	6.80	421	-	-	-	-	-	-	-	-	-	-	-	-	-
Wo4	14.3	6.84	369	223	70	12.3	74.6	10.0	8.2	41	2.5	4.4	2.4	0.15	-4.13	-22.3
Wo5	14.0	6.60	384	-	-	-	-	-	-	-	-	-	-	-	-	-
79055	18.1	6.72	2170	1816	328	41.5	928.1	54.0	60.0	376	22.0	6.4	5.6	0.22	-5.86	-34.6
79056	18.0	6.13	736	431	188	12.9	94.5	17.0	15.0	93	4.3	6.8	4.1	0.19	-5.43	-31.8

[7] Cl^- estimated = E.C. ÷ 3

Table A.8 Piezometer water, bore water and stream water chemistry measured during October 2000.

Location code	Temperature	Field pH	EC	TDS	Cl^-	SO_4^{2-}	Alkalinity as HCO_3^-	Ca^{2+}	Mg^{2+}	Na^+	K^+	$\delta^{18}O$	δ^2H
	°C		µS/cm	mg/L	mg/L	mg/L	mg/L	mg/L	mg/L	mg/L	mg/L	‰	‰
W Brook	12.7	6.39	1377	358	341	87.6	16.6	23.0	35.0	244	6.8	-1.62	-12.3
W1B	20.5	6.78	254	58	53	-	5.4	-	-	-	-	-4.75	-24.1
W2A	20.5	6.15	217	45	39	-	6.0	-	-	-	-	-4.40	-23.2
W2B	21.6	6.03	251	51	47	-	4.4	-	-	-	-	-	-22.5
W3A	21.3	6.06	228	46	39	-	6.6	-	-	-	-	-4.43	-23.9
W3B	17.9	6.66	274	55	45	-	9.5	-	-	-	-	-4.71	-29.3
W4	18.2	7.07	239	46	41	-	4.5	-	-	-	-	-4.87	-19.3
W5	20.5	6.71	486	112	108	-	3.9	-	-	-	-	-5.01	-29.9
WDP1	23.9	-	353	1935	997	135.5	[8]426	67.0	73.0	649	13.0	-2.92	-17.6
WDP2	24.1	-	295	251	115	30.4	[8]76	19.0	12.0	71	4.0	-4.69	-27.7
WDP3	-	-	-	200	80	24.1	[8]114	14.0	12.0	65	4.5	-5.06	-30.6
79059	-	-	-	3411	1285	0.7	[8]3470	34.0	16.0	2062	13.6	-6.59	-41.5
79060	-	-	-	471	164	22.8	[8]484	25.0	16.0	237	5.8	-5.89	-37.5
F Brook	-	-	-	-	-	-	-	-	-	-	-	0.04	-4.7
F1A	15.8	7.10	495	128	113	-	15.1	-	-	-	-	-3.20	-18.9
F1B	17.1	6.82	545	120	106	-	13.7	-	-	-	-		
F3A	17.3	6.91	497	111	98	-	13.4	-	-	-	-	-3.36	-17.0
F3B	15.9	6.96	629	134	120	-	13.8	-	-	-	-		
F5	16.2	7.14	229	41	34	-	7.3	-	-	-	-	-4.31	-24.6
F6	16.9	6.99	3230	885	797	-	87.6	-	-	-	-	-3.30	-20.1

[8] Alkalinity estimated from differences between total cations and anions

Location code	Temperature	Field pH	EC	TDS	Cl^-	SO_4^{2-}	Alkalinity as HCO_3^-	Ca^{2+}	Mg^{2+}	Na^+	K^+	$\delta^{18}O$	δ^2H
	°C		µS/cm	mg/L	mg/L	mg/L	mg/L	mg/L	mg/L	mg/L	mg/L	‰	‰
FoDP1	-	-	1425	598	292	3.1	[9]379	54.0	27.0	219	2.4	-3.97	-24.6
FoDP2	-	-	1215	532	271	1.5	[9]275	26.0	21.0	207	5.5	-3.15	-18.7
FoDP3	-	-	958	400	210	1.8	[9]196	37.0	21.0	127	3.0	-2.57	-16.6
79057	-	-	-	396	76	20.8	[9]687	20.0	19.0	257	3.1	-9.9	-32.1
79058	-	-	-	283	71	19.8	[9]466	68.0	33.0	90	1.0	-5.22	-33.5
Wo Brook	19.3	6.98	428	111	107	9.8	3.9	-	12.0	63.0	4.3	-2.1	-13.4
Wo1B	-	-	-	-	-	-	13.5	-	-	-	-	-	-
Wo2	17.9	6.66	407	-	66	-	-	-	-	-	-	-4.30	-23.2
Wo3A	17.4	6.68	406	80	66	-	13.7	-	-	-	-	-4.3	-24.2
Wo3B	16.7	6.33	394	80	68	-	12.3	-	-	-	-	-4.51	-25.2
Wo4	16.5	6.35	401	86	76	-	10.5	-	-	-	-	-4.60	-22.9
Wo5	17.3	5.97	395	82	80	-	2.4	-	-	-	-	-4.34	-24.3
WoDP1	-	-	-	712	[10]293	3.2	[9]126	26	22	164	5.9	-5.29	-31.6
WoDP2	-	-	-	154	90	2.3	[9]18	11	4.3	44	2.5	-5.67	-35.1
79055	-	-	-	898	316	42.2	[9]989	74	64	377	24.3	-6.11	-35.5
79056	-	-	-	365	202	13.6	[9]76	23	17	105	4.6	-5.61	-32.2

[9] Alkalinity estimated from differences between total cations and anions

[10] Cl^- estimated = $Na^+ \div 0.56$

Table A.9 Piezometer water, bore water and stream water chemistry measured during March 2001.

Location code	Temperature	EC	TDS	Cl^-	SO_4^{2-}	Alkalinity as HCO_3^-	Ca^{2+}	Mg^{2+}	Na^+	K^+	Si	^{222}Rn	Error	$\delta^{18}O$	δ^2H
	°C	µS/cm	mg/L	mg/L	mg/L	mg/L	mg/L	mg/L	mg/L	mg/L	mg/L	Bq/L	Bq/L	‰	‰
W Brook	22.2	484	224	110	13.4	[11]78	10.6	12.8	67	5.8	3.9	0.1	0.01	-2.66	-12.9
W1B	23.8	616	-	100	29.4	72.3	-	-	-	-	-	-	-	-3.06	-17.1
W2B	25.3	474	-	51	26.2	84.2	-	-	-	-	-	4.2	0.23	-3.73	-21.2
W3A	23.5	304	189	42	13.8	72.9	4.9	3.7	43	3.8	5.6	2.8	0.20	-2.76	-12.9
W3B	22.8	309	196	49	2.3	85.7	9.6	9.4	32	3.5	5.1	3.9	0.22	-4.74	-27.9
W4	25.1	155	99	13	16.6	37.5	4.7	2.5	17	3.6	5.0	3.8	0.22	-2.72	-13.7
W5	22.4	175	116	34	9.5	33.5	2.3	2.6	27	2.5	4.7	8.5	0.32	-2.89	-10.2
WDP1	22.3	827	483	[12]268	9.6	179.9	21.0	22.0	150	5.7	4.8	5.5	0.25	-4.81	-28.1
WDP2	22.9	334	198	49	21.9	63.5	12.8	10.2	31	4.5	5.6	5.9	0.28	-4.62	-27.6
WDP3	21.5	522	-	-	-	145.0	-	-	-	-	-			-5.20	-31.4
79059	22.9	6620	3783	[13]2207	<0.4	710.9	20.0	10.5	2100	15.1	6.6	12.9	0.30	-5.09	-29.8
79060	22.0	1712	1155	180	12	531.8	16.7	11.5	390	6.7	6.2	2.3	0.17	-6.34	-38.1
F Brook	-	445	260	100	7.5	65.5	10.0	11.7	56	5.4	3.6	0.1	0.00	-2.50	-12.8
F1B	-	480	302	100	2.8	103.4	12.5	14.6	60	5.4	3.8	-	-	-2.56	-14.3
F3A	-	341	221	70	8.2	73.9	9.6	11.0	40	4.5	3.7	-	-	-2.72	-13.2
F3B	-	709	447	130	<0.4	184.1	17.7	25.3	81	5.4	4.0	-	-	-2.87	-17.1
F5	-	229	182	16	5.9	107.9	6.4	5.5	32	3.6	4.1	-	-	-2.10	-8.7

[11] Alkalinity estimated from differences between total cations and anions

[12] Cl^- estimated = $Na^+ \div 0.56$

[13] Cl^- estimated = E.C. ÷ 3

Location code	Temperature	EC	TDS	Cl^-	SO_4^{2-}	Alkalinity as HCO_3^-	Ca^{2+}	Mg^{2+}	Na^+	K^+	Si	^{222}Rn	Error	$\delta^{18}O$	δ^2H
	°C	µS/cm	mg/L	mg/L	mg/L	mg/L	mg/L	mg/L	mg/L	mg/L	mg/L	Bq/L	Bq/L	‰	‰
F6	-	1955	1280	380	46.6	442.9	49.1	47.7	300	1.8	11.8	-	-	-2.83	-14.5
FoDP1	-	1478	1055	320	<0.4	402.9	54.3	28.9	230	3.2	15.4	-	-	-3.98	-24.9
FoDP2	-	1309	814	280	<0.4	265.1	24.6	21.4	210	6.4	6.5	-	-	-3.29	-20.5
FoDP3	-	585	361	130	5.9	109.2	16.1	16.0	73	6.5	4.4	-	-	-	-
79057	-	1236	311	[14]412	17.7	-	69.0	35.0	92	1.3	21.6	-	-	-	-
79058	-	954	-	-	-	516.5	-	-	-	-	-	-	-	-5.23	-32.9
Wo Brook	-	394	235	86	9.7	60.8	9.9	10.5	49	5.3	3.8	0.2	0.01	-2.94	-14.1
Wo2	21.6	558	280	100	<0.4	92.0	19.1	9.1	53	2.1	5.1	3.4	0.13	-2.88	-14.7
Wo3B	22.0	464	224	87	0.7	66.1	11.8	10.2	41	2.3	4.6	4.6	0.15	-2.92	-15.6
Wo4	21.0	530	258	93	5.4	81.3	14.9	15.3	41	1.7	5.3	2.7	0.11	-3.02	-13.4
Wo5	20.2	418	204	85	16.1	34.3	5.9	8.9	47	1.6	4.4	-	-	-4.04	-22.0
WoDP1	-	-	344	[15]90	8.6	56.4	10.2	10.7	50	3.9	3.6	0.2	0.05	-3.02	-13.4
WoDP2	20.9	265	183	59	3.5	56.2	14.9	5.1	37	2.9	4.3	1.4	0.09	-4.58	-23.2
79055	19.6	2370	1903	330	24.5	983.0	75.3	66.5	390	25.9	7.9	4.3	0.13	-6.03	-34.9
79056	19.2	934	455	200	6.2	99.7	20.0	19.6	100	3.5	6.5	4.6	0.13	-5.76	-32.3

[14] Cl^- estimated = E.C. ÷ 3

[15] Cl^- estimated = Na^+ ÷ 0.56

Table A.10 Piezometer water, bore water and stream water chemistry measured during November 2001.

Location code	Temperature	Field pH	EC	TDS	Cl^-	SO_4^{2-}	Alkalinity as HCO_3^-	Ca^{2+}	Mg^{2+}	Na^+	K^+	Si	^{222}Rn	Error	$\delta^{18}O$	δ^2H
	°C		µS/cm	mg/L	mg/L	mg/L	mg/L	mg/L	mg/L	mg/L	mg/L	mg/L	Bq/L	Bq/L	‰	‰
W Brook	-	-	-	823	310	64.0	196.3	19.0	30.0	195	6.1	3.0	0.1	0.01	-0.94	-8.2
W1B	-	-	-	184	62	10.0	60.6	5.0	6.4	31	2.7	6.1	2.5	0.33	-3.64	-16.1
W2B	-	-	-	197	66	6.9	66.8	7.6	6.4	34	3.3	5.9	3.6	0.37	-3.9	-18.0
W3A	25.0	6.72	320	177	75	17.0	27.4	6.5	2.9	39	3.1	5.8	2.3	0.32	-4.69	-25.3
W3B	22.1	6.96	291	200	71	1.4	75.1	6.9	7.1	30	2.8	6.0	3.7	0.38	-3.07	-20.2
W4	-	6.60	288	190	56	18.0	61.0	7.3	3.0	35	3.6	6.3	2.3	0.33	-3.47	-15.6
W5	24.7	6.41	530	387	103	35.0	153.2	12.0	14.0	60	4.7	5.6	-	-	-4.9	-21.2
WDP1	-	-	-	428	111	0.7	205.6	12.0	13.0	77	3.5	5.9	5.7	0.44	-4.4	-25.7
WDP2	-	6.82	268	194	66	11.0	59.5	7.5	4.9	34	4.7	6.9	3.5	0.39	-3.45	-18.4
WDP3	23.8	6.95	468	342	81	19.0	134.1	15.0	13.0	68	4.4	7.4	5.8	0.43	-4.64	-28.2
79059	22.5	7.55	5910	1941	[16]2827	-	101.9	11.0	8.2	1583	9.7	6.8	16.2	1.06	-4.66	-38.6
79060	23.8	7.24	1874	1712	216	-	1051.4	22.0	17.0	392	6.4	7.4	15.0	0.66	-6.33	-39.1
F Brook	-	-	-	919	420	16.0	195.1	28.0	38.0	213	6.4	2.7	0.1	0.01	-0.76	-9.0
F1B	18.1	6.99	633	419	136	<0.4	170.3	15.0	18.0	71	4.1	4.6	1.6	0.18	-2.88	-16.8
F3A	19.5	7.02	566	399	117	<0.4	177.8	13.0	16.0	67	4.1	4.3	2.9	0.21	-3.36	-16.1
F3B	18.3	6.97	814	536	170	<0.4	211.4	18.0	23.0	104	4.8	4.8	3.5	0.23	-2.69	-18.5
F5	19.2	6.80	316	241	64	3.0	115.4	10.0	7.0	33	3.7	4.9	1.9	0.19	-3.14	-13.4
F6	19.4	6.82	6430	2549	1740	122.0	538.3	27.0	24.0	[17]974	4.8	14.0	2.5	0.19	-3.34	-18.6
FoDP1	-	-	-	1090	310	<0.4	471.0	51.0	28.0	213	2.8	14.0	4.8	0.28	-4.03	-25.0

[16] Cl^- estimated = $Na^+ \div 0.56$

[17] Na^+ estimated = $Cl^- \times 0.56$

Location code	Temperature	Field pH	EC	TDS	Cl^-	SO_4^{2-}	Alkalinity as HCO_3^-	Ca^{2+}	Mg^{2+}	Na^+	K^+	Si	^{222}Rn	Error	$\delta^{18}O$	δ^2H
	°C		µS/cm	mg/L	mg/L	mg/L	mg/L	mg/L	mg/L	mg/L	mg/L	mg/L	Bq/L	Bq/L	‰	‰
FoDP2	-	6.81	1276	821	262	2.8	315.7	21.0	19.0	188	6.0	7.0	4.5	0.27	-3.29	-20.0
FoDP3	18.8	7.06	1222	821	270	0.5	318.3	43.0	31.0	145	3.9	10.0	3.0	0.21	-2.89	-18.2
79057	20.9	6.10	973	1304	81	-	922.6	19.0	20.0	249	2.9	9.0	15.8	0.43	-5.02	-30.8
79058	20.3	7.19	879	710	102	-	387.6	69.0	35.0	91	0.9	25.0	37.8	0.88	-5.02	-32.8
Wo Brook	-	-	-	-	125	-	79.0	-	-	-	-	-	0.3	0.01	-1.68	-9.5
Wo2	20.4	6.88	470	263	76	-	115.6	12.0	8.3	41	2.2	7.7	3.0	0.19	-3.99	-19.8
Wo3B	18.7	6.60	463	248	84	-	93.3	9.4	9.6	43	2.5	6.7	4.9	0.23	-3.78	-21.6
Wo4	19.5	6.58	458	228	84	-	76.3	8.9	10.0	39	2.5	7.3	2.0	0.48	-4.68	-23.7
Wo5	18.0	6.16	395	183	84	-	32.3	4.8	8.4	45	1.9	7.1	6.2	0.26	-4.25	-20.8
WoDP2	17.7	6.58	465	193	81	0.5	51.8	6.2	4.0	41	2.4	6.5	1.6	0.30	-5.95	-33.1
79055	18.8	6.94	2410	1982	333	-	1146.6	64.0	61.0	347	23.0	8.2	0.8	0.25	-6.29	-34.8
79056	19.1	6.46	1088	546	228	-	154.9	20.0	22.0	108	4.7	8.3	3.9	0.41	-5.83	-32.0

Table A.11 Estimates of alluvial groundwater (**AGW**) and regional groundwater (**RGW**) discharge to stream flow based on two component end-member mixing analyses, March - April 2001.

stream reach	TDS	Cl^-	Alkalinity as HCO_3
1 – 2	**AGW:** >3% conc **RGW:** 0 – 1% conc	n/e	**AGW:** >1% conc **RGW:** <1% conc **evaporation:** no
2 – 3	**AGW:** >5% conc **RGW:** 0.5 - 2% conc **T1:** - **evaporation:** partial	n/e	**AGW:** >10% conc **RGW:** 2 - 13% conc **T1:** >69% conc **evaporation:** partial
3 – 4	**AGW:** >4% conc **RGW:** 4 - 9% conc **T2:** 38% conc **evaporation:** partial	**AGW:** >7% conc **RGW:** <6% conc **T2:** 14% conc **evaporation:** partial	**AGW:** 2 - 49% conc **RGW:** <2% conc **T2:** 4% conc **evaporation:** partial
4 – 7	**AGW:** >65% conc **RGW:** 1 - 2% conc **evaporation:** 4 - 5 no, 5 – 7 yes	**AGW:** >2% conc **RGW:** <2% conc **evaporation:** 4 - 5 no, 5 – 7 yes	**AGW:** <2% conc **RGW:** <2% conc **evaporation:** 4 - 5 no, 5 – 7 yes
7 – 8	**AGW:** >4% conc **RGW:** <1% conc	**AGW:** dil **RGW:** -	**AGW:** >1% conc **RGW:** <1% conc **evaporation:** no
8 – 9	**AGW:** >4% dil **RGW:** -	**AGW:** >7% dil **RGW:** -	**AGW:** >2% conc **RGW:** <2% conc **evaporation:** no
9 – 10	**AGW:** >54% dil **RGW:** -	**AGW:** >43% dil **RGW:** -	**AGW:** >12% dil **RGW:** -
10 – 11	**AGW:** - **RGW:** 0.5 - 6% conc **14:** - **T6:** 96% conc	**AGW:** - **RGW:** 5 – 11% conc **14:** - **T6:** - **evaporation:** no	**AGW:** >25% dil **RGW:** - **14:** 40% dil **T6:** -
11 – 12	**AGW:** >12% dil **RGW:** - **T8:** 12% dil **T9:** - **T10:** -	**AGW:** >22% dil **RGW:** - **T8:** 28% dil **T9:** - **T10:** 33% dil	**AGW:** >21% conc **RGW:** 1 - 16% conc **T8:** - **T9:** 21% dil **T10:** 12% dil **evaporation:** no
12 – 13	**evaporation:** yes	n/s	**AGW:** >19% dil **RGW:** -

n/e not evident
n/a data not available
dil dilution
conc concentration
evaporation potential for the evapo-concentration of salts (yes or no) based on shift in water isotopes between consecutive sampling stations

stream reach	SO_4^{2-}	Na^+	Ca^{2+}
1 – 2	**AGW:** >30% conc **RGW:** - **evaporation:** no	**AGW:** >2% conc **RGW:** <1% conc **evaporation:** no	**AGW:** >6% dil **RGW:** -
2 – 3	**AGW:** >17% dil **RGW:** >12% dil **T1:** 24% dil	**AGW:** >7% conc **RGW:** <2% conc **T1:** - **evaporation:** partial	**AGW:** >6% conc **RGW:** 6 - 9% conc **T1:** - **evaporation:** partial
3 – 4	**AGW:** >1% conc **RGW:** <4% conc **T2:** - **evaporation:** partial	**AGW:** >3% conc **RGW:** <21% conc **T2:** 11% conc **evaporation:** partial	**AGW:** >2% conc **RGW:** <2% conc **T2:** 4% conc **evaporation:** partial
4 – 7	**AGW:** >9% dil **RGW:** -	**AGW:** >1% conc **RGW:** <4% conc **evaporation:** 4 – 5 no, 5 – 7 yes	**AGW:** >2% dil **RGW:** -
7 – 8	**AGW:** >1% conc **RGW:** conc **evaporation:** no	**AGW:** >3% conc **RGW:** <1% conc **evaporation:** no	**AGW:** >1% conc **RGW:** <1% conc **evaporation:** no
8 – 9	**AGW:** >4% conc **RGW:** >2% conc **evaporation:** no	**AGW:** dil **RGW:** -	**AGW:** >2% conc **RGW:** <2% conc **evaporation:** no
9 – 10	**AGW:** >61% dil **RGW:** >92% dil	**AGW:** >49% dil **RGW:** -	**AGW:** >55% dil **RGW:** -
10 – 11	**AGW:** - **RGW:** >32% conc **14:** - **T6:** - **evaporation:** no	**AGW:** - **RGW:** 1 - 7% conc **14:** - **T6:** - **evaporation:** no	**AGW:** >15% conc **RGW:** 2 - 13% conc **14:** - **T6:** - **evaporation:** no
11 – 12	**AGW:** >10% dil **RGW:** >15% dil **T8:** 15% dil **T9:** 10% dil **T10:** 83% dil	**AGW:** 24 - 64% dil **RGW:** - **T8:** 22% dil **T9:** 51% dil **T10:** 43% dil	**AGW:** >2% dil **RGW:** - **T8:** 4% dil **T9:** - **T10:** -
12 – 13	n/a	n/a	n/a

stream reach	Mg^{2+}	K^{+}	$SiO_{2\,(aq)}$
1 – 2	**AGW:** >3% dil **RGW:** <11% dil	**AGW:** - **RGW:** 4 - 28% conc **evaporation:** no	**AGW:** 14 – 26% conc **RGW:** 9 - 11% conc **evaporation:** no
2 – 3	**AGW:** >9% conc **RGW:** - **T1:** - **evaporation:** partial	**AGW:** >36% conc **RGW:** 1 – 10% conc **T1:** - **evaporation:** partial	**AGW:** 7 - 11% conc **RGW:** 4 - 5% conc **T1:** 22% conc **evaporation:** partial
3 – 4	**AGW:** >4% conc **RGW:** <6% conc **T2:** 5% conc **evaporation:** partial	**AGW:** >6% conc **RGW:** <6% conc **T2:** 1% conc **evaporation:** partial	**AGW:** <4% conc **RGW:** <1% conc **T2:** - **evaporation:** partial
4 – 7	**AGW:** >1% conc **RGW:** <2% conc **evaporation:** 4 – 5 no, 5 – 7 yes	**AGW:** >11% conc **RGW:** - **evaporation:** 4 – 5 no, 5 – 7 yes	**AGW:** - **RGW:** -
7 – 8	**AGW:** dil **RGW:** -	**AGW:** - **RGW:** >1% conc **evaporation:** no	**AGW:** 49 – 98% conc **RGW:** 27 - 36% conc **evaporation:** no
8 – 9	**AGW:** >2% dil **RGW:** -	**AGW:** - **RGW:** conc **evaporation:** no	**AGW:** - **RGW:** -
9 – 10	**AGW:** >16% dil **RGW:** -	**AGW:** 8 - 23% dil **RGW:** >17% dil	**AGW:** - **RGW:** -
10 – 11	**AGW:** >2% conc **RGW:** <2% conc **14:** - **T6:** 6% conc **evaporation:** no	**AGW:** - **RGW:** >1% conc **14:** - **T6:** 7% conc **evaporation:** no	**AGW:** >51% conc **RGW:** 18 - 27% conc **14:** - **T6:** - **evaporation:** no
11 – 12	**AGW:** >3% dil **RGW:** - **T8:** 16% dil **T9:** - **T10:** -	**AGW:** 10 - 25% dil **RGW:** <20% dil **T8:** 11% dil **T9:** - **T10:** 24% dil	**AGW:** >60% conc **RGW:** 34 - 45% conc **T8:** 57% conc **T9:** - **T10:** - **evaporation:** no
12 – 13	n/a	n/a	n/a

Table A.12 Estimates of alluvial groundwater (**AGW**) and regional groundwater (**RGW**) discharge to stream flow based on two component end-member mixing analyses, September – November 2001.

stream reach	TDS	Cl^-	Alkalinity as HCO_3^-
1 – 2	**AGW**: - **RGW**: 12 - 39% conc **evaporation**: yes	**AGW**: - **RGW**: >4% conc **evaporation**: yes	**AGW**: >85% conc **RGW**: >6% conc **evaporation**: yes
2 – 3	**AGW**: 58 – 85% dil **RGW**: -	**AGW**: 59 – 70% dil **RGW**: -	**AGW**: >32% dil **RGW**: >57% dil
3 – 4	**AGW**: >13% conc **RGW**: <53% conc **evaporation**: yes **T2:** 24% conc **T3:** -	**AGW**: (shallow) >85% conc (deep) 12 - 29% conc **RGW**: (shallow) 3.5% conc **evaporation**: yes **T2:** 23% conc **T3:** -	**AGW**: >14% conc **RGW**: 7 – 23% conc **evaporation**: yes **T2:** 23% conc **T3:** -
4 – 5	**AGW**: >7% conc **RGW**: 24 – 66% conc **evaporation**: no **TB:** 63% conc	**AGW**: (deep) 66 - 95% conc **RGW**: (shallow) 6% conc **evaporation**: no **TB:** 75% conc	**AGW**: >10% conc **RGW**: 6 - 16% conc **evaporation**: no **TB:** 60% conc
5 – 7	**AGW**: >2% conc **RGW**: 7 - 18% conc **evaporation**: yes	**AGW**: (deep) 20 - 26% conc **RGW**: (shallow) 2% conc **evaporation**: yes	**AGW**: 3 – 33% conc **RGW**: 1 - 4% conc **evaporation**: yes
7 – 8	**AGW**: - **RGW**: <2% conc	**AGW**: - **RGW**: <1% conc **evaporation**: partial	**AGW**: >13% conc **RGW**: 1 - 7% conc **evaporation**: partial
8 – 9	**AGW**: 20 - 54% dil **RGW**: -	**AGW**: 23 - 27% dil **RGW**: -	**AGW**: >13% dil **RGW**: -
9 – 10	**AGW**: - **RGW**: <2% conc **evaporation**: partial	**AGW**: - **RGW**: 2 - 4% conc **evaporation**: partial	n/e
10 – 11	**AGW**: 50 - 74% dil **RGW**: - **T6:** - **14:** -	**AGW**: 48 - 53% dil **RGW**: - **T6:** - **14:** 63% dil	**AGW**: >40% dil **RGW**: - **T6:** - **14:** 68% dil
11 – 12	**AGW**: 36 - 45% dil **RGW**: - **T8:** 39% dil **T9:** 60% dil **T10:** -	**AGW**: 36 - 39% dil **RGW**: - **T8:** 37% dil **T9:** 47% dil **T10:** 69% dil	**AGW**: >19% dil **RGW**: - **T8:** 31% dil **T9:** - **T10:** -
12 – 13	**AGW**: - **RGW**: >5% conc **evaporation**: partial	**AGW**: - **RGW**: 22 - 92% conc **evaporation**: partial	**AGW**: - **RGW**: 1 - 34% conc **evaporation:** partial

stream reach	Ca^{2+}	Na^{+}	Mg^{2+}
1 – 2	**AGW**: - **RGW**: >85% conc **evaporation**: yes	**AGW**: - **RGW**: 6 - 33% conc **evaporation**: yes	**AGW**: - **RGW**: - **evaporation**: yes
2 – 3	**AGW**: 59 - 98% dil **RGW**: >78% dil	**AGW**: 56 - 75% dil **RGW**: -	**AGW**: 57 - 82% dil **RGW**: 67-93% dil
3 – 4	**AGW**: >40% conc **RGW**: >26% conc **evaporation**: yes **T2:** 53% conc **T3:** -	**AGW**: >9% conc **RGW**: >73% conc **evaporation**: yes **T2:** 18% conc **T3:** -	**AGW**: - **RGW**: - **evaporation**: yes **T2:** 51% conc **T3:** -
4 – 5	**AGW**: >11% conc **RGW**: 8 - 60% conc **evaporation**: no **TB:** 24% conc	**AGW**: >7% conc **RGW**: >37% conc **evaporation**: no **TB:** -	**AGW**: >40% conc **RGW**: >32% conc **evaporation**: no **TB:** 40% conc
5 – 7	**AGW**: >5% conc **RGW**: <22% conc **evaporation**: yes	**AGW**: >2% conc **RGW**: 11 - 63% conc **evaporation**: yes	**AGW**: >14% conc **RGW**: 12 - 33% conc **evaporation**: yes
7 – 8	**AGW**: >2% dil **RGW**: -	**AGW**: 4 - 6% dil **RGW**: -	**AGW**: 2 - 11% dil **RGW**: -
8 – 9	**AGW**: >19% dil **RGW**: -	**AGW**: 22 - 28% dil **RGW**: -	**AGW**: 12 - 38% dil **RGW**: -
9 – 10	**AGW**: >19% conc **RGW**: <3% conc **evaporation**: partial	**AGW**: - **RGW**: <1% conc **evaporation**: partial	**AGW**: - **RGW**: <2% conc **evaporation**: partial
10 – 11	**AGW**: >53% dil **RGW**: - **T6:** - **14:** 68% dil	**AGW**: 50 - 57% dil **RGW**: - **T6:** - **14:** 64% dil	**AGW**: 29 - 59% dil **RGW**: - **T6:** - **14:** 69% dil
11 – 12	**AGW**: 29 - 52% dil **RGW**: - **T8:** 40% dil **T9:** 61% dil **T10:** -	**AGW**: 40 - 43% dil **RGW**: - **T8:** 37% dil **T9:** 47% dil **T10:** 72% dil	**AGW**: 30 - 46% dil **RGW**: - **T8:** 50% dil **T9:** - **T10:** -
12 – 13	**AGW**: - **RGW**: >4% conc **evaporation:** partial	**AGW**: - **RGW**: >7% conc **evaporation:** partial	**AGW**: - **RGW**: 6 - 73% conc **evaporation:** partial

stream reach	K^+	$SiO_{2\ (aq)}$	Sr^{2+}
1 – 2	**AGW**: - **RGW**: 26 - 86% conc **evaporation**: yes	**AGW**: 1 – 2% conc **RGW**: <1% conc **evaporation**: yes	**AGW**: - **RGW**: 15 - 22% conc **evaporation**: yes
2 – 3	**AGW**: 39 - 85% dil **RGW**: -	**AGW**: 3 - 5% conc **RGW**: <3% conc **evaporation:** partial	**AGW**: >47% dil **RGW**: -
3 – 4	**AGW**: - **RGW**: - **evaporation**: yes **T2:** 10% conc **T3:** -	**AGW**: 5 - 24% conc **RGW**: 2 - 8% conc **evaporation**: yes **T2:** - **T3:** 15% conc	**AGW**: >4% conc **RGW**: 8 - 19% conc **evaporation**: yes **T2:** 10% conc **T3:** -
4 – 5	**AGW**: >15% conc **RGW**: **evaporation**: no **TB:** -	**AGW**: 7 - 27% conc **RGW**: 4 - 11% conc- **evaporation**: no **TB:** 15% conc	**AGW**: >5% conc **RGW**: 8 - 19% conc **evaporation**: no **TB:** 69% conc
5 – 7	**AGW**: >39% conc **RGW**: - **evaporation**: yes	**AGW**: - **RGW**: -	**AGW**: >2% conc **RGW**: 3 - 7% conc **evaporation**: yes
7 – 8	**AGW**: 10 - 12% dil **RGW**: -	**AGW**: 6 – 7% conc **RGW**: <5% conc **evaporation:** partial	**AGW**: >32% conc **RGW**: >10% conc **evaporation:** yes
8 – 9	**AGW**: - **RGW**: - **evaporation:** yes	**AGW**: <1% conc **RGW**: <1% conc **evaporation:** yes	**AGW**: >29% dil **RGW**: >29% dil
9 – 10	**AGW**: - **RGW**: >2% conc **evaporation**: partial	**AGW**: - **RGW**: -	n/e
10 – 11	**AGW**: 3 - 4% dil **RGW**: - **T6:** - **14:** 50% dil	**AGW**: 2 – 3% dil **RGW**: <2% dil **T6:** - **14:** -	**AGW**: >76% dil **RGW**: - **T6:** - **14:** 58% dil
11 – 12	**AGW**: 3 - 4% dil **RGW**: - **T8:** 3% dil **T9:** 47% dil **T10:** -	**AGW**: <1% conc **RGW**: <1% conc **evaporation:** yes **T8:** 1% conc **T9:** 1% conc **T10:** -	**AGW**: 20 - 34% dil **RGW**: >20% dil **T8:** 33% dil **T9:** - **T10:** -
12 – 13	**AGW**: - **RGW**: 3 - 83% conc **evaporation:** partial	**AGW**: 7 – 9% conc **RGW**: 6 - 7% conc **evaporation:** partial	**AGW**: - **RGW**: >82% conc **evaporation:** partial

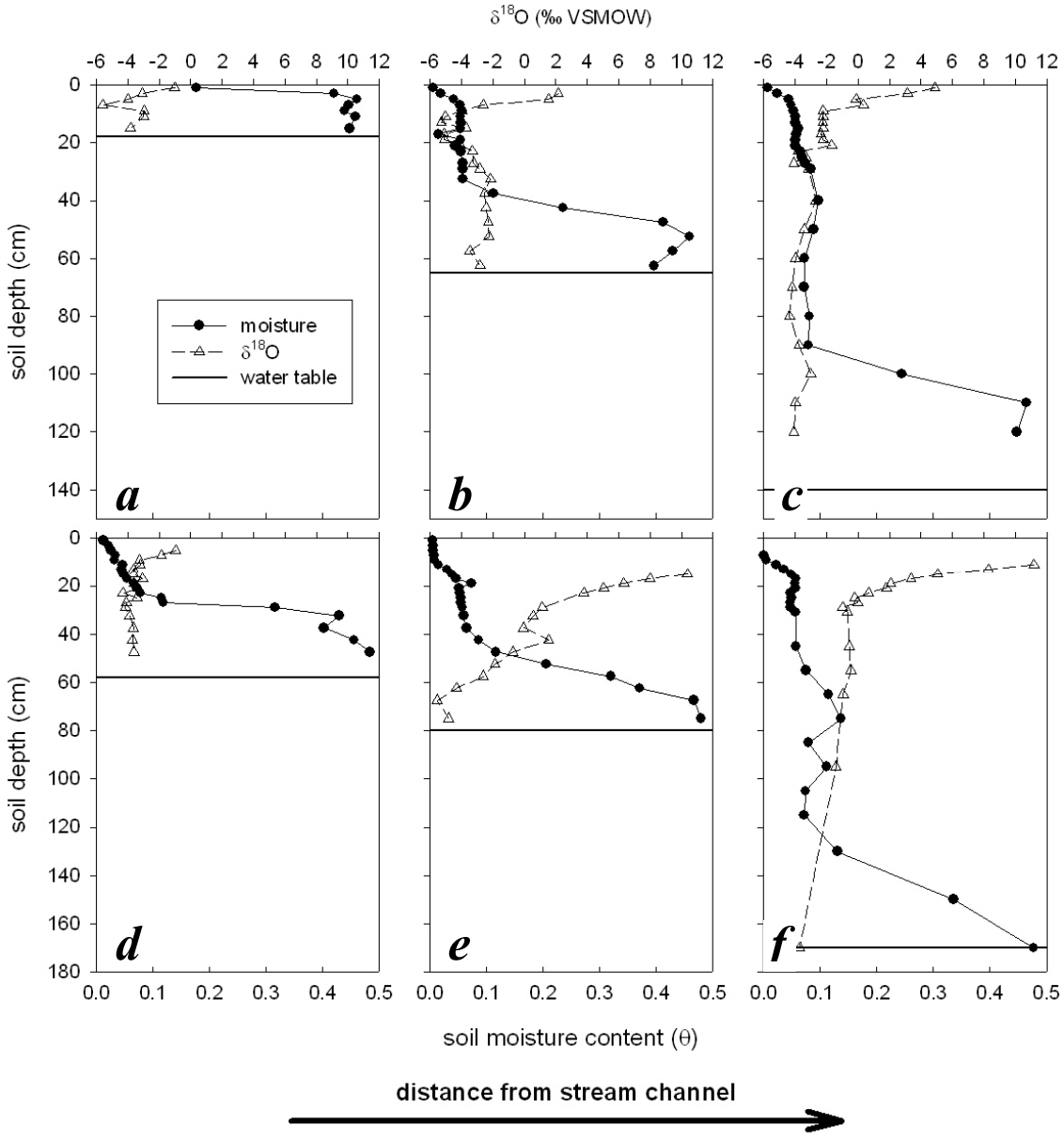

Figure A.1 Soil moisture content and $\delta^{18}O$ signature in unsaturated soils located (***a***) 2 m, (***b***) 6 m, (***c***) 21 m, (***d***) 4 m, (***e***) 10 m and (***f***) 23 m from the stream channel at sampling station 1 (Warkworth) during (***a, b, c***) flood recession (Mar-01) and (***d, e, f***) baseflow (Nov-01) conditions.

APPENDIX B:
PHREEQC GEOCHEMICAL MODELLING OUTPUT

The WEB-PHREEQ (http://www.ndsu.nodak.edu/webphreeq/) interface was used for PHREEQC geochemical modelling

Surface water sampling stations

March 2001

2

Phase	SI	log IAP	log KT	
Anhydrite	-3.68	-8.04	-4.36	CaSO4
Aragonite	-1.71	-10.04	-8.34	CaCO3
Calcite	-1.56	-10.04	-8.48	CaCO3
CH4(g)	-32.41	-76.34	-43.93	CH4
Chalcedony	-0.67	-4.22	-3.55	SiO2
Chrysotile	-8.87	23.33	32.20	Mg3Si2O5(OH)4
CO2(g)	-2.19	-20.34	-18.15	CO2
Dolomite	-2.71	-19.80	-17.09	CaMg(CO3)2
Fe(OH)3(a)	-2.35	15.56	17.91	Fe(OH)3
FeS(ppt)	-28.21	-65.78	-37.56	FeS
Goethite	3.54	15.56	12.02	FeOOH
Gypsum	-3.46	-8.04	-4.58	CaSO4:2H2O
H2(g)	-14.00	-14.00	0.00	H2
H2O(g)	-1.51	-0.00	1.51	H2O
H2S(g)	-32.75	-74.34	-41.59	H2S
Halite	-6.71	-5.12	1.58	NaCl
Hematite	9.09	31.12	22.03	Fe2O3
Jarosite-K	-16.74	13.11	29.85	KFe3(SO4)2(OH)6
Mackinawite	-27.48	-65.78	-38.30	FeS
Melanterite	-7.57	-9.78	-2.21	FeSO4:7H2O
N2(g)	-2.95	-6.21	-3.26	N2
NH3(g)	-19.58	-24.10	-4.52	NH3
O2(g)	-55.12	28.00	83.12	O2
Pyrite	-40.34	-126.12	-85.78	FeS2
Quartz	-0.24	-4.22	-3.98	SiO2
Sepiolite	-7.25	8.51	15.76	Mg2Si3O7.5OH:3H2O
Sepiolite(d)	-10.15	8.51	18.66	Mg2Si3O7.5OH:3H2O
Siderite	-0.89	-11.78	-10.89	FeCO3
SiO2(a)	-1.51	-4.22	-2.71	SiO2
Sulfur	-24.63	-60.34	-35.71	S
Talc	-6.52	14.88	21.40	Mg3Si4O10(OH)2

3

Phase	SI	log IAP	log KT	
Anhydrite	-3.62	-7.98	-4.36	CaSO4
Aragonite	-1.77	-10.11	-8.34	CaCO3
Calcite	-1.63	-10.11	-8.48	CaCO3
CH4(g)	-32.48	-76.41	-43.93	CH4
Chalcedony	-0.68	-4.23	-3.55	SiO2
Chrysotile	-8.99	23.21	32.20	Mg3Si2O5(OH)4
CO2(g)	-2.26	-20.41	-18.15	CO2
Dolomite	-2.87	-19.96	-17.09	CaMg(CO3)2
Fe(OH)3(a)	-1.98	15.94	17.91	Fe(OH)3
FeS(ppt)	-27.79	-65.35	-37.56	FeS
Goethite	3.92	15.94	12.02	FeOOH
Gypsum	-3.40	-7.98	-4.58	CaSO4:2H2O
H2(g)	-14.00	-14.00	0.00	H2
H2O(g)	-1.51	-0.00	1.51	H2O
H2S(g)	-32.70	-74.29	-41.59	H2S
Halite	-6.75	-5.16	1.58	NaCl
Hematite	9.84	31.87	22.03	Fe2O3
Jarosite-K	-15.52	14.33	29.85	KFe3(SO4)2(OH)6
Mackinawite	-27.05	-65.35	-38.30	FeS
Melanterite	-7.14	-9.35	-2.21	FeSO4:7H2O
N2(g)	-2.63	-5.89	-3.26	N2
NH3(g)	-19.42	-23.94	-4.52	NH3
O2(g)	-55.12	28.00	83.12	O2
Pyrite	-39.86	-125.64	-85.78	FeS2
Quartz	-0.25	-4.23	-3.98	SiO2
Sepiolite	-7.35	8.41	15.76	Mg2Si3O7.5OH:3H2O
Sepiolite(d)	-10.25	8.41	18.66	Mg2Si3O7.5OH:3H2O
Siderite	-0.58	-11.47	-10.89	FeCO3
SiO2(a)	-1.52	-4.23	-2.71	SiO2
Sulfur	-24.58	-60.29	-35.71	S
Talc	-6.66	14.74	21.40	Mg3Si4O10(OH)2

4

Phase	SI	log IAP	log KT	
Anhydrite	-3.67	-8.03	-4.36	CaSO4
Aragonite	-1.85	-10.19	-8.34	CaCO3
Calcite	-1.71	-10.19	-8.48	CaCO3
CH4(g)	-32.53	-76.46	-43.93	CH4

```
          Chalcedony       -0.68   -4.23   -3.55  SiO2
          Chrysotile       -9.08   23.12   32.20  Mg3Si2O5(OH)4
          CO2(g)           -2.31  -20.46  -18.15  CO2
          Dolomite         -3.03  -20.12  -17.09  CaMg(CO3)2
          Fe(OH)3(a)       -1.97   15.95   17.91  Fe(OH)3
          FeS(ppt)        -27.79  -65.35  -37.56  FeS
          Goethite          3.93   15.95   12.02  FeOOH
          Gypsum           -3.45   -8.03   -4.58  CaSO4:2H2O
          H2(g)           -14.00  -14.00    0.00  H2
          H2O(g)           -1.51   -0.00    1.51  H2O
          H2S(g)          -32.71  -74.30  -41.59  H2S
          Halite           -6.90   -5.32    1.58  NaCl
          Hematite          9.86   31.89   22.03  Fe2O3
          Jarosite-K      -15.51   14.34   29.85  KFe3(SO4)2(OH)6
          Mackinawite     -27.06  -65.35  -38.30  FeS
          Melanterite      -7.14   -9.35   -2.21  FeSO4:7H2O
          N2(g)            -2.72   -5.98   -3.26  N2
          NH3(g)          -19.47  -23.99   -4.52  NH3
          O2(g)           -55.12   28.00   83.12  O2
          Pyrite          -39.87 -125.65  -85.78  FeS2
          Quartz           -0.25   -4.23   -3.98  SiO2
          Sepiolite        -7.41    8.35   15.76  Mg2Si3O7.5OH:3H2O
          Sepiolite(d)    -10.31    8.35   18.66  Mg2Si3O7.5OH:3H2O
          Siderite         -0.62  -11.51  -10.89  FeCO3
          SiO2(a)          -1.52   -4.23   -2.71  SiO2
          Sulfur          -24.59  -60.30  -35.71  S
          Talc             -6.75   14.65   21.40  Mg3Si4O10(OH)2
-------------------------------------------------------------------------
7
-------------------------------Saturation indices----------------------
          Phase               SI log IAP  log KT
          Anhydrite        -3.64   -8.00   -4.36  CaSO4
          Aragonite        -1.69  -10.03   -8.34  CaCO3
          Calcite          -1.55  -10.03   -8.48  CaCO3
          Chalcedony       -0.67   -4.22   -3.55  SiO2
          Chrysotile       -9.07   23.13   32.20  Mg3Si2O5(OH)4
          CO2(g)           -2.15  -20.30  -18.15  CO2
          Dolomite         -2.71  -19.80  -17.09  CaMg(CO3)2
          Fe(OH)3(a)       -2.12   15.79   17.91  Fe(OH)3
          FeS(ppt)        -27.91  -65.48  -37.56  FeS
          Goethite          3.77   15.79   12.02  FeOOH
          Gypsum           -3.42   -8.00   -4.58  CaSO4:2H2O
          H2(g)           -14.00  -14.00    0.00  H2
          H2O(g)           -1.51   -0.00    1.51  H2O
          H2S(g)          -32.68  -74.26  -41.59  H2S
          Halite           -6.93   -5.35    1.58  NaCl
          Hematite          9.54   31.57   22.03  Fe2O3
          Jarosite-K      -15.94   13.91   29.85  KFe3(SO4)2(OH)6
          Mackinawite     -27.18  -65.48  -38.30  FeS
          Melanterite      -7.27   -9.48   -2.21  FeSO4:7H2O
          N2(g)            -2.66   -5.92   -3.26  N2
          NH3(g)          -19.44  -23.96   -4.52  NH3
          O2(g)           -55.12   28.00   83.12  O2
          Pyrite          -39.96 -125.74  -85.78  FeS2
          Quartz           -0.24   -4.22   -3.98  SiO2
          Sepiolite        -7.38    8.38   15.76  Mg2Si3O7.5OH:3H2O
          Sepiolite(d)    -10.28    8.38   18.66  Mg2Si3O7.5OH:3H2O
          Siderite         -0.62  -11.51  -10.89  FeCO3
          SiO2(a)          -1.51   -4.22   -2.71  SiO2
          Sulfur          -24.55  -60.26  -35.71  S
          Talc             -6.71   14.69   21.40  Mg3Si4O10(OH)2
-------------------------------------------------------------------------
8
-------------------------------Saturation indices----------------------
          Phase               SI log IAP  log KT
          Anhydrite        -3.63   -7.99   -4.36  CaSO4
          Aragonite        -1.85  -10.19   -8.34  CaCO3
          Calcite          -1.71  -10.19   -8.48  CaCO3
          CH4(g)          -32.53  -76.46  -43.93  CH4
          Chalcedony       -0.95   -4.50   -3.55  SiO2
          Chrysotile       -9.61   22.59   32.20  Mg3Si2O5(OH)4
          CO2(g)           -2.31  -20.46  -18.15  CO2
          Dolomite         -3.03  -20.12  -17.09  CaMg(CO3)2
          Fe(OH)3(a)       -2.11   15.80   17.91  Fe(OH)3
          FeS(ppt)        -27.90  -65.46  -37.56  FeS
          Goethite          3.78   15.80   12.02  FeOOH
          Gypsum           -3.41   -7.99   -4.58  CaSO4:2H2O
          H2(g)           -14.00  -14.00    0.00  H2
          H2O(g)           -1.51   -0.00    1.51  H2O
          H2S(g)          -32.67  -74.26  -41.59  H2S
          Halite           -6.94   -5.36    1.58  NaCl
          Hematite          9.57   31.60   22.03  Fe2O3
          Jarosite-K      -15.90   13.95   29.85  KFe3(SO4)2(OH)6
          Mackinawite     -27.16  -65.46  -38.30  FeS
```

```
          Melanterite      -7.25   -9.46   -2.21  FeSO4:7H2O
          N2(g)            -2.46   -5.72   -3.26  N2
          NH3(g)          -19.34  -23.86   -4.52  NH3
          O2(g)           -55.12   28.00   83.12  O2
          Pyrite          -39.94 -125.72  -85.78  FeS2
          Quartz           -0.52   -4.50   -3.98  SiO2
          Sepiolite        -8.20    7.56   15.76  Mg2Si3O7.5OH:3H2O
          Sepiolite(d)    -11.10    7.56   18.66  Mg2Si3O7.5OH:3H2O
          Siderite         -0.77  -11.66  -10.89  FeCO3
          SiO2(a)          -1.79   -4.50   -2.71  SiO2
          Sulfur          -24.55  -60.26  -35.71  S
          Talc             -7.81   13.59   21.40  Mg3Si4O10(OH)2
-------------------------------------------------------------------------
9
-----------------------------Saturation indices----------------------
          Phase               SI log IAP  log KT
          Anhydrite        -3.68   -8.05   -4.36  CaSO4
          Aragonite        -1.89  -10.23   -8.34  CaCO3
          Calcite          -1.75  -10.23   -8.48  CaCO3
          CH4(g)          -32.54  -76.47  -43.93  CH4
          Chalcedony       -0.78   -4.33   -3.55  SiO2
          Chrysotile       -9.27   22.93   32.20  Mg3Si2O5(OH)4
          CO2(g)           -2.32  -20.47  -18.15  CO2
          Dolomite         -3.07  -20.16  -17.09  CaMg(CO3)2
          Fe(OH)3(a)       -2.21   15.70   17.91  Fe(OH)3
          FeS(ppt)        -28.01  -65.58  -37.56  FeS
          Goethite          3.68   15.70   12.02  FeOOH
          Gypsum           -3.46   -8.05   -4.58  CaSO4:2H2O
          H2(g)           -14.00  -14.00    0.00  H2
          H2O(g)           -1.51   -0.00    1.51  H2O
          H2S(g)          -32.70  -74.28  -41.59  H2S
          Halite           -6.93   -5.35    1.58  NaCl
          Hematite          9.38   31.41   22.03  Fe2O3
          Jarosite-K      -16.24   13.61   29.85  KFe3(SO4)2(OH)6
          Mackinawite     -27.28  -65.58  -38.30  FeS
          Melanterite      -7.37   -9.58   -2.21  FeSO4:7H2O
          N2(g)            -2.45   -5.71   -3.26  N2
          NH3(g)          -19.33  -23.86   -4.52  NH3
          O2(g)           -55.12   28.00   83.12  O2
          Pyrite          -40.09 -125.86  -85.78  FeS2
          Quartz           -0.35   -4.33   -3.98  SiO2
          Sepiolite        -7.69    8.07   15.76  Mg2Si3O7.5OH:3H2O
          Sepiolite(d)    -10.59    8.07   18.66  Mg2Si3O7.5OH:3H2O
          Siderite         -0.87  -11.76  -10.89  FeCO3
          SiO2(a)          -1.62   -4.33   -2.71  SiO2
          Sulfur          -24.58  -60.28  -35.71  S
          Talc             -7.13   14.27   21.40  Mg3Si4O10(OH)2
-------------------------------------------------------------------------
10
-----------------------------Saturation indices----------------------
          Phase               SI log IAP  log KT
          Anhydrite        -3.18   -7.54   -4.36  CaSO4
          Aragonite        -1.74  -10.08   -8.34  CaCO3
          Calcite          -1.60  -10.08   -8.48  CaCO3
          CH4(g)          -32.52  -76.45  -43.93  CH4
          Chalcedony       -0.56   -4.12   -3.55  SiO2
          Chrysotile       -8.78   23.42   32.20  Mg3Si2O5(OH)4
          CO2(g)           -2.30  -20.45  -18.15  CO2
          Dolomite         -2.89  -19.98  -17.09  CaMg(CO3)2
          Fe(OH)3(a)       -1.68   16.23   17.91  Fe(OH)3
          FeS(ppt)        -27.11  -64.67  -37.56  FeS
          Goethite          4.21   16.23   12.02  FeOOH
          Gypsum           -2.96   -7.54   -4.58  CaSO4:2H2O
          H2(g)           -14.00  -14.00    0.00  H2
          H2O(g)           -1.51   -0.00    1.51  H2O
          H2S(g)          -32.32  -73.90  -41.59  H2S
          Halite           -6.74   -5.16    1.58  NaCl
          Hematite         10.43   32.46   22.03  Fe2O3
          Jarosite-K      -13.87   15.98   29.85  KFe3(SO4)2(OH)6
          Mackinawite     -26.37  -64.67  -38.30  FeS
          Melanterite      -6.46   -8.67   -2.21  FeSO4:7H2O
          N2(g)            -2.54   -5.80   -3.26  N2
          NH3(g)          -19.38  -23.90   -4.52  NH3
          O2(g)           -55.12   28.00   83.12  O2
          Pyrite          -38.80 -124.58  -85.78  FeS2
          Quartz           -0.14   -4.12   -3.98  SiO2
          Sepiolite        -7.01    8.75   15.76  Mg2Si3O7.5OH:3H2O
          Sepiolite(d)     -9.91    8.75   18.66  Mg2Si3O7.5OH:3H2O
          Siderite         -0.33  -11.22  -10.89  FeCO3
          SiO2(a)          -1.40   -4.12   -2.71  SiO2
          Sulfur          -24.19  -59.90  -35.71  S
          Talc             -6.21   15.19   21.40  Mg3Si4O10(OH)2
```

```
-------------------------------------------------------------------------
11
------------------------------Saturation indices-----------------------
         Phase               SI log IAP  log KT
         Anhydrite        -3.28   -7.64   -4.36  CaSO4
         Aragonite        -1.72  -10.05   -8.34  CaCO3
         Calcite          -1.57  -10.05   -8.48  CaCO3
         CH4(g)          -32.46  -76.39  -43.93  CH4
         Chalcedony       -0.64   -4.19   -3.55  SiO2
         Chrysotile       -8.91   23.29   32.20  Mg3Si2O5(OH)4
         CO2(g)           -2.24  -20.39  -18.15  CO2
         Dolomite         -2.80  -19.89  -17.09  CaMg(CO3)2
         Fe(OH)3(a)       -1.71   16.20   17.91  Fe(OH)3
         FeS(ppt)        -27.21  -64.78  -37.56  FeS
         Goethite          4.18   16.20   12.02  FeOOH
         Gypsum           -3.06   -7.64   -4.58  CaSO4:2H2O
         H2(g)           -14.00  -14.00    0.00  H2
         H2O(g)           -1.51   -0.00    1.51  H2O
         H2S(g)          -32.39  -73.98  -41.59  H2S
         Halite           -6.82   -5.23    1.58  NaCl
         Hematite         10.37   32.40   22.03  Fe2O3
         Jarosite-K      -14.14   15.71   29.85  KFe3(SO4)2(OH)6
         Mackinawite     -26.48  -64.78  -38.30  FeS
         Melanterite      -6.57   -8.78   -2.21  FeSO4:7H2O
         N2(g)            -2.58   -5.84   -3.26  N2
         NH3(g)          -19.40  -23.92   -4.52  NH3
         O2(g)           -55.12   28.00   83.12  O2
         Pyrite          -38.98 -124.76  -85.78  FeS2
         Quartz           -0.21   -4.19   -3.98  SiO2
         Sepiolite        -7.21    8.55   15.76  Mg2Si3O7.5OH:3H2O
         Sepiolite(d)    -10.11    8.55   18.66  Mg2Si3O7.5OH:3H2O
         Siderite         -0.30  -11.19  -10.89  FeCO3
         SiO2(a)          -1.48   -4.19   -2.71  SiO2
         Sulfur          -24.27  -59.98  -35.71  S
         Talc             -6.48   14.91   21.40  Mg3Si4O10(OH)2
-------------------------------------------------------------------------
14
------------------------------Saturation indices-----------------------
         Phase               SI log IAP  log KT
         Anhydrite        -3.99   -8.35   -4.36  CaSO4
         Aragonite        -2.10  -10.43   -8.34  CaCO3
         Calcite          -1.95  -10.43   -8.48  CaCO3
         CH4(g)          -32.62  -76.55  -43.93  CH4
         Chalcedony       -0.63   -4.18   -3.55  SiO2
         Chrysotile       -9.09   23.11   32.20  Mg3Si2O5(OH)4
         CO2(g)           -2.40  -20.55  -18.15  CO2
         Dolomite         -3.40  -20.49  -17.09  CaMg(CO3)2
         Fe(OH)3(a)       -2.49   15.42   17.91  Fe(OH)3
         FeS(ppt)        -28.49  -66.05  -37.56  FeS
         Goethite          3.40   15.42   12.02  FeOOH
         Gypsum           -3.77   -8.35   -4.58  CaSO4:2H2O
         H2(g)           -14.00  -14.00    0.00  H2
         H2O(g)           -1.51   -0.00    1.51  H2O
         H2S(g)          -32.88  -74.47  -41.59  H2S
         Halite           -7.01   -5.43    1.58  NaCl
         Hematite          8.80   30.83   22.03  Fe2O3
         Jarosite-K      -17.49   12.36   29.85  KFe3(SO4)2(OH)6
         Mackinawite     -27.75  -66.05  -38.30  FeS
         Melanterite      -7.84  -10.05   -2.21  FeSO4:7H2O
         N2(g)            -2.28   -5.54   -3.26  N2
         NH3(g)          -19.25  -23.77   -4.52  NH3
         O2(g)           -55.12   28.00   83.12  O2
         Pyrite          -40.74 -126.52  -85.78  FeS2
         Quartz           -0.20   -4.18   -3.98  SiO2
         Sepiolite        -7.31    8.45   15.76  Mg2Si3O7.5OH:3H2O
         Sepiolite(d)    -10.21    8.45   18.66  Mg2Si3O7.5OH:3H2O
         Siderite         -1.24  -12.13  -10.89  FeCO3
         SiO2(a)          -1.47   -4.18   -2.71  SiO2
         Sulfur          -24.76  -60.47  -35.71  S
         Talc             -6.64   14.76   21.40  Mg3Si4O10(OH)2
-------------------------------------------------------------------------
T1
------------------------------Saturation indices-----------------------
         Phase               SI log IAP  log KT
         Anhydrite        -4.13   -8.49   -4.36  CaSO4
         Aragonite        -1.91  -10.24   -8.34  CaCO3
         Calcite          -1.76  -10.24   -8.48  CaCO3
         CH4(g)          -32.38  -76.31  -43.93  CH4
         Chalcedony       -0.61   -4.17   -3.55  SiO2
         Chrysotile       -8.83   23.37   32.20  Mg3Si2O5(OH)4
         CO2(g)           -2.17  -20.31  -18.15  CO2
         Dolomite         -2.90  -19.99  -17.09  CaMg(CO3)2
         Fe(OH)3(a)       -2.22   15.69   17.91  Fe(OH)3
         FeS(ppt)        -28.30  -65.87  -37.56  FeS
```

Goethite	3.67	15.69	12.02	FeOOH
Gypsum	-3.91	-8.49	-4.58	CaSO4:2H2O
H2(g)	-14.00	-14.00	0.00	H2
H2O(g)	-1.51	-0.00	1.51	H2O
H2S(g)	-32.97	-74.56	-41.59	H2S
Halite	-6.91	-5.33	1.58	NaCl
Hematite	9.36	31.39	22.03	Fe2O3
Jarosite-K	-16.81	13.04	29.85	KFe3(SO4)2(OH)6
Mackinawite	-27.57	-65.87	-38.30	FeS
Melanterite	-7.66	-9.87	-2.21	FeSO4:7H2O
N2(g)	-2.75	-6.01	-3.26	N2
NH3(g)	-19.48	-24.01	-4.52	NH3
O2(g)	-55.12	28.00	83.12	O2
Pyrite	-40.65	-126.43	-85.78	FeS2
Quartz	-0.19	-4.17	-3.98	SiO2
Sepiolite	-7.12	8.64	15.76	Mg2Si3O7.5OH:3H2O
Sepiolite(d)	-10.02	8.64	18.66	Mg2Si3O7.5OH:3H2O
Siderite	-0.73	-11.62	-10.89	FeCO3
SiO2(a)	-1.45	-4.17	-2.71	SiO2
Sulfur	-24.85	-60.56	-35.71	S
Talc	-6.36	15.04	21.40	Mg3Si4O10(OH)2

T2

Saturation indices

Phase	SI	log IAP	log KT	
Anhydrite	-3.40	-7.76	-4.36	CaSO4
Aragonite	-0.82	-9.16	-8.34	CaCO3
Calcite	-0.68	-9.16	-8.48	CaCO3
CH4(g)	-31.90	-75.83	-43.93	CH4
Chalcedony	-0.76	-4.31	-3.55	SiO2
Chrysotile	-7.85	24.35	32.20	Mg3Si2O5(OH)4
CO2(g)	-1.69	-19.84	-18.15	CO2
Dolomite	-0.91	-18.00	-17.09	CaMg(CO3)2
Fe(OH)3(a)	-2.50	15.41	17.91	Fe(OH)3
FeS(ppt)	-28.46	-66.02	-37.56	FeS
Goethite	3.39	15.41	12.02	FeOOH
Gypsum	-3.18	-7.76	-4.58	CaSO4:2H2O
H2(g)	-14.00	-14.00	0.00	H2
H2O(g)	-1.51	-0.00	1.51	H2O
H2S(g)	-32.85	-74.44	-41.59	H2S
Halite	-5.64	-4.06	1.58	NaCl
Hematite	8.79	30.83	22.03	Fe2O3
Jarosite-K	-16.97	12.88	29.85	KFe3(SO4)2(OH)6
Mackinawite	-27.73	-66.02	-38.30	FeS
Melanterite	-7.82	-10.03	-2.21	FeSO4:7H2O
N2(g)	-2.52	-5.78	-3.26	N2
NH3(g)	-19.37	-23.89	-4.52	NH3
O2(g)	-55.12	28.00	83.12	O2
Pyrite	-40.68	-126.46	-85.78	FeS2
Quartz	-0.33	-4.31	-3.98	SiO2
Sepiolite	-6.72	9.04	15.76	Mg2Si3O7.5OH:3H2O
Sepiolite(d)	-9.62	9.04	18.66	Mg2Si3O7.5OH:3H2O
Siderite	-0.53	-11.42	-10.89	FeCO3
SiO2(a)	-1.60	-4.31	-2.71	SiO2
Sulfur	-24.73	-60.44	-35.71	S
Talc	-5.68	15.72	21.40	Mg3Si4O10(OH)2

T6

Saturation indices

Phase	SI	log IAP	log KT	
Anhydrite	-4.12	-8.48	-4.36	CaSO4
Aragonite	-1.74	-10.07	-8.34	CaCO3
Calcite	-1.59	-10.07	-8.48	CaCO3
CH4(g)	-32.41	-76.34	-43.93	CH4
Chalcedony	-0.76	-4.32	-3.55	SiO2
Chrysotile	-8.95	23.25	32.20	Mg3Si2O5(OH)4
CO2(g)	-2.19	-20.34	-18.15	CO2
Dolomite	-2.69	-19.78	-17.09	CaMg(CO3)2
Fe(OH)3(a)	-2.35	15.56	17.91	Fe(OH)3
FeS(ppt)	-28.62	-66.18	-37.56	FeS
Goethite	3.54	15.56	12.02	FeOOH
Gypsum	-3.90	-8.48	-4.58	CaSO4:2H2O
H2(g)	-14.00	-14.00	0.00	H2
H2O(g)	-1.51	-0.00	1.51	H2O
H2S(g)	-33.16	-74.74	-41.59	H2S
Halite	-6.76	-5.17	1.58	NaCl
Hematite	9.09	31.13	22.03	Fe2O3
Jarosite-K	-17.36	12.49	29.85	KFe3(SO4)2(OH)6
Mackinawite	-27.88	-66.18	-38.30	FeS
Melanterite	-7.97	-10.18	-2.21	FeSO4:7H2O
N2(g)	-3.11	-6.37	-3.26	N2
NH3(g)	-19.66	-24.18	-4.52	NH3
O2(g)	-55.12	28.00	83.12	O2
Pyrite	-41.15	-126.93	-85.78	FeS2

Quartz	-0.34	-4.32	-3.98	SiO2
Sepiolite	-7.46	8.30	15.76	Mg2Si3O7.5OH:3H2O
Sepiolite(d)	-10.36	8.30	18.66	Mg2Si3O7.5OH:3H2O
Siderite	-0.88	-11.77	-10.89	FeCO3
SiO2(a)	-1.60	-4.32	-2.71	SiO2
Sulfur	-25.03	-60.74	-35.71	S
Talc	-6.78	14.61	21.40	Mg3Si4O10(OH)2

T8

Saturation indices

Phase	SI	log IAP	log KT	
Anhydrite	-3.72	-8.08	-4.36	CaSO4
Aragonite	-1.91	-10.25	-8.34	CaCO3
Calcite	-1.77	-10.25	-8.48	CaCO3
CH4(g)	-32.60	-76.53	-43.93	CH4
Chalcedony	-0.49	-4.04	-3.55	SiO2
Chrysotile	-8.66	23.54	32.20	Mg3Si2O5(OH)4
CO2(g)	-2.38	-20.53	-18.15	CO2
Dolomite	-3.15	-20.24	-17.09	CaMg(CO3)2
Gypsum	-3.50	-8.08	-4.58	CaSO4:2H2O
H2(g)	-14.00	-14.00	0.00	H2
H2O(g)	-1.51	-0.00	1.51	H2O
H2S(g)	-32.77	-74.36	-41.59	H2S
Halite	-7.17	-5.58	1.58	NaCl
N2(g)	-2.64	-5.90	-3.26	N2
NH3(g)	-19.43	-23.95	-4.52	NH3
O2(g)	-55.12	28.00	83.12	O2
Quartz	-0.06	-4.04	-3.98	SiO2
Sepiolite	-6.80	8.96	15.76	Mg2Si3O7.5OH:3H2O
Sepiolite(d)	-9.70	8.96	18.66	Mg2Si3O7.5OH:3H2O
SiO2(a)	-1.33	-4.04	-2.71	SiO2
Sulfur	-24.65	-60.36	-35.71	S
Talc	-5.93	15.47	21.40	Mg3Si4O10(OH)2

T9

Saturation indices

Phase	SI	log IAP	log KT	
Anhydrite	-4.65	-9.01	-4.36	CaSO4
Aragonite	-1.56	-9.89	-8.34	CaCO3
Calcite	-1.41	-9.89	-8.48	CaCO3
CH4(g)	-32.34	-76.27	-43.93	CH4
Chalcedony	-0.67	-4.22	-3.55	SiO2
Chrysotile	-8.59	23.61	32.20	Mg3Si2O5(OH)4
CO2(g)	-2.12	-20.27	-18.15	CO2
Dolomite	-2.39	-19.48	-17.09	CaMg(CO3)2
Fe(OH)3(a)	-2.83	15.08	17.91	Fe(OH)3
FeS(ppt)	-29.74	-67.31	-37.56	FeS
Goethite	3.06	15.08	12.02	FeOOH
Gypsum	-4.43	-9.01	-4.58	CaSO4:2H2O
H2(g)	-14.00	-14.00	0.00	H2
H2O(g)	-1.51	-0.00	1.51	H2O
H2S(g)	-33.80	-75.39	-41.59	H2S
Halite	-6.86	-5.28	1.58	NaCl
Hematite	8.13	30.16	22.03	Fe2O3
Jarosite-K	-20.22	9.63	29.85	KFe3(SO4)2(OH)6
Mackinawite	-29.01	-67.31	-38.30	FeS
Melanterite	-9.10	-11.31	-2.21	FeSO4:7H2O
N2(g)	-3.13	-6.39	-3.26	N2
NH3(g)	-19.67	-24.20	-4.52	NH3
O2(g)	-55.12	28.00	83.12	O2
Pyrite	-42.92	-128.69	-85.78	FeS2
Quartz	-0.24	-4.22	-3.98	SiO2
Sepiolite	-7.06	8.70	15.76	Mg2Si3O7.5OH:3H2O
Sepiolite(d)	-9.96	8.70	18.66	Mg2Si3O7.5OH:3H2O
Siderite	-1.30	-12.19	-10.89	FeCO3
SiO2(a)	-1.51	-4.22	-2.71	SiO2
Sulfur	-25.68	-61.39	-35.71	S
Talc	-6.23	15.16	21.40	Mg3Si4O10(OH)2

T10

Saturation indices

Phase	SI	log IAP	log KT	
Anhydrite	-3.11	-7.47	-4.36	CaSO4
Aragonite	-1.31	-9.65	-8.34	CaCO3
Calcite	-1.17	-9.65	-8.48	CaCO3
CH4(g)	-32.25	-76.18	-43.93	CH4
Chalcedony	-0.76	-4.32	-3.55	SiO2
Chrysotile	-9.00	23.20	32.20	Mg3Si2O5(OH)4
CO2(g)	-2.03	-20.18	-18.15	CO2
Dolomite	-2.13	-19.22	-17.09	CaMg(CO3)2
Fe(OH)3(a)	-2.55	15.36	17.91	Fe(OH)3
FeS(ppt)	-28.07	-65.63	-37.56	FeS
Goethite	3.34	15.36	12.02	FeOOH
Gypsum	-2.89	-7.47	-4.58	CaSO4:2H2O

H2(g)	-14.00	-14.00	0.00	H2
H2O(g)	-1.51	-0.00	1.51	H2O
H2S(g)	-32.41	-74.00	-41.59	H2S
Halite	-6.83	-5.25	1.58	NaCl
Hematite	8.69	30.72	22.03	Fe2O3
Jarosite-K	-16.81	13.04	29.85	KFe3(SO4)2(OH)6
Mackinawite	-27.34	-65.63	-38.30	FeS
Melanterite	-7.43	-9.64	-2.21	FeSO4:7H2O
N2(g)	-2.79	-6.05	-3.26	N2
NH3(g)	-19.50	-24.03	-4.52	NH3
O2(g)	-55.12	28.00	83.12	O2
Pyrite	-39.85	-125.63	-85.78	FeS2
Quartz	-0.34	-4.32	-3.98	SiO2
Sepiolite	-7.48	8.28	15.76	Mg2Si3O7.5OH:3H2O
Sepiolite(d)	-10.38	8.28	18.66	Mg2Si3O7.5OH:3H2O
Siderite	-0.93	-11.82	-10.89	FeCO3
SiO2(a)	-1.60	-4.32	-2.71	SiO2
Sulfur	-24.29	-60.00	-35.71	S
Talc	-6.83	14.57	21.40	Mg3Si4O10(OH)2

November 2001

2

Saturation indices

Phase	SI	log IAP	log KT	
Anhydrite	-4.05	-8.40	-4.36	CaSO4
Aragonite	-0.84	-9.17	-8.33	CaCO3
Calcite	-0.70	-9.17	-8.47	CaCO3
Celestite	-3.91	-10.54	-6.63	SrSO4
CH4(g)	-96.08	-140.21	-44.13	CH4
Chalcedony	-0.80	-4.36	-3.57	SiO2
Chrysotile	-6.06	26.32	32.38	Mg3Si2O5(OH)4
CO2(g)	-2.38	-20.53	-18.15	CO2
Dolomite	-0.96	-18.02	-17.06	CaMg(CO3)2
Gypsum	-3.82	-8.40	-4.58	CaSO4:2H2O
H2(g)	-29.92	-29.92	0.00	H2
H2O(g)	-1.55	-0.00	1.55	H2O
H2S(g)	-97.64	-139.44	-41.80	H2S
Halite	-6.21	-4.63	1.58	NaCl
O2(g)	-23.75	59.84	83.59	O2
Quartz	-0.36	-4.36	-4.00	SiO2
Sepiolite	-5.53	10.27	15.80	Mg2Si3O7.5OH:3H2O
Sepiolite(d)	-8.39	10.27	18.66	Mg2Si3O7.5OH:3H2O
SiO2(a)	-1.64	-4.36	-2.72	SiO2
Strontianite	-2.04	-11.31	-9.27	SrCO3
Sulfur	-73.62	-109.52	-35.90	S
Talc	-3.97	17.59	21.56	Mg3Si4O10(OH)2

4

Saturation indices

Phase	SI	log IAP	log KT	
Anhydrite	-3.85	-8.19	-4.34	CaSO4
Aragonite	-1.21	-9.51	-8.30	CaCO3
Calcite	-1.06	-9.51	-8.45	CaCO3
Celestite	-3.65	-10.27	-6.62	SrSO4
CH4(g)	-90.94	-135.71	-44.77	CH4
Chalcedony	-0.88	-4.50	-3.62	SiO2
Chrysotile	-8.40	24.53	32.93	Mg3Si2O5(OH)4
CO2(g)	-2.18	-20.35	-18.17	CO2
Dolomite	-1.73	-18.68	-16.95	CaMg(CO3)2
Gypsum	-3.61	-8.19	-4.58	CaSO4:2H2O
H2(g)	-28.84	-28.84	0.00	H2
H2O(g)	-1.66	-0.00	1.66	H2O
H2S(g)	-91.91	-134.39	-42.48	H2S
Halite	-6.01	-4.44	1.57	NaCl
O2(g)	-27.43	57.68	85.11	O2
Quartz	-0.43	-4.50	-4.07	SiO2
Sepiolite	-7.06	8.86	15.92	Mg2Si3O7.5OH:3H2O
Sepiolite(d)	-9.80	8.86	18.66	Mg2Si3O7.5OH:3H2O
SiO2(a)	-1.74	-4.50	-2.76	SiO2
Strontianite	-2.32	-11.59	-9.27	SrCO3
Sulfur	-69.02	-105.55	-36.53	S
Talc	-6.54	15.53	22.07	Mg3Si4O10(OH)2

5

Saturation indices

Phase	SI	log IAP	log KT	
Anhydrite	-4.12	-8.49	-4.37	CaSO4
Aragonite	-0.70	-9.04	-8.34	CaCO3
Calcite	-0.56	-9.04	-8.49	CaCO3
Celestite	-4.00	-10.64	-6.64	SrSO4
CH4(g)	-103.24	-146.99	-43.75	CH4
Chalcedony	-1.25	-4.78	-3.54	SiO2

```
          Chrysotile       -4.56   27.49   32.04  Mg3Si2O5(OH)4
          CO2(g)           -2.92  -21.07  -18.15  CO2
          Dolomite         -0.64  -17.76  -17.12  CaMg(CO3)2
          Gypsum           -3.91   -8.49   -4.58  CaSO4:2H2O
          H2(g)           -31.48  -31.48   -0.00  H2
          H2O(g)           -1.48   -0.00    1.48  H2O
          H2S(g)         -105.04 -146.44  -41.40  H2S
          Halite           -6.48   -4.90    1.58  NaCl
          O2(g)           -19.73   62.96   82.69  O2
          Quartz           -0.82   -4.78   -3.96  SiO2
          Sepiolite        -5.37   10.35   15.73  Mg2Si3O7.5OH:3H2O
          Sepiolite(d)     -8.31   10.35   18.66  Mg2Si3O7.5OH:3H2O
          SiO2(a)          -2.08   -4.78   -2.70  SiO2
          Strontianite     -1.92  -11.19   -9.27  SrCO3
          Sulfur          -79.42 -114.96  -35.53  S
          Talc             -3.33   17.92   21.25  Mg3Si4O10(OH)2
------------------------------------------------------------------------
7
------------------------------Saturation indices----------------------
          Phase               SI log IAP  log KT
          Anhydrite        -4.20   -8.55   -4.35  CaSO4
          Aragonite        -1.79  -10.10   -8.31  CaCO3
          Calcite          -1.64  -10.10   -8.46  CaCO3
          Celestite        -4.16  -10.78   -6.62  SrSO4
          CH4(g)          -88.39 -132.88  -44.49  CH4
          Chalcedony       -0.95   -4.55   -3.60  SiO2
          Chrysotile      -10.03   22.66   32.69  Mg3Si2O5(OH)4
          CO2(g)           -2.24  -20.40  -18.16  CO2
          Dolomite         -2.92  -19.92  -17.00  CaMg(CO3)2
          Gypsum           -3.97   -8.55   -4.58  CaSO4:2H2O
          H2(g)           -28.12  -28.12    0.00  H2
          H2O(g)           -1.61   -0.00    1.61  H2O
          H2S(g)          -89.14 -131.32  -42.18  H2S
          Halite           -6.71   -5.14    1.57  NaCl
          O2(g)           -28.21   56.24   84.45  O2
          Quartz           -0.51   -4.55   -4.04  SiO2
          Sepiolite        -8.34    7.53   15.86  Mg2Si3O7.5OH:3H2O
          Sepiolite(d)    -11.13    7.53   18.66  Mg2Si3O7.5OH:3H2O
          SiO2(a)          -1.80   -4.55   -2.74  SiO2
          Strontianite     -3.07  -12.34   -9.27  SrCO3
          Sulfur          -66.95 -103.20  -36.25  S
          Talc             -8.29   13.56   21.85  Mg3Si4O10(OH)2
------------------------------------------------------------------------
8
------------------------------Saturation indices----------------------
          Phase               SI log IAP  log KT
          Anhydrite        -4.12   -8.48   -4.37  CaSO4
          Aragonite        -1.27   -9.62   -8.34  CaCO3
          Calcite          -1.13   -9.62   -8.49  CaCO3
          Celestite        -4.13  -10.76   -6.64  SrSO4
          CH4(g)          -96.21 -139.96  -43.75  CH4
          Chalcedony       -1.13   -4.67   -3.54  SiO2
          Chrysotile       -6.99   25.05   32.04  Mg3Si2O5(OH)4
          CO2(g)           -2.61  -20.76  -18.15  CO2
          Dolomite         -1.79  -18.91  -17.12  CaMg(CO3)2
          Gypsum           -3.90   -8.48   -4.58  CaSO4:2H2O
          H2(g)           -29.80  -29.80   -0.00  H2
          H2O(g)           -1.48   -0.00    1.48  H2O
          H2S(g)          -97.43 -138.82  -41.40  H2S
          Halite           -6.72   -5.13    1.58  NaCl
          O2(g)           -23.09   59.60   82.69  O2
          Quartz           -0.70   -4.67   -3.96  SiO2
          Sepiolite        -6.81    8.92   15.73  Mg2Si3O7.5OH:3H2O
          Sepiolite(d)     -9.74    8.92   18.66  Mg2Si3O7.5OH:3H2O
          SiO2(a)          -1.96   -4.67   -2.70  SiO2
          Strontianite     -2.62  -11.89   -9.27  SrCO3
          Sulfur          -73.49 -109.02  -35.53  S
          Talc             -5.54   15.71   21.25  Mg3Si4O10(OH)2
------------------------------------------------------------------------
9
------------------------------Saturation indices----------------------
          Phase               SI log IAP  log KT
          Anhydrite        -4.06   -8.41   -4.35  CaSO4
          Aragonite        -1.50   -9.82   -8.32  CaCO3
          Calcite          -1.36   -9.82   -8.47  CaCO3
          Celestite        -4.09  -10.71   -6.63  SrSO4
          CH4(g)          -91.58 -135.90  -44.32  CH4
          Chalcedony       -1.08   -4.67   -3.58  SiO2
          Chrysotile       -8.84   23.70   32.54  Mg3Si2O5(OH)4
          CO2(g)           -2.38  -20.54  -18.16  CO2
          Dolomite         -2.33  -19.35  -17.03  CaMg(CO3)2
          Gypsum           -3.83   -8.41   -4.58  CaSO4:2H2O
          H2(g)           -28.84  -28.84    0.00  H2
          H2O(g)           -1.58   -0.00    1.58  H2O
```

```
          H2S(g)          -92.49 -134.49  -42.00  H2S
          Halite           -6.63   -5.05    1.58  NaCl
          O2(g)           -26.36   57.68   84.04  O2
          Quartz           -0.64   -4.67   -4.02  SiO2
          Sepiolite        -7.81    8.03   15.83  Mg2Si3O7.5OH:3H2O
          Sepiolite(d)    -10.63    8.03   18.66  Mg2Si3O7.5OH:3H2O
          SiO2(a)          -1.93   -4.67   -2.73  SiO2
          Strontianite     -2.85  -12.12   -9.27  SrCO3
          Sulfur          -69.57 -105.65  -36.08  S
          Talc             -7.34   14.37   21.71  Mg3Si4O10(OH)2
-------------------------------------------------------------------------
10
------------------------------Saturation indices-----------------------
          Phase               SI log IAP  log KT
          Anhydrite        -4.07   -8.44   -4.36  CaSO4
          Aragonite        -1.54   -9.88   -8.34  CaCO3
          Calcite          -1.40   -9.88   -8.48  CaCO3
          Celestite        -4.06  -10.70   -6.63  SrSO4
          CH4(g)          -91.28 -135.20  -43.92  CH4
          Chalcedony       -1.00   -4.55   -3.55  SiO2
          Chrysotile       -8.59   23.59   32.19  Mg3Si2O5(OH)4
          CO2(g)           -2.33  -20.48  -18.15  CO2
          Dolomite         -2.37  -19.46  -17.09  CaMg(CO3)2
          Gypsum           -3.85   -8.44   -4.58  CaSO4:2H2O
          H2(g)           -28.68  -28.68   -0.00  H2
          H2O(g)           -1.51   -0.00    1.51  H2O
          H2S(g)          -92.18 -133.75  -41.57  H2S
          Halite           -6.65   -5.07    1.58  NaCl
          O2(g)           -25.73   57.36   83.09  O2
          Quartz           -0.57   -4.55   -3.98  SiO2
          Sepiolite        -7.61    8.15   15.76  Mg2Si3O7.5OH:3H2O
          Sepiolite(d)    -10.51    8.15   18.66  Mg2Si3O7.5OH:3H2O
          SiO2(a)          -1.84   -4.55   -2.71  SiO2
          Strontianite     -2.87  -12.14   -9.27  SrCO3
          Sulfur          -69.38 -105.07  -35.70  S
          Talc             -6.89   14.50   21.39  Mg3Si4O10(OH)2
-------------------------------------------------------------------------
11
------------------------------Saturation indices-----------------------
          Phase               SI log IAP  log KT
          Anhydrite        -3.56   -7.92   -4.36  CaSO4
          Aragonite        -1.21   -9.54   -8.33  CaCO3
          Calcite          -1.06   -9.54   -8.48  CaCO3
          Celestite        -3.55  -10.18   -6.63  SrSO4
          CH4(g)          -91.42 -135.40  -43.97  CH4
          Chalcedony       -1.05   -4.60   -3.55  SiO2
          Chrysotile       -8.33   23.91   32.24  Mg3Si2O5(OH)4
          CO2(g)           -2.21  -20.36  -18.15  CO2
          Dolomite         -1.78  -18.86  -17.08  CaMg(CO3)2
          Gypsum           -3.34   -7.92   -4.58  CaSO4:2H2O
          H2(g)           -28.76  -28.76    0.00  H2
          H2O(g)           -1.52   -0.00    1.52  H2O
          H2S(g)          -92.14 -133.78  -41.63  H2S
          Halite           -6.37   -4.79    1.58  NaCl
          O2(g)           -25.70   57.52   83.22  O2
          Quartz           -0.62   -4.60   -3.98  SiO2
          Sepiolite        -7.50    8.27   15.77  Mg2Si3O7.5OH:3H2O
          Sepiolite(d)    -10.39    8.27   18.66  Mg2Si3O7.5OH:3H2O
          SiO2(a)          -1.89   -4.60   -2.71  SiO2
          Strontianite     -2.53  -11.80   -9.27  SrCO3
          Sulfur          -69.27 -105.02  -35.75  S
          Talc             -6.73   14.70   21.43  Mg3Si4O10(OH)2
-------------------------------------------------------------------------
12
------------------------------Saturation indices-----------------------
          Phase               SI log IAP  log KT
          Anhydrite        -3.18   -7.53   -4.35  CaSO4
          Aragonite        -0.86   -9.18   -8.32  CaCO3
          Calcite          -0.72   -9.18   -8.46  CaCO3
          Celestite        -3.25   -9.87   -6.63  SrSO4
          CH4(g)          -94.54 -138.91  -44.38  CH4
          Chalcedony       -1.02   -4.60   -3.59  SiO2
          Chrysotile       -7.13   25.46   32.59  Mg3Si2O5(OH)4
          CO2(g)           -2.36  -20.52  -18.16  CO2
          Dolomite         -1.12  -18.14  -17.02  CaMg(CO3)2
          Gypsum           -2.95   -7.53   -4.58  CaSO4:2H2O
          H2(g)           -29.60  -29.60    0.00  H2
          H2O(g)           -1.59   -0.00    1.59  H2O
          H2S(g)          -95.21 -137.27  -42.06  H2S
          Halite           -6.12   -4.54    1.57  NaCl
          O2(g)           -24.97   59.20   84.17  O2
          Quartz           -0.58   -4.60   -4.03  SiO2
          Sepiolite        -6.54    9.30   15.84  Mg2Si3O7.5OH:3H2O
          Sepiolite(d)     -9.36    9.30   18.66  Mg2Si3O7.5OH:3H2O
```

```
         SiO2(a)          -1.87   -4.60   -2.74  SiO2
         Strontianite     -2.25  -11.52   -9.27  SrCO3
         Sulfur          -71.53 -107.67  -36.14  S
         Talc             -5.50   16.25   21.76  Mg3Si4O10(OH)2
-------------------------------------------------------------------
13
-----------------------------Saturation indices---------------------
         Phase               SI log IAP  log KT
         Anhydrite        -3.33   -7.68   -4.34  CaSO4
         Aragonite        -1.00   -9.31   -8.31  CaCO3
         Calcite          -0.85   -9.31   -8.45  CaCO3
         Celestite        -3.46  -10.09   -6.62  SrSO4
         CH4(g)          -93.49 -138.13  -44.64  CH4
         Chalcedony       -1.17   -4.78   -3.61  SiO2
         Chrysotile       -8.11   24.71   32.82  Mg3Si2O5(OH)4
         CO2(g)           -2.37  -20.53  -18.16  CO2
         Dolomite         -1.44  -18.42  -16.97  CaMg(CO3)2
         Gypsum           -3.09   -7.68   -4.58  CaSO4:2H2O
         H2(g)           -29.40  -29.40    0.00  H2
         H2O(g)           -1.64   -0.00    1.64  H2O
         H2S(g)          -94.16 -136.50  -42.34  H2S
         Halite           -6.24   -4.67    1.57  NaCl
         O2(g)           -25.99   58.80   84.79  O2
         Quartz           -0.73   -4.78   -4.05  SiO2
         Sepiolite        -7.38    8.51   15.89  Mg2Si3O7.5OH:3H2O
         Sepiolite(d)    -10.15    8.51   18.66  Mg2Si3O7.5OH:3H2O
         SiO2(a)          -2.03   -4.78   -2.75  SiO2
         Strontianite     -2.45  -11.72   -9.27  SrCO3
         Sulfur          -70.70 -107.10  -36.40  S
         Talc             -6.81   15.15   21.97  Mg3Si4O10(OH)2
-------------------------------------------------------------------
14
-----------------------------Saturation indices---------------------
         Phase               SI log IAP  log KT
         Anhydrite        -4.48   -8.82   -4.34  CaSO4
         Aragonite        -2.44  -10.74   -8.29  CaCO3
         Calcite          -2.29  -10.74   -8.44  CaCO3
         Celestite        -4.40  -11.02   -6.62  SrSO4
         CH4(g)          -82.52 -127.47  -44.95  CH4
         Chalcedony       -1.03   -4.66   -3.63  SiO2
         Chrysotile      -12.61   20.48   33.09  Mg3Si2O5(OH)4
         CO2(g)           -2.10  -20.27  -18.17  CO2
         Dolomite         -4.15  -21.07  -16.92  CaMg(CO3)2
         Gypsum           -4.24   -8.82   -4.58  CaSO4:2H2O
         H2(g)           -26.80  -26.80    0.00  H2
         H2O(g)           -1.70   -0.00    1.70  H2O
         H2S(g)          -82.89 -125.56  -42.67  H2S
         Halite           -6.85   -5.28    1.57  NaCl
         O2(g)           -31.93   53.60   85.53  O2
         Quartz           -0.58   -4.66   -4.09  SiO2
         Sepiolite       -10.07    5.88   15.95  Mg2Si3O7.5OH:3H2O
         Sepiolite(d)    -12.78    5.88   18.66  Mg2Si3O7.5OH:3H2O
         SiO2(a)          -1.89   -4.66   -2.77  SiO2
         Strontianite     -3.66  -12.93   -9.27  SrCO3
         Sulfur          -62.06  -98.76  -36.70  S
         Talc            -11.06   11.15   22.22  Mg3Si4O10(OH)2
-------------------------------------------------------------------
15
-----------------------------Saturation indices---------------------
         Phase               SI log IAP  log KT
         Anhydrite        -4.62   -8.97   -4.34  CaSO4
         Aragonite        -2.40  -10.70   -8.30  CaCO3
         Calcite          -2.25  -10.70   -8.45  CaCO3
         CH4(g)          -84.68 -129.36  -44.68  CH4
         Chalcedony       -1.05   -4.66   -3.61  SiO2
         Chrysotile      -11.92   20.94   32.86  Mg3Si2O5(OH)4
         CO2(g)           -2.24  -20.40  -18.17  CO2
         Dolomite         -4.05  -21.02  -16.97  CaMg(CO3)2
         Gypsum           -4.38   -8.97   -4.58  CaSO4:2H2O
         H2(g)           -27.24  -27.24    0.00  H2
         H2O(g)           -1.65   -0.00    1.65  H2O
         H2S(g)          -85.24 -127.63  -42.38  H2S
         Halite           -6.91   -5.34    1.57  NaCl
         O2(g)           -30.42   54.48   84.90  O2
         Quartz           -0.61   -4.66   -4.06  SiO2
         Sepiolite        -9.72    6.18   15.90  Mg2Si3O7.5OH:3H2O
         Sepiolite(d)    -12.48    6.18   18.66  Mg2Si3O7.5OH:3H2O
         SiO2(a)          -1.91   -4.66   -2.76  SiO2
         Sulfur          -63.95 -100.39  -36.44  S
         Talc            -10.40   11.61   22.00  Mg3Si4O10(OH)2
-------------------------------------------------------------------
16
-----------------------------Saturation indices---------------------
         Phase               SI log IAP  log KT
```

```
          Anhydrite        -4.52   -8.85   -4.34  CaSO4
          Aragonite        -2.41  -10.69   -8.28  CaCO3
          Calcite          -2.26  -10.69   -8.43  CaCO3
          CH4(g)         -81.34 -126.60  -45.26  CH4
          Chalcedony       -1.16   -4.82   -3.66  SiO2
          Chrysotile      -13.40   19.96   33.36  Mg3Si2O5(OH)4
          CO2(g)           -2.01  -20.20  -18.18  CO2
          Dolomite         -4.15  -21.02  -16.87  CaMg(CO3)2
          Gypsum           -4.27   -8.85   -4.58  CaSO4:2H2O
          H2(g)           -26.60  -26.60    0.00  H2
          H2O(g)           -1.75   -0.00    1.75  H2O
          H2S(g)         -81.76 -124.76  -43.00  H2S
          Halite           -6.79   -5.23    1.56  NaCl
          O2(g)           -33.07   53.20   86.27  O2
          Quartz           -0.71   -4.82   -4.12  SiO2
          Sepiolite       -10.74    5.27   16.01  Mg2Si3O7.5OH:3H2O
          Sepiolite(d)    -13.39    5.27   18.66  Mg2Si3O7.5OH:3H2O
          SiO2(a)          -2.04   -4.82   -2.79  SiO2
          Sulfur          -61.15  -98.16  -37.01  S
          Talc            -12.15   10.32   22.47  Mg3Si4O10(OH)2
------------------------------------------------------------------------
17
-----------------------------Saturation indices----------------------
          Phase               SI log IAP  log KT
          Anhydrite        -5.54   -9.87   -4.34  CaSO4
          Aragonite        -2.26  -10.54   -8.28  CaCO3
          Calcite          -2.11  -10.54   -8.43  CaCO3
          Celestite        -5.50  -12.12   -6.62  SrSO4
          CH4(g)         -82.44 -127.72  -45.28  CH4
          Chalcedony       -0.94   -4.60   -3.66  SiO2
          Chrysotile      -12.54   20.83   33.38  Mg3Si2O5(OH)4
          CO2(g)           -2.02  -20.20  -18.18  CO2
          Dolomite         -3.86  -20.72  -16.87  CaMg(CO3)2
          Gypsum           -5.29   -9.88   -4.58  CaSO4:2H2O
          H2(g)           -26.88  -26.88    0.00  H2
          H2O(g)           -1.76   -0.00    1.76  H2O
          H2S(g)         -84.04 -127.05  -43.02  H2S
          Halite           -6.88   -5.32    1.56  NaCl
          O2(g)           -32.55   53.76   86.31  O2
          Quartz           -0.48   -4.60   -4.12  SiO2
          Sepiolite        -9.79    6.22   16.01  Mg2Si3O7.5OH:3H2O
          Sepiolite(d)    -12.44    6.22   18.66  Mg2Si3O7.5OH:3H2O
          SiO2(a)          -1.81   -4.60   -2.79  SiO2
          Strontianite     -3.51  -12.78   -9.27  SrCO3
          Sulfur          -63.15 -100.17  -37.02  S
          Talc            -10.85   11.63   22.48  Mg3Si4O10(OH)2
------------------------------------------------------------------------
18
-----------------------------Saturation indices----------------------
          Phase               SI log IAP  log KT
          Anhydrite        -4.24   -8.58   -4.34  CaSO4
          Aragonite        -2.11  -10.41   -8.30  CaCO3
          Calcite          -1.96  -10.41   -8.45  CaCO3
          Celestite        -4.26  -10.88   -6.62  SrSO4
          CH4(g)         -83.59 -128.36  -44.77  CH4
          Chalcedony       -0.86   -4.48   -3.62  SiO2
          Chrysotile      -11.72   21.21   32.93  Mg3Si2O5(OH)4
          CO2(g)           -2.04  -20.20  -18.17  CO2
          Dolomite         -3.60  -20.56  -16.95  CaMg(CO3)2
          Gypsum           -4.00   -8.58   -4.58  CaSO4:2H2O
          H2(g)           -27.04  -27.04    0.00  H2
          H2O(g)           -1.66   -0.00    1.66  H2O
          H2S(g)         -84.06 -126.54  -42.48  H2S
          Halite           -6.93   -5.36    1.57  NaCl
          O2(g)           -31.03   54.08   85.11  O2
          Quartz           -0.41   -4.48   -4.07  SiO2
          Sepiolite        -9.24    6.68   15.92  Mg2Si3O7.5OH:3H2O
          Sepiolite(d)    -11.98    6.68   18.66  Mg2Si3O7.5OH:3H2O
          SiO2(a)          -1.72   -4.48   -2.76  SiO2
          Strontianite     -3.44  -12.71   -9.27  SrCO3
          Sulfur          -62.97  -99.50  -36.53  S
          Talc             -9.82   12.25   22.07  Mg3Si4O10(OH)2
------------------------------------------------------------------------
19
-----------------------------Saturation indices----------------------
          Phase               SI log IAP  log KT
          Anhydrite        -4.16   -8.50   -4.34  CaSO4
          Aragonite        -1.96  -10.25   -8.29  CaCO3
          Calcite          -1.81  -10.25   -8.44  CaCO3
          Celestite        -4.22  -10.84   -6.62  SrSO4
          CH4(g)         -82.96 -127.95  -44.99  CH4
          Chalcedony       -0.60   -4.23   -3.64  SiO2
          Chrysotile      -11.27   21.86   33.13  Mg3Si2O5(OH)4
          CO2(g)           -1.94  -20.11  -18.17  CO2
```

```
          Dolomite          -3.34  -20.25  -16.92  CaMg(CO3)2
          Gypsum            -3.92   -8.50   -4.58  CaSO4:2H2O
          H2(g)            -26.96  -26.96    0.00  H2
          H2O(g)            -1.70   -0.00    1.70  H2O
          H2S(g)           -83.48 -126.20  -42.71  H2S
          Halite            -6.79   -5.22    1.57  NaCl
          O2(g)            -31.71   53.92   85.63  O2
          Quartz            -0.14   -4.23   -4.09  SiO2
          Sepiolite         -8.44    7.51   15.96  Mg2Si3O7.5OH:3H2O
          Sepiolite(d)     -11.15    7.51   18.66  Mg2Si3O7.5OH:3H2O
          SiO2(a)           -1.46   -4.23   -2.77  SiO2
          Strontianite      -3.32  -12.59   -9.27  SrCO3
          Sulfur           -62.49  -99.24  -36.74  S
          Talc              -8.86   13.39   22.25  Mg3Si4O10(OH)2
-------------------------------------------------------------------------
20
------------------------------Saturation indices-----------------------
          Phase               SI log IAP  log KT
          Anhydrite         -4.56   -8.89   -4.34  CaSO4
          Aragonite         -2.59  -10.88   -8.29  CaCO3
          Calcite           -2.44  -10.88   -8.44  CaCO3
          CH4(g)           -84.35 -129.36  -45.01  CH4
          Chalcedony        -0.60   -4.23   -3.64  SiO2
          Chrysotile       -11.39   21.75   33.14  Mg3Si2O5(OH)4
          CO2(g)            -2.39  -20.56  -18.17  CO2
          Dolomite          -4.46  -21.37  -16.91  CaMg(CO3)2
          Gypsum            -4.31   -8.89   -4.58  CaSO4:2H2O
          H2(g)            -27.20  -27.20    0.00  H2
          H2O(g)            -1.71   -0.00    1.71  H2O
          H2S(g)           -84.64 -127.37  -42.73  H2S
          Halite            -7.07   -5.51    1.56  NaCl
          O2(g)            -31.27   54.40   85.67  O2
          Quartz            -0.14   -4.23   -4.09  SiO2
          Sepiolite         -8.52    7.44   15.96  Mg2Si3O7.5OH:3H2O
          Sepiolite(d)     -11.22    7.44   18.66  Mg2Si3O7.5OH:3H2O
          SiO2(a)           -1.46   -4.23   -2.77  SiO2
          Sulfur           -63.41 -100.17  -36.76  S
          Talc              -8.99   13.28   22.26  Mg3Si4O10(OH)2
-------------------------------------------------------------------------
21
------------------------------Saturation indices-----------------------
          Phase               SI log IAP  log KT
          Anhydrite         -4.42   -8.76   -4.34  CaSO4
          Aragonite         -2.88  -11.17   -8.28  CaCO3
          Calcite           -2.73  -11.17   -8.43  CaCO3
          CH4(g)           -84.23 -129.51  -45.28  CH4
          Chalcedony        -0.48   -4.14   -3.66  SiO2
          Chrysotile       -11.07   22.31   33.38  Mg3Si2O5(OH)4
          CO2(g)            -2.69  -20.87  -18.18  CO2
          Dolomite          -4.97  -21.84  -16.87  CaMg(CO3)2
          Gypsum            -4.17   -8.76   -4.58  CaSO4:2H2O
          H2(g)            -27.16  -27.16    0.00  H2
          H2O(g)            -1.76   -0.00    1.76  H2O
          H2S(g)           -84.08 -127.10  -43.02  H2S
          Halite            -6.33   -4.77    1.56  NaCl
          O2(g)            -31.99   54.32   86.31  O2
          Quartz            -0.02   -4.14   -4.12  SiO2
          Sepiolite         -8.04    7.97   16.01  Mg2Si3O7.5OH:3H2O
          Sepiolite(d)     -10.69    7.97   18.66  Mg2Si3O7.5OH:3H2O
          SiO2(a)           -1.35   -4.14   -2.79  SiO2
          Sulfur           -62.92  -99.94  -37.02  S
          Talc              -8.46   14.02   22.48  Mg3Si4O10(OH)2
-------------------------------------------------------------------------
22
------------------------------Saturation indices-----------------------
          Phase               SI log IAP  log KT
          Anhydrite         -4.66   -9.01   -4.35  CaSO4
          Aragonite         -2.53  -10.85   -8.32  CaCO3
          Calcite           -2.38  -10.85   -8.47  CaCO3
          CH4(g)           -82.67 -126.98  -44.32  CH4
          Chalcedony        -0.69   -4.27   -3.58  SiO2
          Chrysotile       -11.76   20.78   32.54  Mg3Si2O5(OH)4
          CO2(g)            -2.11  -20.26  -18.16  CO2
          Dolomite          -4.31  -21.34  -17.03  CaMg(CO3)2
          Gypsum            -4.43   -9.01   -4.58  CaSO4:2H2O
          H2(g)            -26.68  -26.68    0.00  H2
          H2O(g)            -1.58   -0.00    1.58  H2O
          H2S(g)           -83.15 -125.14  -42.00  H2S
          Halite            -6.94   -5.37    1.58  NaCl
          O2(g)            -30.68   53.36   84.04  O2
          Quartz            -0.25   -4.27   -4.02  SiO2
          Sepiolite         -9.10    6.73   15.83  Mg2Si3O7.5OH:3H2O
          Sepiolite(d)     -11.93    6.73   18.66  Mg2Si3O7.5OH:3H2O
          SiO2(a)           -1.54   -4.27   -2.73  SiO2
```

```
          Sulfur          -62.38  -98.46  -36.08  S
          Talc             -9.47   12.24   21.71  Mg3Si4O10(OH)2
-----------------------------------------------------------------------
23
-------------------------------Saturation indices----------------------
          Phase               SI log IAP  log KT
          Anhydrite        -4.78   -9.13   -4.35  CaSO4
          Aragonite        -2.73  -11.05   -8.32  CaCO3
          Calcite          -2.59  -11.05   -8.47  CaCO3
          CH4(g)          -81.51 -125.83  -44.32  CH4
          Chalcedony       -0.99   -4.57   -3.58  SiO2
          Chrysotile      -12.85   19.69   32.54  Mg3Si2O5(OH)4
          CO2(g)           -2.08  -20.23  -18.16  CO2
          Dolomite         -4.65  -21.67  -17.03  CaMg(CO3)2
          Gypsum           -4.55   -9.13   -4.58  CaSO4:2H2O
          H2(g)           -26.40  -26.40    0.00  H2
          H2O(g)           -1.58   -0.00    1.58  H2O
          H2S(g)          -81.92 -123.91  -42.00  H2S
          Halite           -7.07   -5.49    1.58  NaCl
          O2(g)           -31.24   52.80   84.04  O2
          Quartz           -0.55   -4.57   -4.02  SiO2
          Sepiolite       -10.33    5.50   15.83  Mg2Si3O7.5OH:3H2O
          Sepiolite(d)    -13.16    5.50   18.66  Mg2Si3O7.5OH:3H2O
          SiO2(a)          -1.84   -4.57   -2.73  SiO2
          Sulfur          -61.43  -97.51  -36.08  S
          Talc            -11.17   10.54   21.71  Mg3Si4O10(OH)2
-----------------------------------------------------------------------
24
-------------------------------Saturation indices----------------------
          Phase               SI log IAP  log KT
          Anhydrite        -4.78   -9.13   -4.35  CaSO4
          Aragonite        -2.55  -10.86   -8.31  CaCO3
          Calcite          -2.40  -10.86   -8.46  CaCO3
          CH4(g)          -84.63 -129.07  -44.43  CH4
          Chalcedony       -1.04   -4.63   -3.59  SiO2
          Chrysotile      -11.97   20.67   32.64  Mg3Si2O5(OH)4
          CO2(g)           -2.27  -20.43  -18.16  CO2
          Dolomite         -4.30  -21.31  -17.01  CaMg(CO3)2
          Gypsum           -4.55   -9.13   -4.58  CaSO4:2H2O
          H2(g)           -27.16  -27.16    0.00  H2
          H2O(g)           -1.60   -0.00    1.60  H2O
          H2S(g)          -85.21 -127.33  -42.12  H2S
          Halite           -7.16   -5.59    1.57  NaCl
          O2(g)           -29.99   54.32   84.31  O2
          Quartz           -0.60   -4.63   -4.03  SiO2
          Sepiolite        -9.79    6.06   15.85  Mg2Si3O7.5OH:3H2O
          Sepiolite(d)    -12.60    6.06   18.66  Mg2Si3O7.5OH:3H2O
          SiO2(a)          -1.89   -4.63   -2.74  SiO2
          Sulfur          -63.97 -100.17  -36.20  S
          Talc            -10.40   11.40   21.80  Mg3Si4O10(OH)2
-----------------------------------------------------------------------
25
-------------------------------Saturation indices----------------------
          Phase               SI log IAP  log KT
          Anhydrite        -4.68   -9.02   -4.34  CaSO4
          Aragonite        -2.59  -10.89   -8.30  CaCO3
          Calcite          -2.44  -10.89   -8.45  CaCO3
          CH4(g)          -83.23 -128.04  -44.81  CH4
          Chalcedony       -1.11   -4.74   -3.62  SiO2
          Chrysotile      -12.89   20.08   32.97  Mg3Si2O5(OH)4
          CO2(g)           -2.19  -20.36  -18.17  CO2
          Dolomite         -4.45  -21.40  -16.95  CaMg(CO3)2
          Gypsum           -4.44   -9.02   -4.58  CaSO4:2H2O
          H2(g)           -26.92  -26.92    0.00  H2
          H2O(g)           -1.67   -0.00    1.67  H2O
          H2S(g)          -83.65 -126.17  -42.52  H2S
          Halite           -7.19   -5.62    1.57  NaCl
          O2(g)           -31.37   53.84   85.21  O2
          Quartz           -0.67   -4.74   -4.07  SiO2
          Sepiolite       -10.43    5.49   15.92  Mg2Si3O7.5OH:3H2O
          Sepiolite(d)    -13.17    5.49   18.66  Mg2Si3O7.5OH:3H2O
          SiO2(a)          -1.97   -4.74   -2.76  SiO2
          Sulfur          -62.68  -99.25  -36.57  S
          Talc            -11.50   10.61   22.11  Mg3Si4O10(OH)2
-----------------------------------------------------------------------
26
-------------------------------Saturation indices----------------------
          Phase               SI log IAP  log KT
          Anhydrite        -5.81  -10.16   -4.34  CaSO4
          Aragonite        -3.21  -11.52   -8.30  CaCO3
          Calcite          -3.07  -11.52   -8.45  CaCO3
          CH4(g)          -77.53 -122.28  -44.75  CH4
          Chalcedony       -1.46   -5.08   -3.62  SiO2
          Chrysotile      -16.06   16.87   32.92  Mg3Si2O5(OH)4
```

CO2(g)	-2.04	-20.20	-18.17	CO2
Dolomite	-5.75	-22.71	-16.96	CaMg(CO3)2
Gypsum	-5.57	-10.16	-4.58	CaSO4:2H2O
H2(g)	-25.52	-25.52	0.00	H2
H2O(g)	-1.66	-0.00	1.66	H2O
H2S(g)	-78.46	-120.92	-42.46	H2S
Halite	-7.68	-6.11	1.57	NaCl
O2(g)	-34.03	51.04	85.07	O2
Quartz	-1.01	-5.08	-4.07	SiO2
Sepiolite	-13.14	2.78	15.91	Mg2Si3O7.5OH:3H2O
Sepiolite(d)	-15.88	2.78	18.66	Mg2Si3O7.5OH:3H2O
SiO2(a)	-2.32	-5.08	-2.76	SiO2
Sulfur	-58.89	-95.40	-36.51	S
Talc	-15.35	6.71	22.06	Mg3Si4O10(OH)2

T2

Saturation indices

Phase	SI	log IAP	log KT	
Anhydrite	-3.78	-8.12	-4.35	CaSO4
Aragonite	0.20	-8.10	-8.31	CaCO3
Calcite	0.35	-8.10	-8.46	CaCO3
Celestite	-3.36	-9.98	-6.62	SrSO4
CH4(g)	-99.92	-144.50	-44.58	CH4
Chalcedony	-1.87	-5.48	-3.60	SiO2
Chrysotile	-5.94	26.83	32.77	Mg3Si2O5(OH)4
CO2(g)	-2.18	-20.34	-18.16	CO2
Dolomite	1.13	-15.85	-16.98	CaMg(CO3)2
Gypsum	-3.54	-8.12	-4.58	CaSO4:2H2O
H2(g)	-31.04	-31.04	0.00	H2
H2O(g)	-1.63	-0.00	1.63	H2O
H2S(g)	-102.24	-144.52	-42.27	H2S
Halite	-4.89	-3.32	1.57	NaCl
O2(g)	-22.58	62.08	84.65	O2
Quartz	-1.43	-5.48	-4.05	SiO2
Sepiolite	-7.12	8.76	15.88	Mg2Si3O7.5OH:3H2O
Sepiolite(d)	-9.90	8.76	18.66	Mg2Si3O7.5OH:3H2O
SiO2(a)	-2.73	-5.48	-2.75	SiO2
Strontianite	-0.70	-9.97	-9.27	SrCO3
Sulfur	-77.14	-113.48	-36.34	S
Talc	-6.04	15.88	21.92	Mg3Si4O10(OH)2

T5

Saturation indices

Phase	SI	log IAP	log KT	
Anhydrite	-5.17	-9.51	-4.34	CaSO4
Aragonite	-5.21	-13.51	-8.30	CaCO3
Calcite	-5.07	-13.51	-8.45	CaCO3
CH4(g)	-67.19	-111.96	-44.77	CH4
Chalcedony	-0.44	-4.06	-3.62	SiO2
Chrysotile	-18.02	14.91	32.93	Mg3Si2O5(OH)4
CO2(g)	-2.28	-20.44	-18.17	CO2
Dolomite	-9.33	-26.28	-16.95	CaMg(CO3)2
Gypsum	-4.93	-9.51	-4.58	CaSO4:2H2O
H2(g)	-22.88	-22.88	0.00	H2
H2O(g)	-1.66	-0.00	1.66	H2O
H2S(g)	-65.49	-107.96	-42.48	H2S
Halite	-7.38	-5.82	1.57	NaCl
O2(g)	-39.35	45.76	85.11	O2
Quartz	0.01	-4.06	-4.07	SiO2
Sepiolite	-12.74	3.17	15.92	Mg2Si3O7.5OH:3H2O
Sepiolite(d)	-15.49	3.17	18.66	Mg2Si3O7.5OH:3H2O
SiO2(a)	-1.30	-4.06	-2.76	SiO2
Sulfur	-48.56	-85.08	-36.53	S
Talc	-15.29	6.79	22.07	Mg3Si4O10(OH)2

T6

Saturation indices

Phase	SI	log IAP	log KT	
Anhydrite	-4.67	-9.01	-4.34	CaSO4
Aragonite	-1.83	-10.12	-8.29	CaCO3
Calcite	-1.68	-10.12	-8.44	CaCO3
Celestite	-4.58	-11.20	-6.62	SrSO4
CH4(g)	-84.60	-129.74	-45.14	CH4
Chalcedony	-0.73	-4.38	-3.65	SiO2
Chrysotile	-10.84	22.42	33.26	Mg3Si2O5(OH)4
CO2(g)	-1.96	-20.14	-18.18	CO2
Dolomite	-2.97	-19.87	-16.89	CaMg(CO3)2
Gypsum	-4.43	-9.01	-4.58	CaSO4:2H2O
H2(g)	-27.40	-27.40	0.00	H2
H2O(g)	-1.73	-0.00	1.73	H2O
H2S(g)	-85.76	-128.63	-42.87	H2S
Halite	-6.36	-4.80	1.56	NaCl
O2(g)	-31.19	54.80	85.99	O2
Quartz	-0.27	-4.38	-4.11	SiO2

Sepiolite	-8.34	7.65	15.98	Mg2Si3O7.5OH:3H2O
Sepiolite(d)	-11.01	7.65	18.66	Mg2Si3O7.5OH:3H2O
SiO2(a)	-1.60	-4.38	-2.78	SiO2
Strontianite	-3.03	-12.31	-9.27	SrCO3
Sulfur	-64.34	-101.23	-36.89	S
Talc	-8.71	13.66	22.37	Mg3Si4O10(OH)2

T7

Saturation indices

Phase	SI	log IAP	log KT	
Anhydrite	-5.07	-9.40	-4.34	CaSO4
Aragonite	-3.33	-11.61	-8.28	CaCO3
Calcite	-3.18	-11.61	-8.43	CaCO3
CH4(g)	-75.65	-121.02	-45.37	CH4
Chalcedony	-0.42	-4.09	-3.67	SiO2
Chrysotile	-14.51	18.94	33.46	Mg3Si2O5(OH)4
CO2(g)	-2.03	-20.22	-18.19	CO2
Dolomite	-5.94	-22.79	-16.85	CaMg(CO3)2
Gypsum	-4.82	-9.40	-4.58	CaSO4:2H2O
H2(g)	-25.20	-25.20	0.00	H2
H2O(g)	-1.77	-0.00	1.77	H2O
H2S(g)	-75.70	-118.81	-43.11	H2S
Halite	-7.02	-5.46	1.56	NaCl
O2(g)	-36.12	50.40	86.52	O2
Quartz	0.04	-4.09	-4.13	SiO2
Sepiolite	-10.21	5.82	16.03	Mg2Si3O7.5OH:3H2O
Sepiolite(d)	-12.84	5.82	18.66	Mg2Si3O7.5OH:3H2O
SiO2(a)	-1.29	-4.09	-2.80	SiO2
Sulfur	-56.50	-93.61	-37.11	S
Talc	-11.79	10.77	22.55	Mg3Si4O10(OH)2

T8

Saturation indices

Phase	SI	log IAP	log KT	
Anhydrite	-4.16	-8.51	-4.34	CaSO4
Aragonite	-1.72	-10.02	-8.30	CaCO3
Calcite	-1.57	-10.02	-8.45	CaCO3
Celestite	-4.04	-10.66	-6.62	SrSO4
CH4(g)	-90.22	-134.96	-44.74	CH4
Chalcedony	-0.45	-4.06	-3.62	SiO2
Chrysotile	-8.51	24.39	32.91	Mg3Si2O5(OH)4
CO2(g)	-2.40	-20.56	-18.17	CO2
Dolomite	-2.78	-19.74	-16.96	CaMg(CO3)2
Gypsum	-3.92	-8.51	-4.58	CaSO4:2H2O
H2(g)	-28.60	-28.60	0.00	H2
H2O(g)	-1.66	-0.00	1.66	H2O
H2S(g)	-91.00	-133.45	-42.45	H2S
Halite	-7.13	-5.56	1.57	NaCl
O2(g)	-27.84	57.20	85.04	O2
Quartz	0.00	-4.06	-4.06	SiO2
Sepiolite	-6.42	9.49	15.91	Mg2Si3O7.5OH:3H2O
Sepiolite(d)	-9.17	9.49	18.66	Mg2Si3O7.5OH:3H2O
SiO2(a)	-1.30	-4.06	-2.76	SiO2
Strontianite	-2.91	-12.18	-9.27	SrCO3
Sulfur	-68.35	-104.85	-36.50	S
Talc	-5.78	16.27	22.05	Mg3Si4O10(OH)2

T9

Saturation indices

Phase	SI	log IAP	log KT	
Anhydrite	-4.98	-9.31	-4.34	CaSO4
Aragonite	-1.85	-10.13	-8.28	CaCO3
Calcite	-1.70	-10.13	-8.43	CaCO3
Celestite	-4.80	-11.42	-6.62	SrSO4
CH4(g)	-82.73	-128.01	-45.28	CH4
Chalcedony	-0.40	-4.06	-3.66	SiO2
Chrysotile	-10.80	22.57	33.38	Mg3Si2O5(OH)4
CO2(g)	-1.82	-20.01	-18.18	CO2
Dolomite	-3.04	-19.91	-16.87	CaMg(CO3)2
Gypsum	-4.73	-9.31	-4.58	CaSO4:2H2O
H2(g)	-27.00	-27.00	0.00	H2
H2O(g)	-1.76	-0.00	1.76	H2O
H2S(g)	-84.17	-127.19	-43.02	H2S
Halite	-6.79	-5.23	1.56	NaCl
O2(g)	-32.31	54.00	86.31	O2
Quartz	0.06	-4.06	-4.12	SiO2
Sepiolite	-7.73	8.28	16.01	Mg2Si3O7.5OH:3H2O
Sepiolite(d)	-10.38	8.28	18.66	Mg2Si3O7.5OH:3H2O
SiO2(a)	-1.27	-4.06	-2.79	SiO2
Strontianite	-2.97	-12.24	-9.27	SrCO3
Sulfur	-63.16	-100.19	-37.02	S
Talc	-8.03	14.45	22.48	Mg3Si4O10(OH)2

```
-------------------------------------------------------------------
T10
------------------------------Saturation indices-------------------
         Phase               SI log IAP  log KT
         Anhydrite        -3.31   -7.66   -4.34  CaSO4
         Aragonite        -0.07   -8.37   -8.31  CaCO3
         Calcite           0.08   -8.37   -8.45  CaCO3
         Celestite        -3.21   -9.84   -6.62  SrSO4
         CH4(g)         -102.25 -146.86  -44.61  CH4
         Chalcedony       -2.18   -5.78   -3.61  SiO2
         Chrysotile       -6.63   26.17   32.79  Mg3Si2O5(OH)4
         CO2(g)           -2.62  -20.78  -18.16  CO2
         Dolomite          0.40  -16.58  -16.98  CaMg(CO3)2
         Gypsum           -3.08   -7.66   -4.58  CaSO4:2H2O
         H2(g)           -31.52  -31.52    0.00  H2
         H2O(g)           -1.63   -0.00    1.63  H2O
         H2S(g)         -103.84 -146.14  -42.31  H2S
         Halite           -6.50   -4.93    1.57  NaCl
         O2(g)           -21.68   63.04   84.72  O2
         Quartz           -1.73   -5.78   -4.05  SiO2
         Sepiolite        -8.08    7.81   15.89  Mg2Si3O7.5OH:3H2O
         Sepiolite(d)    -10.85    7.81   18.66  Mg2Si3O7.5OH:3H2O
         SiO2(a)          -3.03   -5.78   -2.75  SiO2
         Strontianite     -1.28  -10.55   -9.27  SrCO3
         Sulfur          -78.26 -114.62  -36.37  S
         Talc             -7.34   14.60   21.94  Mg3Si4O10(OH)2
-------------------------------------------------------------------
T11
------------------------------Saturation indices-------------------
         Phase               SI log IAP  log KT
         Anhydrite        -3.13   -7.47   -4.34  CaSO4
         Aragonite        -1.34   -9.62   -8.29  CaCO3
         Calcite          -1.19   -9.62   -8.44  CaCO3
         Celestite        -3.06   -9.68   -6.62  SrSO4
         CH4(g)           -83.87 -129.04  -45.17  CH4
         Chalcedony       -0.43   -4.09   -3.65  SiO2
         Chrysotile      -10.11   23.17   33.28  Mg3Si2O5(OH)4
         CO2(g)           -1.74  -19.92  -18.18  CO2
         Dolomite         -2.21  -19.10  -16.89  CaMg(CO3)2
         Gypsum           -2.88   -7.47   -4.58  CaSO4:2H2O
         H2(g)           -27.28  -27.28    0.00  H2
         H2O(g)           -1.74   -0.00    1.74  H2O
         H2S(g)           -83.98 -126.88  -42.90  H2S
         Halite           -6.51   -4.95    1.56  NaCl
         O2(g)           -31.50   54.56   86.06  O2
         Quartz            0.02   -4.09   -4.11  SiO2
         Sepiolite        -7.36    8.63   15.99  Mg2Si3O7.5OH:3H2O
         Sepiolite(d)    -10.03    8.63   18.66  Mg2Si3O7.5OH:3H2O
         SiO2(a)          -1.30   -4.09   -2.78  SiO2
         Strontianite     -2.57  -11.84   -9.27  SrCO3
         Sulfur           -62.69  -99.60  -36.92  S
         Talc             -7.40   15.00   22.40  Mg3Si4O10(OH)2
-------------------------------------------------------------------
T12
------------------------------Saturation indices-------------------
         Phase               SI log IAP  log KT
         Anhydrite        -5.64   -9.99   -4.35  CaSO4
         Aragonite        -3.31  -11.63   -8.31  CaCO3
         Calcite          -3.17  -11.63   -8.46  CaCO3
         CH4(g)           -73.84 -118.28  -44.43  CH4
         Chalcedony       -0.56   -4.16   -3.59  SiO2
         Chrysotile      -14.78   17.86   32.64  Mg3Si2O5(OH)4
         CO2(g)           -1.88  -20.04  -18.16  CO2
         Dolomite         -5.93  -22.94  -17.01  CaMg(CO3)2
         Gypsum           -5.41   -9.99   -4.58  CaSO4:2H2O
         H2(g)           -24.56  -24.56    0.00  H2
         H2O(g)           -1.60   -0.00    1.60  H2O
         H2S(g)           -74.52 -116.64  -42.12  H2S
         Halite           -7.04   -5.46    1.57  NaCl
         O2(g)           -35.19   49.12   84.31  O2
         Quartz           -0.12   -4.16   -4.03  SiO2
         Sepiolite       -10.87    4.98   15.85  Mg2Si3O7.5OH:3H2O
         Sepiolite(d)    -13.68    4.98   18.66  Mg2Si3O7.5OH:3H2O
         SiO2(a)          -1.41   -4.16   -2.74  SiO2
         Sulfur           -55.88  -92.08  -36.20  S
         Talc             -12.25    9.55   21.80  Mg3Si4O10(OH)2
-------------------------------------------------------------------
T13
------------------------------Saturation indices-------------------
         Phase               SI log IAP  log KT
         Anhydrite        -4.26   -8.61   -4.35  CaSO4
         Aragonite        -2.36  -10.68   -8.32  CaCO3
         Calcite          -2.22  -10.68   -8.47  CaCO3
         CH4(g)           -86.29 -130.60  -44.30  CH4
```

Chalcedony	-0.69	-4.27	-3.58	SiO2
Chrysotile	-10.53	22.00	32.53	Mg3Si2O5(OH)4
CO2(g)	-2.36	-20.52	-18.16	CO2
Dolomite	-3.99	-21.02	-17.03	CaMg(CO3)2
Gypsum	-4.03	-8.61	-4.58	CaSO4:2H2O
H2(g)	-27.52	-27.52	0.00	H2
H2O(g)	-1.58	-0.00	1.58	H2O
H2S(g)	-86.54	-128.53	-41.98	H2S
Halite	-6.71	-5.13	1.58	NaCl
O2(g)	-28.96	55.04	84.00	O2
Quartz	-0.25	-4.27	-4.02	SiO2
Sepiolite	-8.29	7.54	15.83	Mg2Si3O7.5OH:3H2O
Sepiolite(d)	-11.12	7.54	18.66	Mg2Si3O7.5OH:3H2O
SiO2(a)	-1.54	-4.27	-2.73	SiO2
Sulfur	-64.93	-101.01	-36.07	S
Talc	-8.25	13.45	21.70	Mg3Si4O10(OH)2

Groundwater bores and piezometers

March 2000

W1A

Saturation indices

Phase	SI	log IAP	log KT	
Anhydrite	-3.81	-8.17	-4.36	CaSO4
Aragonite	-2.31	-10.64	-8.33	CaCO3
Calcite	-2.17	-10.64	-8.47	CaCO3
CH4(g)	-84.59	-128.68	-44.09	CH4
Chalcedony	-0.49	-4.05	-3.56	SiO2
Chrysotile	-10.92	21.42	32.34	Mg3Si2O5(OH)4
CO2(g)	-2.21	-20.36	-18.15	CO2
Dolomite	-4.10	-21.16	-17.06	CaMg(CO3)2
Fe(OH)3(a)	3.16	21.10	17.94	Fe(OH)3
FeS(ppt)	-80.92	-118.65	-37.73	FeS
Goethite	9.01	21.10	12.09	FeOOH
Gypsum	-3.59	-8.17	-4.58	CaSO4:2H2O
H2(g)	-27.08	-27.08	0.00	H2
H2O(g)	-1.54	-0.00	1.54	H2O
H2S(g)	-84.45	-126.21	-41.75	H2S
Halite	-7.53	-5.95	1.58	NaCl
Hematite	20.02	42.19	22.17	Fe2O3
Jarosite-K	-0.04	29.97	30.01	KFe3(SO4)2(OH)6
Mackinawite	-80.19	-118.65	-38.46	FeS
Melanterite	-8.11	-10.33	-2.22	FeSO4:7H2O
N2(g)	-2.00	-5.26	-3.26	N2
NH3(g)	-38.70	-43.25	-4.55	NH3
O2(g)	-29.33	54.16	83.49	O2
Pyrite	-131.64	-217.78	-86.14	FeS2
Quartz	-0.06	-4.05	-4.00	SiO2
Sepiolite	-8.27	7.52	15.79	Mg2Si3O7.5OH:3H2O
Sepiolite(d)	-11.14	7.52	18.66	Mg2Si3O7.5OH:3H2O
Siderite	-1.92	-12.80	-10.88	FeCO3
SiO2(a)	-1.33	-4.05	-2.72	SiO2
Sulfur	-63.27	-99.13	-35.86	S
Talc	-8.22	13.31	21.52	Mg3Si4O10(OH)2

W1B

Saturation indices

Phase	SI	log IAP	log KT	
Anhydrite	-3.91	-8.27	-4.35	CaSO4
Aragonite	-2.58	-10.91	-8.32	CaCO3
Calcite	-2.44	-10.91	-8.47	CaCO3
CH4(g)	-79.15	-123.34	-44.19	CH4
Chalcedony	-0.51	-4.08	-3.57	SiO2
Chrysotile	-12.24	20.18	32.43	Mg3Si2O5(OH)4
CO2(g)	-1.98	-20.14	-18.15	CO2
Dolomite	-4.55	-21.60	-17.05	CaMg(CO3)2
Fe(OH)3(a)	2.44	20.39	17.95	Fe(OH)3
FeS(ppt)	-75.37	-113.20	-37.83	FeS
Goethite	8.27	20.39	12.13	FeOOH
Gypsum	-3.69	-8.27	-4.58	CaSO4:2H2O
H2(g)	-25.80	-25.80	0.00	H2
H2O(g)	-1.56	-0.00	1.56	H2O
H2S(g)	-78.84	-120.70	-41.86	H2S
Halite	-7.34	-5.76	1.58	NaCl
Hematite	18.53	40.79	22.26	Fe2O3
Jarosite-K	-1.56	28.56	30.12	KFe3(SO4)2(OH)6
Mackinawite	-74.64	-113.20	-38.57	FeS
Melanterite	-7.77	-10.00	-2.23	FeSO4:7H2O
N2(g)	-1.65	-4.90	-3.25	N2
NH3(g)	-36.58	-41.15	-4.57	NH3

O2(g)	-32.13	51.60	83.73	O2
Pyrite	-121.74	-208.10	-86.36	FeS2
Quartz	-0.07	-4.08	-4.01	SiO2
Sepiolite	-9.15	6.66	15.81	Mg2Si3O7.5OH:3H2O
Sepiolite(d)	-12.00	6.66	18.66	Mg2Si3O7.5OH:3H2O
Siderite	-1.76	-12.64	-10.88	FeCO3
SiO2(a)	-1.35	-4.08	-2.73	SiO2
Sulfur	-58.94	-94.90	-35.96	S
Talc	-9.58	12.03	21.61	Mg3Si4O10(OH)2

W2A

Saturation indices

Phase	SI	log IAP	log KT	
Anhydrite	-3.94	-8.29	-4.36	CaSO4
Aragonite	-3.12	-11.45	-8.33	CaCO3
Calcite	-2.97	-11.45	-8.47	CaCO3
CH4(g)	-76.70	-120.80	-44.10	CH4
Chalcedony	-0.50	-4.06	-3.57	SiO2
Chrysotile	-14.24	18.11	32.35	Mg3Si2O5(OH)4
CO2(g)	-2.01	-20.16	-18.15	CO2
Dolomite	-5.80	-22.86	-17.06	CaMg(CO3)2
Fe(OH)3(a)	1.75	19.69	17.94	Fe(OH)3
FeS(ppt)	-72.79	-110.54	-37.74	FeS
Goethite	7.60	19.69	12.09	FeOOH
Gypsum	-3.71	-8.29	-4.58	CaSO4:2H2O
H2(g)	-25.16	-25.16	0.00	H2
H2O(g)	-1.54	-0.00	1.54	H2O
H2S(g)	-75.87	-117.64	-41.77	H2S
Halite	-7.43	-5.85	1.58	NaCl
Hematite	17.19	39.37	22.18	Fe2O3
Jarosite-K	-2.81	27.22	30.03	KFe3(SO4)2(OH)6
Mackinawite	-72.06	-110.54	-38.48	FeS
Melanterite	-7.67	-9.90	-2.22	FeSO4:7H2O
N2(g)	-1.98	-5.23	-3.26	N2
NH3(g)	-35.80	-40.36	-4.55	NH3
O2(g)	-33.20	50.32	83.52	O2
Pyrite	-116.85	-203.02	-86.17	FeS2
Quartz	-0.06	-4.06	-4.00	SiO2
Sepiolite	-10.49	5.30	15.79	Mg2Si3O7.5OH:3H2O
Sepiolite(d)	-13.36	5.30	18.66	Mg2Si3O7.5OH:3H2O
Siderite	-2.17	-13.05	-10.88	FeCO3
SiO2(a)	-1.34	-4.06	-2.72	SiO2
Sulfur	-56.61	-92.48	-35.88	S
Talc	-11.55	9.98	21.54	Mg3Si4O10(OH)2

W3A

Saturation indices

Phase	SI	log IAP	log KT	
Anhydrite	-4.08	-8.43	-4.35	CaSO4
Aragonite	-2.44	-10.76	-8.32	CaCO3
Calcite	-2.30	-10.76	-8.47	CaCO3
CH4(g)	-82.62	-126.85	-44.23	CH4
Chalcedony	-0.45	-4.02	-3.58	SiO2
Chrysotile	-11.87	20.60	32.46	Mg3Si2O5(OH)4
CO2(g)	-2.14	-20.29	-18.15	CO2
Dolomite	-4.47	-21.51	-17.04	CaMg(CO3)2
Fe(OH)3(a)	2.44	20.41	17.96	Fe(OH)3
FeS(ppt)	-79.55	-117.43	-37.88	FeS
Goethite	8.26	20.41	12.15	FeOOH
Gypsum	-3.85	-8.43	-4.58	CaSO4:2H2O
H2(g)	-26.64	-26.64	0.00	H2
H2O(g)	-1.56	-0.00	1.56	H2O
H2S(g)	-82.61	-124.52	-41.91	H2S
Halite	-7.49	-5.91	1.58	NaCl
Hematite	18.52	40.81	22.29	Fe2O3
Jarosite-K	-2.12	28.05	30.16	KFe3(SO4)2(OH)6
Mackinawite	-78.82	-117.43	-38.61	FeS
Melanterite	-8.64	-10.87	-2.23	FeSO4:7H2O
N2(g)	-1.86	-5.11	-3.25	N2
NH3(g)	-37.94	-42.51	-4.58	NH3
O2(g)	-30.55	53.28	83.83	O2
Pyrite	-128.85	-215.31	-86.46	FeS2
Quartz	-0.01	-4.02	-4.01	SiO2
Sepiolite	-8.79	7.03	15.82	Mg2Si3O7.5OH:3H2O
Sepiolite(d)	-11.63	7.03	18.66	Mg2Si3O7.5OH:3H2O
Siderite	-2.33	-13.21	-10.88	FeCO3
SiO2(a)	-1.29	-4.02	-2.73	SiO2
Sulfur	-61.88	-97.88	-36.00	S
Talc	-9.09	12.55	21.64	Mg3Si4O10(OH)2

W3B

-----------------------------Saturation indices----------------------

Phase	SI	log IAP	log KT	
Anhydrite	-4.89	-9.24	-4.35	CaSO4
Aragonite	-2.48	-10.79	-8.31	CaCO3
Calcite	-2.33	-10.79	-8.46	CaCO3
CH4(g)	-79.03	-123.53	-44.49	CH4
Chalcedony	-0.46	-4.05	-3.60	SiO2
Chrysotile	-12.65	20.04	32.69	Mg3Si2O5(OH)4
CO2(g)	-1.85	-20.01	-18.16	CO2
Dolomite	-4.41	-21.41	-17.00	CaMg(CO3)2
Fe(OH)3(a)	3.19	21.20	18.01	Fe(OH)3
FeS(ppt)	-75.57	-113.72	-38.15	FeS
Goethite	8.94	21.20	12.25	FeOOH
Gypsum	-4.66	-9.24	-4.58	CaSO4:2H2O
H2(g)	-25.88	-25.88	0.00	H2
H2O(g)	-1.61	-0.00	1.61	H2O
H2S(g)	-79.79	-121.97	-42.18	H2S
Halite	-7.47	-5.90	1.57	NaCl
Hematite	19.87	42.39	22.52	Fe2O3
Jarosite-K	-1.41	29.02	30.44	KFe3(SO4)2(OH)6
Mackinawite	-74.84	-113.72	-38.88	FeS
Melanterite	-7.94	-10.20	-2.26	FeSO4:7H2O
N2(g)	-1.72	-4.97	-3.25	N2
NH3(g)	-36.68	-41.30	-4.62	NH3
O2(g)	-32.69	51.76	84.45	O2
Pyrite	-122.76	-209.81	-87.06	FeS2
Quartz	-0.02	-4.05	-4.04	SiO2
Sepiolite	-9.26	6.60	15.86	Mg2Si3O7.5OH:3H2O
Sepiolite(d)	-12.06	6.60	18.66	Mg2Si3O7.5OH:3H2O
Siderite	-0.88	-11.75	-10.87	FeCO3
SiO2(a)	-1.31	-4.05	-2.74	SiO2
Sulfur	-59.84	-96.09	-36.25	S
Talc	-9.92	11.93	21.85	Mg3Si4O10(OH)2

W4

-----------------------------Saturation indices----------------------

Phase	SI	log IAP	log KT	
Anhydrite	-3.86	-8.20	-4.35	CaSO4
Aragonite	-3.66	-11.97	-8.31	CaCO3
Calcite	-3.51	-11.97	-8.46	CaCO3
CH4(g)	-73.70	-118.15	-44.45	CH4
Chalcedony	-0.45	-4.05	-3.59	SiO2
Chrysotile	-15.65	17.00	32.65	Mg3Si2O5(OH)4
CO2(g)	-2.23	-20.39	-18.16	CO2
Dolomite	-6.99	-24.00	-17.01	CaMg(CO3)2
Fe(OH)3(a)	2.40	20.39	18.00	Fe(OH)3
FeS(ppt)	-68.10	-106.21	-38.10	FeS
Goethite	8.16	20.39	12.24	FeOOH
Gypsum	-3.62	-8.20	-4.58	CaSO4:2H2O
H2(g)	-24.44	-24.44	0.00	H2
H2O(g)	-1.60	-0.00	1.60	H2O
H2S(g)	-72.25	-114.38	-42.14	H2S
Halite	-7.54	-5.96	1.57	NaCl
Hematite	18.31	40.79	22.48	Fe2O3
Jarosite-K	-0.38	30.01	30.39	KFe3(SO4)2(OH)6
Mackinawite	-67.37	-106.21	-38.84	FeS
Melanterite	-6.19	-8.45	-2.25	FeSO4:7H2O
N2(g)	-2.08	-5.33	-3.25	N2
NH3(g)	-34.71	-39.32	-4.62	NH3
O2(g)	-35.46	48.88	84.34	O2
Pyrite	-109.19	-196.15	-86.96	FeS2
Quartz	-0.01	-4.05	-4.03	SiO2
Sepiolite	-11.26	4.59	15.86	Mg2Si3O7.5OH:3H2O
Sepiolite(d)	-14.07	4.59	18.66	Mg2Si3O7.5OH:3H2O
Siderite	-1.35	-12.21	-10.87	FeCO3
SiO2(a)	-1.30	-4.05	-2.74	SiO2
Sulfur	-53.73	-89.94	-36.21	S
Talc	-12.90	8.91	21.81	Mg3Si4O10(OH)2

W5

-----------------------------Saturation indices----------------------

Phase	SI	log IAP	log KT	
Anhydrite	-3.27	-7.62	-4.35	CaSO4
Aragonite	-3.32	-11.63	-8.31	CaCO3
Calcite	-3.17	-11.63	-8.46	CaCO3
CH4(g)	-74.48	-118.98	-44.49	CH4
Chalcedony	-0.46	-4.05	-3.60	SiO2
Chrysotile	-13.96	18.73	32.69	Mg3Si2O5(OH)4
CO2(g)	-2.26	-20.42	-18.16	CO2
Dolomite	-6.10	-23.10	-17.00	CaMg(CO3)2
Fe(OH)3(a)	0.77	18.77	18.01	Fe(OH)3
FeS(ppt)	-70.36	-108.51	-38.15	FeS
Goethite	6.52	18.77	12.25	FeOOH

Gypsum	-3.04	-7.62	-4.58	CaSO4:2H2O
H2(g)	-24.64	-24.64	0.00	H2
H2O(g)	-1.61	-0.00	1.61	H2O
H2S(g)	-72.78	-114.96	-42.18	H2S
Halite	-6.71	-5.13	1.57	NaCl
Hematite	15.03	37.55	22.52	Fe2O3
Jarosite-K	-4.67	25.77	30.44	KFe3(SO4)2(OH)6
Mackinawite	-69.63	-108.51	-38.88	FeS
Melanterite	-7.69	-9.95	-2.26	FeSO4:7H2O
N2(g)	-2.23	-5.48	-3.25	N2
NH3(g)	-35.08	-39.70	-4.62	NH3
O2(g)	-35.17	49.28	84.45	O2
Pyrite	-111.78	-198.83	-87.06	FeS2
Quartz	-0.02	-4.05	-4.04	SiO2
Sepiolite	-10.13	5.73	15.86	Mg2Si3O7.5OH:3H2O
Sepiolite(d)	-12.93	5.73	18.66	Mg2Si3O7.5OH:3H2O
Siderite	-3.10	-13.96	-10.87	FeCO3
SiO2(a)	-1.31	-4.05	-2.74	SiO2
Sulfur	-54.07	-90.32	-36.25	S
Talc	-11.23	10.62	21.85	Mg3Si4O10(OH)2

F1A

Saturation indices

Phase	SI	log IAP	log KT	
Anhydrite	-3.90	-8.26	-4.36	CaSO4
Aragonite	-2.19	-10.52	-8.34	CaCO3
Calcite	-2.05	-10.52	-8.48	CaCO3
CH4(g)	-78.36	-122.31	-43.95	CH4
Chalcedony	-0.72	-4.27	-3.55	SiO2
Chrysotile	-12.25	19.96	32.21	Mg3Si2O5(OH)4
CO2(g)	-1.60	-19.75	-18.15	CO2
Dolomite	-3.68	-20.77	-17.09	CaMg(CO3)2
Fe(OH)3(a)	1.65	19.57	17.91	Fe(OH)3
FeS(ppt)	-75.72	-113.30	-37.58	FeS
Goethite	7.54	19.57	12.03	FeOOH
Gypsum	-3.68	-8.26	-4.58	CaSO4:2H2O
H2(g)	-25.64	-25.64	0.00	H2
H2O(g)	-1.51	-0.00	1.51	H2O
H2S(g)	-78.44	-120.04	-41.60	H2S
Halite	-6.79	-5.21	1.58	NaCl
Hematite	17.09	39.13	22.04	Fe2O3
Jarosite-K	-3.58	26.29	29.86	KFe3(SO4)2(OH)6
Mackinawite	-74.98	-113.30	-38.31	FeS
Melanterite	-8.53	-10.74	-2.21	FeSO4:7H2O
N2(g)	-2.02	-5.28	-3.26	N2
NH3(g)	-36.57	-41.10	-4.53	NH3
O2(g)	-31.87	51.28	83.15	O2
Pyrite	-121.89	-207.70	-85.81	FeS2
Quartz	-0.29	-4.27	-3.98	SiO2
Sepiolite	-9.58	6.18	15.76	Mg2Si3O7.5OH:3H2O
Sepiolite(d)	-12.48	6.18	18.66	Mg2Si3O7.5OH:3H2O
Siderite	-2.11	-13.00	-10.89	FeCO3
SiO2(a)	-1.56	-4.27	-2.71	SiO2
Sulfur	-58.68	-94.40	-35.72	S
Talc	-10.00	11.41	21.41	Mg3Si4O10(OH)2

F1B

Saturation indices

Phase	SI	log IAP	log KT	
Anhydrite	-4.67	-9.02	-4.35	CaSO4
Aragonite	-2.17	-10.49	-8.32	CaCO3
Calcite	-2.02	-10.49	-8.46	CaCO3
CH4(g)	-78.16	-122.50	-44.35	CH4
Chalcedony	-0.64	-4.22	-3.59	SiO2
Chrysotile	-12.38	20.18	32.56	Mg3Si2O5(OH)4
CO2(g)	-1.63	-19.78	-18.16	CO2
Dolomite	-3.71	-20.73	-17.02	CaMg(CO3)2
Fe(OH)3(a)	2.73	20.71	17.98	Fe(OH)3
FeS(ppt)	-75.17	-113.17	-38.00	FeS
Goethite	8.51	20.71	12.19	FeOOH
Gypsum	-4.44	-9.02	-4.58	CaSO4:2H2O
H2(g)	-25.68	-25.68	0.00	H2
H2O(g)	-1.59	-0.00	1.59	H2O
H2S(g)	-79.01	-121.04	-42.03	H2S
Halite	-6.59	-5.01	1.58	NaCl
Hematite	19.02	41.41	22.39	Fe2O3
Jarosite-K	-2.26	28.02	30.28	KFe3(SO4)2(OH)6
Mackinawite	-74.44	-113.17	-38.73	FeS
Melanterite	-8.21	-10.45	-2.24	FeSO4:7H2O
N2(g)	-2.16	-5.41	-3.25	N2
NH3(g)	-36.63	-41.23	-4.60	NH3
O2(g)	-32.74	51.36	84.10	O2
Pyrite	-121.80	-208.53	-86.73	FeS2
Quartz	-0.20	-4.22	-4.02	SiO2

Sepiolite	-9.42	6.42	15.84	Mg2Si3O7.5OH:3H2O
Sepiolite(d)	-12.24	6.42	18.66	Mg2Si3O7.5OH:3H2O
Siderite	-1.04	-11.92	-10.87	FeCO3
SiO2(a)	-1.49	-4.22	-2.74	SiO2
Sulfur	-59.25	-95.36	-36.11	S
Talc	-9.99	11.74	21.73	Mg3Si4O10(OH)2

F2

Saturation indices

Phase	SI	log IAP	log KT	
Anhydrite	-4.07	-8.43	-4.36	CaSO4
Aragonite	-1.41	-9.75	-8.34	CaCO3
Calcite	-1.27	-9.75	-8.48	CaCO3
CH4(g)	-88.62	-132.51	-43.89	CH4
Chalcedony	-0.66	-4.21	-3.55	SiO2
Chrysotile	-8.52	23.65	32.16	Mg3Si2O5(OH)4
CO2(g)	-2.04	-20.19	-18.15	CO2
Dolomite	-2.16	-19.26	-17.10	CaMg(CO3)2
Fe(OH)3(a)	1.68	19.58	17.90	Fe(OH)3
FeS(ppt)	-88.12	-125.64	-37.52	FeS
Goethite	7.58	19.58	12.00	FeOOH
Gypsum	-3.85	-8.43	-4.58	CaSO4:2H2O
H2(g)	-28.08	-28.08	-0.00	H2
H2O(g)	-1.50	-0.00	1.50	H2O
H2S(g)	-89.64	-131.19	-41.54	H2S
Halite	-6.74	-5.16	1.58	NaCl
Hematite	17.17	39.17	22.00	Fe2O3
Jarosite-K	-5.55	24.25	29.81	KFe3(SO4)2(OH)6
Mackinawite	-87.39	-125.64	-38.25	FeS
Melanterite	-11.12	-13.32	-2.21	FeSO4:7H2O
N2(g)	-1.95	-5.21	-3.26	N2
NH3(g)	-40.21	-44.73	-4.52	NH3
O2(g)	-26.86	56.16	83.02	O2
Pyrite	-143.07	-228.75	-85.68	FeS2
Quartz	-0.23	-4.21	-3.98	SiO2
Sepiolite	-7.01	8.75	15.75	Mg2Si3O7.5OH:3H2O
Sepiolite(d)	-9.91	8.75	18.66	Mg2Si3O7.5OH:3H2O
Siderite	-3.76	-14.65	-10.89	FeCO3
SiO2(a)	-1.50	-4.21	-2.71	SiO2
Sulfur	-67.44	-103.11	-35.67	S
Talc	-6.14	15.23	21.36	Mg3Si4O10(OH)2

F3A

Saturation indices

Phase	SI	log IAP	log KT	
Anhydrite	-4.25	-8.61	-4.36	CaSO4
Aragonite	-1.93	-10.26	-8.33	CaCO3
Calcite	-1.78	-10.26	-8.48	CaCO3
CH4(g)	-82.71	-126.69	-43.99	CH4
Chalcedony	-0.65	-4.21	-3.56	SiO2
Chrysotile	-10.78	21.48	32.25	Mg3Si2O5(OH)4
CO2(g)	-1.82	-19.97	-18.15	CO2
Dolomite	-3.19	-20.27	-17.08	CaMg(CO3)2
Gypsum	-4.03	-8.61	-4.58	CaSO4:2H2O
H2(g)	-26.68	-26.68	0.00	H2
H2O(g)	-1.52	-0.00	1.52	H2O
H2S(g)	-83.40	-125.05	-41.65	H2S
Halite	-6.74	-5.16	1.58	NaCl
N2(g)	-1.94	-5.19	-3.26	N2
NH3(g)	-38.08	-42.62	-4.53	NH3
O2(g)	-29.89	53.36	83.25	O2
Quartz	-0.22	-4.21	-3.99	SiO2
Sepiolite	-8.47	7.30	15.77	Mg2Si3O7.5OH:3H2O
Sepiolite(d)	-11.36	7.30	18.66	Mg2Si3O7.5OH:3H2O
SiO2(a)	-1.50	-4.21	-2.72	SiO2
Sulfur	-62.60	-98.37	-35.76	S
Talc	-8.39	13.06	21.44	Mg3Si4O10(OH)2

F3B

Saturation indices

Phase	SI	log IAP	log KT	
Anhydrite	-4.69	-9.04	-4.35	CaSO4
Aragonite	-1.92	-10.23	-8.32	CaCO3
Calcite	-1.77	-10.23	-8.46	CaCO3
CH4(g)	-80.43	-124.76	-44.33	CH4
Chalcedony	-0.63	-4.21	-3.58	SiO2
Chrysotile	-11.39	21.16	32.55	Mg3Si2O5(OH)4
CO2(g)	-1.64	-19.80	-18.16	CO2
Dolomite	-3.15	-20.17	-17.02	CaMg(CO3)2
Fe(OH)3(a)	2.77	20.75	17.98	Fe(OH)3
FeS(ppt)	-77.96	-115.94	-37.98	FeS
Goethite	8.56	20.75	12.19	FeOOH
Gypsum	-4.46	-9.04	-4.58	CaSO4:2H2O
H2(g)	-26.24	-26.24	0.00	H2

H2O(g)	-1.58	-0.00	1.58	H2O
H2S(g)	-81.56	-123.57	-42.01	H2S
Halite	-6.44	-4.87	1.58	NaCl
Hematite	19.11	41.49	22.38	Fe2O3
Jarosite-K	-2.55	27.72	30.27	KFe3(SO4)2(OH)6
Mackinawite	-77.23	-115.94	-38.72	FeS
Melanterite	-8.74	-10.99	-2.24	FeSO4:7H2O
N2(g)	-1.98	-5.23	-3.25	N2
NH3(g)	-37.38	-41.98	-4.59	NH3
O2(g)	-31.59	52.48	84.07	O2
Pyrite	-126.58	-213.27	-86.69	FeS2
Quartz	-0.19	-4.21	-4.02	SiO2
Sepiolite	-8.74	7.09	15.83	Mg2Si3O7.5OH:3H2O
Sepiolite(d)	-11.57	7.09	18.66	Mg2Si3O7.5OH:3H2O
Siderite	-1.30	-12.17	-10.87	FeCO3
SiO2(a)	-1.47	-4.21	-2.74	SiO2
Sulfur	-61.23	-97.33	-36.10	S
Talc	-8.98	12.74	21.72	Mg3Si4O10(OH)2

F4

Saturation indices

Phase	SI	log IAP	log KT	
Anhydrite	-4.05	-8.41	-4.36	CaSO4
Aragonite	-2.09	-10.43	-8.34	CaCO3
Calcite	-1.95	-10.43	-8.48	CaCO3
CH4(g)	-79.63	-123.47	-43.85	CH4
Chalcedony	-0.69	-4.23	-3.54	SiO2
Chrysotile	-11.68	20.45	32.13	Mg3Si2O5(OH)4
CO2(g)	-1.64	-19.79	-18.15	CO2
Dolomite	-3.48	-20.58	-17.10	CaMg(CO3)2
Fe(OH)3(a)	2.44	20.34	17.90	Fe(OH)3
FeS(ppt)	-76.60	-114.07	-37.48	FeS
Goethite	8.36	20.34	11.98	FeOOH
Gypsum	-3.83	-8.41	-4.58	CaSO4:2H2O
H2(g)	-25.92	-25.92	-0.00	H2
H2O(g)	-1.49	-0.00	1.49	H2O
H2S(g)	-79.95	-121.45	-41.50	H2S
Halite	-6.70	-5.11	1.58	NaCl
Hematite	18.72	40.68	21.96	Fe2O3
Jarosite-K	-1.63	28.13	29.76	KFe3(SO4)2(OH)6
Mackinawite	-75.86	-114.07	-38.21	FeS
Melanterite	-8.19	-10.39	-2.20	FeSO4:7H2O
N2(g)	-1.86	-5.13	-3.26	N2
NH3(g)	-36.94	-41.44	-4.51	NH3
O2(g)	-31.08	51.84	82.92	O2
Pyrite	-124.02	-209.60	-85.59	FeS2
Quartz	-0.26	-4.23	-3.97	SiO2
Sepiolite	-9.17	6.57	15.74	Mg2Si3O7.5OH:3H2O
Sepiolite(d)	-12.09	6.57	18.66	Mg2Si3O7.5OH:3H2O
Siderite	-1.52	-12.41	-10.89	FeCO3
SiO2(a)	-1.53	-4.23	-2.71	SiO2
Sulfur	-59.90	-95.53	-35.63	S
Talc	-9.35	11.98	21.33	Mg3Si4O10(OH)2

F5

Saturation indices

Phase	SI	log IAP	log KT	
Anhydrite	-3.87	-8.23	-4.36	CaSO4
Aragonite	-2.40	-10.73	-8.33	CaCO3
Calcite	-2.25	-10.73	-8.48	CaCO3
CH4(g)	-80.59	-124.60	-44.00	CH4
Chalcedony	-0.61	-4.17	-3.56	SiO2
Chrysotile	-11.78	20.48	32.26	Mg3Si2O5(OH)4
CO2(g)	-1.97	-20.12	-18.15	CO2
Dolomite	-4.17	-21.24	-17.08	CaMg(CO3)2
Gypsum	-3.65	-8.23	-4.58	CaSO4:2H2O
H2(g)	-26.12	-26.12	0.00	H2
H2O(g)	-1.52	-0.00	1.52	H2O
H2S(g)	-80.43	-122.09	-41.66	H2S
Halite	-7.25	-5.67	1.58	NaCl
N2(g)	-2.04	-5.30	-3.26	N2
NH3(g)	-37.30	-41.83	-4.54	NH3
O2(g)	-31.05	52.24	83.29	O2
Quartz	-0.18	-4.17	-3.99	SiO2
Sepiolite	-9.06	6.71	15.77	Mg2Si3O7.5OH:3H2O
Sepiolite(d)	-11.95	6.71	18.66	Mg2Si3O7.5OH:3H2O
SiO2(a)	-1.45	-4.17	-2.72	SiO2
Sulfur	-60.20	-95.97	-35.78	S
Talc	-9.31	12.15	21.46	Mg3Si4O10(OH)2

Wo1A

Saturation indices

Phase	SI	log IAP	log KT	
Anhydrite	-3.53	-7.88	-4.35	CaSO4

Aragonite	-1.99	-10.32	-8.33	CaCO3
Calcite	-1.85	-10.32	-8.47	CaCO3
CH4(g)	-79.37	-123.53	-44.16	CH4
Chalcedony	-0.72	-4.29	-3.57	SiO2
Chrysotile	-12.95	19.45	32.40	Mg3Si2O5(OH)4
CO2(g)	-1.70	-19.85	-18.15	CO2
Dolomite	-3.77	-20.82	-17.05	CaMg(CO3)2
Fe(OH)3(a)	3.27	21.21	17.95	Fe(OH)3
FeS(ppt)	-75.04	-112.84	-37.80	FeS
Goethite	9.10	21.21	12.12	FeOOH
Gypsum	-3.30	-7.88	-4.58	CaSO4:2H2O
H2(g)	-25.92	-25.92	0.00	H2
H2O(g)	-1.55	-0.00	1.55	H2O
H2S(g)	-79.27	-121.10	-41.83	H2S
Halite	-7.11	-5.54	1.58	NaCl
Hematite	20.20	42.43	22.23	Fe2O3
Jarosite-K	1.06	31.15	30.09	KFe3(SO4)2(OH)6
Mackinawite	-74.30	-112.84	-38.54	FeS
Melanterite	-6.93	-9.16	-2.23	FeSO4:7H2O
N2(g)	-1.80	-5.05	-3.25	N2
NH3(g)	-36.84	-41.41	-4.56	NH3
O2(g)	-31.82	51.84	83.66	O2
Pyrite	-121.72	-208.02	-86.30	FeS2
Quartz	-0.28	-4.29	-4.00	SiO2
Sepiolite	-9.98	5.82	15.80	Mg2Si3O7.5OH:3H2O
Sepiolite(d)	-12.84	5.82	18.66	Mg2Si3O7.5OH:3H2O
Siderite	-0.72	-11.60	-10.88	FeCO3
SiO2(a)	-1.56	-4.29	-2.73	SiO2
Sulfur	-59.24	-95.18	-35.93	S
Talc	-10.70	10.88	21.58	Mg3Si4O10(OH)2

Wo1B

Saturation indices

Phase	SI	log IAP	log KT	
Anhydrite	-4.71	-9.07	-4.36	CaSO4
Aragonite	-2.21	-10.55	-8.33	CaCO3
Calcite	-2.07	-10.55	-8.48	CaCO3
CH4(g)	-77.87	-121.86	-43.99	CH4
Chalcedony	-0.54	-4.10	-3.56	SiO2
Chrysotile	-12.56	19.69	32.25	Mg3Si2O5(OH)4
CO2(g)	-1.63	-19.78	-18.15	CO2
Dolomite	-3.95	-21.03	-17.08	CaMg(CO3)2
Fe(OH)3(a)	2.17	20.10	17.92	Fe(OH)3
FeS(ppt)	-75.43	-113.05	-37.62	FeS
Goethite	8.05	20.10	12.04	FeOOH
Gypsum	-4.49	-9.07	-4.58	CaSO4:2H2O
H2(g)	-25.52	-25.52	0.00	H2
H2O(g)	-1.52	-0.00	1.52	H2O
H2S(g)	-78.74	-120.39	-41.65	H2S
Halite	-7.01	-5.43	1.58	NaCl
Hematite	18.11	40.19	22.08	Fe2O3
Jarosite-K	-3.89	26.02	29.91	KFe3(SO4)2(OH)6
Mackinawite	-74.70	-113.05	-38.36	FeS
Melanterite	-8.76	-10.97	-2.21	FeSO4:7H2O
N2(g)	-1.65	-4.91	-3.26	N2
NH3(g)	-36.20	-40.74	-4.53	NH3
O2(g)	-32.21	51.04	83.25	O2
Pyrite	-122.01	-207.92	-85.91	FeS2
Quartz	-0.11	-4.10	-3.99	SiO2
Sepiolite	-9.47	6.30	15.77	Mg2Si3O7.5OH:3H2O
Sepiolite(d)	-12.36	6.30	18.66	Mg2Si3O7.5OH:3H2O
Siderite	-1.56	-12.45	-10.89	FeCO3
SiO2(a)	-1.38	-4.10	-2.72	SiO2
Sulfur	-59.10	-94.87	-35.76	S
Talc	-9.95	11.49	21.44	Mg3Si4O10(OH)2

Wo2

Saturation indices

Phase	SI	log IAP	log KT	
Anhydrite	-3.49	-7.84	-4.36	CaSO4
Aragonite	-1.87	-10.20	-8.33	CaCO3
Calcite	-1.73	-10.20	-8.48	CaCO3
CH4(g)	-79.44	-123.47	-44.03	CH4
Chalcedony	-0.80	-4.36	-3.56	SiO2
Chrysotile	-12.74	19.55	32.29	Mg3Si2O5(OH)4
CO2(g)	-1.64	-19.79	-18.15	CO2
Dolomite	-3.49	-20.57	-17.07	CaMg(CO3)2
Fe(OH)3(a)	3.18	21.11	17.93	Fe(OH)3
FeS(ppt)	-75.30	-112.97	-37.67	FeS
Goethite	9.05	21.11	12.06	FeOOH
Gypsum	-3.26	-7.85	-4.58	CaSO4:2H2O
H2(g)	-25.92	-25.92	0.00	H2
H2O(g)	-1.53	-0.00	1.53	H2O
H2S(g)	-79.42	-121.11	-41.69	H2S

```
          Halite           -7.13   -5.55    1.58  NaCl
          Hematite         20.10   42.21   22.12  Fe2O3
          Jarosite-K        0.83   30.78   29.95  KFe3(SO4)2(OH)6
          Mackinawite     -74.57 -112.97  -38.40  FeS
          Melanterite      -7.07   -9.29   -2.22  FeSO4:7H2O
          N2(g)            -1.88   -5.14   -3.26  N2
          NH3(g)          -36.91  -41.45   -4.54  NH3
          O2(g)           -31.52   51.84   83.36  O2
          Pyrite         -122.16 -208.16  -86.01  FeS2
          Quartz           -0.37   -4.36   -3.99  SiO2
          Sepiolite       -10.02    5.76   15.78  Mg2Si3O7.5OH:3H2O
          Sepiolite(d)    -12.90    5.76   18.66  Mg2Si3O7.5OH:3H2O
          Siderite         -0.76  -11.64  -10.89  FeCO3
          SiO2(a)          -1.65   -4.36   -2.72  SiO2
          Sulfur          -59.39  -95.19  -35.81  S
          Talc            -10.66   10.82   21.48  Mg3Si4O10(OH)2
-------------------------------------------------------------------------
Wo3A
------------------------------Saturation indices----------------------
          Phase               SI log IAP  log KT
          Anhydrite        -3.80   -8.16   -4.35  CaSO4
          Aragonite        -2.19  -10.51   -8.32  CaCO3
          Calcite          -2.04  -10.51   -8.47  CaCO3
          CH4(g)          -78.12 -122.37  -44.25  CH4
          Chalcedony       -0.75   -4.33   -3.58  SiO2
          Chrysotile      -13.50   18.97   32.48  Mg3Si2O5(OH)4
          CO2(g)           -1.66  -19.81  -18.15  CO2
          Dolomite         -4.07  -21.11  -17.04  CaMg(CO3)2
          Fe(OH)3(a)        3.19   21.16   17.96  Fe(OH)3
          FeS(ppt)        -73.78 -111.68  -37.89  FeS
          Goethite          9.01   21.16   12.15  FeOOH
          Gypsum           -3.58   -8.16   -4.58  CaSO4:2H2O
          H2(g)           -25.64  -25.64    0.00  H2
          H2O(g)           -1.57   -0.00    1.57  H2O
          H2S(g)          -78.09 -120.02  -41.92  H2S
          Halite           -7.07   -5.50    1.58  NaCl
          Hematite         20.01   42.32   22.31  Fe2O3
          Jarosite-K        0.64   30.81   30.18  KFe3(SO4)2(OH)6
          Mackinawite     -73.05 -111.68  -38.63  FeS
          Melanterite      -6.88   -9.12   -2.24  FeSO4:7H2O
          N2(g)            -1.92   -5.18   -3.25  N2
          NH3(g)          -36.47  -41.05   -4.58  NH3
          O2(g)           -32.58   51.28   83.86  O2
          Pyrite         -119.56 -206.05  -86.50  FeS2
          Quartz           -0.32   -4.33   -4.01  SiO2
          Sepiolite       -10.39    5.43   15.82  Mg2Si3O7.5OH:3H2O
          Sepiolite(d)    -13.23    5.43   18.66  Mg2Si3O7.5OH:3H2O
          Siderite         -0.60  -11.47  -10.88  FeCO3
          SiO2(a)          -1.60   -4.33   -2.73  SiO2
          Sulfur          -58.36  -94.38  -36.01  S
          Talc            -11.34   10.31   21.65  Mg3Si4O10(OH)2
-------------------------------------------------------------------------
Wo3B
------------------------------Saturation indices----------------------
          Phase               SI log IAP  log KT
          Anhydrite        -4.26   -8.61   -4.36  CaSO4
          Aragonite        -2.48  -10.81   -8.33  CaCO3
          Calcite          -2.34  -10.81   -8.48  CaCO3
          CH4(g)          -77.47 -121.47  -44.00  CH4
          Chalcedony       -0.88   -4.44   -3.56  SiO2
          Chrysotile      -13.43   18.84   32.26  Mg3Si2O5(OH)4
          CO2(g)           -1.72  -19.87  -18.15  CO2
          Dolomite         -4.37  -21.44  -17.08  CaMg(CO3)2
          Fe(OH)3(a)        3.09   21.01   17.92  Fe(OH)3
          FeS(ppt)        -73.32 -110.96  -37.64  FeS
          Goethite          8.96   21.01   12.05  FeOOH
          Gypsum           -4.03   -8.61   -4.58  CaSO4:2H2O
          H2(g)           -25.40  -25.40    0.00  H2
          H2O(g)           -1.52   -0.00    1.52  H2O
          H2S(g)          -77.61 -119.27  -41.66  H2S
          Halite           -7.02   -5.44    1.58  NaCl
          Hematite         19.93   42.02   22.09  Fe2O3
          Jarosite-K        0.05   29.97   29.92  KFe3(SO4)2(OH)6
          Mackinawite     -72.59 -110.96  -38.37  FeS
          Melanterite      -7.14   -9.36   -2.22  FeSO4:7H2O
          N2(g)            -1.87   -5.13   -3.26  N2
          NH3(g)          -36.13  -40.66   -4.54  NH3
          O2(g)           -32.49   50.80   83.29  O2
          Pyrite         -118.89 -204.83  -85.94  FeS2
          Quartz           -0.45   -4.44   -3.99  SiO2
          Sepiolite       -10.61    5.16   15.77  Mg2Si3O7.5OH:3H2O
          Sepiolite(d)    -13.50    5.16   18.66  Mg2Si3O7.5OH:3H2O
          Siderite         -0.67  -11.56  -10.89  FeCO3
          SiO2(a)          -1.72   -4.44   -2.72  SiO2
```

Sulfur	-58.09	-93.87	-35.78	S
Talc	-11.49	9.96	21.46	Mg3Si4O10(OH)2

May 2000

W1B

Phase	SI	log IAP	log KT	
Anhydrite	-3.66	-8.00	-4.34	CaSO4
Aragonite	-1.06	-9.34	-8.28	CaCO3
Calcite	-0.91	-9.34	-8.43	CaCO3
CH4(g)	-102.41	-147.78	-45.37	CH4
Chalcedony	-0.59	-4.26	-3.67	SiO2
Chrysotile	-4.86	28.60	33.46	Mg3Si2O5(OH)4
CO2(g)	-3.19	-21.38	-18.19	CO2
Dolomite	-1.49	-18.34	-16.85	CaMg(CO3)2
Fe(OH)3(a)	2.76	20.91	18.15	Fe(OH)3
FeS(ppt)	-102.26	-141.32	-39.06	FeS
Goethite	8.29	20.91	12.62	FeOOH
Gypsum	-3.41	-8.00	-4.58	CaSO4:2H2O
H2(g)	-31.60	-31.60	0.00	H2
H2O(g)	-1.77	-0.00	1.77	H2O
H2S(g)	-103.32	-146.43	-43.11	H2S
Halite	-7.13	-5.57	1.56	NaCl
Hematite	18.54	41.82	23.28	Fe2O3
Jarosite-K	-4.91	26.45	31.35	KFe3(SO4)2(OH)6
Mackinawite	-101.53	-141.32	-39.80	FeS
Melanterite	-12.59	-14.92	-2.34	FeSO4:7H2O
N2(g)	-2.25	-5.48	-3.23	N2
NH3(g)	-45.36	-50.14	-4.78	NH3
O2(g)	-23.32	63.20	86.52	O2
Pyrite	-167.10	-256.15	-89.06	FeS2
Quartz	-0.13	-4.26	-4.13	SiO2
Sepiolite	-4.07	11.96	16.03	Mg2Si3O7.5OH:3H2O
Sepiolite(d)	-6.70	11.96	18.66	Mg2Si3O7.5OH:3H2O
Siderite	-5.44	-16.27	-10.83	FeCO3
SiO2(a)	-1.47	-4.26	-2.80	SiO2
Sulfur	-77.72	-114.83	-37.11	S
Talc	-2.48	20.07	22.55	Mg3Si4O10(OH)2

W2A

Phase	SI	log IAP	log KT	
Anhydrite	-3.66	-7.99	-4.34	CaSO4
Aragonite	-1.06	-9.34	-8.28	CaCO3
Calcite	-0.91	-9.34	-8.43	CaCO3
CH4(g)	-101.07	-146.52	-45.44	CH4
Chalcedony	-0.37	-4.04	-3.68	SiO2
Chrysotile	-5.70	27.83	33.52	Mg3Si2O5(OH)4
CO2(g)	-3.05	-21.24	-18.19	CO2
Dolomite	-1.77	-18.61	-16.84	CaMg(CO3)2
Fe(OH)3(a)	4.63	22.79	18.16	Fe(OH)3
FeS(ppt)	-98.89	-138.04	-39.14	FeS
Goethite	10.14	22.79	12.65	FeOOH
Gypsum	-3.41	-7.99	-4.58	CaSO4:2H2O
H2(g)	-31.32	-31.32	0.00	H2
H2O(g)	-1.79	-0.00	1.79	H2O
H2S(g)	-101.97	-145.17	-43.19	H2S
Halite	-7.60	-6.04	1.56	NaCl
Hematite	22.23	45.58	23.35	Fe2O3
Jarosite-K	0.96	32.39	31.43	KFe3(SO4)2(OH)6
Mackinawite	-98.16	-138.04	-39.88	FeS
Melanterite	-10.41	-12.76	-2.34	FeSO4:7H2O
N2(g)	-2.03	-5.26	-3.22	N2
NH3(g)	-44.81	-49.61	-4.79	NH3
O2(g)	-24.06	62.64	86.70	O2
Pyrite	-162.66	-251.89	-89.23	FeS2
Quartz	0.10	-4.04	-4.14	SiO2
Sepiolite	-4.22	11.82	16.04	Mg2Si3O7.5OH:3H2O
Sepiolite(d)	-6.84	11.82	18.66	Mg2Si3O7.5OH:3H2O
Siderite	-3.28	-14.11	-10.82	FeCO3
SiO2(a)	-1.24	-4.04	-2.80	SiO2
Sulfur	-76.66	-113.85	-37.19	S
Talc	-2.87	19.74	22.61	Mg3Si4O10(OH)2

W2B

Phase	SI	log IAP	log KT	
Anhydrite	-4.14	-8.48	-4.34	CaSO4
Aragonite	-0.43	-8.72	-8.29	CaCO3
Calcite	-0.28	-8.72	-8.44	CaCO3
CH4(g)	-102.88	-148.01	-45.13	CH4

Chalcedony	-0.50	-4.15	-3.65	SiO2
Chrysotile	-4.71	28.54	33.25	Mg3Si2O5(OH)4
CO2(g)	-2.95	-21.13	-18.18	CO2
Dolomite	-0.67	-17.57	-16.89	CaMg(CO3)2
Fe(OH)3(a)	4.64	22.75	18.11	Fe(OH)3
FeS(ppt)	-102.07	-140.88	-38.81	FeS
Goethite	10.23	22.75	12.52	FeOOH
Gypsum	-3.89	-8.48	-4.58	CaSO4:2H2O
H2(g)	-31.72	-31.72	0.00	H2
H2O(g)	-1.73	-0.00	1.73	H2O
H2S(g)	-104.91	-147.77	-42.86	H2S
Halite	-7.18	-5.62	1.56	NaCl
Hematite	22.42	45.50	23.07	Fe2O3
Jarosite-K	-0.96	30.14	31.10	KFe3(SO4)2(OH)6
Mackinawite	-101.33	-140.88	-39.54	FeS
Melanterite	-11.68	-14.00	-2.31	FeSO4:7H2O
N2(g)	-1.76	-4.99	-3.23	N2
NH3(g)	-45.34	-50.07	-4.74	NH3
O2(g)	-22.51	63.44	85.95	O2
Pyrite	-168.42	-256.92	-88.51	FeS2
Quartz	-0.04	-4.15	-4.10	SiO2
Sepiolite	-3.87	12.11	15.98	Mg2Si3O7.5OH:3H2O
Sepiolite(d)	-6.55	12.11	18.66	Mg2Si3O7.5OH:3H2O
Siderite	-3.40	-14.24	-10.84	FeCO3
SiO2(a)	-1.37	-4.15	-2.78	SiO2
Sulfur	-79.17	-116.05	-36.87	S
Talc	-2.12	20.24	22.36	Mg3Si4O10(OH)2

W3A

Saturation indices

Phase	SI	log IAP	log KT	
Anhydrite	-3.35	-7.69	-4.34	CaSO4
Aragonite	-1.10	-9.38	-8.28	CaCO3
Calcite	-0.95	-9.38	-8.43	CaCO3
CH4(g)	-101.15	-146.59	-45.44	CH4
Chalcedony	-0.36	-4.03	-3.68	SiO2
Chrysotile	-5.54	27.98	33.52	Mg3Si2O5(OH)4
CO2(g)	-3.12	-21.31	-18.19	CO2
Dolomite	-1.83	-18.68	-16.84	CaMg(CO3)2
Fe(OH)3(a)	4.74	22.90	18.16	Fe(OH)3
FeS(ppt)	-98.51	-137.66	-39.14	FeS
Goethite	10.25	22.90	12.65	FeOOH
Gypsum	-3.10	-7.69	-4.58	CaSO4:2H2O
H2(g)	-31.32	-31.32	0.00	H2
H2O(g)	-1.79	-0.00	1.79	H2O
H2S(g)	-101.70	-144.90	-43.19	H2S
Halite	-7.61	-6.05	1.56	NaCl
Hematite	22.45	45.80	23.35	Fe2O3
Jarosite-K	2.00	33.43	31.43	KFe3(SO4)2(OH)6
Mackinawite	-97.78	-137.66	-39.88	FeS
Melanterite	-10.03	-12.38	-2.34	FeSO4:7H2O
N2(g)	-1.86	-5.08	-3.22	N2
NH3(g)	-44.73	-49.52	-4.79	NH3
O2(g)	-24.06	62.64	86.70	O2
Pyrite	-162.00	-251.23	-89.23	FeS2
Quartz	0.10	-4.03	-4.14	SiO2
Sepiolite	-4.11	11.93	16.04	Mg2Si3O7.5OH:3H2O
Sepiolite(d)	-6.73	11.93	18.66	Mg2Si3O7.5OH:3H2O
Siderite	-3.24	-14.07	-10.82	FeCO3
SiO2(a)	-1.23	-4.03	-2.80	SiO2
Sulfur	-76.39	-113.58	-37.19	S
Talc	-2.70	19.92	22.61	Mg3Si4O10(OH)2

W3B

Saturation indices

Phase	SI	log IAP	log KT	
Anhydrite	-4.73	-9.08	-4.34	CaSO4
Aragonite	-1.19	-9.49	-8.30	CaCO3
Calcite	-1.04	-9.49	-8.45	CaCO3
CH4(g)	-95.49	-140.30	-44.81	CH4
Chalcedony	-0.45	-4.07	-3.62	SiO2
Chrysotile	-6.68	26.29	32.97	Mg3Si2O5(OH)4
CO2(g)	-2.62	-20.78	-18.17	CO2
Dolomite	-1.85	-18.79	-16.95	CaMg(CO3)2
Fe(OH)3(a)	3.84	21.90	18.06	Fe(OH)3
FeS(ppt)	-94.45	-132.94	-38.49	FeS
Goethite	9.51	21.90	12.39	FeOOH
Gypsum	-4.49	-9.08	-4.58	CaSO4:2H2O
H2(g)	-29.88	-29.88	0.00	H2
H2O(g)	-1.67	-0.00	1.67	H2O
H2S(g)	-97.37	-139.89	-42.52	H2S
Halite	-7.23	-5.66	1.57	NaCl
Hematite	21.00	43.80	22.80	Fe2O3
Jarosite-K	-2.42	28.35	30.77	KFe3(SO4)2(OH)6

Mackinawite	-93.72	-132.94	-39.22	FeS
Melanterite	-11.13	-13.42	-2.29	FeSO4:7H2O
N2(g)	-1.60	-4.84	-3.24	N2
NH3(g)	-42.56	-47.24	-4.68	NH3
O2(g)	-25.45	59.76	85.21	O2
Pyrite	-155.16	-242.95	-87.79	FeS2
Quartz	-0.00	-4.07	-4.07	SiO2
Sepiolite	-5.18	10.74	15.92	Mg2Si3O7.5OH:3H2O
Sepiolite(d)	-7.92	10.74	18.66	Mg2Si3O7.5OH:3H2O
Siderite	-2.97	-13.83	-10.85	FeCO3
SiO2(a)	-1.31	-4.07	-2.76	SiO2
Sulfur	-73.45	-110.01	-36.57	S
Talc	-3.96	18.15	22.11	Mg3Si4O10(OH)2

W4

-----Saturation indices-----

Phase	SI	log IAP	log KT	
Anhydrite	-3.57	-7.91	-4.34	CaSO4
Aragonite	-1.50	-9.80	-8.30	CaCO3
Calcite	-1.35	-9.80	-8.45	CaCO3
CH4(g)	-102.67	-147.53	-44.86	CH4
Chalcedony	-0.46	-4.08	-3.63	SiO2
Chrysotile	-6.10	26.91	33.01	Mg3Si2O5(OH)4
CO2(g)	-3.44	-21.61	-18.17	CO2
Dolomite	-2.77	-19.71	-16.94	CaMg(CO3)2
Fe(OH)3(a)	3.94	22.01	18.07	Fe(OH)3
FeS(ppt)	-100.84	-139.37	-38.53	FeS
Goethite	9.60	22.01	12.41	FeOOH
Gypsum	-3.33	-7.91	-4.58	CaSO4:2H2O
H2(g)	-31.48	-31.48	0.00	H2
H2O(g)	-1.68	-0.00	1.68	H2O
H2S(g)	-103.07	-145.64	-42.57	H2S
Halite	-7.69	-6.12	1.57	NaCl
Hematite	21.18	44.01	22.84	Fe2O3
Jarosite-K	-0.44	30.38	30.82	KFe3(SO4)2(OH)6
Mackinawite	-100.11	-139.37	-39.27	FeS
Melanterite	-11.16	-13.45	-2.29	FeSO4:7H2O
N2(g)	-1.79	-5.03	-3.24	N2
NH3(g)	-45.04	-49.73	-4.69	NH3
O2(g)	-22.36	62.96	85.32	O2
Pyrite	-165.64	-253.54	-87.89	FeS2
Quartz	-0.01	-4.08	-4.08	SiO2
Sepiolite	-4.80	11.14	15.93	Mg2Si3O7.5OH:3H2O
Sepiolite(d)	-7.52	11.14	18.66	Mg2Si3O7.5OH:3H2O
Siderite	-4.49	-15.34	-10.85	FeCO3
SiO2(a)	-1.32	-4.08	-2.77	SiO2
Sulfur	-77.55	-114.16	-36.61	S
Talc	-3.40	18.75	22.14	Mg3Si4O10(OH)2

W5

-----Saturation indices-----

Phase	SI	log IAP	log KT	
Anhydrite	-3.31	-7.65	-4.34	CaSO4
Aragonite	-1.75	-10.05	-8.30	CaCO3
Calcite	-1.60	-10.05	-8.45	CaCO3
CH4(g)	-99.13	-143.93	-44.80	CH4
Chalcedony	-0.45	-4.07	-3.62	SiO2
Chrysotile	-6.25	26.71	32.96	Mg3Si2O5(OH)4
CO2(g)	-3.20	-21.37	-18.17	CO2
Dolomite	-2.85	-19.80	-16.95	CaMg(CO3)2
Gypsum	-3.07	-7.65	-4.58	CaSO4:2H2O
H2(g)	-30.64	-30.64	0.00	H2
H2O(g)	-1.67	-0.00	1.67	H2O
H2S(g)	-99.03	-141.54	-42.51	H2S
Halite	-7.37	-5.80	1.57	NaCl
N2(g)	-2.84	-6.08	-3.24	N2
NH3(g)	-44.32	-49.00	-4.68	NH3
O2(g)	-23.90	61.28	85.18	O2
Quartz	-0.00	-4.07	-4.07	SiO2
Sepiolite	-4.91	11.01	15.92	Mg2Si3O7.5OH:3H2O
Sepiolite(d)	-7.65	11.01	18.66	Mg2Si3O7.5OH:3H2O
SiO2(a)	-1.31	-4.07	-2.76	SiO2
Sulfur	-74.34	-110.90	-36.55	S
Talc	-3.54	18.56	22.10	Mg3Si4O10(OH)2

F1A

-----Saturation indices-----

Phase	SI	log IAP	log KT	
Anhydrite	-3.66	-7.99	-4.33	CaSO4
Aragonite	-1.14	-9.40	-8.27	CaCO3
Calcite	-0.98	-9.40	-8.42	CaCO3
CH4(g)	-97.56	-143.35	-45.80	CH4
Chalcedony	-0.38	-4.08	-3.70	SiO2
Chrysotile	-6.65	27.18	33.83	Mg3Si2O5(OH)4

CO2(g)	-2.75	-20.95	-18.20	CO2
Dolomite	-1.79	-18.58	-16.78	CaMg(CO3)2
Fe(OH)3(a)	3.37	21.60	18.22	Fe(OH)3
FeS(ppt)	-96.14	-135.65	-39.51	FeS
Goethite	8.79	21.60	12.80	FeOOH
Gypsum	-3.41	-7.99	-4.59	CaSO4:2H2O
H2(g)	-30.60	-30.60	0.00	H2
H2O(g)	-1.85	-0.00	1.85	H2O
H2S(g)	-98.37	-141.94	-43.57	H2S
Halite	-7.41	-5.86	1.55	NaCl
Hematite	19.53	43.19	23.66	Fe2O3
Jarosite-K	-2.55	29.25	31.80	KFe3(SO4)2(OH)6
Mackinawite	-95.41	-135.65	-40.24	FeS
Melanterite	-10.87	-13.25	-2.38	FeSO4:7H2O
N2(g)	-1.86	-5.08	-3.22	N2
NH3(g)	-43.58	-48.44	-4.86	NH3
O2(g)	-26.34	61.20	87.54	O2
Pyrite	-156.96	-246.99	-90.03	FeS2
Quartz	0.09	-4.08	-4.17	SiO2
Sepiolite	-4.79	11.32	16.11	Mg2Si3O7.5OH:3H2O
Sepiolite(d)	-7.34	11.32	18.66	Mg2Si3O7.5OH:3H2O
Siderite	-3.85	-14.66	-10.81	FeCO3
SiO2(a)	-1.26	-4.08	-2.82	SiO2
Sulfur	-73.81	-111.34	-37.53	S
Talc	-3.88	19.02	22.90	Mg3Si4O10(OH)2

F1B

Saturation indices

Phase	SI	log IAP	log KT	
Anhydrite	-4.02	-8.36	-4.33	CaSO4
Aragonite	-0.99	-9.27	-8.28	CaCO3
Calcite	-0.84	-9.27	-8.43	CaCO3
CH4(g)	-94.67	-140.16	-45.49	CH4
Chalcedony	-0.52	-4.20	-3.68	SiO2
Chrysotile	-6.89	26.67	33.56	Mg3Si2O5(OH)4
CO2(g)	-2.45	-20.64	-18.19	CO2
Dolomite	-1.38	-18.22	-16.84	CaMg(CO3)2
Gypsum	-3.77	-8.36	-4.59	CaSO4:2H2O
H2(g)	-29.88	-29.88	0.00	H2
H2O(g)	-1.79	-0.00	1.79	H2O
H2S(g)	-96.00	-139.25	-43.24	H2S
Halite	-6.80	-5.25	1.56	NaCl
N2(g)	-1.94	-5.16	-3.22	N2
NH3(g)	-42.60	-47.40	-4.80	NH3
O2(g)	-27.05	59.76	86.81	O2
Quartz	-0.06	-4.20	-4.14	SiO2
Sepiolite	-5.27	10.78	16.05	Mg2Si3O7.5OH:3H2O
Sepiolite(d)	-7.88	10.78	18.66	Mg2Si3O7.5OH:3H2O
SiO2(a)	-1.40	-4.20	-2.80	SiO2
Sulfur	-72.14	-109.37	-37.23	S
Talc	-4.38	18.27	22.65	Mg3Si4O10(OH)2

F3A

Saturation indices

Phase	SI	log IAP	log KT	
Anhydrite	-3.70	-8.03	-4.33	CaSO4
Aragonite	-0.96	-9.22	-8.26	CaCO3
Calcite	-0.80	-9.22	-8.42	CaCO3
CH4(g)	-98.50	-144.40	-45.90	CH4
Chalcedony	-0.55	-4.26	-3.71	SiO2
Chrysotile	-6.15	27.77	33.92	Mg3Si2O5(OH)4
CO2(g)	-2.83	-21.04	-18.21	CO2
Dolomite	-1.39	-18.16	-16.77	CaMg(CO3)2
Fe(OH)3(a)	2.65	20.89	18.24	Fe(OH)3
FeS(ppt)	-98.12	-137.74	-39.62	FeS
Goethite	8.04	20.89	12.85	FeOOH
Gypsum	-3.44	-8.03	-4.59	CaSO4:2H2O
H2(g)	-30.84	-30.84	0.00	H2
H2O(g)	-1.87	-0.00	1.87	H2O
H2S(g)	-99.53	-143.21	-43.69	H2S
Halite	-6.73	-5.18	1.55	NaCl
Hematite	18.03	41.78	23.75	Fe2O3
Jarosite-K	-5.11	26.80	31.91	KFe3(SO4)2(OH)6
Mackinawite	-97.39	-137.74	-40.36	FeS
Melanterite	-12.00	-14.38	-2.39	FeSO4:7H2O
N2(g)	-2.14	-5.35	-3.21	N2
NH3(g)	-44.06	-48.94	-4.88	NH3
O2(g)	-26.12	61.68	87.80	O2
Pyrite	-159.83	-250.12	-90.28	FeS2
Quartz	-0.08	-4.26	-4.19	SiO2
Sepiolite	-4.71	11.41	16.13	Mg2Si3O7.5OH:3H2O
Sepiolite(d)	-7.25	11.41	18.66	Mg2Si3O7.5OH:3H2O
Siderite	-4.77	-15.57	-10.81	FeCO3
SiO2(a)	-1.44	-4.26	-2.83	SiO2

```
          Sulfur          -74.73 -112.37  -37.64  S
          Talc             -3.73   19.25   22.99  Mg3Si4O10(OH)2
-------------------------------------------------------------------------
F3B
------------------------------Saturation indices-----------------------
          Phase               SI log IAP  log KT
          Anhydrite        -4.57   -8.91   -4.33  CaSO4
          Aragonite        -0.87   -9.14   -8.27  CaCO3
          Calcite          -0.72   -9.14   -8.42  CaCO3
          CH4(g)          -95.49 -141.12  -45.63  CH4
          Chalcedony       -0.54   -4.24   -3.69  SiO2
          Chrysotile       -6.53   27.15   33.68  Mg3Si2O5(OH)4
          CO2(g)           -2.44  -20.64  -18.20  CO2
          Dolomite         -1.09  -17.90  -16.81  CaMg(CO3)2
          Fe(OH)3(a)        2.49   20.69   18.20  Fe(OH)3
          FeS(ppt)        -95.92 -135.26  -39.33  FeS
          Goethite          7.96   20.69   12.73  FeOOH
          Gypsum           -4.32   -8.91   -4.59  CaSO4:2H2O
          H2(g)           -30.12  -30.12    0.00  H2
          H2O(g)           -1.82   -0.00    1.82  H2O
          H2S(g)          -97.50 -140.88  -43.39  H2S
          Halite           -6.41   -4.86    1.56  NaCl
          Hematite         17.87   41.38   23.51  Fe2O3
          Jarosite-K       -6.75   24.88   31.62  KFe3(SO4)2(OH)6
          Mackinawite      -95.19 -135.26  -40.07  FeS
          Melanterite      -12.42  -14.78   -2.36  FeSO4:7H2O
          N2(g)            -1.94   -5.16   -3.22  N2
          NH3(g)           -42.93  -47.76   -4.83  NH3
          O2(g)            -26.90   60.24   87.14  O2
          Pyrite          -156.37 -246.02  -89.65  FeS2
          Quartz           -0.08   -4.24   -4.16  SiO2
          Sepiolite        -5.03   11.04   16.07  Mg2Si3O7.5OH:3H2O
          Sepiolite(d)     -7.62   11.04   18.66  Mg2Si3O7.5OH:3H2O
          Siderite         -4.19  -15.01  -10.82  FeCO3
          SiO2(a)          -1.42   -4.24   -2.81  SiO2
          Sulfur          -73.40 -110.76  -37.37  S
          Talc             -4.08   18.68   22.76  Mg3Si4O10(OH)2
-------------------------------------------------------------------------
F6
------------------------------Saturation indices-----------------------
          Phase               SI log IAP  log KT
          Anhydrite        -2.69   -7.03   -4.34  CaSO4
          Aragonite        -1.92  -10.21   -8.29  CaCO3
          Calcite          -1.77  -10.21   -8.44  CaCO3
          CH4(g)           -89.91 -135.00  -45.08  CH4
          Chalcedony       -0.15   -3.80   -3.65  SiO2
          Chrysotile       -6.65   26.55   33.21  Mg3Si2O5(OH)4
          CO2(g)           -3.22  -21.40  -18.18  CO2
          Dolomite         -3.32  -20.22  -16.90  CaMg(CO3)2
          Fe(OH)3(a)        3.91   22.01   18.10  Fe(OH)3
          FeS(ppt)         -85.24 -124.01  -38.76  FeS
          Goethite          9.51   22.01   12.50  FeOOH
          Gypsum           -2.44   -7.03   -4.58  CaSO4:2H2O
          H2(g)            -28.40  -28.40    0.00  H2
          H2O(g)           -1.72   -0.00    1.72  H2O
          H2S(g)           -89.01 -131.82  -42.81  H2S
          Halite           -5.18   -3.62    1.56  NaCl
          Hematite         20.99   44.02   23.03  Fe2O3
          Jarosite-K        1.65   32.70   31.05  KFe3(SO4)2(OH)6
          Mackinawite      -84.51 -124.01  -39.50  FeS
          Melanterite      -8.10  -10.41   -2.31  FeSO4:7H2O
          N2(g)            -1.74   -4.97   -3.23  N2
          NH3(g)           -40.36  -45.09   -4.73  NH3
          O2(g)            -29.05   56.80   85.85  O2
          Pyrite          -139.02 -227.42  -88.40  FeS2
          Quartz            0.30   -3.80   -4.10  SiO2
          Sepiolite        -4.60   11.37   15.97  Mg2Si3O7.5OH:3H2O
          Sepiolite(d)     -7.29   11.37   18.66  Mg2Si3O7.5OH:3H2O
          Siderite         -2.75  -13.59  -10.84  FeCO3
          SiO2(a)          -1.02   -3.80   -2.78  SiO2
          Sulfur          -66.59 -103.42  -36.83  S
          Talc             -3.36   18.96   22.32  Mg3Si4O10(OH)2
-------------------------------------------------------------------------
Wo1C
------------------------------Saturation indices-----------------------
          Phase               SI log IAP  log KT
          Anhydrite        -3.44   -7.78   -4.34  CaSO4
          Aragonite        -2.48  -10.74   -8.26  CaCO3
          Calcite          -2.33  -10.74   -8.41  CaCO3
          CH4(g)           -80.04 -126.16  -46.12  CH4
          Chalcedony       -0.32   -4.05   -3.73  SiO2
          Chrysotile      -13.08   21.04   34.11  Mg3Si2O5(OH)4
          CO2(g)           -2.02  -20.24  -18.22  CO2
          Dolomite         -4.53  -21.27  -16.73  CaMg(CO3)2
```

Fe(OH)3(a)	2.72	21.00	18.28	Fe(OH)3
FeS(ppt)	-75.59	-115.44	-39.85	FeS
Goethite	8.06	21.00	12.94	FeOOH
Gypsum	-3.19	-7.78	-4.59	CaSO4:2H2O
H2(g)	-26.48	-26.48	0.00	H2
H2O(g)	-1.91	-0.00	1.91	H2O
H2S(g)	-79.28	-123.20	-43.92	H2S
Halite	-7.47	-5.92	1.55	NaCl
Hematite	18.06	42.00	23.94	Fe2O3
Jarosite-K	-1.22	30.92	32.14	KFe3(SO4)2(OH)6
Mackinawite	-74.86	-115.44	-40.58	FeS
Melanterite	-7.11	-9.52	-2.41	FeSO4:7H2O
N2(g)	-1.66	-4.87	-3.21	N2
NH3(g)	-37.24	-42.15	-4.91	NH3
O2(g)	-35.35	52.96	88.31	O2
Pyrite	-121.38	-212.16	-90.78	FeS2
Quartz	0.15	-4.05	-4.21	SiO2
Sepiolite	-8.90	7.27	16.17	Mg2Si3O7.5OH:3H2O
Sepiolite(d)	-11.39	7.27	18.66	Mg2Si3O7.5OH:3H2O
Siderite	-1.69	-12.48	-10.80	FeCO3
SiO2(a)	-1.22	-4.05	-2.84	SiO2
Sulfur	-58.87	-96.72	-37.85	S
Talc	-10.23	12.93	23.16	Mg3Si4O10(OH)2

Wo4

Saturation indices

Phase	SI	log IAP	log KT	
Anhydrite	-3.43	-7.76	-4.33	CaSO4
Aragonite	-2.12	-10.40	-8.28	CaCO3
Calcite	-1.97	-10.40	-8.43	CaCO3
CH4(g)	-84.29	-129.79	-45.50	CH4
Chalcedony	-0.45	-4.14	-3.68	SiO2
Chrysotile	-11.58	21.99	33.57	Mg3Si2O5(OH)4
CO2(g)	-2.16	-20.35	-18.19	CO2
Dolomite	-3.83	-20.67	-16.83	CaMg(CO3)2
Fe(OH)3(a)	4.53	22.71	18.18	Fe(OH)3
FeS(ppt)	-78.92	-118.13	-39.21	FeS
Goethite	10.03	22.71	12.68	FeOOH
Gypsum	-3.18	-7.76	-4.59	CaSO4:2H2O
H2(g)	-27.36	-27.36	0.00	H2
H2O(g)	-1.80	-0.00	1.80	H2O
H2S(g)	-83.90	-127.16	-43.26	H2S
Halite	-7.07	-5.51	1.56	NaCl
Hematite	22.01	45.41	23.40	Fe2O3
Jarosite-K	3.81	35.30	31.50	KFe3(SO4)2(OH)6
Mackinawite	-78.19	-118.13	-39.94	FeS
Melanterite	-6.34	-8.69	-2.35	FeSO4:7H2O
N2(g)	-2.33	-5.56	-3.22	N2
NH3(g)	-39.01	-43.82	-4.80	NH3
O2(g)	-32.13	54.72	86.85	O2
Pyrite	-128.56	-217.93	-89.37	FeS2
Quartz	0.01	-4.14	-4.14	SiO2
Sepiolite	-8.28	7.77	16.05	Mg2Si3O7.5OH:3H2O
Sepiolite(d)	-10.89	7.77	18.66	Mg2Si3O7.5OH:3H2O
Siderite	-0.51	-11.33	-10.82	FeCO3
SiO2(a)	-1.33	-4.14	-2.80	SiO2
Sulfur	-62.55	-99.80	-37.25	S
Talc	-8.94	13.72	22.66	Mg3Si4O10(OH)2

79055

Saturation indices

Phase	SI	log IAP	log KT	
Anhydrite	-2.54	-6.88	-4.34	CaSO4
Aragonite	-0.58	-8.87	-8.30	CaCO3
Calcite	-0.43	-8.87	-8.44	CaCO3
CH4(g)	-81.74	-126.67	-44.93	CH4
Chalcedony	-0.34	-3.97	-3.63	SiO2
Chrysotile	-9.37	23.71	33.08	Mg3Si2O5(OH)4
CO2(g)	-0.98	-19.15	-18.17	CO2
Dolomite	-0.55	-17.48	-16.93	CaMg(CO3)2
Gypsum	-2.30	-6.88	-4.58	CaSO4:2H2O
H2(g)	-26.88	-26.88	0.00	H2
H2O(g)	-1.69	-0.00	1.69	H2O
H2S(g)	-82.03	-124.68	-42.65	H2S
Halite	-5.52	-3.95	1.57	NaCl
N2(g)	-1.65	-4.88	-3.24	N2
NH3(g)	-38.06	-42.76	-4.70	NH3
O2(g)	-31.73	53.76	85.49	O2
Quartz	0.12	-3.97	-4.08	SiO2
Sepiolite	-6.76	9.19	15.95	Mg2Si3O7.5OH:3H2O
Sepiolite(d)	-9.47	9.19	18.66	Mg2Si3O7.5OH:3H2O
SiO2(a)	-1.20	-3.97	-2.77	SiO2
Sulfur	-61.11	-97.80	-36.68	S
Talc	-6.44	15.77	22.20	Mg3Si4O10(OH)2

```
-------------------------------------------------------------------------
79056
------------------------------Saturation indices-----------------------
         Phase               SI log IAP  log KT
         Anhydrite        -3.28   -7.62   -4.34  CaSO4
         Aragonite        -2.79  -11.08   -8.29  CaCO3
         Calcite          -2.64  -11.08   -8.44  CaCO3
         CH4(g)          -72.94 -117.89  -44.95  CH4
         Chalcedony       -0.31   -3.95   -3.63  SiO2
         Chrysotile      -14.31   18.78   33.09  Mg3Si2O5(OH)4
         CO2(g)           -1.64  -19.81  -18.17  CO2
         Dolomite         -5.08  -22.00  -16.92  CaMg(CO3)2
         Fe(OH)3(a)        2.76   20.84   18.08  Fe(OH)3
         FeS(ppt)        -67.22 -105.84  -38.62  FeS
         Goethite          8.40   20.84   12.45  FeOOH
         Gypsum           -3.03   -7.62   -4.58  CaSO4:2H2O
         H2(g)           -24.52  -24.52    0.00  H2
         H2O(g)           -1.70   -0.00    1.70  H2O
         H2S(g)          -71.76 -114.42  -42.67  H2S
         Halite           -6.31   -4.75    1.57  NaCl
         Hematite         18.77   41.68   22.92  Fe2O3
         Jarosite-K        1.06   31.97   30.91  KFe3(SO4)2(OH)6
         Mackinawite     -66.48 -105.84  -39.36  FeS
         Melanterite      -5.46   -7.76   -2.30  FeSO4:7H2O
         N2(g)            -1.20   -4.44   -3.24  N2
         NH3(g)          -34.29  -39.00   -4.70  NH3
         O2(g)           -36.49   49.04   85.53  O2
         Pyrite         -107.64 -195.74  -88.10  FeS2
         Quartz            0.14   -3.95   -4.09  SiO2
         Sepiolite       -10.00    5.95   15.95  Mg2Si3O7.5OH:3H2O
         Sepiolite(d)    -12.71    5.95   18.66  Mg2Si3O7.5OH:3H2O
         Siderite         -0.38  -11.23  -10.85  FeCO3
         SiO2(a)          -1.17   -3.95   -2.77  SiO2
         Sulfur          -53.20  -89.90  -36.70  S
         Talc            -11.32   10.89   22.22  Mg3Si4O10(OH)2
-------------------------------------------------------------------------
79057
------------------------------Saturation indices-----------------------
         Phase               SI log IAP  log KT
         Anhydrite        -3.18   -7.51   -4.34  CaSO4
         Aragonite        -0.65   -8.91   -8.25  CaCO3
         Calcite          -0.50   -8.91   -8.41  CaCO3
         CH4(g)          -88.46 -134.74  -46.28  CH4
         Chalcedony       -0.12   -3.87   -3.74  SiO2
         Chrysotile       -8.74   25.51   34.25  Mg3Si2O5(OH)4
         CO2(g)           -1.48  -19.71  -18.23  CO2
         Dolomite         -0.82  -17.53  -16.71  CaMg(CO3)2
         Gypsum           -2.92   -7.51   -4.59  CaSO4:2H2O
         H2(g)           -28.76  -28.76    0.00  H2
         H2O(g)           -1.94   -0.00    1.94  H2O
         H2S(g)          -89.26 -133.35  -44.09  H2S
         Halite           -6.26   -4.72    1.54  NaCl
         N2(g)            -1.44   -4.64   -3.20  N2
         NH3(g)          -40.52  -45.46   -4.94  NH3
         O2(g)           -31.17   57.52   88.69  O2
         Quartz            0.36   -3.87   -4.22  SiO2
         Sepiolite        -5.64   10.56   16.20  Mg2Si3O7.5OH:3H2O
         Sepiolite(d)     -8.10   10.56   18.66  Mg2Si3O7.5OH:3H2O
         SiO2(a)          -1.02   -3.87   -2.85  SiO2
         Sulfur          -66.58 -104.59  -38.01  S
         Talc             -5.52   17.77   23.29  Mg3Si4O10(OH)2
-------------------------------------------------------------------------
79058
------------------------------Saturation indices-----------------------
         Phase               SI log IAP  log KT
         Anhydrite        -2.57   -6.91   -4.34  CaSO4
         Aragonite        -1.31   -9.61   -8.30  CaCO3
         Calcite          -1.16   -9.61   -8.45  CaCO3
         CH4(g)          -88.06 -132.86  -44.80  CH4
         Chalcedony        0.21   -3.42   -3.62  SiO2
         Chrysotile       -6.69   26.27   32.96  Mg3Si2O5(OH)4
         CO2(g)           -2.54  -20.70  -18.17  CO2
         Dolomite         -2.34  -19.28  -16.95  CaMg(CO3)2
         Gypsum           -2.33   -6.91   -4.58  CaSO4:2H2O
         H2(g)           -28.04  -28.04    0.00  H2
         H2O(g)           -1.67   -0.00    1.67  H2O
         H2S(g)          -87.65 -130.16  -42.51  H2S
         Halite           -6.30   -4.73    1.57  NaCl
         N2(g)            -2.62   -5.86   -3.24  N2
         NH3(g)          -40.31  -44.99   -4.68  NH3
         O2(g)           -29.10   56.08   85.18  O2
         Quartz            0.65   -3.42   -4.07  SiO2
         Sepiolite        -4.10   11.82   15.92  Mg2Si3O7.5OH:3H2O
         Sepiolite(d)     -6.84   11.82   18.66  Mg2Si3O7.5OH:3H2O
```

SiO2(a)	-0.65	-3.42	-2.76	SiO2
Sulfur	-65.57	-102.12	-36.55	S
Talc	-2.66	19.44	22.10	Mg3Si4O10(OH)2

79059

Saturation indices

Phase	SI	log IAP	log KT	
Anhydrite	-3.87	-8.21	-4.34	CaSO4
Aragonite	-0.23	-8.54	-8.31	CaCO3
Calcite	-0.08	-8.54	-8.45	CaCO3
CH4(g)	-94.34	-138.97	-44.62	CH4
Chalcedony	-0.38	-3.99	-3.61	SiO2
Chrysotile	-6.26	26.54	32.81	Mg3Si2O5(OH)4
CO2(g)	-1.76	-19.93	-18.16	CO2
Dolomite	0.02	-16.96	-16.98	CaMg(CO3)2
Gypsum	-3.64	-8.22	-4.58	CaSO4:2H2O
H2(g)	-29.76	-29.76	0.00	H2
H2O(g)	-1.64	-0.00	1.64	H2O
H2S(g)	-96.32	-138.64	-42.32	H2S
Halite	-4.31	-2.74	1.57	NaCl
N2(g)	-1.37	-4.61	-3.24	N2
NH3(g)	-42.30	-46.95	-4.65	NH3
O2(g)	-25.24	59.52	84.76	O2
Quartz	0.06	-3.99	-4.05	SiO2
Sepiolite	-4.85	11.04	15.89	Mg2Si3O7.5OH:3H2O
Sepiolite(d)	-7.62	11.04	18.66	Mg2Si3O7.5OH:3H2O
SiO2(a)	-1.24	-3.99	-2.75	SiO2
Sulfur	-72.50	-108.88	-36.38	S
Talc	-3.40	18.56	21.95	Mg3Si4O10(OH)2

79060

Saturation indices

Phase	SI	log IAP	log KT	
Anhydrite	-3.28	-7.62	-4.34	CaSO4
Aragonite	-1.54	-9.85	-8.30	CaCO3
Calcite	-1.39	-9.85	-8.45	CaCO3
CH4(g)	-92.78	-137.52	-44.74	CH4
Chalcedony	-0.34	-3.96	-3.62	SiO2
Chrysotile	-7.20	25.71	32.91	Mg3Si2O5(OH)4
CO2(g)	-2.80	-20.96	-18.17	CO2
Dolomite	-2.64	-19.60	-16.96	CaMg(CO3)2
Fe(OH)3(a)	2.37	20.41	18.05	Fe(OH)3
FeS(ppt)	-91.05	-129.45	-38.41	FeS
Goethite	8.06	20.41	12.36	FeOOH
Gypsum	-3.04	-7.62	-4.58	CaSO4:2H2O
H2(g)	-29.14	-29.14	0.00	H2
H2O(g)	-1.66	-0.00	1.66	H2O
H2S(g)	-92.85	-135.30	-42.45	H2S
Halite	-5.51	-3.94	1.57	NaCl
Hematite	18.09	40.83	22.74	Fe2O3
Jarosite-K	-3.54	27.16	30.70	KFe3(SO4)2(OH)6
Mackinawite	-90.31	-129.45	-39.14	FeS
Melanterite	-10.62	-12.90	-2.28	FeSO4:7H2O
N2(g)	-2.71	-5.95	-3.24	N2
NH3(g)	-42.02	-46.69	-4.67	NH3
O2(g)	-26.76	58.28	85.04	O2
Pyrite	-147.99	-235.61	-87.63	FeS2
Quartz	0.11	-3.96	-4.06	SiO2
Sepiolite	-5.37	10.54	15.91	Mg2Si3O7.5OH:3H2O
Sepiolite(d)	-8.12	10.54	18.66	Mg2Si3O7.5OH:3H2O
Siderite	-4.26	-15.12	-10.86	FeCO3
SiO2(a)	-1.20	-3.96	-2.76	SiO2
Sulfur	-69.66	-106.16	-36.50	S
Talc	-4.26	17.79	22.05	Mg3Si4O10(OH)2

March 2001

W3A

Saturation indices

Phase	SI	log IAP	log KT	
Anhydrite	-3.64	-8.00	-4.35	CaSO4
Aragonite	-2.08	-10.41	-8.33	CaCO3
Calcite	-1.94	-10.41	-8.47	CaCO3
Celestite	-3.10	-9.73	-6.63	SrSO4
CH4(g)	-32.24	-76.38	-44.14	CH4
Chalcedony	-0.46	-4.03	-3.57	SiO2
Chrysotile	-10.25	22.14	32.39	Mg3Si2O5(OH)4
CO2(g)	-2.23	-20.38	-18.15	CO2
Dolomite	-3.67	-20.73	-17.06	CaMg(CO3)2
Fe(OH)3(a)	-0.80	17.15	17.95	Fe(OH)3
FeS(ppt)	-26.03	-63.82	-37.79	FeS
Goethite	5.04	17.15	12.11	FeOOH

Gypsum	-3.42	-8.00	-4.58	CaSO4:2H2O
H2(g)	-14.00	-14.00	0.00	H2
H2O(g)	-1.55	-0.00	1.55	H2O
H2S(g)	-32.15	-73.97	-41.81	H2S
Halite	-7.29	-5.71	1.58	NaCl
Hematite	12.08	34.30	22.22	Fe2O3
Jarosite-K	-11.61	18.47	30.07	KFe3(SO4)2(OH)6
Mackinawite	-25.30	-63.82	-38.52	FeS
Melanterite	-5.59	-7.82	-2.23	FeSO4:7H2O
N2(g)	-1.89	-5.14	-3.25	N2
NH3(g)	-19.01	-23.57	-4.56	NH3
O2(g)	-55.63	28.00	83.63	O2
Pyrite	-37.52	-123.79	-86.27	FeS2
Quartz	-0.03	-4.03	-4.00	SiO2
Sepiolite	-7.76	8.04	15.80	Mg2Si3O7.5OH:3H2O
Sepiolite(d)	-10.62	8.04	18.66	Mg2Si3O7.5OH:3H2O
Siderite	0.65	-10.23	-10.88	FeCO3
SiO2(a)	-1.31	-4.03	-2.72	SiO2
Strontianite	-2.87	-12.14	-9.27	SrCO3
Sulfur	-24.05	-59.97	-35.92	S
Talc	-7.50	14.08	21.57	Mg3Si4O10(OH)2

W3B

Saturation indices

Phase	SI	log IAP	log KT	
Anhydrite	-4.14	-8.49	-4.35	CaSO4
Aragonite	-1.72	-10.04	-8.32	CaCO3
Calcite	-1.57	-10.04	-8.47	CaCO3
Celestite	-3.73	-10.35	-6.63	SrSO4
CH4(g)	-32.08	-76.32	-44.25	CH4
Chalcedony	-0.49	-4.07	-3.58	SiO2
Chrysotile	-9.20	23.27	32.48	Mg3Si2O5(OH)4
CO2(g)	-2.17	-20.32	-18.15	CO2
Dolomite	-2.85	-19.89	-17.04	CaMg(CO3)2
Fe(OH)3(a)	-0.93	17.03	17.96	Fe(OH)3
FeS(ppt)	-26.85	-64.74	-37.89	FeS
Goethite	4.88	17.03	12.15	FeOOH
Gypsum	-3.91	-8.49	-4.58	CaSO4:2H2O
H2(g)	-14.00	-14.00	0.00	H2
H2O(g)	-1.57	-0.00	1.57	H2O
H2S(g)	-32.85	-74.77	-41.92	H2S
Halite	-7.35	-5.77	1.58	NaCl
Hematite	11.76	34.06	22.31	Fe2O3
Jarosite-K	-13.71	16.47	30.18	KFe3(SO4)2(OH)6
Mackinawite	-26.12	-64.74	-38.63	FeS
Melanterite	-6.51	-8.74	-2.24	FeSO4:7H2O
N2(g)	-1.29	-4.54	-3.25	N2
NH3(g)	-18.69	-23.27	-4.58	NH3
O2(g)	-55.86	28.00	83.86	O2
Pyrite	-39.02	-125.51	-86.50	FeS2
Quartz	-0.06	-4.07	-4.01	SiO2
Sepiolite	-7.09	8.73	15.82	Mg2Si3O7.5OH:3H2O
Sepiolite(d)	-9.93	8.73	18.66	Mg2Si3O7.5OH:3H2O
Siderite	0.59	-10.29	-10.88	FeCO3
SiO2(a)	-1.34	-4.07	-2.73	SiO2
Strontianite	-2.63	-11.90	-9.27	SrCO3
Sulfur	-24.76	-60.77	-36.01	S
Talc	-6.52	15.13	21.65	Mg3Si4O10(OH)2

W4

Saturation indices

Phase	SI	log IAP	log KT	
Anhydrite	-3.52	-7.88	-4.36	CaSO4
Aragonite	-2.33	-10.67	-8.34	CaCO3
Calcite	-2.19	-10.67	-8.48	CaCO3
Celestite	-3.26	-9.89	-6.63	SrSO4
CH4(g)	-32.73	-76.64	-43.92	CH4
Chalcedony	-0.53	-4.08	-3.55	SiO2
Chrysotile	-10.60	21.59	32.19	Mg3Si2O5(OH)4
CO2(g)	-2.50	-20.64	-18.15	CO2
Dolomite	-4.30	-21.40	-17.09	CaMg(CO3)2
Fe(OH)3(a)	-0.97	16.94	17.91	Fe(OH)3
FeS(ppt)	-26.36	-63.91	-37.55	FeS
Goethite	4.93	16.94	12.01	FeOOH
Gypsum	-3.30	-7.88	-4.58	CaSO4:2H2O
H2(g)	-14.00	-14.00	-0.00	H2
H2O(g)	-1.51	-0.00	1.51	H2O
H2S(g)	-32.28	-73.85	-41.57	H2S
Halite	-8.19	-6.61	1.58	NaCl
Hematite	11.87	33.88	22.02	Fe2O3
Jarosite-K	-11.77	18.06	29.84	KFe3(SO4)2(OH)6
Mackinawite	-25.63	-63.91	-38.28	FeS
Melanterite	-5.70	-7.91	-2.21	FeSO4:7H2O
N2(g)	-1.55	-4.81	-3.26	N2

NH3(g)	-18.89	-23.41	-4.52	NH3
O2(g)	-55.09	28.00	83.09	O2
Pyrite	-38.02	-123.77	-85.75	FeS2
Quartz	-0.10	-4.08	-3.98	SiO2
Sepiolite	-8.16	7.59	15.76	Mg2Si3O7.5OH:3H2O
Sepiolite(d)	-11.07	7.59	18.66	Mg2Si3O7.5OH:3H2O
Siderite	0.19	-10.70	-10.89	FeCO3
SiO2(a)	-1.37	-4.08	-2.71	SiO2
Strontianite	-3.41	-12.68	-9.27	SrCO3
Sulfur	-24.16	-59.85	-35.70	S
Talc	-7.96	13.43	21.39	Mg3Si4O10(OH)2

W5

Saturation indices

Phase	SI	log IAP	log KT	
Anhydrite	-4.08	-8.43	-4.35	CaSO4
Aragonite	-2.73	-11.05	-8.32	CaCO3
Calcite	-2.58	-11.05	-8.47	CaCO3
Celestite	-3.20	-9.83	-6.63	SrSO4
CH4(g)	-32.42	-76.72	-44.30	CH4
Chalcedony	-0.53	-4.11	-3.58	SiO2
Chrysotile	-10.92	21.61	32.53	Mg3Si2O5(OH)4
CO2(g)	-2.56	-20.72	-18.16	CO2
Dolomite	-4.80	-21.83	-17.03	CaMg(CO3)2
Fe(OH)3(a)	-2.82	15.15	17.97	Fe(OH)3
FeS(ppt)	-28.00	-65.95	-37.95	FeS
Goethite	2.97	15.15	12.18	FeOOH
Gypsum	-3.85	-8.43	-4.58	CaSO4:2H2O
H2(g)	-14.00	-14.00	0.00	H2
H2O(g)	-1.58	-0.00	1.58	H2O
H2S(g)	-32.12	-74.10	-41.98	H2S
Halite	-7.57	-5.99	1.58	NaCl
Hematite	7.94	30.30	22.36	Fe2O3
Jarosite-K	-18.20	12.03	30.24	KFe3(SO4)2(OH)6
Mackinawite	-27.26	-65.95	-38.69	FeS
Melanterite	-7.71	-9.95	-2.24	FeSO4:7H2O
N2(g)	-1.95	-5.20	-3.25	N2
NH3(g)	-19.01	-23.60	-4.59	NH3
O2(g)	-56.00	28.00	84.00	O2
Pyrite	-39.42	-126.05	-86.63	FeS2
Quartz	-0.09	-4.11	-4.02	SiO2
Sepiolite	-8.27	7.56	15.83	Mg2Si3O7.5OH:3H2O
Sepiolite(d)	-11.10	7.56	18.66	Mg2Si3O7.5OH:3H2O
Siderite	-1.70	-12.57	-10.87	FeCO3
SiO2(a)	-1.37	-4.11	-2.73	SiO2
Strontianite	-3.18	-12.45	-9.27	SrCO3
Sulfur	-24.03	-60.10	-36.07	S
Talc	-8.30	13.39	21.70	Mg3Si4O10(OH)2

F1B

Saturation indices

Anhydrite	-4.02	-8.38	-4.36	CaSO4
Aragonite	-1.55	-9.88	-8.34	CaCO3
Calcite	-1.41	-9.88	-8.48	CaCO3
CH4(g)	-32.29	-76.22	-43.93	CH4
Chalcedony	-0.65	-4.20	-3.55	SiO2
Chrysotile	-8.64	23.56	32.20	Mg3Si2O5(OH)4
CO2(g)	-2.07	-20.22	-18.15	CO2
Dolomite	-2.36	-19.45	-17.09	CaMg(CO3)2
Fe(OH)3(a)	-1.39	16.52	17.91	Fe(OH)3
FeS(ppt)	-27.64	-65.20	-37.56	FeS
Goethite	4.50	16.52	12.02	FeOOH
Gypsum	-3.80	-8.38	-4.58	CaSO4:2H2O
H2(g)	-14.00	-14.00	0.00	H2
H2O(g)	-1.51	-0.00	1.51	H2O
H2S(g)	-33.13	-74.72	-41.59	H2S
Halite	-6.78	-5.20	1.58	NaCl
Hematite	11.01	33.04	22.03	Fe2O3
Jarosite-K	-14.63	15.22	29.85	KFe3(SO4)2(OH)6
Mackinawite	-26.90	-65.20	-38.30	FeS
Melanterite	-6.99	-9.20	-2.21	FeSO4:7H2O
N2(g)	-1.98	-5.24	-3.26	N2
NH3(g)	-19.10	-23.62	-4.52	NH3
O2(g)	-55.12	28.00	83.12	O2
Pyrite	-40.14	-125.92	-85.78	FeS2
Quartz	-0.22	-4.20	-3.98	SiO2
Sepiolite	-7.05	8.71	15.76	Mg2Si3O7.5OH:3H2O
Sepiolite(d)	-9.95	8.71	18.66	Mg2Si3O7.5OH:3H2O
Siderite	0.19	-10.70	-10.89	FeCO3
SiO2(a)	-1.49	-4.20	-2.71	SiO2
Sulfur	-25.01	-60.72	-35.71	S
Talc	-6.24	15.16	21.40	Mg3Si4O10(OH)2

F3A

-----------------------------Saturation indices----------------------

Phase	SI	log IAP	log KT	
Anhydrite	-3.59	-7.95	-4.36	CaSO4
Aragonite	-1.75	-10.09	-8.34	CaCO3
Calcite	-1.61	-10.09	-8.48	CaCO3
CH4(g)	-32.43	-76.36	-43.93	CH4
Chalcedony	-0.66	-4.21	-3.55	SiO2
Chrysotile	-9.03	23.18	32.20	Mg3Si2O5(OH)4
CO2(g)	-2.21	-20.36	-18.15	CO2
Dolomite	-2.83	-19.92	-17.09	CaMg(CO3)2
Fe(OH)3(a)	-1.86	16.05	17.91	Fe(OH)3
FeS(ppt)	-27.61	-65.17	-37.56	FeS
Goethite	4.03	16.05	12.02	FeOOH
Gypsum	-3.37	-7.95	-4.58	CaSO4:2H2O
H2(g)	-14.00	-14.00	0.00	H2
H2O(g)	-1.51	-0.00	1.51	H2O
H2S(g)	-32.64	-74.23	-41.59	H2S
Halite	-7.11	-5.52	1.58	NaCl
Hematite	10.07	32.11	22.03	Fe2O3
Jarosite-K	-15.11	14.74	29.85	KFe3(SO4)2(OH)6
Mackinawite	-26.88	-65.17	-38.30	FeS
Melanterite	-6.96	-9.17	-2.21	FeSO4:7H2O
N2(g)	-1.87	-5.13	-3.26	N2
NH3(g)	-19.04	-23.56	-4.52	NH3
O2(g)	-55.12	28.00	83.12	O2
Pyrite	-39.62	-125.40	-85.78	FeS2
Quartz	-0.23	-4.21	-3.98	SiO2
Sepiolite	-7.33	8.43	15.76	Mg2Si3O7.5OH:3H2O
Sepiolite(d)	-10.23	8.43	18.66	Mg2Si3O7.5OH:3H2O
Siderite	-0.42	-11.31	-10.89	FeCO3
SiO2(a)	-1.50	-4.21	-2.71	SiO2
Sulfur	-24.52	-60.23	-35.71	S
Talc	-6.64	14.75	21.40	Mg3Si4O10(OH)2

F3B

-----------------------------Saturation indices----------------------

Phase	SI	log IAP	log KT	
Aragonite	-1.16	-9.50	-8.34	CaCO3
Calcite	-1.02	-9.50	-8.48	CaCO3
CH4(g)	-32.05	-75.98	-43.93	CH4
Chalcedony	-0.62	-4.18	-3.55	SiO2
Chrysotile	-8.01	24.19	32.20	Mg3Si2O5(OH)4
CO2(g)	-1.83	-19.98	-18.15	CO2
Dolomite	-1.54	-18.63	-17.09	CaMg(CO3)2
Fe(OH)3(a)	-0.81	17.10	17.91	Fe(OH)3
Goethite	5.08	17.10	12.02	FeOOH
H2(g)	-14.00	-14.00	0.00	H2
H2O(g)	-1.51	-0.00	1.51	H2O
Halite	-6.55	-4.97	1.58	NaCl
Hematite	12.17	34.20	22.03	Fe2O3
N2(g)	-1.76	-5.02	-3.26	N2
NH3(g)	-18.99	-23.51	-4.52	NH3
O2(g)	-55.12	28.00	83.12	O2
Quartz	-0.20	-4.18	-3.98	SiO2
Sepiolite	-6.60	9.16	15.76	Mg2Si3O7.5OH:3H2O
Sepiolite(d)	-9.50	9.16	18.66	Mg2Si3O7.5OH:3H2O
Siderite	1.01	-9.88	-10.89	FeCO3
SiO2(a)	-1.46	-4.18	-2.71	SiO2
Talc	-5.56	15.83	21.40	Mg3Si4O10(OH)2

F4

-----------------------------Saturation indices----------------------

Phase	SI	log IAP	log KT	
Anhydrite	-3.88	-8.24	-4.36	CaSO4
Aragonite	-1.76	-10.09	-8.34	CaCO3
Calcite	-1.61	-10.09	-8.48	CaCO3
CH4(g)	-32.26	-76.19	-43.93	CH4
Chalcedony	-0.61	-4.17	-3.55	SiO2
Chrysotile	-9.79	22.42	32.20	Mg3Si2O5(OH)4
CO2(g)	-2.04	-20.19	-18.15	CO2
Dolomite	-2.95	-20.04	-17.09	CaMg(CO3)2
Fe(OH)3(a)	-1.41	16.50	17.91	Fe(OH)3
FeS(ppt)	-27.27	-64.84	-37.56	FeS
Goethite	4.48	16.50	12.02	FeOOH
Gypsum	-3.66	-8.24	-4.58	CaSO4:2H2O
H2(g)	-14.00	-14.00	0.00	H2
H2O(g)	-1.51	-0.00	1.51	H2O
H2S(g)	-32.75	-74.34	-41.59	H2S
Halite	-7.83	-6.25	1.58	NaCl
Hematite	10.97	33.00	22.03	Fe2O3
Jarosite-K	-14.10	15.75	29.85	KFe3(SO4)2(OH)6
Mackinawite	-26.54	-64.84	-38.30	FeS

Melanterite	-6.63	-8.84	-2.21	FeSO4:7H2O
N2(g)	-2.03	-5.29	-3.26	N2
NH3(g)	-19.12	-23.64	-4.52	NH3
O2(g)	-55.12	28.00	83.12	O2
Pyrite	-39.39	-125.17	-85.78	FeS2
Quartz	-0.19	-4.17	-3.98	SiO2
Sepiolite	-7.76	8.00	15.76	Mg2Si3O7.5OH:3H2O
Sepiolite(d)	-10.66	8.00	18.66	Mg2Si3O7.5OH:3H2O
Siderite	0.20	-10.69	-10.89	FeCO3
SiO2(a)	-1.45	-4.17	-2.71	SiO2
Sulfur	-24.63	-60.34	-35.71	S
Talc	-7.32	14.08	21.40	Mg3Si4O10(OH)2

F6

Saturation indices

Phase	SI	log IAP	log KT	
Anhydrite	-2.48	-6.84	-4.36	CaSO4
Aragonite	-0.47	-8.81	-8.34	CaCO3
Calcite	-0.33	-8.81	-8.48	CaCO3
CH4(g)	-31.69	-75.62	-43.93	CH4
Chalcedony	-0.15	-3.70	-3.55	SiO2
Chrysotile	-6.50	25.70	32.20	Mg3Si2O5(OH)4
CO2(g)	-1.47	-19.62	-18.15	CO2
Dolomite	-0.31	-17.40	-17.09	CaMg(CO3)2
Fe(OH)3(a)	-0.63	17.28	17.91	Fe(OH)3
FeS(ppt)	-25.81	-63.37	-37.56	FeS
Goethite	5.26	17.28	12.02	FeOOH
Gypsum	-2.26	-6.84	-4.58	CaSO4:2H2O
H2(g)	-14.00	-14.00	0.00	H2
H2O(g)	-1.51	-0.00	1.51	H2O
H2S(g)	-32.07	-73.66	-41.59	H2S
Halite	-5.56	-3.98	1.58	NaCl
Hematite	12.54	34.57	22.03	Fe2O3
Jarosite-K	-10.72	19.13	29.85	KFe3(SO4)2(OH)6
Mackinawite	-25.08	-63.37	-38.30	FeS
Melanterite	-5.17	-7.38	-2.21	FeSO4:7H2O
N2(g)	-1.91	-5.17	-3.26	N2
NH3(g)	-19.06	-23.58	-4.52	NH3
O2(g)	-55.12	28.00	83.12	O2
Pyrite	-37.25	-123.03	-85.78	FeS2
Quartz	0.28	-3.70	-3.98	SiO2
Sepiolite	-4.79	10.97	15.76	Mg2Si3O7.5OH:3H2O
Sepiolite(d)	-7.69	10.97	18.66	Mg2Si3O7.5OH:3H2O
Siderite	1.55	-9.34	-10.89	FeCO3
SiO2(a)	-0.99	-3.70	-2.71	SiO2
Sulfur	-23.95	-59.66	-35.71	S
Talc	-3.10	18.30	21.40	Mg3Si4O10(OH)2

FDP1

Saturation indices

Phase	SI	log IAP	log KT	
Aragonite	-0.42	-8.76	-8.34	CaCO3
Calcite	-0.28	-8.76	-8.48	CaCO3
CH4(g)	-31.72	-75.65	-43.93	CH4
Chalcedony	-0.05	-3.60	-3.55	SiO2
Chrysotile	-6.86	25.34	32.20	Mg3Si2O5(OH)4
CO2(g)	-1.50	-19.65	-18.15	CO2
Dolomite	-0.47	-17.56	-17.09	CaMg(CO3)2
Fe(OH)3(a)	-1.73	16.18	17.91	Fe(OH)3
Goethite	4.16	16.18	12.02	FeOOH
H2(g)	-14.00	-14.00	0.00	H2
H2O(g)	-1.51	-0.00	1.51	H2O
Halite	-5.74	-4.16	1.58	NaCl
Hematite	10.33	32.36	22.03	Fe2O3
N2(g)	-1.55	-4.81	-3.26	N2
NH3(g)	-18.88	-23.41	-4.52	NH3
O2(g)	-55.12	28.00	83.12	O2
Quartz	0.38	-3.60	-3.98	SiO2
Sepiolite	-4.87	10.89	15.76	Mg2Si3O7.5OH:3H2O
Sepiolite(d)	-7.77	10.89	18.66	Mg2Si3O7.5OH:3H2O
Siderite	0.42	-10.47	-10.89	FeCO3
SiO2(a)	-0.89	-3.60	-2.71	SiO2
Talc	-3.26	18.14	21.40	Mg3Si4O10(OH)2

FDP2

Saturation indices

Phase	SI	log IAP	log KT	
Aragonite	-0.91	-9.25	-8.34	CaCO3
Calcite	-0.77	-9.25	-8.48	CaCO3
CH4(g)	-31.90	-75.83	-43.93	CH4
Chalcedony	-0.41	-3.96	-3.55	SiO2
Chrysotile	-7.94	24.26	32.20	Mg3Si2O5(OH)4
CO2(g)	-1.68	-19.83	-18.15	CO2
Dolomite	-1.26	-18.35	-17.09	CaMg(CO3)2

Fe(OH)3(a)	-0.75	17.16	17.91	Fe(OH)3
Goethite	5.14	17.16	12.02	FeOOH
H2(g)	-14.00	-14.00	0.00	H2
H2O(g)	-1.51	-0.00	1.51	H2O
Halite	-5.83	-4.25	1.58	NaCl
Hematite	12.29	34.33	22.03	Fe2O3
N2(g)	-1.28	-4.54	-3.26	N2
NH3(g)	-18.75	-23.27	-4.52	NH3
O2(g)	-55.12	28.00	83.12	O2
Quartz	0.02	-3.96	-3.98	SiO2
Sepiolite	-6.19	9.57	15.76	Mg2Si3O7.5OH:3H2O
Sepiolite(d)	-9.09	9.57	18.66	Mg2Si3O7.5OH:3H2O
Siderite	1.22	-9.67	-10.89	FeCO3
SiO2(a)	-1.25	-3.96	-2.71	SiO2
Talc	-5.07	16.33	21.40	Mg3Si4O10(OH)2

FDP3

Saturation indices

Phase	SI	log IAP	log KT	
Anhydrite	-3.60	-7.96	-4.36	CaSO4
Aragonite	-1.41	-9.75	-8.34	CaCO3
Calcite	-1.27	-9.75	-8.48	CaCO3
CH4(g)	-32.27	-76.20	-43.93	CH4
Chalcedony	-0.58	-4.14	-3.55	SiO2
Chrysotile	-8.47	23.73	32.20	Mg3Si2O5(OH)4
CO2(g)	-2.05	-20.20	-18.15	CO2
Dolomite	-2.19	-19.28	-17.09	CaMg(CO3)2
Fe(OH)3(a)	-2.07	15.84	17.91	Fe(OH)3
FeS(ppt)	-28.01	-65.57	-37.56	FeS
Goethite	3.82	15.84	12.02	FeOOH
Gypsum	-3.38	-7.96	-4.58	CaSO4:2H2O
H2(g)	-14.00	-14.00	0.00	H2
H2O(g)	-1.51	-0.00	1.51	H2O
H2S(g)	-32.82	-74.41	-41.59	H2S
Halite	-6.59	-5.01	1.58	NaCl
Hematite	9.64	31.67	22.03	Fe2O3
Jarosite-K	-15.97	13.88	29.85	KFe3(SO4)2(OH)6
Mackinawite	-27.27	-65.57	-38.30	FeS
Melanterite	-7.36	-9.57	-2.21	FeSO4:7H2O
N2(g)	-1.70	-4.96	-3.26	N2
NH3(g)	-18.96	-23.48	-4.52	NH3
O2(g)	-55.12	28.00	83.12	O2
Pyrite	-40.20	-125.98	-85.78	FeS2
Quartz	-0.15	-4.14	-3.98	SiO2
Sepiolite	-6.83	8.93	15.76	Mg2Si3O7.5OH:3H2O
Sepiolite(d)	-9.73	8.93	18.66	Mg2Si3O7.5OH:3H2O
Siderite	-0.47	-11.36	-10.89	FeCO3
SiO2(a)	-1.42	-4.14	-2.71	SiO2
Sulfur	-24.70	-60.41	-35.71	S
Talc	-5.93	15.46	21.40	Mg3Si4O10(OH)2

Wo2

Saturation indices

Phase	SI	log IAP	log KT	
Aragonite	-1.47	-9.78	-8.32	CaCO3
Calcite	-1.32	-9.78	-8.46	CaCO3
CH4(g)	-31.90	-76.32	-44.42	CH4
Chalcedony	-0.48	-4.07	-3.59	SiO2
Chrysotile	-9.47	23.16	32.63	Mg3Si2O5(OH)4
CO2(g)	-2.16	-20.32	-18.16	CO2
Dolomite	-2.66	-19.67	-17.01	CaMg(CO3)2
Fe(OH)3(a)	-0.44	17.55	17.99	Fe(OH)3
Goethite	5.33	17.55	12.22	FeOOH
H2(g)	-14.00	-14.00	0.00	H2
H2O(g)	-1.60	-0.00	1.60	H2O
Halite	-6.83	-5.26	1.57	NaCl
Hematite	12.65	35.11	22.46	Fe2O3
N2(g)	-1.25	-4.50	-3.25	N2
NH3(g)	-18.64	-23.25	-4.61	NH3
O2(g)	-56.28	28.00	84.28	O2
Quartz	-0.04	-4.07	-4.03	SiO2
Sepiolite	-7.20	8.65	15.85	Mg2Si3O7.5OH:3H2O
Sepiolite(d)	-10.01	8.65	18.66	Mg2Si3O7.5OH:3H2O
Siderite	1.11	-9.76	-10.87	FeCO3
SiO2(a)	-1.33	-4.07	-2.74	SiO2
Talc	-6.77	15.02	21.79	Mg3Si4O10(OH)2

Wo3B

Saturation indices

Phase	SI	log IAP	log KT	
Anhydrite	-4.62	-8.97	-4.35	CaSO4
Aragonite	-1.79	-10.11	-8.32	CaCO3
Calcite	-1.65	-10.11	-8.46	CaCO3
CH4(g)	-32.09	-76.45	-44.36	CH4

Chalcedony	-0.53	-4.12	-3.59	SiO2
Chrysotile	-9.35	23.23	32.58	Mg3Si2O5(OH)4
CO2(g)	-2.30	-20.45	-18.16	CO2
Dolomite	-3.06	-20.08	-17.02	CaMg(CO3)2
Fe(OH)3(a)	-0.47	17.51	17.98	Fe(OH)3
FeS(ppt)	-26.79	-64.81	-38.01	FeS
Goethite	5.31	17.51	12.20	FeOOH
Gypsum	-4.39	-8.97	-4.58	CaSO4:2H2O
H2(g)	-14.00	-14.00	0.00	H2
H2O(g)	-1.59	-0.00	1.59	H2O
H2S(g)	-33.27	-75.32	-42.04	H2S
Halite	-7.00	-5.42	1.58	NaCl
Hematite	12.62	35.02	22.41	Fe2O3
Jarosite-K	-13.66	16.64	30.30	KFe3(SO4)2(OH)6
Mackinawite	-26.06	-64.81	-38.75	FeS
Melanterite	-6.56	-8.81	-2.25	FeSO4:7H2O
N2(g)	-1.37	-4.62	-3.25	N2
NH3(g)	-18.71	-23.31	-4.60	NH3
O2(g)	-56.14	28.00	84.14	O2
Pyrite	-39.36	-126.12	-86.76	FeS2
Quartz	-0.09	-4.12	-4.03	SiO2
Sepiolite	-7.22	8.62	15.84	Mg2Si3O7.5OH:3H2O
Sepiolite(d)	-10.04	8.62	18.66	Mg2Si3O7.5OH:3H2O
Siderite	0.93	-9.94	-10.87	FeCO3
SiO2(a)	-1.38	-4.12	-2.74	SiO2
Sulfur	-25.19	-61.32	-36.13	S
Talc	-6.75	14.99	21.74	Mg3Si4O10(OH)2

Wo4

-----Saturation indices-----

Phase	SI	log IAP	log KT	
Anhydrite	-3.68	-8.02	-4.35	CaSO4
Aragonite	-1.64	-9.95	-8.31	CaCO3
Calcite	-1.49	-9.95	-8.46	CaCO3
CH4(g)	-31.88	-76.38	-44.51	CH4
Chalcedony	-0.46	-4.05	-3.60	SiO2
Chrysotile	-8.87	23.84	32.70	Mg3Si2O5(OH)4
CO2(g)	-2.22	-20.38	-18.16	CO2
Dolomite	-2.69	-19.68	-17.00	CaMg(CO3)2
Fe(OH)3(a)	-0.40	17.61	18.01	Fe(OH)3
FeS(ppt)	-25.68	-63.84	-38.16	FeS
Goethite	5.35	17.61	12.26	FeOOH
Gypsum	-3.44	-8.02	-4.58	CaSO4:2H2O
H2(g)	-14.00	-14.00	0.00	H2
H2O(g)	-1.61	-0.00	1.61	H2O
H2S(g)	-32.26	-74.45	-42.20	H2S
Halite	-6.97	-5.40	1.57	NaCl
Hematite	12.69	35.22	22.53	Fe2O3
Jarosite-K	-11.92	18.53	30.45	KFe3(SO4)2(OH)6
Mackinawite	-24.95	-63.84	-38.90	FeS
Melanterite	-5.58	-7.84	-2.26	FeSO4:7H2O
N2(g)	-1.59	-4.84	-3.25	N2
NH3(g)	-18.79	-23.42	-4.63	NH3
O2(g)	-56.48	28.00	84.48	O2
Pyrite	-37.21	-124.30	-87.09	FeS2
Quartz	-0.01	-4.05	-4.04	SiO2
Sepiolite	-6.73	9.13	15.87	Mg2Si3O7.5OH:3H2O
Sepiolite(d)	-9.53	9.13	18.66	Mg2Si3O7.5OH:3H2O
Siderite	1.09	-9.77	-10.87	FeCO3
SiO2(a)	-1.31	-4.05	-2.75	SiO2
Sulfur	-24.18	-60.45	-36.27	S
Talc	-6.13	15.73	21.86	Mg3Si4O10(OH)2

Wo5

-----Saturation indices-----

Phase	SI	log IAP	log KT	
Anhydrite	-3.55	-7.90	-4.34	CaSO4
Aragonite	-2.41	-10.71	-8.31	CaCO3
Calcite	-2.26	-10.71	-8.45	CaCO3
CH4(g)	-32.13	-76.75	-44.62	CH4
Chalcedony	-0.53	-4.14	-3.61	SiO2
Chrysotile	-9.77	23.04	32.81	Mg3Si2O5(OH)4
CO2(g)	-2.59	-20.75	-18.16	CO2
Dolomite	-4.06	-21.03	-16.98	CaMg(CO3)2
Fe(OH)3(a)	-0.69	17.34	18.03	Fe(OH)3
FeS(ppt)	-25.31	-63.60	-38.29	FeS
Goethite	5.03	17.34	12.31	FeOOH
Gypsum	-3.32	-7.90	-4.58	CaSO4:2H2O
H2(g)	-14.00	-14.00	0.00	H2
H2O(g)	-1.64	-0.00	1.64	H2O
H2S(g)	-31.62	-73.94	-42.32	H2S
Halite	-6.94	-5.37	1.57	NaCl
Hematite	12.05	34.68	22.63	Fe2O3
Jarosite-K	-11.84	18.73	30.57	KFe3(SO4)2(OH)6

Mackinawite	-24.58	-63.60	-39.02	FeS
Melanterite	-5.33	-7.60	-2.27	FeSO4:7H2O
N2(g)	-1.31	-4.55	-3.24	N2
NH3(g)	-18.63	-23.27	-4.65	NH3
O2(g)	-56.76	28.00	84.76	O2
Pyrite	-36.18	-123.53	-87.36	FeS2
Quartz	-0.08	-4.14	-4.05	SiO2
Sepiolite	-7.42	8.47	15.89	Mg2Si3O7.5OH:3H2O
Sepiolite(d)	-10.19	8.47	18.66	Mg2Si3O7.5OH:3H2O
Siderite	0.45	-10.41	-10.86	FeCO3
SiO2(a)	-1.38	-4.14	-2.75	SiO2
Sulfur	-23.55	-59.94	-36.38	S
Talc	-7.19	14.77	21.95	Mg3Si4O10(OH)2

WoDP1

Saturation indices

Phase	SI	log IAP	log KT	
Anhydrite	-3.66	-8.02	-4.36	CaSO4
Aragonite	-1.92	-10.26	-8.34	CaCO3
Calcite	-1.78	-10.26	-8.48	CaCO3
CH4(g)	-32.55	-76.49	-43.93	CH4
Chalcedony	-0.67	-4.22	-3.55	SiO2
Chrysotile	-9.17	23.03	32.20	Mg3Si2O5(OH)4
CO2(g)	-2.34	-20.49	-18.15	CO2
Dolomite	-3.16	-20.25	-17.09	CaMg(CO3)2
Fe(OH)3(a)	-1.67	16.24	17.91	Fe(OH)3
FeS(ppt)	-27.45	-65.01	-37.56	FeS
Goethite	4.22	16.24	12.02	FeOOH
Gypsum	-3.44	-8.02	-4.58	CaSO4:2H2O
H2(g)	-14.00	-14.00	0.00	H2
H2O(g)	-1.51	-0.00	1.51	H2O
H2S(g)	-32.66	-74.25	-41.59	H2S
Halite	-6.06	-4.48	1.58	NaCl
Hematite	10.45	32.48	22.03	Fe2O3
Jarosite-K	-14.68	15.17	29.85	KFe3(SO4)2(OH)6
Mackinawite	-26.71	-65.01	-38.30	FeS
Melanterite	-6.80	-9.01	-2.21	FeSO4:7H2O
N2(g)	-1.87	-5.13	-3.26	N2
NH3(g)	-19.04	-23.57	-4.52	NH3
O2(g)	-55.12	28.00	83.12	O2
Pyrite	-39.48	-125.26	-85.78	FeS2
Quartz	-0.24	-4.22	-3.98	SiO2
Sepiolite	-7.45	8.31	15.76	Mg2Si3O7.5OH:3H2O
Sepiolite(d)	-10.35	8.31	18.66	Mg2Si3O7.5OH:3H2O
Siderite	-0.36	-11.25	-10.89	FeCO3
SiO2(a)	-1.51	-4.22	-2.71	SiO2
Sulfur	-24.54	-60.25	-35.71	S
Talc	-6.82	14.58	21.40	Mg3Si4O10(OH)2

79055

Saturation indices

Phase	SI	log IAP	log KT	
Anhydrite	-2.65	-7.00	-4.34	CaSO4
Aragonite	-0.06	-8.36	-8.30	CaCO3
Calcite	0.09	-8.36	-8.45	CaCO3
CH4(g)	-30.62	-75.33	-44.71	CH4
Chalcedony	-0.26	-3.88	-3.62	SiO2
Chrysotile	-7.21	25.67	32.88	Mg3Si2O5(OH)4
CO2(g)	-1.17	-19.33	-18.17	CO2
Dolomite	0.41	-16.55	-16.96	CaMg(CO3)2
Fe(OH)3(a)	-1.87	16.17	18.04	Fe(OH)3
FeS(ppt)	-26.41	-64.79	-38.38	FeS
Goethite	3.82	16.17	12.35	FeOOH
Gypsum	-2.42	-7.00	-4.58	CaSO4:2H2O
H2(g)	-14.00	-14.00	0.00	H2
H2O(g)	-1.65	-0.00	1.65	H2O
H2S(g)	-31.55	-73.96	-42.41	H2S
Halite	-5.51	-3.94	1.57	NaCl
Hematite	9.63	32.34	22.71	Fe2O3
Jarosite-K	-14.33	16.33	30.67	KFe3(SO4)2(OH)6
Mackinawite	-25.68	-64.79	-39.11	FeS
Melanterite	-6.52	-8.80	-2.28	FeSO4:7H2O
N2(g)	-1.06	-4.30	-3.24	N2
NH3(g)	-18.49	-23.15	-4.66	NH3
O2(g)	-56.97	28.00	84.97	O2
Pyrite	-37.20	-124.76	-87.56	FeS2
Quartz	0.18	-3.88	-4.06	SiO2
Sepiolite	-5.25	10.65	15.90	Mg2Si3O7.5OH:3H2O
Sepiolite(d)	-8.01	10.65	18.66	Mg2Si3O7.5OH:3H2O
Siderite	0.70	-10.16	-10.86	FeCO3
SiO2(a)	-1.12	-3.88	-2.76	SiO2
Sulfur	-23.50	-59.96	-36.47	S
Talc	-4.11	17.92	22.03	Mg3Si4O10(OH)2

```
-------------------------------------------------------------------------
79056
------------------------------Saturation indices-----------------------
         Phase               SI log IAP  log KT
         Anhydrite        -3.57   -7.91   -4.34  CaSO4
         Aragonite        -1.50   -9.80   -8.30  CaCO3
         Calcite          -1.35   -9.80   -8.45  CaCO3
         Celestite        -3.23   -9.86   -6.62  SrSO4
         CH4(g)          -31.55  -76.32  -44.77  CH4
         Chalcedony       -0.34   -3.97   -3.62  SiO2
         Chrysotile       -8.64   24.29   32.93  Mg3Si2O5(OH)4
         CO2(g)           -2.16  -20.32  -18.17  CO2
         Dolomite         -2.43  -19.39  -16.95  CaMg(CO3)2
         Fe(OH)3(a)       -0.37   17.69   18.05  Fe(OH)3
         FeS(ppt)        -25.31  -63.75  -38.44  FeS
         Goethite          5.31   17.69   12.37  FeOOH
         Gypsum           -3.33   -7.91   -4.58  CaSO4:2H2O
         H2(g)           -14.00  -14.00    0.00  H2
         H2O(g)           -1.66   -0.00    1.66  H2O
         H2S(g)          -31.96  -74.44  -42.48  H2S
         Halite           -6.27   -4.70    1.57  NaCl
         Hematite         12.61   35.37   22.76  Fe2O3
         Jarosite-K      -11.64   19.09   30.73  KFe3(SO4)2(OH)6
         Mackinawite     -24.58  -63.75  -39.17  FeS
         Melanterite      -5.47   -7.75   -2.28  FeSO4:7H2O
         N2(g)            -0.97   -4.21   -3.24  N2
         NH3(g)          -18.43  -23.10   -4.67  NH3
         O2(g)           -57.11   28.00   85.11  O2
         Pyrite          -36.49 -124.19  -87.69  FeS2
         Quartz            0.10   -3.97   -4.07  SiO2
         Sepiolite        -6.33    9.59   15.92  Mg2Si3O7.5OH:3H2O
         Sepiolite(d)     -9.07    9.59   18.66  Mg2Si3O7.5OH:3H2O
         Siderite          1.22   -9.64  -10.85  FeCO3
         SiO2(a)          -1.20   -3.97   -2.76  SiO2
         Strontianite     -2.47  -11.74   -9.27  SrCO3
         Sulfur          -23.91  -60.44  -36.53  S
         Talc             -5.71   16.36   22.07  Mg3Si4O10(OH)2
-------------------------------------------------------------------------
79059
------------------------------Saturation indices-----------------------
         Phase               SI log IAP  log KT
         Aragonite        -0.85   -9.17   -8.32  CaCO3
         Calcite          -0.70   -9.17   -8.47  CaCO3
         CH4(g)          -31.23  -75.46  -44.23  CH4
         Chalcedony       -0.37   -3.95   -3.58  SiO2
         Chrysotile       -9.56   22.90   32.46  Mg3Si2O5(OH)4
         CO2(g)           -1.31  -19.46  -18.15  CO2
         Dolomite         -1.32  -18.36  -17.04  CaMg(CO3)2
         H2(g)           -14.00  -14.00    0.00  H2
         H2O(g)           -1.57   -0.00    1.56  H2O
         Halite           -4.03   -2.45    1.58  NaCl
         N2(g)            -1.62   -4.87   -3.25  N2
         NH3(g)          -18.86  -23.44   -4.58  NH3
         O2(g)           -55.83   28.00   83.83  O2
         Quartz            0.06   -3.95   -4.01  SiO2
         Sepiolite        -7.13    8.69   15.82  Mg2Si3O7.5OH:3H2O
         Sepiolite(d)     -9.97    8.69   18.66  Mg2Si3O7.5OH:3H2O
         Siderite         -0.60  -11.47  -10.88  FeCO3
         SiO2(a)          -1.22   -3.95   -2.73  SiO2
         Strontianite     -1.08  -10.35   -9.27  SrCO3
         Talc             -6.63   15.01   21.64  Mg3Si4O10(OH)2
-------------------------------------------------------------------------
79060
------------------------------Saturation indices-----------------------
         Phase               SI log IAP  log KT
         Anhydrite        -3.43   -7.78   -4.35  CaSO4
         Aragonite        -0.85   -9.17   -8.32  CaCO3
         Calcite          -0.71   -9.17   -8.46  CaCO3
         Celestite        -2.61   -9.24   -6.63  SrSO4
         CH4(g)          -31.19  -75.55  -44.36  CH4
         Chalcedony       -0.40   -3.98   -3.59  SiO2
         Chrysotile       -9.29   23.29   32.58  Mg3Si2O5(OH)4
         CO2(g)           -1.40  -19.56  -18.16  CO2
         Dolomite         -1.29  -18.31  -17.02  CaMg(CO3)2
         Gypsum           -3.20   -7.78   -4.58  CaSO4:2H2O
         H2(g)           -14.00  -14.00    0.00  H2
         H2O(g)           -1.59   -0.00    1.59  H2O
         H2S(g)          -32.12  -74.17  -42.04  H2S
         Halite           -5.69   -4.11    1.58  NaCl
         N2(g)            -1.71   -4.96   -3.25  N2
         NH3(g)          -18.88  -23.48   -4.60  NH3
         O2(g)           -56.14   28.00   84.14  O2
         Quartz            0.04   -3.98   -4.03  SiO2
         Sepiolite        -6.96    8.88   15.84  Mg2Si3O7.5OH:3H2O
```

Sepiolite(d)	-9.78	8.88	18.66	Mg2Si3O7.5OH:3H2O
SiO2(a)	-1.25	-3.98	-2.74	SiO2
Strontianite	-1.36	-10.63	-9.27	SrCO3
Sulfur	-24.04	-60.17	-36.13	S
Talc	-6.42	15.32	21.74	Mg3Si4O10(OH)2

November 2001

W1B

Phase	SI	log IAP	log KT	
Anhydrite	-3.76	-8.12	-4.36	CaSO4
Aragonite	-2.12	-10.46	-8.34	CaCO3
Calcite	-1.98	-10.46	-8.48	CaCO3
CH4(g)	-32.51	-76.44	-43.93	CH4
Chalcedony	-0.44	-3.99	-3.55	SiO2
Chrysotile	-9.26	22.94	32.20	Mg3Si2O5(OH)4
CO2(g)	-2.30	-20.44	-18.15	CO2
Dolomite	-3.50	-20.59	-17.09	CaMg(CO3)2
Fe(OH)3(a)	-2.79	15.12	17.91	Fe(OH)3
FeS(ppt)	-28.43	-65.99	-37.56	FeS
Goethite	3.10	15.12	12.02	FeOOH
Gypsum	-3.54	-8.12	-4.58	CaSO4:2H2O
H2(g)	-14.00	-14.00	0.00	H2
H2O(g)	-1.51	-0.00	1.51	H2O
H2S(g)	-32.52	-74.11	-41.59	H2S
Halite	-7.26	-5.68	1.58	NaCl
Hematite	8.20	30.23	22.03	Fe2O3
Jarosite-K	-17.91	11.94	29.85	KFe3(SO4)2(OH)6
Mackinawite	-27.69	-65.99	-38.30	FeS
Melanterite	-7.78	-9.99	-2.21	FeSO4:7H2O
N2(g)	-1.96	-5.22	-3.26	N2
NH3(g)	-19.09	-23.61	-4.52	NH3
O2(g)	-55.12	28.00	83.12	O2
Pyrite	-40.32	-126.10	-85.78	FeS2
Quartz	-0.01	-3.99	-3.98	SiO2
Sepiolite	-7.12	8.64	15.76	Mg2Si3O7.5OH:3H2O
Sepiolite(d)	-10.02	8.64	18.66	Mg2Si3O7.5OH:3H2O
Siderite	-1.44	-12.33	-10.89	FeCO3
SiO2(a)	-1.28	-3.99	-2.71	SiO2
Sulfur	-24.40	-60.11	-35.71	S
Talc	-6.44	14.96	21.40	Mg3Si4O10(OH)2

W2B

Phase	SI	log IAP	log KT	
Anhydrite	-3.75	-8.11	-4.36	CaSO4
Aragonite	-1.90	-10.23	-8.34	CaCO3
Calcite	-1.75	-10.23	-8.48	CaCO3
CH4(g)	-32.47	-76.40	-43.93	CH4
Chalcedony	-0.46	-4.01	-3.55	SiO2
Chrysotile	-9.29	22.91	32.20	Mg3Si2O5(OH)4
CO2(g)	-2.25	-20.40	-18.15	CO2
Dolomite	-3.24	-20.33	-17.09	CaMg(CO3)2
Fe(OH)3(a)	-1.95	15.96	17.91	Fe(OH)3
FeS(ppt)	-27.76	-65.32	-37.56	FeS
Goethite	3.94	15.96	12.02	FeOOH
Gypsum	-3.53	-8.11	-4.58	CaSO4:2H2O
H2(g)	-14.00	-14.00	0.00	H2
H2O(g)	-1.51	-0.00	1.51	H2O
H2S(g)	-32.69	-74.28	-41.59	H2S
Halite	-7.19	-5.61	1.58	NaCl
Hematite	9.88	31.91	22.03	Fe2O3
Jarosite-K	-15.64	14.21	29.85	KFe3(SO4)2(OH)6
Mackinawite	-27.02	-65.32	-38.30	FeS
Melanterite	-7.11	-9.32	-2.21	FeSO4:7H2O
N2(g)	-1.73	-4.99	-3.26	N2
NH3(g)	-18.97	-23.49	-4.52	NH3
O2(g)	-55.12	28.00	83.12	O2
Pyrite	-39.82	-125.60	-85.78	FeS2
Quartz	-0.03	-4.01	-3.98	SiO2
Sepiolite	-7.17	8.59	15.76	Mg2Si3O7.5OH:3H2O
Sepiolite(d)	-10.07	8.59	18.66	Mg2Si3O7.5OH:3H2O
Siderite	-0.55	-11.44	-10.89	FeCO3
SiO2(a)	-1.30	-4.01	-2.71	SiO2
Sulfur	-24.57	-60.28	-35.71	S
Talc	-6.51	14.89	21.40	Mg3Si4O10(OH)2

W3A

-----------------------------Saturation indices----------------------

Phase	SI	log IAP	log KT	
Anhydrite	-3.42	-7.78	-4.36	CaSO4
Aragonite	-2.70	-11.03	-8.34	CaCO3
Calcite	-2.55	-11.03	-8.48	CaCO3
CH4(g)	-84.16	-128.09	-43.93	CH4
Chalcedony	-0.46	-4.02	-3.55	SiO2
Chrysotile	-12.02	20.18	32.20	Mg3Si2O5(OH)4
CO2(g)	-2.42	-20.57	-18.15	CO2
Dolomite	-5.11	-22.20	-17.09	CaMg(CO3)2
Fe(OH)3(a)	3.70	21.61	17.91	Fe(OH)3
FeS(ppt)	-79.09	-116.66	-37.56	FeS
Goethite	9.59	21.61	12.02	FeOOH
Gypsum	-3.20	-7.78	-4.58	CaSO4:2H2O
H2(g)	-26.88	-26.88	0.00	H2
H2O(g)	-1.51	-0.00	1.51	H2O
H2S(g)	-83.25	-124.83	-41.59	H2S
Halite	-7.08	-5.50	1.58	NaCl
Hematite	21.20	43.23	22.03	Fe2O3
Jarosite-K	2.96	32.81	29.85	KFe3(SO4)2(OH)6
Mackinawite	-78.36	-116.66	-38.30	FeS
Melanterite	-6.93	-9.14	-2.21	FeSO4:7H2O
N2(g)	-1.82	-5.08	-3.26	N2
NH3(g)	-38.34	-42.86	-4.52	NH3
O2(g)	-29.36	53.76	83.12	O2
Pyrite	-128.84	-214.61	-85.78	FeS2
Quartz	-0.03	-4.02	-3.98	SiO2
Sepiolite	-9.00	6.76	15.76	Mg2Si3O7.5OH:3H2O
Sepiolite(d)	-11.90	6.76	18.66	Mg2Si3O7.5OH:3H2O
Siderite	-1.51	-12.40	-10.89	FeCO3
SiO2(a)	-1.30	-4.02	-2.71	SiO2
Sulfur	-62.25	-97.95	-35.71	S
Talc	-9.25	12.15	21.40	Mg3Si4O10(OH)2

W3B

-----------------------------Saturation indices----------------------

Phase	SI	log IAP	log KT	
Anhydrite	-4.49	-8.84	-4.35	CaSO4
Aragonite	-1.98	-10.30	-8.32	CaCO3
Calcite	-1.84	-10.30	-8.46	CaCO3
CH4(g)	-87.36	-131.71	-44.35	CH4
Chalcedony	-0.42	-4.00	-3.59	SiO2
Chrysotile	-9.73	22.83	32.56	Mg3Si2O5(OH)4
CO2(g)	-2.19	-20.35	-18.16	CO2
Dolomite	-3.35	-20.37	-17.02	CaMg(CO3)2
Fe(OH)3(a)	3.47	21.45	17.98	Fe(OH)3
FeS(ppt)	-84.72	-122.72	-38.00	FeS
Goethite	9.26	21.45	12.19	FeOOH
Gypsum	-4.26	-8.84	-4.58	CaSO4:2H2O
H2(g)	-27.84	-27.84	0.00	H2
H2O(g)	-1.59	-0.00	1.59	H2O
H2S(g)	-88.22	-130.25	-42.03	H2S
Halite	-7.21	-5.64	1.58	NaCl
Hematite	20.51	42.90	22.39	Fe2O3
Jarosite-K	-0.92	29.37	30.28	KFe3(SO4)2(OH)6
Mackinawite	-83.99	-122.72	-38.73	FeS
Melanterite	-9.11	-11.36	-2.24	FeSO4:7H2O
N2(g)	-1.56	-4.81	-3.25	N2
NH3(g)	-39.57	-44.16	-4.60	NH3
O2(g)	-28.42	55.68	84.10	O2
Pyrite	-138.40	-225.12	-86.73	FeS2
Quartz	0.02	-4.00	-4.02	SiO2
Sepiolite	-7.28	8.55	15.84	Mg2Si3O7.5OH:3H2O
Sepiolite(d)	-10.11	8.55	18.66	Mg2Si3O7.5OH:3H2O
Siderite	-1.94	-12.82	-10.87	FeCO3
SiO2(a)	-1.26	-4.00	-2.74	SiO2
Sulfur	-66.29	-102.41	-36.11	S
Talc	-6.90	14.83	21.73	Mg3Si4O10(OH)2

W4

-----------------------------Saturation indices----------------------

Phase	SI	log IAP	log KT	
Anhydrite	-3.34	-7.70	-4.36	CaSO4
Aragonite	-2.46	-10.79	-8.34	CaCO3
Calcite	-2.31	-10.79	-8.48	CaCO3
CH4(g)	-81.81	-125.74	-43.93	CH4
Chalcedony	-0.43	-3.98	-3.55	SiO2
Chrysotile	-12.63	19.57	32.20	Mg3Si2O5(OH)4
CO2(g)	-1.99	-20.14	-18.15	CO2
Dolomite	-4.67	-21.76	-17.09	CaMg(CO3)2
Fe(OH)3(a)	3.49	21.40	17.91	Fe(OH)3
FeS(ppt)	-76.89	-114.45	-37.56	FeS

Goethite	9.38	21.40	12.02	FeOOH
Gypsum	-3.12	-7.70	-4.58	CaSO4:2H2O
H2(g)	-26.40	-26.40	0.00	H2
H2O(g)	-1.51	-0.00	1.51	H2O
H2S(g)	-81.06	-122.65	-41.59	H2S
Halite	-7.26	-5.67	1.58	NaCl
Hematite	20.76	42.79	22.03	Fe2O3
Jarosite-K	2.78	32.63	29.85	KFe3(SO4)2(OH)6
Mackinawite	-76.15	-114.45	-38.30	FeS
Melanterite	-6.64	-8.85	-2.21	FeSO4:7H2O
N2(g)	-1.91	-5.17	-3.26	N2
NH3(g)	-37.66	-42.19	-4.52	NH3
O2(g)	-30.32	52.80	83.12	O2
Pyrite	-124.92	-210.70	-85.78	FeS2
Quartz	0.00	-3.98	-3.98	SiO2
Sepiolite	-9.34	6.42	15.76	Mg2Si3O7.5OH:3H2O
Sepiolite(d)	-12.24	6.42	18.66	Mg2Si3O7.5OH:3H2O
Siderite	-1.05	-11.94	-10.89	FeCO3
SiO2(a)	-1.27	-3.98	-2.71	SiO2
Sulfur	-60.54	-96.25	-35.71	S
Talc	-9.78	11.61	21.40	Mg3Si4O10(OH)2

W5

Saturation indices

Phase	SI	log IAP	log KT	
Anhydrite	-2.94	-7.30	-4.36	CaSO4
Aragonite	-2.16	-10.50	-8.33	CaCO3
Calcite	-2.02	-10.50	-8.48	CaCO3
CH4(g)	-78.22	-122.20	-43.97	CH4
Chalcedony	-0.48	-4.03	-3.55	SiO2
Chrysotile	-12.03	20.21	32.24	Mg3Si2O5(OH)4
CO2(g)	-1.49	-19.64	-18.15	CO2
Dolomite	-3.63	-20.71	-17.08	CaMg(CO3)2
Gypsum	-2.72	-7.30	-4.58	CaSO4:2H2O
H2(g)	-25.64	-25.64	0.00	H2
H2O(g)	-1.52	-0.00	1.52	H2O
H2S(g)	-77.37	-119.00	-41.63	H2S
Halite	-6.77	-5.19	1.58	NaCl
N2(g)	-2.37	-5.63	-3.26	N2
NH3(g)	-36.74	-41.27	-4.53	NH3
O2(g)	-31.94	51.28	83.22	O2
Quartz	-0.05	-4.03	-3.98	SiO2
Sepiolite	-9.01	6.76	15.77	Mg2Si3O7.5OH:3H2O
Sepiolite(d)	-11.90	6.76	18.66	Mg2Si3O7.5OH:3H2O
SiO2(a)	-1.32	-4.03	-2.71	SiO2
Sulfur	-57.61	-93.36	-35.75	S
Talc	-9.28	12.15	21.43	Mg3Si4O10(OH)2

WDP1

Saturation indices

Phase	SI	log IAP	log KT	
Anhydrite	-4.65	-9.01	-4.36	CaSO4
Aragonite	-1.27	-9.60	-8.34	CaCO3
Calcite	-1.12	-9.60	-8.48	CaCO3
CH4(g)	-31.99	-75.92	-43.93	CH4
Chalcedony	-0.46	-4.01	-3.55	SiO2
Chrysotile	-8.49	23.71	32.20	Mg3Si2O5(OH)4
CO2(g)	-1.78	-19.92	-18.15	CO2
Dolomite	-1.86	-18.95	-17.09	CaMg(CO3)2
Fe(OH)3(a)	-1.07	16.84	17.91	Fe(OH)3
FeS(ppt)	-27.92	-65.49	-37.56	FeS
Goethite	4.82	16.84	12.02	FeOOH
Gypsum	-4.43	-9.01	-4.58	CaSO4:2H2O
H2(g)	-14.00	-14.00	0.00	H2
H2O(g)	-1.51	-0.00	1.51	H2O
H2S(g)	-33.74	-75.33	-41.59	H2S
Halite	-6.64	-5.05	1.58	NaCl
Hematite	11.65	33.68	22.03	Fe2O3
Jarosite-K	-15.07	14.78	29.85	KFe3(SO4)2(OH)6
Mackinawite	-27.19	-65.49	-38.30	FeS
Melanterite	-7.28	-9.49	-2.21	FeSO4:7H2O
N2(g)	-1.58	-4.84	-3.26	N2
NH3(g)	-18.90	-23.42	-4.52	NH3
O2(g)	-55.12	28.00	83.12	O2
Pyrite	-41.04	-126.82	-85.78	FeS2
Quartz	-0.03	-4.01	-3.98	SiO2
Sepiolite	-6.63	9.13	15.76	Mg2Si3O7.5OH:3H2O
Sepiolite(d)	-9.53	9.13	18.66	Mg2Si3O7.5OH:3H2O
Siderite	0.81	-10.08	-10.89	FeCO3
SiO2(a)	-1.30	-4.01	-2.71	SiO2
Sulfur	-25.62	-61.33	-35.71	S
Talc	-5.70	15.70	21.40	Mg3Si4O10(OH)2

```
-------------------------------------------------------------------------
WDP2
------------------------------Saturation indices-----------------------
         Phase               SI log IAP  log KT
         Anhydrite        -3.55   -7.91   -4.36  CaSO4
         Aragonite        -2.17  -10.51   -8.34  CaCO3
         Calcite          -2.03  -10.51   -8.48  CaCO3
         CH4(g)          -85.50 -129.43  -43.93  CH4
         Chalcedony       -0.39   -3.94   -3.55  SiO2
         Chrysotile      -10.58   21.62   32.20  Mg3Si2O5(OH)4
         CO2(g)           -2.16  -20.31  -18.15  CO2
         Dolomite         -3.90  -20.99  -17.09  CaMg(CO3)2
         Fe(OH)3(a)        3.14   21.05   17.91  Fe(OH)3
         FeS(ppt)        -81.85 -119.41  -37.56  FeS
         Goethite          9.03   21.05   12.02  FeOOH
         Gypsum           -3.33   -7.91   -4.58  CaSO4:2H2O
         H2(g)           -27.28  -27.28    0.00  H2
         H2O(g)           -1.51   -0.00    1.51  H2O
         H2S(g)          -85.24 -126.83  -41.59  H2S
         Halite           -7.20   -5.61    1.58  NaCl
         Hematite         20.08   42.11   22.03  Fe2O3
         Jarosite-K        0.77   30.62   29.85  KFe3(SO4)2(OH)6
         Mackinawite     -81.12 -119.41  -38.30  FeS
         Melanterite      -8.09  -10.30   -2.21  FeSO4:7H2O
         N2(g)            -2.06   -5.32   -3.26  N2
         NH3(g)          -39.06  -43.58   -4.52  NH3
         O2(g)           -28.56   54.56   83.12  O2
         Pyrite         -133.19 -218.96  -85.78  FeS2
         Quartz            0.04   -3.94   -3.98  SiO2
         Sepiolite        -7.92    7.84   15.76  Mg2Si3O7.5OH:3H2O
         Sepiolite(d)     -10.82    7.84   18.66  Mg2Si3O7.5OH:3H2O
         Siderite         -2.01  -12.90  -10.89  FeCO3
         SiO2(a)          -1.23   -3.94   -2.71  SiO2
         Sulfur           -63.84  -99.55  -35.71  S
         Talc             -7.66   13.74   21.40  Mg3Si4O10(OH)2
-------------------------------------------------------------------------
WDP3
------------------------------Saturation indices-----------------------
         Phase               SI log IAP  log KT
         Anhydrite        -3.11   -7.46   -4.36  CaSO4
         Aragonite        -1.43   -9.75   -8.33  CaCO3
         Calcite          -1.28   -9.75   -8.47  CaCO3
         CH4(g)          -87.17 -131.28  -44.10  CH4
         Chalcedony       -0.34   -3.91   -3.57  SiO2
         Chrysotile       -8.73   23.62   32.35  Mg3Si2O5(OH)4
         CO2(g)           -1.92  -20.08  -18.15  CO2
         Dolomite         -2.29  -19.35  -17.06  CaMg(CO3)2
         Fe(OH)3(a)        2.17   20.11   17.94  Fe(OH)3
         FeS(ppt)        -85.03 -122.78  -37.74  FeS
         Goethite          8.02   20.11   12.09  FeOOH
         Gypsum           -2.88   -7.46   -4.58  CaSO4:2H2O
         H2(g)           -27.80  -27.80    0.00  H2
         H2O(g)           -1.54   -0.00    1.54  H2O
         H2S(g)          -87.22 -128.99  -41.77  H2S
         Halite           -6.82   -5.24    1.58  NaCl
         Hematite         18.04   40.22   22.18  Fe2O3
         Jarosite-K       -2.31   27.72   30.03  KFe3(SO4)2(OH)6
         Mackinawite     -84.30 -122.78  -38.48  FeS
         Melanterite      -9.35  -11.58   -2.22  FeSO4:7H2O
         N2(g)            -2.16   -5.42   -3.26  N2
         NH3(g)          -39.86  -44.41   -4.55  NH3
         O2(g)           -27.92   55.60   83.52  O2
         Pyrite         -137.80 -223.96  -86.17  FeS2
         Quartz            0.09   -3.91   -4.00  SiO2
         Sepiolite        -6.56    9.23   15.79  Mg2Si3O7.5OH:3H2O
         Sepiolite(d)     -9.43    9.23   18.66  Mg2Si3O7.5OH:3H2O
         Siderite         -2.99  -13.87  -10.88  FeCO3
         SiO2(a)          -1.19   -3.91   -2.72  SiO2
         Sulfur           -65.31 -101.19  -35.88  S
         Talc             -5.74   15.80   21.54  Mg3Si4O10(OH)2
-------------------------------------------------------------------------
F1B
------------------------------Saturation indices-----------------------
         Phase               SI log IAP  log KT
         Anhydrite        -4.94   -9.28   -4.34  CaSO4
         Aragonite        -1.38   -9.67   -8.30  CaCO3
         Calcite          -1.23   -9.67   -8.44  CaCO3
         CH4(g)          -86.98 -131.91  -44.93  CH4
         Chalcedony       -0.48   -4.12   -3.63  SiO2
         Chrysotile       -9.21   23.86   33.08  Mg3Si2O5(OH)4
         CO2(g)           -1.90  -20.07  -18.17  CO2
         Dolomite         -2.12  -19.04  -16.93  CaMg(CO3)2
         Fe(OH)3(a)        3.83   21.91   18.08  Fe(OH)3
         FeS(ppt)        -84.98 -123.59  -38.61  FeS
```

Goethite	9.47	21.91	12.44	FeOOH
Gypsum	-4.70	-9.28	-4.58	CaSO4:2H2O
H2(g)	-27.96	-27.96	0.00	H2
H2O(g)	-1.69	-0.00	1.69	H2O
H2S(g)	-88.87	-131.52	-42.65	H2S
Halite	-6.57	-5.00	1.57	NaCl
Hematite	20.92	43.83	22.90	Fe2O3
Jarosite-K	-1.55	29.35	30.90	KFe3(SO4)2(OH)6
Mackinawite	-84.25	-123.59	-39.34	FeS
Melanterite	-9.45	-11.75	-2.30	FeSO4:7H2O
N2(g)	-1.68	-4.91	-3.24	N2
NH3(g)	-39.70	-44.40	-4.70	NH3
O2(g)	-29.57	55.92	85.49	O2
Pyrite	-139.08	-227.15	-88.06	FeS2
Quartz	-0.03	-4.12	-4.08	SiO2
Sepiolite	-6.90	9.05	15.95	Mg2Si3O7.5OH:3H2O
Sepiolite(d)	-9.61	9.05	18.66	Mg2Si3O7.5OH:3H2O
Siderite	-1.29	-12.14	-10.85	FeCO3
SiO2(a)	-1.35	-4.12	-2.77	SiO2
Sulfur	-66.88	-103.56	-36.68	S
Talc	-6.57	15.63	22.20	Mg3Si4O10(OH)2

F3A

Saturation indices

Phase	SI	log IAP	log KT	
Anhydrite	-5.16	-9.51	-4.34	CaSO4
Aragonite	-1.36	-9.66	-8.30	CaCO3
Calcite	-1.21	-9.66	-8.45	CaCO3
CH4(g)	-87.65	-132.38	-44.73	CH4
Chalcedony	-0.53	-4.14	-3.62	SiO2
Chrysotile	-9.05	23.84	32.90	Mg3Si2O5(OH)4
CO2(g)	-1.89	-20.06	-18.17	CO2
Dolomite	-2.05	-19.01	-16.96	CaMg(CO3)2
Fe(OH)3(a)	3.13	21.17	18.04	Fe(OH)3
FeS(ppt)	-86.70	-125.10	-38.39	FeS
Goethite	8.82	21.17	12.35	FeOOH
Gypsum	-4.93	-9.51	-4.58	CaSO4:2H2O
H2(g)	-28.08	-28.08	0.00	H2
H2O(g)	-1.66	-0.00	1.65	H2O
H2S(g)	-89.80	-132.23	-42.43	H2S
Halite	-6.66	-5.09	1.57	NaCl
Hematite	19.62	42.34	22.72	Fe2O3
Jarosite-K	-3.98	26.70	30.68	KFe3(SO4)2(OH)6
Mackinawite	-85.97	-125.10	-39.13	FeS
Melanterite	-10.50	-12.78	-2.28	FeSO4:7H2O
N2(g)	-1.77	-5.01	-3.24	N2
NH3(g)	-39.96	-44.62	-4.67	NH3
O2(g)	-28.84	56.16	85.00	O2
Pyrite	-141.65	-229.24	-87.59	FeS2
Quartz	-0.08	-4.14	-4.06	SiO2
Sepiolite	-6.92	8.99	15.91	Mg2Si3O7.5OH:3H2O
Sepiolite(d)	-9.67	8.99	18.66	Mg2Si3O7.5OH:3H2O
Siderite	-2.07	-12.93	-10.86	FeCO3
SiO2(a)	-1.39	-4.14	-2.76	SiO2
Sulfur	-67.67	-104.15	-36.48	S
Talc	-6.49	15.55	22.04	Mg3Si4O10(OH)2

F3B

Saturation indices

Phase	SI	log IAP	log KT	
Anhydrite	-5.38	-9.72	-4.34	CaSO4
Aragonite	-1.25	-9.54	-8.30	CaCO3
Calcite	-1.10	-9.54	-8.45	CaCO3
CH4(g)	-86.58	-131.48	-44.90	CH4
Chalcedony	-0.47	-4.10	-3.63	SiO2
Chrysotile	-9.01	24.04	33.05	Mg3Si2O5(OH)4
CO2(g)	-1.79	-19.96	-18.17	CO2
Dolomite	-1.83	-18.76	-16.93	CaMg(CO3)2
Fe(OH)3(a)	4.02	22.10	18.07	Fe(OH)3
FeS(ppt)	-84.93	-123.50	-38.58	FeS
Goethite	9.67	22.10	12.43	FeOOH
Gypsum	-5.14	-9.72	-4.58	CaSO4:2H2O
H2(g)	-27.88	-27.88	0.00	H2
H2O(g)	-1.69	-0.00	1.69	H2O
H2S(g)	-89.05	-131.66	-42.62	H2S
Halite	-6.32	-4.75	1.57	NaCl
Hematite	21.32	44.20	22.88	Fe2O3
Jarosite-K	-1.84	29.02	30.87	KFe3(SO4)2(OH)6
Mackinawite	-84.19	-123.50	-39.31	FeS
Melanterite	-9.69	-11.99	-2.29	FeSO4:7H2O
N2(g)	-1.72	-4.96	-3.24	N2
NH3(g)	-39.60	-44.30	-4.70	NH3
O2(g)	-29.66	55.76	85.42	O2
Pyrite	-139.29	-227.29	-88.00	FeS2

Quartz	-0.02	-4.10	-4.08	SiO2
Sepiolite	-6.74	9.20	15.94	Mg2Si3O7.5OH:3H2O
Sepiolite(d)	-9.46	9.20	18.66	Mg2Si3O7.5OH:3H2O
Siderite	-0.95	-11.80	-10.85	FeCO3
SiO2(a)	-1.33	-4.10	-2.77	SiO2
Sulfur	-67.13	-103.78	-36.66	S
Talc	-6.33	15.85	22.18	Mg3Si4O10(OH)2

F5

Saturation indices

Phase	SI	log IAP	log KT	
Anhydrite	-4.02	-8.36	-4.34	CaSO4
Aragonite	-1.89	-10.19	-8.30	CaCO3
Calcite	-1.74	-10.19	-8.45	CaCO3
CH4(g)	-84.10	-128.87	-44.77	CH4
Chalcedony	-0.47	-4.09	-3.62	SiO2
Chrysotile	-11.28	21.66	32.93	Mg3Si2O5(OH)4
CO2(g)	-1.90	-20.07	-18.17	CO2
Dolomite	-3.36	-20.31	-16.95	CaMg(CO3)2
Fe(OH)3(a)	3.54	21.59	18.05	Fe(OH)3
FeS(ppt)	-80.61	-119.05	-38.44	FeS
Goethite	9.22	21.59	12.37	FeOOH
Gypsum	-3.78	-8.36	-4.58	CaSO4:2H2O
H2(g)	-27.20	-27.20	0.00	H2
H2O(g)	-1.66	-0.00	1.66	H2O
H2S(g)	-84.57	-127.04	-42.48	H2S
Halite	-7.21	-5.64	1.57	NaCl
Hematite	20.42	43.19	22.76	Fe2O3
Jarosite-K	0.31	31.04	30.73	KFe3(SO4)2(OH)6
Mackinawite	-79.88	-119.05	-39.17	FeS
Melanterite	-7.97	-10.25	-2.28	FeSO4:7H2O
N2(g)	-2.05	-5.29	-3.24	N2
NH3(g)	-38.77	-43.44	-4.67	NH3
O2(g)	-30.71	54.40	85.11	O2
Pyrite	-131.20	-218.89	-87.69	FeS2
Quartz	-0.02	-4.09	-4.07	SiO2
Sepiolite	-8.29	7.62	15.92	Mg2Si3O7.5OH:3H2O
Sepiolite(d)	-11.04	7.62	18.66	Mg2Si3O7.5OH:3H2O
Siderite	-1.22	-12.08	-10.85	FeCO3
SiO2(a)	-1.33	-4.09	-2.76	SiO2
Sulfur	-63.32	-99.84	-36.53	S
Talc	-8.59	13.48	22.07	Mg3Si4O10(OH)2

F6

Saturation indices

Phase	SI	log IAP	log KT	
Anhydrite	-3.35	-7.70	-4.34	CaSO4
Aragonite	-0.86	-9.16	-8.30	CaCO3
Calcite	-0.71	-9.16	-8.45	CaCO3
CH4(g)	-83.81	-128.55	-44.74	CH4
Chalcedony	-0.01	-3.63	-3.62	SiO2
Chrysotile	-8.85	24.05	32.91	Mg3Si2O5(OH)4
CO2(g)	-1.26	-19.43	-18.17	CO2
Dolomite	-1.19	-18.15	-16.96	CaMg(CO3)2
Fe(OH)3(a)	1.82	19.87	18.05	Fe(OH)3
FeS(ppt)	-82.45	-120.86	-38.41	FeS
Goethite	7.51	19.87	12.36	FeOOH
Gypsum	-3.12	-7.70	-4.58	CaSO4:2H2O
H2(g)	-27.28	-27.28	0.00	H2
H2O(g)	-1.66	-0.00	1.66	H2O
H2S(g)	-84.64	-127.09	-42.45	H2S
Halite	-6.57	-5.00	1.57	NaCl
Hematite	17.00	39.74	22.74	Fe2O3
Jarosite-K	-4.16	26.53	30.70	KFe3(SO4)2(OH)6
Mackinawite	-81.72	-120.86	-39.14	FeS
Melanterite	-9.46	-11.74	-2.28	FeSO4:7H2O
N2(g)	-1.43	-4.67	-3.24	N2
NH3(g)	-38.59	-43.26	-4.67	NH3
O2(g)	-30.48	54.56	85.04	O2
Pyrite	-133.04	-220.67	-87.63	FeS2
Quartz	0.43	-3.63	-4.06	SiO2
Sepiolite	-5.93	9.98	15.91	Mg2Si3O7.5OH:3H2O
Sepiolite(d)	-8.68	9.98	18.66	Mg2Si3O7.5OH:3H2O
Siderite	-2.34	-13.20	-10.86	FeCO3
SiO2(a)	-0.87	-3.63	-2.76	SiO2
Sulfur	-63.31	-99.81	-36.50	S
Talc	-5.26	16.79	22.05	Mg3Si4O10(OH)2

FDP1

Saturation indices

Phase	SI	log IAP	log KT	
Anhydrite	-4.10	-8.46	-4.36	CaSO4
Aragonite	-0.38	-8.72	-8.34	CaCO3
Calcite	-0.24	-8.72	-8.48	CaCO3

CH4(g)	-31.65	-75.58	-43.93	CH4
Chalcedony	-0.08	-3.63	-3.55	SiO2
Chrysotile	-6.97	25.23	32.20	Mg3Si2O5(OH)4
CO2(g)	-1.43	-19.58	-18.15	CO2
Dolomite	-0.38	-17.47	-17.09	CaMg(CO3)2
Fe(OH)3(a)	-1.41	16.50	17.91	Fe(OH)3
FeS(ppt)	-28.27	-65.83	-37.56	FeS
Goethite	4.48	16.50	12.02	FeOOH
Gypsum	-3.88	-8.47	-4.58	CaSO4:2H2O
H2(g)	-14.00	-14.00	0.00	H2
H2O(g)	-1.51	-0.00	1.51	H2O
H2S(g)	-33.74	-75.33	-41.59	H2S
Halite	-5.79	-4.20	1.58	NaCl
Hematite	10.96	32.99	22.03	Fe2O3
Jarosite-K	-16.23	13.62	29.85	KFe3(SO4)2(OH)6
Mackinawite	-27.54	-65.83	-38.30	FeS
Melanterite	-7.63	-9.84	-2.21	FeSO4:7H2O
N2(g)	-1.48	-4.74	-3.26	N2
NH3(g)	-18.85	-23.37	-4.52	NH3
O2(g)	-55.12	28.00	83.12	O2
Pyrite	-41.39	-127.17	-85.78	FeS2
Quartz	0.35	-3.63	-3.98	SiO2
Sepiolite	-4.99	10.77	15.76	Mg2Si3O7.5OH:3H2O
Sepiolite(d)	-7.89	10.77	18.66	Mg2Si3O7.5OH:3H2O
Siderite	0.80	-10.09	-10.89	FeCO3
SiO2(a)	-0.92	-3.63	-2.71	SiO2
Sulfur	-25.62	-61.33	-35.71	S
Talc	-3.43	17.97	21.40	Mg3Si4O10(OH)2

FDP2

Saturation indices

Phase	SI	log IAP	log KT	
Anhydrite	-3.91	-8.27	-4.36	CaSO4
Aragonite	-1.12	-9.46	-8.34	CaCO3
Calcite	-0.98	-9.46	-8.48	CaCO3
CH4(g)	-84.62	-128.55	-43.93	CH4
Chalcedony	-0.38	-3.93	-3.55	SiO2
Chrysotile	-9.13	23.07	32.20	Mg3Si2O5(OH)4
CO2(g)	-1.45	-19.60	-18.15	CO2
Dolomite	-1.65	-18.74	-17.09	CaMg(CO3)2
Fe(OH)3(a)	3.77	21.68	17.91	Fe(OH)3
FeS(ppt)	-81.74	-119.30	-37.56	FeS
Goethite	9.66	21.68	12.02	FeOOH
Gypsum	-3.69	-8.27	-4.58	CaSO4:2H2O
H2(g)	-27.24	-27.24	0.00	H2
H2O(g)	-1.51	-0.00	1.51	H2O
H2S(g)	-85.78	-127.37	-41.59	H2S
Halite	-5.90	-4.32	1.58	NaCl
Hematite	21.34	43.37	22.03	Fe2O3
Jarosite-K	1.34	31.19	29.85	KFe3(SO4)2(OH)6
Mackinawite	-81.00	-119.30	-38.30	FeS
Melanterite	-8.13	-10.34	-2.21	FeSO4:7H2O
N2(g)	-1.19	-4.45	-3.26	N2
NH3(g)	-38.56	-43.08	-4.52	NH3
O2(g)	-28.64	54.48	83.12	O2
Pyrite	-133.65	-219.43	-85.78	FeS2
Quartz	0.05	-3.93	-3.98	SiO2
Sepiolite	-6.93	8.83	15.76	Mg2Si3O7.5OH:3H2O
Sepiolite(d)	-9.83	8.83	18.66	Mg2Si3O7.5OH:3H2O
Siderite	-0.64	-11.53	-10.89	FeCO3
SiO2(a)	-1.22	-3.93	-2.71	SiO2
Sulfur	-64.42	-100.13	-35.71	S
Talc	-6.19	15.21	21.40	Mg3Si4O10(OH)2

FDP3

Saturation indices

Phase	SI	log IAP	log KT	
Anhydrite	-4.40	-8.74	-4.34	CaSO4
Aragonite	-0.62	-8.92	-8.30	CaCO3
Calcite	-0.47	-8.92	-8.45	CaCO3
CH4(g)	-87.99	-132.82	-44.83	CH4
Chalcedony	-0.15	-3.78	-3.62	SiO2
Chrysotile	-7.48	25.50	32.99	Mg3Si2O5(OH)4
CO2(g)	-1.69	-19.86	-18.17	CO2
Dolomite	-0.82	-17.76	-16.94	CaMg(CO3)2
Fe(OH)3(a)	3.67	21.74	18.06	Fe(OH)3
FeS(ppt)	-86.52	-125.02	-38.50	FeS
Goethite	9.34	21.74	12.40	FeOOH
Gypsum	-4.16	-8.74	-4.58	CaSO4:2H2O
H2(g)	-28.24	-28.24	0.00	H2
H2O(g)	-1.67	-0.00	1.67	H2O
H2S(g)	-90.10	-132.64	-42.54	H2S
Halite	-5.99	-4.42	1.57	NaCl
Hematite	20.66	43.47	22.81	Fe2O3

Jarosite-K	-1.93	28.85	30.79	KFe3(SO4)2(OH)6
Mackinawite	-85.79	-125.02	-39.23	FeS
Melanterite	-9.78	-12.07	-2.29	FeSO4:7H2O
N2(g)	-1.52	-4.76	-3.24	N2
NH3(g)	-40.06	-44.74	-4.68	NH3
O2(g)	-28.77	56.48	85.25	O2
Pyrite	-141.60	-229.42	-87.83	FeS2
Quartz	0.30	-3.78	-4.07	SiO2
Sepiolite	-5.22	10.71	15.93	Mg2Si3O7.5OH:3H2O
Sepiolite(d)	-7.95	10.71	18.66	Mg2Si3O7.5OH:3H2O
Siderite	-1.39	-12.25	-10.85	FeCO3
SiO2(a)	-1.01	-3.78	-2.76	SiO2
Sulfur	-67.82	-104.40	-36.58	S
Talc	-4.17	17.95	22.12	Mg3Si4O10(OH)2

Wo2

Saturation indices

Phase	SI	log IAP	log KT	
Anhydrite	-4.83	-9.18	-4.34	CaSO4
Aragonite	-1.70	-10.01	-8.31	CaCO3
Calcite	-1.55	-10.01	-8.46	CaCO3
CH4(g)	-85.61	-130.20	-44.59	CH4
Chalcedony	-0.29	-3.89	-3.61	SiO2
Chrysotile	-10.05	22.73	32.78	Mg3Si2O5(OH)4
CO2(g)	-1.96	-20.12	-18.16	CO2
Dolomite	-2.97	-19.95	-16.98	CaMg(CO3)2
Fe(OH)3(a)	4.32	22.34	18.02	Fe(OH)3
FeS(ppt)	-82.53	-120.79	-38.26	FeS
Goethite	10.04	22.34	12.30	FeOOH
Gypsum	-4.60	-9.18	-4.58	CaSO4:2H2O
H2(g)	-27.52	-27.52	0.00	H2
H2O(g)	-1.63	-0.00	1.63	H2O
H2S(g)	-87.08	-129.37	-42.29	H2S
Halite	-7.05	-5.48	1.57	NaCl
Hematite	22.07	44.68	22.61	Fe2O3
Jarosite-K	0.50	31.04	30.54	KFe3(SO4)2(OH)6
Mackinawite	-81.80	-120.79	-38.99	FeS
Melanterite	-8.44	-10.71	-2.27	FeSO4:7H2O
N2(g)	-1.83	-5.08	-3.24	N2
NH3(g)	-39.18	-43.82	-4.64	NH3
O2(g)	-29.65	55.04	84.69	O2
Pyrite	-135.35	-222.64	-87.29	FeS2
Quartz	0.16	-3.89	-4.05	SiO2
Sepiolite	-7.22	8.67	15.88	Mg2Si3O7.5OH:3H2O
Sepiolite(d)	-9.99	8.67	18.66	Mg2Si3O7.5OH:3H2O
Siderite	-0.68	-11.54	-10.86	FeCO3
SiO2(a)	-1.14	-3.89	-2.75	SiO2
Sulfur	-65.50	-101.85	-36.35	S
Talc	-6.99	14.95	21.93	Mg3Si4O10(OH)2

Wo3B

Saturation indices

Phase	SI	log IAP	log KT	
Anhydrite	-5.07	-9.41	-4.34	CaSO4
Aragonite	-2.29	-10.58	-8.30	CaCO3
Calcite	-2.14	-10.58	-8.45	CaCO3
CH4(g)	-80.79	-125.63	-44.84	CH4
Chalcedony	-0.33	-3.95	-3.63	SiO2
Chrysotile	-11.87	21.13	33.00	Mg3Si2O5(OH)4
CO2(g)	-1.86	-20.03	-18.17	CO2
Dolomite	-4.00	-20.94	-16.94	CaMg(CO3)2
Fe(OH)3(a)	4.02	22.09	18.06	Fe(OH)3
FeS(ppt)	-77.06	-115.57	-38.52	FeS
Goethite	9.68	22.09	12.40	FeOOH
Gypsum	-4.83	-9.41	-4.58	CaSO4:2H2O
H2(g)	-26.40	-26.40	0.00	H2
H2O(g)	-1.68	-0.00	1.68	H2O
H2S(g)	-81.90	-124.46	-42.56	H2S
Halite	-6.98	-5.41	1.57	NaCl
Hematite	21.34	44.17	22.83	Fe2O3
Jarosite-K	0.11	30.92	30.80	KFe3(SO4)2(OH)6
Mackinawite	-76.32	-115.57	-39.25	FeS
Melanterite	-7.68	-9.97	-2.29	FeSO4:7H2O
N2(g)	-1.63	-4.87	-3.24	N2
NH3(g)	-37.35	-42.03	-4.69	NH3
O2(g)	-32.48	52.80	85.28	O2
Pyrite	-125.77	-213.63	-87.86	FeS2
Quartz	0.12	-3.95	-4.08	SiO2
Sepiolite	-8.43	7.50	15.93	Mg2Si3O7.5OH:3H2O
Sepiolite(d)	-11.16	7.50	18.66	Mg2Si3O7.5OH:3H2O
Siderite	-0.30	-11.15	-10.85	FeCO3
SiO2(a)	-1.19	-3.95	-2.76	SiO2
Sulfur	-61.46	-98.06	-36.60	S
Talc	-8.91	13.22	22.13	Mg3Si4O10(OH)2

Wo4

-----------------------------Saturation indices----------------------

Phase	SI	log IAP	log KT	
Anhydrite	-4.01	-8.35	-4.34	CaSO4
Aragonite	-2.41	-10.71	-8.30	CaCO3
Calcite	-2.26	-10.71	-8.45	CaCO3
CH4(g)	-80.65	-125.38	-44.73	CH4
Chalcedony	-0.30	-3.92	-3.62	SiO2
Chrysotile	-11.76	21.13	32.90	Mg3Si2O5(OH)4
CO2(g)	-1.93	-20.10	-18.17	CO2
Dolomite	-4.20	-21.16	-16.96	CaMg(CO3)2
Fe(OH)3(a)	4.04	22.08	18.04	Fe(OH)3
FeS(ppt)	-75.70	-114.10	-38.39	FeS
Goethite	9.73	22.08	12.35	FeOOH
Gypsum	-3.77	-8.35	-4.58	CaSO4:2H2O
H2(g)	-26.32	-26.32	0.00	H2
H2O(g)	-1.66	-0.00	1.65	H2O
H2S(g)	-80.59	-123.02	-42.43	H2S
Halite	-7.03	-5.46	1.57	NaCl
Hematite	21.44	44.16	22.72	Fe2O3
Jarosite-K	2.44	33.12	30.68	KFe3(SO4)2(OH)6
Mackinawite	-74.97	-114.10	-39.13	FeS
Melanterite	-6.54	-8.82	-2.28	FeSO4:7H2O
N2(g)	-2.05	-5.29	-3.24	N2
NH3(g)	-37.46	-42.12	-4.67	NH3
O2(g)	-32.36	52.64	85.00	O2
Pyrite	-123.20	-210.80	-87.59	FeS2
Quartz	0.15	-3.92	-4.06	SiO2
Sepiolite	-8.34	7.56	15.91	Mg2Si3O7.5OH:3H2O
Sepiolite(d)	-11.10	7.56	18.66	Mg2Si3O7.5OH:3H2O
Siderite	-0.32	-11.18	-10.86	FeCO3
SiO2(a)	-1.16	-3.92	-2.76	SiO2
Sulfur	-60.22	-96.70	-36.48	S
Talc	-8.73	13.30	22.04	Mg3Si4O10(OH)2

Wo5

-----------------------------Saturation indices----------------------

Phase	SI	log IAP	log KT	
Anhydrite	-4.09	-8.43	-4.34	CaSO4
Aragonite	-3.70	-12.00	-8.29	CaCO3
Calcite	-3.55	-12.00	-8.44	CaCO3
CH4(g)	-73.89	-118.84	-44.95	CH4
Chalcedony	-0.29	-3.93	-3.63	SiO2
Chrysotile	-14.71	18.38	33.09	Mg3Si2O5(OH)4
CO2(g)	-2.11	-20.28	-18.17	CO2
Dolomite	-6.61	-23.53	-16.92	CaMg(CO3)2
Fe(OH)3(a)	2.79	20.87	18.08	Fe(OH)3
FeS(ppt)	-68.09	-106.72	-38.62	FeS
Goethite	8.43	20.87	12.45	FeOOH
Gypsum	-3.84	-8.43	-4.58	CaSO4:2H2O
H2(g)	-24.64	-24.64	0.00	H2
H2O(g)	-1.70	-0.00	1.70	H2O
H2S(g)	-72.60	-115.27	-42.67	H2S
Halite	-6.96	-5.39	1.57	NaCl
Hematite	18.83	41.75	22.92	Fe2O3
Jarosite-K	0.11	31.02	30.91	KFe3(SO4)2(OH)6
Mackinawite	-67.36	-106.72	-39.36	FeS
Melanterite	-5.86	-8.16	-2.30	FeSO4:7H2O
N2(g)	-1.70	-4.94	-3.24	N2
NH3(g)	-34.72	-39.43	-4.70	NH3
O2(g)	-36.25	49.28	85.53	O2
Pyrite	-109.25	-197.34	-88.10	FeS2
Quartz	0.16	-3.93	-4.09	SiO2
Sepiolite	-10.24	5.71	15.95	Mg2Si3O7.5OH:3H2O
Sepiolite(d)	-12.95	5.71	18.66	Mg2Si3O7.5OH:3H2O
Siderite	-0.88	-11.73	-10.85	FeCO3
SiO2(a)	-1.16	-3.93	-2.77	SiO2
Sulfur	-53.93	-90.63	-36.70	S
Talc	-11.69	10.52	22.22	Mg3Si4O10(OH)2

79055

-----------------------------Saturation indices----------------------

Phase	SI	log IAP	log KT	
Anhydrite	-3.34	-7.68	-4.34	CaSO4
Aragonite	-0.14	-8.44	-8.30	CaCO3
Calcite	0.01	-8.44	-8.45	CaCO3
CH4(g)	-85.43	-130.26	-44.83	CH4
Chalcedony	-0.24	-3.86	-3.62	SiO2
Chrysotile	-7.75	25.23	32.99	Mg3Si2O5(OH)4
CO2(g)	-1.05	-19.22	-18.17	CO2
Dolomite	0.27	-16.68	-16.94	CaMg(CO3)2
Fe(OH)3(a)	3.17	21.24	18.06	Fe(OH)3
FeS(ppt)	-83.64	-122.14	-38.50	FeS

Goethite	8.84	21.24	12.40	FeOOH
Gypsum	-3.10	-7.68	-4.58	CaSO4:2H2O
H2(g)	-27.76	-27.76	0.00	H2
H2O(g)	-1.67	-0.00	1.67	H2O
H2S(g)	-86.96	-129.50	-42.54	H2S
Halite	-5.55	-3.99	1.57	NaCl
Hematite	19.66	42.47	22.81	Fe2O3
Jarosite-K	-0.37	30.42	30.79	KFe3(SO4)2(OH)6
Mackinawite	-82.91	-122.14	-39.23	FeS
Melanterite	-8.82	-11.11	-2.29	FeSO4:7H2O
N2(g)	-1.14	-4.38	-3.24	N2
NH3(g)	-39.15	-43.83	-4.68	NH3
O2(g)	-29.73	55.52	85.25	O2
Pyrite	-136.06	-223.89	-87.83	FeS2
Quartz	0.21	-3.86	-4.07	SiO2
Sepiolite	-5.54	10.39	15.93	Mg2Si3O7.5OH:3H2O
Sepiolite(d)	-8.27	10.39	18.66	Mg2Si3O7.5OH:3H2O
Siderite	-1.01	-11.87	-10.85	FeCO3
SiO2(a)	-1.10	-3.86	-2.76	SiO2
Sulfur	-65.16	-101.74	-36.58	S
Talc	-4.61	17.51	22.12	Mg3Si4O10(OH)2

79059

Saturation indices

Phase	SI	log IAP	log KT	
Anhydrite	-5.10	-9.45	-4.35	CaSO4
Aragonite	-1.07	-9.39	-8.32	CaCO3
Calcite	-0.92	-9.39	-8.47	CaCO3
CH4(g)	-97.26	-141.55	-44.29	CH4
Chalcedony	-0.37	-3.95	-3.58	SiO2
Chrysotile	-6.04	26.47	32.51	Mg3Si2O5(OH)4
CO2(g)	-2.60	-20.75	-18.16	CO2
Dolomite	-1.65	-18.68	-17.03	CaMg(CO3)2
Gypsum	-4.87	-9.45	-4.58	CaSO4:2H2O
H2(g)	-30.20	-30.20	0.00	H2
H2O(g)	-1.58	-0.00	1.58	H2O
H2S(g)	-99.65	-141.61	-41.97	H2S
Halite	-5.93	-4.36	1.58	NaCl
N2(g)	-1.21	-4.46	-3.25	N2
NH3(g)	-42.95	-47.53	-4.59	NH3
O2(g)	-23.57	60.40	83.97	O2
Quartz	0.07	-3.95	-4.02	SiO2
Sepiolite	-4.76	11.07	15.83	Mg2Si3O7.5OH:3H2O
Sepiolite(d)	-7.59	11.07	18.66	Mg2Si3O7.5OH:3H2O
SiO2(a)	-1.21	-3.95	-2.73	SiO2
Sulfur	-75.36	-111.41	-36.06	S
Talc	-3.11	18.58	21.69	Mg3Si4O10(OH)2

79060

Saturation indices

Phase	SI	log IAP	log KT	
Anhydrite	-4.01	-8.36	-4.36	CaSO4
Aragonite	-0.19	-8.52	-8.33	CaCO3
Calcite	-0.05	-8.52	-8.47	CaCO3
CH4(g)	-91.19	-135.29	-44.10	CH4
Chalcedony	-0.34	-3.91	-3.57	SiO2
Chrysotile	-7.03	25.33	32.35	Mg3Si2O5(OH)4
CO2(g)	-1.30	-19.46	-18.15	CO2
Dolomite	0.13	-16.93	-17.06	CaMg(CO3)2
Gypsum	-3.78	-8.36	-4.58	CaSO4:2H2O
H2(g)	-28.96	-28.96	0.00	H2
H2O(g)	-1.54	-0.00	1.54	H2O
H2S(g)	-93.36	-135.13	-41.77	H2S
Halite	-5.69	-4.11	1.58	NaCl
N2(g)	-1.84	-5.09	-3.26	N2
NH3(g)	-41.43	-45.99	-4.55	NH3
O2(g)	-25.61	57.92	83.52	O2
Quartz	0.09	-3.91	-4.00	SiO2
Sepiolite	-5.42	10.37	15.79	Mg2Si3O7.5OH:3H2O
Sepiolite(d)	-8.29	10.37	18.66	Mg2Si3O7.5OH:3H2O
SiO2(a)	-1.19	-3.91	-2.72	SiO2
Sulfur	-70.30	-106.17	-35.88	S
Talc	-4.03	17.51	21.54	Mg3Si4O10(OH)2

APPENDIX C:
PREDICTED COMPARED TO MEASURED ^{222}Rn CONCENTRATIONS IN STREAM WATER

Table C.1 Measured and predicted ^{222}Rn concentration (mBq L^{-1}) after ^{222}Rn losses caused by turbulent gas exchange and radioactive decay (numerical modeling) in stream water during March 2001 (flood recession).

stream reach	Measured ^{222}Rn	Predicted ^{222}Rn
1 – 2	122	10^{-22}
2 – 3	119	10^{-8}
3 – 4	70	10^{-5}
4 – 5	59	2
5 – 7	79	5
7 – 8	80	58
8 – 9	123	119
9 – 10	181	62
10 – 11	220	10^{-3}
11 – 12	196	10^{-3}
12 – 13	149	0.06
10 – 14	220	76
2 – T1	119	10^{-7}
10 – T6	220	0.06
11 – T8	196	5
11 – T9	196	10^{-3}
11 – T10	196	10^{-6}

Table C.2 Measured and predicted ^{222}Rn concentration (mBq L^{-1}) after ^{222}Rn losses caused by turbulent gas exchange and radioactive decay (numerical modeling) in stream water during November 2001 (baseflow).

stream reach	Measured ^{222}Rn	Predicted ^{222}Rn
1 – 2	127	10^{-245}
2 – 3	233	10^{-26}
3 – 4	62	10^{-16}
4 – 5	272	10^{-4}
5 – 7	106	10^{-2}
7 – 8	44	11
8 – 9	67	62
9 – 10	153	41
10 – 11	278	10^{-4}
11 – 12	339	10^{-5}
12 – 13	170	0.06
10 – 14	278	20
14 – 15	532	0.3
15 – 22	53	0.03
22 – 23	228	0.5
23 – 24	173	0.1
24 – 25	151	10^{-3}
25 – 26	253	10^{-137}
15 – 16	53	10^{-5}
16 – 17	319	0.02
17 – 18	388	10^{-5}
18 – 19	73	10^{-6}
19 – 20	564	10^{-13}
20 – 21	82	0
7 – T4	44	160
10 – T6	278	10^{-7}
T6 – T7	209	10^{-15}

stream reach	Measured ^{222}Rn	Predicted ^{222}Rn
11 – T10	339	10^{-16}
T10 – T11	57	10^{-36}
3 – T3	62	10^{-9}
3 – T2	62	10^{-12}
4 – TB	272	10^{-87}
23 – T13	173	10^{-3}
11 – T8	339	0.6
11 – T9	339	10^{-5}